LEABHARLANN CHOLÁISTE NA TRÍONÓIDE, BAILE ÁTHA CLIATH | TRINITY COLLEGE LIBRARY DUBLIN
Ollscoil Átha Cliath | The University of Dublin

Terms and Conditions of Use of Digitised Theses from Trinity College Library Dublin

Copyright statement

All material supplied by Trinity College Library is protected by copyright (under the Copyright and Related Rights Act, 2000 as amended) and other relevant Intellectual Property Rights. By accessing and using a Digitised Thesis from Trinity College Library you acknowledge that all Intellectual Property Rights in any Works supplied are the sole and exclusive property of the copyright and/or other IPR holder. Specific copyright holders may not be explicitly identified. Use of materials from other sources within a thesis should not be construed as a claim over them.

A non-exclusive, non-transferable licence is hereby granted to those using or reproducing, in whole or in part, the material for valid purposes, providing the copyright owners are acknowledged using the normal conventions. Where specific permission to use material is required, this is identified and such permission must be sought from the copyright holder or agency cited.

Liability statement

By using a Digitised Thesis, I accept that Trinity College Dublin bears no legal responsibility for the accuracy, legality or comprehensiveness of materials contained within the thesis, and that Trinity College Dublin accepts no liability for indirect, consequential, or incidental, damages or losses arising from use of the thesis for whatever reason. Information located in a thesis may be subject to specific use constraints, details of which may not be explicitly described. It is the responsibility of potential and actual users to be aware of such constraints and to abide by them. By making use of material from a digitised thesis, you accept these copyright and disclaimer provisions. Where it is brought to the attention of Trinity College Library that there may be a breach of copyright or other restraint, it is the policy to withdraw or take down access to a thesis while the issue is being resolved.

Access Agreement

By using a Digitised Thesis from Trinity College Library you are bound by the following Terms & Conditions. Please read them carefully.

I have read and I understand the following statement: All material supplied via a Digitised Thesis from Trinity College Library is protected by copyright and other intellectual property rights, and duplication or sale of all or part of any of a thesis is not permitted, except that material may be duplicated by you for your research use or for educational purposes in electronic or print form providing the copyright owners are acknowledged using the normal conventions. You must obtain permission for any other use. Electronic or print copies may not be offered, whether for sale or otherwise to anyone. This copy has been supplied on the understanding that it is copyright material and that no quotation from the thesis may be published without proper acknowledgement.

NITROGEN CONTAINING AROMATIC LIGANDS

NITROGEN-HETEROSUPERBENZENE AND DERIVATIVES

BY

DANIEL J. GREGG

A thesis submitted in the fulfilment of the requirements for the Degree of Doctor of Philosophy at the University of Dublin, Trinity College. Submitted April 2003

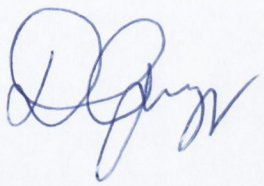
TRINITY COLLEGE
13 OCT 2003
LIBRARY DUBLIN
THESIS
7477
7360

DECLARATION

This thesis has never been submitted as an exercise for a degree at this or any other university.

Except where otherwise stated, the experimental work described herein has been carried out by the author alone.

I agree that the Library of Trinity College may lend or copy this thesis upon request.



Daniel Gregg

ACKNOWLEDGEMENTS

I would like to sincerely thank my supervisor, Dr. Sylvia Draper, for all her support, advice, and encouragement throughout my time here at Trinity College. Thanks to Professor John Kelly and Professor John Corish, for the use of the departmental equipment, and for accepting me into the College.

Thanks to my Family, especially my parents, for their support both financial and emotional.

Thanks to all the members of my group, Anne, Denise, Elise, Eileen, Gareth, Cecille, Rethi, Angelica and Chris for their help and friendship, and to the rest of the Post Graduate crew, "cheers".

Thanks to Dr. Marko Duati, Dr. Wesley Browne, and Professor Han Vos for their collaboration and helpful discussion of the Ruthenium complex formed in this work.

To Dr. John O'Brien for working so hard on all my NMRs, thanks loads!!! Thanks to the great TCD technical support team, especially Dr Martin Feeney, who are always so happy to help, and thanks to Dr. Tom McCabe and Dr. Chris Fitchett for their hard work on the X-ray structural analysis.

Thank you Dr. Emma Schofield for your most helpful discussion and support, Dr. Graeme Watson for calculating the ground state dipole moment of N-HBC, and Sandy Flemming for work on the low concentration electronic spectroscopy and enlightening aggregation discussions!!

Thanks Hollie, once again, for everything!! Thanks Subgenera!!

Finally I would like to thank the Krieble Fund, BOC Gases, Enterprise Ireland, Trinity Association and Trust and the Broad Curriculum Exercise for financial support.

Thanks!

SUMMARY

In Chapter 1, the potentially terdentate C,N,N'-chelating monoanionic aryl diamine ligand "Diam" is manipulated, resulting in the synthesis of several novel compounds. This includes DiamZnEt, the first organometallic complex of an alkylated Zn(II) centre, which is intramolecularly stabilised by the pendant di-nitrogen arm of this ligand.

Chapter 2 establishes the synthetic route representative of molecularly controlled intrinsic doping of two-dimensional soft organic materials to produce N-doped graphite analogues. The formation of the first N-functionalized heterosuperbenzene has been proven through the isolation and spectroscopic characterization of N-HBC **(17)**.
The absorption and emission spectra of N-HBC show similarities to hexa-*peri*-benzocoronene, indicating that N-HBC maintains the HBC chromophore. The introduction of four electron withdrawing imine nitrogen atoms causes a depletion of the π-electron density within the core, and gives N-HBC overall electron-accepting properties. Kasha's criteria are used to assign the bands in the UV-vis spectrum of N-HBC as either $n \rightarrow \pi^*$ or $\pi \rightarrow \pi^*$ electronic transitions.
The fluorescence spectra of N-HBC are more diffuse and red-shifted in a polar solvent relative to that in a nonpolar solvent. This is due to the charge transfer character of the electronic transition (large μ_e value). The polar N-HBC molecule has structurally opposing electronegative nitrogen atoms and weakly donating *tert*-butyl groups. Solvatochromic studies allow estimation of the change in dipole moment upon excitation (μ_g and μ_e) by way of a Lippert Mataga Plot.
Because of the incorporation of pyrimidine nitrogens within the carbon framework, N-HBC is sensitive toward external triggers, as seen in the electronic spectra upon addition of acid (TFA) or the amine donor aniline. Thermogravimetric analysis demonstrates the extremely high thermal stability of the central unit of N-HBCs, and cyclic voltammetry experiments show an increase in the ease of reduction compared to HBC, further demonstrating the electron acceptor properties of the N-doped derivative.
Electronic and NMR spectroscopic analyses suggest that these systems spontaneously aggregate, even at very low concentration.
I have also presented, in this chapter, my synthetic contribution toward the establishment of a family of N-heterosuperbenzenes with intrinsic carbon-nitrogen frameworks.

In Chapter 3, I have succeeded in the synthesis of two new transition metal complexes of N-HBC with Ru(II) and Pd(II).

$[Ru(bpy)_2(N\text{-}HBC_{17})](PF_6)_2$ was synthesized and fully characterized. The visible region of the UV-vis spectra of $[Ru(bpy)_2(N\text{-}HBC_{17})]^{2+}$ is dominated by two MLCT transitions, assigned as transitions due to bpy or N-HBC. The low-lying π^* acceptor orbitals of N-HBC provide the low-energy MLCT absorption bands at 615 nm and the emission maxima at 816 nm. Electrochemical results suggest that oxidation of the metal centre is more difficult in $[Ru(bpy)_2(N\text{-}HBC_{17})](PF_6)_2$ than in $[Ru(bpy)_3]^{2+}$. This is due to the presence of the electron accepting N-HBC ligand. The complex also shows better π-acceptor properties than the ligand.

$[AllylPd(N\text{-}HBC_{17})](PF_6)$ has also been prepared and characterised. Coordination is found to have a profound electronic effect on the π-electron density throughout the ligand system, as seen by large red-shifts in the absorption spectrum that mimic ligand protonation. Metal perturbed LC absorption bands are detected in the 340-700 nm spectral region. The fluorescent emission from N-HBC is quenched upon complexation.

In Chapter 4, new ferrocenyl complexes with polyphenylene derivatives have been prepared and characterised, and the molecular structures of 1,2,3,4-tetraphenyl-5-ferrocenylbenzene **(40)** and 1,2-dipyrimidyl-3,6-bis-(4-*tert*-butylphenyl)-4-phenyl-5-ferrocenyl benzene **(45)** have been elucidated by single-crystal X-ray analyses. The work demonstrates for the first time that cyclodehydrogenation is possible in the presence of an organometallic unit, with the synthesis of tetra-*peri*-benzo-*peri*-ferrocenylcoronene **(41)** *via* treatment of 1,2,3,4-tetraphenyl-5-ferrocenylbenzene with $CuCl_2$ and $AlCl_3$ in CS_2.

In general, the UV-vis spectrum of ferrocenyl complex **(41)** is dominated by $\pi \rightarrow \pi^*$ transitions, attributed to the corresponding polycyclic aromatic substituent.

The cyclic voltammograms of these ferrocenyl derivatives each exhibit the one-electron reversible oxidation wave associated with ferrocene/ferrocenium couple and an E° value that is influenced by the electronic effects of the substituent. The latter are also evident in the NMR data.

As the three dimensional extension to nitrogen doped PAHs, Chapter 5 describes the synthesis of the aza[60]fullerene dimer $(C_{59}N)_2$, and attempts its functionalization with acetylenic units.

Chapter 6 gives an account of the experimental details of this work.

CONTENTS

Declaration ii
Acknowledgements iii
Summary iv
Abbreviations and Symbols vi
List of Tables and Figures vii

Chapter One: **COMPLEXES OF AN ARYL DIAMINE LIGAND**

1.1 Introduction 1
1.2 Results and Discussion 5
1.2.1 Formation of $(DiamLi)_2$ 5
1.2.2 Intramolecularly stabilised arylzincates, DiamZnCl and DiamZnEt 6
1.2.3 Ethynyl Substituted Diam 8
1.3 References 13

Chapter Two: **NITROGEN-HETEROSUPERBENZENES (2-D POLYAROMATIC SYSTEMS)**

2.1 Introduction 14
2.1.1 Synthesis 14
2.1.2 HBC Properties and Material Application 20
2.2 Results and Discussion 25
2.2.1 The Synthesis of N-Heterosuperbenzene, N-HBC **(17)** 25
2.2.1.1 The Cyclodehydrogenation reaction of Hexaphenylbenzene 25
2.2.1.2 Nitrogen Doping of an Organic Semiconductor: Discrete Control at a Molecular Level 26
2.2.1.3 Synthetic Extension To N-HBC **(17)** 29
2.2.2 The Generation of the N-Heterosuperbenzene Family 34
2.2.2.1 The Synthetic Control 34
2.2.2.2 Incorporating Alkyne Functionalities 35
2.2.2.3 Functionalised Polyarylbenzenes 39
2.2.2.4 Propeller Frameworks 45
2.2.2.5 UV-vis Absorption Spectroscopy 48
2.2.2.6 Alternative Synthesis 51
2.2.3 General Properties of N-HBC **(17)** 52
2.2.3.1 Solubility 52
2.2.3.2 Thermal Stability 52
2.2.3.3 Electrochemistry 53
2.2.4 Photophysical Properties of N-HBC **(17)** 54
2.2.4.1 UV-vis Absorption Spectroscopy 54
2.2.4.2 Emission Spectroscopy 61
2.2.4.3 Absorption and Fluorescence Properties of the Protonated Form of N-HBC **(17)** 72
2.2.4.4 Absorption and Fluorescence Properties of an Exciplex of N-HBC **(17)** 77
2.2.5 Spectral Summary For N-HBC **(17)** 79
2.2.6 Self-Association: Aggregation of N-HBC **(17)** in Solution 81
2.2.7 Cyclodehydrogenation to N-Heterosuperbenzene Derivatives 87
2.2.7.1 Synthesis of N-HBC **(21)** 87
2.2.7.2 Photophysical Properties of N-HBC **(21)** 88

2.2.7.3 Attempted Cyclodehydrogenation of **(23)**, **(29)** and **(31)** to N-HBC 92
2.2.7.4 Photophysical Properties of Spirocyclic **(24)** 96
2.3 Summary 97
2.4 Future Applications 100
2.5 References 102

Chapter Three: **TRANSITION METAL COMPLEXES OF NITROGEN-HETEROSUPERBENZENES**
3.1 Introduction 105
3.1.1 Ruthenium 106
3.1.2 Palladium 108
3.2 Results and Discussion 110
3.2.1 Synthesis of the Ligand N-HBC **(17)** 110
3.2.2 Ruthenium Complex **(35)** 110
3.2.2.1 Synthesis and Characterisation 110
3.2.2.2 Electrochemistry 114
3.2.2.3 Photophysical Properties of **(35)** 119
3.2.2.4 Spectroelectrochemistry 126
3.2.2.5 Acid-Base Properties 126
3.2.2.6 Photodissociation 127
3.2.3 Ruthenium Complex **(34)** 128
3.2.3.1 Synthesis and Characterisation 128
3.2.4 Palladium Complex **(36)** 131
3.2.4.1 Synthesis and Characterisation 131
3.2.4.2 Photophysical Properties of **(36)** 133
3.3 Summary 137
3.4 Future Work 139
3.5 References 141

Chapter Four: **POLYARYL FERROCENE COMPOUNDS (TOWARD THE SYNTHESIS OF FERROCENE SUBSTITUTED PAHs)**
4.1 Introduction 143
4.2 Results and Discussion 146
4.2.1 Synthesis and Characterisation 146
4.2.1.1 Derivative Comparisons 158
4.2.1.2 X-Ray Crystallographic Analysis 159
4.2.2 UV-vis Absorption Spectroscopy 162
4.2.3 Electrochemistry 165
4.3 Summary 169
4.4 Future Work 170
4.5 References 171

Chapter Five: **THE HETEROFULLERENE, AZA[60]FULLERENE**
5.1 Introduction 172
5.2 Results and Discussion 176
5.3 References 180

Chapter Six: **EXPERIMENTAL**

General comments 181

6.1 COMPLEXES OF AN ARYL DIAMINE LIGAND 183

6.1.1 DiamBr, **(1)** 183

6.1.2 DiamLi, **(2)** 183

6.1.3 DiamZnCl, **(3)** 184

6.1.4 DiamZnEt, **(4)** 184

6.1.5 Tributyl(phenylethynyl)tin, **(5)** 185

6.1.6 $DiamSn(Bu)_3$, **(6)** 185

6.1.7 DiamI, **(7)** 186

6.1.8 Attempted Synthesis of Ethynyl substituted Diam, **(8)** 187

6.2 NITROGEN-HETEROSUPERBENZENES 188

6.2.1 Hexaphenylbenzene, **(10)** 188

6.2.2 Hexabenzocoronene, **(11)** 188

6.2.3 Dipyrimidinyl acetylene, **(12)** 188

6.2.4 1,2-bis-(4-*tert*-butylphenyl)ethane-1,2-dione, **(13)** 189

6.2.5 1,3-bis-(4-*tert*-butylphenyl)propan-2-one, **(14)** 190

6.2.6 2,3,4,5-tetra-(4-*tert*-butylphenyl)cyclopenta-2,4-dienone, **(15)** 190

6.2.7 1,2-dipyrimidyl-3,4,5,6-tetra-(4-*tert*-butylphenyl)benzene, **(16)** 191

6.2.8 Tetra-*peri*-(*tert*-butyl-benzo)-di-*peri*-(pyrimidino)-coronene, **(17)** 191

6.2.9 1,2-bis-(4-methyl-phenyl)ethane-1,2-dione, **(18)** 192

6.2.10 2,5-bis-(4-*tert*-butylphenyl)-3,4-bis-(4-methyl-phenyl)cyclopenta-2,4-dienone, **(19)** 193

6.2.11 1,2-dipyrimidyl-3,6-bis-(4-*tert*-butylphenyl)-4,5-bis-(4-methyl-phenyl)benzene, **(20)** 193

6.2.12 Di-*peri*-(*tert*-butyl-benzo)-di-*peri*-(methyl-benzo)-di-*peri*-(pyrimidino)-coronene, **(21)** 194

6.2.13 2,5-bis-(4-*tert*-butylphenyl)-3,4-bis-(4-methoxyphenyl)cyclopenta-2,4-dienone, **(22)** 194

6.2.14 1,2-dipyrimidyl-3,6-bis-(4-*tert*-butylphenyl)-4,5-bis-(4-methoxyphenyl)benzene, **(23)** 195

6.2.15 Attempted Synthesis of Di-*peri*-(*tert*-butyl-benzo)-di-*peri*-(methoxy-benzo)-di-*peri*-(pyrimidino)-coronene, **(24)** 196

6.2.16 1,2-bis(4-trimethylsilylethynylphenyl)ethane-1,2-dione, **(25)** 196

6.2.17 3,4-bis(4-ethynylphenyl)-2,5-bis(4-*tert*-butylphenyl)cyclopenta-2,4-dienone, **(26)** 197

6.2.18 1,2-bis(4-triisopropylsilylethynylphenyl)ethane-1,2-dione, **(27)** 198

6.2.19 2,5-bis(4-*tert*-butylphenyl)-3,4-bis(4-triisopropylsilylethynylphenyl)cyclopenta-2,4-dienone, **(28)** 198

6.2.20 1,2-dipyrimidyl-3,6-bis-(4-*tert*-butylphenyl)-4,5-bis-(4-triisopropylsilylethynylphenyl)benzene, **(29)** 199

6.2.21 2,5-bis-(4-*tert*-butylphenyl)-3,4-bis-(4-bromo-phenyl)cyclopenta-2,4-dienone, **(30)** 199

6.2.22 1,2-dipyrimidyl-3,6-bis-(4-*tert*-butylphenyl)-4,5-bis-(4-bromo-phenyl)benzene, **(31)** 200

6.2.23 1,2-dipyrimidyl-3,6-bis-(4-*tert*-butylphenyl)-4,5-bis-(4-(3-methyl-3-hydroxy-butynyl)phenyl)benzene, **(32)** 200

6.3 TRANSITION METAL COMPLEXES OF N-HETEROSUPERBENZENES 202
6.3.1 $[Ru(bpy)_2(16)](PF_6)_2$, **(34)** 202
6.3.2 $[Ru(bpy)_2(N\text{-}HBC_{17})](PF_6)_2$, **(35)** 202
6.3.3 $[Pd(\eta^3\text{-}C_3H_5)(N\text{-}HBC_{17})]PF_6$, **(36)** 203

6.4 POLYARYL FERROCENE COMPOUNDS 204
6.4.1 Ethynylferrocene, **(37)** 204
6.4.2 Phenylethynylferrocene, **(38)** 205
6.4.3 1,4-bis(ferrocenyl)butadiyne, **(39)** 205
6.4.4 1,2,3,4-tetraphenyl-5-ferrocenylbenzene, **(40)** 206
6.4.5 Tetra-*peri*-benzo-*peri*-ferrocenylcoronene, **(41)** 206
6.4.6 1,2,3,4,5-pentaphenyl-6-ferrocenylbenzene, **(42)** 207
6.4.7 1-ferrocenyl-2-phenylethane-1,2-dione, **(43)** 208
6.4.8 2,5-bis-(4-*tert*-butylphenyl)-3-ferrocenyl-4-phenylcyclopenta-2,4-dienone, **(44)** 209
6.4.9 1,2-dipyrimidyl-3,6-bis-(4-*tert*-butylphenyl)-4-ferrocenyl-5-phenylbenzene, **(45)** 209
6.4.10 1,2,3,4-tetraphenyl-5-ferrocenyl-6-ferrocenylethynylbenzene, **(46)** 210

6.5 THE HETEROFULLERENE, AZA[60]FULLERENE 212
6.5.1 Diazabis-(1,6);(1,9)-homofullerene, **(47)** 212
6.5.2 Aza[60]fullerene dimer, $(C_{59}N)_2$, **(48)** 212

6.6 References 213

APPENDICIES 214
Appendix 1 214
Tables A1-A6: Crystal Data and Structure Refinement for **(23)** 214
Tables B1-B6: Crystal Data and Structure Refinement for **(29)** 223
Tables C1-C6: Crystal Data and Structure Refinement for **(31)** 234
Tables D1-D6: Crystal Data and Structure Refinement for **(24)** 242
Tables E1-E6: Crystal Data and Structure Refinement for **(40)** 256
Tables F1-F6: Crystal Data and Structure Refinement for **(45)** 265
Appendix 2 276
Semi-empirical quantum mechanic calculations of various Dipole moments (AM1 parameter set) 276

ABBREVIATIONS AND SYMBOLS

bpy	2,2′-bipyridine	*m/z*	Mass/charge value
br	Broad (NMR)	N-HBC	Nitrogen-heterosuperbenzene
Cat	Catalyst	NMR	Nuclear magnetic resonance
$CDCl_3$	Deuterated chloroform	ODCB	1,2-dichlorobenzene
Cp	Cyclopentadiene	PAH	Polycyclic aromatic hydrocarbon
CT	Charge transfer	phen	1,10-phenanthroline
CV	Cyclic voltammetry	ppm	Parts per million
d	Doublet (NMR)	*p*-TsOH	Toluene-*p*-sulfonic acid
	Days (Experimental)	s	Singlet (NMR)
DBU	1,8-Diazabicyclo[5.4.0]undec-7-ene	SCE	Saturated calomel reference electrode
DMF	Dimethyl formamide		
DMPD	Dimethylpiperazinedione	SWNT	Single-walled carbon nanotubes
DPV	Differential Pulse Voltammetry	st	Stretching vibration
Et	Ethyl	sy	Symmetric
Fc	Ferrocenyl	t	Triplet (NMR)
FMO	Frontier Molecular Orbitals	TBA	Tetrabutyl ammonium ion
h	Hours (Experimental)	*tert*-butyl	Tertiarybutyl
HBC	Hexa-*peri*-hexabenzocoronene	TFA	Trifluoroacetic acid
HOMO	Highest occupied molecular orbital	TG	Thermogravimetric
IC	Internal conversion	THF	Tetrahydrofuran
IR	Infrared	TiPSA	Triisopropylsilyl acetylene
ISC	Intersystem crossing	TMEDA	Tetramethylethylenediamine
LC	Ligand centred	TMSA	Trimethylsilyl acetylene
LED	Light emitting diode	tpy	2,2′:6′2″-terpyridine
LMCT	Ligand to metal charge transfer	Quat	Quaternary
LUMO	Lowest unoccupied molecular orbital	UV-vis	Ultra Violet-visible
m	Multiplet (NMR)	ν	Stretching frequency
Me	Methyl	δ	Chemical shift (NMR)
MEM	Methoxyethoxymethyl		Deformation frequency (IR)
MO	Molecular orbital	μ_g	Ground state dipole moment
MLCT	Metal to ligand charge transfer	μ_e	Excited state dipole moment
MC	Metal centred		

TABLES AND FIGURES

Chapter One: **COMPLEXES OF AN ARYL DIAMINE LIGAND** **Page**

Figure 1.1. (a) Bidentate, (b) terdentate *trans* pincer (N,C,N) and (c) terdentate *cis* pincer (C,N,N') monoanionic aryl ligands with heteroatom containing substituents.[2,3] If R'=R''=R'''=Me then (c) is 'Diam'. 1

Figure 1.2. The fluxional process showing coordination and decoordination of the hemi-labile – $CH_2CH_2NMe_2$ arm.[8] 2

Figure 1.3. Diam complexes showing (a) the octahedral complex $[TiMe_2(CNN')(O\text{-}i\text{-}Pr)]$[8] and (b) the square planar complex [PtCl(CNN')].[9] 3

Figure 1.4. The mixed aryl copper-copper bromide aggregates (a) $[Cu_3BrL_2]$ and (b) $[Cu_4Br_2L_2]$.[14] 3

Figure 1.5. (a) The 3-coordinate $Me_2Zn.OEt_2$[16] and (b) The 4-coordinate $(^nBu)_2Zn.TMEDA$.[17] 4

Figure 1.6. The 4-coordinate 1:1 zincates (a) $LiZn(dmba)_3.THF$[18] and (b) DiamZnCl.[19] 4

Figure 1.7. DiamBr, **(1)**, and the dimer $(DiamLi)_2$, **(2)**. 5

Table 1.1. Selected ^{1} H NMR spectroscopic data for DiamBr and $(DiamLi)_2$ (RT, 400 MHz). 5

Figure 1.8. **(3)** DiamZnCl, [ZnCl(CNN')], and **(4)** Diam ZnEt, [ZnEt(CNN')]. 6

Table 1.2: Selected ^{1}H NMR spectroscopic data for transition metal complexes of Diam (RT). 7

Table 1.3. Selected ^{13}C NMR spectroscopic data for complexes of Diam in C_6D_6 (RT, 100 MHz). 8

Figure 1.9. Attempted synthesis of ethynyl Diam **(8)** compounds. Conditions: (i) $Pd(OAc)_2$, PPh_3, CuI, di-isopropylamine. (ii)/(iii) $Pd(PPh_3)_2Cl_2$, CuI, diethylamine. (iv)/(v) diethyl ether/benzene, 200 K. 9

Figure 1.10. The synthesis of tributyl(phenylethynyl)tin **(5)**. 9

Figure 1.11. The synthesis of DiamI **(7)** *via* tributyltinDiam **(6)**. 9

Table 1.4. Selected NMR spectroscopic data for DiamBr, $DiamSn(Bu)_3$ and DiamI (RT, ^{1}H NMR 400 MHz, ^{13}C NMR 100 MHz). 10

Figure 1.12. The attempted Stille reaction of Ar-I **(7)** with tributyl(phenylethynyl)tin **(5)**. 10

Figure 1.13. The ESI-mass spectrum showing the new species at *m/z*=424.9. 11

Figure 1.14. Pd Catalytic cycle[29]. 11

Chapter Two: **NITROGEN-HETEROSUPERBENZENES** **Page**

Figure 2.1. (a) Vollhardt's polycyclic benzenoid hydrocarbons and (b) Müllen's graphitic sheets. 14

Figure 2.2. (a) The distribution of the carbon $2p_z$ electrons, (b) and (c) the Clar formulae, (d) the single Clar formula for coronene. 14

Figure 2.3. Construction techniques for PAHs. 15

Figure 2.4. Oligophenyls with high melting points (i) 470°C and (ii) 375°C. 16

Figure 2.5. The Frontier-Orbital diagram showing the thermally allowed [2+4]-cycloaddition. 16

Figure 2.6. The proposed mechanism of the Diels-Alder reaction. 17

Figure 2.7. Route to oligophenylenes by intermolecular Diels-Alder reactions. 17

Figure 2.8. Route to larger oligophenylene derivatives by multiple intermolecular Diels-Alder reactions. 18

Figure 2.9. Prototypical [2+2+2]-cycloaddition. 18

Figure 2.10. Proposed oxidative cationic mechanism for dehydrogenation reactions using metal halides. 19

Figure 2.11. The oxidative cyclodehydrogenation reaction to hexa-*peri*-hexabenzocoronene (R=H or alkyl). 20

Figure 2.12. Stacks of small triphenylene type discs compared to stacks of larger hexabenzocoronene type discs. 21

Table 2.1. The theorectically predicted effect of the selective N-doping of hexabenzocoronene on λ_{max}. 22

Figure 2.13. A coronenemonoimide.[39] 23
Figure 2.14. The synthesis of hexaphenylbenzene **(10)**. 25
Figure 2.15. The synthesis of hexabenzocoronene **(11)**. 25
Table 2.2. The UV-vis spectral data for HBC **(11)** and hexabenzocoronene[8] in 1,2,4-trichlorobenzene. 25
Figure 2.16. The synthesis of dipyrimidine acetylene **(12).** 26
Figure 2.17. The synthesis of *tert*-butyl substituted tetraphenylcyclopentadienone **(15)**. 27
Figure 2.18. The synthesis of substituted N-doped hexaphenylbenzene **(16)**. 27
Figure 2.19. (a) ^{1}H NMR (400 MHz) and (b) ^{13}C NMR (100 MHz) spectra of the aromatic areas of **(16)** ($CDCl_3$, RT). 28
Figure 2.20. The atom labelling scheme of **(16)**. 28
Table 2.3. Assignment of ^{13}C and ^{1}H NMR signals from HMQC experiments on **(16)**. 29
Table 2.4. Assignment of ^{1}H NMR signals using coupling information from TOCSY experiments on **(16)**. 29
Figure 2.21. The synthesis of N-HBC **(17)**, *via* the cyclodehydrogenation of **(16)**. 29
Figure 2.22. The atom labelling scheme of **(17)**. 30
Figure 2.23. The ^{1}H NMR spectrum of **(17)** ($CDCl_3$, RT, 400 MHz). 31
Figure 2.24. The ^{13}C NMR spectrum of heterosuperbenzene **(17)** showing the assigned 23 signals ($CDCl_3$, RT, 100 MHz). 32
Table 2.5. Assignment of ^{13}C and ^{1}H NMR signals from HMQC experiments on **(17)**. 32
Table 2.6. Assignment of ^{13}C and ^{1}H NMR signals from HMBC experiments on **(17)**. 32
Figure 2.25. The ESI-mass spectrum of heterosuperbenzene **(17)** in toluene. 33
Figure 2.26. The synthesis of substituted tetraarylcyclopentadienones. 34
Figure 2.27. The synthesis of substituted N-doped hexaarylbenzenes. 35
Figure 2.28. Ethynyl substituted polyarylbenzene **(49)**. 36
Figure 2.29. The synthesis of triisopropylsilylethynyl substituted polyarylbenzene **(29)** *via* the [2+4]-cycloaddition reaction. 36
Figure 2.30. The synthesis of conjugated 1,2-dipyrimidyl-3,6-bis-(4-tert-butylphenyl)-4,5-bis-(4-(3-methyl-3-hydroxy-butynyl)phenyl)benzene, **(32b)**, by Pd-mediated cross-coupling reactions. 38
Figure 2.31. Various novel nitrogen-containing polyphenylene derivatives and hexaphenylbenzene **(10)**. 39
Table 2.7. Reaction yields from the Diels-Alder cycloaddition step in the formation of nitrogen containing polyphenylenes and ESI-mass spectral analysis of the polyphenylene. 40
Figure 2.32. The atom labelling scheme of the novel N-doped polyphenylenes. 41
Figure 2.33. The ^{1}H NMR spectra of the aromatic region of (a) **(16)**, (b) **(20)**, (c) **(23)**, (d) **(29)**, (e) **(31)**, (f) **(32b)** and (g) **(32a)** ($CDCl_3$, RT, 400 MHz). 42
Table 2.8. ^{1}H NMR chemical shifts for the alkyl substituents of the N-doped polyphenylenes ($CDCl_3$, RT, 400 MHz). 43
Table 2.9. Assignment of ^{13}C and ^{1}H NMR signals from TOCSY, HMQC and HMBC COSY experiments on **(16)**, **(23)**, **(29)** and **(31)**. 43
Table 2.10. The ^{13}C NMR chemical shifts of the aromatic CH carbons for the various N-doped polyphenylene derivatives ($CDCl_3$, RT, 100 MHz). 44
Figure 2.34. The X-ray crystal structure of polyphenylene **(23)** (disorder in the *tert*-butyl group results in two forms described by either solid or hollow bonds). 46
Figure 2.35. The X-ray crystal structure of polyphenylene **(29)**. 46
Figure 2.36. The X-ray crystal structure of polyphenylene **(31)**. 47
Figure 2.37. The normalized absorption spectra for the various N-doped polyphenylene derivatives and hexaphenylbenzene, in diethyl ether. 48

Table 2.11. The UV-vis spectral characteristics of hexaphenylbenzene and the N-doped polyphenylenes in 1,2-dichloroethane. 49
Table 2.12. The absorption wavelengths for the N-doped polyphenylenes and hexaphenylbenzene in diethyl ether. 50
Figure 2.38. The synthesis of pyrimidine-5-carboxaldehyde. 51
Figure 2.39. Thermogravimetric analysis of heterosuperbenzene **(17)** showing 5-10% solvent loss and *tert*-butyl decomposition. 53
Figure 2.40. The cyclic voltammogram for **(17)** in chloroform showing two quasi-reversible reductions. 53
Table 2.13. Electrochemical information obtained from the cyclic voltammogram. Supporting electrolyte: $(TBA)PF_6$ (0.1 M); [a]glassy carbon working electrode, Pt wire auxiliary electrode, SCE reference electrode; [b]Au working and auxiliary electrode, SCE reference electrode.[31] $E^{\circ}=1/2(E_{pa}+E_{pc})$, where E_{pa} and E_{pc} denote anodic and cathodic peak potentials, respectively. $E_{1/2}=E_p+1.11(RT/nF)$ 54
Figure 2.41. The UV-vis absorption spectra of (a) Hexabenzocoronene[8] and (b) N-HBC **(17)**, in 1,2,4-trichlorobenezene. 55
Table 2.14. The molar extinction coefficient for the absorption maxima at each wavelength of N-HBC **(17)** in toluene solution. 56
Figure 2.42. (a)-(d). Absorption spectra of N-HBC **(17)** in various solvents. The arrows indicate the direction that the absorption band below has shifted on increasing solvent polarity. 58
Table 2.15. Peaks for the absorption bands for N-HBC **(17)** in a variety of solvents of increasing polarity. 59
Table 2.16. Peaks for the absorption bands for N-HBC **(17)** in the mixed solvent experiment. 60
Figure 2.43. The combined absorption and emission spectra of Hexa-*peri*-hexabenzocoronene in 1,2,4-trichlorobenzene.[8] 61
Figure 2.44. The combined absorption and emission spectra of N-HBC **(17)** in hexane. 61
Figure 2.45. Absorption and fluorescence spectra of N-HBC **(17)** in (a) hexane and (b) toluene. 63
Table 2.17. The lowest-energy absorption wavelength, highest-energy emission wavelength and Stokes' shift for N-HBC **(17)** in hexane or toluene. 64
Figure 2.46. Fluorescence spectrum of N-HBC **(17)** in (a) toluene and (b) chloroform with various λ_{ex}. 65
Figure 2.47. The normalized fluorescence spectra for N-HBC **(17)** in solvents of increasing polarity. 66
Table 2.18. The absorption and emission data of N-HBC **(17)** in various solvents. 66
Figure 2.48. The (a) absorption and (b) emission spectra for **(17)** in toluene:methanol solution mixtures; (i) 100:0, (ii) 98.8:1.2, (iii) 96:4, (iv) 90:10, (v) 80:20, (vi) 50:50, (vii) 0:100. 68
Figure 2.49. $\Delta\overline{\nu}$ as a function of the solvent polarity Δf for N-HBC **(17)** in various solvents. 70
Figure 2.50. N-HBC **(17)** photographed under a UV lamp and the normalized fluorescence emission spectra in (a) toluene, (b) chloroform and (c) methanol. 71
Figure 2.51. The fluorescence spectrum for N-HBC **(17)** in the highly polar methanol:ethanol solvent mix at room temperature and at liquid nitrogen temperature. 72
Figure 2.52. The absorbtion spectra of **(17)** in toluene (4 mL, $6.66x10^{-7}$ M) on addition of (i) 0 μLs, (ii) 5 μLs, (iii) 10 μLs, (iv) 50 μLs, (v) 110 μLs of trifluoroacetic acid (0.1 M). 73
Figure 2.53. The fluorescence spectra of **(17)** in toluene (4 mL, $6.66x10^{-7}$ M) on addition of (i) 0 μLs, (ii) 5 μLs, (iii) 10 μLs, (iv) 50 μLs, (v) 110 μLs, (vi) 200 μLs, (vii) 450 μLs of trifluoroacetic acid (0.1 M). 74
Figure 2.54. Normalised changes in fluorescence at (i) 494 nm, and absorption at (ii) 376.5 nm and (iii) 521.5 nm upon incremental addition of trifluoroacetic acid to a toluene solution of N-HBC **(17)** (4 mL, $6.66x10^{-7}$ M). 75

Table 2.19. Fluorescence data for **(17)** and the protonated species in toluene at room temperature. 76
Figure 2.55. (a) The fluorescence spectra of **(17)** in toluene (4 mL, $6.66x10^{-7}$ M) on addition of (i) 0 μLs, (ii) 5 μLs, (iii) 10 μLs, (iv) 20 μLs, (v) 60 μLs, (vi) 160 μLs of aniline (4.39 M, toluene) and (b) the normalized changes in fluorescence at 494 nm. 78
Figure 2.56. Dipole moment (arrow direction) and one orientation of the N-HBC **(17)** in H-aggregate form. 82
Figure 2.57. Hypochromic effects of the various absorption bands of N-HBC **(17)** in toluene, (a) 339.0, (b) 355.0, (c) 376.5, (d) 393.0, (e) 414.0, (f) 452.0 and (g) 481.5 nm. 84
Figure 2.58. Models of association based on the alignment of transition dipoles of (π,π^*) bands (black) and (n,π^*) bands (unshaded).[59] 85
Figure 2.59. The aromatic region for the ^{1}H NMR spectra of N-HBC **(17)**, (a) $16.379x10^{-3}$ M, 30°C, (b) $0.819\ x10^{-3}$ M, 30°C, (c) $16.379x10^{-3}$ M, 21°C, (d) $16.379x10^{-3}$ M, 40°C ($CDCl_3$, 400 MHz). 86
Table 2.20. ^{1}H NMR data for N-HBC **(17)** showing variations in chemical shift with concentration and temperature ($CDCl_3$, 400 MHz). 86
Figure 2.60. The synthesis of N-HBC **(21)**, *via* the cyclodehydrogenation of **(20)**. 87
Figure 2.61. The ESI-mass spectrum of heterosuperbenzene **(21)** in toluene. 88
Figure 2.62. The normalized absorption spectra of N-HBCs **(17)** and **(21)** in chloroform. 89
Table 2.21. Peaks for the absorption bands for N-HBCs **(21)** and **(17)** in chloroform. 89
Figure 2.63. The normalized fluorescence spectra of N-HBCs **(17)** and **(21)** in chloroform. 90
Table 2.22. Fluorescence data of N-HBCs **(21)** and **(17)** in chloroform. 90
Figure 2.64. The normalized fluorescence spectra of N-HBCs **(17)** and **(21)** in toluene. 91
Figure 2.65. Hexaarylbenzenes for oxidative cyclodehydrogenation. 92
Figure 2.66. Reaction of N-doped polyphenylene **(23)** under milder cyclodehydrogenation conditions. 93
Figure 2.67. The aromatic region of the ^{1}H NMR spectra for polyphenylenes (a) **(23)** and (b) **(24)** ($CDCl_3$, RT, 400 MHz). 94
Figure 2.68. Atom labelling scheme for **(24)**. 94
Figure 2.69. Expected result through dienone/phenol rearrangement. 95
Figure 2.70. The X-ray crystal structure of spirocyclic compound **(24)** showing one of the two enantiomeric forms of the unit cell (the other enantiomer and solvent have been removed for clarity). 96
Figure 2.71. The absorption spectra of polyphenylene compound **(23)** and spirocyclic **(24)** in dichloroethane. 96
Figure 2.72. Incorporation of corannulene into the polyaryl benzene. 101

Chapter Three: **TRANSITION METAL COMPLEXES OF NITROGEN-HETEROSUPERBENZENES** **Page**

Figure 3.1. Schematic energy-level diagram for an octahedral transition metal complex (*e.g.* Ru(II), d^6) with various electronic transition types indicated. 106
Figure 3.2. Commonly used bidentate (bpy) and tridentate (tpy) ligands. 107
Figure 3.3. Oxidative cyclodehydrogenation of N-doped polyphenylene **(16)** to yield the novel N-HBC ligand **(17)**. 110
Figure 3.4. Chemdraw depiction of the synthesis of ruthenium(II) complex $[Ru(bpy)_2(N\text{-}HBC_{17})]^{2+}$, **(35)**, from $[Ru(bpy)_2Cl_2]$. 110
Figure 3.5. Chemdraw representation for the optical isomers of ruthenium complex **(35)**, counterions omitted. 111
Figure 3.6. The ESI-mass spectrum of ruthenium complex **(35)** in acetonitrile. 111
Figure 3.7. The low-field, aromatic region of the ^{1}H NMR spectra of (a) ligand N-HBC **(17)** and (b) $[Ru(bpy)_2(N\text{-}HBC_{17})](PF_6)_2$ **(35)** ($CDCl_3$, RT, 400 MHz). 112

Figure 3.8. The aromatic region of the ^1H NMR spectrum of $[Ru(bpy)_2(N\text{-}HBC_{17})](PF_6)_2$ (CD_3CN, RT, 400 MHz). 113
Figure 3.9. The atom labelling scheme for the bipyridyl protons of **(35)**. 113
Table 3.1. ^1H-^1H coupling information from the TOCSY experiment of **(35)** (CD_3CN, RT, 400 MHz). 113
Figure 3.10. Cyclic voltammograms of (a) **(17)** in chloroform and (b) **(35)** in chloroform. Supporting electrolyte: $(TBA)PF_6$ (0.1 M); glassy carbon working electrode, Pt wire auxiliary electrode, SCE reference electrode. 116
Table 3.2. Electrochemical information obtained from the cyclic voltammogram. Supporting electrolyte: $(TBA)PF_6$ (0.1 M) in chloroform; glassy carbon working electrode, Pt wire auxiliary electrode, SCE reference electrode. 116
Figure 3.11. Cyclic voltammograms of $[Ru(bpy)_2(N\text{-}HBC_{17})](PF_6)_2$ **(35)** in CH_3CN solution (scan rate=500 mV s^{-1}). Supporting electrolyte: $(TBA)PF_6$ (0.1 M); glassy carbon working electrode, Pt wire auxiliary electrode, SCE reference electrode. 117
Table 3.3. Electrochemical data for **(35)** and $[Ru(bpy)_3]^{2+}$[7] in acetonitrile. [a]Supporting electrolyte: $(TBA)PF_6$ (0.1 M); glassy carbon working electrode, Pt wire auxiliary electrode, SCE reference electrode. [b]Supporting electrolyte: $(TBA)ClO_4$ (0.1 M); Pt disc electrode, Pt wire auxiliary electrode, SCE reference electrode. 117
Figure 3.12. The DPV experiment for ruthenium complex **(35)** in CH_3CN showing two oxidation processes. Supporting electrolyte: $(TBA)PF_6$ (0.1 M); glassy carbon working electrode, Pt wire auxiliary electrode, SCE reference electrode. 118
Figure 3.13. The absorption spectrum of (a) ligand N-HBC **(17)** and (b) $[Ru(bpy)_2(N\text{-}HBC_{17})]^{2+}$ and $[Ru(bpy)_3]^{2+}$ in acetonitrile. 119
Table 3.4. The principle bands in the absorption spectrum of the $[Ru(bpy)_2(N\text{-}HBC_{17})]^{2+}$ complex **(35)** and $[Ru(bpy)_3]^{2+}$[38] in acetonitrile. 120
Figure 3.14. Absorption spectra of $[Ru(bpy)_2(N\text{-}HBC_{17})]^{2+}$ in various solvents. 121
Figure 3.15. The normalized emission spectra of $[Ru(bpy)_2(N\text{-}HBC_{17})]^{2+}$, **(35)**, and $[Ru(bpy)_3]^{2+}$ in CH_3CN at 298 K. 122
Table 3.5. Spectroscopic properties of the Near-Infrared emitter **(35)** in various de-aerated solvents together with $[Ru(bpy)_3]^{2+}$[7] at RT or at 77 K*. 122
Figure 3.16. Emission spectra of $[Ru(bpy)_2(N\text{-}HBC_{17})]^{2+}$ (a) in various solvents and (b) at various temperatures. 123
Scheme 3.1. Deactivation pathways for Ru(II) polypyridines. 125
Figure 3.17. Visible and near-IR (a) absorption spectra and (b) "differential" spectra of **(35)** in dichloromethane with 0.1 M $(TBA)PF_6$ at 2.2 V (*vs* pseudo-Ag/AgCl). The arrows indicate the changes over time. 126
Figure 3.18. The (a) absorption and (b) emission spectra of Ru(II) complex **(35)** in acetonitrile on addition of perchloric acid. 127
Figure 3.19. Chemdraw representation of the synthesis of Ru(II) complex **(34)** incorporating the N-doped polyphenylene ligand **(16)**. 129
Figure 3.20. Chemdraw representation of the steric hindrance between protons at H_6 and $H_{6'}$ in **(34)**. 129
Figure 3.21. The ESI-mass spectrum of **(34)** in acetonitrile after (a) 0 and (b) 200 seconds of irradiation. 130
Figure 3.22. Chemdraw representation of the synthesis of $[Pd(\eta^3\text{-}C_3H_5)(N\text{-}HBC_{17})]PF_6$, complex **(36)**. 131
Figure 3.23. The ^1H NMR spectra of (a) N-HBC ligand **(17)** and (b) $[Pd(\eta^3\text{-}C_3H_5)(N\text{-}HBC_{17})]PF_6$, **(36)** ($CDCl_3$, RT, 400 MHz). 132
Figure 3.24. The atom labelling scheme of $[Pd(\eta^3\text{-}C_3H_5)(N\text{-}HBC_{17})]PF_6$, **(36)**. 132
Table 3.6. The ^1H NMR spectral data of $[Pd(\eta^3\text{-}C_3H_5)(N\text{-}HBC_{17})]PF_6$, **(36)** ($CDCl_3$, RT, 400 MHz). 132
Figure 3.25. The ESI-mass spectrum of $[Pd(\eta^3\text{-}C_3H_5)(N\text{-}HBC_{17})]^+$ **(36)** in methanol. 133

Table 3.7. Peaks for the absorption bands for $[Pd(\eta^3\text{-}C_3H_5)(N\text{-}HBC_{17})]PF_6$ in various solvents. 134
Figure 3.26. The normalised absorption spectrum of $[Pd(\eta^3\text{-}C_3H_5)(N\text{-}HBC_{17})]PF_6$ in methanol or tetrahydrofuran. 134
Figure 3.27. The (a) absorption and (b) emission spectra of ligand **(17)** in tetrahydrofuran (4 mL, $6.66x10^{-7}$ M) on addition of (i) 0 μLs, (ii) 20 μLs and (iii) 180 μLs of $[Pd(\eta^3\text{-}C_3H_5)(CH_3CN)_2]^+$ ($4.37x10^{-4}$ M). 135

Chapter Four: **POLYARYL FERROCENE COMPOUNDS** **Page**

Figure 4.1. The synthesis of tricarbonyl(arene)chromium complex.[13] 144
Figure 4.2. The structure of 4-(2-ferrocenyl-vinyl)-pyrene. 144
Figure 4.3. The synthesis of ethynylferrocene **(37)**. 146
Figure 4.4. The synthesis of 1,2,3,4-tetraphenyl-5-ferrocenylbenzene **(40)**. 147
Figure 4.5. The atom labelling scheme and NMR spectroscopic data for 1,2,3,4-tetraphenyl-5-ferrocenylbenzene **(40).** 147
Figure 4.6. The cyclodehydrogenation of **(40)** to produce ferrocenyl PAH derivative **(41)**. 148
Figure 4.7. The atom labelling scheme of tetra-*peri*-benzo-*peri*-ferrocenylcoronene, **(41)**. 149
Figure 4.8. The ^1H NMR spectrum of ferrocenyl compound **(41)** ($CDCl_3$, RT, 400 MHz). 149
Table 4.1. Coupling information from the ^1H NMR and TOCSY experiments on **(41)**. 150
Table 4.2. Assignment of major ^{13}C and ^1H NMR signals from HMQC experiments on **(41)**. 151
Figure 4.9. The ESI-mass spectrum of ferrocenyl PAH complex **(41)** in toluene. 151
Figure 4.10. The synthesis of ferrocene substituted polyphenylbenzene **(42)**, *via* phenylethynylferrocene **(38)**. 153
Figure 4.11. Synthetic route to the *tert*-butyl substituted ferrocenyl cyclopentadienone **(44)**. 154
Figure 4.12. The synthesis of ferrocene substituted N-doped polyphenylbenzene **(45)**. 155
Figure 4.13. The atom labelling scheme and the aromatic region of the ^1H NMR spectrum of ferrocenyl compound **(45)** ($CDCl_3$, RT, 400 MHz). 155
Figure 4.14. The synthesis of diferrocenyl substituted polyphenylbenzene **(46)**. 156
Figure 4.15. The ^1H NMR spectrum of diferrocenyl polyphenylene **(46)** ($CDCl_3$, RT, 400 MHz). 156
Figure 4.16. The atom labelling scheme of diferrocenyl derivative **(46)**. 157
Table 4.3. Assignment of major ^{13}C and ^1H NMR signals from HMQC experiments on **(46)**. 157
Table 4.4. Assignment of ^{13}C and ^1H NMR signals from HMBC experiments on **(46)**. 158
Table 4.5. Spectroscopic data for complexes **(37)**, **(38)**, **(39)**, **(40)**, **(41)**, **(42)**, **(45)** and **(46)**. 158
Figure 4.17. The X-ray crystal structures of ferrocenyl polyphenylenes (a) **(40)** and (b) **(45)**. 160
Table 4.6. The UV-vis data for ferrocenyl complexes **(37)**, **(38)**, **(39)**, **(40)**, **(41)**, **(42)**, **(45)** and **(46)** in toluene. 162
Figure 4.18. The UV-vis absorption spectrum of ferrocenyl complexes **(40)**, **(42)**, **(45)** and **(46)** in toluene, with ferrocene for comparison. 163
Figure 4.19. The UV-vis absorption spectrum of ferrocenyl complex **(41)** in toluene. 164
Figure 4.20. Ferrocenyl PAH **(41)** and PAH **(50)**. 164
Table 4.7. UV-vis data comparing **(41)** (toluene) and **(50)**[18] (chloroform). 164
Table 4.8. Electrochemical data for complexes **(37)**, **(38)**, **(40)**, **(41)**, **(42)**, **(45)** and **(46)**. Supporting electrolyte: $(TBA)PF_6$ (0.1 M) in CH_2Cl_2; platinum disc working electrode, Pt wire auxiliary electrode, Ag/AgCl reference electrode, 100 mV s^{-1} scan rate; measured for $(0.2\text{-}1.0)x10^{-4}$ M solutions. ΔE_p is given by $(E_{pa}\text{-}E_{pc})$. 166
Figure 4.21. The cyclic voltammetric response of a $(0.2\text{-}1.0)x10^{-4}$ M solution of ferrocene complexes (a) **(41)** and (b) **(46)**. Supporting electrolyte: $(TBA)PF_6$ (0.1 M) in CH_2Cl_2; platinum disc working electrode, Pt wire auxiliary electrode, Ag/AgCl reference electrode, 100 mV s^{-1} scan rate. 167

Chapter Five: **THE HETEROFULLERENE, AZA[60]FULLERENE** **Page**

Figure 5.1. (a) fullerene, C_{60}, (b) endohedral fullerene, $N@C_{60}$, (c) exohedral fullerene, 1-ferrocenylethynyl-2-hydro-1,2-dihydro-[60]fullerene.[5] 172

Figure 5.2. (a) The aza[60]fullerene $C_{59}N^{\bullet}$ radical and its dimer (b). 172

Figure 5.3. The formation of bisazafulleroid (c) from C_{60}, *via* the triazoline intermediate (b) MEM=$CH_2O(CH_2)_2OMe$. 173

Figure 5.4. The formation of heterofullerene **(48)** and adduct $C_{59}NO(CH_2)_2OMe$, *via* the green aminofullerides. 174

Figure 5.5. The (a) photochemical[16] and (b) thermal[17] cleavage of the heterofullerene dimer. 174

Figure 5.6. ^1H NMR spectroscopic data for bisazafulleroid **(47)**, MEM=$CH_2O(CH_2)_2OMe$ (RT, 400 MHz). 176

Figure 5.7. The attempted thermal synthesis of $C_{59}N$ ethynyl benzene, **(51)**, using *p*-TsOH, and oxygen. 177

Figure 5.8. The attempted photochemical synthesis of $C_{59}N$ ethynyl benzene, **(51)**. 178

Figure 5.9. The 780 – 940 *m/z* region of the ESI-mass spectrum showing the products of the photochemical reaction of $(C_{59}N)_2$ and tributyl(phenylethynyl)tin. 178

CHAPTER ONE

COMPLEXES OF AN ARYL DIAMINE LIGAND

1.1 INTRODUCTION

The search for Inorganic and Organometallic systems which have their metal centres encapsulated in a specifically modelled organic environment is the focus of much research. Natures metal-containing systems, for example metal porphyrins, have proven to be a source of inspiration in this area. The desire to develop chiral ligands that impose geometric restrictions on a complexed metal centre, has led researchers to the monoanionic aryl ligands with functionalized heteroatom containing substituents (figure 1.1).[1]

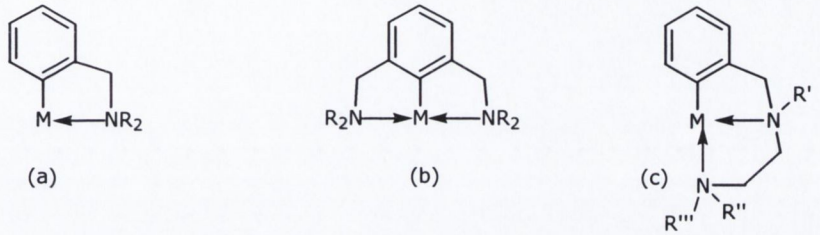


Figure 1.1. (a) Bidentate, (b) terdentate *trans* pincer (N,C,N) and (c) terdentate *cis* pincer (C,N,N') monoanionic aryl ligands with heteroatom containing substituents.[2,3] If R'=R''=R'''=Me then (c) is 'Diam'.

The potentially terdentate C,N,N'-chelating monoanionic aryl diamine ligand 'Diam' $[2\text{-}(Me_2NCH_2CH_2N(Me)CH_2)C_6H_4]^-$ was chosen in this study for several reasons. In general, aryl ligands of this type have chelating properties (the formation of complexes containing an M-C bond that is supported by intramolecular (heteroatom) coordination to the metal centre[4]). Diam has the potential to stabilise a variety of metal oxidation states because of its chelating side arm which provides additional kinetic stability, as compared to a complex which has an equivalent number of monodentate ligands.

Diam has a two-fold effect, which tunes the reactivity of a complexed metal atom. The first has to do with the electronic properties of the set of donor atoms. The choice of hard, carbon and nitrogen, donor atoms provides an extremely electron-rich system, which consequently enhances the nucleophilicity of a complexed metal centre.[5] The second effect is the stereochemistry of the aryl ligand, which severely limits the degree of spatial freedom of the diamine donor for coordination. The amine side arm creates channels of access so that the incoming ligands are guided to positions either *trans* or *cis* to the *ortho*-carbon ligand. Diam is therefore a potentially terdentate C,N,N', *cis* pincer ligand system.[1] It is also possible to incorporate chirality into Diam through the appropriate choice or R'' and R''' (see figure 1.1). Thus terdentate chelating ligands have proven to be very useful in organometallic chemistry, with capabilities that include stabilisation of a variety of metal oxidation states, and control of reaction and complex stereochemistry.[6,7] They have thus found use as catalytic materials in processes such as ring opening metathesis polymerisation.[7]

When coordinated as a terdentate ligand, the nitrogen donor atoms are positioned mutually *cis* and therefore perfectly set for pseudofacial coordination to the metal.[8] This bonding, along with the σ metal-carbon bond, to the ipso carbon, produces a conformationally rigid metal complex.

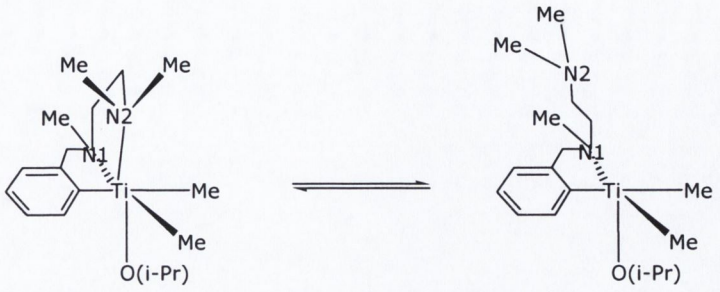


Figure 1.2. The fluxional process showing coordination and decoordination of the hemi-labile $-CH_2CH_2NMe_2$ arm.[8]

When the $-CH_2CH_2NMe_2$ arm is not coordinating (see figure 1.2), its flexibility still enables the nitrogen donor atom to approach the metal centre closely. In fact, stereochemistry demands that N1 be held in a fixed orientation with its lone pair of electrons orientated toward the metal centre. Thus in this situation this arm may become an active spectator, Lewis base moiety and be involved in an anchimeric type of assistance in metal-centred reactions. As such this system can be envisaged as a model for the early stages of an S_N2 type process.[9]

The most generally useful synthetic method for the preparation of organometallic compounds involves the alkylation of metal salts (*e.g.* ZnX_2), by organolithium or Grignard reagents,[10] *i.e.*:

$$R\text{-}Br + R'\text{-}Li \rightleftharpoons R\text{-}Li + R'\text{-}Br \qquad (1.1)$$

The equilibrium involved in the formation of organolithium species is shifted to the right if R is superior to R′ at stabilising a negative charge. Therefore this reaction is particularly practical for R-Br=aryl bromide. The metal halogen exchange is a comparatively fast reaction and is favoured at low temperatures (Kinetic control). Once the organolithium reagent has been formed, metal exchange with the halide of a second metal (M) will lead to the formation of a new species M-R, if the metal M is less electropositive than Li, *i.e.*:

$$R\text{-}Li + M\text{-}Cl \rightarrow R\text{-}M + LiCl \qquad (1.2)$$

This procedure has wide applicability since the formation of LiCl makes a large contribution to the driving force.

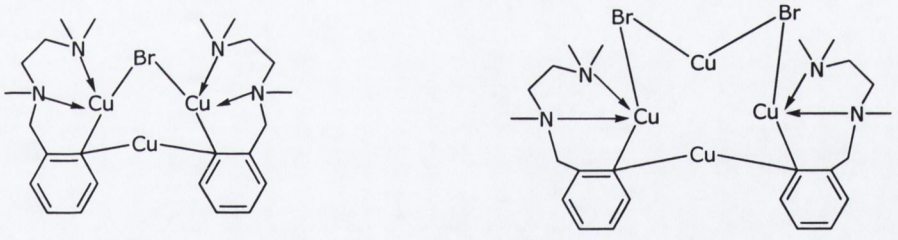
Diam can bind to a variety of transition metal species through both bidentate (C,N) or terdentate (C,N,N') coordination modes, and can exist in a variety of geometric configurations (see figure 1.3). In fact the transmetalation of the lithium complex of this ligand system has enabled the synthesis of metal complexes of the transition metals Ti(IV), Ta(V), W(II), Pd(II), Ir(I), Rh(I), and Pt(II).[7-9,11-13]



(a) (b)

Figure 1.3. Diam complexes showing (a) the octahedral complex $[TiMe_2(CNN')(O\text{-}i\text{-}Pr)]$[8] and (b) the square planar complex $[PtCl(CNN')]$.[9]

Up until 1996 no first row transition metals had been incorporated into this ligand system. In 1996 van Koten *et al.* synthesized the mixed air-sensitive aryl copper-copper bromide aggregates $[Cu_3BrL_2]$ and $[Cu_4Br_2L_2]$ from the reaction of different ratios of $(DiamLi)_2$ with Cu(1)Br.[14] These can be described as comprising of a $[CuR_2]^-$ unit stabilised by a $[Cu_2Br]^+$ or a $[Cu_3Br_2]^+$ cation, respectively. The bromide anions complete the structure by bridging two copper atoms.



(a) (b)

Figure 1.4. The mixed aryl copper-copper bromide aggregates (a) $[Cu_3BrL_2]$ and (b) $[Cu_4Br_2L_2]$.[14]

The work described in this chapter is concerned with the synthesis of mononuclear DiamZn(II) compounds. Zinc metal has the electron configuration $[Ar]3d^{10}4s^2$. The loss of two electrons in the formation of organometallic derivatives renders a net $3d^{10}$ electron configuration. Dialkylzinc compounds are generally linear and 2-coordinate.[15] The zinc-carbon bonds in a typical organozinc compound can be thought of as generated from two electron pairs occupying two equivalent sp-hybridised molecular

orbitals. The 2-coordinate Zn(II) centres in dialkylzinc compounds are both electronically and coordinatively unsaturated. As such they react readily with a number of donor ligands (L), to form 3-coordinate,[16] and 4-coordinate[17] adducts of type R_2ZnL and R_2ZnL_2, of which the 4-coordinate complexes are the more common (see figure 1.5 (b)). In this case the Zn(II) atom is tetrahedral with sp^3 hybridisation.

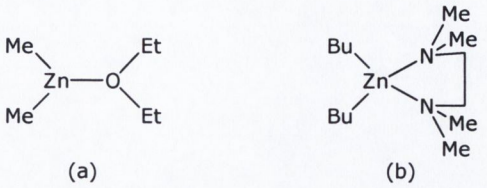


Figure 1.5. (a) The 3-coordinate $Me_2Zn.OEt_2$[16] and (b) The 4-coordinate $(^nBu)_2Zn.TMEDA$.[17]

Little work has been done to isolate and characterise arylzinc compounds, largely due to their instability. Among the limited number of reported studies on their structural aspects, few complexes contain potentially intramolecularly coordinating groups in the ligands. This intramolecular coordination should produce more stable organozinc adducts as the sites required for decomposition reactions are blocked.

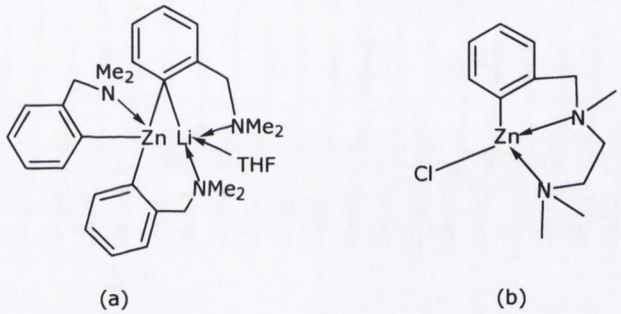


Figure 1.6. The 4-coordinate 1:1 zincates (a) $LiZn(dmba)_3.THF$[18] and (b) DiamZnCl.[19]

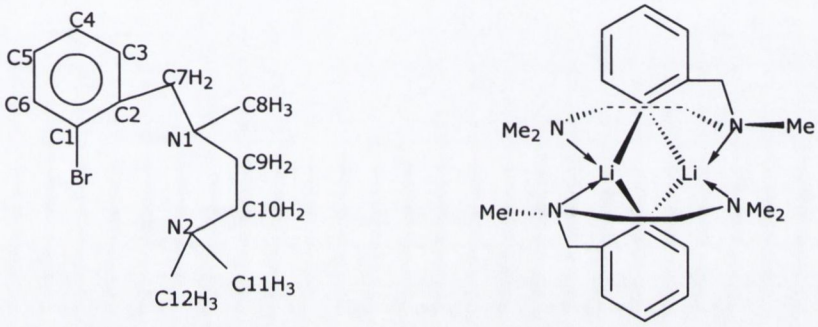
In 1997, two examples of four coordinate zincates, involving this type of pincer ligand, were formed (figure 1.6), one of which was formed within our research group figure 1.6 (b). These have distorted tetrahedral geometries, caused by the presence of the intramolecularly coordinating groups. To extend the number of zincate complexes within the C,N,N'-chelating manifold, I have investigated the synthesis of Zn(II) complexes with the $[2\text{-}(Me_2NCH_2CH_2N(Me)CH_2)C_6H_4]^-$, **(1)**, pincer ligand. In this regard a new monoarylzinc complex, which is intramolecularly stabilised by a dinitogen arm, has been synthesized.

1.2 RESULTS AND DISCUSSION

1.2.1 FORMATION OF (DiamLi)$_2$

The *o*-diamine-substituted aryl bromide DiamBr, **(1)**, was obtained in 65% yield from a substitution reaction of bromobenzyl bromide and trimethylethylenediamine in the presence of a large excess of triethylamine as base.[1] Pure DiamBr, **(1)**, is a pale yellow oil that is somewhat air-sensitive and best stored at 273 K under an argon atmosphere.

The bromine-lithium exchange reaction of **(1)** with an equivalent of *n*-BuLi, was carried out according to the procedure of van Koten.[1] It occurs in a hexane/diethyl ether solvent mix at low temperature and affords the *ortho*-lithiated species (DiamLi)$_2$, **(2)**, quantitatively. This aryllithium complex is a white air and moisture sensitive microcrystalline solid which exists as a dimer.[1]



(1) **(2)**

Figure 1.7. DiamBr, **(1)**, and the dimer (DiamLi)$_2$, **(2)**.

Selected ^{1}H NMR Chemical Shifts		
	DiamBr (C_6D_6)	**[DiamLi]$_2$ (C_6D_6)**
C(6)-H_{aryl}	7.65 d 1H	8.32 d 1H
C(7)-H_2	3.69 s 2H	4.23 d 1H
		3.28 d 1H
C(9)-H_2	2.61 t 2H	2.75 m 1H
		2.10 m 1H
C(10)-H_2	2.46 t 2H	1.70 m 1H
		1.55 m 1H
C(11,12)-H_3	2.19 s 6H	1.53 br s 6H

Table 1.1. Selected ^{1}H NMR spectroscopic data for DiamBr and (DiamLi)$_2$ (RT, 400 MHz).

The NMR spectra of **(1)** and **(2)** were identical to those reported in literature.[1] In the ^{1}H NMR spectrum of **(2)**, (see table 1.1) there is a characteristic lowfield doublet

resonance at δ 8.32 for the lithium complex. This is indicative of an aromatic proton positioned *ortho* to a metal atom. The coordination of the –NMe- moiety to the lithium is clear due to the stereogenic nature of the benzylic protons and their low-field shift. This causes distinct peaks for each set of methylene protons at C(7), C(9), and C(10). The $-NMe_2$ unit affords a broad resonance at δ 1.53 which is evidence for fluxional behaviour between coordinated and non coordinated $-NMe_2$ situations.[1]

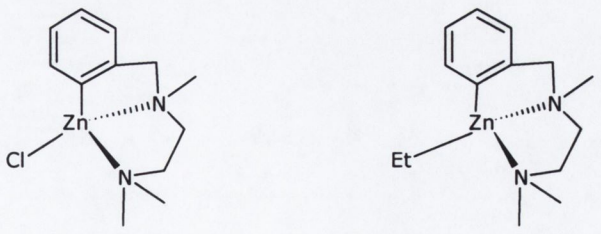
With this organolithium compound new transition metal complexes are accessible *via* transmetalation reactions with the corresponding metal salts.

1.2.2 INTRAMOLECULARLY STABILISED ARYLZINCATES, DiamZnCl and DiamZnEt

Organozincs (RZnX) and especially diorganozincs (R_2Zn) have found use as organometallic intermediates in organic synthesis. They react, in the presence of an appropriate transition metal catalyst, with a range of organic electrophiles.[20-22]

The transmetalation reaction of **(2)** with 2 molar equivalents of $ZnCl_2$ readily affords a white precipitate of LiCl and the mononuclear tetrahedral zinc(II) complex, DiamZnCl (**(3)**, figure 1.8) as colourless, air-sensitive crystals.[19] Treatment of this complex with a further equivalent of organolithium does not result in the formation of a bis-DiamZn complex by removal of the second chlorine atom. It was found that DiamZnCl only converts back to DiamH.

In an attempt to produce a tetra-coordinate zincate complex with no halogen present, the synthesis of the mixed arylethylzinc, DiamZnEt **(4)**, was carried out. $(DiamLi)_2$ **(2)** was added to a solution of ethylzinc chloride, which was prepared *in situ* from zinc chloride and diethylzinc. This transmetalation reaction again yields LiCl along with the mononuclear zinc(II) complex DiamZnEt as a white air-sensitive crystalline solid (compound **(4)** figure 1.8).



(3) **(4)**

Figure 1.8. **(3)** DiamZnCl, [ZnCl(CNN')], and **(4)** Diam ZnEt, [ZnEt(CNN')].

The aromatic protons of **(4)** provide a diagnostic probe for metalation. The important evidence for the change in substituent at the *ortho* position of the aryl ligand is the chemical shift in the ^1H NMR spectra of the doublet associated with the proton at C(6) (figure 1.7). For the transition metals Pd[12] and Pt,[9] this resonates upfield with respect to DiamBr, whereas in the zincate complexes the signal appears downfield at δ 8.02 for DiamZnCl, and δ 8.03 for DiamZnEt (see table 1.2). Corresponding shifts occur for the protons in the diamine arm, in Pd and Pt they shift downfield and in the zincate complexes they are shifted upfield.

Selected ^1H NMR Chemical Shifts ([a]400 MHz and C_6D_6; [b]200 MHz and $CDCl_3$)					
	[a]DiamBr	[b]DiamPtCl[9]	[b]DiamPdCl[12]	[a]DiamZnCl	[a]DiamZnEt
C(6)-H_{aryl}	7.65 d 1H	7.27 d 1H	7.46 m 1H	8.02 d 1H	8.03 d 1H
C(7)-H_2	3.69 s 2H	3.82 d 1H	3.67 d 1H	3.00 d 1H	3.16 d 1H
		4.30 d 1H	4.55 d 1H	3.44 d 1H	3.66 d 1H
C(9)-H_2	2.61 t 2H	3.23 td 1H	3.64 td 1H	1.36 td 1H	1.62 td 1H
		3.57 td 1H	3.16 td 1H	1 18 td 1H	1.50 td 1H
C(10)-H_2	2.46 t 2H	2.80 m 2H	2.63 m 2H	1.92 d 1H	2.35 td 1H
				2.02 d 1H	2.01 td 1H
C(11,12)-H_3	2.19 s 6H	2.78 s 3H	2.89 s 3H	2.12 s 3H	2.14 s 3H
		2.82 s 3H	2.76 s 3H	2.16 s 3H	2.18 s 3H

Table 1.2: Selected ^1H NMR spectroscopic data for transition metal complexes of Diam (RT).

Further evidence for the coordination of the diamine side arm comes from the signals produced by its diastereotopic methylene and methyl groups. These groups are no longer equivalent as the nitrogen atoms are coordinated in a rigid system. This is evident in the ^1H NMR spectra as two distinct methyl signals are produced for the $-NMe_2$ unit. The benzyl protons (C(7)), and the methylene protons, C(9) and C(10) are split into an AB pattern, *i.e.* these CH_2 hydrogens are diastereotopic. The diastereotopicity of the NMe_2 methyl groups establishes that intramolecular M-N coordination is rigid on the NMR timescale.

Fluxionality within these compounds, initiated by dissociation of the M-N bonds, would scramble the benzyl ligand signals.[23] It is interesting to note that previous reports indicate that their intra- and intermolecular fluxional processes cause coalescence of the NMR signals for the diamine chain in metal complexes at elevated temperatures.[5]

Selected ^{13}C NMR Chemical Shifts				
	DiamH	**DiamBr**	**DiamZnCl**	**DiamZnEt**
Ar C(1)	128.6	138.7	154.2	161.2
Ar C(7)	62.5	61.4	65.0	66.0
Ar C(11,12)	45.4	45.2	43.4, 48.2	42.9, 46.1

Table 1.3. Selected ^{13}C NMR spectroscopic data for complexes of Diam in C_6D_6 (RT, 100 MHz).

In the ^{13}C NMR experiment the aryl C(1) peak in the zincate complexes resonates downfield with respect to the equivalent C(1) resonance in DiamBr. This indicates the loss of electron density to the metal in the formation of the organometallic bond. Smaller downfield shifts are observed in the diamine side-chain, especially at C(7). Again the $-NMe_2$ group is split into two distinct methyl resonances, showing the coordination of N2.

The organozinc complex **(4)** thus contains the pincer ligand in the C,N,N'-terdentate binding mode, established by the comparison of spectroscopic data of **(4)** with those of related complexes. DiamZnEt is the first organometallic complex of an alkylated Zn(II) centre which is intramolecularly stabilised by the pendant di-nitrogen arm of this ligand. The Zn(II) centre is embedded in the coordination pocket of the terdentate C,N,N' framework of the pincer ligand. It decomposes slowly on contact with air, but can be stored under argon at 243 K for months. Similar pincer ligand systems to those formed in this study, have been used to study the mechanism involved in alkylation reactions using alkyl and aryl zincates.[24]

1.2.3 ETHYNYL SUBSTITUTED Diam

Alkynes react easily with $Co_2(CO)_8$ to give deeply coloured diamagnetic compounds $[Co_2(CO)_6(\mu_2\text{-}\eta^2,\eta^2\text{-alkyne})]$. Robinson *et al.*[25] have shown that these clusters promote long-range electronic communication and have use as components for material of technological interest. If an ethynyl substituent could be coupled to Diam at the *ortho* position, it may provide a route for the introduction of $Co_2(CO)_8$, and the formation of a cluster complex, which could set up interesting interactions between the metal centre and the nitrogen donor atoms. Alternatively, an ethynyl substituted Diam may also undergo Diels-Alder [2+4]-cycloaddition with tetracyclone (see Chapter 2). This would produce polyphenylenes with a coordinating diamine side arm.

Attempts at the synthesis of ethynyl substituted Diam **(8)**, using the methods below, were unsuccessful, as either no reaction occurs or DiamH is produced. A less direct route, which has allowed the formation and NMR characterisation of two new Diam products, was therefore undertaken. The synthesis involves four steps:

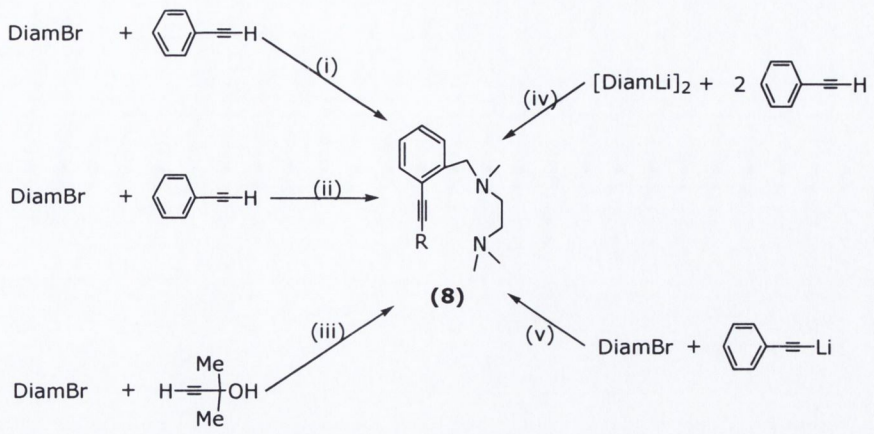
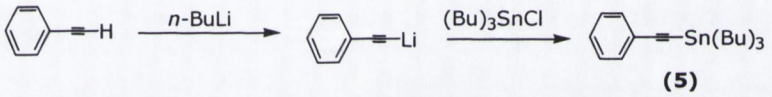


Figure 1.9. Attempted synthesis of ethynyl Diam **(8)** compounds. Conditions: (i) $Pd(OAc)_2$, PPh_3, CuI, di-isopropylamine. (ii)/(iii) $Pd(PPh_3)_2Cl_2$, CuI, diethylamine. (iv)/(v) diethyl ether/benzene, 200 K.

1: Formation of tributyl(phenylethynyl)tin **(5)**, as reported in literature,[26] *via* the reaction of lithiumphenylacetylide with tributyltinchloride. Tributyl(phenylethynyl)tin was produced as a colourless oil.

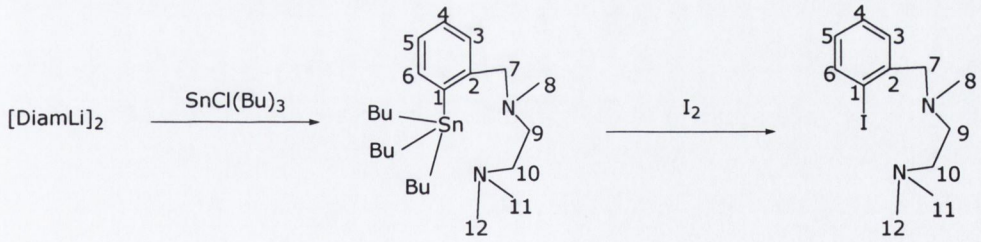


(5)

Figure 1.10. The synthesis of tributyl(phenylethynyl)tin **(5)**.

2: TributyltinDiam **(6)** was synthesized as a yellow oil, from reaction of $(DiamLi)_2$ and tributyltinchloride (figure 1.11).

3: Formation of DiamI **(7)** *via* the substitution of tin by iodine in **(6)**. DiamI was produced as an orange oil (figure 1.11).



(6) **(7)**

Figure 1.11. The synthesis of DiamI **(7)** *via* tributyltinDiam **(6)**.

The ^1H NMR spectra shows that the diamine arm is not coordinating to the tin centre in **(6)**, as there is equivalence within the methylene, and $-NMe_2$ groups as shown in table 1.4. In the tetraorganotin compound, **(6)**, the Lewis acidity of the tin centre is too low to result in coordination of the nitrogen donors, as found likewise in similar tin

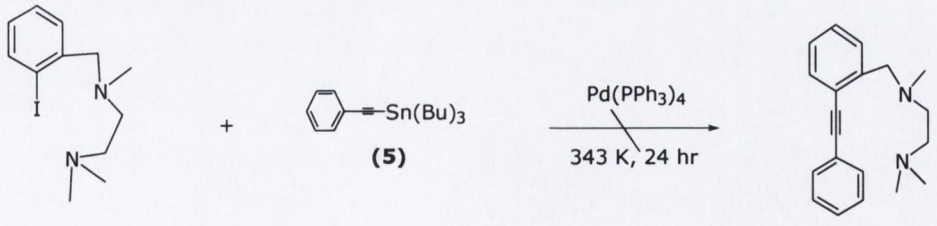
complexes.[6] There are also characteristic shifts in the ^{13}C NMR at C(1), most notably for C(1) in DiamI which is shifted upfield to δ 100.5. C(11) and C(12) are equivalent, showing again that N2 remains uncoordinated.

	Selected NMR Chemical Shifts		
	DiamBr (C_6D_6)	**DiamSn(Bu)$_3$** (C_6D_6)	**DiamI** ($CDCl_3$)
^1H NMR - Selected peaks			
C(7)-H	3.69 s 2H	3.62 s 2H	3.62 s 2H
C(9)-H	2.61 t 2H	2.67 t 2H	3.27 t 2H
C(10)-H	2.46 t 2H	2.53 t 2H	2.91 t 2H
C(11,12)-H	2.19 s 6H	2.22 s 6H	2.84 s 6H
^{13}C NMR - Selected peaks			
Ar C(1)	138.7	146.3	100.5
Ar C(11,12)	45.2	45.9	43.4

Table 1.4. Selected NMR spectroscopic data for DiamBr, DiamSn(Bu)$_3$ and DiamI (RT, ^1H NMR 400 MHz, ^{13}C NMR 100 MHz).

4: The Stille coupling[27] of **(7)** and tributyl(phenylethynyl)tin, utilising the $Pd(PPh_3)_4$ catalysis.

Aromatic acetylenes have been prepared by a wide variety of efficient methods,[28] most relying on transition metal catalysed couplings of aromatic halides with trimethylsilylacetylene (TMSA) or 2-methyl-3-butyn-2-ol, to form the protected aromatic acetylenes, which can be subsequently deprotected prior to further use. Alternatively the Stille coupling of aromatic iodides Ar-I and tributyl(ethynyl)tin directly affords aromatic acetylides Ar-C≡CH with tributyltin iodide as side product. This palladium-catalysed cross-coupling reaction is nowdays, one of the most used and versatile procedures to form carbon-carbon bonds by transition metal catalysis.[29,30]



(7) **(5)** **(8)**

Figure 1.12. The attempted Stille reaction of Ar-I **(7)** with tributyl(phenylethynyl)tin **(5)**.

DiamI **(7)** and tributyl(phenylethynyl)tin **(5)** were reacted in the presence of 5 mol.% of $Pd(PPh_3)_4$ catalyst in THF solvent. Following overnight stirring at 343 K, under argon,

the reaction was cooled and the solvent removed *in vacuo*. This gave a mixture of products, which did not contain the desired product **(8)**.

Analysis of the ESI-mass spectrum indicates the presence, among other products, of triphenylphosphine, unreacted DiamI **(7)** (*m/z*=318), and evidence for a new palladium complex **(9)** (*m/z*=424.6). Although further isolation and characterisation of **(9)** was not attempted, it is believed to be of the form shown in figure 1.13.

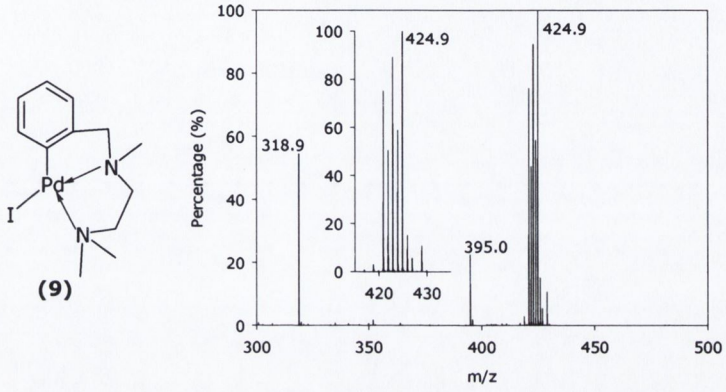


Figure 1.13. The ESI-mass spectrum showing the new species at *m/z*=424.9.

There are three steps in the currently accepted catalytic cycle for the cross-coupling reaction of organostannanes with aryl halides.[29] These are: a) oxidative addition of an aryl halide to an electron-rich Pd(0) complex, b) transmetalation of the resulting electrophilic Pd(II) complex with a nucleophilic organostannane, and c) reductive elimination to give a cross-coupled product and regenerate the Pd(0) complex.[29] The palladium ligands *e.g.* triphenylphosphine, dissociate from the Pd(II) intermediate to create the vacant coordination site that is needed for the rate determining step of transmetalation. Some experimental evidence for this cycle is a) if additional ligands are present, an inhibitory effect is observed, and b) the rate can be modified by using palladium ligands of varying donor strength.[31]

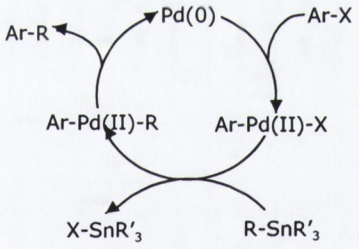


Figure 1.14. Pd Catalytic cycle[29].

The oxidative addition of **(7)** to the Pd(0) complex would be expected to form the stable complex **(9)**, with the metal inserted into the C_{aryl}-I bond. In addition to this, coordination of the pendant nitrogen donor atoms of diam encapsulate the metal within a stable 4-coordinate atmosphere. Diam has restricted the number of coordination sites that are available for incoming reagents, thus frustrating the normal course of reaction, and leading to the trapped intermediate. Complex **(9)**, once formed, must remain stable at 343 K, preventing the rate-determining transmetalation step in the cycle.[31]

As a result the palladium catalyst is consumed. This reaffirms the currently accepted catalytic cycle for the Stille cross-coupling, with the intermediate (Ar-Pd(II)-X) effectively trapped as the stable species **(9)**. This also demonstrates the remarkable stability of metal complexes formed from this ligand. Terdentate-bound organopalladium complexes are seen to be extremely stable solids (decomposition temperature>473 K).[12] This type of reaction is not without precedence. Metal insertion into the C_{aryl}-halide bond, has been used very recently to form η^3-N,C,N-coordinated palladium complexes, *via* the oxidative addition of $[Pd(PPh_3)_4]$.[32]

The Sonogashira cross-coupling reaction of (trimethylsilyl)acetylene, in the presence of catalytic amounts of CuI and $[PdCl_2(PPh_3)_2]$ has been used successfully to couple acetylenes to the *meta*-position of these pincer type ligands, although only when the ipso carbon and the pendant nitrogen donors have been previously engaged in metal coordination.[32] This provides further evidence for the destructive effect of the pendant nitrogen donors on the cross-coupling reaction.

In conclusion, the terdentate C,N,N'-chelating monoanionic aryl diamine ligand 'Diam', **(1)**, has been studied as a versatile synthon for organic and/or organometallic synthesis. The remarkable stability of metal complexes of this pincer ligand has been demonstrated with the formation of a stable arylethylzinc **(4)** complex and a palladium complex **(9)**. The latter is the result of an attempted palladium cross-coupling reaction. The presence of intramolecular Zn-N coordination in **(4)**, in solution, is supported by the diastereotopicity of the CH_2N methylene hydrogen atoms, and the NMe_2 methyl groups.

1.3 REFERENCES

1. M. Rietveld, I. Wehman-Ooyevar, G. Kapteijn, D. M. Grove, W. Smeets, A. L. Spek, G. van Koten, *Organometallics*, **1994**, *13*, 3782-3787
2. J. Brandts, M. van Leur, R. Gossage, J. Boersma, A. L. Spek, G. van Koten, *Organometallics*, **1999**, *18*, 2633-2648
3. I. Rio, R. Gossage, M. Hannu, M. Lutz, A. L. Spek, G. van Koten, *Organometallics*, **1999**, *18*, 1097-1105
4. J. Dehand, M. Pfeffer, *Coord. Chem. Rev.*, **1976**, *18*, 327-352
5. J. Terheijden, G. van Koten, P. Mul, D. Stufkers, F. Muller, C. Stam, *Organometallics*, **1986**, *5*, 519-525
6. G. van Koten, *Pure Appl. Chem.*, **1989**, *61*, 1681-1694
7. M. Rietveld, W. Teunissen, H. Hagen, L. van de Water, D. M. Grove, P. van de Schaaf, A. Mühlebach, H. Kooijman, W. Smeets, N. Veldman, A. L. Spek, G. van Koten, *Organometallics*, **1997**, *16*, 1674-1684
8. J. Donkervoort, C. Kronenburg, B. Deelman, J. Jastrzebski, N. Veldman, A. L. Spek, G. van Koten, *J. Organomet. Chem.*, **1997**, *547*, 349-355
9. I. Wehman-Ooyevar, G. Kapteijn, D. M. Grove, W. Smeets, A. L. Spek, G. van Koten, *J. Chem. Soc., Dalton Trans.*, **1994**, 703-711
10. M. Schlosser, *Angew. Chem., Int. Ed. Engl.*, **1964**, *3*, 287-306
11. B. Buffin, M. Poss, A. Arif, T. Richmond, *Inorg. Chem.*, **1993**, *32*, 3805-3806
12. P. Alsters, P. Engel, M. Hogerheide, M. Copijn, A. L. Spek, G. van Koten, *Organometallics*, **1993**, *12*, 1831-1844
13. M. Rietveld, H. Hagen, L. van de Water, D. M. Grove, H. Kooijman, N. Veldman, A. L. Spek, G. van Koten, *Organometallics*, **1997**, *16*, 168-177
14. M. Janssen, M. Corsten, A. L. Spek, D. M. Grove, G. van Koten, *Organometallics*, **1996**, *15*, 2810-2820
15. M. Westerhaussen, B. Radmacher, W. Poll, *J. Organomet. Chem.*, **1991**, *421*, 175-188
16. K. Thiel, *Z. Anorg. Allg. Chem.*, **1962**, *319*, 183
17. J. Noltes, J. van de Hurk, *J. Organomet. Chem.*, **1964**, *1*, 377
18. E. Rijnberg, J. Jastrzebski, J. Boersma, H. Kooijman, N. Veldman, A. L. Spek, G. van Koten, *Organometallics*, **1997**, *16*, 2239-2245
19. J. J. Bryne, Ph.D. Thesis, Trinity College Dublin, **1996**
20. P. Knochel, J. J. Almena-Perea, P. Jones, *Tetrahedron*, **1998**, *54*, 8275-8319
21. P. Knochel, R. Singer, *Chem. Rev.*, **1993**, *93*, 2117-2188
22. E. Rijnberg, N. J. Hovestad, A. W. Kleij, J. Jastrzebski, J. Boersma, M. D. Janssen, A. L. Spek, G. van Koten, *Organometallics*, **1997**, *16*, 2847-2857
23. H. C. L. Abbenhuis, D. M. Grove, G. P. M. van Mier, A. L. Spek, G. van Koten, *Chem. Commun.*, **1989**, 1581-1583
24. E. Wissing, M. Kaupp, J. Boersma, A. L. Spek, G. van Koten, *Organometallics*, **1994**, *13*, 2349-2356
25. N. Duffy, B. Robinson, J. Simpson, *J. Organomet. Chem.*, **1999**, *573*, 36-46
26. J. Lorberth, *J. Organomet. Chem.*, **1969**, *16*, 327-329
27. J. K. Stille, *Pure Appl. Chem.*, **1985**, *57*, 1771-1780
28. T. X. Neenan, G. M. Whitesides, *J. Org. Chem.*, **1988**, *53*, 2489-2496
29. V. Farina, B. Krishnan, *J. Am. Chem. Soc.*, **1991**, *113*, 9585-9595
30. E. Antonelli, P. Rosi, C. L. Sterzo, E. Viola, *J. Organomet. Chem.*, **1999**, *578*, 210-222
31. E. Shirakawa, T. Hiyama, *J. Organomet. Chem.*, **1999**, *576*, 169-178
32. G. Rodríguez, M. Albrecht, J. Schoenmaker, A. Ford, M. Lutz, A. L. Spek, G. van Koten, *J. Am. Chem. Soc.*, **2002**, *124*, 5127-5138

CHAPTER TWO

NITROGEN-HETEROSUPERBENZENES
2-DIMENSIONAL POLYAROMATIC SYSTEMS

2.1 INTRODUCTION

2.1.1 SYNTHESIS

Chemists have continually attempted to link molecules using weak intermolecular forces to produce supramolecular structures with novel geometries.[1] The synthesis of rod-like, spherical and disc-shaped molecules has recently been an area of avid interest.[3,4] Examples include Vollhardt's polycyclic benzenoid hydrocarbons,[2] or Müllen's graphitic sheets (figure 2.1).[1] The latter group includes polycyclic aromatic hydrocarbons which are characterized by their stacking in columnar discotic mesophases.[1,5]

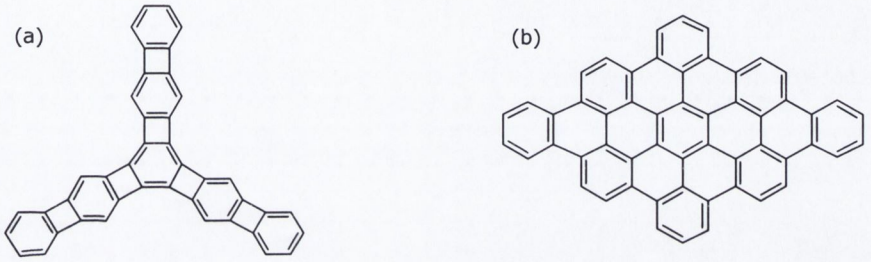


Figure 2.1. (a) Vollhardt's polycyclic benzenoid hydrocarbons and (b) Müllen's graphitic sheets.

As part of the on-going development of molecular materials within the electronics industry, there has been a strategic shift in research and development toward so-called 'soft' materials. These are essentially organic materials capable of the same function as more traditional inorganic semiconductors. Despite continuing research into planar multidimensional carbon systems, graphite, with its network of mobile π-electrons, is still the best organic conductor. Electrons are free to move within the sheets, in the delocalised π-orbitals formed from the unhybridised *p*-orbitals of the carbon atoms. By extension it is believed that polycyclic aromatic hydrocarbons (PAHs) will find extensive and valuable use in the area of molecular electronics[3] and optoelectronics.[6]

PAHs are all-benzenoid hydrocarbons, which can be differentiated from the other alternating aromatics by their benzene-like character, first described in Clar's model of the sextet.[3] The rule of the aromatic sextet can be understood by considering the $2p_z$ electrons of a fused aromatic, *e.g.* anthracene, figure 2.2 (a)-(c). Clar formulae are the mesomeric limiting structures that contain the largest possible number of electron sextets.

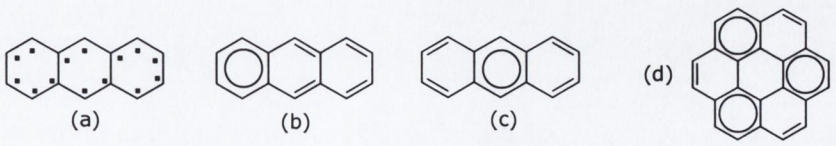


Figure 2.2. (a) The distribution of the carbon $2p_z$ electrons, (b) and (c) the Clar formulae, (d) the single Clar formula for coronene.

All-benzenoid aromatic hydrocarbons are distinct in that they have only one Clar formula, (*e.g.* coronene, figure 2.2 (d)) and are thus made up of a C_{6n} skeleton. The olefinic character is completely suppressed in all-benzenoid hydrocarbons, giving them exclusively aromatic character. Clar predicted that the all-benzenoid hydrocarbons would have the greatest stability and lowest reactivity of all PAHs.[7] It is therefore not surprising that these PAHs are insoluble in sulfuric acid and have extreme thermal stability. Coronene itself is one of the carbon-bearing molecules present through the diffuse interstellar bands.[8]

PAHs are thermally and chemically stable two-dimensional graphite sections, which were first synthesized under drastic conditions at high temperatures, in strongly oxidising reaction melts, with low or variable yields.[7] Only in the mid to late 1990's, and early this century, have synthetic breakthroughs allowed the selective formation of PAHs under mild conditions at room temperature.[4,6] Various procedures have been employed for the selective formation of aromatic hydrocarbons:[3] the coupling of suitable smaller PAHs to extended PAHs (concept (a), figure 2.3); the addition of C_n fragments to smaller PAHs, and subsequent aromatisation (concept (b), figure 2.3); the complete intramolecular cyclodehydrogenation of suitable precursors (concept (c), figure 2.3).

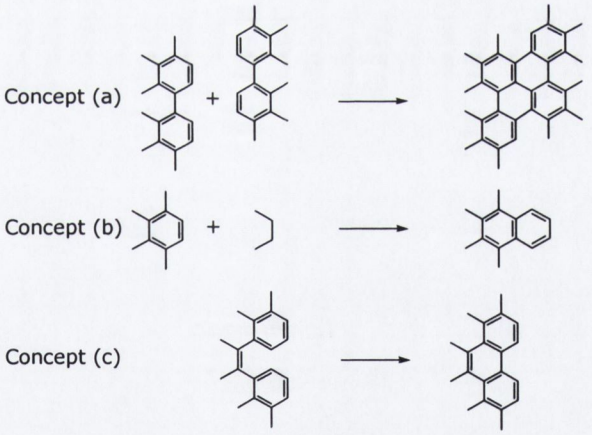


Figure 2.3. Construction techniques for PAHs.

Concept (a) is not feasible as a possible synthetic route in this work as highly unreactive all-benzenoid PAHs are required as starting materials. Concept (b) is also not considered, as a considerable number of addition steps would be required to synthesize extended carbon PAHs. For this work it was decided that concept (c) was the best route to extended, all-benzenoid PAHs *via* specific oligophenylene precursors. Our synthesis of these materials, is therefore based on Müllen's two steps:[9]

Step A) construction of a soluble polyphenylene precursor of well-defined structure and a close spatial arrangement of the phenyl rings, using the Diels-Alder reaction. Step B) planarisation of this precursor to the PAH by intramolecular cyclodehydrogenation.

A) The [2+4]-cycloaddition Reaction

The Diels-Alder reaction of tetraphenylcyclopentadienones with arylacetylenes is a well established method for the controlled construction of polyaryl compounds (such as those shown in figure 2.4).[9,10] It is one of the most fundamental and useful reactions in modern organic synthesis,[11] and has been proven to play a major role in the synthesis of natural products[12,13] and heat resistant polymers.[10] The method is widely used for the formation of carbon-carbon, carbon-heteroatom, and heteroatom-heteroatom bonds. In the [2+4]-cycloaddition, a dienophile stereospecifically adds 1,4 to a conjugated diene component, to generate a six-membered ring through two C-C bond formations.

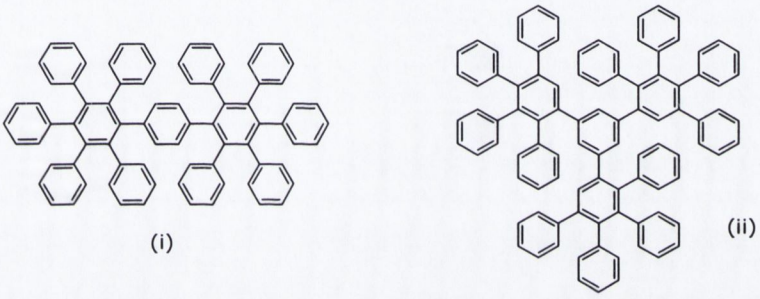


Figure 2.4. Oligophenyls with high melting points (i) 470°C and (ii) 375°C.

The reactivity of the diene, which is the 4π component of the Diels-Alder reaction, is influenced by its substituents. For example a terminal methyl substituent destabilizes both the *cisoid* conformation of the diene and the transition state through steric effects, causing a decrease in the reactivity.[14] The methyl substituent also has an electronic influence on the diene's reactivity in the Diels-Alder reaction. Whereas electron-donating substituents on the diene cause an increase of reactivity in a 'normal demand' Diels-Alder reaction, electron-withdrawing groups cause the opposite effect. An increase in the reactivity of the dienophile, the 2π reacting partner in a Diels-Alder reaction, is afforded by attaching electron-withdrawing groups. This is due to the lowering of the energy gap between the interacting Frontier Molecular Orbitals (FMOs).

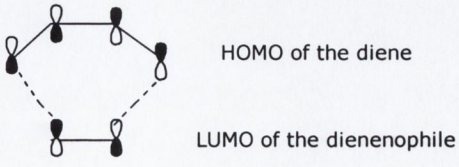


Figure 2.5. The Frontier-Orbital diagram showing the thermally allowed [2+4]-cycloaddition.

In the 'normal demand' Diels-Alder reaction, the dominating orbital interaction (corresponding to the lowest HOMO-LUMO energy separation) is the HOMO diene-LUMO dienophile,[14] figure 2.5.

There have been many mechanistic investigations into the Diels-Alder reaction, however the bulk of the evidence supports the concerted, one-step mechanism shown in figure 2.6.[14] In this mechanism there is a cyclic, six-centred transition state, and no intermediate.

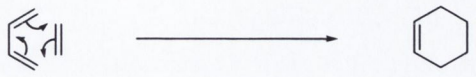


Figure 2.6. The proposed mechanism of the Diels-Alder reaction.

The synthetic strategy that has been adopted for the formation of the polyphenyl systems in this work, is based on the symmetry-allowed Diels-Alder reaction, in which acetylenes are reacted thermally with suitably substituted tetraphenylcyclopentadienones in a [2+4]-cycloaddition reaction. During this reaction carbon monoxide is evolved, to produce the corresponding hexaphenylbenzene[15] (see figure 2.7).

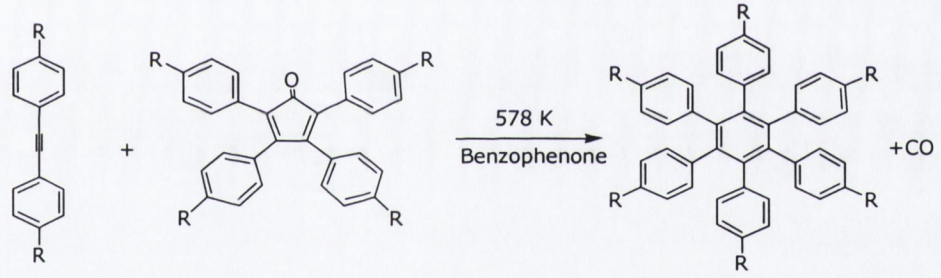


Figure 2.7. Route to oligophenylenes by intermolecular Diels-Alder reactions.

The scope of this reaction can be extended using other phenylene/ethynyl derivatives as precursors for larger, all benzenoid hydrocarbons with various topologies. The double Diels-Alder reaction in figure 2.8 produces quinquiphenylene in an almost quantitative yield.[10] Again this system can be further extended.[9] So by altering the number of acetylene spacers in the starting alkyne we can tune the size and dimension of the poly substituted product. The power of this method lies in its extraordinary specificity: it is chemoselective, in that the dienophile prefers to react with the diene and not competitively in an intermolecular reaction with itself; it is regioselective, unsymmetrical dienes choosing only one conformation for cycloaddition to unsymmetrical dienophiles; and it is stereoselective, mostly following the *endo*-rule.[16]

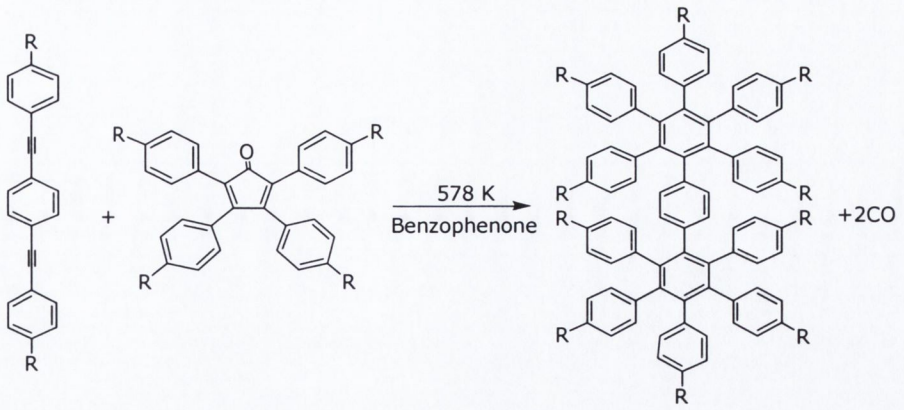


Figure 2.8. Route to larger oligophenylene derivatives by multiple intermolecular Diels-Alder reactions.

As a less effective synthetic strategy to polyphenylenes, the intermolecular [2+2+2]-cycloaddition of three unsaturated moieties (figure 2.9) constructs three new bonds in one step.[16] The cyclotrimerisation is catalysed by a large number of transition metal systems (for example $CpCo(CO)_2$).[16]

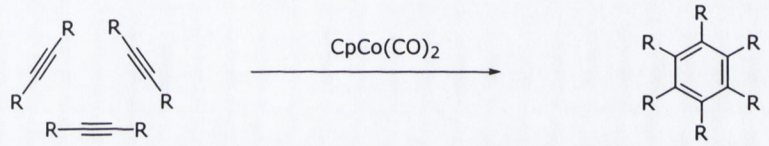


Figure 2.9. Prototypical [2+2+2]-cycloaddition.

This synthetic concept allows only the identical functionalization of all six phenyl substituents of the hexaphenylbenzene, or product mixes have to be tolerated. Selectively functionalized products are best accomplished *via* the [2+4]-cycloaddition of the suitably substituted diphenylacetylenes and 2,3,4,5-tetraarylcyclopenta-2,4-dien-1-ones, which allows the formation of well-defined unsymmetrical hexaphenylbenzene derivatives in excellent yields.

B) Oxidative Cyclodehydrogenation

On the route to all-benzenoid hydrocarbons, the oxidation cyclodehydrogenation of the oligophenylene is the final step of the synthesis. This flattens the polyphenylene precursors to obtain planar PAHs. The most frequently reported examples of oxidative cyclodehydrogenation are with vanadium(v) salts,[17] with thallium(III) salts,[18] iron(III) chloride[19] or photochemical cyclodehydrogenation.[20] Reductive cyclodehydrogenation with elemental lithium[21] or potassium[22] has been used less often and in exceptional cases platinum(0)- or palladium(0)-catalysed cyclodehydrogenation reactions have also been reported.[23]

The photocyclisation of stilbene-like compounds is well known, and such transformations have been widely used to prepare complex ring systems.[20] However, this radical process can be low yielding, with the formation of several products due to rearrangements such as 1,2-phenyl shifts.[24] An alternative method for the coupling of aromatics was developed in 1965 by Kovacic.[25] His conditions employed Lewis acid catalyst-oxidants, such as ferric chloride, molybdenum pentachloride, or aluminium chloride/cupric chloride.[25] Under such conditions he coupled benzene, to form *p*-polyphenyls, and naphthalene, binaphthyls, ternaphthyls and higher molecular weight materials.[26] He proposed the oxidative cationic mechanism shown in figure 2.10 for the single reaction step.

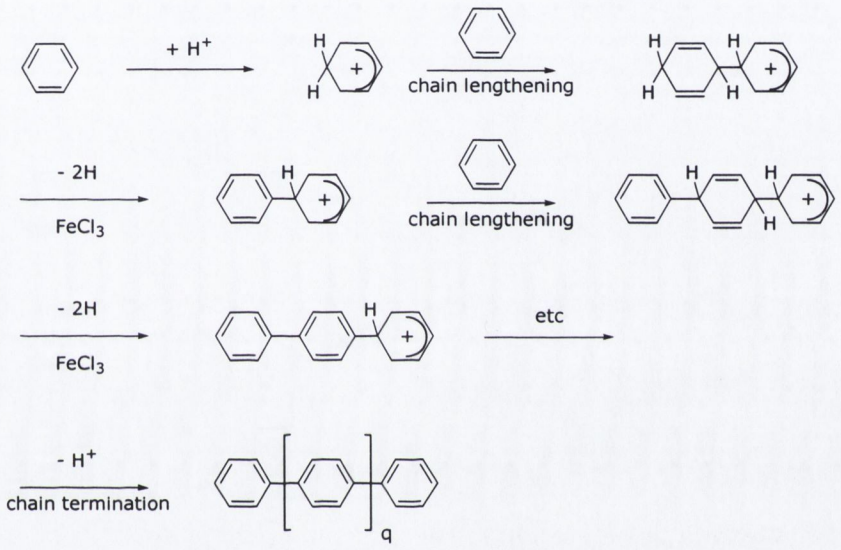


Figure 2.10. Proposed oxidative cationic mechanism for dehydrogenation reactions using metal halides.

In the initiation and propagation phases of the nuclear coupling, aluminium chloride is thought to be the catalyst and copper(II) chloride the oxidant. Ferric chloride and molybdenum pentachloride will function as both. The strength of the Lewis acid catalyst is a crucial factor. For example no reaction occurs with stannic chloride or titanium tetrachloride.

Optimal conditions use aluminium(III) chloride and carbon disulfide at RT with copper(II) chloride as oxidant instead of oxygen. The use of these mild conditions allows the formation of, for example, hexa-*peri*-hexabenzocoronene (HBC) at room temperature (see figure 2.11).[9] The driving force for intramolecular cyclodehydrogenation is the considerable gain in stability of the planar PAH compared to the more energetic oligophenylene precursor.[6] This synthetic strategy has been

used to produce all-benzenoid hydrocarbons of varying topology and up to 222 carbon atoms.[27]

Large PAHs often exhibit poor solubility, preventing their complete charaterisation or investigation of their physical properties. The introduction of bulky solubilising side-chains (R in figure 2.11) in some cases enables characterisation of the coronenes by NMR spectroscopy.[28,29] Purity can be obtained as their high thermal stability enables purification by fractional sublimation at high vacuum and temperature.

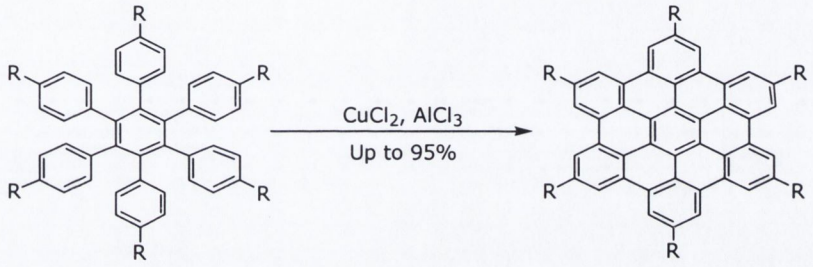


Figure 2.11. The oxidative cyclodehydrogenation reaction to hexa-*peri*-hexabenzocoronene (R=H or alkyl).

2.1.2 HBC PROPERTIES AND MATERIAL APPLICATION

PAHs are characterised by their stacking in discotic mesophases.[1,5] Hexabenzocoronene has a diameter of 15 Å and may be considered to be a nanoscale version of an infinite, two-dimensional graphite sheet.[30] In the crystalline form the molecule is not strictly planar and forms dimers with an interplanar distance of 3.44 Å due to strong π interactions.[31] This distance is only slightly larger than in graphite (3.35 Å). Scanning tunnelling microscopy (STM) has also revealed the ability of HBC derivatives to form highly ordered monomolecular layers with diode like electrical behaviour when adsorbed on suitable substrates.[32] These aspects of the behaviour of HBC molecules open possibilities for their future use as molecular nanowires.

There is currently a drive in the electronics industry toward molecular materials which self-assemble with little external assistance, to form electronic and optical devices such as nanowires and molecular transistors.[30] This makes aggregation (the process of energy minimization through molecular interaction) an important property for potentially useful systems. The discotic material HBC, with its small permanent dipole moment and large polarisability, offers a well-defined, self-arranging system that can be modified at the periphery.[30] Due to strong π-π interactions, substituted HBC molecules self-assemble into highly ordered columnar stacks. The optimal stacking arrangement is staggered and constrained by side chains.[30] For comparison, the packing order of hexabenzocoronenes within the columns is lower than in the corresponding triphenylenes. This can be rationalized in terms of the area of the

aromatic core of the hexabenzocoronene, which is approximately three times that of the triphenylene moiety.[5] Larger discs are able to maintain substantial overlap of their aromatic regions even in the staggered conformation shown in figure 2.12.[5] Although hexabenzocoronenes exhibit extremely broad columnar mesophases, they are still less ordered within the columns than conventional triphenylenes.



Figure 2.12. Stacks of small triphenylene type discs compared to stacks of larger hexabenzocoronene type discs.

If the flat, disc-like cores are peripherally substituted with long alkyl chains, the molecules still self-assemble into columnar aggregates and above *ca.* 65°C (thermotropic phase transition) form a discotic liquid-crystalline phase.[5] Here the aromatic cores stack orthogonally, and gain mobility to spin about the axis to form columns, surrounded by saturated hydrocarbons. This insulated, coaxial structure can be regarded as a nanowire. Electronic charge transport is expected to be mediated by the overlap of π-orbitals of adjacent units and is therefore one-dimensional with very little lateral dispersion.[33] Recently it has been found that mesomorphic derivatives of hexabenzocoronene display liquid crystalline mesophases over an extensive temperature range,[33] and possess charge-carrier mobilities along the columnar axis, that are larger than any mobility value previously found for liquid-crystalline discotic materials (1.13 $cm^2\ V^{-1}\ s^{-1}$).[34] This makes them particularly attractive materials for applications in one-dimensional transport processes such as in conducting layers in molecular electronic devices,[33,35] in photoconductivity[36,37] and solar cells.[38]

There have been numerous attempts to change the electronic properties of PAHs and to prepare fully conjugated, organic π-systems. One way is to produce PAHs with a large number of benzene rings, since the electronic bandgap (ΔE) decreases with the increasing size of the PAH.[22] Another way to enhance the electronic properties of

traditional semiconducting and molecular materials is to 'dope' them. Although large polycyclic materials incorporating up to 222 carbon atoms, or 37 separate benzene units (3 nm diameter), have been characterised using the synthetic strategy described,[3,27] very few of these systems include a heteroatom. Nitrogen atoms represent ideal electron-rich dopants.

The research in this thesis will investigate a new family of N-doped molecular materials which will be generated from N-containing alkynyl compounds. They will serve as model compounds for the study of optical and electronic properties of larger multicomponent systems.

Compound	a_1	a_2	b_1	b_2	c_1	C_2	λ_{max} (nm)
1	C	C	CH	CH	CH	CH	330
2	N	C	CH	CH	CH	CH	420
3	N	N	CH	CH	CH	CH	417
4	C	C	N	CH	CH	CH	423
5	C	C	N	N	CH	CH	385
6	C	C	CH	CH	N	CH	422
7	C	C	CH	CH	N	N	423

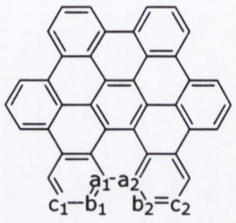


Table 2.1. The theorectically predicted effect of the selective N-doping of hexabenzocoronene on λ_{max}.

We have undertaken a preliminary theoretical study in conjunction with Dr. Davey in the Physics department at Dublin City University. This has shown that one way to enhance the electronic properties of hexabenzocoronene is to 'dope' with nitrogen. Optimised geometries were calculated using the semi-empirical AM1 parameter set and the electronic spectra of the model compounds were calculated using a single excitation configuration interaction with the ZINDO/S parameter set.

If such systems are genuine analogues of doped organic semiconductors, the appearance of red-shifted absorptions due to 'quasi-midgap' states would be expected. This is exactly what is observed theoretically, with a substantial increase in the λ_{max} from 330 nm when nitrogen atoms are substituted for carbon atoms. Currently methods of extrinsic doping have been unsuccessful as they tend to be non-selective or introduce defects. The route we have developed to synthesize these novel compounds represents for the first time the intrinsic doping of an organic semiconductor in a controlled and systematic fashion. Not only is nitrogen electron-withdrawing, producing electroactive compounds, but its lone pair of electrons is also a potential donor site for metal atoms. Further, the presence of heteroatoms is also expected to affect the liquid crystalline properties of the material.[15] Imido substituted aromatic compounds, for

example coronene-monoimide (figure 2.13), have been shown to have *n*-type (*i.e.* electron conducting) semiconductive characteristics,[39] in contrast to the more usual *p*-type (*i.e.* hole transport) behaviour of other discotic materials.

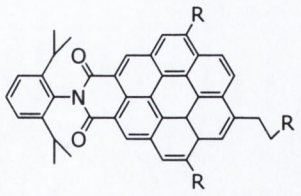


Figure 2.13. A coronenemonoimide.[39]

With charge carrier mobilities up to 0.3 $cm^2 V^{-1} s^{-1}$, liquid crystalline properties even at room temperature, and with a readily accessible fluid phase mesophase (the isotropic phase has a high degree of columnar order) at higher temperatures, this coronene-monoimide is of interest for many practical applications.[39] Extending this rationale to HBC derivatives would suggest that the N-doping of HBC would have a profound effect on the semi-conductor characteristics, the liquid crystalline phase, and the charge carrier mobility rates of such large aromatic compounds.

Materials with both strong fluorescence and carrier transporting ability are particularly suitable for the fabrication of organic light-emitting diodes (LEDs).[40,41] In this regard, coronene has already proved to be a good hole transporting material and is suitable as the emitting layer in multilayer LEDs. A critical element in designing and fabricating suitable materials is the control of their emission wavelength, obtained through changes in length, substitution, regioregularity and degree of conjugation.[40] In this way it is possible to utilize one family of modular chromophores and tune their photophysical characteristics. This could be applied to a novel family of highly fluorescent N-doped coronene derivatives. It is likely that the emission wavelength of any derivative would be dictated by the nature of its substituents. It would also be of interest to investigate the influence of nitrogen-heterosuperbenzenes (N-HBC) functionalization upon supramolecular ordering in both two-dimensional and three-dimensional motifs, as vast differences have been observed for the mesoscopic properties by changes at the periphery of HBC aromatic cores.[37,42] In order to provide suitable model systems, the synthetic approach to synthesize functionalized, nitrogen-doped HBC derivatives has been further investigated. This was accomplished through the formation of the bromo-substituted polyphenylene, by the [2+4]-cycloaddition of dipyrimidine acetylenes and suitably bromo-substituted 2,3,4,5-tetraarylcyclopenta-2,4-dien-1-ones. The bromo substituents serve as "handles" for further functionalization, *i.e.* to introduce substituents at the aromatic core using palladium catalysed coupling reactions.

In the following section the synthesis and investigation is discussed of the new family of nitrogen-functionalized (intrinsically doped) graphitic molecules, of predefined size and shape and tunable opto-electronic properties. These are called N-HBCs. Also reported is the synthetic work towards the establishment of a host of unique N-HBC derivatives and various physical data such as CV, TG, UV-vis and fluorescence spectra. The aim of the current research is to synthesize highly processable, novel nitrogen-doped derivatives based on the planar HBC molecule. We expected these to show advantages in terms of good solubility, synthetic tuneabilty, thermal stability and enhanced electrical conductivity, as well as to exhibit the ability to self assemble into columnar arrays.

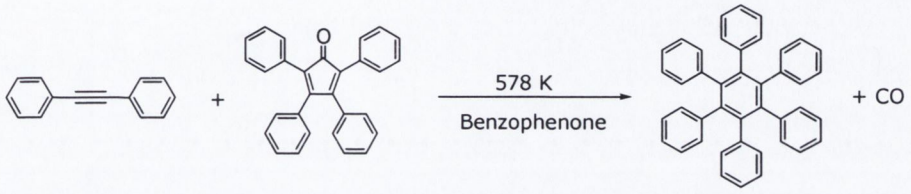
We expect these materials to be uniquely sensitive toward external triggers and highly processable. The high solubility of the N-HBCs has made it possible to measure the optical properties of the materials at varying concentrations, yielding information on the aggregation of the molecules. In this study, the electronic spectra of the materials are recorded at very low concentrations (10^{-15} M), where the effects of aggregation are still seen.

2.2 RESULTS AND DISCUSSION

2.2.1 THE SYNTHESIS OF N-HETEROSUPERBENZENE, N-HBC (17)

2.2.1.1 The Cyclodehydrogenation reaction of Hexaphenylbenzene

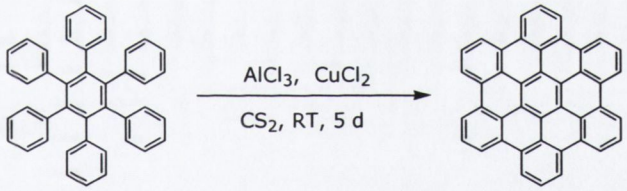
In order to check the synthetic conditions of the cyclodehydrogenation reaction, hexabenzocoronene **(11)** was synthesized. First hexaphenylbenzene **(10)** was formed from tetraphenylcyclopentadienone and diphenylacetylene in a Diels-Alder reaction at 578 K in a benzophenone melt.



(10)

Figure 2.14. The synthesis of hexaphenylbenzene **(10)**.

The white crystalline product **(10)**, which is insoluble in most common organic solvents, was treated with $AlCl_3$, and $CuCl_2$ in CS_2 to produce hexabenzocoronene (HBC) **(11)**. Being completely insoluble in most organic solvents it was purified by fractional sublimation to afford a pale yellow crystalline solid in 40% yield.



(11)

Figure 2.15. The synthesis of hexabenzocoronene **(11)**.

The UV-vis absorption spectrum obtained for HBC **(11)** matched those wavelengths reported in the literature for hexabenzocoronene, see table 2.2.

Wavelength (nm)	
HBC (11)	**HBC[8]**
342.5	342.5
358.5	359.5
388.5	387.5

Table 2.2. The UV-vis spectral data for HBC **(11)** and hexabenzocoronene[8] in 1,2,4-trichlorobenzene.

2.2.1.2 Nitrogen-Doping of an Organic Semiconductor: Discrete Control at a Molecular Level

The method for the intrinsic nitrogen-doping of hexabenzocoronene in a controlled and systematic fashion is introduced here. In an attempt to enhance the electrical conductivity of PAHs, nitrogen atoms were incorporated into the aromatic system to produce N-HBCs. It is essential that the products are processable with the focus on solubility, thermal stability and dimension control. Müllen's synthetic procedure, which allows control in size and dimension, has been developed here to allow the synthesis of N-HBCs for the first time.

One modification is to incorporate a heteroatom into the alkyne moiety, in a stepwise manner *via* pyrimidine substituents. See figure 2.16.

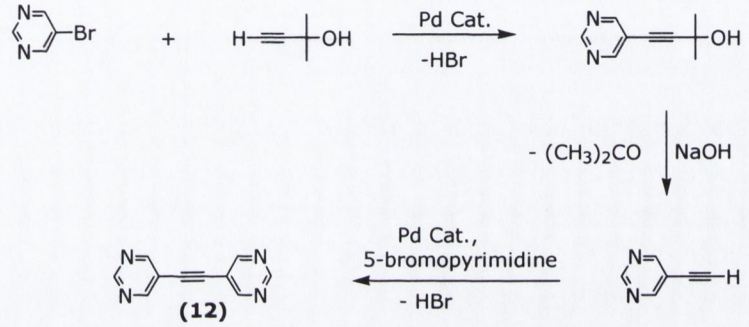


Figure 2.16. The synthesis of dipyrimidine acetylene **(12).**

Various conjugated pyrimidine alkyne moieties can be synthesized *via* this method, which employs the use of a Pd coupling catalyst. The synthesis of dipyrimidine acetylene **(12)** was accomplished by a sequence of Sonogashira coupling reactions[43] (figure 2.16). In the first step 5-bromopyrimidine was coupled with 2-methyl-3-butyn-2-ol to give 2-methyl-4-pyrimidin-5-yl-but-3-yn-2-ol in 88% yield. After deprotection of the triple bond with NaOH in toluene,[44] the alkyne 5-ethynylpyrimidine (produced in 55% yield) was coupled with 5-bromopyrimidine, yielding the symmetrically substituted building block dipyrimidine acetylene **(12)** as an air stable, off-white crystalline compound in 74% yield.

In an attempt to avoid future solubility problems after cyclodehydrogenation to the coronene derivative, the tertiary butyl substituted tetraphenylcyclopentadienone was synthesized as the diene for Diels-Alder reaction with dipyrimidine acetylene. The alkyl substitution is a key step toward the synthesis of soluble PAH derivatives. The 1,2-diketone synthesis by Mueller-Westerhoff,[45] and the synthesis of 1,3-diarylacetones,

based on the synthesis of des Abbayes,[46] permit the synthesis of alkyl-substituted tetraphenylcyclopentadienones, figure 2.17.

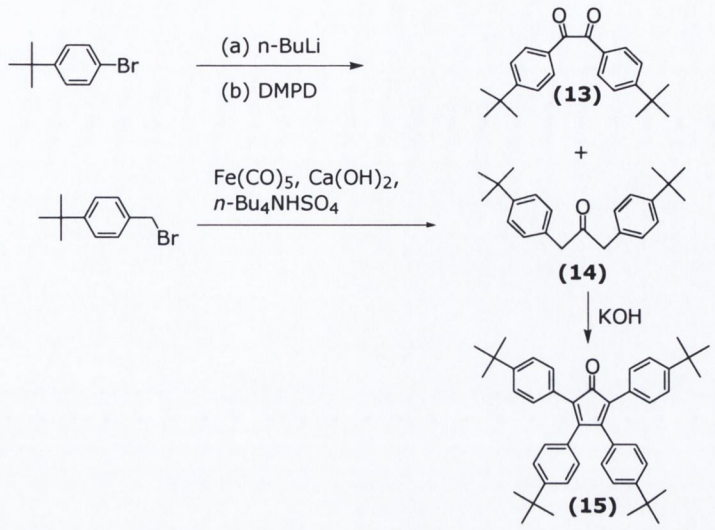


Figure 2.17. The synthesis of *tert*-butyl substituted tetraphenylcyclopentadienone **(15)**.

Treatment of 1,4-*tert*-butylbromobenzene with *n*-BuLi at 195 K, followed by the addition of DMPD afforded the white crystalline product 1,2-diaryl-1,2-diketone, **(13)**. 4-*tert*-butylbromobenzyl bromide was converted to the 1,3-diaryl-2-propanone **(14)**, using catalytic amounts of iron pentacarbonyl in a liquid-liquid phase transfer system. The two-fold Knoevenagel condensation[1] of **(13)** and **(14)** in refluxing ethanol with KOH, yielded the tetraarylcyclopentadienone building block **(15)** as a dark red crystalline solid in 65% yield.

Central to the work is the introduction of heteroatoms into a polyphenylene precursor. Polyphenylene **(16)**, the precursor of the N-HBC compound **(17)**, was synthesized in an 81% yield, in a stepwise manner *via* Diels-Alder [2+4]-cycloaddition of di-(pyrimidin-3,5-yl)ethyne **(12)** to 2,3,4,5-tetra-(4-*tert*-butylphenyl)cyclopentadien-1-one **(15)** (figure 2.18). The careful choice of starting materials and the established stereochemistry of the [2+4]-cycloaddition reactions meant that the system was chemioselective, ensuring the *ortho*-arrangement of the pyrimidine subunits on the generated benzene core of **(16)**.

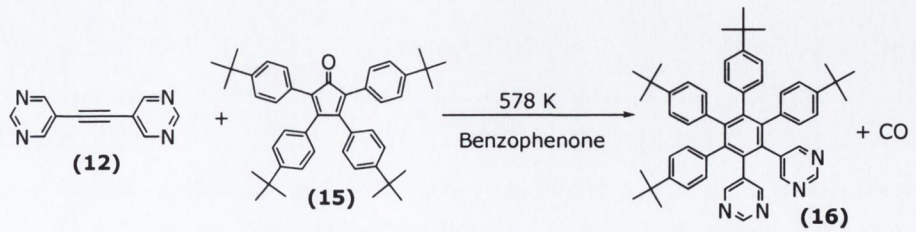


Figure 2.18. The synthesis of substituted N-doped hexaphenylbenzene **(16)**.

Polyphenylene **(16)** was purified by column chromatography and multiple recrystallisations from ethyl acetate and petroleum ether to give colourless crystals.

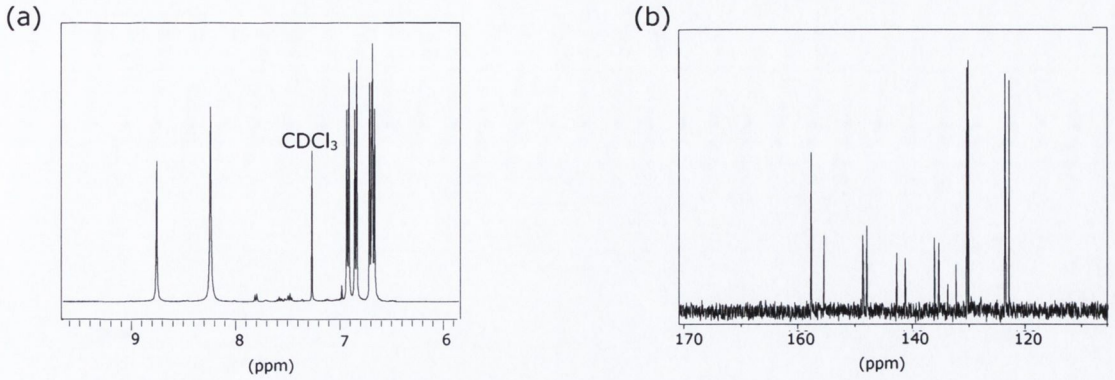


Figure 2.19. (a) ^{1}H NMR (400 MHz) and (b) ^{13}C NMR (100 MHz) spectra of the aromatic areas of **(16)** ($CDCl_3$, RT).

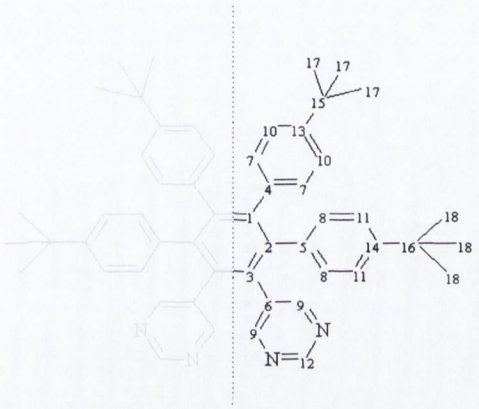


Figure 2.20. The atom labelling scheme of **(16)**.

The structure of **(16)** has a C_2 axis of symmetry running through the molecule (see figure 2.20), which considerably simplifies the NMR spectra.

There are two sets of signals in the aromatic region of the ^{1}H NMR spectrum of **(16)**, see figure 2.19 (a). The two lowfield singlets at δ 8.77 and δ 8.26, in an integral ratio of 2:4 hydrogen atoms, respectively, are assigned to the hydrogen atoms of the pyrimidine ring. The lowest field signal (δ 8.77) is specifically assigned to the protons between the nitrogens of the pyrimidine ring at C12. The electron-withdrawing properties of the nitrogen atoms have shifted the signal for these protons to this lowfield position. The second set of signals comprises four doublets in the region δ 6.6 - δ 7.0. These are assigned to the aromatic protons of carbons C7, C8, C10 and C11. Vicinal coupling of the adjacent aromatic proton causes the multiplicity in each case. The phenyl rings are free to rotate around their single bonds to the central carbon ring, which creates equivalence within each ring. The methyl groups of each *tert*-butyl group can also rotate, rendering them equivalent on the NMR time-scale. This gives rise to only two methyl proton signals, at δ 1.13 and δ 1.11, which integrate to 18 protons each (not shown in figure 2.19 (a)).

The aromatic region of the ^{13}C NMR spectrum of **(16)** is shown in figure 2.19 (b). This shows eight quaternary carbon signals in the region δ 132 - δ 149, which are assigned to the eight chemically distinct carbons, C1-6 and C13-14. According to 135° DEPT NMR spectroscopy there are six aromatic CH signals, four of which are in the δ 120 –

δ 130 area, and are assigned as the phenyl carbons C7, C8, C10 and C11. The two lowfield signals at δ 157.6 and δ 155.4 are assigned as the deshielded aromatic carbon atoms of the pyrimidine ring, C9 and C12, respectively. There are four signals in the aliphatic region of the ^{13}C NMR spectrum, which are allocated to the two distinct *tert*-butyl groups. Each *tert*-butyl comprises of a quaternary peak, C15 or C16 (δ 33.7 or δ 33.6), and a methyl group signal, C17 or C18 (δ 30.70 or δ 30.68).

Heteronuclear CH COSY (HMQC), and Homonuclear HH COSY (TOCSY) experiments were carried out to assist in the assignment of **(16)**. The results of these NMR experiments are given in tables 2.3 and 2.4.

Carbon atom Label	^{1}H NMR assignment (ppm)	^{13}C NMR assignment (ppm)
C7 or C10, CH	6.69	130.1
C8 or C11, CH	6.71	130.4
C7 or C10, CH	6.86	122.9
C8 or C11, CH	6.93	123.7
C9, CH	8.26	157.6
C12, CH	8.77	155.4

Table 2.3. Assignment of ^{13}C and ^{1}H NMR signals from HMQC experiments on **(16)**.

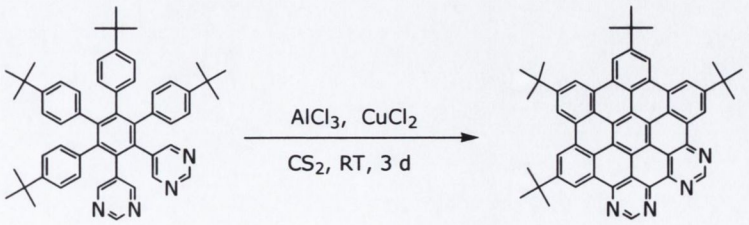
Carbon atom Label	^{1}H NMR (ppm)	^{1}H NMR (ppm)
C7 or C10, CH	6.86	6.69
C8 or C11, CH	6.93	6.71

Table 2.4. Assignment of ^{1}H NMR signals using coupling information from TOCSY experiments on **(16)**.

The coupling information from the COSY experiments has allowed further assignment of the aromatic proton signals of the phenyl rings of **(16)**. Vicinal coupling between the protons at C7 and C10 and between the protons at C8 and C11 is clear in the TOCSY experiment (see table 2.4).

2.2.1.3 Synthetic Extension To N-HBC (17)

Subsequent oxidative cyclodehydrogenation of **(16)** generated the first N-functionalized heterosuperbenzene, **(17)**, figure 2.21, which we published in 2002.[47]



(16) **(17)**

Figure 2.21. The synthesis of N-HBC **(17)**, *via* the cyclodehydrogenation of **(16)**.

N-HBC **(17)** was purified by chromatography, and extracted into $CHCl_3$. Coronene and its derivatives are insoluble in this solvent, ensuring that such graphene materials were not present in the sample. Finally, multiple recrystallisations from toluene and methanol gave the N-heterosuperbenzene **(17)** as a dark red/brown microcrystalline solid in 49% yield. The low yield obtained for **(17)** is explained through intermolecular aryl-aryl couplings and dealkylation, which could not be suppressed under these conditions. From a thermodynamic point of view, incomplete cyclisation would be unfavourable because the formation of a fully dehydrogenated system gains the largest increase of resonance energy.[28] Therefore it is not expected that partially cyclodehydrogenated compounds are also formed. Due to HCl formation in the course of the cyclodehydrogenation reaction, the side products are predicted to be chlorinated, cyclised products.[9] Nevertheless it was possible to isolate the non-chlorinated, fully cyclised product from these mixtures.

The four *tert*-butyl groups along with the four peripheral nitrogen atoms of **(17)** provide sufficient solubility for characterization, so that the proposed structure could be proven unambiguously. Accurate mass spectral data, ^{13}C and ^{1}H NMR spectra, heteronuclear CH COSY (HMQC, HMBC) and 135° DEPT NMR spectra in $CDCl_3$ were obtained of **(17)**. All data were cooperative and no signals other than those attributable to **(17)** were observed.

Like **(16)**, the proposed structure of **(17)** is simplified by the presence of a C_2 axis of symmetry running through the molecule, as shown in figure 2.22.

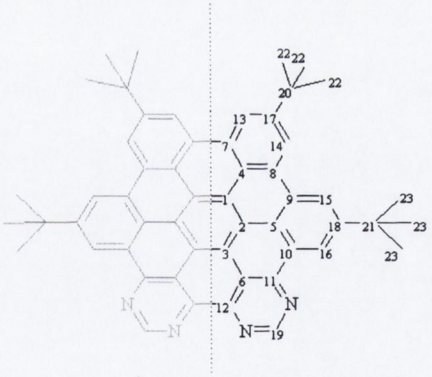


Figure 2.22. The atom labelling scheme of **(17)**.

The methyl groups of each *tert*-butyl group rotate, rendering them equivalent on the NMR time-scale. The atom labelling scheme shows the 23 chemically distinct carbon atoms of the heterosuperbenzene **(17)**. There are 5 chemically distinct aromatic protons at carbon positions 13, 14, 15, 16 and 19, and 2 distinct methyl protons from carbons 22 and 23.

This is in agreement with the ^{1}H NMR spectra (figure 2.23), and the ^{13}C NMR spectra (figure 2.24). The ^{1}H NMR spectrum of **(17)** shows two sets of aliphatic signals at δ 1.95 and δ 1.87, integrating for 18 hydrogen atoms each corresponding to the two sets of equivalent *tert*-butyl protons. There are five aromatic signals, each integrating for

two hydrogen atoms. The aromatic signal at lowest field is assigned to the two hydrogen atoms located between the pyrimidine nitrogens, at carbon position C19.

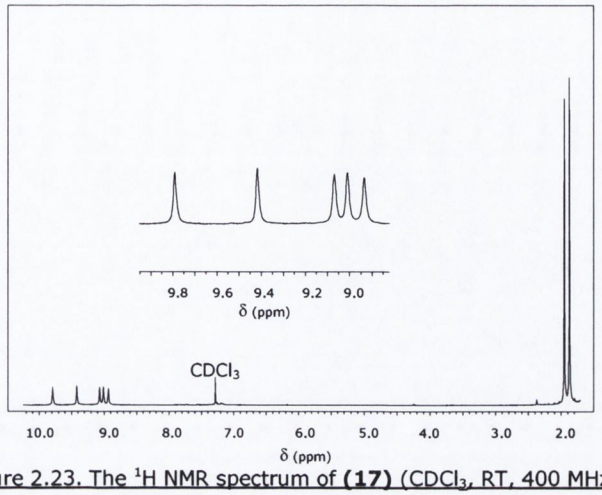


Figure 2.23. The ^{1}H NMR spectrum of **(17)** ($CDCl_3$, RT, 400 MHz).

It is possible to interpret the broadening of the aromatic signals as the result of placement of these ring protons in the shielding region of a neighbouring disk-type π-system, which would occur if the molecules aggregated. Strong π-π interactions between single molecules favour aggregation, leading to the broadening of resonance signals. The observed chemical shifts of the aromatic protons result from a complex interplay between both ring current-induced deshielding and van der Waals shielding effects. It is difficult to make comparisons between the chemical shifts for these protons in N-HBC (δ 8.9 – δ 9.8) and HBC derivatives due to N-HBCs additional N-functionality. Most HBC derivatives have D_{6h} symmetry and display a single peak for the aromatic protons in the ^{1}H NMR. However, the chemical shifts for these protons in N-HBC are at a slightly higher-field when compared to the coronene derivative 2,2′-bis-(5,8,11,14,17-penta-*tert*-butylhexa-*peri*-hexabenzocoronene) which is known not to undergo significant aggregation (δ 9.3 - δ 10.1).[29] Thus it is possible that N-HBC is experiencing intermolecular shielding of the aromatic core through aggregation in $CDCl_3$.

The ^{13}C NMR spectrum of heterosuperbenzene **(17)** shows 23 distinct signals. Four of these signals are in the aliphatic region at δ 31.58, 31.67, 35.40 and 35.42. The former two signals are assigned as the methyl carbon atoms of the two chemically distinct *tert*-butyl groups and the latter two signals are assigned to the quaternary carbon atoms. In the aromatic region the remaining 19 signals can be divided into 5 aromatic CH and 14 quaternary carbon atoms by use of 135° DEPT NMR spectroscopy. The carbons labelled C13-16 and C19 are given at δ 155.5, 122.3, 121.6, 118.7 and 118.4, with the lowest field signal (δ 155.5) expected to have resulted from the deshielded carbon atom C19, situated between the pyrimidine nitrogen atoms.

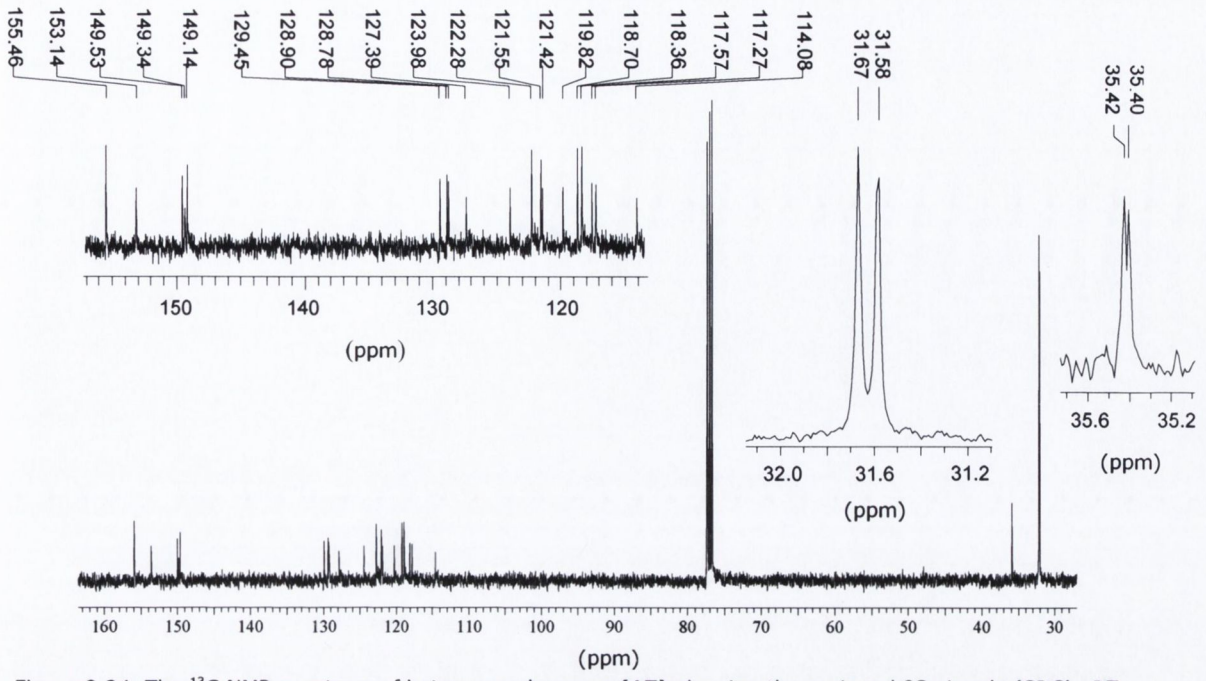


Figure 2.24. The ^{13}C NMR spectrum of heterosuperbenzene **(17)** showing the assigned 23 signals ($CDCl_3$, RT, 100 MHz).

Heteronuclear CH COSY (HMQC and HMBC) experiments have allowed further detailed ^1H and ^{13}C NMR assignments. The results of these NMR experiments are given in tables 2.5 and 2.6.

Carbon atom Label	^1H NMR assignment (ppm)	^{13}C NMR assignment (ppm)
C22, CH_3	1.87	31.6
C23, CH_3	1.95	31.7
C13 or C14, CH	8.94	118.4
C13 or C14, CH	9.01	118.7
C15, CH	9.07	122.3
C16, CH	9.42	121.6
C19, CH	9.79	155.5

Table 2.5. Assignment of ^{13}C and ^1H NMR signals from HMQC experiments on **(17)**.

^1H NMR assignment (ppm)	Carbon atom label, ^{13}C NMR assignment (ppm)	Carbon atom label, ^{13}C NMR assignment (ppm) Long-range Coupling HMBC Data
1.87	C22, 31.6	C17, 149.1; C20, 35.40
1.95	C23, 31.7	C18, 149.5; C21, 35.42
8.94	C13 or C14, 118.4	C17, 149.1; C20, 35.40; C7 or C8, 128.8; C13 or C14, 118.7
9.01	C13 or C14, 118.7	C17, 149.1; C20, 35.40; C7 or C8, 129.5; C13 or C14, 118.4
9.07	C15, 122.3	C18, 149.5; C21, 35.42; C9, 128.9; C10, 124.0
9.42	C16, 121.6	C11, 153.1; C10, 124.0; C15, 122.3; C21, 35.42
9.79	C19, 155.5	C11, 153.1; C12, 149.3; C6, 117.3

Table 2.6. Assignment of ^{13}C and ^1H NMR signals from HMBC experiments on **(17)**.

Due to the lack of resolution of some of the coupling information, it is impossible to distinguish between the carbon atoms labelled C13 and C14, or between the quaternary carbon atoms labelled C7 and C8. In addition, the long-range coupling CH COSY (HMBC) experiment is no assistance in assigning the quaternary carbon atoms labelled 1-5; however several assignments using these experiments have been possible, see table 2.6.

Mass spectrometry and accurate mass analysis give satisfying results, and are in full accordance with the theoretically expected values. The ESI-mass spectrum of N-heterosuperbenzene **(17)** in toluene (figure 2.25) shows an isotopic distribution pattern for the $[MH]^+$ ion at 751.3. The presence of Na^+ ions produces the isotopic distribution pattern for the $[MNa]^+$ ion at 774.3.

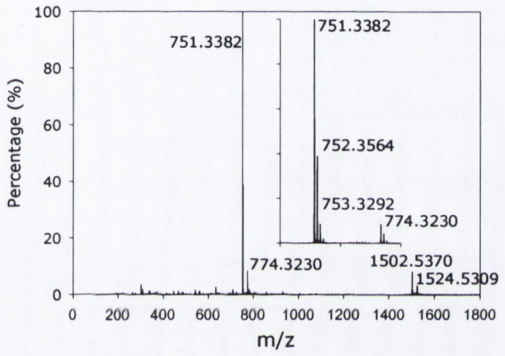


Figure 2.25. The ESI-mass spectrum of heterosuperbenzene **(17)** in toluene.

The envelopes at 1502.5 and 1524.5 are assigned to the bimolecular ions $[M_2H]^+$ and $[M_2Na]^+$. This is support for the existence of dimers of **(17)** in toluene solutions. No peaks other than those assigned to **(17)** were observed in the ESI-MS. This suggests that the N-heterosuperbenzene sample was pure.

Elemental analysis, a method usually well suited to the analysis of solid materials, could not be obtained for **(17)**, due to the extremely high thermal stability of the aromatic core. Incomplete combustion of this carbon rich type of molecule led to inaccurate results.[27] Non-invasive methods of analysis have been employed for analogous thermally stable graphene systems.[9] In the absence of Elemental Analysis data an accurate mass spectrum was obtained for **(17)** in toluene, which gave a $[C_{54}H_{47}N_4]^+$ peak of 751.3840, correct to within 5 ppm for that calculated.

2.2.2 THE GENERATION OF THE N-HETEROSUPERBENZENE FAMILY

2.2.2.1 The Synthetic Control

In the development of the N-heterosuperbenzene family, it is important to subject N-HBCs to functionalization and investigate the influence of variations in the molecular structure on their properties. Different functional groups (electron donating or withdrawing) connected to the aromatic core of the N-HBCs would be expected to influence the supramolecular ordering[37,42,48] and the photophysical characteristics.[40] Analogous to HBCs, N-HBC derivatives with electron donating substituents may possess better photoconductive properties in the discotic mesophase.[37] In order to provide suitable systems, various nitrogen containing polyphenylene derivatives with electron donating and electron withdrawing substituents have been synthesized in this work.

The best method to obtain selectively funtionalized polyphenylene precursors is *via* the [2+4]-cycloaddition of the dipyrimidine acetylene with a suitably substituted 2,3,4,5-tetraarylcyclopenta-2,4-dien-1-one. Figure 2.26 shows the general scheme for the selective formation of these substituted 2,3,4,5-tetraarylcyclopenta-2,4-dien-1-ones.

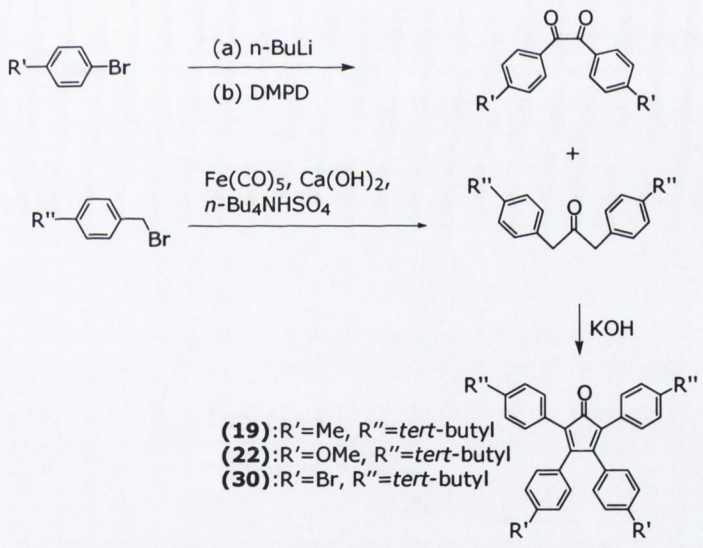
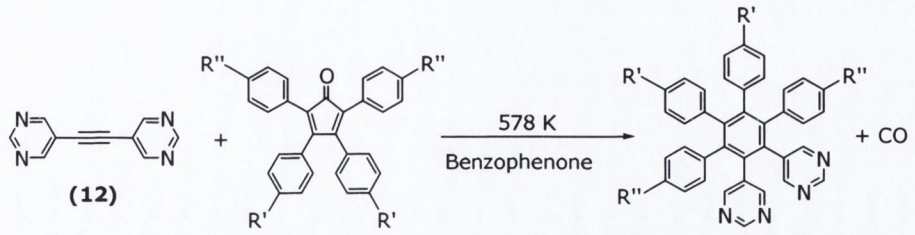


Figure 2.26. The synthesis of substituted tetraarylcyclopentadienones.

Suitable combinations of the synthesized dipyrimidine acetylene **(12)** and the appropriately substituted tetraarylcylopentadienones **(19)**, **(22)** and **(30)** can then be reacted in the [2+4]-cycloaddition, in refluxing benzophenone. By this method, the three functionalized hexaarylbenzenes **(20)**, **(23)** and **(31)**, were synthesized (see figure 2.27).



(19):R'=Me, R''=*tert*-butyl
(22):R'=OMe, R''=*tert*-butyl
(30):R'=Br, R''=*tert*-butyl

(20):R'=Me, R''=*tert*-butyl
(23):R'=OMe, R''=*tert*-butyl
(31):R'=Br, R''=*tert*-butyl

Figure 2.27. The synthesis of substituted N-doped hexaarylbenzenes.

All the N-doped polyphenylenes were unambiguously characterised by NMR spectroscopy, mass spectrometry and elemental analysis.

With the right combination of diarylacetylene and tetraarylcyclopentadienone, this synthetic approach, using the intermolecular Diels-Alder reaction, affords well-defined hexaarylbenzene derivatives in excellent yields. Cyclodehydrogenation of these derivatives would offer the possibility of synthesizing a variety of funtionalised N-HBCs for spectroscopic and electronic investigations.

2.2.2.2 Incorporating Alkyne Functionalities

We hypothesized that increasing the conjugation along the axis (substitution at R', figure 2.27) may provide highly fluorescent derivatives with emission in the visible range. Acetylenic linkages are attractive candidates for this purpose as they have been shown previously to affect electron delocalisation substantially in the excited state of conjugated arenes and to provide intensely fluorescent chromophores.[40] For example, substituting anthracene (λ_{em}=388 nm, ϕ_F=0.25 in benzene) with two phenylethynyl groups at the 9 and 10 positions results in a 100 nm red-shift in the emission wavelength and considerably enhanced fluorescence intensity (λ_{em}=486 nm, ϕ_F=0.96 in benzene). In contrast, the addition of phenyl rings in the form of 9,10-diphenylanthracene, while improving fluorescence quantum yield, produces only a moderate shift in emission wavelength (λ_{em}=407 nm, ϕ_F=0.84 in benzene).[40]

The novel synthesis of the ethynyl substituted polyarylbenzene **(49)** (shown in figure 2.28) has been selected in this work as a target molecule. It was expected that cyclodehydrogenation of this compound would produce an ethynyl substituted N-HBC, as a highly fluorescent chromophore.

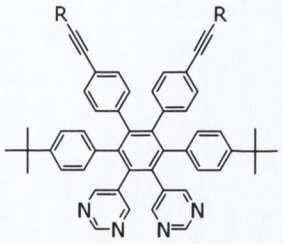


Figure 2.28. Ethynyl substituted polyarylbenzene **(49)**.

Two complementary routes have been utilized for the synthesis of **(49)**: **route a)** built-in, or **route b)** cross-coupling, palladium catalysed reactions of the bromo-substituted polyarylbenzene, **(31)**, with substituted acetylenes.

Built-in, route a) Figure 2.29 shows the synthesis of 1,2-dipyrimidyl-3,6-bis-(4-*tert*-butylphenyl)-4,5-bis-(4-triisopropylsilylethynylphenyl) benzene, **(29)**.

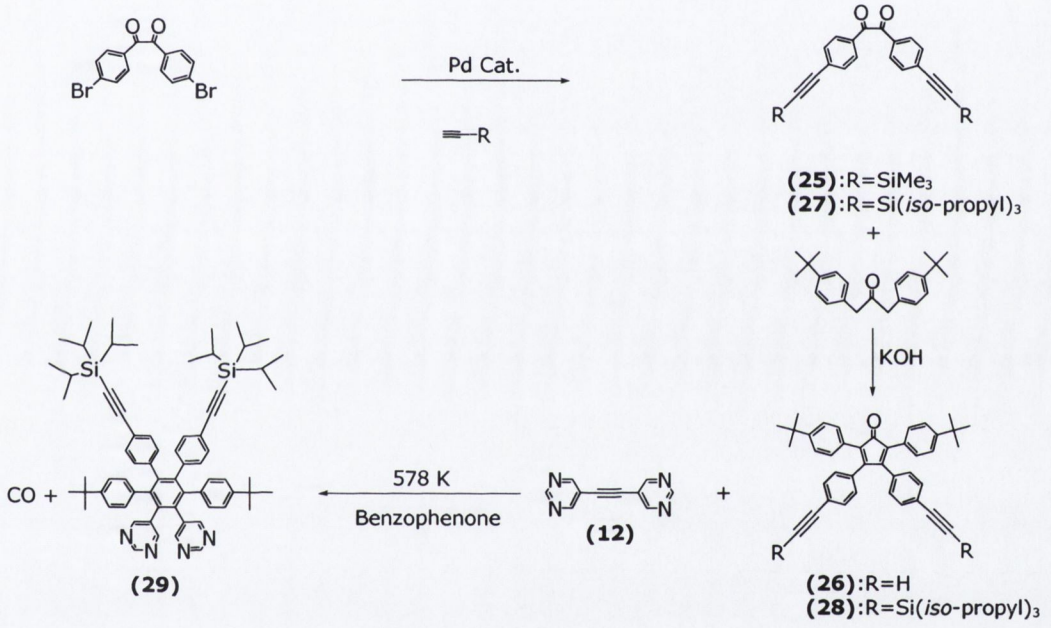


Figure 2.29. The synthesis of triisopropylsilylethynyl substituted polyarylbenzene **(29)** *via* the [2+4]-cycloaddition reaction.

Acetylenic units such as trimethylsilylethynyl or triisopropylsilylethynyl, can be incorporated into the dione by coupling trimethylsilylacetylene (TMSA) or triisopropylsilylacetylene (TiPSA) with dibromobenzil, using the method of Sonogashira *et al.*,[43] to form **(25)** and **(27)**, respectively. The benzil derivatives **(25)** and **(27)** are obtained in a 62% and 87% yield, respectively. The appropriate dione is then condensed with the ketone **(14)** in the presence of KOH to afford the substituted cyclopentadienones **(26)** or **(28)**. The diethynyl cyclopentadienone derivatives **(26)** and **(28)** each contain one diene as well as two dienophile functions. However,

participation of the triple bonds in the cycloaddition can be prevented by protecting them with bulky substituents such as triisopropylsilyl (TiPS) substituents.[1] TiPS is sterically very demanding, and does not favour the cycloaddition process. However the bulky trimethylsilyl (TMS) groups were lost in the condensation reaction to **(26)** and only the simple ethynyl functionality remained. The bulky protecting group, TiPS, proved to be much more robust in the condensation reaction, and **(28)** was achieved in an 81% yield. Unfortunately it is not possible to couple TMSA or TiPSA directly to a brominated cyclopentadienone (*e.g.* to **(30)**), as hydrogenation of a double bond in the cyclopentadienone is likely.[1]

The attempted [2+4]-cycloaddition reaction of dipyrimidine acetylene **(12)** with the ethynyl substituted cyclopentadienone **(26)** led only to an insoluble brown crystalline product, which is likely to be polymeric. Multiple chloroform washes were performed, removing benzophenone and any unreacted starting materials, and leaving the brown solid. This solid remained insoluble in all available solvents. Analysis of the chloroform washings showed the presence of large quantities of dipyrimidine acetylene, which was recovered almost quantitatively.

The electron-withdrawing properties of the nitrogen atoms in the pyrimidine rings is expected to cause an increase in reactivity of dipyrimidine acetylene, in a 'normal demand' Diels-Alder reaction. Thus the selective [2+4]-cycloaddition, as a result of preferential reactivity of dipyrimidine acetylene as compared to the acetylenes of **(26)**, was expected. The ethynyl substituent on the cyclopentadienone, however, is in a two-fold excess and is the least sterically demanding dienophile. It is therefore not surprising that the cyclopentadienone would prefer to self-react, and it is presumed that polymerization to large, dense, hyperbranched polyphenyls has occurred.[49] The dense packing of the benzene rings in these high generation polymers would account for the complete insolubility of the product. However, IR spectroscopy reveals the loss of the characteristic carbonyl resonance, which is replaced by a more complex aromatic region, caused by the increase in the number of benzene rings. This has been seen with similar cyclopentadienone units by Müllen *et al.*[49]

The [2+4]-cycloaddition reaction of dipyrimidine acetylene **(12)** and the substituted tetraarylcyclopentadienone **(28)**, was much more successful. The bulky TiPS ethynyl groups prevent much of the polymerisation of **(28)** in the Diels-Alder reaction under these conditions, and the polyphenylene product **(29)** was obtained in 65% yield after column chromatography and recrystallisation from acetone and water. After the Diels-Alder addition giving **(29)** the TiPS groups can be removed, if desired, and the

diethynyl functions thus activated for further Diels-Alder cycloadditions or for further functionalization.

Palladium cross-coupling, route b) Having at hand the bromo-substituted polyarylbenzene compound **(31)**, it is possible to exchange the bromo substituents at the aromatic core to introduce various electron donating and electron withdrawing groups. The solubilizing substituents (*tert*-butyl groups) are maintained as a prerequisite for any chemical transformations at the aromatic core.

The addition of lithiated trimethylsilylacetylene, formed from trimethylsilylacetylene and *n*-butyl lithium in tetrahydrofuran, did not yield the desired product, but resulted in almost quantitative return of the bromo-substituted polyarylbenzene, **(31)**. However, it was possible to introduce acetylenes onto the aromatic core by using Pd-catalysed coupling reactions, see figure 2.30.

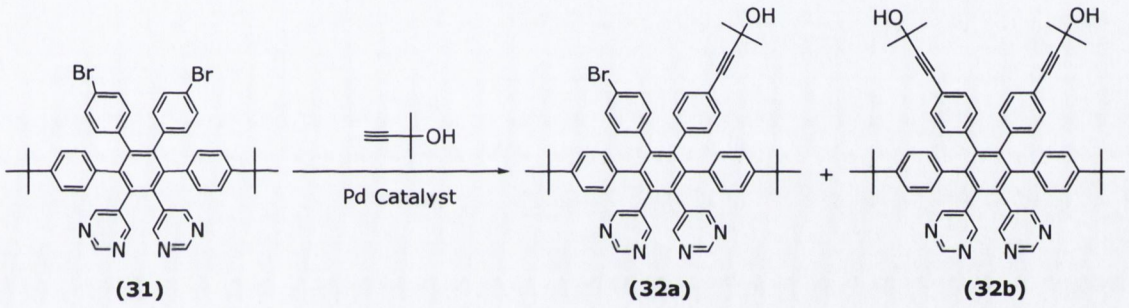


Figure 2.30. The synthesis of conjugated 1,2-dipyrimidyl-3,6-bis-(4-tert-butylphenyl)-4,5-bis-(4-(3-methyl-3-hydroxy-butynyl)phenyl)benzene, **(32b)**, by Pd-mediated cross-coupling reactions.

It was possible to cross couple 2-methyl-3-butyn-2-ol with the bromo-substituted polyarylbenzene **(31)** under Sonogashira catalysis[43] with $Pd(PPh_3)_2Cl_2$ and CuI. The mono-substituted derivative **(32a)** was produced as the major product, and significant amounts of polyarylbenzene starting material **(31)** was recovered (30%), even in the presence of a four-fold excess of 2-methyl-3-butyn-2-ol. The synthesis was repeated and similar results were obtained each time, suggesting that the bromo substituted polyarylbenzene **(31)** has been somewhat deactivated toward the Pd mediated cross-coupling process. This could be due to decreased lability of the bromine substituent when attached to an electron rich, aromatic core. Alternatively, the low yield of the alkynylation could suggest that the bromo substituted polyarylbenzene may function as a ligand for Pd(II).

Although high temperatures (343 K) and long reaction times (24 h) were necessary for the reaction to progress, with this method I was able to obtain **(32a)** and **(32b)** in 38% and 30% yields, respectively.

2.2.2.3 Functionalized Polyarylbenzenes

The controlled synthesis of nitrogen containing polyphenylene precursors is central to the formation of the extended N-heterosuperbenzene family. Functionalization at the periphery of the polyphenylene is expected to have dramatic effects on the physical and chemical properties of the N-HBC. Here we can compare the NMR and UV-vis spectroscopy, and X-ray crystallographic structures of the various synthesized nitrogen containing polyphenylene derivatives with electron donating and electron withdrawing substituents.

The novel nitrogen containing polyphenylene derivatives synthesized in this work are shown in figure 2.31, with hexaphenylbenzene **(10)**.

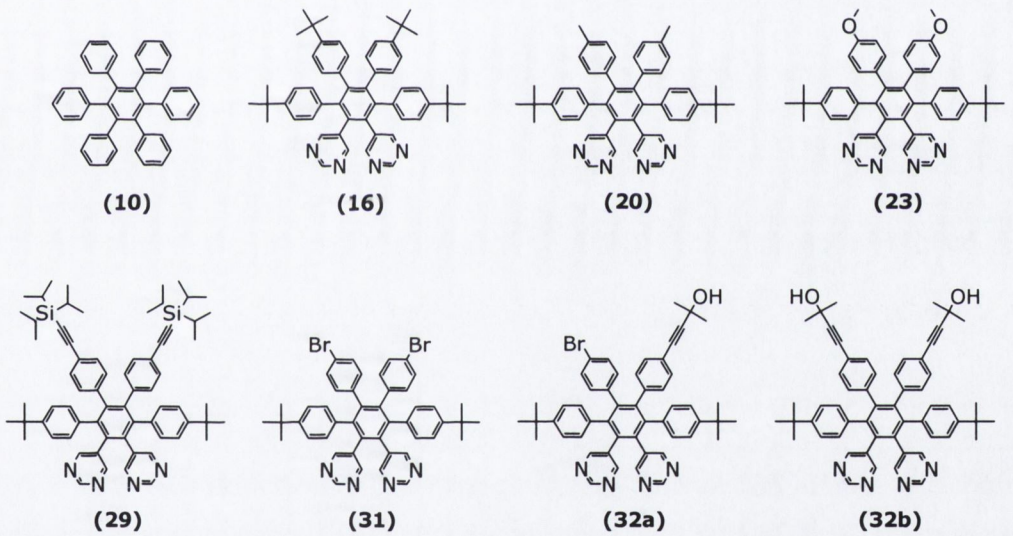


Figure 2.31. Various novel nitrogen-containing polyphenylene derivatives and hexaphenylbenzene **(10)**.

The synthesis of all the N-doped polyphenylenes, except that of **(32a/b)**, employed the Diels-Alder [2+4]-cycloaddition reaction from the appropriately substituted tetraarylcyclopentadienone and dipyrimidine acetylene **(12)**. The intermolecular Diels-Alder reaction, with expulsion of carbon monoxide, was carried out at 578 K in a benzophenone melt. Column chromatography followed by multiple recrystallisations from ethyl acetate/pet. ether or acetone/water afforded the well-defined hexaarylbenzene derivatives as colourless crystals in excellent yields, see table 2.7.

The Diels-Alder step is high-yielding, with hexaarylbenzene derivatives formed in 72–85% yields with the exception of **(29)** which is formed in a 65% yield. This lower yield, in comparison to the other hexaarylbenzene derivatives, could be as a result of competition from the protected acetylenic functionality of the tetraarylcyclopentadienone. Although these acetylenes are protected with bulky TiPS groups there may still be some self-reaction in competition with the intermolecular reaction with dipyrimidine acetylene **(12)**, resulting in a yield reduction of the desired ethynyl substituted hexaarylbenzene derivative **(29)**.

REACTION YIELDS AND ESI-MASS SPECTRAL ANALYSIS				
Substituents	**Polyphenylene**	**Yield (%)**	**Molar Mass ($gmol^{-1}$)**	**ESI-mass spectrum, $[MH]^+$, (%)**
None	**(10)**	75	534.660	
tert-butyl	**(16)**	81	763.044	763.5, (100)
methyl	**(20)**	72	678.880	679.4, (100)
methoxy	**(23)**	77	710.896	711.5, (100); 733.5, (5)
TiPSA	**(29)**	65	1011.547	1011.6, (100)
bromo	**(31)**	85	808.628	809.2, (100)
bromo, 3-methyl-3-hydroxy-butynyl	**(32a)**	38, Pd coupling reaction from **(31)**	811.836	812.6, (100); 834.6, (40)
3-methyl-3-hydroxy-butynyl	**(32b)**	30, Pd coupling reaction from **(31)**	815.044	815.4, (100)

Table 2.7. Reaction yields from the Diels-Alder cycloaddition step in the formation of nitrogen containing polyphenylenes and ESI-mass spectral analysis of the polyphenylene.

All the aryl-heteroarylbenzenes are colourless and, as with previously reported polyphenylenes, their melting points are extremely high. Compounds **(20)**, **(23)**, **(32a)** and **(32b)** all melt within the 250 – 300°C range, while derivatives **(16)**, **(29)** and **(31)** all melt above 300°C.

Unambiguous characterisation of all the N-doped polyphenylenes was achieved by NMR spectroscopy, mass spectrometry and elemental analysis.

ESI-mass spectrometry results are in agreement with the theoretically expected values (table 2.7). The isotopic distribution pattern assigned to the $[MH]^+$ ion dominates the spectrum. In fact it is the only signal observed in all cases apart from **(23)** and **(32a)**, which show one other signal assigned to the $[MNa]^+$ ion (5% and 40%, respectively).

As already discussed for hexaarylbenzene derivative **(16)**, the structures for all the novel N-doped polyphenylene derivatives (except that of **(32a)**) have a C_2 axis of symmetry running through the molecule (see figure 2.32), which simplifies their NMR spectra.

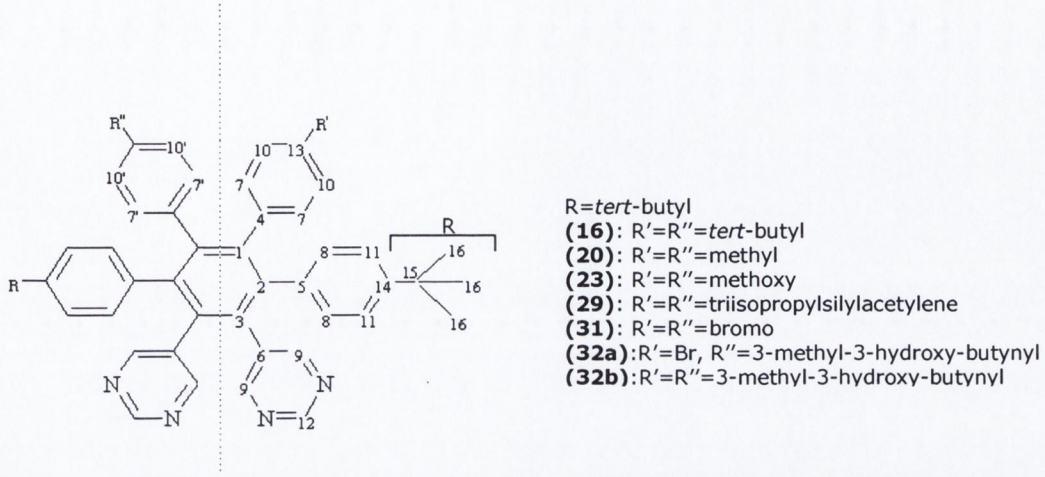


Figure 2.32. The atom labelling scheme of the novel N-doped polyphenylenes.

For polyphenylene **(32a)** the C_2 axis of symmetry is removed through the non-equivalence of the substituents in the R′ and R″ positions. This is, of course, reflected in the NMR spectroscopic analysis.

Figure 2.33 shows the aromatic regions of the ^{1}H NMR spectrum of the novel N-doped polyphenylenes **(16)**, **(20)**, **(23)**, **(29)**, **(31)** and **(32a/b)**. All the NMR spectra were carried out in $CDCl_3$, hence the small peak at δ 7.28. The lowest field signal in the ^{1}H NMR spectra for all the N-doped polyphenylenes is attributed to the aromatic protons situated between the nitrogens of the pyrimidine at C12. There is little variation in the chemical shift for these proton signals, with a range of δ 8.75 – δ 8.77 for polyphenylenes **(16)**, **(23)**, **(29)**, **(31)** and **(32a/b)**. Only **(20)** shows some deviation, resonating at higher field δ 8.66. Similarly the signals for the pyrimidine protons at C9 fall within the range of δ 8.20 – δ 8.26 for polyphenylenes **(16)**, **(23)**, **(29)**, **(31)** and **(32a/b)**, with **(20)** again resonating at slightly higher field δ 8.14. The aromatic proton signals for the phenyl rings at C7, C8, C10 and C11 prove to be more interesting. Their chemical shifts show a clear dependence on the nature of the substituent R′ or R″ (see figure 2.33 and table 2.9). It should be noted that hexaphenyl benzene displays only a single multiplet in the ^{1}H NMR at δ 6.83.

The aliphatic region of the ^{1}H NMR spectra of the polyphenylene derivatives show the various alkyl substituents, as summarized in table 2.8.

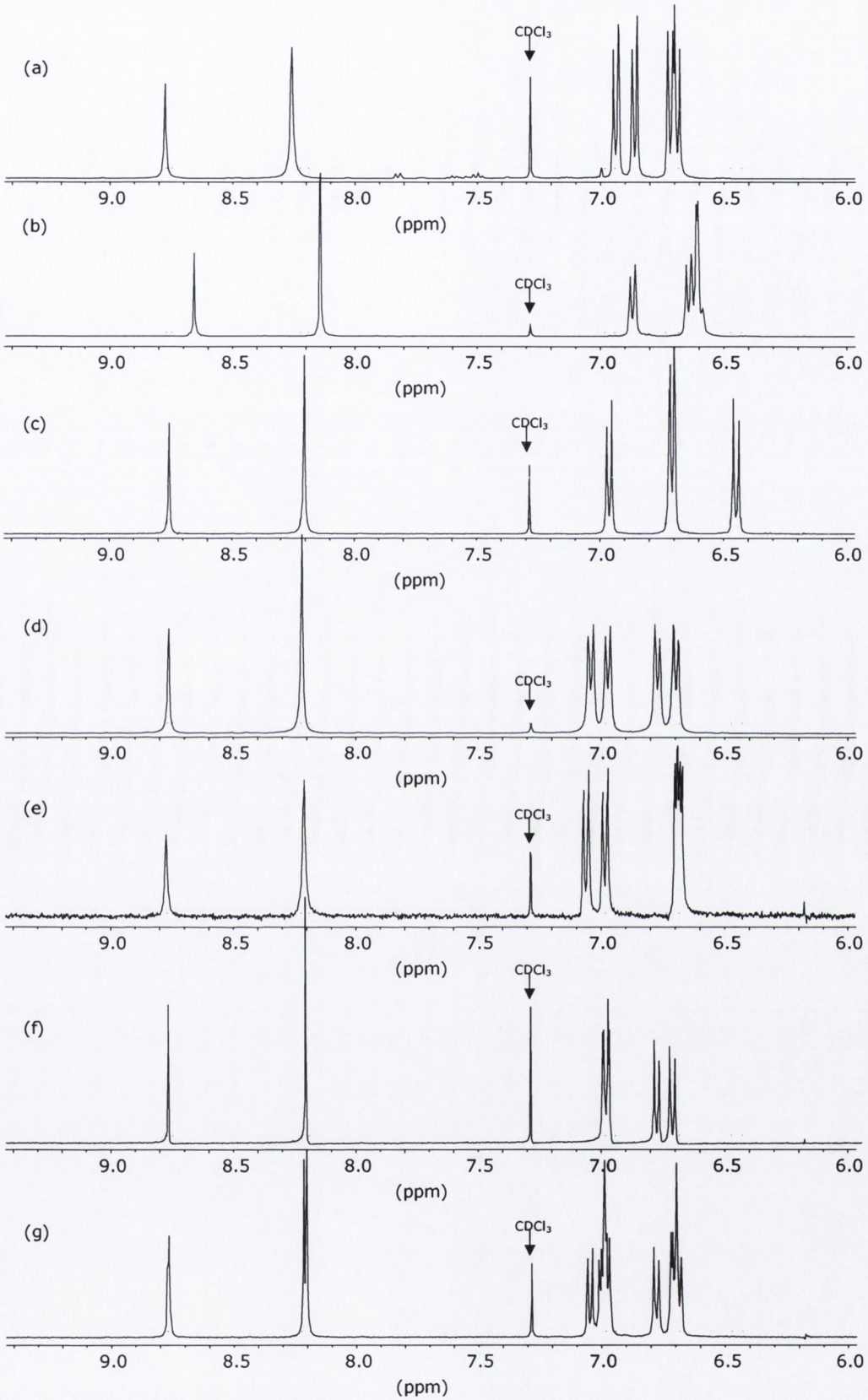


Figure 2.33. The ^{1}H NMR spectra of the aromatic region of (a) **(16)**, (b) **(20)**, (c) **(23)**, (d) **(29)**, (e) **(31)**, (f) **(32b)** and (g) **(32a)** ($CDCl_3$, RT, 400 MHz).

Polyphenylene	R, ^{1}H NMR (ppm)	R', ^{1}H NMR (ppm)	R'', ^{1}H NMR (ppm)
(16)	*tert*-butyl, 1.13	*tert*-butyl, 1.11	R''=R'
(20)	*tert*-butyl, 1.06	methyl, 2.02	R''=R'
(23)	*tert*-butyl, 1.15	methoxy, 3.63	R''=R'
(29)	*tert*-butyl, 1.15	TiPS, 1.08	R''=R'
(31)	*tert*-butyl, 1.15	Br, -	R''=R'
(32a)	*tert*-butyl, 1.15	3-methyl-3-hydroxy-butynyl, 1.57, 1.74	Br, -
(32b)	*tert*-butyl, 1.16	3-methyl-3-hydroxy-butynyl, 1.58, 1.97	R''=R'

Table 2.8. ^{1}H NMR chemical shifts for the alkyl substituents of the N-doped polyphenylenes ($CDCl_3$, RT, 400 MHz).

The *tert*-butyl groups in the R position are dispersed within the range of δ 1.13 – δ 1.16 for **(16)**, **(23)**, **(29)**, **(31)** and **(32)**. Again only **(20)** shows slight deviation from this range, resonating upfield at δ 1.06. The other aliphatic signals for the alkyl substituents in the R' and R'' positions are characteristic of the particular alkyl sustituent.

	HH COSY (TOCSY)	CH COSY (HMBC)	HH COSY (TOCSY)	CH COSY (HMBC)	
	Aromatic H at C7/10	C13	Aromatic H at C8/11	C15	C14
(16)	6.86, 6.69	147.9 or 148.6	6.93, 6.71	33.7	147.9 or 148.6
(23)	6.71, 6.45	156.8	6.96, 6.70	33.8	148.7
(29)	7.04, 6.77	120.5	6.97, 6.70	33.8	149.2
(31)	7.06, 6.68	119.9	6.98, 6.69	33.9	149.3

Table 2.9. Assignment of ^{13}C and ^{1}H NMR signals from TOCSY, HMQC and HMBC COSY experiments on **(16)**, **(23)**, **(29)** and **(31)**.

In the ^{1}H NMR spectrum, polyphenylene **(16)** shows two pairs of coupled aromatic protons, which indicate two distinct *para*-substituted phenyl rings (see figure 2.33 and table 2.9). One set is at δ 6.86 and δ 6.69, while the other is at δ 6.93 and δ 6.71. From the HMBC NMR experiment, it is possible to assign the ^{13}C NMR signals at δ 147.9 and δ 148.6 to the quaternary carbons at positions C13 and C14, although these signals are too close to distinguish. The quaternary carbon C15 is assigned to the signal at δ 33.7.

As expected, derivative **(23)** also shows two pairs of coupled aromatic protons in the ^{1}H NMR experiment. The set at δ 6.96 and δ 6.70 remains unshifted with respect to that of **(16)** (δ 6.93 and δ 6.71). These are assigned to the signals for the aromatic protons at C8 and C11 as they couple to the carbons at C14 (δ 148.7, ^{13}C NMR) and C15 (δ 33.8, ^{13}C NMR) in the HMBC experiment. The second set of aromatic proton signals, at δ 6.71 and δ 6.45, are assigned to the aromatic protons at positions C7 and C10. These resonate considerably upfield with respect to **(16)** due to the electronic effect of the

methoxy substituents (see figure 2.33 (c)). The HMBC experiment allows assignment of the signal at δ 156.8, in the ^{13}C NMR experiment, to the carbon at C13.

Similarly, the bromine compound **(31)** (see figure 2.33 (e)), shows the two pairs of coupled aromatic protons in the ^{1}H NMR experiment. Again, the signals at δ 6.98 and δ 6.69 remain unshifted with respect to **(16)**. These signals are assigned, once again, to the aromatic protons at positions C8 and C11, with coupling in the HMBC experiment to the carbons at C14 (δ 149.3, ^{13}C NMR) and C15 (δ 33.9, ^{13}C NMR). The second set of aromatic protons at δ 7.06 and δ 6.68 (the aromatic protons at positions C7 and C10) is shifted slightly downfield with respect to **(16)** due to the electronic effect of the bromine substituent. Once again the HMBC experiment allows characterization of the carbon signal at δ 119.9 as quaternary carbon, C13.

Likewise, in the ^{1}H NMR spectrum of the acetylene substituted polyphenylene, **(29)**, there are two pairs of coupled aromatic protons. As above, the set at δ 6.97 and δ 6.70, which are again unshifted with respect to **(16)**, are assigned as the signals for the aromatic protons at positions C8 and C11, coupled to the carbons C14 (δ 149.2, ^{13}C NMR) and C15 (δ 33.8, ^{13}C NMR) in the HMBC experiment. The second set of aromatic protons, the signals for the aromatic protons at C7 and C10, are shifted slightly downfield to δ 7.04 and δ 6.77, with respect to **(16)**, due to the electronic effect of the acetylenic substituent. The HMBC experiment allows characterization of the signal in the ^{13}C NMR at δ 120.5 as the carbon at C13. The ^{1}H NMR of the acetylene substituted derivative, **(32b)**, shows the same pattern as **(29)**, with a smaller downfield shift for the ^{1}H NMR signals of the aromatic protons at C7 and C10 (δ 6.98 and δ 6.77). The asymmetrical **(32a)** is the spectral sum of the bromine derivative, **(31)**, and the acetylene derivative **(32b)**, thus by direct comparison the doublet in the ^{1}H NMR at δ 7.05 is assigned to the aromatic proton at either C7 or C10 and the doublet at δ 6.78 to C7′ or C10′.

Polyphenylene	C12	C9	C7, C8, C10, C11
(16)	155.4	157.6	130.4, 130.1, 123.7, 122.9
(20)	155.3	157.4	130.3, 130.2, 126.9, 123.6
(23)	156.8	157.5	131.6, 130.3, 123.9, 111.9
(29)	155.6	157.4	130.3, 130.3, 130.2, 124.1
(31)	155.6	157.4	132.0, 130.1, 129.8, 124.1
(32a)	155.6, 155.5	157.4, 157.3	132.0, 130.3, 130.1, 130.1, 130.0, 129.7, 124.1, 124.1
(32b)	155.5	157.4	130.4, 130.2, 130.0, 124.1

Table 2.10. The ^{13}C NMR chemical shifts of the aromatic CH carbons for the various N-doped polyphenylene derivatives ($CDCl_3$, RT, 100 MHz).

Table 2.10 summarizes the information from the ^{13}C NMR spectra on the aromatic carbons of the various N-doped polyphenylene derivatives. With little or no effect observed in the chemical shifts of the pyrimidine carbons C9 and C12, there is slightly more variation in the phenyl carbons at C7, C8, C10 and C11. The most significant shifts are seen if we compare the data on **(16)**, **(23)** and **(31)**. As expected, the electron-donating properties of the methoxy substituents of polyarylbenzene **(23)** have caused a highfield shift to δ 111.9 as compared to **(16)**, with the electron-withdrawing bromine substituent of **(31)** causing an opposite and less pronounced downfield shift to δ 124.1. Polyarylbenzene **(32a)**, as in the ^{1}H NMR spectrum, seems to be a simple superimposition of the signals from polyphenylenes **(31)** and **(32b)**.

2.2.2.4 Propeller Frameworks

Colourless crystals suitable for X-ray crystallographic structure analyses were obtained from acetone/water, in the case of **(23)** and **(29)**, and from ethyl acetate/petroleum ether in the case of **(31)**. Crystals of **(23)** belong to the $P2_1/n$ space group, while those of **(29)** and **(31)** belong to the $P2_1/c$ space group. The structures were refined to give R_1 values of 4.19, 7.97, and 4.58% for **(23)**, **(29)** and **(31)**, respectively. A summary of the crystallographic data is given in tables A to C in Appendix 1.

In solution, each phenyl substituent is believed to be free to rotate at small angle intervals about its carbon-carbon single bond to the central phenyl unit. It is clear from the molecular structures, however, that in the solid-state the outer phenyl substituents are strongly twisted with respect to the central phenyl unit (average twisting angles are 66.8, 66.1 and 66.6° for **(23)**, **(29)** and **(31)**, respectively), see figures 2.34 - 2.36. In order to relieve the strain between the aromatic hydrogens of the outer phenyl rings, these rings twist apart from each other, in the same direction, like propeller blades. These structures can be compared closely to the regular propeller array adopted by hexaphenyl benzene **(10)**, which has approximate interplanar angles of 67° between the phenyl groups and the central ring.

Furthermore, we see that the outer phenyl rings are in close proximity, so that with cyclodehydrogenation and planarisation, PAH structures can be formed.

In addition, the methoxy substituted polyphenylene derivative **(23)** displays disorder in the *tert*-butyl group attached to the phenyl carbon, C42 (figure 2.34). This is due to rotation about the carbon-carbon single bond between C42 and C45. As a result, compound **(23)** crystallizes in an approximately 1:1 ratio of the two forms displayed in figure 2.34.

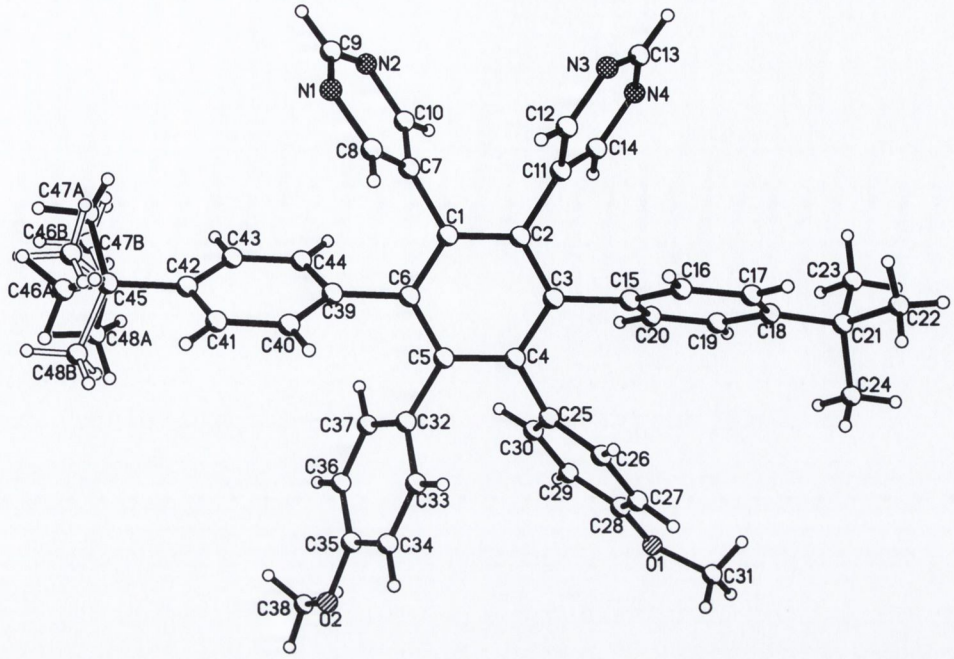


Figure 2.34. The X-ray crystal structure of polyphenylene **(23)** (disorder in the *tert*-butyl group results in two forms described by either solid or hollow bonds).

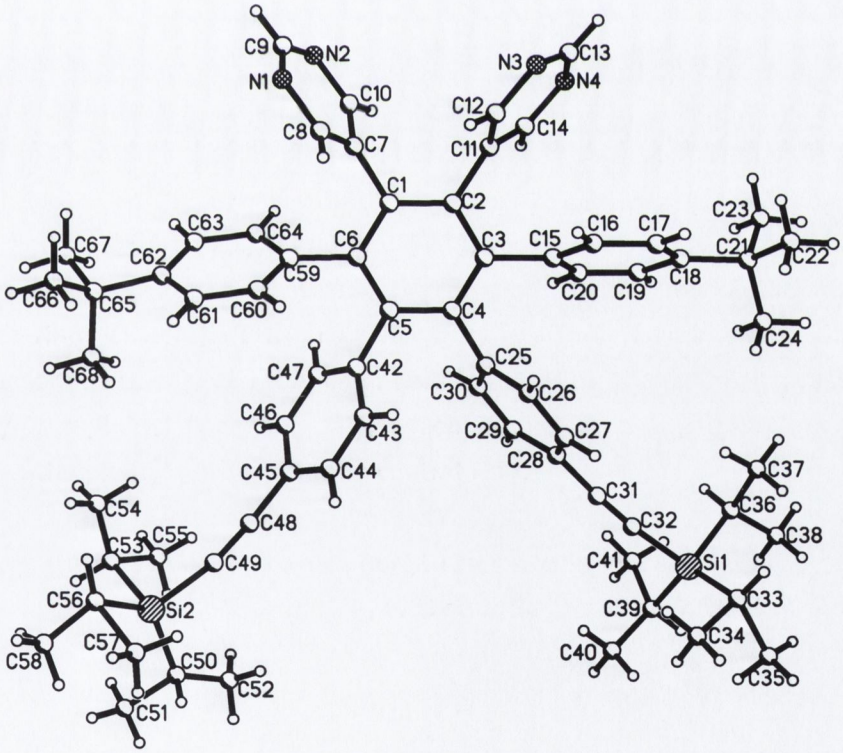


Figure 2.35. The X-ray crystal structure of polyphenylene **(29)**.

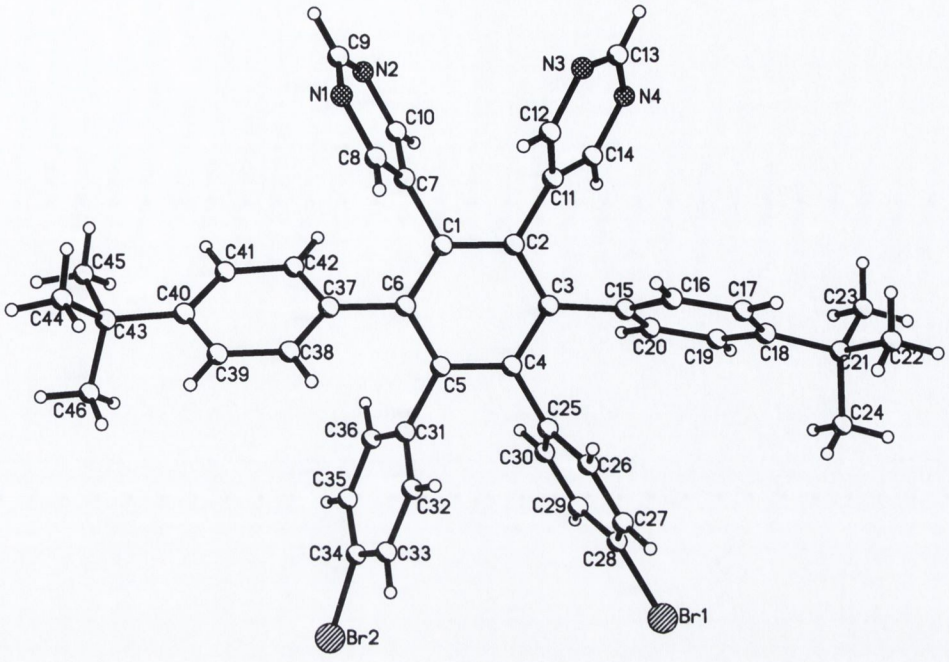


Figure 2.36. The X-ray crystal structure of polyphenylene **(31)**.

There is evidence for intermolecular hydrogen-bonding in polyphenylene **(23)**. The distance between an oxygen (O1) of one molecule and an aromatic hydrogen of the pyrimidine ring (H10) of another unit, which is offset stacked above the first, is 2.7(1) Å. This is indicative of a moderately strong hydrogen bond.[50] Similarly we see an intermolecular interaction to a third unit between O1 and H48E as well as O2 and H24A. The bond distances involved in these hydrogen bond interactions are 2.7(1) Å and 2.6(1) Å, respectively. Again these are moderately strong hydrogen bonds.

Intermolecular hydrogen-bonding is evident in compound **(29)**, between N3 of one molecule and H10 of a second unit. Once again the distance (2.6(3) Å) is indicative of a moderately strong hydrogen bond. In pyrimidine, a reduction of π-electron density at carbon positions C8 and C10 (as labelled in figure 2.35) is caused by the electron withdrawing nitrogen atoms (N1 and N2).[51] This contributes to the enhanced acidity of pyrimidine (pK_a of pyrimidine=1.31 *cf.* pK_a of pyridine=5.2)[51] and may increase the potential for hydrogen-bonding through H8 and H10 in **(29)** and **(23)**.

The bromine derivative, **(31)**, exhibits a displaced, stacked configuration with hydrogen-bonding between N2 and H35 (2.7(1) Å) on one face, and between N3 and H38 (2.7(1) Å) and between N1 and H26 (2.4(1) Å) on the other face.

2.2.2.5 UV-vis Absorption Spectroscopy

The normalized UV-vis spectra for the N-doped polyphenylene derivatives, in diethyl ether, are shown in figure 2.37, together with hexaphenylbenzene for comparison.

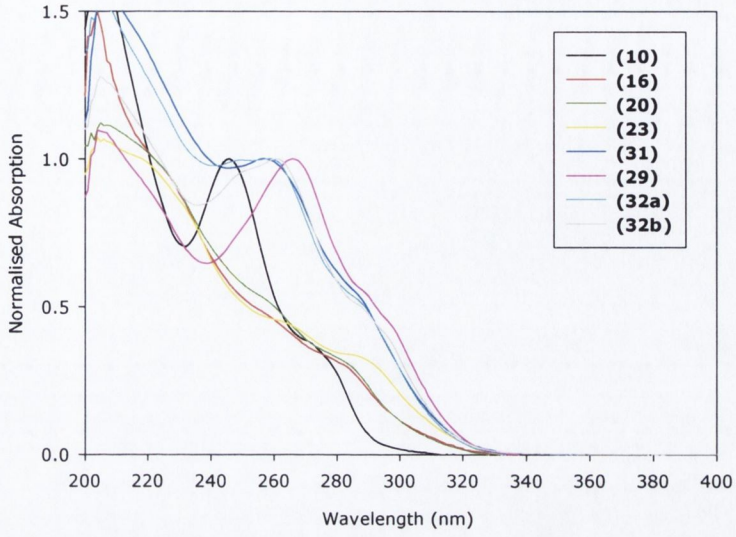


Figure 2.37. The normalized absorption spectra for the various N-doped polyphenylene derivatives and hexaphenylbenzene, in diethyl ether.

Molecular structure plays a major role in determining the shape and position of absorption maxima in the electronic spectra of aromatic molecules. Ogliaruso proposed structural rigidity and the angle between the outer rings as important factors in the elucidation of the electronic spectra of polyphenylenes.[52] Non-planar molecules usually have structureless absorption and emission spectra, while planar, rigid molecules, with high symmetry show well-resolved vibrational bands. In the case of biphenyl which is non-planar in solution,[53] a wide structureless absorption band and a structured fluorescence spectrum is observed. Like many oligophenylenes, it exhibits a large change in conformation between the ground and first excited states; the molecule becomes more planar upon excitation. The UV-vis absorption spectrum of biphenyl contains a broad structureless *p*-band (λ_{max}=250 nm) and the forbidden α and α^* bands which are partially submerged in the long-wavelength end of the *p*-band at 270 nm.[53] The vibrational freedom of the phenyl rings causes the wide "bell-like" structure of the *p*-band. In order to force the phenyl rings into a planar position a bridging group or bond can be introduced resulting in a sharp absorption and fluorescence. We will see this effect later when we look at the planar N-HBC **(17)**.

Hexaphenylbenzene exhibits electronic characteristics typical of a non-planar molecule, with an absorption maximum at 246.5 nm, and a shoulder at 271.0 nm.[54] It has a slightly structured absorption spectrum, and there is no effective conjugation between

the rings. Interestingly, the principal absorption of hexaphenylbenzene is exactly the same as the major absorption band for biphenyl and many other oligophenylenes.[55]

The electronic spectra for polyphenylenes **(16)**, **(20)**, **(23)**, **(29)**, **(31)** and **(32a/b)** are very broad, and exhibit no fine-structure, so it becomes difficult to estimate the 0-0 transition.[54] The spectra are mostly structureless because in the ground state steric hindrance is expected to impose a non-planar configuration on the chromophore.[54] In general the spectra show absorption bands around 250 nm and a shoulder around 280 nm, with molar extinction coefficients (see table 2.11, dichloroethane) that remain consistently higher than that of hexaphenylbenzene. It has been known for some time that the maximum value of the molar extinction coefficient ε_{max} of the oligophenylene chromophore increases with the number of phenyl rings.[54]

Compound	Wavelength (nm), Molar Extinction Coefficient ($x10^3$ L mol^{-1} cm^{-1})	
hexaphenylbenzene	246.0, 46	268.0, 18
(16)	-	282.0, 19
(20)	-	281.0, 22
(23)	-	287.0, 22
(29)	267.0, 80	290.0, 49 and 297.0, 39
(31)	255.0, 35	286.0, 21
(32a)	249.0, 55 and 261.0, 57	286.0, 30
(32b)	251.0, 57 and 259.0, 65	290.0, 43

Table 2.11. The UV-vis spectral characteristics of hexaphenylbenzene and the N-doped polyphenylenes in 1,2-dichloroethane.

We can separate the N-doped polyphenylenes into two groups in terms of molar absorptivity. The polyphenylenes **(16)**, **(20)**, **(23)** and **(31)** are N-doped polyphenylenes with alkyl or bromo substituents. These compounds have a molar absorptivity of the order of hexaphenylbenzene. The N-doped polyphenylenes with acetylenic functionalities, compounds **(29)**, **(32a)** and **(32b)**, have larger molar absorptivities than that of hexaphenylbenzene. There is also a corresponding increase in the molar absorptivity with the number of acetylenic groups from **(32a)** (ε=30 $x10^3$ L mol^{-1} cm^{-1}) to **(32b)** and **(29)** (ε=43 $x10^3$ and 49 $x10^3$ L mol^{-1} cm^{-1}, respectively).

A decrease in the planarity of the basic chromophore will cause a blue-shift and a reduction of the value of ε_{max}. If we increase the planarity, the absorption spectrum becomes more structured, red-shifted, and the intensity of the transitions is generally increased.[54] In our series of compounds the possibility that any two of the phenyl rings within the polyphenylene moieties are coplanar is highly unlikely. The absence of

higher absorption wavelengths indicates the lack of appreciable conjugation in the system. For example, in **(23)**, X-ray diffraction studies have shown that the peripheral rings are at an angle of 67° to the central ring in the solid state, although in solution it is expected that the outer rings would oscillate at intervals between smaller angle limits. Planarity is reduced by steric hindrance between *o*-hydrogen atoms on adjacent rings.

Although substituents on the N-doped polyphenylenes may interfere with the planarity of the chromophore, more importantly they affect its dipole moment in either the ground and/or first excited state, thus altering the spectroscopic characteristics.[54] Increased crowding at the periphery, which we would predict to be greatest for the acetylenic functionalized **(29)**, would further restrict the oscillation of the phenyl rings. However, by enhancing the permanent dipole moment through the correct choice of substituent, we increase the static dipole moment of the ground and first excited singlet state. This would correspond to a red-shift in the absorption spectra, and enhancement of the molar extinction coefficient. This sensitivity to substitution has been seen for *p*-oligophenylenes[54] and is in accord with the belief that the transitions producing all of the long-wavelength absorption bands are long-axis polarized. The N-doped polyphenylenes, with their electron-withdrawing nitrogen atoms have a permanent dipole moment along the plane of the molecule. Any change that affects this dipole moment is expected to modify the electronic spectrum.

Table 2.12 shows the positions of the absorption bands of polyphenylenes **(16)**, **(20)**, **(23)**, **(29)**, **(31)** and **(32a/b)**, in diethyl ether, together with hexaphenylbenzene.

Compound	Absorption Wavelength (nm)				
hexaphenylbenzene	-	-	246.5	268.0	-
(16)	224.0	-	256.0	282.0	-
(20)	219.0	-	258.0	281.0	-
(23)	215.0	-	260.0	284.0	-
(29)	-	-	266.0	288.0	297.0
(31)	-	-	257.0	285.0	-
(32a)	-	248.0	260.0	285.0	-
(32b)	-	251.0	261.0	287.0	296.0

Table 2.12. The absorption wavelengths for the N-doped polyphenylenes and hexaphenylbenzene in diethyl ether.

The absorption bands for all the N-doped polyphenylenes are red-shifted, and exhibit a slight increase of fine structure on comparison with hexaphenylbenzene. The effect is most notable if we compare the acetylene fuctionalised derivative **(29)** with

hexaphenylbenzene. Polyphenylene **(29)** has an approximately 20 nm red-shifted *p*-band, a 20 nm red-shifted α or α* band, and an additional shoulder has become apparent at 297 nm.

For compounds **(16)**, **(20)** and **(23)** there is evidence of a band in the 220 nm region although, because this is in the region of the solvent cutoff, it is difficult to be certain. For these, the band around 258 nm appears to be a shoulder, rather than the principal absorption band, and it is submerged when the solvent is dichloroethane rather than diethyl ether, thus an accurate molar absorptivity is hard to ascertain.

In summary, the differences in the electronic spectra between the aryl-heteroarylbenzenes and hexaphenylbenzene can be explained in terms of both the steric arrangement of the aryl-heteroaryl substituents and, more importantly, the increase in the permanent dipole moment of the ground state in the plane of the molecule. Variation within the N-doped polyphenylene family is explained through modification of this permanent dipole moment *via* changes in the substituent at the *para*-position to the pyrimidine rings of the polyarylbenzene. The incorporation of acetylenes induces a further red-shift, indicating an extension of the π-system.

2.2.2.6 Alternative Synthesis

As an alternative synthetic method toward N-doped polyphenylenes, pyrimidine subunits can be incorporated into the cyclopentadienone. This increases the number of options available for the positioning and number of pyrimidine subunits, and opens up the possibility of firstly generating structural isomers of **(17)** and secondly systematically increasing the degree of N-doping in the resultant heterosuperbenzene. The one-pot synthesis of pyrimidine-5-carboxaldehyde was achieved in a 59% yield, figure 2.38, by following the literature procedure.[56]

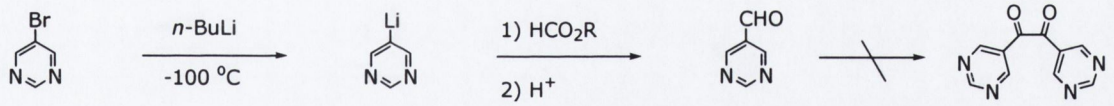


Figure 2.38. The synthesis of pyrimidine-5-carboxaldehyde.

Unfortunately the attempted benzoin condensation reaction of pyrimidine-5-carboxaldehyde in ethanol, in the presence of KCN, did not produce the desired 1,2-dipyrimidin-5-yl-ethane-1,2-dione. This can be explained through the redox potential of the carbonyl group of the carboxaldehyde. 3-Pyridyl residues have keto groups which are the least susceptible to reduction, thus pyrimidine-5-carboxaldehyde is unable to form the intermediate associated with the pyridoin condensation reaction and therefore the 1,2-dione.[57]

2.2.3 GENERAL PROPERTIES OF N-HBC (17)

All the results obtained so far for N-HBC **(17)** provide reliable proof for the structure of the heterosuperbenzene. Our interest, however, focuses not only on the synthesis and characterization of the PAHs, but also on their optical and chemical properties.

The selective synthesis, enhanced conductivity and processability of these N-heterosuperbenzenes were the three criteria set as the driving force at the beginning of this thesis. We have discussed the success of the selective synthetic approach used in this work; the following will focus on the properties of N-HBC **(17)**.

In the solid state, N-HBC **(17)** is a deep brown/black colour, with a reddish luster. Toluene solutions of **(17)** are green/yellow and have a noticeable green fluorescence.

2.2.3.1 Solubility

One of the difficulties of working with the all-carbon HBCs is their insolubility in most available solvents. This requires the use of high boiling solvents such as dichlorobenzene or tetrachloroethane to obtain spectroscopic data, and until recently it has been virtually impossible to obtain any NMR spectroscopic data at room temperature.[31] N-HBC **(17)**, with its built-in *tert*-butyl and nitrogen solubilising units, shows a dramatic increase in solubility compared with reported all-carbon analogues. It is soluble in a wide variety of common organic solvents such as benzene, chloroform, acetone, methanol and acetonitrile, with a solubility of greater than 20 g/L in tetrahydrofuran while that for HBC-$PhC_{12}H_{25}$ is 10 g/L.[58]

2.2.3.2 Thermal Stability

Thermogravimetric analysis of **(17)** indicates compound stability to around 450°C (see figure 2.39). There is an initial 5-10% mass loss, attributed to the removal of trapped solvent molecules (130-220°C). Decomposition around 450°C agrees with the mass loss of the flexible *tert*-butyl groups.[47] This suggests that the simplest heterosuperbenzenes, without substituents, are likely to be highly thermally stable, beyond 1000°C and the scope of this experiment. This is not surprising however, as it is believed that the all-carbon PAH derivative, coronene, is formed in the interstellar media at many thousand °C. The extremely high thermal stability of the central unit of N-HBCs would make them particularly suitable for many LED applications where thermally sensitive polymer materials can fail.

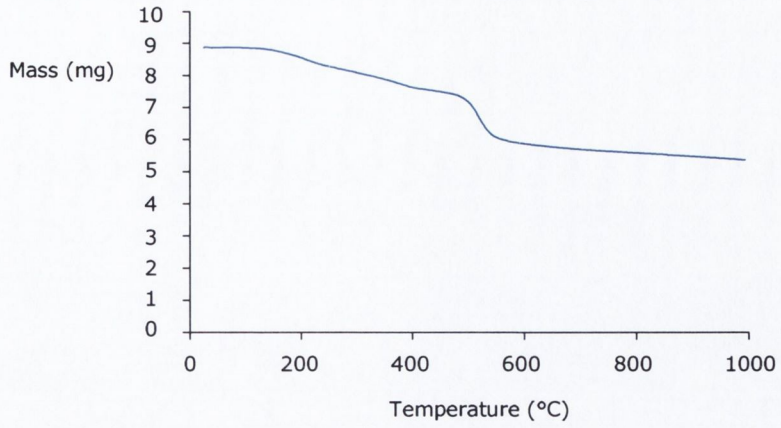


Figure 2.39. Thermogravimetric analysis of heterosuperbenzene **(17)** showing 5-10% solvent loss and *tert*-butyl decomposition.

2.2.3.3 Electrochemistry

The semiconducting properties of N-HBC were studied initially by electrochemical methods. Figure 2.40 shows the cyclic voltammograms (CVs) of the reduction of N-HBC in solution. It is observed that N-HBC exhibits two quasi-reversible one electron processes. The first reduction has an anodic peak at E_{pa}=-1.02 V *vs* SCE and a cathodic peak at E_{pc}=-1.34 V *vs* SCE. These potentials are shifted away from each other with a difference in peak potential (ΔE_p) of 0.32 V. The second quasi-reversible reduction has an E_{pa}=-1.45 V, an E_{pc}=-1.78 V and ΔE_p of 0.33 V.

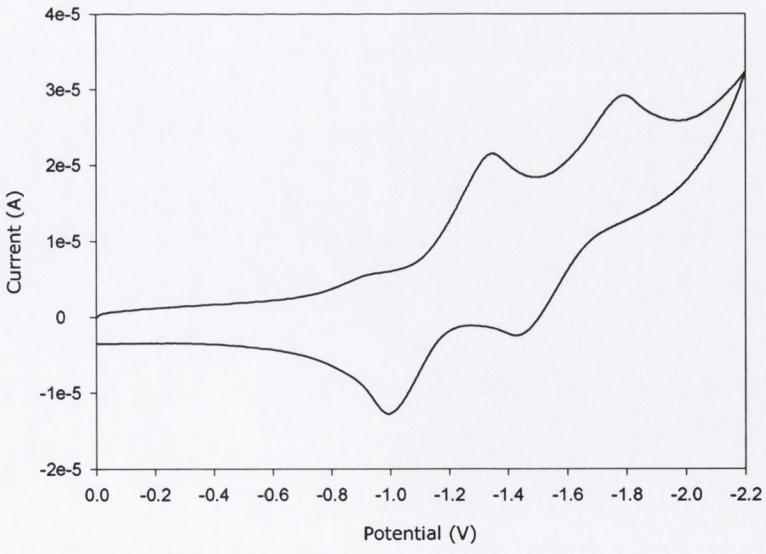


Figure 2.40. The cyclic voltammogram for **(17)** in chloroform showing two quasi-reversible reductions.

Results from the cyclic voltammogram are summarized in table 2.13, and compared to the all-carbon HBC derivative.

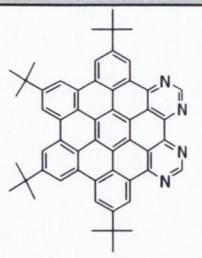
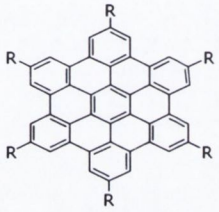
	Solvent	$E_{1/2}^1$	$E_{1/2}^2$	E^{o1}	E^{o2}
	$CHCl_3$	-1.31 V[a]	-1.75 V[a]	-1.18 V[a]	-1.62 V[a]
 R=*tert*-butyl	THF	-2.10 V[b]	-2.40 V[b]	-	-

Table 2.13. Electrochemical information obtained from the cyclic voltammogram. Supporting electrolyte: $(TBA)PF_6$ (0.1 M); [a]glassy carbon working electrode, Pt wire auxiliary electrode, SCE reference electrode; [b]Au working and auxiliary electrode, SCE reference electrode.[31] $E°=1/2(E_{pa}+E_{pc})$, where E_{pa} and E_{pc} denote anodic and cathodic peak potentials, respectively. $E_{1/2}=E_0+1.11(RT/nF)$

Similar to the all-carbon derivative *tert*-butyl substituted HBC,[31] N-HBC **(17)** has two quasi-reversible, one electron reductions showing the reversible formation of the mono- and the dianion. However, distinction between the two comes with a comparison of the peak potentials. N-HBC **(17)** shows a vast increase in the ease of reduction, with reduction potentials considerably less negative than –2.0 V. This observation is in agreement with the depletion of π-electron density as a result of the incorporation of the electron-withdrawing nitrogens, thus rendering the molecule with overall electron-acceptor characteristics.

In contrast to the all-carbon derivative, which has two irreversible oxidation potentials,[31] **(17)** shows no oxidation chemistry in chloroform.

2.2.4 PHOTOPHYSICAL PROPERTIES OF N-HBC (17)

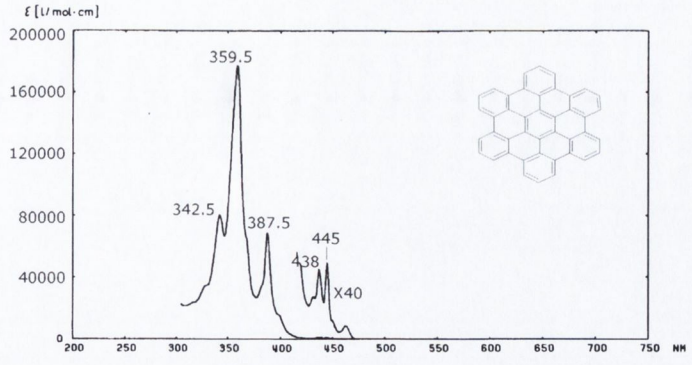
2.2.4.1 UV-vis Absorption Spectroscopy

A Comparison of N-HBC with HBC

UV-vis spectroscopy of PAHs can provide information as to the electronic structure of the compounds. We can see from the absorption spectra of the "cyclised" N-HBC derivative (figure 2.41 (b)), that the increase in planarity and rigidity of the system has

resulted in well-resolved bands, compared with the polyphenylene precursor **(16)** (see earlier figure 2.37).

(a)



(b)

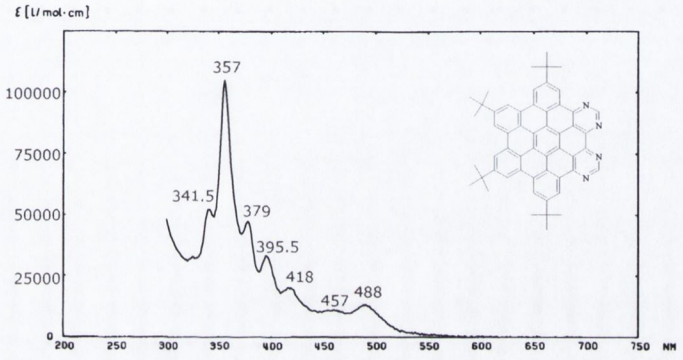


Figure 2.41. The UV-vis absorption spectra of (a) Hexabenzocoronene[8] and (b) N-HBC **(17)**, in 1,2,4-trichlorobenezene.

The highly structured electronic absorption spectrum of N-HBC in trichlorobenzene (figure 2.41 (b)) can be directly compared to that of the parent hydrocarbon, hexa-*peri*-hexabenzocoronene in the same solvent (HBC, figure 2.41 (a)). N-HBC **(17)** shows greater resolution of the series of red-shifted absorption bands. The typical line shape of the UV-vis spectra of **(17)** indicate that, despite the chemical modification, the HBC chromophore is still intact.

The UV-vis spectrum of **(17)** has a λ_{max}=357 nm, which is slightly blue-shifted by 2.5 nm in comparison to HBC. There is an additional absorption band in **(17)** at 379 nm, which is not found in the all-benzene analogue, and a large increase in the molar absorptivity for the weak bands toward the red end of the spectrum at 418, 457 and 488 nm.

PAHs typically show three types of bands, α, β and *p* bands, in agreement with Clar's results.[7] The β-bands (at 360 nm for HBC) correspond to the electronic interaction between the benzoid rings of the PAH. A red-shift in these bands is a consequence of increasing the electronic interaction, for example by extending the π-system.

The *p*-bands (around 390 nm for HBC) involve the localization of the π-electrons in the excited state. As localization takes place in different positions in different PAHs, comparisons do not show regularities.

The extremely weak α-band at 463 nm (ε=220) for HBC, is assigned as the 0-0 transition, which is strictly forbidden in D_{6h} symmetry and coincides with the first fluorescence band for HBC at 462.5 nm.[8] This assignment has been verified through the synthesis and comparison of a methyl substituted HBC derivative with D_{2h} symmetry,[8] which showed a significant enhancement of the 0-0 transition, as expected on the basis of the lower molecular symmetry. N-HBC **(17)** has a more intense 0-0 transition (α-band) due to a further lifting of molecular symmetry to C_{2v}. Thus the red-shifted α-band at 488 nm is assigned to the 0-0, $^1(\pi,\pi^*)$ transition, with enhanced molar absorptivity as compared to HBC.

For other HBC derivatives where the 0-0 band is apparently absent, its position can be estimated at around 430-435 nm by using the approximate mirror image relationship between absorption and emission. This is considerably red-shifted from that of benzene (270 nm in cyclohexane solution).[29]

The molar extinction coefficients of N-HBC were recorded in toluene and are presented in table 2.14. HBC is insoluble in toluene so comparison with HBC spectra in trichlorobenzene was made. From this comparison it is clear that the molar extinction coefficients for N-HBC show a more than fifty-fold increase in the intensity of the 0-0, $^1(\pi,\pi^*)$ transition (table 2.14) compared to HBC. In contrast there is a reduction in the intensity of λ_{max} at 355 nm (ε_{max}=137000, toluene) compared to hexa-*peri*-hexabenzocoronene (ε_{max}=177000, trichlorobenzene). This is a result of the introduction of four electron withdrawing nitrogen atoms, which as expected, has depleted the π-electron density within the N-HBC core, as compared to HBC. This is a similar phenomenon to that seen on comparison of pyrimidine and benzene.[59] In accordance with the electrochemistry result, this demonstrates the molecule's overall electron-accepting character.

Wavelength (nm)	289.5	323.5	339.0	354.5	376.5	393.5	414.5	451.5	481.0
Molar Absorptivity (M^{-1} cm^{-1})	50000	26000	57000	137000	54000	32000	15000	10000	14000

Table 2.14. The molar extinction coefficient for the absorption maxima at each wavelength of N-HBC **(17)** in toluene solution.

The Electronic Transitions Of N-HBC

In general, a nitrogen containing aromatic (like **(17)**) has π and n-orbitals, where n represents the non-bonding orbital on the nitrogen atom and the two electrons in it are the "lone-pair", which are close in energy. The lowest energy unfilled orbitals are π^*-orbitals.[60,61,62] Promotion of an electron from the n to the π^* orbital ($n\rightarrow\pi^*$) leads to excitation with an excited state in which the electron is delocalised over the entire aromatic system. The latter, with no restriction on unpairing of spins, will give excited singlet $^1(n,\pi^*)$ and triplet $^3(n,\pi^*)$ states. Similarly a $\pi\rightarrow\pi^*$ transition will lead to the excited states $^1(\pi,\pi^*)$ and $^3(\pi,\pi^*)$.[60]

The UV-vis spectra of **(17)** in various organic solvents shows two types of bands, the $\pi\rightarrow\pi^*$ bands and the $n\rightarrow\pi^*$ bands. These appear overlapped, to generate an overall spectrum which is complex and shows several component bands.

In molecules such as **(17)**, where both $n\rightarrow\pi^*$ and $\pi\rightarrow\pi^*$ transitions are possible, the two possibilities may often be distinguished. There are many methods to elucidate the nature of the absorption bands, one of the simplest methods is to apply Kasha's criteria and compare the UV-vis absorption spectra of HBC with N-HBC.[60] According to Kasha an $n\rightarrow\pi^*$ transition is absent in the analogous hydrocarbon. By comparing the absorption spectra of HBC and N-HBC (figure 2.41) we have already been able to assign the low energy bands at 457 and 488 nm (in 1,2,4-trichlorobenzene) as $\pi\rightarrow\pi^*$ transitions, with the 0-0 transition at 488 nm. In fact direct comparison would suggest that all bands in N-HBC are of $\pi\rightarrow\pi^*$ character, except the band at 379 nm (in trichlorobenzene). This is the only clearly new band in the absorption spectrum of N-HBC and can thereby be assigned as an $n\rightarrow\pi^*$ transition.

The $n\rightarrow\pi^*$ and $\pi\rightarrow\pi^*$ transitions may also be distinguished by the effect of polar and nonpolar solvents on the wavelengths of the absorption bands.[60] Formally only one electron is available on the heteroatom in an excited (n,π^*) state, so polar solvents are more strongly hydrogen-bonded to the heteroatoms in the ground state than in the excited state. The energy of the ground state is therefore lowered more by interaction with polar solvent than is the excited state, causing an increase in the energy gap between the two levels. Hence a shift in the absorption maximum to shorter wavelengths (a blue-shift) is observed for an $n\rightarrow\pi^*$ transition in polar solvents. The typical energy change associated with the blue-shift of an (n,π^*) state by solvation in polar solvents is of the order of 2000 cm^{-1} for a solvent change from hydrocarbon to water.[62] In contrast, a red-shift is observed in some $\pi\rightarrow\pi^*$ transitions in polar

solvents: the excited state is more polar than the ground state, hence its interaction with a polar solvent reduces the energy difference between the two states.[60]

Figure 2.42 shows the normalized absorption spectra of **(17)** in solvents of varying polarity. Notable features of the spectra are (i) loss of fine structure in some solvents and (ii) marked solvent shifts.

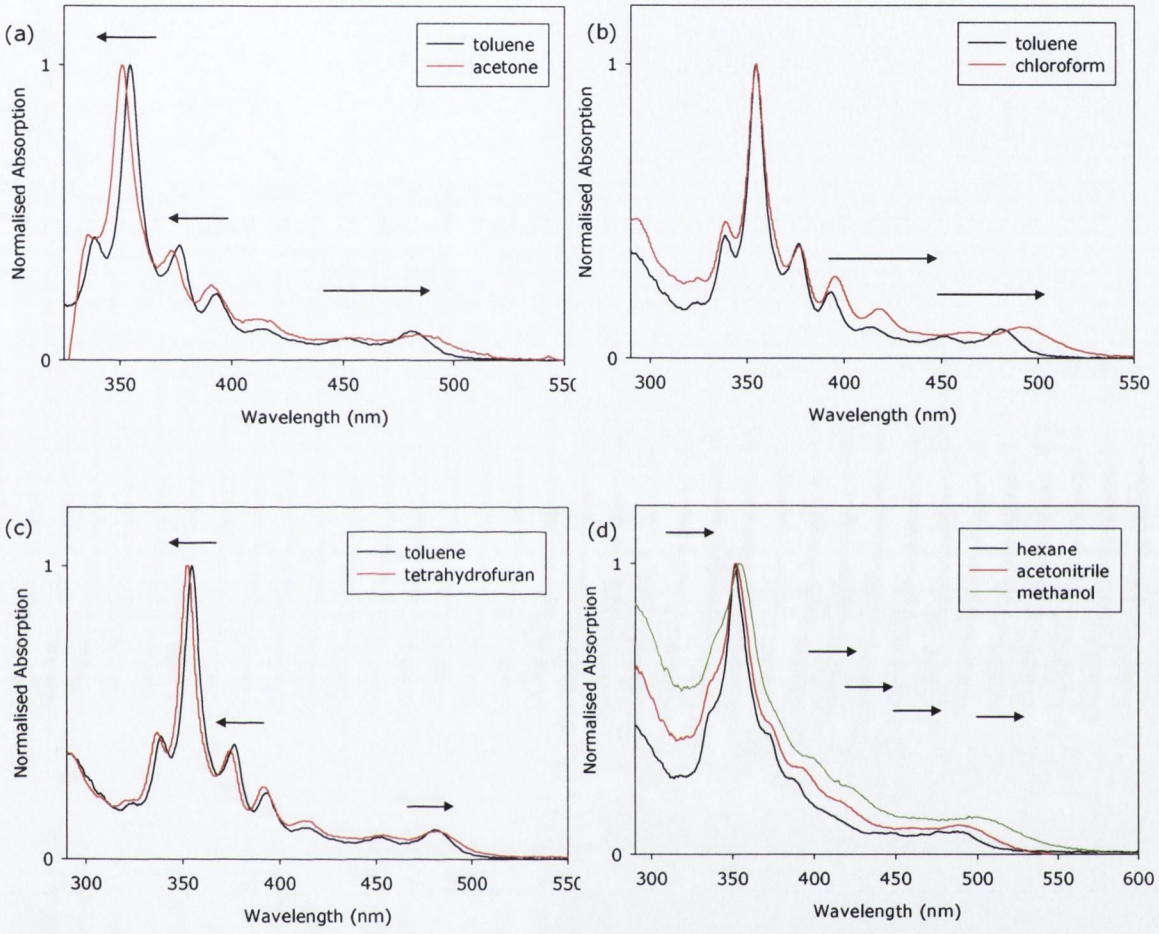


Figure 2.42. (a)-(d). Absorption spectra of N-HBC **(17)** in various solvents. The arrows indicate the direction that the absorption band below has shifted on increasing solvent polarity.

Figure 2.42 (a) compares the absorption spectra of **(17)** in toluene and in the more polar solvent acetone. There is a significant blue-shift in the λ_{max} from 354.5 nm in toluene to 351.0 nm in acetone. The band at 376.5 nm in toluene has also been blue-shifted to 373.0 nm as has the band at 393.5 nm which shifts to 391.0 nm. The bands in the red region at 414.5 nm, 451.5, and 481.0 nm in toluene have all undergone a red-shift by 2-3 nm in acetone. On applying Kasha's criteria, this would indicate that the absorption bands in the red region (400-500 nm) are in fact $\pi \rightarrow \pi^*$ transitions, and the bands at 354.5 nm and 376.5 nm in toluene are $n \rightarrow \pi^*$ transitions or at least have some $n \rightarrow \pi^*$ character.

Figure 2.42 (b) shows extremely large red-shifts in the $\pi \rightarrow \pi^*$ transitions at the low energy end of the absorption spectrum of **(17)**, in chloroform. These shifts are larger than those expected from the magnitude of the polarity change from toluene to chloroform, see table 2.15. This would indicate the existence of solvent-specific effects in addition to polarity ones.

In **Figure 2.42 (c)**, comparison of the absorption spectra of **(17)** in toluene to that in tetrahydrofuran again shows some small shifts which agree with the $n \rightarrow \pi^*$ and $\pi \rightarrow \pi^*$ transition allocations. Small hypsochromic shifts for the λ_{max} from 354.5 nm in toluene to 352.5 nm in tetrahydrofuran, and for the peak at 376.5 nm in toluene, which is blue-shifted to 374.5 nm in tetrahydrofuran, again indicate the $n \rightarrow \pi^*$ character of these two bands. The red-shift in the long-wavelength region from 481.0 nm in toluene to 482.0 nm in tetrahydrofuran is extremely small, but consistent with the allocation of this band as a $\pi \rightarrow \pi^*$transition.

Figure 2.42 (d) compares the absorption spectra of **(17)** in hexane, in acetonitrile and in methanol. This comparison provides the largest polarity index range (see table 2.15). Although the peaks are in general much broader than those already observed, it is still possible to extract many of the absorption band centres. In moving from nonpolar hexane, through acetonitrile to the polar methanol, we see large bathochromic shifts for all the absorption bands. It is not possible to comment on the peak at around 371 nm (hexane), as it seems to be disappearing through acetonitrile and has been completely swamped underneath the broad λ_{max} in methanol. It may be that this absorption at about 371 nm, being an $n \rightarrow \pi^*$ transition, has blue-shifted underneath the λ_{max} in the more polar solvent.

It is possible to summarise the spectral trends *i.e.* the solvatochroism (see table 2.15).

Solvent	Polarity Index	Wavelength (nm)								
hexane	0.06	288.5	318.0	337.0	351.5	371.0	386.0	411.0	446.0	475.5
toluene	2.40	289.5	323.5	339.0	354.5	376.5	393.5	414.5	451.5	481.0
benzene	3.00	288.5	324.5	339.0	354.5	376.5	393.0	414.0	451.5	481.5
dichloromethane	3.40	292.0	322.5	337.5	353.0	375.5	393.0	416.0	461.5	489.0
tetrahydrofuran	4.20	290.0	325.0	336.5	352.5	374.5	392.0	414.0	450.0	482.0
chloroform	4.40	292.0	325.0	339.0	354.5	376.5	395.0	418.5	463.5	493.5
acetone	5.40	-	-	336.0	351.0	373.0	391.0	417.0	453.5	483.5
acetonitrile	6.20	291.5	322.0	337.5	352.0	372.5	391.0	417.0	458.5	489.0
methanol	6.60	290.5	-	340.0	353.5	-	399.0	419.0	460.5	499.5

Table 2.15. Peaks for the absorption bands for N-HBC **(17)** in a variety of solvents of increasing polarity.

In general the bands at 386.0, 411.0, 446.0 and 475.5 nm in hexane are red-shifted in solvents of higher polarity in accordance with these bands being $\pi \rightarrow \pi^*$ transitions. Although for dichloromethane, chloroform and methanol these shifts are larger than expected (from the magnitudes of the polarity constants of the solvents) suggesting the existence of solvent-specific effects in addition to polarity effects in these cases. Similarly, the band at 376.5 nm in toluene shows a general blue-shift with increasing solvent polarity to 372.5 nm in acetonitrile. This band disappears beneath the large and broad λ_{max} in methanol, in accord with this band being assigned as an $n \rightarrow \pi^*$ transition. It should be noted however, that hexane does not follow this trend.

The results for mixed solvent experiments reveal the gradual increase in absorption wavelength with increasing percentage of polar solvent, for low energy bands at 393.5, 414.5, 451.5 and 481.0 nm, and the band at 323.5 nm in toluene (see table 2.16). Again the red-shift with increasing solvent polarity is indicative of $\pi \rightarrow \pi^*$ transitions.

Solvent Ratio	**Wavelength (nm)**								
toluene:methanol; 100:0	289.5	323.5	339.0	354.5	376.5	393.5	414.5	451.5	481.0
toluene:methanol; 98.8:1.2	290.0	324.5	339.0	355.0	377.0	394.0	415.5	454.0	486.0
toluene:methanol; 96:4	291.0	325.0	339.5	355.0	377.0	394.5	416.5	457.5	488.0
toluene:methanol; 90:10	293.0	325.5	339.5	355.0	377.5	395.0	417.5	459.5	492.5
toluene:methanol; 80:20	294.0	326.5	339.5	355.0	377.5	395.5	418.5	463.5	492.0
toluene:methanol; 50:50	-	-	340.0	355.0	377.5	395.5	419.0	465.0	494.5
toluene:methanol; 0:100	290.5	-	340.0	353.5	-	399.0	419.0	460.5	499.5

Table 2.16. Peaks for the absorption bands for N-HBC **(17)** in the mixed solvent experiment.

As a result of the above solvatochroism tentative assignments can be made for the absorption peaks in the UV-vis spectrum. The low energy bands in the red end of the spectrum at 393.5, 414.5, 451.5 and 481.0 nm in toluene and the band at 323.5 nm, are expected to be $\pi \rightarrow \pi^*$ transitions. The absorption band at 376.5 nm in toluene which is not present in the analogous hydrocarbon, HBC, is expected to be an $n \rightarrow \pi^*$ transition. This band blue-shifts in higher polarity solvents in agreement with Kasha's criteria and is relatively weak compared with the $\pi \rightarrow \pi^*$ bands. The λ_{max} at 354.5 nm in toluene is expected to have both $\pi \rightarrow \pi^*$ and $n \rightarrow \pi^*$ character. Although it is present in the analogous hydrocarbon, it undergoes sporadic shifts in solvents of varying polarity. It is suggested that an $n \rightarrow \pi^*$ transition is submerged beneath the larger, more dominant $\pi \rightarrow \pi^*$ transition.

2.2.4.2 Emission Spectroscopy

A Comparison of N-HBC with HBC

The combined absorption and fluorescence spectra of HBC and of N-HBC **(17)** are shown in figures 2.43 and 2.44, respectively. For both compounds the fluorescence spectra is highly structured, although for **(17)** there is some degree of broadening which becomes more obvious at the low energy end of the emission.

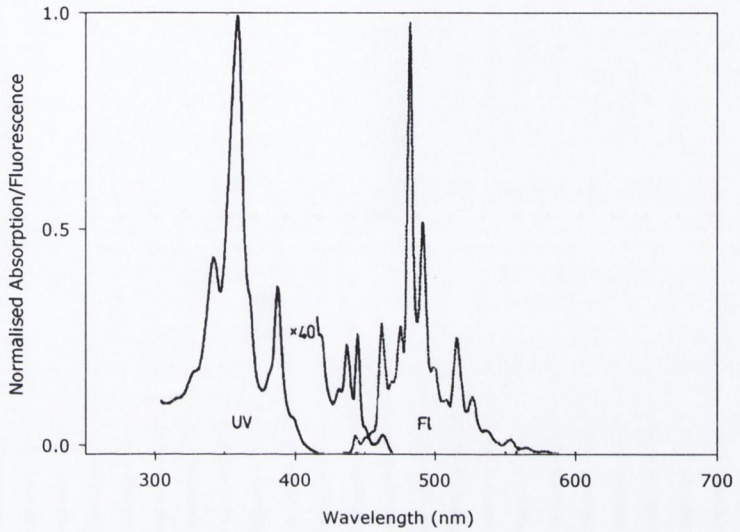


Figure 2.43. The combined absorption and emission spectra of Hexa-*peri*-hexabenzocoronene in 1,2,4-trichlorobenzene.[8]

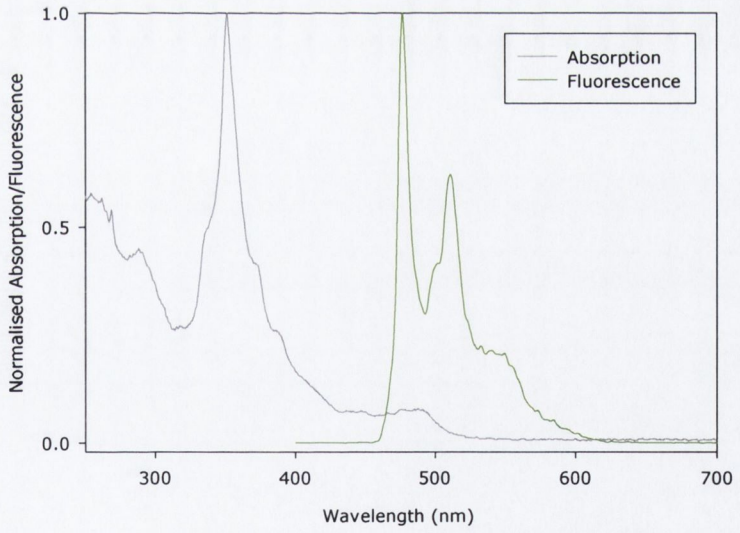


Figure 2.44. The combined absorption and emission spectra of N-HBC **(17)** in hexane.

All the bands in the fluorescence spectra of **(17)** are shifted significantly to the red by around 20 nm when compared to hexabenzocoronene. However, as these spectra were carried out in different solvents, we cannot infer much from these shifts. The most important difference between the two fluorescence spectra is the significant

enhancement of the 0-0 transition, as expected on the basis of the removal of molecular symmetry from D_{6h} for HBC to C_{2v} for N-HBC. This can be verified through the comparison of the methyl substituted HBC derivative with D_{2h} symmetry,[8] which also experiences enhancement of the (0,0) transition band in the fluorescence spectrum.

As the absorption at 475.5 nm in hexane is the 0-0, $\pi \rightarrow \pi^*$ transition, a mirror image relationship would thus suggest that the λ_{max} at 477.0 nm in the emission spectrum of **(17)** is from $^1(\pi,\pi^*)$ excited state, and that there is little solvent stabilization of this excited state in hexane. As the first excited state in this solvent is $^1(\pi,\pi^*)$, the fluorescence spectrum should resemble that of the parent hydrocarbon, HBC. This is indeed the case.

General Characteristics

Fluorescence of organic compounds usually originates from the *lowest excited singlet* level, S_1, even though absorption may initially populate a higher singlet state (S_2, S_3, ...S_n).[60] This is due to rapid internal conversion (IC) from S_n to S_1, followed by vibrational degradation. Radiationless IC $S_1 \rightsquigarrow S_0$ may now occur, although this process must be of the same order or slower than for $S_n \rightsquigarrow S_1$, otherwise fluorescence from S_1 would not occur. The forbidden Intersystem Crossing (ISC) $S_1 \rightsquigarrow T_1$ can also compete and lead to a phosphorescent emission. For many aromatic molecules direct IC $S_1 \rightsquigarrow S_0$ is unimportant, as seen in their ϕ_F and ϕ_{ISC} values which add to approximately one (*e.g.* anthracene: ϕ_F=0.72, ϕ_{ISC}=0.32).[60]

The electronic absorption spectra, and (n,π^*) and (π,π^*) nature of the excited singlet and triplet states, have been studied in detail for diazabenzenes. These molecules, for example pyrimidine, are reported to have $^1(n,\pi^*)$ states as the lowest energy singlet excited state and $^3(n,\pi^*)$ as the lowest triplet state. The diazanaphthalenes have $^1(n,\pi^*)$ as the lowest singlet excited state, and $^3(\pi,\pi^*)$ as the lowest triplet state. All the above exhibit a weak fluorescence but are found to show a strong phosphorescence.[61]

Although it is generally accepted that luminescence from (n,π^*) excited states of diazabenzenes occurs at lower energy than that derived from (π,π^*) states of the parent hydrocarbon,[62] this is not the case for 1,10-phenanthroline. The fluorescence maximum for 1,10-phenanthroline is shifted toward lower energy in non-polar solvents, which is characteristic of an increased contribution from an $^1(n,\pi^*)$ state.[62] Indeed,

the sensitivity of the fluorescence efficiency and lifetime to the nature of the solvent is indicative of a close proximity of $^1(n,\pi^*)$ and $^1(\pi,\pi^*)$ excited states, which are said mix to varying degrees in 1,10-phenanthroline and hence influence the observed photophysical properties of this compound.[62] In polar solvents, however, the first excited state for 1,10-phenanthroline is $^1(\pi,\pi^*)$.[62] As additional aromatic rings are added to the N-containing aromatic system, additional bonding and antibonding levels are introduced with a resulting reduction of the energy of the lowest $\pi \rightarrow \pi^*$ transition.[63] Thus, it is expected that N-HBC's first excited state is $^1(\pi,\pi^*)$.

Figure 2.45 shows the combined absorption and fluorescence spectra of **(17)** in (a) hexane and (b) toluene. The fluorescence spectrum is highly structured in hexane while in toluene the broadened emission has undergone a significant bathochromic shift. The lowest-energy absorption ((0,0), $\pi \rightarrow \pi^*$) and the highest-energy emission peaks are also collected in table 2.17, allowing comparison for the varying solvents.

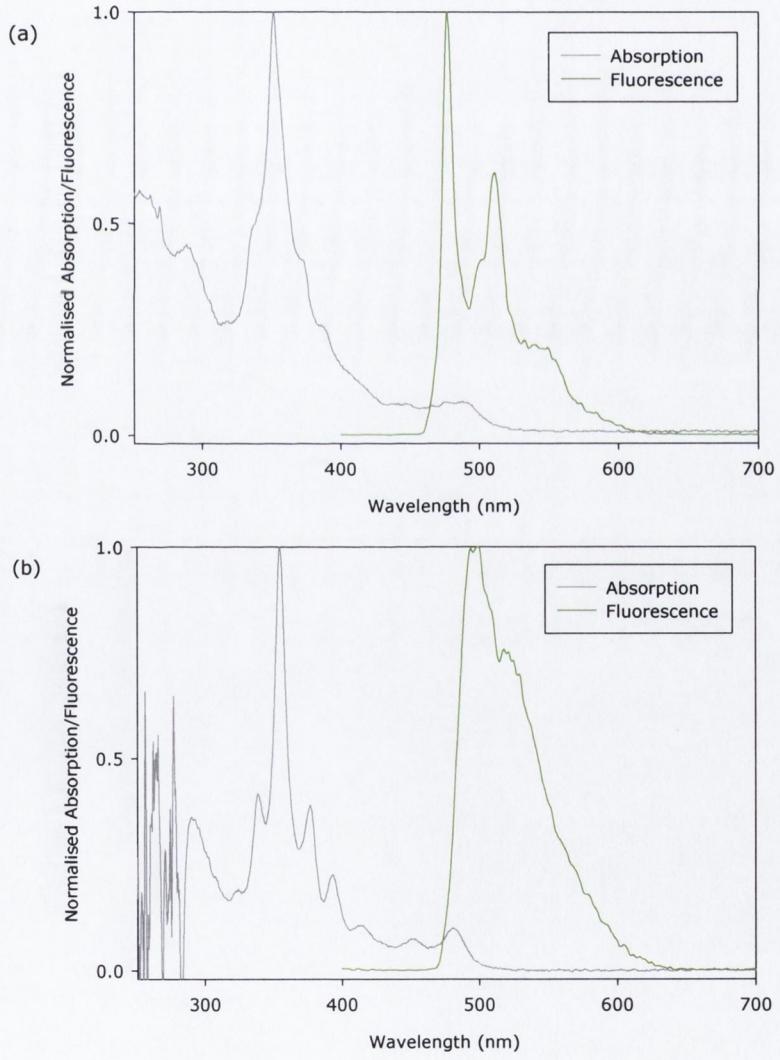


Figure 2.45. Absorption and fluorescence spectra of N-HBC **(17)** in (a) hexane and (b) toluene.

As photons emitted by fluorescence have less energy than those absorbed, absorption spectra always occur at shorter wavelengths than emission spectra. The wavelength difference, or Stokes' shift, between absorption and emission is given in table 2.17.

	λ_{abs} (nm)	λ_{em} (nm)	λ_{em}-λ_{abs} (nm)
hexane	475.5	477.0	1.5
toluene	481.0	494.0	13.0

Table 2.17. The lowest-energy absorption wavelength, highest-energy emission wavelength and Stokes' shift for N-HBC **(17)** in hexane or toluene.

The (0,0) bands in figure 2.45 (a) are seen to lie at only slightly different wavelengths in absorption and in emission; figure 2.45 (b) shows a more pronounced separation of the (0,0) bands. These separations are thought to be caused by energy loss to the solvent environment,[60] as solvent molecules reorientate themselves around the excited state molecule and stabilize it. This occurs faster than the emission process. The equilibrium interactions of **(17)** with the solvent are therefore different for the ground state and the excited states of the solvated molecule. These interactions are mainly electrical interactions, *via* the dipole moment of **(17)**, as the molecular dimensions for the ground and excited states are expected to be similar. Although the species cannot relax to the equilibrium interaction energy during the absorption process (*i.e.* in about 10^{-15} s), it can do so before fluorescent emission occurs. Thus, the energy of equilibrium, $v'=0$, is lower than that of $v'=0$ populated by the absorption process. Consequently there is separation of the (0,0) bands.

The magnitude of the separation depends on the dipole moment of the excited state of **(17)**, and on the polarity of the solvent.[60] Thus, in nonpolar hexane there is little stabilization of the excited state and only a small shift of 2 nm between the (0,0) bands results. In toluene however, the higher polarity of the solvent stabilizes the excited state, and there is a red-shift in the fluorescence emission. The (0,0) bands are now separated by 13 nm. At very low temperatures these separations are expected to become smaller because molecular movements are reduced.

The emission from N-HBC **(17)** is independent of the wavelength of excitation. A solution of **(17)** was irradiated at all absorption band wavelengths and, in each case, the corrected emission spectrum could be superimposed, suggesting a single fluorescing species (see figure 2.46). The highest intensity emission spectrum of **(17)** is generated on irradiating at $\lambda=355$ nm, which is the λ_{max} in the absorption spectrum.

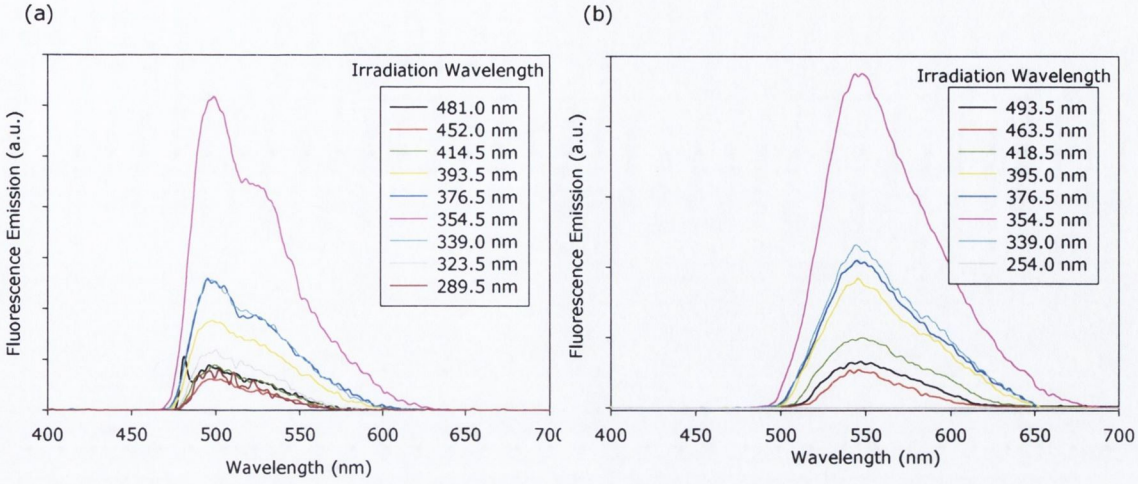


Figure 2.46. Fluorescence spectrum of N-HBC **(17)** in (a) toluene and (b) chloroform with various λ_{ex}.

Solvent Dependence

Although for a hexane solution of N-HBC **(17)** the general characteristics of HBC fluorescence are retained, we have also seen that the emission maximum (λ_F) and the extent of fine structure of **(17)** do depend upon the nature of the solvent. So whereas a solution of **(17)** in toluene displays green fluorescence with maxima at 494 and 523 nm, in chloroform there is a single maximum at 544 nm and the solution emits with a yellow fluorescence.

The effects of solvent on the absorption and emission spectra are also markedly different. These anomalies in the photophysical properties of **(17)** have been investigated in some detail and several models have been proposed to explain its photophysical behaviour.

The normalized fluorescence spectra for **(17)** are shown in figure 2.47 for a variety of solvents of differing polarity. The close mirror image relationship with the absorption spectra that was observed in hexane has disappeared in more polar solvents, as the bands become more diffuse and red-shifted. For example a solution of **(17)** in methanol shows only one broad band located at 590 nm.

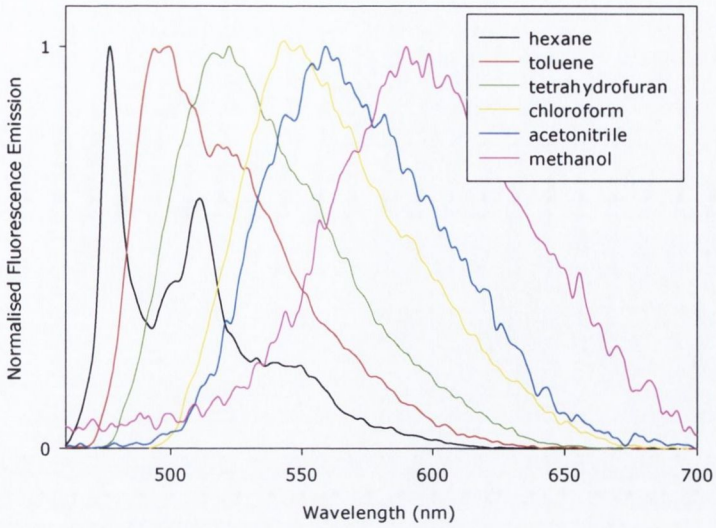


Figure 2.47. The normalized fluorescence spectra for N-HBC **(17)** in solvents of increasing polarity.

The emission spectrum of **(17)** does not mirror the absorption spectrum in polar solvents, but is broader and less structured. Table 2.18 highlights the remarkably large red-shift, in the emission maxima of **(17)** when dissolved in solvents of increasing polarity.

		ABSORPTION		EMISSION		
Solvent	**Polarity Index**	**λ_{max} (nm)**	**ε_{max} (L mol^{-1} cm^{-1})**	**λ_F (nm)**	**ϕ_F**	**τ (ns)**
hexane	0.06	351.5	51000	477.0	0.31	
toluene	2.40	354.5	137000	494.0	0.40	13
dichlorobenzene	2.70	357.0	93000	536.0	0.28	
benzene	3.00	354.5	143000	501.5	0.39	
dichloromethane	3.40	353.0	101000	544.5	0.23	
tetrahydrofuran	4.20	352.5	146000	522.5	0.33	
chloroform	4.40	354.5	146000	544.0	0.21	12
acetone	5.40	351.0	86000	547.0	0.28	
acetonitrile	6.20	352.0	66000	559.5	0.22	11, 26
methanol	6.60	353.5	53000	590.0	0.06	

Table 2.18. The absorption and emission data of N-HBC **(17)** in various solvents.

The fluorescence quantum yield, ϕ_F, of **(17)** is 0.40 in toluene solution (*cf.* 0.23 for coronene in ethanol[64]). Like the fluorescence maximum, the singlet excited state lifetime (τ_s) of N-HBC **(17)**, varies substantially with the nature of the solvent (see table 2.18). The shift in the fluorescence maximum toward lower energy (longer λ_F) in more polar solvents is accompanied by a large decrease of the fluorescence quantum

yield, which may be interpreted as a decrease in the degree of radiative decay and an an increase in non-radiative processes.[65]

The bi-exponential fluorescence decay that is observed for **(17)** in CH_3CN has been reported before in HBC derivatives, and is likewise attributed here to emission from the aggregate (11 ns) and emission from the monomer (26 ns).[64]

The emission maximum of **(17)** in hexane is found to be at 477 nm, whilst in methanol the emission maximum is red-shifted to 590 nm. Such large spectral shifts in emission wavelengths cannot be attributed to solvent relaxation. This indicates the formation of a charge transfer state, resulting in emission taking place from a state of lower energy.[66]

Degassing (to remove oxygen, the known triplet quencher) gave a 10-15% increase in the quantum yield, with no change in shape of the emission spectra.

Importantly, the weak emission of 1,10-phenanthroline is blue-shifted upon increasing solvent polarity. This behaviour has been attributed to the close proximity of the (π,π^*) and (n,π^*) singlet excited states, with the latter making a greater contribution in non-polar solvents.[62] This may explain the low fluorescence quantum efficiency of 1,10-phenanthroline (*ca.* ϕ_F=0.001-0.010),[62] since the (n,π^*) excited states often decay by nonradiative pathways.[60] In contrast, **(17)** exhibits high fluorescence quantum efficiencies in various solvents and short excited state lifetimes (13 ns in toluene, table 2.18), supporting the assignment of the emitting excited state as a $^1(\pi,\pi^*)$ species.[40]

The results of a mixed solvent experiment reveal a gradual increase in wavelength of the emission maximum with an increasing proportion of the more polar solvent, as shown in figure 2.48.

The results of the absorption and emission spectra show that the wavelength of the highest-energy fluorescence band and the wavelength of the lowest-energy absorption band are both very much dependent on the solvent system. This strong solvent dependence implies strong electric dipole moments for both absorption and fluorescence emission processes. However, the solvent effect on emission is more pronounced than on absorption, for example the red-shift of the longest wavelength absorption is 770 cm^{-1}, when passing from toluene to methanol, while the shift of the fluorescence maximum is 3294 cm^{-1}. This experimental data agrees with the assignment of the first excited singlet state, S_1 as having (π-π^*) character.[67] The

much larger bathochromic displacement of the fluorescence maximum upon increase of solvent polarity relative to the displacement of the absorption maximum is also evidence of the formation of a partial intramolecular charge transfer (ICT) state on excitation.[67] It is probable that the formation of this charge-transfer state is enhanced by increasing the solvent dielectric constant.

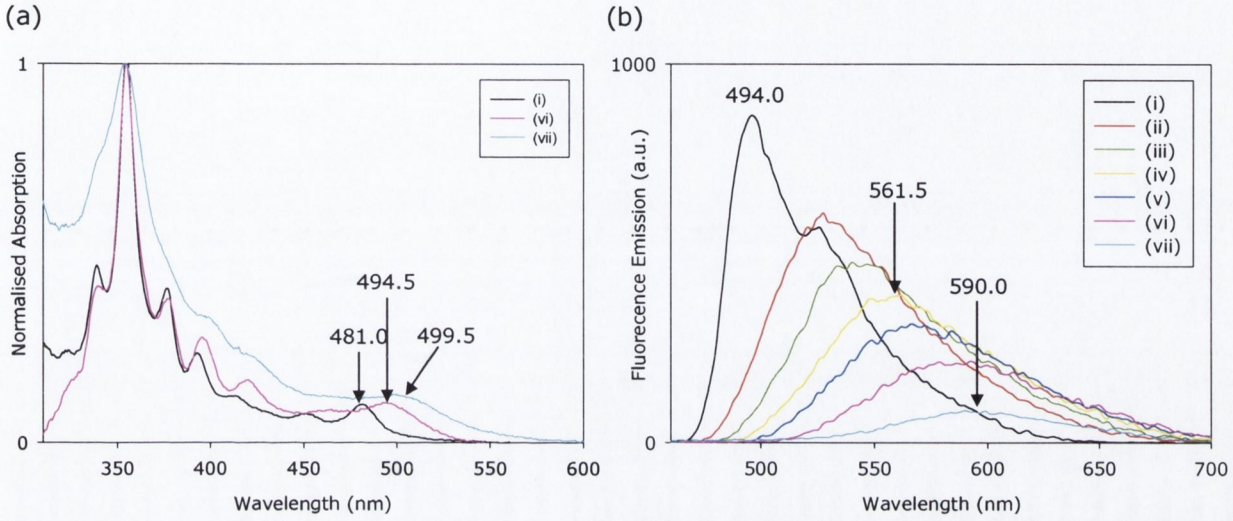


Figure 2.48. The (a) absorption and (b) emission spectra for **(17)** in toluene:methanol solution mixtures; (i) 100:0, (ii) 98.8:1.2, (iii) 96:4, (iv) 90:10, (v) 80:20, (vi) 50:50, (vii) 0:100.

These results suggest that upon excitation to the lowest energy $^1(\pi,\pi^*)$ state, electron density is displaced from the *tert*-butyl groups through the aromatic ring system to the nitrogen (*i.e.*, the LUMO now has a higher electron density on the nitrogen atoms than the HOMO).

Confirmation of the formation of the CT state

The observed solvent-induced shifts of the electronic absorption and emission bands of organic compounds are commonly an indication that charge reorganization is taking place in the compound upon electronic excitation or radiative deactivation.[67] A detailed consideration of solvent-solute interactions describe solvent shifts in the electronic absorption spectra as "an indication of the extent of inertial solvent reorganization on the instantaneous charge reorganization of the molecule upon electronic excitation". Solvent shifts of the emission (fluorescence) bands reflect "the influence of the equilibrium solvent arrangement around the excited molecule, rearrangement inertially due to the instantaneous charge redistribution upon radiative deactivation to the ground electronic state".[67]

Dipole moments (μ) are influenced by electronic excitation not only through changes in geometry of the molecular skeleton, but also through the redistribution of electrons themselves. A change in the dipole moment upon excitation or deactivation is often observed through the effects of polar solvents on the absorption and emission spectra. The simplest visualisation of an $n \rightarrow \pi^*$ transition is that the excited n-electron is completely delocalised over the entire ring system and thus the transition should therefore be accompanied by a large decrease in the dipole moment, *i.e.* $(\mu_e) < (\mu_g)$. This is in contrast to $\pi \rightarrow \pi^*$ transitions, where usually $(\mu_e) > (\mu_g)$.

We have seen that solvent polarity has some influence on the absorption maxima of **(17)** and a profound effect on the emission behaviour. The magnitude of (μ_e) is therefore much greater than that of (μ_g). The red-shift observed for **(17)** upon increasing solvent polarity is therefore indicative of the greater stabilization of the excited state dipole, and indicates that the excited state has charge-transfer character.[40] It has in fact been shown that a large excited state dipole moment (μ_e) value with respect to the ground state (μ_g) is a favourable condition to obtain efficiently fluorescent systems.[68]

The large increase of dipole moment on excitation of **(17)** is in part a consequence of the molecule possessing electron-donor and electron-acceptor groups linked through a conjugated system. When the electron-accepting nitrogen nuclei are linked to the electron-donating *tert*-butyl groups, an intramolecular charge transfer state is favoured.[68] The bathochromic effect observed for **(17)** (*i.e.*, the red-shift observed for the emission maxima of **(17)** on increasing solvent polarity) can thus be attributed to the internal extended π-electronic conjugation between the donor *tert*-butyl groups and the nitrogen acceptor nuclei.

As large (μ_e) values reflect the formation of a partially charge-seperated state, the solvatochromic studies performed were used to determine the change in dipole moment of **(17)** upon excitation. In order to estimate the change in the dipole moment of **(17)**, we have used the method of Lippert and Mataga,[68,69] which consists of studying the influence of solvents of differing polarity upon the absorption and emission features of polar organic compounds. If, as in this case, there is no specific interaction (such as hydrogen-bonding between solute and solvent molecules) the dispersion-dipole theory of solvent effects is applicable to the frequency shifts.[70] The stokes shifts $(\bar{\nu}_a - \bar{\nu}_e)$ are expressed as a function of the dipole moments of the molecule in the excited state (μ_e), the ground state (μ_g), the dielectric constant (ε) and the refractive index (n) of the solvent (equation 2.1):

$$(\bar{\nu}_a - \bar{\nu}_e) = \frac{2}{hc}(\mu_e-\mu_g)^2 a^{-3}\left\{\frac{\varepsilon-1}{2\varepsilon+1} - \frac{n^2-1}{2n^2+1}\right\} \quad (2.1)$$

Where $\bar{\nu}_a$ and $\bar{\nu}_e$ are the wavenumbers of the absorption and emission, respectively.

h is the Planck constant.

c is the velocity of light

a is the radius of the Onsager cavity, which corresponds to the molecular volume for **(17)**.

Using the assumption of Lippert, that the radius *a* can be derived from the length of the molecule multiplied by a reduction factor of 0.8, a value of 11.55 Å for **(17)** is obtained (as deduced from X-ray chrystallographic analysis of precursor **(16)**).

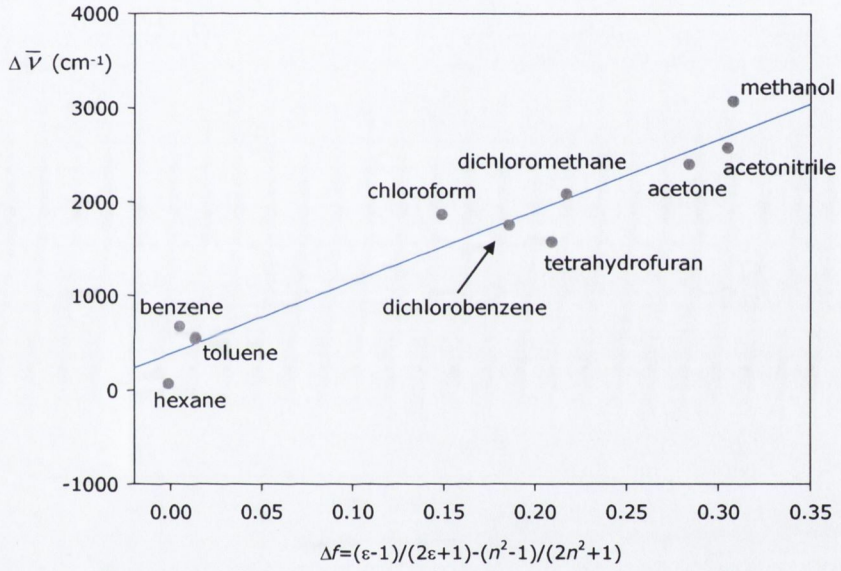


Figure 2.49. $\Delta\bar{\nu}$ as a function of the solvent polarity Δf for N-HBC **(17)** in various solvents.

Application of equation 2.1 in the case of N-HBC **(17)** leads to a satisfactory result. In polar solvents, the red-shift of the emission is reasonably linear with the solvent parameter $f(\varepsilon,n)$ confirming the dipolar nature of the excited state of **(17)**. Deviations from the linear fit (*e.g.* chloroform and methanol) could point toward the existence of solvent-specific effects in addition to polarity ones. By estimating a value of 11.55 Å for the Onsager cavity (*a* value), it was deduced from the slope of the plot (figure 2.49) that **(17)** has a $\Delta\mu$ value ($(\mu_e)-(\mu_g)$) as high as 34 D. This corresponds to a strong charge transfer in the excited state.

The ground state dipole moment (μ_g) for **(17)** can be estimated as 6 D, using semi-empirical quantum mechanics AM1 parameter set (see Appendix 2), which leads to a

large (μ_e)=40 D. This dramatic increase is largely attributed to the significant size of the molecule (for comparison 4-nitroaniline: (μ_g)=6 D, (μ_e)=14 D,[60] while 4-dimethylaminobenzil-4'-nitroanilin: (μ_g)=3.6 D, (μ_e)=38 D[69]).

These results emphasize the effect of the dipolar donor-acceptor structure of the N-HBC chromophore on its optical response.

The above feature allows the control of the emission colour *via* solvent polarity. Thus, **(17)** exhibits a green emission in toluene, a yellow emission in chloroform and in methanol displays a red light emission, see figure 2.50.

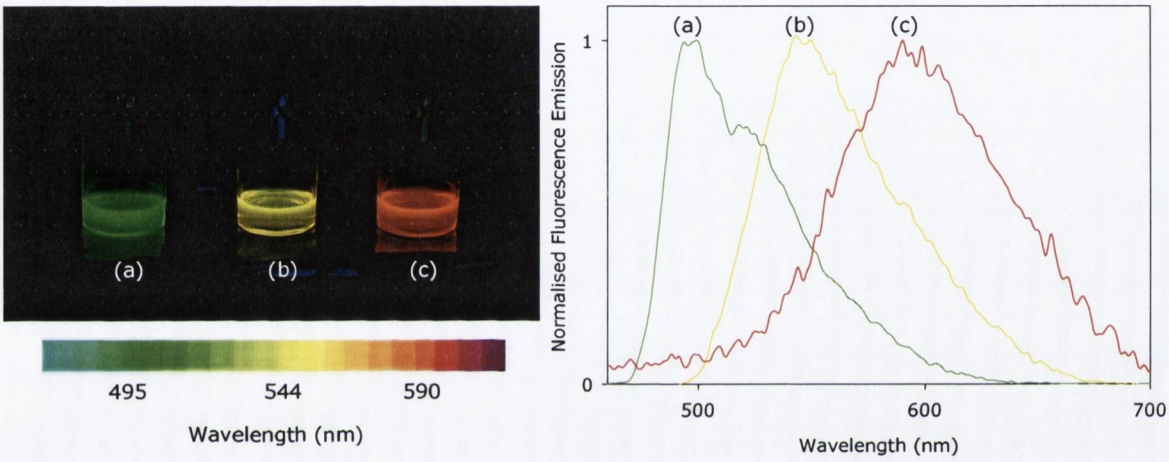


Figure 2.50. N-HBC **(17)** photographed under a UV lamp and the normalized fluorescence emission spectra in (a) toluene, (b) chloroform and (c) methanol.

An attempt was made to probe the excited state further by means of fluorescence spectra analysis at room temperature and at liquid nitrogen temperatures in a rigid matrix. At liquid nitrogen temperature, molecular motion is strongly slowed because of the high increase of the solvent viscosity.[65]

Figure 2.51 shows the fluorescence spectrum of **(17)** in the highly polar methanol:ethanol solvent mix at room temperature and at 77 K. At low temperature there is an increase in the structure of the emission spectra. At room temperature we see the broad and structureless charge transfer state emission. These results seem to indicate that the major emitting state at low temperature in the highly polar solvent is still the charge transfer state.

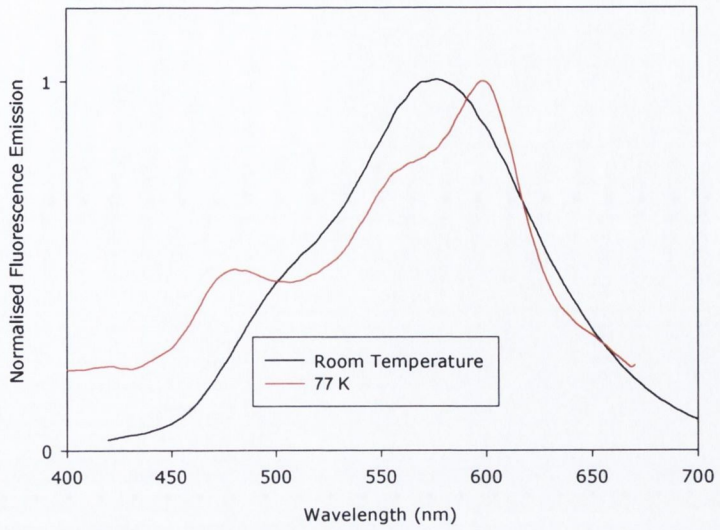


Figure 2.51. The fluorescence spectrum for N-HBC **(17)** in the highly polar methanol:ethanol solvent mix at room temperature and at liquid nitrogen temperature.

The different behaviour in the rigid matrix at 77 K can be attributed to the repolarization of the solvent around the excited state, a process which takes place in fluid solution, but is at least in part prevented in the rigid matrix.

The increase in the structure of the emission at low temperature in the polar solvent system may originate from three different excited states, nevertheless, in highly polar solvents the intramolecular charge transfer state persists, even at 77 K, again suggesting a strong dipole moment in the excited state. Analysis of the emission lifetime (τ) at 77 K is required to confirm this hypothesis.

2.2.4.3 Absorption and Fluorescence Properties of the Protonated Form of N-HBC (17)

To understand better the behaviour of the chromophoric unit of N-HBC **(17)**, the effect of protonation on the nitrogen atoms of the coordinating unit of **(17)** was studied. N-HBC **(17)** contains four nitrogen atoms each of which is capable of acting as a proton acceptor.

The absorption spectra of **(17)** in toluene solution is shown in figure 2.52 (i). Addition of triethyl amine base to the solution does not cause any spectral change. By contrast, the addition of trifluoroacetic acid causes strong changes over the entire spectrum. In particular, the low energy bands move to the red. There is no further variation in the spectra at high acid concentrations.

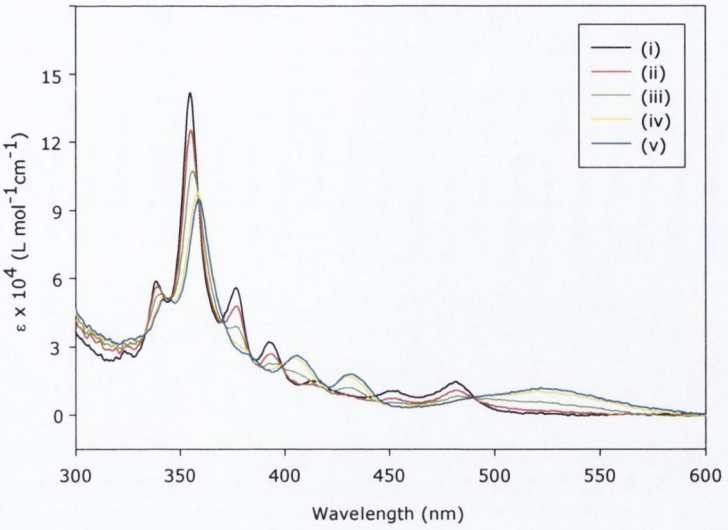


Figure 2.52. The absorbtion spectra of **(17)** in toluene (4 mL, 6.66×10^{-7} M) on addition of (i) 0 μLs, (ii) 5 μLs, (iii) 10 μLs, (iv) 50 μLs, (v) 110 μLs of trifluoroacetic acid (0.1 M).

Protonation of the peripheral nitrogen atoms by the gradual addition of trifluoroacetic acid causes major changes in the absorption spectrum (figure 2.52). The decrease in intensity of the 355 nm absorption band along with the disappearance of the 376 nm band in the UV-vis spectrum indicates that nitrogen protonation has a profound electronic effect on the π-electron density throughout the system.

As discussed earlier, the lowest-energy band in the absorption spectrum of **(17)** can be assigned, similarly to phenanthroline,[62,71] as a spin-allowed $\pi \rightarrow \pi^*$ transition. The red-shift observed for the lowest-energy absorption bands upon protonation of **(17)** shows that the lowest-energy $\pi \rightarrow \pi^*$ transitions display charge-transfer character (*i.e.*, the LUMO has a higher electron density on the nitrogen atoms than the HOMO), as seen for various phenanthroline derivatives.[71]

The changes in the absorption spectrum upon addition of acid are reversed upon addition of triethylamine base. This suggests that an equilibrium (equation 2.2) is established in the ground state:

$$A + BH \rightleftharpoons AH^+ + B^- \qquad (2.2)$$

In equation 2.2, A is **(17)** and BH is trifluoroacetic acid.

The fluorescence spectrum, like the absorption spectrum, is dependent on pH, with large changes to the spectrum on addition of trifluoroacteic acid. In toluene solution at

room temperature **(17)** displays a structured fluorescence band (figure 2.53 (i)) that is assigned to the lowest-energy $^1(\pi,\pi^*)$ level of **(17)** with charge transfer character (this assignment has already been discussed). On addition of acid, the intensity of this band decreases, and a new, unstructured, shorter-lived luminescence band arises at longer wavelength.

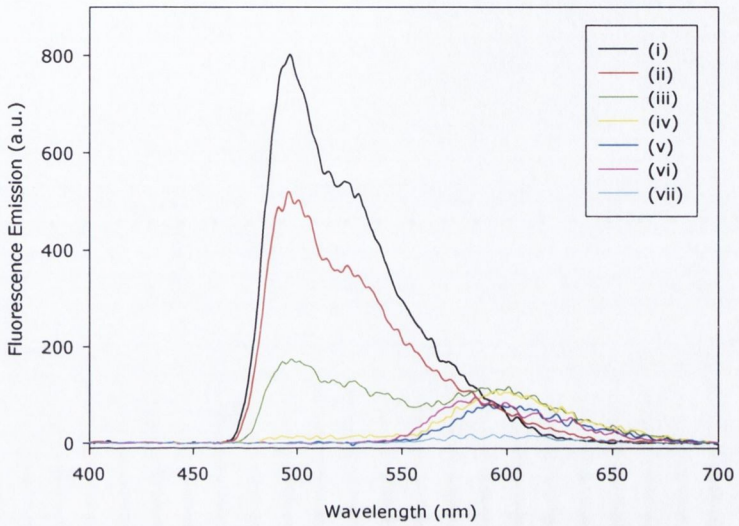


Figure 2.53. The fluorescence spectra of **(17)** in toluene (4 mL, 6.66×10^{-7} M) on addition of (i) 0 μLs, (ii) 5 μLs, (iii) 10 μLs, (iv) 50 μLs, (v) 110 μLs, (vi) 200 μLs, (vii) 450 μLs of trifluoroacetic acid (0.1 M).

On addition of trifluoroacteic acid the fluorescence from the neutral compound (λ_F=494 nm) is replaced by fluorescence from the monoprotonated species (λ_F=595 nm). This is in direct correlation to the behaviour of various phenanthroline compounds,[62,71] until, on the addition of excess trifluoroacteic acid, the fluorescence emission becomes completely quenched.

The spectral variations have been summarized in figure 2.54, which shows the normalized variations of two UV-vis absorption maxima of **(17)** and one fluorescence maximum. As can be seen in the absorption spectra, the decrease in the intensity of the absorption band at 376 nm is accompanied by a parallel increase (within experimental error) of the intensity of the 521 nm band. The intensity decrease of the fluorescence band at 494 nm closely follows the trace for the absorption at 376 nm. Unfortunately due to the overlap of the emission band at 494 nm and the lower-energy band for the mono-protonated form of **(17)** at 595 nm, the error in this trace makes it less reliable and this band has not been added to figure 2.54.

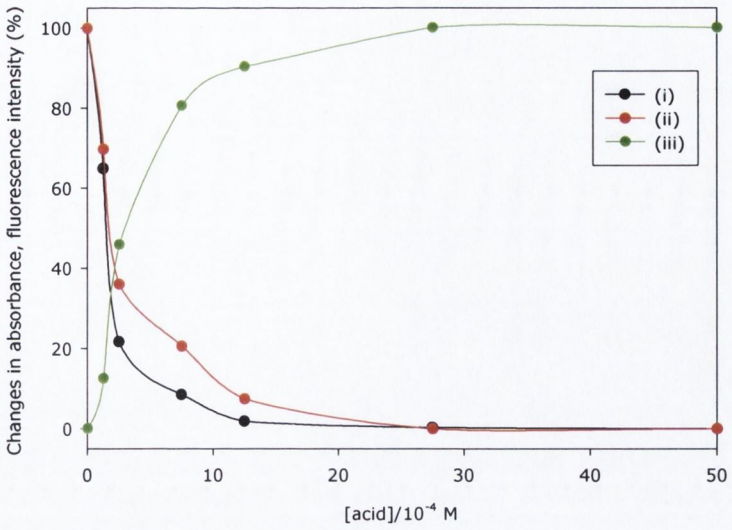


Figure 2.54. Normalised changes in fluorescence at (i) 494 nm, and absorption at (ii) 376.5 nm and (iii) 521.5 nm upon incremental addition of trifluoroacetic acid to a toluene solution of N-HBC **(17)** (4 mL, 6.66x10^{-7} M).

Firstly, these results confirm the assignment of the 376 nm band in the absorption spectrum as an n→π* transition. According to Kasha's criteria an n→π* transition will disappear in acidic media.[60] The decrease of the band at 355 nm would suggest that, although this band appears to be dominated by a π→π* transition, it does contain some n→π* character, which is removed upon protonation.

These results also indicate that the lowest $^1(\pi,\pi^*)$ level of **(17)** is stabilized by protonation of the pyrimidine nitrogens because of its partial charge transfer. This has been seen for various phenanthroline derivatives.[62,71]

The removal of all fluorescence at higher acid concentrations (11 x 10^{-3} M) may indicate that further protonation to give diprotonated, triprotonated, or terprotonated species may be occurring, and with the extension of the above hypothesis has reduced K_r (the radiative rate constant) to an undetectable level.

Acid-Base Properties

The changes in the absorption reflect the position of the acid-base equilibrium in the ground state, equation 2.2, whereas the changes in the fluorescence intensity reflect the position of the acid-base equilibrium in the excited state, equation 2.3, at the time the emission takes place:

$$*A + BH \rightleftharpoons *AH^+ + B^- \qquad (2.3)$$

In figure 2.54 we see that for **(17)** the changes in absorption upon protonation seem to parallel the changes in the fluorescence intensity under the same conditions. It is probable, however, that the equilibrium constants for the ground state equation 2.2, and the excited states, equation 2.3, are different as reflected by their different charge-transfer characters (*i.e.*, different amounts of negative charge on the nitrogens). Using a Förster cycle,[62] the changes in the equilibrium constants on going from the ground to the excited state can be estimated from equation 2.4:

$$\Delta pK = pK^* - pK = \frac{(\bar{\nu}_P - \bar{\nu}_{PH^+})Nhc}{2.303RT} \qquad (2.4)$$

Where N is Avagadro's number, *h* is the Planck constant, *c* is the velocity of light, R is the gas constant, T is the temperature and ($\bar{\nu}_P - \bar{\nu}_{PH+}$) is the energy difference (cm^{-1}) of the absorption of A and AH^+ measured in the (0,0) band. $\Delta\bar{\nu}$ is found to be 1611 cm^{-1} for **(17)** and the corresponding ΔpK_a value is calculated to be 3.4 ± 0.1. The occurrence of a singlet, excited-state, prototropic equilibrium for **(17)** is very unlikely, however, as its lifetime is of the order of nanoseconds. Also, the calculated increase in the pK_a of the excited state is not reflected in figure 2.54, so we believe that there is little or no chance that protonation or deprotonation will occur within the excited state lifetime, and hence the fluorescence reflects the ground state equilibrium mixture.

The Radiative decrease

The decrease in fluorescence yields with decreasing pH is due either to an increase in the singlet-state IC or to an enhancement in the ISC process (or both). The decrease of the radiative rate constant, k_r (table 2.19), on going from the unprotonated to the protonated forms has been related, for phenanthroline derivatives, to the increase in the charge-transfer character of the electronic transitions.[71] A similar argument could be used to explain the decrease of k_r for **(17)**. The lowest energy $^1(\pi,\pi^*)$ of **(17)** is stabilized by protonation because of its partial charge transfer character.

Compound	λ_{max} (nm)	τ (ns)	ϕ_F	k_r (s^{-1})= ϕ_F/τ
(17)	494	13	0.40	$3.0x10^7$
(17).H$^+$	595	9	0.11	$1.2x10^7$
(17).xH$^+$	-	-	0	0

Table 2.19. Fluorescence data for **(17)** and the protonated species in toluene at room temperature.

Other authors have related the low fluorescence quantum yield of diaza aromatic compounds to the position of the (n,π*) transition.[62] It is the "lone-pair" electrons of aromatic nitrogen heterocyclic molecules which usually determine the nature of the radiative and radiationless paths for deactivation of the excited states formed from these compounds.[61] The low fluorescence quantum yield observed for mono-protonated phenanthroline was found to be consistent with an (n,π*) lowest excited singlet state.[62] Apparently, for phenanthroline the $^1(n,\pi^*)$ state has moved below the $^1(\pi,\pi^*)$ during protonation, so that the lowest excited singlet state becomes (n,π*). Often fluorescence efficiency is much lower for (n,π*) singlets than for the corresponding (π,π*) singlets so that decay processes are fast.[62] (For example ISC to the T_1 state and radiationless energy loss.)

In fact, the electronic configuration resulting from an n→π* transition, *i.e.* an electrophilic heteroatom, is responsible for photoreduction in many analogous systems and may contribute to the low fluorescence quantum yield obtained for **(17)** in some solvents.[62]

Likewise, the presence of good hydrogen atom donors, such as aliphatic alcohols, will stabilize the charge transfer state, and increase radiationless decay through similar mechanisms to those described above. Thus a solution of **(17)** in methanol produces fluorescence with low quantum efficiency.

2.2.4.4 Absorption and Fluorescence Properties of an Exciplex of N-HBC (17)

It has been known for some time that tertiary amines quench the fluorescence of arenes in non-polar solvents and an exciplex emission with charge transfer character is observed.[72] The charge transfer complex, A^-D^+, is stabilized by an electron transfer from the donor (amine) to the acceptor (arene). It has been found that different amines quench the fluorescence with different solvent dependent efficiencies. In polar solvents such as acetonitrile, the arene-tertiary amine exciplex undergoes rapid dissociation to give solvent separated ion pairs ($A^-_s...D^+_s$), and the exciplex emission is largely quenched.[65]

The absorption spectra of **(17)**, in the presence of incremental amounts of the donor aniline, are unchanged. There are, however, drastic changes in the fluorescence spectra of **(17)** as aniline is added (see figure 2.55).

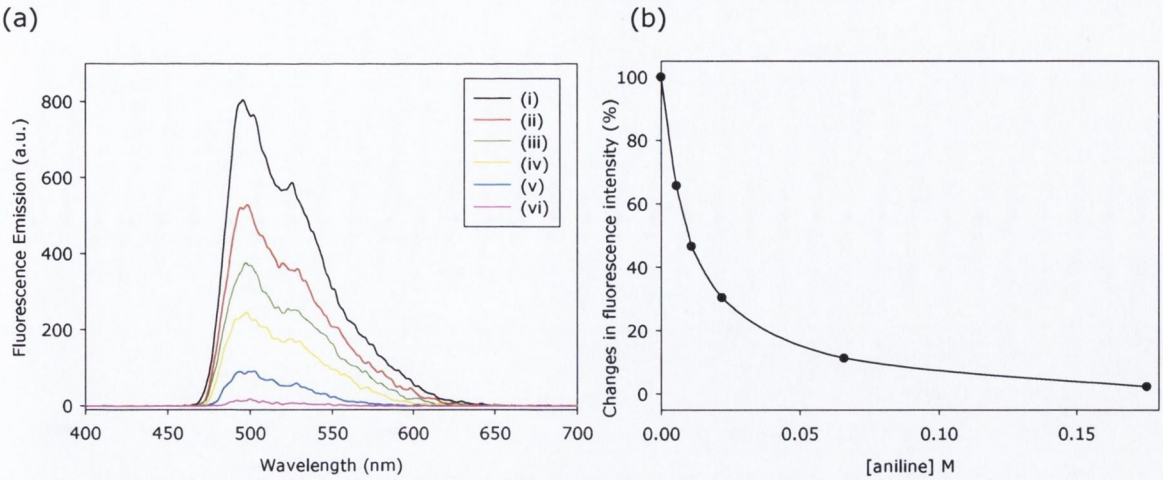


Figure 2.55. (a) The fluorescence spectra of **(17)** in toluene (4 mL, 6.66×10^{-7} M) on addition of (i) 0 μLs, (ii) 5 μLs, (iii) 10 μLs, (iv) 20 μLs, (v) 60 μLs, (vi) 160 μLs of aniline (4.39 M, toluene) and (b) the normalized changes in fluorescence at 494 nm.

It is generally known that photoinduced electron transfer reactions between neutral molecules form a contact ion pair.[65] These ions may recombine in the solvent cage or may form solvent separated ion pairs and free solvated ions depending on the solvent polarity. These species will decay non-radiatively to the ground state.[65] Exciplex emission is observed if the excited state is a contact ion pair.[65] The luminescence of N-HBC **(17)** is effectively quenched on addition of aniline. It is postulated that this is due to the formation of an exciplex between the donor aniline and the acceptor **(17)**. That the exciplex emission is not observed could be due to the formation of non-fluorescent solvent shared ion-pairs even in the weakly polar solvent toluene.[65] This may suggest a weak electrostatic interaction energy for the contact ion pair.

2.2.5 SPECTRAL SUMMARY FOR N-HBC (17)

The electronic absorption spectrum of N-HBC displays the typical line shape of the parent hydrocarbon, HBC, indicating that despite the chemical modification, the HBC chromophore is still intact. For N-HBC, the red-shifted α-band at 481 nm (in toluene) is assigned to the 0-0, $^1(\pi,\pi^*)$ transition. Strictly forbidden for HBC, due to its D_{6h} symmetry, this transition is significantly enhanced for N-HBC on the basis of its lower molecular symmetry. The introduction of four electron withdrawing nitrogen atoms causes a depletion of the π-electron density within the N-HBC core, as compared to HBC, and results in a reduction in ε_{max} (355 nm, ε_{max} 137000) compared to HBC (ε_{max} 177000). This gives N-HBC overall electron-accepting properties. By applying Kasha's criteria it is possible to assign the bands in the UV-vis spectrum as either $n\rightarrow\pi^*$ or $\pi\rightarrow\pi^*$ electronic transitions. There is only one, clearly new absorption band in the UV-vis spectrum of N-HBC, as compared to HBC. This appears at 377 nm (in toluene) and is therefore assigned as an $n\rightarrow\pi^*$ transition. Solvatochroism confirms this assignment, and it is suggested that all other bands in the electronic spectrum of N-HBC, like HBC, are $\pi\rightarrow\pi^*$ transitions, although the band at 355 nm, which conveys sporadic behaviour in solvents of varying polarity, has some $n\rightarrow\pi^*$ character.

Like HBC, N-HBC displays a highly structured fluorescence spectra (in hexane), with significant enhancement of the 0-0 transition, as expected on the basis of the reduction of molecular symmetry from D_{6h} for HBC, to C_{2v} for N-HBC. It is deduced, from the mirror image relationship with the absorption spectra, that the λ_{max} at 477 nm in the emission spectra of N-HBC is from the $^1(\pi,\pi^*)$ excited state, with little solvent stabilization of this excited state in hexane. That the lowest energy excited state is a $^1(\pi,\pi^*)$ is expected for this N-containing system with a large number of aromatic rings. The fluorescence spectra of N-HBC display a marked solvatochroism. The mirror image relationship with the absorption spectrum that was observed for hexane disappears in more polar solvents as the bands become more diffuse and red-shifted. Also, the solvent effect on the emission spectra is more pronounced than on the absorption spectra. For example the red-shift of the longest wavelength absorption is 770 cm^{-1}, when passing from toluene to methanol, while the shift of the fluorescence maximum is 3294 cm^{-1}. Such large spectral shifts in emission wavelengths indicate the formation of a charge transfer state (*i.e.*, the LUMO now has a higher electron density on the nitrogen atoms than the HOMO). Increasing the solvent dielectric constant enhances the formation of this charge-transfer state. The bathochrome effect observed for N-HBC is attributed to the extended internal π-electronic conjugation between the donor *tert*-butyl groups and the nitrogen acceptor nuclei, thus a large increase in the dipole moment and the formation of a charge-transfer state upon excitation occurs. It is

possible to estimate the change in dipole moment ($\Delta\mu$) between the ground and excited state by studying the solvatochroism of N-HBC. A Lippert-Mataga plot reveals a ($\Delta\mu$) value as large as 34 D for N-HBC. As a direct consequence it is possible to control the emission colour of N-HBC *via* solvent polarity. A solution of N-HBC in toluene displays a green fluorescence, in chloroform it is a yellow fluorescence and in methanol it is a red fluorescence. In the highly polar methanol:ethanol solvent mix, the charge-transfer state persists even at 77 K. The reduction of solvent repolarisation around the excited state at low temperature, however, has resulted in an increase in the structure of the emission spectrum.

There is a profound effect on both the absorption and the emission spectra of N-HBC upon the addition of acid. In the absorption spectra we see red-shifts for the lowest-energy absorption bands, after protonation of the peripheral nitrogen atoms by the gradual addition of trifluoroacetic acid. This indicates that the α-bands are stabilized by protonation of the pyrimidine nitrogens, because of their partial charge-transfer. The disappearance of the 376 nm absorption band is further evidence for its $n\rightarrow\pi^*$ origin, according to Kasha's criteria. Likewise, the decrease in intensity of the absorption band at 355 nm would suggest that, although this band appears to be dominated by a $\pi\rightarrow\pi^*$ transition, it does contain some $n\rightarrow\pi^*$ character. These changes on protonation can be reversed by the addition of triethylamine base, suggesting an equilibrium in the ground state between N-HBC and its protonated form. On the addition of trifluoroacetic acid the fluorescence from the neutral compound (λ_{max}=494 nm, ϕ_F=0.40) is replaced by the fluorescence of the monoprotonated species (λ_{max}=522 nm, ϕ_F=0.11). On the addition of excess acid the fluorescence emission becomes completely quenched, perhaps due to further protonation to the di-, tri- or terprotonated species. The decrease in the ϕ_F upon protonation of the nitrogens is related to either the stabilization of the $^1(\pi,\pi^*)$ state of N-HBC due to its partial charge-transfer character or to the relative positions of the $^1(n,\pi^*)$ and $^1(\pi,\pi^*)$ states, which may mix to varying degrees. Changes in the UV-vis spectra parallel the changes in the fluorescence spectra upon protonation, suggesting that protonation or deprotonation does not occur within the excited state lifetime.

Although the donor compound aniline has no effect on the absorption spectra of N-HBC, the fluorescent emission of N-HBC is quenched on the addition of aniline due to the formation of a non-fluorescent exciplex.

2.2.6 SELF-ASSOCIATION: AGGREGATION OF N-HBC (17) IN SOLUTION

Nano-scale electronic circuitry could be constructed from self-assembling molecules, the components of which would be required to self-assemble with little external assistance. Due to its aggregation and electron accepting properties, N-HBC **(17)** may have importance as a self-assembling molecular material for the construction of nano-wires.

An aggregate is formed when two or more molecules interact strongly enough that spontaneous separation becomes energetically unfavourable. Aggregation is controlled by random molecular collisions and is therefore concentration dependent.[30] In this work, we have studied the self-association (aggregation) of N-HBC in toluene by electronic spectroscopy. By studying changes in the absorption wavelengths, fine structure and molar absorptivity of the UV-vis spectrum at various concentrations, we can obtain information as to the aggregation properties of these molecules. We have also investigated the concentration dependence of N-HBC using ^{1}H NMR spectroscopy as a technique to investigate its aromatic stacking in deuterated chloroform.

N-HBCs have two structural domains that determine their association process. Firstly, they have a planar aromatic system that may lead to the stacking of the rings similar to the columnar aggregates of HBCs. Alternatively, the nitrogen atoms provide potential hydrogen bonding sites that may lead to colinear interactions. Although the methods used in this work give evidence for N-HBCs spontaneous aggregation, the mode of aggregation is still unclear. We can only draw conclusions from comparisons with results reported for HBC derivatives, which are said to aggregate in columnar stacks.[4,30]

At extremely low concentrations (10^{-15} M), any single non-aggregated HBC type molecules present in solution are expected to be sufficiently separated to prevent any attractive intermolecular interactions, which would lead to aggregation,[30] hence the electronic spectra should correspond to single molecules in solution. As the concentration is increased and single molecules in solution are depleted in favour of aggregates, changes to the spectra should be observed, and the aggregate spectrum should gradually replace the single molecule spectrum. Dramatic changes in the excitation and luminescence spectra, with varying concentration of HBCs, have been attributed to the aggregation process of HBCs which lead to the formation of columnar stacks.[30] Broad featureless excitation spectra have been assigned to single molecule HBCs in solution, whereas aggregates are responsible for the blue-shifted, sharper spectra, which are observed at higher concentrations ($>10^{-8}$ M).

In conjunction with Alex Fleming, Physics Department Trinity College, the excitation spectra of **(17)** were studied in a similar manner, over a wide concentration range ($5.3x10^{-5}$ - $3.5x10^{-15}$ M), and no spectral divergence was observed. The spectrum maintained its fine structure, with no significant shift in the wavelength of any of the band maxima, and no evidence for the appearance of unstructured single molecule bands, even at 10^{-15} M. This suggests that **(17)** is aggregating even at these extremely low concentrations. Detector limits prevented us from studying the excitation spectra below $3.5x10^{-15}$ M, so we were unable to obtain the spectrum for the single molecule. Similarly for the luminescence spectra, no spectral shifts were observed for N-HBC **(17)** in the concentration range studied ($1.4x10^{-6}$ – $9.7x10^{-14}$ M) in toluene.

HBC derivatives have a high polarisability. This, along with the small dipole moment of the large aromatic core, means dispersion interactions are the major contributors to the interaction energy between molecules. N-HBC **(17)** is considered to have a similarly high polarisability when compared to HBC derivatives with a similar sized aromatic core. In contrast however, **(17)** also has a permanent dipole moment, due to the electron-withdrawing properties of the pyrimidine nitrogens, suggesting a large electrostatic contribution to the dimer interaction energy. This, along with the large aromatic core, ensures extensive π-π overlap of neighbouring molecules in columnar stacks.

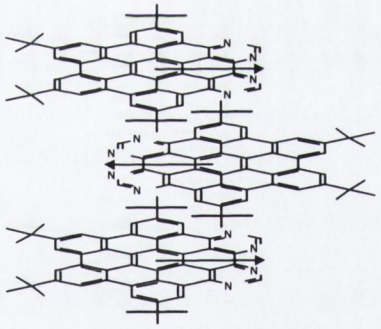


Figure 2.56. Dipole moment (arrow direction) and one orientation of the N-HBC **(17)** in H-aggregate form.

π-π Stacking to form face-to-face (H) or edge-to-face (J) aggregates is a well known and understood phenomenon.[73] Although the exact geometry of the nanoscaled aggregates is still under investigation, one suggestion is that each planar array is stacked on top of another with a rotation of 180°, in a staggered arrangement so as to maximize the overlap of the dipole's opposite charges, *e.g.* figure 2.56 for **(17)**.

The sharpening of an HBC aggregate absorption and fluorescence spectra is thought to show an increase in stack order.[30] It would follow that the sharp peaks obtained from

the absorption spectra of N-HBC **(17)** aggregates are also indicative of highly ordered stacks, which could follow through to the solid state.

The variation in molar absorptivity with concentration was measured for the $\pi \rightarrow \pi^*$ bands and for the bands with $n \rightarrow \pi^*$ character. Hypochromic deviations from Beer's law with increasing concentration were detected. These effects can be interpreted in terms of the self-association process.[59,74] The occurrence of hyperchromic and hypochromic effects can be analysed in terms of vertical and horizontal interactions, to elucidate the nature of the self-association process.

The existence of four nitrogen atoms in N-HBC, as compared to none in HBC, is likely to introduce modifications in the electronic structure. Therefore, N-doping of HBC would be expected to affect the aromaticity of the resulting N-HBC similar to the benzene/pyrimidine system.[59] This may also exert an influence on the self-association behaviour of this compound.

The spectrum of N-HBC in toluene shows two types of bands, the $\pi \rightarrow \pi^*$ bands at 339.0 nm, 355.0 nm, 393.0 nm, 414.0 nm, 452.0 nm, 481.5 nm and the $n \rightarrow \pi^*$ band at 376.5 nm. The band at 355 nm has some $n \rightarrow \pi^*$ character, as determined previously. The $n \rightarrow \pi^*$ band at 377 nm is relatively weak and partially submerged within the more intense $\pi \rightarrow \pi^*$ bands. Although with increasing concentration the component bands do not show significant shifts, the apparent molar absorptivity undergoes notable variations, supporting the assumption that self-association is taking place. In solution all bands show significant hypochromic deviations from the Beer law.

In figure 2.57, plots of the variation of molar absorptivity as a function of concentration for N-HBC in toluene are given, showing the hypochromic behaviour of the $\pi \rightarrow \pi^*$ bands, curves (a), (b), (d), (e), (f) and (g), and the $n \rightarrow \pi^*$ band, curve (c). These effects can be interpretated according to the theory of hypochromism.[74] For an absorbing chromophore the direction of the transition dipole moment is the direction in which the electrons are shifted in a spectral transition. The transition dipole moment of this chromophore will interact with the induced dipoles of the neighbouring chromophores, depending on their relative orientation.[74] If the dipoles are parallel and adjacent, a decrease in the intensity of the absorption band occurs, and hypochromism is observed. Conversely, if the dipoles are along the same axis and one behind the other, then the intensity of the absortion band is increased, and hyperchromism is observed.

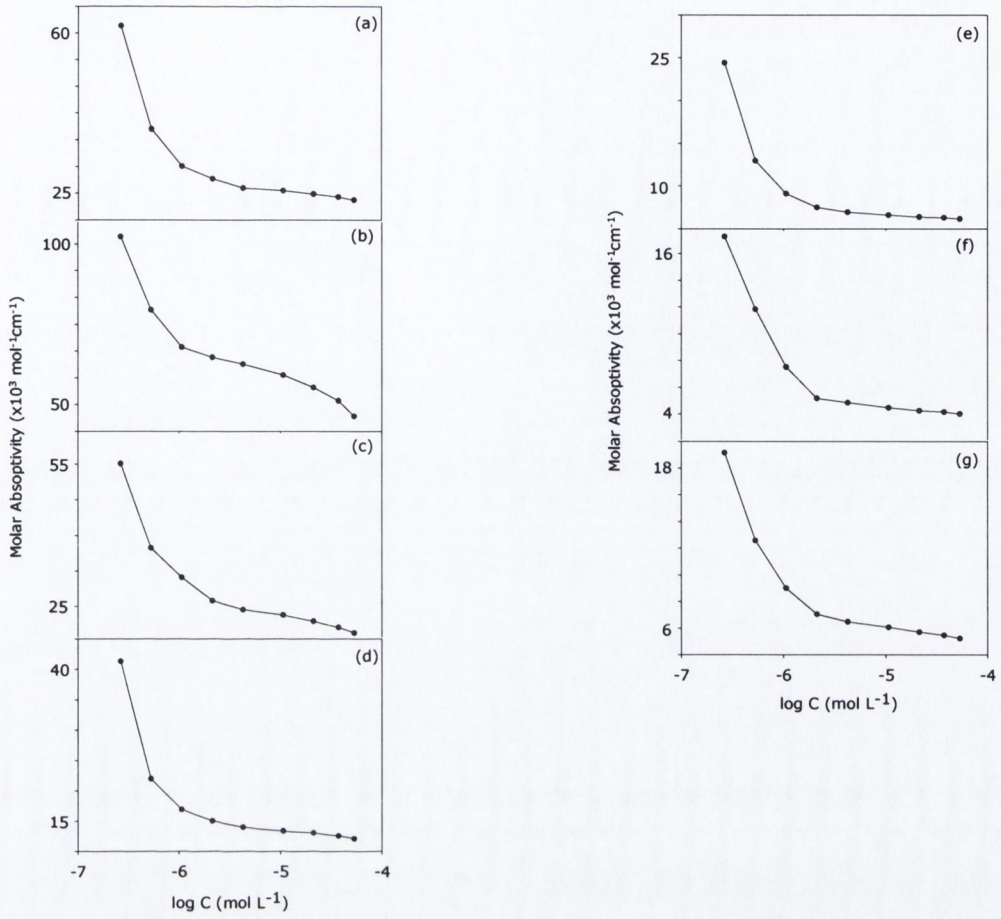
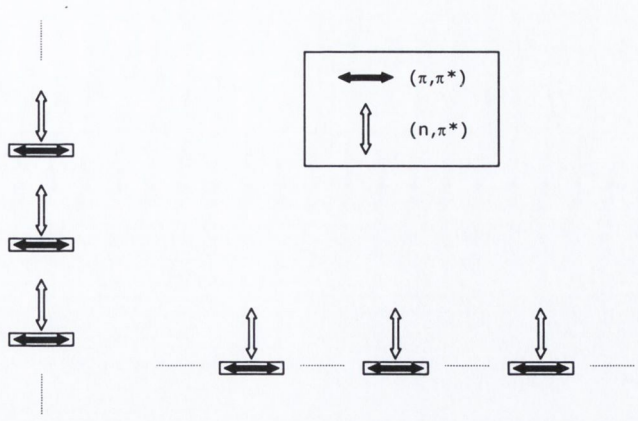


Figure 2.57. Hypochromic effects of the various absorption bands of N-HBC **(17)** in toluene, (a) 339.0, (b) 355.0, (c) 376.5, (d) 393.0, (e) 414.0, (f) 452.0 and (g) 481.5 nm.

According to the results above, hypochromic effects have been observed supporting the assumption of self-association in this molecule. We can interpret the mechanism of self-association in relation to "horizontal" (colinear), or "vertical" (stacked) molecular interactions. The $\pi \rightarrow \pi^*$ transitions have transition moments polarized in the plane of the molecules, whereas the $n \rightarrow \pi^*$ transition moments are polarized perpendicular to the base plane.[59] If the transition moments of the interacting groups are randomly orientated with respect to each other, there is no net-effect on the spectrum. If the aggregate contains colinear transition moments there will be an increase in absorption (hyperchromism), while parallel stacking of the moments will cause a decrease in absorption (hypochromism). Therefore, the vertical stacking of N-HBC will result in hypochromism for the $\pi \rightarrow \pi^*$ bands and hyperchromism for the $n \rightarrow \pi^*$ bands. A colinear interaction will show the converse (see figure 2.58). This type of hyperchromism, related to the self-association of heteroaromatics, was first detected through similar studies of pyrimidine in aqueous solution.[59]



(a) Vertical Stacking (b) Colinear Interaction

Figure 2.58. Models of association based on the alignment of transition dipoles of (π,π*) bands (black) and (n,π*) bands (unshaded).[59]

N-HBC **(17)** shows hypochromic effects in all the (π,π*) bands, which is compatible with the formation of vertical structures and the parallel stacking of the aromatic planes. This interpretation is consistent with the structure of heterosuperbenzenes, with their extensive conjugated system in which dispersion forces would be especially favoured. However, hypochromism is dominant at all wavelengths, and we do not see hyperchromism for the n→π* band at 377 nm. This could be because the effect on the n→π* band is relatively weak, or it could be involved in an interaction with the solvent molecules.

NMR spectroscopy has been used as an important tool to investigate the π-π aggregation of phenylacetylene macrocycles[75] and columnar structures formed by HBC derivatives in the solid state, and in solution.[4] For N-HBC **(17)** the downfield signals at δ 8.9 - δ 9.8, due to the aromatic protons of the compound clearly show the diatropic character of N-HBCs. For PAHs these chemical shifts are seen to originate from a complex interplay of aromatic core size, perimeter type and columnar aggregation. It was expected that the chemical shifts of N-HBC protons would show a similar dependence.

^{1}H NMR spectroscopy has been used in this work to qualitatively assess the influence of concentration and temperature on the aggregation of these aromatic compounds in solution. As depicted in figure 2.59 (a) and (b), by decreasing the concentration from 16.379x10^{-3} M to 0.819 x10^{-3} M we see shifts to lower field in the range of Δδ=0.20-0.32 ppm (see table 2.20) for the signals arising from the core protons. The largest shifts come from the protons between the pyrimidine nitrogens and on the ring adjacent, positions 19 and 16, respectively.

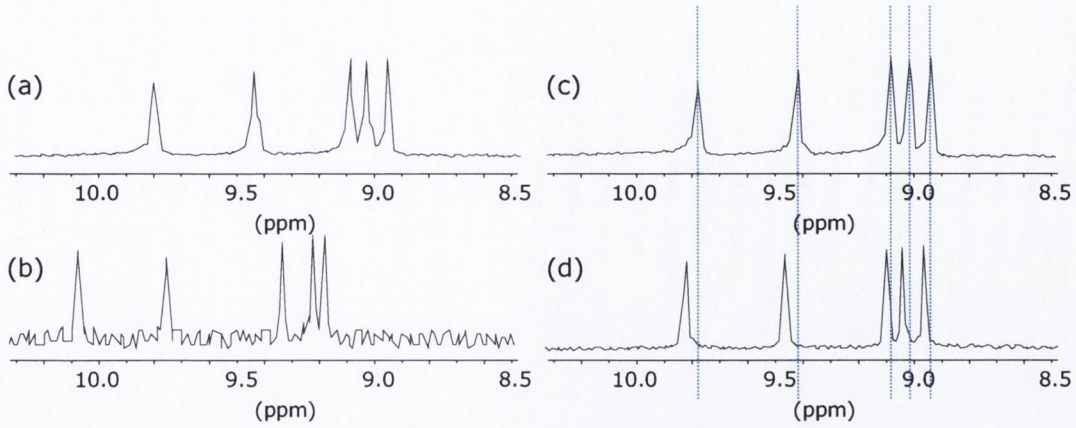


Figure 2.59. The aromatic region for the ^{1}H NMR spectra of N-HBC **(17)**, (a) 16.379x10^{-3} M, 30°C, (b) 0.819 x10^{-3} M, 30°C, (c) 16.379x10^{-3} M, 21°C, (d) 16.379x10^{-3} M, 40°C ($CDCl_3$, 400 MHz).

Concentration Dependence		Temperature Dependence			
16.379x10^{-3} M	**0.819 x10^{-3} M**	**21°C**	**24°C**	**30°C**	**40°C**
1.87	1.89	1.87	1.87	1.87	1.88
1.95	1.93	1.94	1.94	1.95	1.95
8.94	9.17	8.93	8.93	8.94	8.96
9.01	9.21	9.01	9.01	9.01	9.03
9.07	9.33	9.07	9.07	9.07	9.09
9.42	9.74	9.40	9.40	9.42	9.45
9.78	10.06	9.77	9.77	9.78	9.81

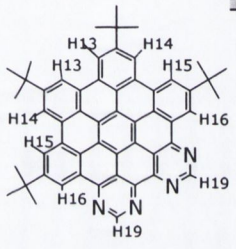


Table 2.20. ^{1}H NMR data for N-HBC **(17)** showing variations in chemical shift with concentration and temperature ($CDCl_3$, 400 MHz).

Less pronounced shifts are observed for the methyl protons of the *tert*-butyl side chains at δ 1.87 and δ 1.95. The shifts observed here, for varying concentrations of N-HBC **(17)**, are of similar magnitude to the downfield shifts published for the all-carbon derivatives.[4] Likewise, we can attribute these downfield shifts to a decrease in aggregation number with decreasing concentration.

Similar shifts to lower fields are observed with increasing temperature (for a constant concentration). Shifts of up to 0.05 ppm were seen even over the very small temperature range used in this work (21-40°C). These shifts are again attributed to a decrease in aggregation number with increasing temperature.

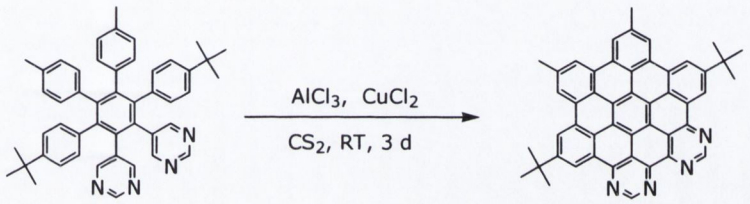
The above shifts of the aromatic protons are all explained by the intermolecular stacking interaction of the aromatic core of N-HBC, as observed for other molecules containing delocalised π-ring systems.[4]

2.2.7 CYCLODEHYDROGENATION TO N-HETEROSUPERBENZENE DERIVATIVES

As the first member of the N-heterosuperbenzene family, **(17)** has shown interesting properties such as enhanced solubility, high fluorescence yields and the tendency to aggregate at even low concentrations. It was the aim of this thesis not only to prepare **(17)**, but to extend the synthesis route to produce a family of N-HBC molecules. Some progress has been made in this regard.

2.2.7.1 Synthesis of N-HBC (21)

Following the conditions established in the synthesis of N-HBC **(17)**, the oxidative cyclodehydrogenation of **(20)** generated the N-functionalized heterosuperbenzene, **(21)**, figure 2.60.



(20) **(21)**

Figure 2.60. The synthesis of N-HBC **(21)**, *via* the cyclodehydrogenation of **(20)**.

N-HBC **(21)** was purified by chromatography, and extracted into $CHCl_3$. The solid was washed with 10% HCl solution, water, 10% NH_4OH solution, water, and diethyl ether, and dried *in vacuo* to afford **(21)** as a red/brown powder in a 30% yield.

It was immediately apparent that there was a huge decrease in the solubility of **(21)** compared to its precursor **(20)** and to N-HBC **(17)**. The replacement of two of the four *tert*-butyl groups with methyl groups, in conjunction with the four peripheral nitrogen atoms of **(21)**, provides only sparing solubility in toluene and chlorinated solvents such as chloroform. Several attempts to obtain NMR data on N-HBC **(21)** were unsuccessful due to its poor solubility in the wide range of deuterated solvents tried. Similar to many of the all-benzenoid HBC derivatives reported in literature, insufficient solubility has prevented a comprehensive characterization of **(21)**.[3,9] For this reason, and in conjunction with the analysis of HBC derivatives, mass spectrometry and accurate mass analysis was used to provide reliable proof of the synthesis of N-HBC **(21)**.

Mass spectrometry and accurate mass analysis give consistent results and are in full accord with the theoretically expected values. The ESI-mass spectrum of heterosuperbenzene **(21)** in toluene (figure 2.61) shows the isotopic distribution pattern for the $[MH]^+$ ion at 667.0.

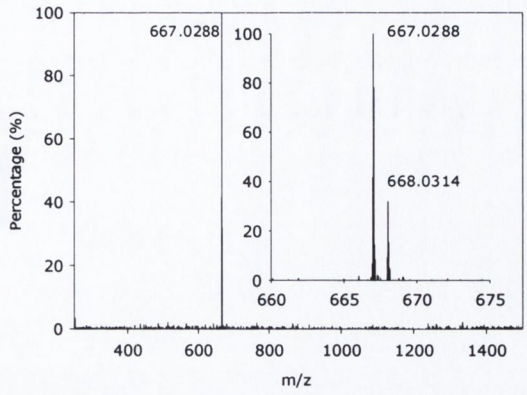


Figure 2.61. The ESI-mass spectrum of heterosuperbenzene **(21)** in toluene.

There is no mass spectral evidence for the formation of higher mass species of **(21)** in toluene solutions. The ESI-mass spectrum also gave an indication of the purity of the N-heterosuperbenzene sample, as it was the only signal observed.

Again, it was not possible to obtain elemental analysis of **(21)** due to the extremely high thermal stability of the aromatic core, and incomplete combustion in the analysis. An accurate mass spectrum was obtained for **(21)**, in toluene, as a non-invasive method of mass analysis. The result gave a $[C_{48}H_{35}N_4]^+$ peak of 667.2915, correct to within 8 ppm for that calculated.

2.2.7.2 Photophysical Properties of N-HBC (21)

As the second member of the N-heterosuperbenzene family, it is interesting to compare the optical behaviour of N-HBC **(21)** with the established N-HBC **(17)**. Therefore, the UV-vis absorption and emission spectra of N-HBC **(21)** were measured in solution, and compared to compound **(17)**.

The UV-vis absorption spectrum of **(21)** bears a marked similarity to the parent N-heterosuperbenzene compound, as shown in figure 2.62. Again a highly structured electronic absorption spectrum is obtained, with only small shifts to the peak maxima.

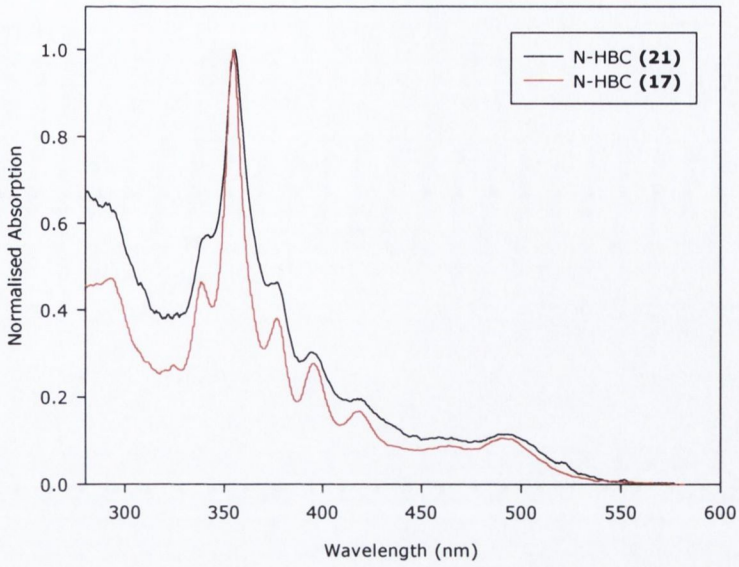


Figure 2.62. The normalized absorption spectra of N-HBCs **(17)** and **(21)** in chloroform.

Although broadening has occurred, the line shape typical of an N-HBC UV-vis spectrum is reproduced by N-HBC **(21)**. The slight chemical modification at the periphery of the N-HBC chromophore results in only minor shifts of the peak maxima (see table 2.21).

Compound	**Wavelength (nm)**							
N-HBC **(21)**	281.0	342.0	355.5	375.5	394.5	418.0	459.0	496.0
N-HBC **(17)**	292.0	339.0	354.5	376.5	395.0	418.5	463.5	493.5

Table 2.21. Peaks for the absorption bands for N-HBCs **(21)** and **(17)** in chloroform.

Shifts of 1-3 nm are seen for the main absorption bands of **(21)**, and there are no additional or missing bands, as expected due to the small modification at the periphery. The UV-vis spectrum of N-HBC **(21)** has a λ_{max}=355.5 nm, which is slightly red-shifted by 1.0 nm in comparison to N-HBC **(17)**. The band at 376.5 nm for **(17)**, not found in analogous all-carbon derivatives, is again present in **(21)** although blue-shifted by 1.0 nm. It is assumed that this band, as it is in **(17)**, is an $n \rightarrow \pi^*$ transition of **(21)**. Again, the α-bands, toward the red end of the spectrum at 418, 459 and 496 nm, are prominent, as they are in N-HBC **(17)**, as C_{2v} symmetry is maintained. Presumably the band at 496 nm is the (0,0) transition, formally forbidden in D_{6h} symmetry, and which is not usually seen for the all-carbon derivatives. N-HBC **(21)** has a molar extinction coefficient of 12300, which is a ten-fold decrease in molar absorptivity when compared with **(17)**.

In toluene the absorption spectrum of **(21)** is considerably broadened and the bands less well-defined. The λ_{max} (356 nm) is little affected by the change of solvent from

chloroform to toluene. Broadening of the electronic spectra in both chloroform and especially toluene may indicate an increase in the ratio of monomers of **(21)** in solution to aggregates. This is confirmed by the bi-exponential fluorescence decay observed for **(21)** (see table 2.22) and may also explain the reduction in molar extinction coefficient for **(21)**.[64]

The emission spectrum of N-HBC **(21)** was obtained in chloroform (figure 2.63) and, like **(17)**, the corrected emission was independent of the wavelength of excitation.

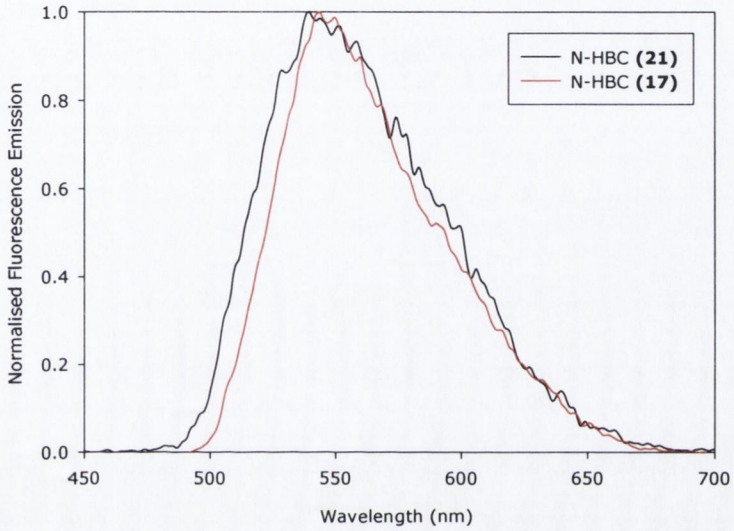


Figure 2.63. The normalized fluorescence spectra of N-HBCs **(17)** and **(21)** in chloroform.

The emission of N-HBC **(21)** has a λ_{max} at 539 nm in chloroform and a quantum yield of 0.19. This band is diffuse and blue-shifted by 4.5 nm compared to the emission produced by **(17)** in chloroform.

Compound	λ_{max} (nm)	ϕ_F	τ (ns)
N-HBC **(21)**	539.5	0.19	9, 22
N-HBC **(17)**	544.0	0.21	12

Table 2.22. Fluorescence data of N-HBCs **(21)** and **(17)** in chloroform.

A decrease in the stabilization energy of the charge transfer state would imply a smaller dipole moment in the excited state. However, this shift is extremely small (154 cm^{-1}), suggesting that the charge transfer state of **(21)** has a similar dipole moment to that of **(17)**, which interacts to a similar extent with the polar chloroform solvent. The quantum yield of **(21)** is slightly less than that of **(17)**. The bi-exponential fluorescence decay observed for **(21)** in $CHCl_3$ is thus assigned as the emission from

the aggregate (9 ns) and emission from the monomer (22 ns) (table 2.22), similarly to HBC derivatives reported in literature.[64] This is different to the single-exponential fluorescence decay observed for **(17)** suggesting that **(21)** has a different aggregation behaviour to that of **(17)**.

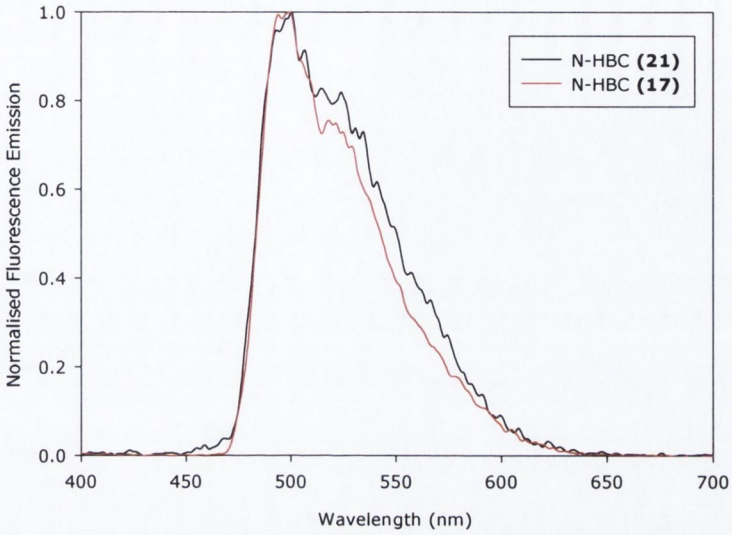


Figure 2.64. The normalized fluorescence spectra of N-HBCs **(17)** and **(21)** in toluene.

In toluene, N-HBC **(21)** is characterized by two emission bands (see figure 2.64), with maxima at around 500 nm and 520 nm. This is also very similar to N-HBC **(17)**, however the broadness of the emission peaks makes it difficult to determine the exact peak maxima.

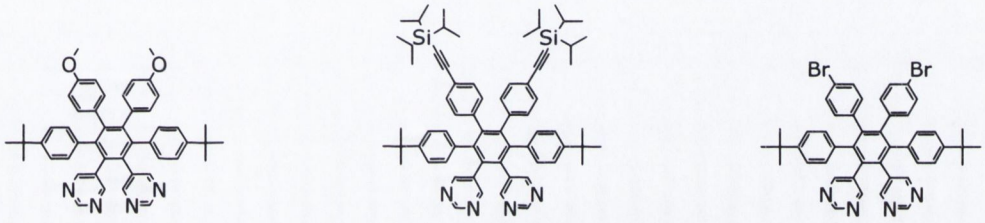
There is a large shift in the absorption maximum from around 500 nm in toluene, to 540 nm in chloroform. The large spectral shift is again attributed to the presence of a partial intramolecular charge transfer in the excited state. Again, these results emphasise the effect of the dipolar donor-acceptor structure of the N-HBC chromophore on its optical response, features which allow the control of the emission wavelength *via* the electron-donating ability of the R group. Larger shifts in the emission spectra are thus expected with more dramatic electronic changes in the R groups at the periphery.

The addition of trifluoroacetic acid to N-HBC **(21)** in toluene or chloroform had the same fluorescence quenching effect as it did on N-HBC **(17)**. This is not surprising on considering that the structural and optical properties of the two N-HBCs are so similar. In fact it is surprising that changing two of the peripheral *tert*-butyl groups to methyl substituents has had such a profound effect on the solubility of the N-heterosuperbenzene. It was found that although **(21)** was only sparingly soluble in chloroform, it was mostly insoluble in deuterated chloroform, suggesting that hydrogen-bonding plays a substantial role in solubility. Interestingly, **(17)** showed a

large increase in solubility in toluene when a small percentage of methanol (1%) was added to the solvent mix, even though the N-HBC is only sparingly soluble in methanol alone, indicating the importance of solvent polarity and perhaps hydrogen-bonding in the dissolution of N-HBCs.

2.2.7.3 Attempted Cyclodehydrogenation of (23), (29) and (31) to N-HBC

The N-HBC compounds are formed when cyclodehydrogenation is undertaken of the precursor so as to "close" the rings and flatten the system. Attempts have been made to transform the functionalized hexaarylbenzenes **(23)**, **(29)** and **(31)** into the corresponding N-HBC derivatives by applying the oxidative cyclodehydrogenation conditions ($AlCl_3/CuCl_2$ in CS_2) suitable for synthesizing the alkyl-substituted N-HBC derivatives, **(17)** and **(21)**.



(23) **(29)** **(31)**

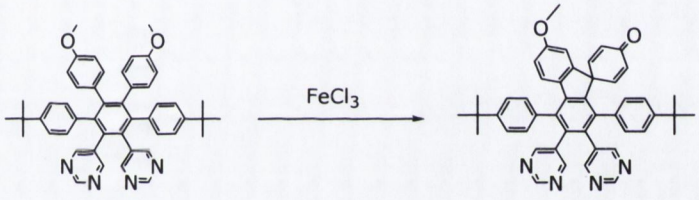
Figure 2.65. Hexaarylbenzenes for oxidative cyclodehydrogenation.

Attempts to perform analogous oxidative cyclodehydrogenation of the above N-doped polyphenylenes (**(23)**, **(29)** and **(31)**) led, in most cases, to insoluble, and uncharacterisable black solids. Unfortunately, Lewis acids, in addition to favouring the oxidative cyclodehydrogenation of suitable oligophenylenes, also promote the reverse Friedal-Crafts alkylation.[3,9,48] Thus, under aluminium(III) chloride catalysis, dealkylation, migration of the alkyl side chain, or even chlorination of the aromatic system are prominent processes that may occur.[9] Due to HCl formation in the course of the reaction, chlorinated, cyclised products are invariably obtained.[9] All of these factors are thought to have contributed here. We have seen the pronounced influence that changing the *tert*-butyl groups of N-HBC **(17)** to the methyl groups of **(21)** had on the solubility of the N-HBC derivative. It is believed that dealkylation in the above cases is having a severe effect on the solubility, resulting in uncharacterisable black solids.

Although the reaction of the bromo-substituted hexaphenylbenzene under these oxidative conditions failed to yield the desired product, analysis of the reaction mixture was more encouraging. According to mass spectral analyses of the soluble fractions of the product mix, partially cyclised products were formed. This was found similarly by

Müllen *et al.*[48] when applied to their bromo-substituted all-carbon hexaphenylbenzenes. They had more success with iron(III) chloride. By analogy the addition of an iron(III) chloride solution in nitromethane to a solution of the bromo-substituted precursor in dichloromethane, and purging out the HCl evolved during the course of the reaction, was expected to prevent the formation of mixtures of N-HBC derivatives and chlorinated by-products; however, after quenching with methanol, this route led only to the return of the hexaarylbenzene starting material. A similar negative result was obtained under the iron(III) chloride reaction conditions for the N-doped polyphenylene **(29)**, with the formation of various dealkylated hexaarylbenzenes. Interestingly, when these same conditions were applied to the N-doped polyphenylene **(16)**, the corresponding N-HBC derivative **(17)** was produced, but in a much reduced yield, possibly suggesting that the milder conditions of oxidative cyclodehydrogenation obtained with iron(III) chloride are less efficient for these systems.

An interesting result was obtained, however, when the iron(III) chloride conditions were applied to the N-doped polyphenylene **(23)**. The product isolated was not the expected N-HBC derivative, but the spirocyclic dienone **(24)** (see figure 2.66).



(23) **(24)**

Figure 2.66. Reaction of N-doped polyphenylene **(23)** under milder cyclodehydrogenation conditions.

Attempts to perform the cyclodehydrogenation of **(23)** under $AlCl_3$ and $CuCl_2$ in CS_2 resulted in unidentified product mixtures because of the inherent high acidity of the reaction mixture. The use of iron(III) chloride was employed under significantly milder conditions without side reactions (such as alkyl group migrations or chlorinations). Hydrogen chloride was continuously removed from the reaction mixture by a steady flow of argon. Quenching the reaction with methanol, followed by column chromatography, yielded a white solid. Recrystallization from dichloromethane:hexane 1:1, gave colourless crystals, suitable for X-ray diffraction. Under these conditions **(24)** was obtained in an 86% yield.

Methoxy substituted aromatic compounds have resulted in similar products under such oxidative dehydrogenation conditions, *e.g.* in the formation of alkoxytriphenylenes *via* the coupling of biphenyl and benzene derivatives, spirocyclic dienones are obtained.[19]

NMR spectroscopy was the first indication of incomplete cyclisation. The loss of the C_{2v} symmetry axis was immediately evident in the ^1H NMR spectra. Figure 2.67 shows the aromatic region of the ^1H NMR spectra for (a) **(23)** where C_{2v} symmetry holds, and (b) **(24)** where loss of symmetry is seen through an increase in the number of proton signals.

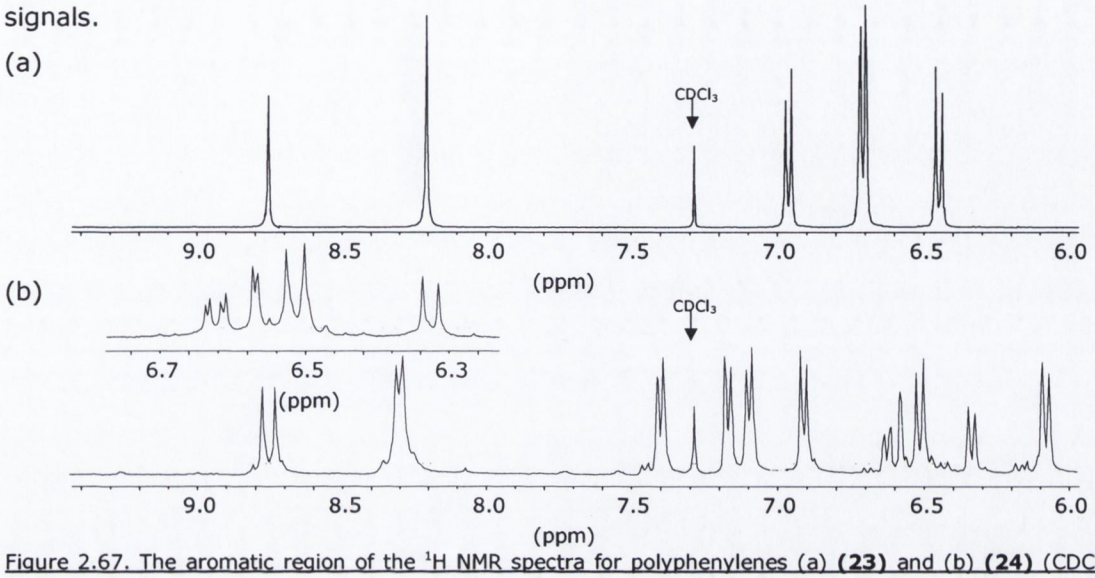


Figure 2.67. The aromatic region of the ^1H NMR spectra for polyphenylenes (a) **(23)** and (b) **(24)** ($CDCl_3$, RT, 400 MHz).

For **(24)** we see two peaks for the chemically distinct aromatic protons of the pyrimidine rings at positions 1 and 13 (in the region of δ 8.8), and two peaks for the chemically distinct aromatic protons on the pyrimidine rings at positions 2 and 12 (in the region of δ 8.3) (see atom labelling scheme, figure 2.68). This is due to loss of the C_{2v} symmetry in **(24)** through the formation of the 5-membered ring as shown in figure 2.68.

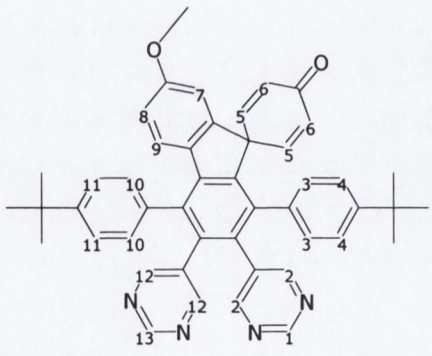


Figure 2.68. Atom labelling scheme for **(24)**.

The three proton system at positions 7, 8 and 9 in the atom labelling scheme show well resolved coupling information in the ^1H NMR spectrum, which allows the precise assignment of these signals. Vicinal coupling ($^3J_{HH}$=8.52 Hz) between signals at δ 6.62 and δ 6.32 allows the assignment of protons at positions 8 and 9. The long-range coupling ($^4J_{HH}$=2.52 Hz) between protons at positions 7 and 8 is also evident in the signals at δ 6.62 and δ 6.57.

This allows the unambiguous assignment of proton resonances at positions 7, 8 and 9 as ^1H NMR signals δ 6.57, δ 6.62 and δ 6.32, respectively. All other aromatic signals (positions 3-4 and 10-11) as well as the quinone type resonances (positions 5-6) appear as doublets of integal two.

The ESI-mass spectrum of **(24)** in toluene shows the isotopic distribution pattern for the $[MH]^+$ ion at 695.3. The presence of Na^+ ions produces the isotopic distribution pattern for the $[MNa]^+$ ion at 717.2. An envelope at 1390.5 is assigned to the bimolecular ion $[M_2H]^+$. This may give support for the existence of dimers of **(24)** in toluene solutions. No other peaks were observed in the mass spectrum. The accurate mass spectrum obtained for **(24)** in acetonitrile gave a peak of 695.3411 $[C_{47}H_{43}N_4O_2]^+$, correct to within 5 ppm for that calculated.

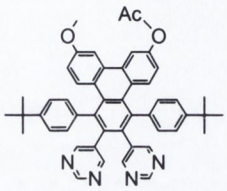


Figure 2.69. Expected result through dienone/phenol rearrangement.

It is expected that a dienone/phenol rearrangement[19] may allow the formation of the partially cyclised compound of figure 2.69, by heating **(24)** in acetic anhydride/concentrated sulfuric acid. This may provide a route to site-specific cyclodehydrogenation. The spirocyclic compound **(24)** is also interesting in itself. The 6,5,6 membered ring system is actually a dienone and could lead to further strategic substitutions and new systems which incorporate a 5-membered ring, *via* a cycloaddition reaction with an appropriate diene.

Colourless crystals of **(24)**, suitable for X-ray crystallographic structure analysis, were obtained from dichloromethane/hexane. The spirocyclic compound crystallised in the space group P-1, and the structure was refined to give an R_1 value of 15.97%. The crystallographic data is given in table D in Appendix 1. The four outer phenyl rings at carbon positions C1, C2, C3 and C6 are free to rotate about their carbon-carbon single bonds to the central phenyl unit. In the molecular structure of **(24)**, these rings are practically orthogonal to the central phenyl unit (average twisting angle of 85°), see figure 2.70. This is in contrast to the regular propeller arrays adopted by the polyphenylenes (see **2.2.2.4**), which have approximate interplanar angles of only 67° between the outer phenyl groups and the central ring. The spirocyclic forms a flat 6,5,6 membered ring system with the cyclohexa-2,5-dienone unit orthogonal at carbon C25. The poorly refined nature of the structure has not allowed a comprehensive investigation of the intermolecular interactions. Another data collection may be necessary to gain further insight into these interactions.

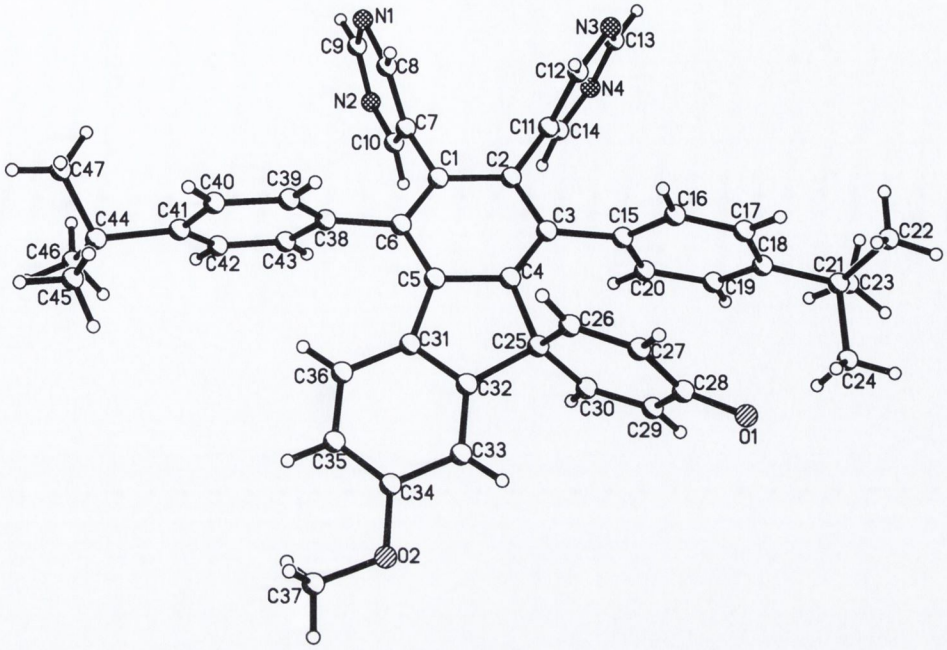


Figure 2.70. The X-ray crystal structure of spirocyclic compound **(24)** showing one of the two enantiomeric forms of the unit cell (the other enantiomer and solvent have been removed for clarity).

2.2.7.4 Photophysical Properties of Spirocyclic (24)

The UV-vis spectrum of spirocyclic compound **(24)** can be compared to polyphenylene **(23)**. The spectra are shown in figure 2.71.

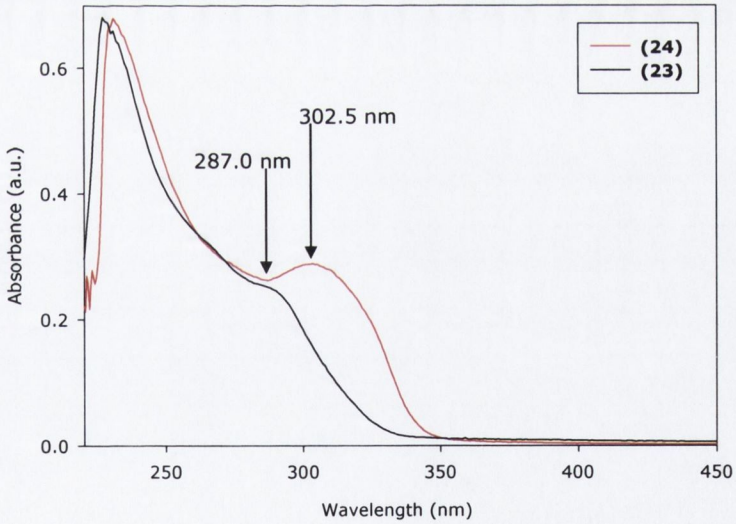


Figure 2.71. The absorption spectra of polyphenylene compound **(23)** and spirocyclic **(24)** in dichloroethane.

The absorption spectrum of the spirocyclic dienone **(24)** shows a red-shift of 15.5 nm to 302.5 nm, and an increase in molar absorptivity from 22×10^3 to 27×10^3 L mol^{-1} cm^{-1}. Both effects are believed to be due to the increased conjugation of **(24)**.

2.3 SUMMARY

The synthesis of molecules having unusual electronic properties has been a continuing goal in chemistry. At present organic semiconductors are often extrinsically 'doped' *via* chemical oxidation or reduction to enhance their conducting properties. This process is often unselective and leads to unstable materials, which, despite having desirable electronic properties, suffer from huge processing problems. The research presented here provides an alternative means to doping soft organic materials *via* nanoscale, controlled intrinsic doping. This process provides far more stable materials with more defined electronic properties. The value of N-incorporation into polyaromatic hydrocarbon systems has been proven through the isolation and spectroscopic characterization of the first N-functionalized heterosuperbenzene **(17),** a nitrogen-doped analogue of molecular graphite.

The synthetic routes to produce N-doped graphite analogues have been established in this work, which builds on the known stereochemistry associated with [2+4]-cycloadditions and oxidative cyclodehydrogenation reaction using $AlCl_3$ and $CuCl_2$.

N-HBC **(17)** formally combines superbenzene and bipyrimidine and experimentally exhibits desirable properties of both. The enhanced π-electron mobility of **(17)** is evident from the polar nature of the molecule, which support structurally opposing electronegative nitrogen atoms and weakly donating *tert*-butyl groups. As important characteristics dramatically enhanced solubility and processability are imparted when *tert*-butyl groups and pyrimidine nitrogen atoms are positioned at the periphery of the hexabenzocoronene. Cyclic voltammetry experiments on N-HBC **(17)** show an increase in the ease of reduction, further demonstrating the electron acceptor properties of the N-doped derivative.

Both the absorption and emission features of the donor-acceptor molecule **(17)** are presented. The absorption and emission spectra are in general similar to HBC, except for large solvent induced shifts. Differences can be explained by the presence of additional excited states introduced by the nitrogen substituents. The fluorescence spectra of these compounds in a polar solvent relative to that in a nonpolar solvent are more diffuse and red-shifted. The fluorescence spectrum shows some fine structure in the nonpolar solvent hexane with a small Stokes' shift (1.5 nm). In more polar solvents there is little overlap between the absorption and emission spectra. It is probable that these solvent effects are produced by an interaction between the dipole moment of the solute and solvent. The unstructured nature of the band suggests strong interaction between the solvent and the polarized compound in the excited state. The appropriately shifted emission peak in solvents of different polarity have been

described and the magnitude of the red-shift related to the electron-withdrawing character of the pyrimidine nitrogens, and the charge transfer character of the excited state (large (μ_e) value). The bathochrome effect observed is attributed to an internal extended π-electronic conjugation between the donor *tert*-butyl groups and the nitrogen acceptor nuclei. Solvatochromic studies were performed, in order to determine the changes in dipole moments under excitation.

Addition of trifluoroacetic acid to toluene solutions of **(17)** causes strong changes in the absorption and fluorescence spectra. The low energy absorption bands move to the red, and the intensity of the structured, short-lived $^1(\pi,\pi^*)$ fluorescence band decreases and a new unstructured shorter-lived fluorescence band arises at longer wavelength.

Organic polymers and conjugated molecular systems have made an impression recently as photo- and electro-luminescent materials for optical technologies.[76] Although most of the well-developed systems are red to green light emitting materials based on polyphenylene and polyfluorene conjugated systems, N-HBC **(17)** may contribute as a blue-green emitting material with extremely high thermal stability.

The aggregation of N-HBC **(17)** was investigated. The electronic spectra of **(17)** were studied over a wide concentration range ($5.3x10^{-5}$ - $3.5x10^{-15}$ M), and no significant shifts of the absorption bands or changes to the fine structure were observed. N-HBC **(17)** did not exhibit any spectral divergence down to the lowest concentration studied here ($3.5x10^{-15}$ M), suggesting that it is aggregating even at these low concentrations. NMR studies and molar absorptivity changes reinforce the belief that these systems spontaneously aggregate.

The combination of the highly coordinating bipyridyl functionality and the extended conjugation, through the π-electron system, provides a unique family of tunable intrinsic fluorophores, where changes in the electronic polarization, solvation and coordination (Chapter 3) are translated into dramatic spectral changes. The simple synthesis together with the availability of numerous precursors and cross-coupling methodologies make the preparation of other N-HBC chromophores with diverse absorption and emission characteristics possible. I have presented my synthetic contribution toward the establishment of a host of heterosuperbenzenes (N-HBC) with intrinsic carbon-nitrogen frameworks.

The members of this new heterosuperbenzene family are molecular models of active graphitic nanostructures with electroactive nitrogens on the periphery. The

incorporation of nitrogen within the carbon framework renders these materials sensitive toward external triggers and enhances solubility. These N-HBC systems consist of donor and acceptor end groups, D and A, connected by an unsaturated conjugated unit, highly delocalised molecular orbitals and relatively small energy separation between ground and the excited states. Excitation of these molecules from their ground states results in the appearance of very strong absorption bands, a redistribution of electronic charge within the molecule, and a change in the molecular dipole moment. This would give the systems interesting Non-Linear Optical (NLO) properties.[77] As well as this, active soft materials are also making their presence felt in the form of polymer and organic light emitting diodes, stable electrically conducting polymers, liquid crystals and high speed polymer electrooptic signal modulators already used in electronics, display and telecommunications.[78] In the context of LED applications, the systematic replacement of carbon atoms with electronegative nitrogen atoms is expected to enhance the carrier transport of the system. There is a paucity of processable forms of electron-acceptor materials with the desired thermal stability. Our N-heterosuperbenzenes offer a significant advance in this regard.[47]

In the context of this work, there is still a large amount of research required to produce useable forms of conducting soft materials (especially nanometric materials). The main issue addressed here is how to control structural parameters at the molecular level. Carefully designed chemical synthesis is the most promising way to achieve this since it offers the ability to tailor electronic properties with complete control at a molecular level.

In conclusion the essential steps in the formation of intrinsically nitrogen-doped graphite nanostructures in a controlled and systematic manner have been proven. The presence of pyrimidine nitrogen atoms has rendered overall electron-accepting properties to **(17)** compared to its all-carbon analogue. The preliminary emission studies undertaken on **(17)** suggest that the opto-electronic properties of this emerging heterosuperbenzene family will be promising. Synthetic control, such as demonstrated here, allows molecular tuning of the opto-electronic properties of the resultant material and provides the potential for ligand-based functionality.

2.4 FUTURE APPLICATIONS

The synthetic strategy introduced in this work opens up possibilities in the development of the N-heterosuperbenzene family. With the synthesis and characterization of N-HBCs **(17)** and **(21)** proven, there is still much investigation to be carried out into the physical properties of these novel N-HBC materials and in the synthesis of further N-HBC derivatives. Although the electronic absorption and emission characteristics of the N-HBCs discovered in this work are promising, investigation into the triplet state emissions have yet to be explored. The charge carrier mobility rate, ordering of two-dimensional crystals (investigated by scanning tunnelling microscopy), the discotic liquid crystalline mesophase (measured using differential scanning calorimetry), the stacking pattern (measured through X-ray investigations), the non-linear optics, and the alignment of the N-HBC derivatives under the influence of a magnetic field, are all physical properties which need to be investigated further. It may also be interesting to link an all-carbon HBC derivative covalently to N-HBC **(17)** and spectroscopically examine for single-molecule energy transfer.[79]

The emission characteristics of the various polyphenylene compounds **(10)**, **(16)**, **(20)**, **(23)**, **(29)**, **(31)**, **(32a)** and **(32b)** should also be investigated. Being nonplanar and of reasonably low symmetry in the S_0 ground state, if they become increasingly planar in the S_1 excited state, they could make effective fluorescent dyes to be used in dye lasers.

The significant advantage of the synthetic strategy is that it allows flexibility and discrete control at a molecular level, and therefore the further development of the N-HBC family. From a synthetic chemist's view-point, it offers considerable scope for the synthesis and characterization of various functionalized N-heterosuperbenzenes. Complexation of the peripheral pyrimidine nitrogens could produce metal complexes with interesting properties. Palladium mediated cross-coupling reactions using the activated polyaryl bromide derivative **(31)** could be used to functionalize the polyphenylene further, for example bulky water soluble units could be attached in an attempt to induce water solubility. The pendant alkynyl groups, protected from initial cyclisation using triisopropylsilyl groups, have been shown to survive the reaction conditions of the [2+4]-cycloaddition reaction and to yield polyphenylene **(29)**. These groups can be subsequently deprotected for further functionalization.

The position of the heteroatom in the pyridyl moiety (1,2-, 1,3- or 1,4-) could be altered systematically. This permits a detailed study into the relationship between the position of the dopant N atom and the resultant electronic properties of the material. In addition the synthetic strategy proposed allows control of the number of N-dopant

atoms, *e.g.* alkynes incorporating pyrimidine, quinoline or phenanthroline could be used. It may also be possible for some of these alkynes to undergo cyclotrimerisation under metal catalysis as a quick and convenient route to N-doped polyphenylenes.

An alternative route to introduce the N-dopant is to incorporate the N atoms in the cyclopentadienone rather than (or as well as) the alkyne. α,β-Diketones may be formed from dipyridyl (or dipyrimidyl) alkynes using I_2 in DMSO,[80] which in turn will generate the desired dipyridyl (or dipyrimidyl) diphenyl cyclopentadienone. A combination of dipyrimidine acetylene with pyrimidyl cyclopentadienones should result in up to 8 N-donor atoms being introduced into the graphitic sheet. In each case only one isomer is generated due to the stereochemistry associated with the [2+4]-cycloaddition reaction. Thus the complexity of the system can be controlled in a systematic manner.

The key features (fused ring rigidity, aromaticity, and N—heteroatoms) could be incorporated into a new series of polyheterocyclic-C,N molecules which could be developed as molecular models of active fullerene substructures with a corannulene core and electroactive nitrogens on the periphery.

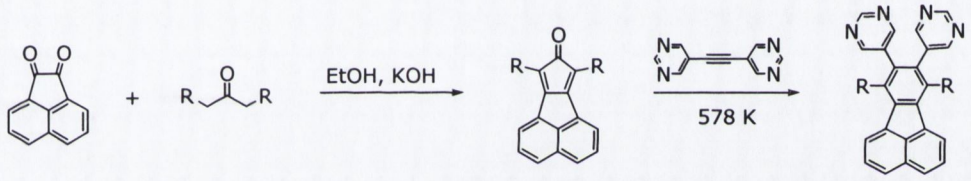


Figure 2.72. Incorporation of corannulene into the polyaryl benzene.

The incorporation of corannulene into the core of polyaromatic superbenzenes has not been investigated, yet it offers the distinct advantage of 3-D curvature. The extension of the synthetic strategy used in this work could be used to build corannulene supported materials (figure 2.72) which, after cyclodehydrogenation, may act as building blocks for larger fused-ring heterocyclic systems and allow access to a range of non-planar curved aromatics.

N-HBCs may find use in solubilising single-walled carbon nanotubes (SWNTs) *via* a *nonwrapping* approach. The solubilisation of SWNTs *via* a π-π stacking interaction between short, rigid, conjugated polymers, poly(aryleneethynylene)s (with backbone lengths less than 15 nm) and the nanotube surface, have led to the highest reported solubility of SWNTs. This occurs by mixing the polymer with the SWNTs in chloroform, followed by shaking and bath-sonication.[81] The highly soluble material N-HBC **(17)** would be expected to form strong π-π interactions with the SWNT surface and increase the solubility and processability of these important materials.

2.5 REFERENCES

1. F. Morgenroth, E. Reuthler, K. Müllen, *Angew. Chem., Int. Ed. Engl.*, **1997**, *36*, 631-634
2. R. Boese, A. Matzger, D. Mohler, K. P. C. Vollhardt, *Angew. Chem., Int. Ed. Engl.*, **1995**, *34*, 1478-1481
3. (a) M. Müller, C. Kübel, K. Müllen, *Chem. Eur. J.*, **1998**, *4*, 2099-2109; (b) A. Thünemann, D. Ruppelt, S. Ito, K. Müllen, *J. Mater. Chem.*, **1999**, *9*, 1055-1057
4. A. Fechtenkötter, N. Tchebotareva, M. D. Watson, K. Müllen, *Tetrahedron*, **2001**, *57*, 3769-3783
5. P. T. Herwig, C. W. Kayser, K. Müllen, H. W. Spiess, *Adv. Mater.*, **1996**, *8*, 510-513
6. (a) M. Müller, V. Iyer, C. Kübel, V. Enkelmann, K. Müllen, *Angew. Chem., Int. Ed. Engl.*, **1997**, *36*, 1607-1610; (b) V. Iyer, K. Yoshimura, V. Enkelmann, R. Epsch, J. Rabe, K. Müllen, *Angew. Chem., Int. Ed. Engl.*, **1998**, *37*, 2696-2699
7. E. Clar, C. Ironside, M. Zander, *J. Chem. Soc.*, **1959**, *81*, 142-147
8. W. Hendel, Z. H. Khan, W. Schmidt, *Tetrahedron*, **1986**, *42*, 1127-1134
9. V. Iyer, M. Wehmeir, J. D. Brand, M. Keegstra, K. Müllen, *Angew. Chem., Int. Ed. Engl.*, **1997**, *36*, 1604-1607
10. W. Reid, D. Freitag, *Angew. Chem., Int. Ed. Engl.*, **1968**, *7*, 835-845
11. J. Sauer, R. Sustmann, *Angew. Chem., Int. Ed. Engl.*, **1980**, *19*, 779-807
12. R. B. Woodward, F. Sondheimer, D. Taub, K. Heusler, W. M. McLamore, *J. Am. Chem. Soc.*, **1951**, *73*, 2403-2404
13. G. Stork, E. F. van Tamelen, L. J. Friedman, A. W. Burgstahler, *J. Am. Chem. Soc.*, **1951**, *73*, 4501-4501
14. F. Fringuelli, A. Taticchi, in *Dienes in the Diels-Alder Reaction*, John Wiley & Sons, **1990**
15. L. Fieser, *Org. Synth.*, **1966**, *46*, 44-47
16. K. P. C. Vollhardt, *Angew. Chem., Int. Ed. Engl.*, **1984**, *23*, 539-644
17. A. Brown P. Edwards, *Tetrahedron Lett.*, **1990**, *31*, 6581-6584
18. P. Magnus, J. Schultz, T. Gallagher, *J. Am. Chem. Soc.*, **1985**, *107*, 4984-4988
19. N. Boden, R. Bushby, A. Cammidge, G. Headdock, *Synthesis*, **1995**, 31-32
20. L. Liu, B. Yang, T. Katz, M. Poindexter, *J. Org. Chem.*, **1991**, *56*, 3769-3775
21. W. Jaworek, F. Vögtle, *Chem. Ber.*, **1991**, *124*, 347-352
22. K. Koch, K. Müllen, *Chem. Ber.*, **1991**, *124*, 2091-2100
23. P. Copeland, R. Dean, D. McNeil, *J. Chem. Soc.*, **1960**, 1689-1691
24. A. H. A. Tinnemans, W. H. Laarhoven, *J. Am. Chem. Soc.*, **1974**, *96*, 4617-4622
25. P. Kovacic, F. W. Koch, *J. Org. Chem.*, **1965**, *30*, 3176-3181
26. P. Kovacic, A. Kyriakis, *J. Am. Chem. Soc.*, **1963**, *85*, 454-458
27. C. D. Simpson, J. D. Brand, A. J. Berresheim, L. Przybilla, H. J. Räder, K. Müllen, *Chem. Eur. J.*, **2002**, *8*, 1424-1429
28. F. Dötz, J. D. Brand, S. Ito, L. Gherghel, K. Müllen, *J. Am. Chem. Soc.*, **2000**, *122*, 7707-7717
29. S. Ito, P. T. Herwig, T. Böhme, J. P. Rabe, W. Rettig, K. Müllen, *J. Am. Chem. Soc.*, **2000**, *122*, 7698-7706
30. A. Fleming, J. N. Coleman, A. B. Dalton, A. Fechtenkötter, M. D. Watson, K. Müllen, H. J. Byrne, W. J. Blau, *J. Phys. Chem. B*, **2003**, *107*, 37-43
31. P. T. Herwig, V. Enkelmann, O. Schmelz, K. Müllen, *Chem. Eur. J.*, **2000**, *6*, 1834-1839
32. A. Stabel, P. T. Herwig, K. Müllen, J. Rabe, *Angew. Chem., Int. Ed. Engl.*, **1995**, *34*, 1609-1611
33. A. M. van de Craats, J. M. Warman, K. Müllen, Y. Geerts, J. D. Brand, *Adv. Mater.*, **1998**, *10*, 36-38
34. A. M. van de Craats, J. M. Warman, A. Fechtenkötter, J. D. Brand, M. Harbison, K. Müllen, *Adv. Mater.*, **1999**, *11*, 1469-1472
35. N. Boden, R. J. Bushby, J. Clements, M. V. Jesudason, P. F. Knowles, G. Williams, *Chem. Phys. Lett.*, **1988**, *152*, 94-99
36. D. Adam, F. Closs, T. Frey, D. Funhoff, D. Haarer, H. Ringsdorf, P. Schuhmacher, K. Siemensmeyer, *Phys. Rev. Lett.*, **1993**, *70*, 457-460

37. D. Adam, P. Schuhmacher, J. Simmerer, L. Häussling, K. Siemensmeyer, K. H. Etzbach, H. Ringsdorf, D. Haarer, *Nature*, **1994**, *371*, 141-143
38. L. Scmidt-Mende, A. Fechtenkötter, K. Müllen, E. Moons, R. H. Friend, J. D. Mackenzie, *Science*, **2001**, *293*, 1119-1122
39. U. Rohr, C. Kohl, K. Müllen, A. van de Craats, J. Warman, *J. Mater. Chem.*, **2001**, *11*, 1789-1799
40. H. S. Joshi, R. Jamshidi, Y. Tor, *Angew. Chem., Int. Ed. Engl.*, **1999**, *38*, 2721-2725
41. R. Zhang, H. Zheng, J. Shen, *Synth. Met.*, **1999**, *105*, 49-53
42. J. Simmerer, B. Glüsen, W. Paulus, A. Kettner, P. Schuhmacher, D. Adam, K. H. Etzbach, K. Siemensmeyer, J. H. Wendorff, H. Ringsdorf, D. Haarer, *Adv. Mater.*, **1996**, *8*, 815-819
43. S. Takahashi, Y. Kuroyma, K. Sonogashira, N. Hagihara, *Synthesis*, **1980**, 627-630
44. L. D. Ciana, A. Haim, *J. Heterocycl. Chem.*, **1984**, *21*, 607-608
45. U. T. Mueller-Westerhoff, M. Zhou, *J. Org. Chem.*, **1994**, *59*, 4988-4992
46. H. des Abbayes, J. Clement, P. Laurent, G. Tanguy, N. Thilmont, *Organometallics*, **1988**, *7*, 2293-2299
47. S. M. Draper, D. J. Gregg, R. Madathil, *J. Am. Chem. Soc.*, **2002**, *124*, 3486-3487
48. S. Ito, M. Wehmeier, J. D. Brand, C. Kübel, R. Epsch, J. P. Rabe, K. Müllen, *Chem. Eur. J.*, **2000**, *6*, 4327-4342
49. F. Morgenroth, K. Müllen, *Tetrahedron*, **1997**, *53*, 15349-15366
50. T. Steiner, *Angew. Chem., Int. Ed. Engl.*, **2002**, *41*, 48-76
51. A. J. Boulton, A. McKillop (Eds.), in *Comprehensive Heterocyclic Chemistry*, Vol. 3., Part 2B, Pergamon Press, Oxford, **1984**, p. 59-61
52. M. A. Ogliaruso, E. I. Becker, *J. Org. Chem.*, **1965**, *30*, 3354-3360
53. N. I. Nijegorodov, W. S. Downey, *J. Phys. Chem.*, **1994**, *98*, 5639-5643
54. I. B. Berlman, H. O. Wirth, O. J. Steingraber, *J. Phys. Chem.*, **1971**, *75*, 318-325
55. A. E. Gillam, D. H. Hey, *J. Chem. Soc.*, **1939**, 1170-1177
56. T. Rho, Y. F. Abuh, *Synth. Commun.*, **1994**, *24*, 253-256
57. A. Clerici, O. Porta, *Tetrahedron*, **1982**, *38*, 1293-1297
58. A. Fechtenkötter, K. Saalwachter, M. A. Harbison, K. Müllen, H. W. Spiess, *Angew. Chem., Int. Ed. Engl.*, **1999**, *38*, 3039-3042
59. F. Peral, E. Gallego, *J. Mol. Struct.*, **1995**, *372*, 101-112
60. R. P. Wayne, in *Principles and Applications of Photochemistry*, Oxford University Press, **1980**
61. D. V. Bent, E. Hayon, P. N. Moorthy, *J. Am. Chem. Soc.*, **1975**, *97*, 5065-5071
62. B. N. Bandyopadhyay, A. Harriman, *J. Chem. Soc., Faraday Trans.*, **1977**, *73*, 663-674
63. S. K. Lee, Y. Zu, A. Herrmann, Y. Geerts, K. Müllen, A. Bard, *J. Am. Chem. Soc.*, **1999**, *121*, 3513-3520
64. M. A. Biasutti, J. Rommens, A. Vaes, S. De Feyter, F. D. de Schryver, P. T. Herwig, K. Müllen, *Bull. Soc. Chim. Belg.*, **1997**, *106*, 659-664
65. N. Ghoneim, *Spectrochim. Acta, Part A*, **2001**, *57*, 483-489
66. R. B. Cundall, I. Johnson, M. W. Jones, E. W. Thomas, *Chem. Phys. Lett.*, **1979**, *64*, 39-42
67. S. Bakalova, J. Kaneti, *Spectrochim. Acta, Part A*, **2000**, *56*, 1443-1452
68. M. C. Castex, C. Olivero, G. Pichler, D. Adés, E. Cloutet, A. Siove, *Synth. Met.*, **2001**, *122*, 59-61
69. E. Lippert, *Z. Naturforsch.*, **1957**, *61*, 962-975
70. H. Baba, L. Goodman, P. C. Valenti, *J. Am. Chem. Soc.*, **1966**, *88*, 5410-5415
71. N. Armaroli, L. De Cola, V. Balzani, J. P. Sauvage, C. O. Dietrich-Buchecker, J. Kern, *J. Chem. Soc., Faraday Trans.*, **1992**, *88*, 553-556
72. N. C. Yang, J. Libman, *J. Am. Chem. Soc.*, **1973**, *95*, 5783-5784
73. C. A. Hunter, K. R. Lawson, J. Perkins, C. J. Urch, *J. Chem. Soc., Perkin Trans. 2*, **2001**, 651-669
74. F. Peral, E. Gallego, *Spectrochim. Acta, Part A*, **2000**, *56*, 2149-2155
75. A. S. Shetty, J. Zhang, J. S. Moore, *J. Am. Chem. Soc.*, **1996**, *118*, 1019-1027
76. J. Wang, D. R. Miller, E. G. Gillan, *Chem. Commun.*, 2002, *19*, 2258-2259

77. T. Verbiest, S. Houbrechts, M. Kauranen, K. Clays, A. Persoons, *J. Mater. Chem.*, **1997**, *7*, 2175-2189
78. (a) C. Ego, D. Marsitzky, S. Becker, J. Y. Zhang, A. C. Grimsdale, K. Müllen, J. D. MacKenzie, C. Silva, R. H. Friend, *J. Am. Chem. Soc.*, **2003**, *125*, 437-443; (b) P. Leclere, E. Hennebicq, A. Calderone, P. Brocorens, A. C. Grimsdale, K. Müllen, J. L. Bredas, R. Lazzaroni, *Prog. Polymer Science*, **2003**, *28*, 55-81
79. P. Schlichting, B. Duchscherer, G. Seisenberger, T. Basché, C. Bräuchle, K. Müllen, *Chem. Eur. J.*, **1999**, *5*, 2388-2394
80. M. S. Yusubov, V. D. Filimonov, *Synthesis*, **1991**, 131-132
81. J. Chen, H. Liu, W. A. Weimer, M. D. Halls, D. H. Waldeck, G. C. Walker, *J. Am. Chem. Soc.*, **2002**, *124*, 9034-9035

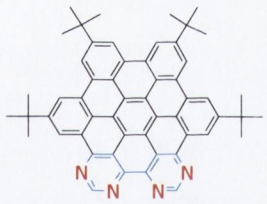
CHAPTER THREE

TRANSITION METAL COMPLEXES OF NITROGEN-HETEROSUPERBENZENES

3.1 INTRODUCTION

Transition metal complexes are a diverse class of compounds with interesting electrochemical, photochemical and photophysical properties.[1] It is now possible to prepare stable transition metal complexes *via* simple synthetic routes, making these metal-containing species a convenient source of new molecular materials with physical properties that make them suitable for electro-optical applications. Within the complex, the interaction between the metal and the ligand is often weak enough to allow the manifestation of intrinsic metal and ligand properties (*e.g.* ligand-centred (LC) and metal-centred (MC) absorption bands and redox processes), yet it is also strong enough to cause the appearance of new properties which are characteristic of the whole compound (*e.g.* metal-to-ligand (MLCT) or ligand-to-metal (LMCT) charge-transfer bands). These electronic properties can be tuned through selection of appropriate ligands and metals.[1] The metal complexes synthesized as a result of this work may prove attractive for many future applications. Currently new types of metal complexes are the subject of intense research in the areas of molecular electronics,[2] non-linear optics[3] and superconductivity.[4]

The systematic control inherent in the synthesis of N-HBC systems means that the N atoms can be positioned so as to allow the graphene analogue to function as a N-donor ligand. The ability of the nitrogen heteroatoms of **(17)** to behave as Lewis bases (see Chapter 2) is further evidence for their suitability as ligands for the formation of metal complexes. The scope of such complex formation is limited with homocyclic PAHs due to the absence of appropriate donor atoms. In fact no ligand has ever before been synthetically accessible which has the same degree of electronic delocalisation as is present in N-HBC. Heterosuperbenzenes, therefore, form a new class of nitrogen containing donor ligand, which possess an unprecedented degree of electronic delocalisation: in N-HBC **(17)** this extends over 13 fused rings. The physical, chemical and spectroscopic properties of **(17)** make it suitable for incorporation into a variety of transition metal complexes. This work therefore links two topical developments: the generation of dendritic graphene molecules in organic chemistry and the building of nano-structures with pre-defined geometries in transition metal coordination chemistry.



N-HBC, **(17)**

We will direct our attention initially to metallic arrays containing the Ru(II)-polypyridine chromophores which have outstanding redox and spectroscopic properties,[1,5] and to the synthesis of (η^3-allyl)Pd(II) complexes.[6]

3.1.1 RUTHENIUM

Ruthenium(II) is the most widely studied photoactive metal in the field of coordination chemistry. It has unique electronic and spectroscopic properties which make it suitable for incorporation into photoresponsive materials, for example as a sensitizer in photochemical and chemiluminescent processes.[5,7,8] In particular Ru(II) polypyridine complexes are currently playing a key role in the development of multicomponent, supramolecular systems capable of performing photo- and/or redox-triggered functions. Examples include artificial antenna systems,[1,9] charge separation devices for photochemical solar energy conversion[1,9] and information storage devices.[5,10]

The effect of varying the steric and electronic properties of diimine type ligands on the excited-state properties of their ruthenium(II) complexes has remained an active area of investigation.[11] Indeed numerous studies[5,7,12] have shown that it is possible to gradually change several ground- and excited-state properties over a broad range of values. However, the improvement of one specific property can compromise other properties. For example, a higher photochemical stability is usually accompanied by a shorter excited-state lifetime.[7]

The typical molecular orbital (MO) diagram of an octahedral complex is shown in figure 3.1, where each MO is labelled as metal (M) or ligand (L) according to its predominant localisation.[1]

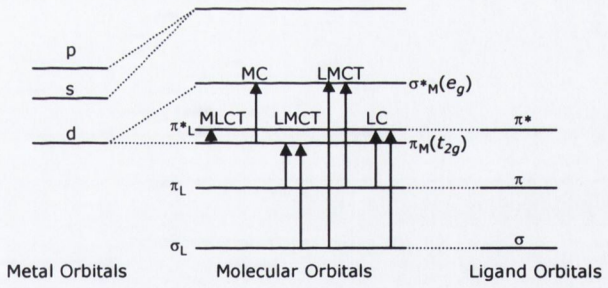
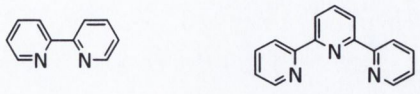


Figure 3.1. Schematic energy-level diagram for an octahedral transition metal complex (*e.g.* Ru(II), d^6) with various electronic transition types indicated.

The order of the excited-states is sensitive to the ligand type and ruthenium oxidation state.[1] There is considerable spin-orbit coupling between the charge transfer (CT) states (singlet and triplet). This effect is a result of the presence of the central heavy metal atom, and depends on the type of excited state. For example, spin-orbit coupling hardly effects the almost pure LC states, whereas it is extremely influential in the MC and CT states of ruthenium(II).[1]

Polypyridine complexes of Ru(II) are characterised by strong ^{1}MLCT absorptions and long-lived, emissive ^{3}MLCT excited states, which make these complexes ideal "photosensitizer" molecular components.[2] The most commonly reported ligands are bidentate ligands such as 2,2′-bipyridine (bpy) and tridentate ligands such as 2,2′:6′2″-terpyridine (tpy).[1,9]



bpy tpy

Figure 3.2. Commonly used bidentate (bpy) and tridentate (tpy) ligands.

The emission lifetime and quantum yield of the ^{3}MLCT excited states are known to be dependent on (i) the energy of the state ("energy gap law") and (ii) the proximity of a higher-energy metal-centred (^{3}MC) excited state.[5]

A small energy gap between the ^{3}MLCT and the ^{3}MC levels allows fast, thermally-activated radiationless decay through the upper ^{3}MC level. This small energy gap can be caused, for example, by an unfavourable bite angle which perturbs the ligand field.[13] This occurs with tris chelating tpy ligands, which do not coordinate with ideal octahedral geometry.[1] The result is a relatively weak ligand field around the metal centre, a low energy MC state and an efficient thermally activated decay pathway.[5,14] As a consequence the tpy complexes tend to have relatively short-lived MLCT excited states and produce a weaker emission, as compared to their bpy complex counterparts.

Strategies to increase the excited-state lifetimes of Ru(II) complexes therefore involve increasing the energy gap between the emissive ^{3}MLCT state and the upper-lying ^{3}MC states. One way to increase the gap is to lower the energy of the ^{3}MLCT state. π-Delocalised fragments have been found to cause such stabilisation of the ^{3}MLCT resulting in lifetime enhancements.[15] N-HBC **(17)**, which has a rigid structure and considerable π-delocalisation, would be expected to be an ideal ligand to give a complex with effective ^{3}MLCT state and ^{3}MC state separation.

As MLCT absorption and MLCT excited states in polypyridyl complexes of Ru(II) continue to be investigated, one issue to evolve is the use of new acceptor ligands and heteroleptic synthetic strategies in the design of complexes which are low energy light absorbers or "black" absorbers. These absorb throughout the visible absorption spectrum and produce low energy emissions.[11,16] Low energy emitters incorporate different acceptor ligands with extended π/π^* frameworks, which lowers the energy of the π^* acceptor level without significantly decreasing the σ electron donor ability.[11]

The result is a complex which emits from the ^{3}MLCT excited state in the near-infrared region. There are limited examples in the literature of near-infrared emitters but these include singlet oxygen,[17] coordinatively labile complexes of the lanthanide and actinide ions,[18] photosensitive highly conjugated organic molecules,[19] and anionic complexes of Mo(III) and Re(IV).[20] Only recently have Ru(II) and Os(II) based near-infrared emitters been developed.[11] N-HBC, with its extended π-system, should provide a further example of this type of low energy, near-IR emission and "black" absorption in Ru(II) chemistry.

Aside from their photophysical properties, ruthenium(II) complexes have also been shown to exhibit strong DNA-binding and -photocleavage properties.[21] Bio-inorganic investigations of $[Ru(phen)_2L]^{2+}$ complexes, where L is, for example, 1,10-phenanthroline (phen) or dipyrido[3,2-a:2',3'-c]-phenazine (dppz), have shown that the planar aryl N-moieties allow a metal complex to intercalate between the base-pairs of DNA. This is the mechanism by which such systems prevent the replication of tumour cells.[22] The N-doped graphene **(17)**, in which 2,2'-bipyridyl and hexabenzocoronene subunits are combined, is an analogue of 1,10-phenanthroline with an extended π-system, thus a similar mode of DNA intercalation might be envisaged for Ru(II)-centred complexes containing this ligand. The bio-medical applications of such a complex are worthy of investigation, as suitable ligands with high DNA-binding affinity and high photo-cleavage efficiency are increasingly sought.[21]

The current Chapter reports on the synthesis, characterisation, spectroscopic, redox and photophysical behaviour of a novel ruthenium(II) complex **(35)**, $[Ru(bpy)_2(N\text{-}HBC_{17})](PF_6)_2$ (where N-HBC_{17} is the N-HBC derivative, **(17)**, described in Chapter 2). The absorption spectra, emission spectra, luminescence lifetimes, luminescence quantum yields, photochemical behaviour and redox potentials of the ruthenium complex $[Ru(bpy)_2(N\text{-}HBC_{17})]^{2+}$ have been studied and compared with those of $[Ru(bpy)_3]^{2+}$. The uncyclised N-doped polyphenylene **(16)** was also used as a ligand in the formation of **(34)**, a model complex for **(35)**.

3.1.2 PALLADIUM

Palladium complexes are excellent catalysts for a variety of organic reactions.[23,24] Allylic alkylation is a classical and useful carbon-carbon bond forming process that involves both Pd(II) and Pd(0) catalytic complexes[25] and currently ranks among the most intensively studied catalytic transformations. Since the first reports on the palladium-mediated C-C bond formations between allylic substrates and carbon nucleophiles, by Tsuji[26] and Trost,[27] this area has seen development in reaction

scope, catalyst structure, nucleophile diversity and ligand design.[23,24] The ligands coordinated to palladium play an important role, affecting the metal electronically and sterically.[6,28] The resulting complex can, therefore, be used to control the reactivity of substrates and selectivity of products, both of which are important factors if a complex is to be applied to catalysis.[23] The ligand characteristics of **(17)** could, therefore, infer unique catalytic properties on the $[Pd(\eta^3\text{-}C_3H_5)(\text{N-HBC}_{17})]PF_6$ complex.

Another aspect of (η^3-allyl)palladium complexes that has attracted much interest in recent years is the study of the fluxional behaviour of these systems.[23,29] The allyl group, for example, is known to undergo a mutual exchange of *syn* and *anti* protons *via* a $\eta^3\text{-}\eta^1\text{-}\eta^3$ dynamic process,[29] and in complexes bearing ligands with less σ-donor character the apparent rotation of the allyl group, a second dynamic process, is also frequently observed.[29]

In the work described here a new cationic (η^3-allyl)palladium complex **(36)** with the N,N-donor chelating bipyridine type ligand N-HBC **(17)** is synthesized. The work mainly focuses on the study of the photophysical properties of N-HBC **(17)** and the effect of palladium coordination.

3.2 RESULTS AND DISCUSSION

3.2.1 SYNTHESIS OF THE LIGAND N-HBC (17)

As already discussed in Chapter 2, the synthesis of N-HBC **(17)** results in a thermally stable and highly conjugated new ligand system, as shown in figure 3.3.

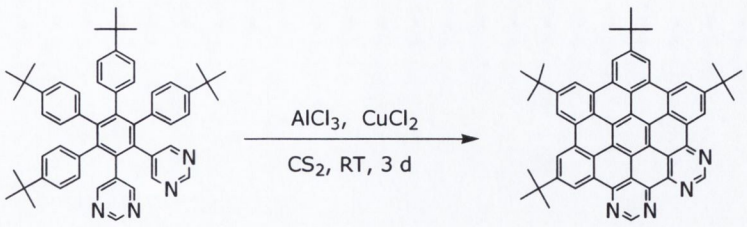


Figure 3.3. Oxidative cyclodehydrogenation of N-doped polyphenylene **(16)** to yield the novel N-HBC ligand **(17)**.

The imine nitrogens of **(17)** have been carefully positioned to give the electron-rich graphene product ligand-based functionality. The N-donor atoms are ideally arranged for bidentate metal chelation, thus similar pathways to those used for 1,10-phenanthroline are envisaged for the coordination of **(17)** to obtain the ruthenium(II) centred complexes of this ligand species.

3.2.2 RUTHENIUM COMPLEX (35)

3.2.2.1 Synthesis and Characterisation

Several synthetic approaches were employed, following literature pathways, in an attempt to coordinate N-HBC **(17)** to Ru(II). These included alcoholic or ethylene glycol reflux[21,30,31,32] with either $[Ru(bpy)_2Cl_2]$ or $[Ru(bpy)_2(CH_3CN)_2]^{2+}$. These attempts, however, led only to quantitative return of uncomplexed ligand **(17)**. Success was only obtained by using a solvent employed by the Sauvage group.[33]

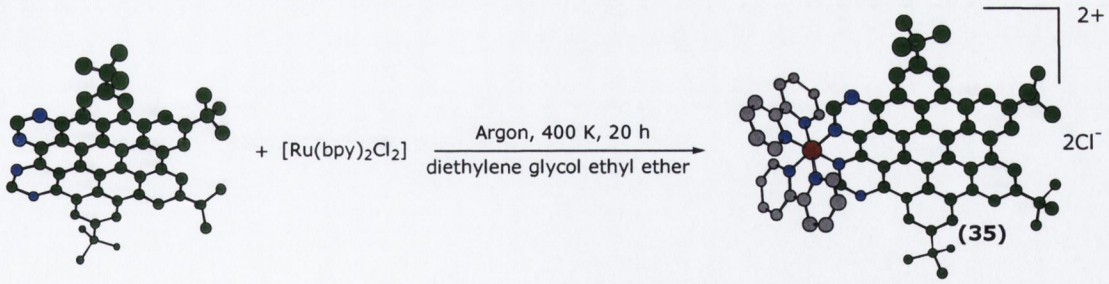


Figure 3.4. Chemdraw depiction of the synthesis of ruthenium(II) complex $[Ru(bpy)_2(N\text{-}HBC_{17})]^{2+}$, **(35)**, from $[Ru(bpy)_2Cl_2]$.

The $[Ru(bpy)_2(N\text{-}HBC_{17})]^{2+}$ complex, **(35)**, was synthesized in high yield by heating $[Ru(bpy)_2Cl_2]$ and a stoichiometric amount of the ligand in degassed diethylene glycol ethyl ether under an argon atmosphere (see figure 3.4). The reaction mixture was heated at 400 K for 20 h to form a dark green solution, which was filtered to remove

any unreacted $[Ru(bpy)_2Cl_2]$. An excess of aqueous NH_4PF_6 was added to precipitate the green complex **(35)** as its PF_6^- salt. Purification by column chromatography on silica using acetonitrile:water:KNO_3 (100:10:1) as the solvent system, followed by anion exchange gave $[Ru(bpy)_2(N\text{-}HBC_{17})](PF_6)_2$ as a black-green solid in 60% yield.

Due to their bidentate nature, bipyridyl type ligands are known to give rise to stereoisomerism at six-coordinate centres. Therefore, like any $[M(bpy)_3]^{n+}$ based octahedral complex, $[Ru(bpy)_2(N\text{-}HBC_{17})](PF_6)_2$ is expected to exist in two enantiomeric forms. The chiral structures of $[Ru(bpy)_2(N\text{-}HBC_{17})]^{2+}$, which were not separated, are shown in figure 3.5.

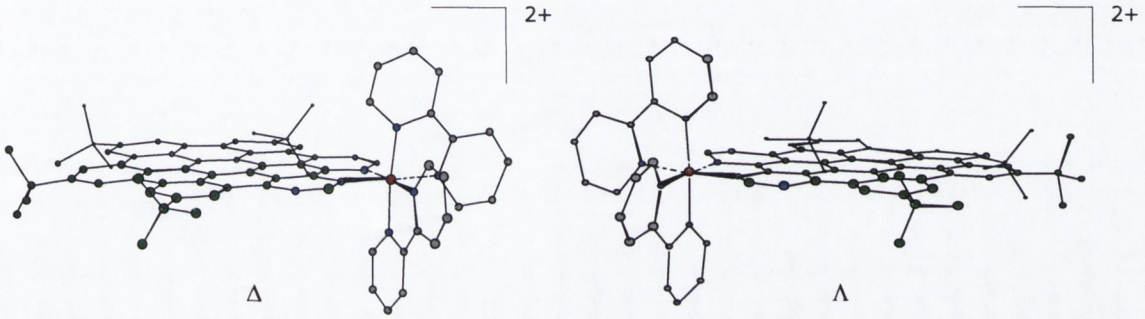


Figure 3.5. Chemdraw representation for the optical isomers of ruthenium complex **(35)**, counterions omitted.

$[Ru(bpy)_2(N\text{-}HBC_{17})](PF_6)_2$ **(35)** was characterised, initially, by ^1H and ^{13}C NMR spectroscopy, and ESI-MS and accurate mass spectrometry. In accordance with the theoretically expected value for **(35)** (m/z=582.2) the ESI-mass spectra showed a base peak at m/z=581.6, assigned to $[M\text{-}2PF_6]^{2+}$ with peaks in the envelope at 1/2 m.u. intervals confirming the 2+ charge of the molecular ion (figure 3.6). The spectrum also gave an indication of the purity of complex **(35)**, as it was the only signal observed.

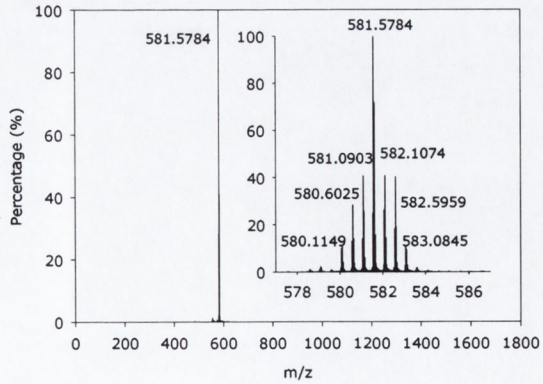


Figure 3.6. The ESI-mass spectrum of ruthenium complex **(35)** in acetonitrile.

Elemental analysis of **(35)** could not be obtained, due to the extremely high thermal stability of the aromatic core of the N-HBC ligand **(17)**, which results in incomplete combustion. Consequently an accurate mass analysis was obtained instead for **(35)** in acetonitrile, which gave a $(C_{74}H_{62}N_8Ru)^{2+}$ peak of 582.2042, accurate to within 5 ppm of that calculated.

Figures 3.7 (a) and (b) compare the low-field region of the ^{1}H-NMR spectra of ligand **(17)** with that of $[Ru(bpy)_2(N\text{-}HBC_{17})](PF_6)_2$ **(35)** in $CDCl_3$.

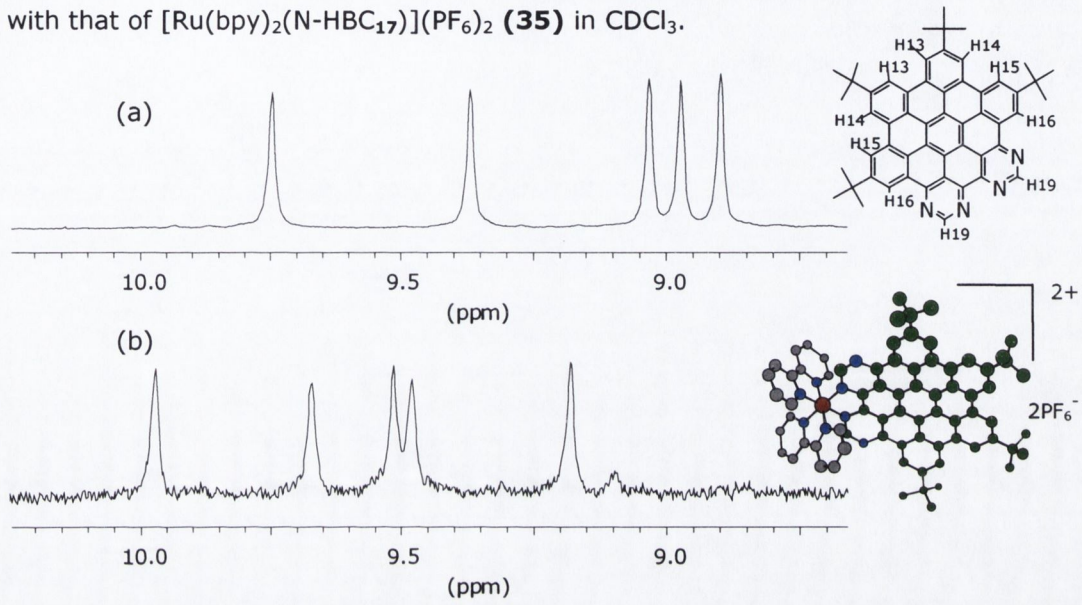


Figure 3.7. The low-field, aromatic region of the ^{1}H NMR spectra of (a) ligand N-HBC **(17)** and (b) $[Ru(bpy)_2(N\text{-}HBC_{17})](PF_6)_2$ **(35)** ($CDCl_3$, RT, 400 MHz).

The complexation of N-HBC **(17)** is evident in the general downfield shift of the aromatic protons of **(17)** from the region of δ 8.8 - δ 9.8 in the free ligand to the region of δ 9.2 – δ 10.0 in the complex (see figure 3.7 (a) and (b), respectively). These five signals are assigned to the five aromatic protons of coordinated **(17)** at positions H13/14/15/16 and 19 (see inset figure 3.7 (a)), each integrating for two hydrogen atoms. In the complex these protons experience, primarily, a deshielding effect due to the formation of the coordinate bonds. In the uncoordinated ligand, H19 is the lowest field resonance (δ 9.79 in ^{1}H NMR spectrum, see figure 3.7 (a)) due to a combination of inductive and resonance deshielding at this position. These effects are over-ridden in the ruthenium complex, however, and this proton moves a substantial 0.6 ppm upfield, to δ 9.18, as a result of its being pointed directly toward the shielding face of a pyridine ring of the adjacent bpy ligand. The remaining proton signals, H13-16, cannot be assigned precisely because NOe experiments were unsuccessful. The ^{1}H NMR spectrum of **(35)** has two sets of aliphatic signals at δ 1.89 and δ 1.80 (not shown in figure 3.7 (b)), integrating for 18 hydrogen atoms each, which correspond to the two pairs of

equivalent *tert*-butyl protons of coordinated **(17)**. N-HBC **(17)** has thus maintained its C_{2v} symmetry in the Ru(II) complex.

Figure 3.8 shows the aromatic region of the ^{1}H-NMR spectrum of ruthenium complex $[Ru(bpy)_2(N\text{-}HBC_{17})](PF_6)_2$ **(35)** in CD_3CN.

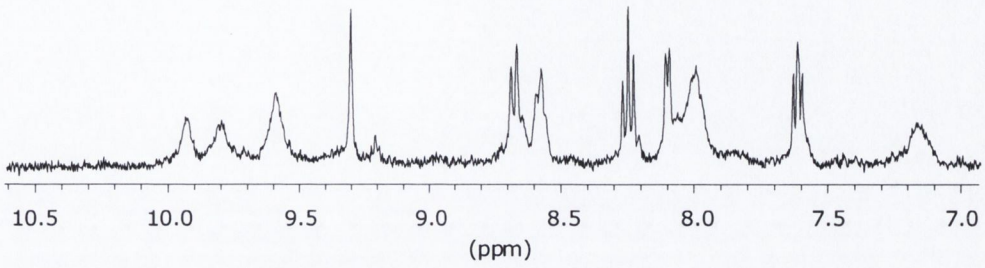


Figure 3.8. The aromatic region of the ^{1}H NMR spectrum of $[Ru(bpy)_2(N\text{-}HBC_{17})](PF_6)_2$ (CD_3CN, RT, 400 MHz).

The chemical shifts for the aromatic protons of the two bpy ligands are chemically equivalent in the ^{1}H NMR spectra of **(35)**. The ^{1}H NMR spectral data for the bpy protons are given in table 3.1, using the atom labelling scheme in figure 3.9, and illustrate the symmetrical nature of the complex. All these assignments are based on comparison with those already reported for similar complexes,[34,35] and the coupling patterns and ^{1}H-^{1}H COSY spectra obtained for **(35)**.

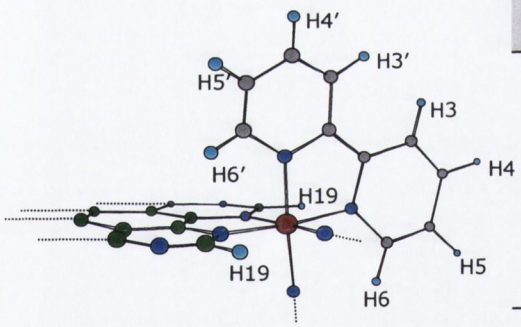


Figure 3.9. The atom labelling scheme for the bipyridyl protons of **(35)**.

Proton Label	^{1}H NMR (ppm)	Coupled Nuclei, ^{1}H NMR (ppm)
H3	d, 8.67 (2H)	8.25
H3′	br. d, 8.58 (2H)	8.00
H4	t, 8.25 (2H)	7.63, 8.67
H6	d, 8.10 (2H)	7.63
H4′, H6′	br. s, 8.00 (4H)	8.58, 7.17
H5	t, 7.63 (2H)	8.10, 8.25
H5′	Br. s, 7.17 (2H)	8.00

Table 3.1. ^{1}H-^{1}H coupling information from the TOCSY experiment of **(35)** (CD_3CN, RT, 400 MHz).

In the ^{1}H NMR spectra of uncoordinated bpy, the lowest field proton resonance is assigned to H6′ (=H6, δ 8.65 in CD_3CN). As occurs for H19, the shift of this proton is due to inductive and resonance deshielding at this position. In ruthenium complex **(35)**, this proton (H6′) resonates considerably upfield, at δ 8.00. The magnitude of this shift difference is 0.7 ppm, which is the result of the proton being pushed deep into the shielding conjugated π-system of the pyrimidine rings of the adjacent N-HBC ligand

(see figure 3.9). In fact the signals for the protons H4′ and H6′ are both observed at δ 8.00 with extensive overlap, which contributes to the signals' broad appearance.

The signal for the bpy proton at H5′ also resonates significantly upfield in complex **(35)**. H5′ is found at δ 7.17, upfield of δ 7.36 (the signal for H5 in the free bpy ligand). This is because H5′ is pushed close to the shielding face of the adjacent N-HBC π-system, which also causes its broad featureless appearance.

The four signals at δ 8.67, δ 8.25, δ 7.63 and δ 8.10 in the ^{1}H NMR of **(35)** can be assigned as protons at H3, H4, H5 and H6 (figure 3.9). These assignments correlate well with the equivalent protons reported for $[Ru(bpy)_2(phen)]^{2+}$ (CD_3COCD_3) at δ 8.88, δ 8.25, δ 7.64 and δ 8.18.[34] A similar comparison can be made for the four signals at δ 8.58, δ 8.00, δ 7.17 and δ 8.00 which can be assigned as protons H3′, H4′, H5′ and H6′. These appear at δ 8.84, δ 8.14, δ 7.39 and δ 7.89 in $[Ru(bpy)_2(phen)]^{2+}$ (CD_3COCD_3). The proton chemical shifts of the H3′-H6′ ring are more upfield than those of the H3-H6 ring in the bpy ligand. This can be explained by ligand interaction. Because N-HBC is a large, rigid, aromatic ligand, its ring current has a very strong effect on the H3′-H6′ pyridine ring of bpy. As a consequence of the smaller π-system in the bpy moiety, the effect of the ring current of the bpy ligand (the bpy not shown in figure 3.9) on the H3-H6 pyridine ring is not as strong.

^{1}H-^{1}H TOCSY experiments reveal coupling between the bpy protons of **(35)**, as summarised in table 3.1. These verify the above results. NOe experiments were unsuccessful.

3.2.2.2 Electrochemistry

Oxidation and reduction processes are viewed as metal or ligand centred,[1] with the HOMO usually being metal centred, and the LUMO either metal or ligand centred. Reduction takes place on the ligand if the ligand field is sufficiently strong and/or if the ligands can be easily reduced. Oxidation or reduction can lead to decomposition of the complex, although reversibility is a fundamental requirement for most device applications.[1] The oxidation of Ru(II)-polypyridine complexes often leads to Ru(III) compounds (low-spin $\pi_M(t_{2g})^5$ configuration).[1]

$$[Ru^{II}(L)_3]^{2+} \rightarrow [Ru^{III}(L)_3]^{3+} + e^- \qquad (3.1)$$

Usually, only the first metal-centred oxidation process is observed in the potential window available in common solvents (*e.g.* acetonitrile). The Ru(III)/Ru(II) redox

potential of most polypyridine-type Ru(II) complexes falls around +1.25 V (*vs* SCE, acetonitrile solution),[1] for example $[Ru(bpy)_3]^{2+}$ which has an Ru(III)/Ru(II) redox potential of 1.26 V.[7] Substitution of one bpy ligand in $[Ru(bpy)_3]^{2+}$ by two Cl^- ions lowers the potential to +0.32 V. On the other hand, substitution of CO, a strong π-acceptor, increases the value above +1.9 V.[1]

For Ru^{II}-polypyridine complexes, reduction takes place on a π*-orbital of the polypyridine ligands. Therefore the reduced form keeps its low-spin $\pi_M(t_{2g})^6$ configuration, which is usually inert and reduction is reversible:

$$[Ru^{II}(L)_3]^{2+} + e^- \rightarrow [Ru^{II}(L)_2(L^{\bullet-})]^+ \qquad (3.2)$$

Several reduction steps are often observed, for example $[Ru(bpy)_3]^{2+}$ in DMF at 219 K has up to six reduction waves between −1.33 and −2.85 V (*vs* SCE). These are assigned to the successive first and second reduction processes of the three bpy ligands.[1]

The π^*_L and σ^*_M orbitals which accept an electron in the reduction process (redox orbitals) are the same orbitals as are involved in the MLCT and MC transitions, respectively (spectroscopic orbitals), according to Koopman's theorem (see figure 3.1).[1] Reversibility of the first reduction step can be used as an indication of a ligand centred LUMO.[1] This is because reduction on a π*-orbital of the ligand allows the low-spin $\pi_M(t_{2g})^6$ configuration to be maintained, which is usually inert. This also implies that the lowest energy excited state is an MLCT transition. Thus, electrochemical measurements show the relationship between the ability of the ligand to accept an electron and the wavelength of the lowest energy ^{1}MLCT absorption band, the presence of a more easily reduced ligand leading to a further red-shifted ^{1}MLCT absorbtion band.

To allow comparison of **(35)**'s electrochemistry to the electrochemistry of the free ligand **(17)**, cyclic voltammograms of **(35)** were carried out in chloroform. In chloroform containing 0.1 M $(TBA)PF_6$, the free ligand **(17)** shows two well-defined, "pseudo"-reversible one-electron-reduction waves at −1.20 V and −1.64 V *vs* SCE as seen in figure 3.10 (a). Reduction waves for complexed **(17)** within $[Ru(bpy)_2(N\text{-}HBC_{17})](PF_6)_2$, when measured in chloroform, occur at −0.52 V and −1.10 V *vs* SCE ("pseudo"-reversible one-electron transfer) followed by the successive bpy reductions at around −1.7 V and −2.1 V (figure 3.10 (b), and table 3.2), (as found through Differential Pulse Voltammetry (DPV) analysis).

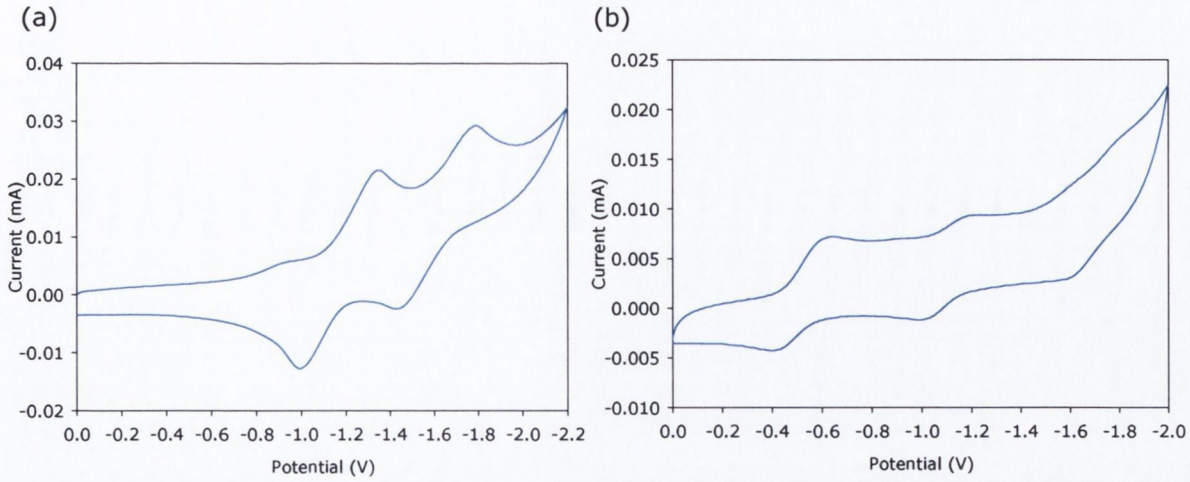


Figure 3.10. Cyclic voltammograms of (a) **(17)** in chloroform and (b) **(35)** in chloroform. Supporting electrolyte: $(TBA)PF_6$ (0.1 M); glassy carbon working electrode, Pt wire auxiliary electrode, SCE reference electrode.

Complex	Redox Potentials (V *vs* SCE)			
	E^{o1}	E^{o2}	E^{o3}	E^{o4}
(17)	-1.20	-1.64	-	-
(35)	-0.52	-1.10	approx. -1.7	approx. -2.1

Table 3.2. Electrochemical information obtained from the cyclic voltammogram. Supporting electrolyte: $(TBA)PF_6$ (0.1 M) in chloroform; glassy carbon working electrode, Pt wire auxiliary electrode, SCE reference electrode.

The small wave at about −0.9 V *vs* SCE in the cyclic voltammogram of **(17)** (figure 3.10 (a)) is believed to be due to the reduction of a small amount of dissolved oxygen. This could not be removed from the electrolyte solution even after prolonged degassing with nitrogen.

By comparing the redox potentials of the free and complexed N-HBC ligand, we see that, as expected, N-HBC has become easier to reduce on coordination. This is due to charge depletion in the ring system, resulting from the formation of the coordinative bonds. This is in agreement with the downfield shifts observed in the ^1H NMR spectrum of **(35)**, indicating deshielding of the aromatic protons.

To allow comparison of **(35)**'s electrochemistry to other Ru(II) polypyridyl complexes, cyclic voltammograms of **(35)** were also carried out in acetonitrile. In acetonitrile, within the redox window investigated (between +2.0 and −2.0 V *vs* SCE), the electrochemical measurements show that complex **(35)** follows the general behaviour observed for that of Ru(II) polypyridine complexes,[7] with a metal-centred oxidation process and a series of reduction waves, corresponding to successive one-electron

reductions of the three bidentate ligands. Figure 3.11 shows the cyclic voltammograms and table 3.3 collects the potential values. The observed waves are quasi-reversible (ΔE_p *ca.* 110 mV for the oxidation process and 130 mV for reduction) indicating the formation of stable oxidized and reduced species.

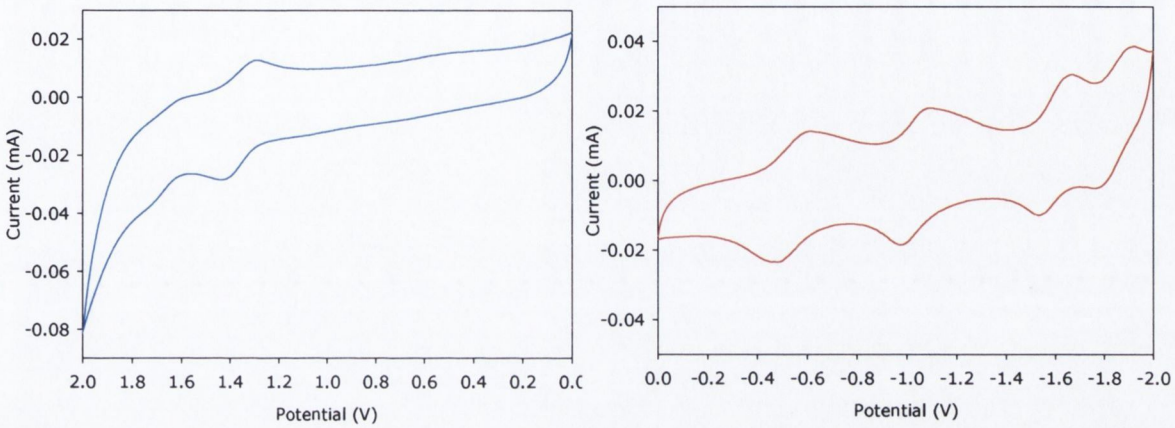


Figure 3.11. Cyclic voltammograms of $[Ru(bpy)_2(N\text{-}HBC_{17})](PF_6)_2$ **(35)** in CH_3CN solution (scan rate=500 mV s^{-1}). Supporting electrolyte: $(TBA)PF_6$ (0.1 M); glassy carbon working electrode, Pt wire auxiliary electrode, SCE reference electrode.

The redox potentials for **(35)** and $[Ru(bpy)_3]^{2+}$, in acetonitrile, are collected and summarized in table 3.3.

Complex	Redox Potentials (V *vs* SCE)				
	Ru(II)/Ru(III)	Ligand Reduction Processes			
[a]**(35)**	+1.35	-0.54	-1.01	-1.59	-1.83
[b]$[Ru(bpy)_3]^{2+}$	+1.26	-1.35		-1.54	-1.79

Table 3.3. Electrochemical data for **(35)** and $[Ru(bpy)_3]^{2+}$[7] in acetonitrile. [a]Supporting electrolyte: $(TBA)PF_6$ (0.1 M); glassy carbon working electrode, Pt wire auxiliary electrode, SCE reference electrode. [b]Supporting electrolyte: $(TBA)ClO_4$ (0.1 M); Pt disc electrode, Pt wire auxiliary electrode, SCE reference electrode.

For **(35)**, the two reductions at −0.54 V and −1.01 V are reasonably attributed to two consecutive one-electron reductions on the complexed N-HBC ligand. Literature comparisons allow the assignment of the redox potentials at −1.59 V and −1.83 V of **(35)** to the successive one-electron reductions of the two bpy ligands (equivalent to -1.54 V and −1.79 V in $[Ru(bpy)_3]^{2+}$[7]). An analysis of these data suggests, not surprisingly, that the lowest unoccupied π*-orbital of **(17)** lies at a lower energy than that of the bpy making **(17)** easier to reduce. This is due to the electron accepting properties of $N\text{-}HBC_{17}$. The π*-orbital of $N\text{-}HBC_{17}$ is in fact so much lower in energy than the π*-orbital of bpy that we see two reduction processes on the heterosuperbenzene ligand (to form $[Ru(bpy)_2(N\text{-}NBC_{17}^{2-})]$) before reduction of a bpy

ligand. This is an unusual feature in Ru(II) polypyridyl electrochemistry, for example $[Ru(bpy)_2(dppz)]^{2+}$ undergoes consecutive one electron reductions for each ligand (redox potentials -1.02 V, -1.44 V and -1.67 V *vs* SCE).[35]

Upon reduction the electron is localised in the π^* level of the complexed N-HBC ligand, rather than being delocalised over the π-system of the three ligands in $[Ru(bpy)_2(N\text{-}HBC_{17})]^{2+}$. This supposition is in line with DeArmond's proposal for $[Ru(bpy)_3]^{2+}$.[36] These electrochemical data support the assignment of the lowest energy absorption band at 615 nm to the Ru→N-HBC_{17} MLCT transition (see section **3.2.2.3**).

It was found that N-HBC **(17)** cannot be oxidised within the potential window investigated (up to +2.0 V) in either dichloromethane or in tetrahydrofuran. In the presence of 0.1 M $(TBA)PF_6$. $[Ru(bpy)_2(N\text{-}HBC_{17})]^{2+}$ **(35)**, however, undergoes a clear oxidation process at 1.35 V *vs* SCE. By comparison with literature data this oxidation wave can be assigned as the metal centred (Ru^{II}/Ru^{III}) process.[1,7,21,30,37,38] The variation of this potential value, observed for various ruthenium(II) complexes, can be explained on the basis of differences in the donor/acceptor properties of the ligands. Thus, the (Ru^{II}/Ru^{III}) oxidation process of **(35)** occurs at more positive potential than that of $[Ru(bpy)_3]^{2+}$ (see table 3.3) because of the better π-acceptor properties of the N-HBC ring. This makes electron abstraction from the metal centre more difficult.

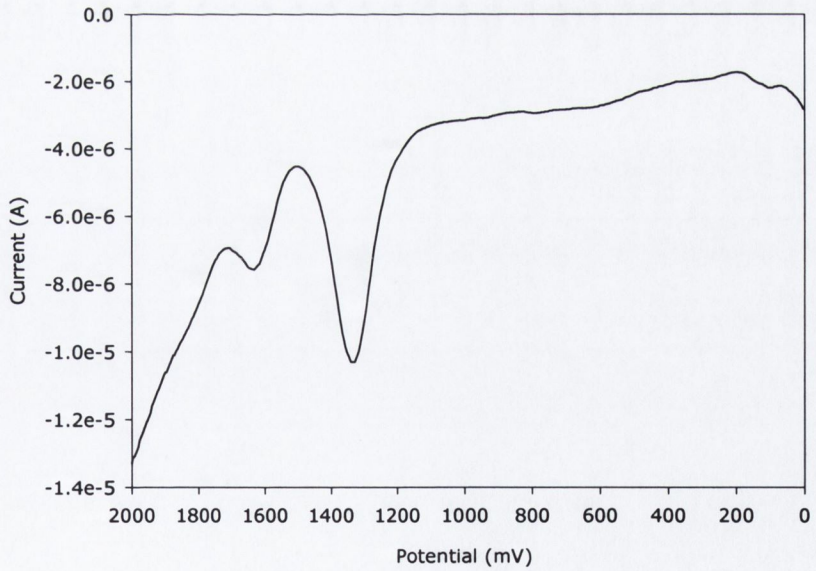


Figure 3.12. The DPV experiment for ruthenium complex **(35)** in CH_3CN showing two oxidation processes. Supporting electrolyte: $(TBA)PF_6$ (0.1 M); glassy carbon working electrode, Pt wire auxiliary electrode, SCE reference electrode.

There is evidence for a second oxidation process at +1.63 V *vs* SCE in the CV and DPV electrochemical experiments, carried out in acetonitrile. This may be an oxidation process occurring at the coordinated N-HBC **(17)**. Although there is no evidence of an analogous process occurring in the free ligand, its low solubility meant electrochemical experiments could not be performed in acetonitrile.

3.2.2.3 Photophysical Properties of (35)

UV-vis Absorption Spectroscopy

The complexity in the electronic structure of transition metal complexes often makes it difficult to assign the various bands appearing in the absorption spectra of these molecules. It is possible, however, to class the various types of electronic transition according to the localization of the MO's involved. The three fundamental types of electronic transitions observed in complexes of this type are metal-centred (MC, *e.g. d-d* transitions), ligand-centred (LC, *e.g.* π-π^* transitions, as seen for N-HBC **(17)** in Chapter 2), and transitions between MO's of different localization.[1] Transitions of this last class cause the displacement of the electronic charge from ligands to metal (LMCT) or *vice versa* (MLCT).

The absorption spectrum of $[Ru(bpy)_3]^{2+}$, figure 3.13 (b)(-), is well known.[7] The bands at 185 nm (not shown) and at 285 nm have been assigned to LC $\pi \rightarrow \pi^*$ transitions of the bpy ligands. The two remaining intense bands at 240 and 450 nm have been assigned to MLCT $d \rightarrow \pi^*$ transitions. The two shoulders between 300 and 350 nm are most likely due to MC $d \rightarrow d$ transitions. For the purpose of our discussion the most interesting band is that in the visible region, assigned to the lowest energy singlet MLCT absortion.

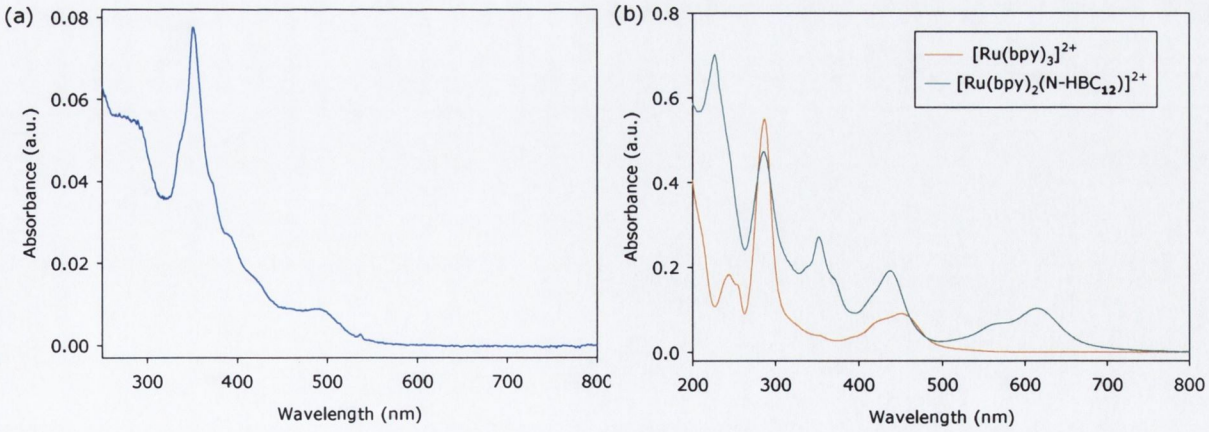


Figure 3.13. The absorption spectrum of (a) ligand N-HBC **(17)** and (b) $[Ru(bpy)_2(N\text{-}HBC_{17})]^{2+}$ and $[Ru(bpy)_3]^{2+}$ in acetonitrile.

The absorption spectra of **(17)** (figure 3.13 (a)) in acetonitrile shows its most intense band at 352.0 nm (see Chapter 2). The UV-vis absorption spectra of the complex **(35)** in acetonitrile (figure 3.13 (b)(-), table 3.4) shows intense bands in the UV region at 226.5 and 285.5 nm, and moderately less intense bands in the visible region at 351.5, 436.5 and 615.0 nm. As one can see from figure 3.13 (b), in the case of **(35)** a second absorption band has appeared in the visible region, which is considerably red-shifted to 615 nm.

Compound	Wavelength (nm)								
$[Ru(bpy)_2(N\text{-}HBC_{17})]^{2+}$	226.5	285.5	335.0 shoulder	351.5	370.0 shoulder	416.0 shoulder	436.5	564.5 shoulder	615.0
$[Ru(bpy)_3]^{2+}$	242.	284.0	320, shoulder	350, shoulder		436.0 shoulder	450.5	-	-

Table 3.4. The principle bands in the absorption spectrum of the $[Ru(bpy)_2(N\text{-}HBC_{17})]^{2+}$ complex **(35)** and $[Ru(bpy)_3]^{2+}$[38] in acetonitrile.

Analogous to other polypyridyl ruthenium complexes, the ultraviolet region of the absorption spectrum of **(35)** (figure 3.13 (b)(-)) is dominated by the intra ligand, LC $\pi\rightarrow\pi^*$ transitions due to both bpy (226.5 nm, $171x10^3$ L mol^{-1} cm^{-1} and 285.5 nm, $123.5x10^3$ L mol^{-1} cm^{-1}) and **(17)** (351.5 nm, $64x10^3$ L mol^{-1} cm^{-1}). The visible region of the spectrum of the new complex is characterized by the presence of the two broad $d\rightarrow\pi^*$ MLCT transitions, located at 436.5 (close to the corresponding transition of $[Ru(bpy)_3]^{2+}$, (450 nm)) and at 615 nm, each with a less intense shoulder at shorter wavelength. The intense band at 436.5 nm has a molar extinction coefficient of $47x10^3$ M^{-1} cm^{-1}, and is assigned, by comparison with $[Ru(bpy)_3]^{2+}$, to the MLCT due to coordinated bpy. The red-shifted absorption band at 615 nm, which is not present in the free ligand spectra, has a molar extinction coefficient of $26.5x10^3$ M^{-1} cm^{-1}. This band is associated with the promotion of a ruthenium *d* electron into a π^*-orbital of the N-HBC ligand. The presence of two MLCT bands for **(35)**, one for each type of ligand, is also seen in $[Ru(bpy)_2(CN_2\text{-}np)]^{2+}$ (CN_2-np=naphtho[2,3-*f*][1,ω]phenanthroline-9,14-dicarbonitrile),[37] but not in $[Ru(phen)_2(dicnq)]^{2+}$ (dicnq=6,7-dicyanodipyrido[2,2-*d*:2′,3′-*f*]-quinoxaline)[30] in which only one MLCT band is observed. It has been well established that such ruthenium MLCT states are not delocalized over all the ligands, but are localized on an individual ligand with a preference for the one with the lowest energy π^* state.[38]

The MLCT band at 615 nm is considerably red-shifted compared to that of $[Ru(bpy)_3]^{2+}$, because of the extended conjugation and enhanced electron affinity of the N-HBC ligand. Since highly conjugated N-HBC is more delocalised than bpy, there are lower-

lying π^* acceptor orbitals which stabilize the excited electron and lead to lower energy MLCT states.

These results explain the unusual green colour of this Ru(II) complex. Ruthenium polypyridyl complexes are usually orange, due to the single MLCT absorption band in the region of 450 nm, which absorbs blue light. Complex **(35)** on the other hand is an unusual strong black/green colour, as a result of the spectral sum of the yellow $[Ru(bpy)_2]^{2+}$ chromophore and the blue $[Ru(N\text{-}HBC_{17})]^{2+}$ chromophore.

The $[Ru(bpy)_2(N\text{-}HBC_{17})]^{2+}$ complex **(35)** does not exhibit pronounced solvatochromic behaviour, however there is variation, especially at the low energy end of the spectrum. The absorption spectra in acetonitrile, chloroform, methanol and tetrahydrofuran are shown in figure 3.14. The wavelengths of the lowest energy absorption band maximum, λ_{max}^{abs} (298 K), are collected in table 3.5.

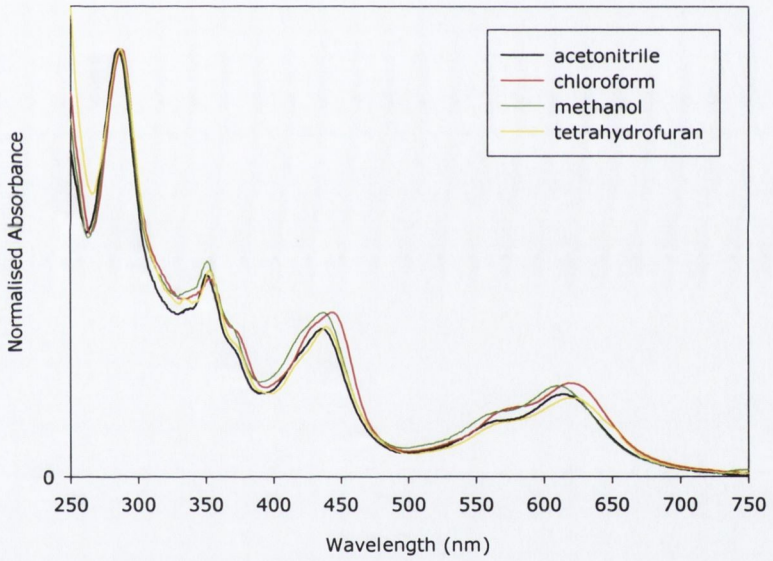


Figure 3.14. Absorption spectra of $[Ru(bpy)_2(N\text{-}HBC_{17})]^{2+}$ in various solvents.

Emission Spectroscopy

Uncoordinated N-HBC **(17)** emits strongly in the 500 – 600 nm range (see Chapter 2). N-HBC **(17)** is uniquely sensitive toward external triggers, thus chemically triggered emission changes were expected upon coordination of the N atoms. This was observed with the loss of the principal ligand emission in **(35)** and the observation of a new luminescent band in the 816 nm range. Figure 3.15 shows the normalised emission spectra of $[Ru(bpy)_2(N\text{-}HBC_{17})]^{2+}$ and $[Ru(bpy)_3]^{2+}$ in acetonitrile at room temperature.

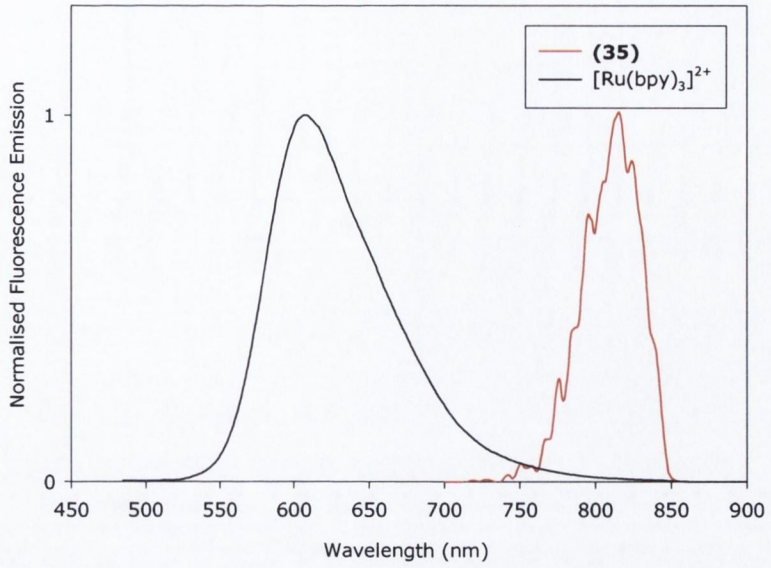


Figure 3.15. The normalized emission spectra of $[Ru(bpy)_2(N\text{-}HBC_{17})]^{2+}$, **(35)**, and $[Ru(bpy)_3]^{2+}$ in CH_3CN at 298 K.

When excited within the MLCT absorption band at 615 nm, in acetonitrile solution, complex **(35)** exhibits a broad emission centred at 816 nm (figure 3.15) with a lifetime of 13 ns (±1 ns). It should be noted that the complex has a relatively low emission quantum yield hence structure in the emission spectrum of **(35)** is due to the decrease in signal to noise ratio. These results are summarized along with the excited state lifetimes and emission quantum yields in table 3.5. The $[Ru(bpy)_2(N\text{-}HBC_{17})]^{2+}$ complex, with its emission maximum appearing around 816 nm, is considerably red-shifted in comparison to that measured for $[Ru(bpy)_3]^{2+}$ under similar experimental conditions of solvent and excitation wavelength. The data given in table 3.5 also reveal that the emission quantum yield for the complex is much lower than that of $[Ru(bpy)_3]^{2+}$ ($\phi_{em}=6.2\times10^{-2}$ in dry acetonitrile).

Complex	Solvent	λ_{max}^{abs} (nm)	λ_{max}^{em} (nm)	τ (ns)	ϕ_{em}
(35)	tetrahydrofuran	622.5	-	-	-
(35)	chloroform	618.0	811	39	5×10^{-3}
(35)	acetonitrile	615	816	13	1×10^{-4}
(35)	methanol	609.5	813	-	-
(35)	methanol:ethanol*	-	790	323	-
$[Ru(bpy)_3]^{2+}$	acetonitrile	452	615	800	6.2×10^{-2}

Table 3.5. Spectroscopic properties of the Near-Infrared emitter **(35)** in various de-aerated solvents together with $[Ru(bpy)_3]^{2+}$[7] at RT or at 77 K*.

Luminescent lifetimes of **(35)** at room temperature are in the 10-40 ns time domain. Luminescent quantum yields at room temperature are of the order of 10^{-3} to 10^{-4} (table

3.5), although the weak intensity and low energy of the luminescence of these complexes rendered an accurate determination of their ϕ_{em} values difficult.

At room temperature in fluid solution $[Ru(bpy)_2(N\text{-}HBC_{17})]^{2+}$ exhibits emission in all solvents investigated, although with varying intensity (see figure 3.16 (a)). The energy of the emission, λ_{em} (298 K), does not appear to be solvent dependent, however the decay of the emission, which always follows appreciably single exponential behaviour, gives lifetimes, τ (298 K), that do seem to depend strongly on the solvent (table 3.5). So whereas the emission in acetonitrile has a quantum yield of $1x10^{-4}$ and a lifetime of 13 ns, in chloroform these are $5x10^{-3}$ and 39 ns, respectively. Thus the relative emission intensity parallels the variation in lifetime.

Based on results reported in the literature for other ruthenium polypyridine complexes containing bpy ligands, this emission is more than likely N-HBC based with the bpy ligands acting as spectator ligands.[7,11] The luminescence of **(35)** is considerably red-shifted compared to $[Ru(bpy)_3]^{2+}$ (figure 3.15) as expected because of the lower-energy of the ^{1}MLCT (seen in the absorption spectra). This confirms the ^{3}MLCT luminescence nature of the emission of **(35)**. It is noted from the lifetime data (table 3.5) however, that the chromophoric group of the complex has a much shorter lifetime than that of $[Ru(bpy)_3]^{2+}$. This is assumed to be due to the energy-gap law.

In rigid glasses at 77 K, under these experimental conditions, the emission is strongly blue-shifted as a consequence of the lack of solvent relaxation (see figure 3.16 (b)).

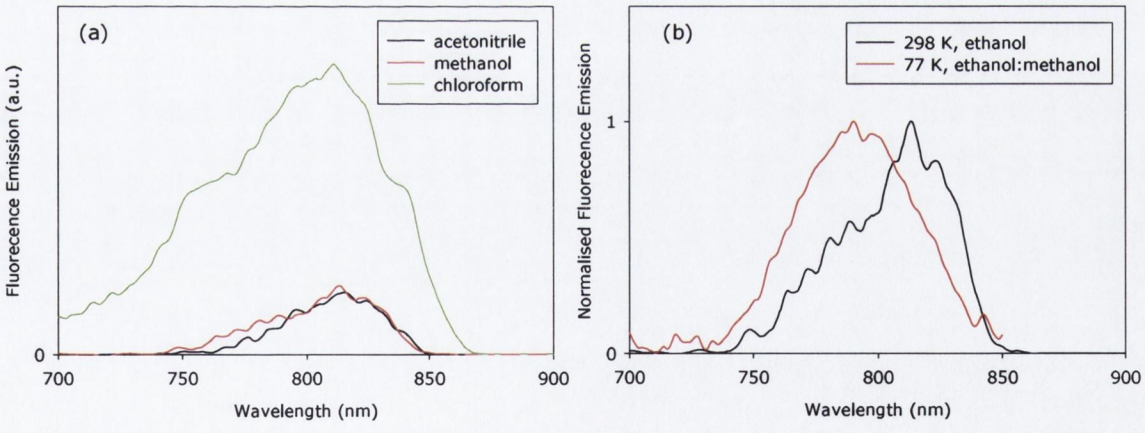


Figure 3.16. Emission spectra of $[Ru(bpy)_2(N\text{-}HBC_{17})]^{2+}$ (a) in various solvents and (b) at various temperatures.

The lifetime, τ (77 K), is greatly increased in the glassy solvent (table 3.5). This is explained by the energy-gap law, and the increase in energy of the ^{3}MLCT state.

Although this would decrease the gap between the ^{3}MLCT and the higher energy ^{3}MC excited states, the thermally activated decay pathway, *via* the ^{3}MC state is less accessible at lower temperature.

When ruthenium complex **(35)** is excited at 350 nm, a LC emission from the coordinated N-HBC is observed. This LC emission shows a vastly reduced quantum yield with a magnitude change from 0.22 for the free ligand to 0.001 for the complexed ligand in acetonitrile (99.5% reduction).

Discussion

Whilst ligand-based, $\pi \rightarrow \pi^*$ transitions dominate the near-UV region of the absorption spectrum of a Ru(II) complex,[5] the visible light absorption arises primarily from the charge transfer transitions from $d\pi(Ru^{II})$ to multiple, low-lying π^*(polypyridyl) energy levels. In the formation of these MLCT excited states, there is formally oxidation at the metal and reduction at the acceptor ligand, *e.g.* equation (3.3).[11,16]

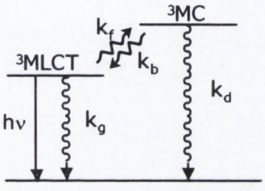
$$[Ru^{II}(bpy)_2(L)]^{2+} \xrightarrow{h\nu} [Ru^{III}(bpy)_2(L^{\bullet-})]^{2+*} \qquad (3.3)$$

For $[Ru(bpy)_3]^{2+}$, the $d\pi \rightarrow \pi_1^*$ transition occurs at 450 nm and $d\pi \rightarrow \pi_2^*$ transition at 243 nm in acetonitrile.[5] In the absorption spectrum, MLCT transitions produce excited states that are largely singlet in character, *e.g.* $^1(d\pi^5\pi^{*1})$, however emission occurs from an excited triplet state due to spin-orbit coupling.[8] The photophysical properties of $[Ru(bpy)_3]^{2+}$ have been the object of extensive investigations over many years, and it is well established that the lowest excited states of $[Ru(bpy)_3]^{2+}$ are mainly of triplet character (^{3}MLCT), hence the long emission lifetime.[39] A heteroleptic complex normally possesses separate ^{1}MLCT absorptions for each of the ligands, but rapid intramolecular electron transfer leads ultimately to a ^{3}MLCT state in which the excited electron is localized on the ligand having the lowest π^*-acceptor orbital.[16] Recently chemists have used these fundamental concepts in the design strategy of black absorbers,[11] to shift the $d\pi \rightarrow \pi^*$ bands systematically toward the red region of the spectrum. One way to do this is to provide low energy acceptor π^* levels for example by adding electron-withdrawing groups to a polypyridyl ligand, or by extending the conjugated π-framework.[11] Another way is to stabilize the "hole" at Ru^{III} in the MLCT state by introducing electron-donating ligands directly onto the metal.[16]

Complex **(35)** is simultaneously providing low energy π^* levels and "hole" stabilization. The relatively electron rich bipyridine ligands stabilize the excited-state hole at $*Ru^{III}$ by electron donation, while low energy π^* acceptor orbitals on the N-HBC ligand **(17)**

stabilize the excited electron. A combination of the two results in a small excited-to-ground-state energy gap and a near-IR emitter.[11,16]

The absorption and emission characteristics of **(35)** can be interpreted within the generally accepted scheme for the photophysics of Ru(II) polypyridine complexes (Scheme 3.1), where the emitting ^{3}MLCT state deactivates along two main competing channels: (i) direct radiationless transition to the ground state (k_g) and (ii) conversion to the lowest metal centred (^{3}MC) excited state (k_f and k_b are the forward and backward processes, respectively) and, from there, to the ground state (k_d).[5,14,39]



Scheme 3.1. Deactivation pathways for Ru(II) polypyridines.

Both deactivation channels are sensitive to changes in the energy of the ^{3}MLCT state. For k_g, the energy gap law of radiationless transitions predicts an exponential decrease in deactivation rate (k_g) with increasing ^{3}MLCT energy ($v^*=0 \rightarrow v=0$).[39] For the thermally activated pathway, on the other hand, the decay rate is expected to increase with increasing ^{3}MLCT energy because the increase in energy of the ^{3}MLCT state would result in a decrease of the ^{3}MLCT-to-^{3}MC separation. Thus, for a higher energy Ru^{II}-based MLCT emitter, the major contribution to decreased lifetimes occurs as a result of thermal population and nonradiative decay through low-lying, metal-centred *d-d* states.[5,14] For the lower energy near-IR emitter, **(35)**, these states are expected to be too high in energy to be thermally populated, so the decay of low energy emitters is generally dominated by the nonradiative process K_g.[11] It is possible to decrease this rate through increases in the delocalised nature and rigidity of the π^* framework of the acceptor ligands.[11] N-HBC **(17)** would be expected to help in this regard, with its large delocalised π-system and rigid planar structure. These two features decrease vibrational overlap between the ground and excited states and with it the rate of nonradiative decay. Similar magnitude red-shifts in the emission spectra have been seen for $[Ru(bpy)_2(dpop)]^{2+}$ (λ_{max}^{em}=802 nm in CH_3CN, dpop=dipyrido[2,3-*a*;2′,3′-*h*]phenazine) and for complexes with anionic ligands.[16] Anionic ligands stabilize the excited states by electron donation to Ru(III), causing a general shift in the MLCT bands.

3.2.2.4 Spectroelectrochemistry

Combining electrochemistry with diverse spectroscopic methods may yield valuable information about the identity and localization of the primary redox sites within a more complex molecule and the changes in structure and bonding associated with electron transfer. As already stated, oxidation is primarily a metal based process and may be regarded as the Ru(II/III) couple.

The visible-near-infrared spectra of **(35)** and of the electrochemically generated oxidized species are shown in figure 3.17 (a). The formation of the oxidized species is identified by a decrease in the intensity of the ^{1}MLCT bands at around 416 and 615 nm and the formation of new weak bands at around 400, 500, and 850 nm. The spectra show clear isobestic points at 379, 408, 463, 545 and 665 nm, indicating quantitative conversion.

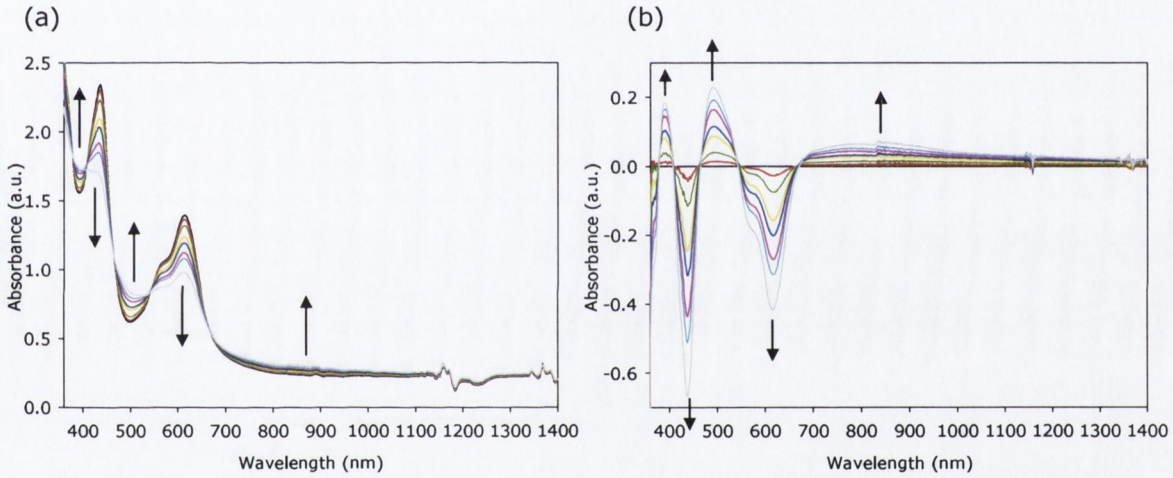


Figure 3.17. Visible and near-IR (a) absorption spectra and (b) "differential" spectra of **(35)** in dichloromethane with 0.1 M (TBA)PF_6 at 2.2 V (*vs* pseudo-Ag/AgCl). The arrows indicate the changes over time.

Although these processes were nonreversible in dichloromethane, reversibility was obtained in acetonitrile.

3.2.2.5 Acid-Base Properties

Preliminary studies show that the spectroscopic properties of **(35)** are dependent on the protonation state of the complex. For **(35)** in acetonitrile protonation is expected to occur on the two remaining, uncoordinated imine nitrogens of the complexed ligand **(17)**.

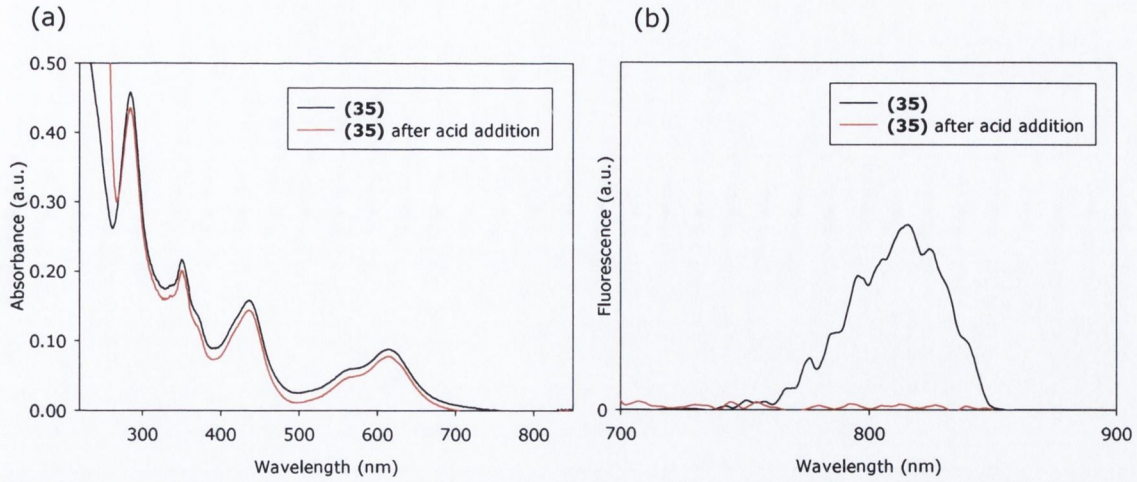


Figure 3.18. The (a) absorption and (b) emission spectra of Ru(II) complex **(35)** in acetonitrile on addition of perchloric acid.

Complex **(35)** shows little change to its UV-vis spectrum upon addition of acid (figure 3.18 (a)), however, total quenching of the ^{3}MLCT emission is observed (figure 3.18 (b)). This is unusual, as we would expect to see some change in the energy of the N-HBC$_{17}$ π^* LUMO upon acidification and therefore a change in the energy of the ^{1}MLCT excited state.[31]

The dramatic reduction in emission of **(35)** may be related to a decrease in the σ-donor strength of **(17)** upon acidification, which results in a lowering in the energy of the ^{3}MC level. The increased proximity of the ^{3}MLCT and ^{3}MC states could lead to rapid deactivation of the luminescent ^{3}MLCT state by thermally activated processes.[5,14]

3.2.2.6 Photodissociation

The main drawbacks in using $[Ru(bpy)_3]^{2+}$ as an ideal lumophore or photosensitiser are, firstly, the relatively fast radiationless decay of its lowest-energy ^{3}MLCT excited state and secondly, the occurrence of ligand photodissociation.[7] Manipulation of the ligand coordination sphere, *i.e.* by replacing bpy with other polypyridine ligands, has been used in an attempt to prevent such problems,[5,7,12] however, the improvement of a specific property can compromise other properties. For example, a higher photochemical stability is usually accompanied by a shorter excited-state lifetime (see below).

The ligand photodissociation of $[Ru(bpy)_3]^{2+}$ proceeds *via* a thermally activated radiationless transition from the luminescent ^{3}MLCT level to an upper lying, distorted ^{3}MC level (refer back to scheme 3.1). This level can undergo fast deactivation to the

ground state and/or cleavage of one Ru-N bond to form an intermediate containing a monodentate bpy ligand.[5] Such an intermediate can then undergo either loss of bpy, to form ligand dissociation products, or chelate ring closure, with reformation of $[Ru(bpy)_3]^{2+}$. A commonly used strategy to improve the photochemical stability of this type of complex is to reduce the population of the ^{3}MC state by increasing the energy gap between the ^{3}MC and the ^{3}MLCT levels. As said in the introduction, there are two ways to achieve this:

(i) Raise the energy of the ^{3}MC state: this is difficult as the energy of the ^{3}MC level is dependent on ligand field strength, which generally decreases when bpy is replaced by other polypyridine ligands.

(ii) Lower the energy of the ^{3}MLCT level: the disadvantage to this is that it increases the rate of the temperature-independent nonradiative decay from ^{3}MLCT directly to the ground state (k_g, scheme 3.1), with a consequent decrease of the excited-state lifetime and of the luminescence quantum yield,[7] both of which are observed for **(35)**.

This can be used to explain the photo-stability of **(35)**. The emitting ^{3}MLCT excited state is stabilized by the N-HBC ligand and lowered in energy. This creates a large ^{3}MC to ^{3}MLCT energy gap such that the ^{3}MC excited state is not easily accessible in this complex. This, as well as the fast radiationless decay of the ^{3}MLCT directly to the ground state, prevents population of the ^{3}MC state and photodissociation.

3.2.3 RUTHENIUM COMPLEX (34)

3.2.3.1 Synthesis and Characterisation

It was intended that the synthesis of the ruthenium(II) complex, **(34)**, incorporating two identical bpy bidentate ligands and the bidentate, uncyclised, N-doped polyphenylene **(16)** (see figure 3.19) would act as a suitable model complex when studying the photophysical properties of $[Ru(bpy)_2(N\text{-}HBC_{17})]^{2+}$. However its synthesis proved very challenging, and was only achieved *via* an *n*-butanol reflux of the acetone complex, $[Ru(bpy)_2(CH_3COCH_3)_2]^{2+}$, with **(16)** for several hours. Ruthenium complex **(34)** was synthesized as shown in figure 3.19.

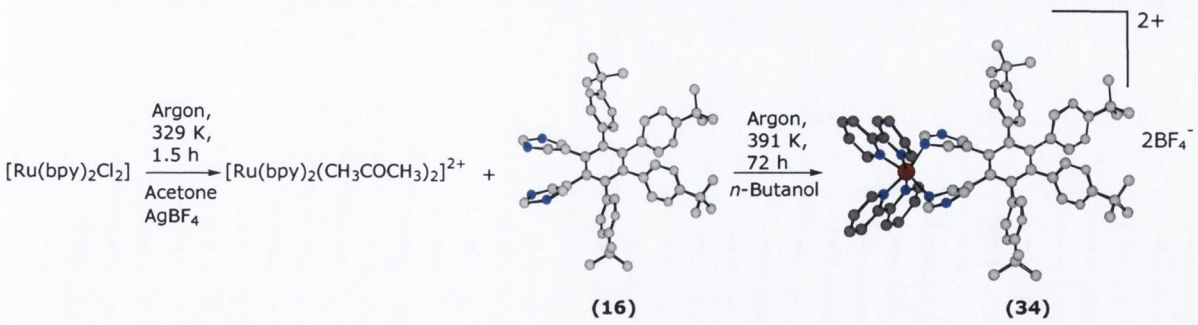


Figure 3.19. Chemdraw representation of the synthesis of Ru(II) complex **(34)** incorporating the N-doped polyphenylene ligand **(16)**.

The PF_6^- salt of the complex **(34)** was formed by addition of excess aqueous NH_4PF_6 to a solution of **(34)** in a minimum of acetonitrile. Crude **(34)** was isolated as a red-brown solid which was filtered and washed with water and diethyl ether. Several attempts to purify the solid were unsuccessful due to the instability of the complex in several solvents.

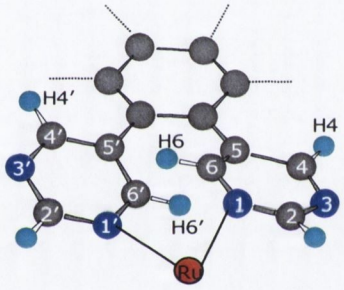


Figure 3.20. Chemdraw representation of the steric hindrance between protons at H_6 and $H_{6'}$ in **(34)**.

The difficulty in this synthesis of **(34)** is likely to arise from the steric interaction required by the coordination bond of **(16)** and Ru(II). Generally coordination has a flattening effect upon the bidentate ligand,[38] however, flattening of the pyrimidine rings of **(16)** is prevented due to the steric hindrance created at the 4 and 6 positions of the pyrimidine rings (see figure 3.20). These protons are not present in complex **(35)**.

The ^1H NMR spectrum of **(34)** shows evidence for a mixture of compounds in solution (CD_3CN) including chemical shifts for $[Ru(bpy)_2(CD_3CN)_2]^{2+}$. The formation of **(34)** could therefore only be confirmed through ESI-mass spectral analysis and accurate mass analysis.

The instability of the complex when subjected to column chromatography is also likely to be related to its distorted structure. Strong steric interactions between the protons of the pyrimidine rings results in a twisting of these rings and possibly an extension of the Ru-N**(16)** bond distances. Such a distortion has been found for the similar system $[Ru(bpy)_2(dppH)]^{2+}$ (dppH=2,9-diphenyl-1,10-phenanthroline), which undergoes clean and selective ligand substitution under irradiation with visible light.[32] Hindering bidentate ligands with poor σ-donor character are considered to decrease the ligand

field. This decreases the energy of the ^{3}MC level allowing significant overlap with the ^{3}MLCT state,[38,40] making photochemical instability a significant problem.

Photolabilisation is most likely to occur on the weakest ligand field axis.[32] Excitation in the MLCT region leads to a charge-transfer excited state, allowing the thermal population of low-lying dissociative *d-d* states,[32] and ligand substitution.

As expected, irradiation of **(34)** with visible light (300-800 nm) in degassed acetonitrile led very selectively to substitution of the bidentate ligand **(16)** by two molecules of solvent.

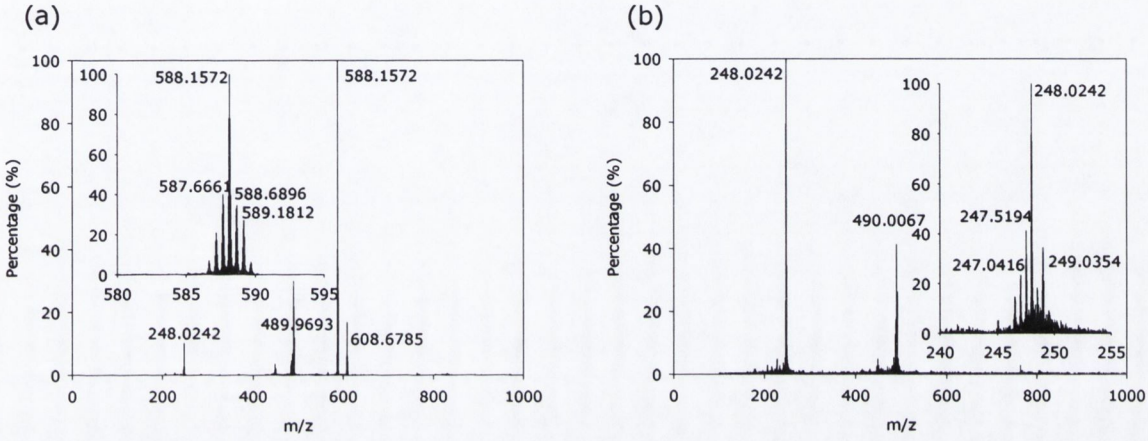


Figure 3.21. The ESI-mass spectrum of **(34)** in acetonitrile after (a) 0 and (b) 200 seconds of irradiation.

As illustrated in figure 3.21, after a few minutes of irradiation (125-W Mercury lamp) in acetonitrile, complex **(34)** ($[M\text{-}2PF_6]^{2+}$=588.2) is transformed into the $[Ru(bpy)_2(CH_3CN)_2]^{2+}$ species ($[M\text{-}2PF_6]^{2+}$=248.0) (The envelope in both spectra at *m/z*=490 is assigned to the unreacted starting material $[Ru(bpy)_2Cl_2]$). This result can be shown using the following equation (3.4):[32]

$$[Ru(bpy)_2\mathbf{(16)}]^{2+} \xrightarrow[CH_3CN]{h\nu} [Ru(bpy)_2(CH_3CN)_2]^{2+} + \mathbf{(16)} \qquad (3.4)$$

Cleavage of an Ru-N bond occurs *via* the ^{3}MC excited state.[5] This species can reform the starting material, in the absence of a ligating group, or in the presence of a ligating group, such as acetonitrile, form a monodentate intermediate.[5,8] This species can then undergo loss of **(16)** with the formation of $[Ru(bpy)_2(CH_3CN)_2]^{2+}$. Preference for the loss of **(16)**, over bpy, is due to its poor σ-donor character and high steric strain.

Development of materials capable of signal processing and information storage at the molecular level is based on molecules able to exist in two stable states, with fast and quantitative interconversion between these states.[32] Photolabilisation of a ligand

followed by its recoordination in the dark could be the key steps in the construction of photoswitchable molecular devices. Although it is capable of clean photo-expulsion of a given ligand with a high quantum efficiency, unfortunately complex **(34)** is too difficult to synthesize and far too unstable for it to be useful for devices.

3.2.4 PALLADIUM COMPLEX (36)

3.2.4.1 Synthesis and Characterisation

The (η^3-allyl)Pd(II) complex **(36)** was prepared as shown in figure 3.22. After treatment of the dimer $[Pd(\eta^3\text{-}C_3H_5)(\mu\text{-}Cl)]_2$ with $AgNO_3$ in acetonitrile solution, the AgCl formed in the reaction was filtered and N-HBC **(17)** was subsequently added as a toluene solution. After stirring for 12 h, the red precipitate was collected. An excess of aqueous NH_4PF_6 was added to an acetonitrile solution of crude (η^3-allyl)palladium complex, to precipitate the red/black solid of **(36)** as the PF_6^- salt.

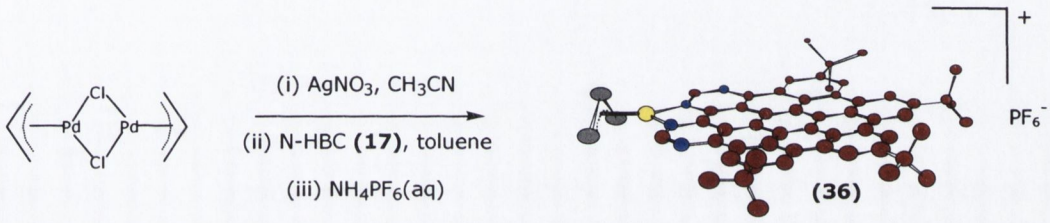


Figure 3.22. Chemdraw representation of the synthesis of $[Pd(\eta^3\text{-}C_3H_5)(N\text{-}HBC_{17})]PF_6$, complex **(36)**.

The $[Pd(\eta^3\text{-}C_3H_5)(N\text{-}HBC_{17})]PF_6$ complex, **(36)**, was characterized by NMR and IR spectroscopy and by ESI-mass spectral analysis and accurate mass analysis. UV-vis and fluorescence spectroscopic analyses are also included. The IR spectrum shows the characteristic vibrational bands of the allyl group, and N-HBC **(17)**, see Chapter 6. The complex $[Pd(\eta^3\text{-}C_3H_5)(N\text{-}HBC_{17})]PF_6$, **(36)**, is only sparingly soluble in acetone, tetrahydrofuran, and more polar solvents such as methanol. Attempts to measure ^1H NMR spectra of **(36)** were hampered by poor solubility in a wide range of deuterated solvents. However, ^1H NMR spectroscopy was carried out in $CDCl_3$, and indicates the C_s symmetry of **(36)** due to equivalence in the allyl moiety. The ^1H NMR spectrum of the complex is shown in figure 3.23 (b) with the data given in table 3.6. Assignment of the different signals was made by literature comparisons.[28,29,41] The atom labelling scheme is shown in figure 3.24.

The (η^3-allyl)Pd(II) unit is chelated by two nitrogens of the N-HBC ligand **(17)**. Although broad peaks are displayed for the coordinated N-HBC ligand, evidence for complexation of **(17)** in the (η^3-allyl)Pd(II) complex is provided by the observation of positive coordination-induced shifts for N-HBC when compared to those of the free ligand. There is a general downfield shift of the aromatic protons of **(17)**, H13-H16,

from the region of δ 8.9 - δ 9.4 in the free ligand to the region of δ 9.2 – δ 9.45 in the complex (see figure 3.23, (a) and (b)). This is due to deshielding through charge depletion upon coordination. It is believed that the signal at δ 8.56 in the ^{1}H NMR spectrum of **(36)** is due to the aromatic proton H19. Similarly to the Ru(II) complex of **(17)**, the chemical shift of H19 is shifted a substantial 1.2 ppm upfield upon coordination, from δ 9.79 to δ 8.56. This is as a result of its being pointed directly toward the shielding region of the allyl ligand.

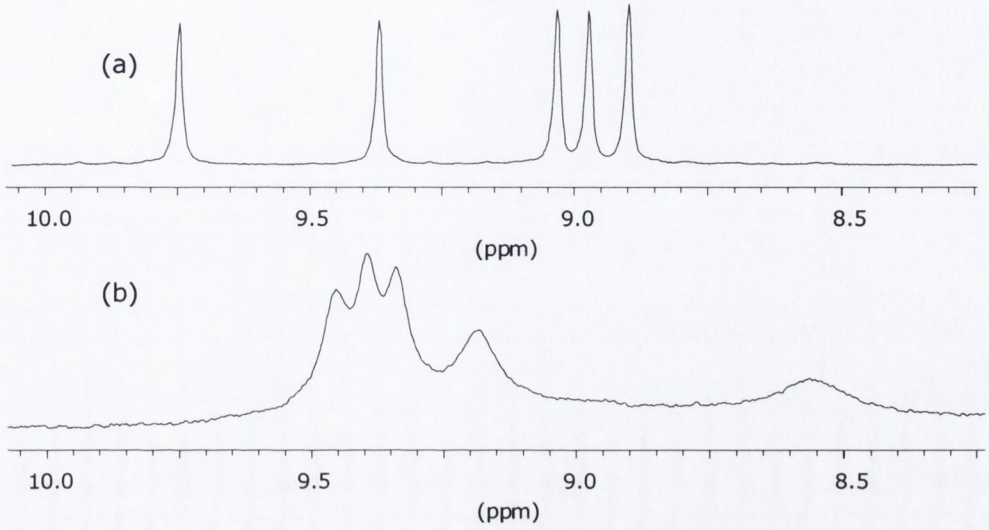


Figure 3.23. The ^{1}H NMR spectra of (a) N-HBC ligand **(17)** and (b) $[Pd(\eta^3\text{-}C_3H_5)(N\text{-}HBC_{17})]PF_6$, **(36)** ($CDCl_3$, RT, 400 MHz).

In the ^{1}H NMR spectra of **(36)** three signals for the allyl ligand are observed (see table 3.6). The two *syn* protons are equivalent and the two *anti* protons are equivalent. The allyl moiety, therefore, displays two broad singlets for the terminal *syn* and *anti* protons and a third broad singlet for the central H2 proton. Broadening of the spectrum may indicate an incipient fluxional behaviour, probably involving an $\eta^1\text{-}\eta^3\text{-}\eta^1$ isomerism.[41c] Rapid apparent rotation of the allyl ligand is also likely.[29]

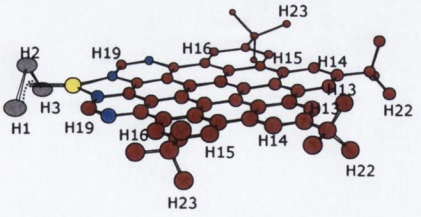


Figure 3.24. The atom labelling scheme of $[Pd(\eta^3\text{-}C_3H_5)(N\text{-}HBC_{17})]PF_6$, **(36)**.

^{1}H NMR	Chemical shift for (36)	Integration
H22, H23	1.86, 1.96; s	2x18H
H1, $H3^{anti}$	2.87; br s	2H
H1, $H3^{syn}$	4.24; br s	2H
H2	5.61; br s	1H
H19	8.56; br s	2H
H13-H16	9.18, 9.34, 9.40, 9.45; br s	4x2H

Table 3.6. The ^{1}H NMR spectral data of $[Pd(\eta^3\text{-}C_3H_5)(N\text{-}HBC_{17})]PF_6$, **(36)** ($CDCl_3$, RT, 400 MHz).

In the case of the cationic complex **(36)**, an NOe between H19 and $H1^{syn}$ and $H3^{syn}$ was not observed at room temperature. This may also be as a result of fluxionality of the η^3-allyl moiety.[29,41] Low-temperature NMR analysis might serve to verify this hypothesis.[41]

A downfield shift of H2, when compared to other reported (η^3-allyl)Pd(II) complexes, would indicate a reduction of electron density for this proton. The chemical shift of H2 (δ 5.61) suggests the electron withdrawing nature of the N-HBC ligand is analogous to that of other published ligands (*e.g.* 2-(3-methylpyridin-2-yl)-imidazole[41]) since this signal does not appear downfield of those reported for other (η^3-allyl)Pd(II) complexes.[28,41]

The ESI-mass spectrum, in methanol, shows a base peak at *m/z*=898.1, assigned to $[M\text{-}PF_6]^+$ (figure 3.25). This is in agreement with the calculated value for **(36)** (*m/z*=898.4).

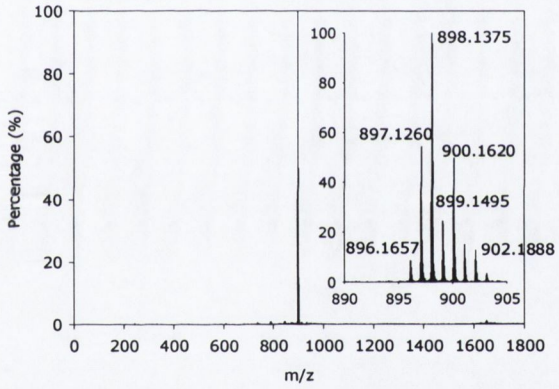


Figure 3.25. The ESI-mass spectrum of $[Pd(\eta^3\text{-}C_3H_5)(N\text{-}HBC_{17})]^+$ **(36)** in methanol.

The presence of only a single signal in the ESI-mass spectrum of complex **(36)** gives an indication of the purity of the sample, although it has not been possible to obtain confirmation by elemental analysis. The non-invasive method of accurate mass analysis, in methanol, gave a $[C_{57}H_{51}N_4Pd]^+$ peak of 897.3182, correct to within 5 ppm of that calculated for **(36)**.

3.2.4.2 Photophysical Properties of (36)

The electronic absorption spectra of **(36)**, covering the 280-900 nm range in methanol and tetrahydrofuran, are shown in figure 3.26. The intense absorption bands in the 340-700 nm region are also featured in the free ligand **(17)**, and are reasonably attributed to the metal-perturbed, $\pi \rightarrow \pi^*$ transitions within the coordinated ligand

molecule. These bands experience a general red-shift in solvents of higher polarity, in compliance with Kasha's criteria for $\pi \rightarrow \pi^*$ transitions and their charge transfer character (see Chapter 2). The absorption maxima are reported in table 3.7.

Solvent	Wavelength (nm)							
toluene	-	-	343.5	359.0	410.0	436.0	505 (sh)	539.5
tetrahydrofuran	-	-	343.0	359.0	412.0	436.5	512 (sh)	546.5
methanol	214.0	283.5	347.5	359.0	416.0	441.0	525 (sh)	550.0

Table 3.7. Peaks for the absorption bands for $[Pd(\eta^3\text{-}C_3H_5)(N\text{-}HBC_{17})]PF_6$ in various solvents.

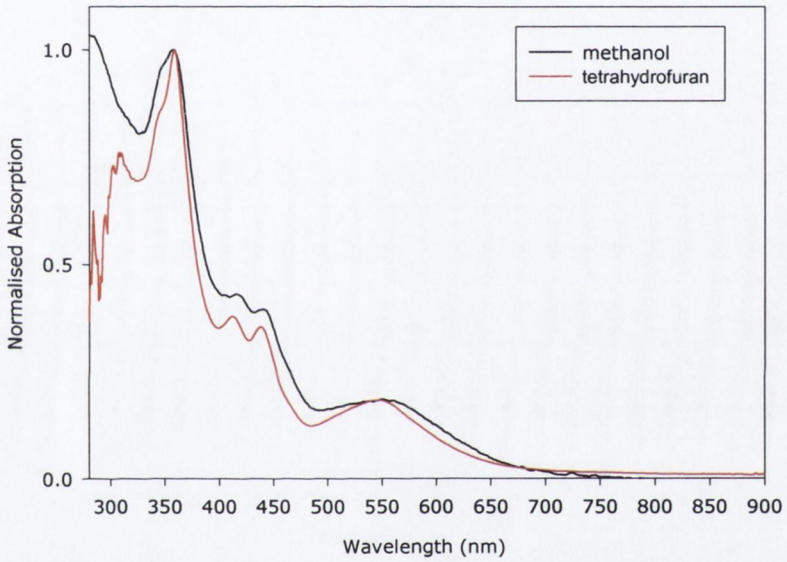


Figure 3.26. The normalised absorption spectrum of $[Pd(\eta^3\text{-}C_3H_5)(N\text{-}HBC_{17})]PF_6$ in methanol or tetrahydrofuran.

The fluorescence properties of the complex **(36)** were investigated in tetrahydrofuran solution at room temperature, and no emission was observed.

Coordination of two of the peripheral nitrogen atoms by the gradual addition of $[Pd(\eta^3\text{-}C_3H_5)(CH_3CN)_2]NO_3$ to **(17)**, causes major changes in the absorption and emission spectra, as seen in figure 3.27. These effects (on the absorption and emission spectra of (η^3-allyl)Pd(II) coordination to N-HBC **(17)**) bear a strong resemblance to those of acid addition (see Chapter 2).

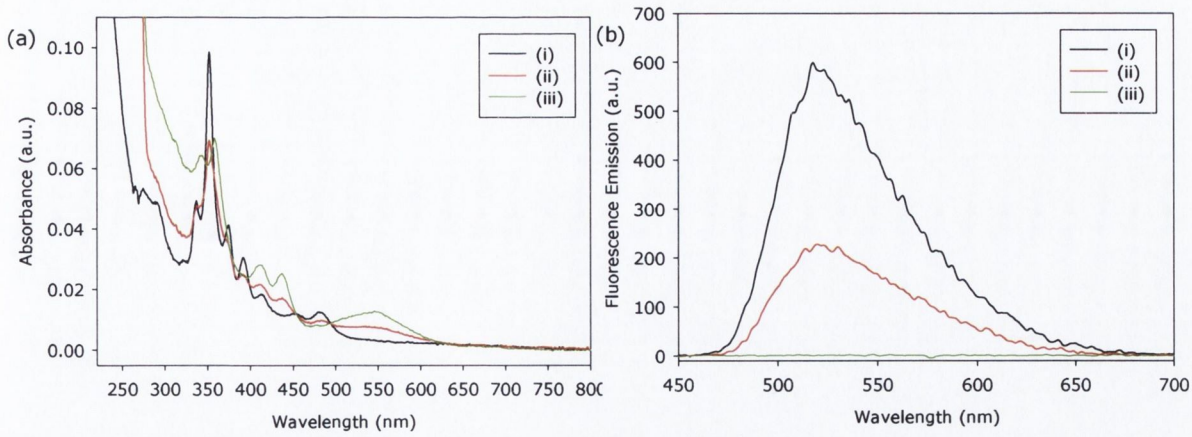


Figure 3.27. The (a) absorption and (b) emission spectra of ligand **(17)** in tetrahydrofuran (4 mL, 6.66×10^{-7} M) on addition of (i) 0 μLs, (ii) 20 μLs and (iii) 180 μLs of $[Pd(\eta^3\text{-}C_3H_5)(CH_3CN)_2]^+$ (4.37×10^{-4} M).

The addition of $[Pd(\eta^3\text{-}C_3H_5)(CH_3CN)_2]^+$ to **(17)** causes strong changes over the entire absorption spectrum (figure 3.27 (a)), in particular, in the low energy region where the bands move to the red. There is a decrease in intensity of the 355 nm absorption band along with the disappearance of the 376 nm band. These results again confirm the assignment of the 376 nm band in the absorption spectrum of **(17)** as an $n \rightarrow \pi^*$ transition, according to Kasha's criteria, with the decrease of the 355 nm band suggesting it is a $\pi \rightarrow \pi^*$ transition which has some $n \rightarrow \pi^*$ character.

The fluorescence spectrum (figure 3.27 (b)), like the absorption spectrum, undergoes changes upon coordination of (η^3-allyl)Pd(II). For similar Pd(II) complexes,[42] it has been found that their luminescence mainly involves electronic transitions centred on the organic ligands. In tetrahydrofuran solution, at room temperature, **(17)** displays a fluorescence band centred at 522.5 nm. As discussed in Chapter 2, this was assigned to the $^1(\pi,\pi^*)$ state of **(17)**. Upon coordination to Pd(II) the emission is efficiently quenched.

These changes in the UV-vis and fluorescence spectra mimic the behaviour seen on addition of trifluoroacetic acid to **(17)**. This would seem to indicate that a similar process is occurring that enables efficient radiationless deactivation of the resulting complex. As discussed earlier, the lowest-energy band in the absorption spectrum of **(17)** can be assigned to the spin-allowed $\pi \rightarrow \pi^*$ transition. It is likely that this $^1(\pi,\pi^*)$ state of **(17)** becomes stabilized upon coordination of the imine nitrogens to Pd(II), because of its partial charge transfer. Hence this absorption is shifted to the red region of the absorption spectrum. The decrease in the radiative rate constant on coordination can thus be related to the decrease in energy of the electronic transition.[43]

Alternatively the $^1(n,\pi^*)$ state of **(17)** may have moved below the $^1(\pi,\pi^*)$ during coordination, becoming the lowest excited singlet state and providing a fast decay pathway.[44]

A third explanation for the quenching of the fluorescent emission from $[Pd(\eta^3\text{-}C_3H_5)(N\text{-}HBC_{17})]PF_6$ is that the MC excited states, which presumably lie at low energies, are thermally populated and undergo radiationless deactivation.[42] This mode of quenching is found in similar Pd(II) complexes.[42]

The Pd(II) ion possesses a d^8 electronic configuration which can alter the ground-state energies of the bonded ligands so allowing, in some cases, MLCT transitions (*ca.* 350-550 nm).[42] This does not appear to be the case, however, for (η^3-allyl)Pd(II) complex **(36)**. The absorption spectra of **(36)** were measured up to the detector limit (1100 nm). On comparison with the spectral data of **(17)**, **(36)** shows no evidence for any MLCT process involving the Pd(II) metal atom.

3.3 SUMMARY

The new ligand N-HBC **(17)**, while retaining the basic HBC structure, also possesses electron withdrawing imine nitrogens in its architecture. Until now N-HBC **(17)** has not been tested as a ligand for metal complexation. I have succeeded in the synthesis of two new complexes with the transition metals Ru(II) and Pd(II). The ligand successfully undergoes metal complexation to form octahedral and square planar complexes in good yield. These compounds are air-stable solids with unusual photophysical properties.

The ruthenium(II) complex containing the N-HBC ligand was synthesized by heating the appropriate mole ratio of the precursor complex and ligand in diethylene glycol ethyl ether at reflux and precipitating the product as the PF_6^- salt. The mono ruthenium(II) octahedral complex **(35)** of the novel ligand N-HBC was fully characterised by ^{1}H-NMR spectroscopy, ESI-MS and accurate mass spectrometry and cyclic voltammetric methods. Results of UV-vis absorption spectra are also included and lifetimes and fluorescence emission spectra were measured at room temperature and at 77 K.

NMR spectra give evidence that coordination has occurred. In these spectra, resonances due to the protons of coordinated bpy and **(17)** are seen to be shifted (to both downfield and upfield regions) compared to those of the free ligand, indicating complexation.

The Ru(II) complex **(35)** has interesting spectroscopic, photophysical and electrochemical properties. In the UV-vis spectra of $[Ru(bpy)_2(N\text{-}HBC_{17})]^{2+}$, the ultraviolet regions show intense bands arising from the intra-ligand $\pi \rightarrow \pi^*$ transitions due to coordinated bpy and N-HBC **(17)**. The visible spectrum of $[Ru(bpy)_2(N\text{-}HBC_{17})]^{2+}$ is dominated by MLCT transitions at 437 and 615 nm as a result of promotion of an electron from filled metal *d*-orbitals to low-lying π^* acceptor orbitals on the N-HBC ligand, **(17)**. MLCT states are responsible for the low energy absorption bands at 615 nm in acetonitrile and emission maxima (λ_{max}) at 816 nm. The near-IR emitter has a lifetime of 13 ns, and like other black MLCT absorbers is photochemically inert.[16]

The emission spectrum of **(35)** has the typical spectral and photophysical features of a Ru(II) polypyridine ^{3}MLCT transition and does not shift significantly with solvent. However, the lifetime and intensity of the emission are strongly pH and solvent-dependent. In low-temperature rigid glasses, a blue-shifted emission from $[Ru(bpy)_2(N\text{-}HBC_{17})]^{2+}$ is observed. In this complex the emission has been shifted into

the infrared, with appreciable absorption throughout the near-UV and visible spectral regions.

Electrochemical results suggest that electron abstraction from the metal centre is more difficult in **(35)** than in $[Ru(bpy)_3]^{2+}$. This is due to the presence of the electron accepting ligand **(17)**. Complex **(35)** shows better π-acceptor properties than the ligand **(17)**.

By coordinating polyphenylene **(16)**, instead of N-HBC **(17)**, to the Ru(II) centre, we add to the steric strain within the ligand. In contrast to complex **(35)**, the photochemically active Ru(II) complex **(34)** undergoes selective photoexpulsion and solvent coordination under light irradiation. With development, this photolabile complex could be incorporated as a building block into multi-component systems.

The new cationic $[Pd(\eta^3\text{-}C_3H_5)(N\text{-}HBC_{17})]PF_6$ complex has also been prepared and isolated. The stable cationic (η^3-allyl)palladium(II)(N-HBC_{17}) complex **(36)** was synthesized from the dimer $[Pd(\eta^3\text{-}C_3H_5)(\mu\text{-}Cl)]_2$ and fully characterised by ^1H NMR spectroscopy and ESI-MS and accurate mass spectrometry.

Again ^1H NMR spectra give a good indication that coordination had occurred, with the resonances due to bound **(17)** shifted to both downfield and upfield regions compared to those for the free ligand.

Coordination has a profound electronic effect on the π-electron density throughout the ligand system, as seen by large red-shifts in the absorption spectrum that mimic those observed on protonation. Metal perturbed LC bands are detected in the 340-700 nm spectral region and the fluorescent emission from **(17)** is quenched upon complexation. It is believed that this occurs through a similar mechanism of non-radiative decay to that found on protonation.

3.4 FUTURE WORK

The work described in this Chapter has opened several avenues by which to extend the use of N-HBC as a ligand in the synthesis of complexes with materials applications.

With regard to the mononuclear Ru(II) complex **(35)**, the synthesis of bis- and tris-(N-HBC_{17}) ruthenium complexes may give access to a family of black MLCT absorbers, with potential use as photosensitisers. Within this family, the progressive replacement of bpy with N-HBC_{17} ligand is likely to have considerable effect on the photophysical properties of the resulting complex, which should be assessed. The DNA-binding ability of ruthenium complex **(35)** should also be investigated. N-HBC **(17)** has a larger extended π-system than the DNA intercalator dppz, which has well documented DNA-binding and photocleavage properties.[45] Its unique architecture and extended π-system may give **(35)** unusual DNA-binding properties, which could be studied, initially, by absorption titration (*e.g.* with calf-thymus DNA).

The non-linear optical responses of both the Ru(II) complex **(35)** and the Pd(II) complex **(36)** are worthy of study. Both will be an integral part of further investigations.

With regard to the Pd(II) complex **(36)**, its influence in the palladium-catalysed allylic substitution should be analysed (through catalytic investigations). The allyl fluxionality could be investigated (using low temperature NMR studies) and its liquid crystallinity assessed. Discotic liquid crystals of organic transition metal complexes have been shown recently to exhibit columnar liquid crystalline phases,[46] for example the octa-alkyl bis(diphenyldithiolene)nickel complexes which are the first examples of π-acceptor columnar liquid crystals.[47] Liquid crystallinity has been shown to be greatly affected by the central metal species,[46] with the Pd complexes exhibiting higher clearing points, a broader temperature range of the mesophase and better π-acceptor columnar mesogens than the corresponding Ni or Pt complexes.[46]

The scope of the research could be extended to polynuclear transition metal complexes. The synthetic strategy used to prepare N-HBCs gives control over the amount of N-doping and thus the possible number of metal coordination sites. This should facilitate the synthesis of polynuclear transition metal complexes using bridging N-HBC ligands. Polynuclear transition metal complexes not only exhibit properties related to each metal-based component, but also properties related to the structure and composition of the array.[1] There is particular interest in the design and construction of multicomponent systems capable of performing light- and/or redox-induced

functions.[1] For example, the coupling of photo-reactive groups *e.g.* Ru(II) and Os(II). The electronic nature of the bridging ligand (N-HBC in this case) is key in determining the electronic coupling between metal centres.[48] Polynuclear complexes involving N-HBC may ensure unusually strong coupling between metal centres, and thus offer long-range electronic communication. Once formed, dinuclear complexes may also show a metal interaction strongly dependent on the protonation state of the bridging ligand,[31] which could incorporate up to eight uncoordinated nitrogen atoms. These would have potential as components in proton gated redox active and emitting devices.

A final extension of this work could involve variation of the metal centre. A number of suitable metal reagents are envisaged for the synthesis of a variety of metal complexes; using the bpy type coordinating region of N-HBC (*e.g.* complexes $[Fe(N\text{-}HBC_{\mathbf{17}})_3]^{2+}$ and $[Cu(N\text{-}HBC_{\mathbf{17}})_2]^{+}$); using the π-system of N-HBC, (*e.g.* tricarbonylchromium complexes similar to that synthesized with *tert*-butyl substituted HBC[49]); and using an alkyne moiety for the introduction of metal clusters into N-HBC derivatives (*e.g. via* the N-doped alkyne substituted polyphenylene **(29)**).

3.5 REFERENCES

1. V. Balzani, A. Juris, M. Venturi, S. Campagna, S. Serroni, *Chem. Rev.*, **1996**, *96*, 759-833 (and References therein)
2. V. Balzani, F. Scandola, in *Supramolecular Photochemistry*, Ellis Horwood, Chichester, UK, **1991**
3. N. Long, *Angew. Chem., Int. Ed. Engl.*, **1995**, *34*, 21-38
4. H. Kobayashi, *Curr. Opin. Solid State and Mater. Science*, **1997**, *2*, 440-445
5. A. Juris, V. Balzani, F. Barigelletti, S. Campagna, P. Belser, A. von Zelewsky, *Coord. Chem. Rev.*, **1988**, *84*, 85-277
6. U. Nettekoven, M. Widhalm, H. Kalchhauser, P. C. J. Kamer, P. W. N. van Leeuwen, M. Lutz, A. L. Spek, *J. Org. Chem.*, **2001**, *66*, 759-770
7. F. Barigelletti, L. De Cola, V. Balzani, P. Belser, A. von Zelewsky, F. Vögtle, F. Ebmeyer, S. Grammenudi, *J. Am. Chem. Soc.*, **1989**, *111*, 4662-4668
8. (a) R. J. Watts, *J. Chem. Educ.*, **1983**, *60*, 834-842, (b) K. Kalyanasundaram, *Coord. Chem. Rev.*, **1982**, *46*, 159-244
9. Y. Z. Hu, S. Tsukiji, S. Shinkai, S. Oishi, I. Hamachi, *J. Am. Chem. Soc.*, **2000**, *122*, 241-253
10. L. De Cola, P. Belser, *Coord. Chem. Rev.*, **1998**, *177*, 301-346
11. J. A. Treadway, G. F. Strouse, R. R. Ruminski, T. J. Meyer, *Inorg. Chem.*, **2001**, *40*, 4508-4509
12. G. H. Allen, R. P. White, D. P. Rillema, T. J. Meyer, *J. Am. Chem. Soc.*, **1984**, *106*, 2613-2620
13. M. T. Indelli, C. A. Bignozzi, F. Scandola, J. P. Collin, *Inorg. Chem.*, **1998**, *37*, 6084-6089
14. J. M. Calvert, J. V. Caspar, R. A. Binstead, T. D. Westmoreland, T. J. Meyer, *J. Am. Chem. Soc.*, **1982**, *104*, 6620-6627
15. F. Barigelletti, L. Flamigni, M. Guardigli, J. P. Sauvage, J. P. Collin, A. Sour, *Chem. Commun.*, **1996**, 1329-1330
16. P. A. Anderson, G. F. Strouse, J. A. Treadway, F. R. Keene, T. J. Meyer, *Inorg. Chem.*, **1994**, *33*, 3863-3864
17. A. N. Macpherson, P. H. Turner, T. G. Truscott, *Appl. Spectrosc.*, **1994**, *48*, 539
18. W. D. Horrocks, J. P. Bolender, W. D. Smith, R. M. Supkowski, *J. Am. Chem. Soc.*, **1997**, *119*, 5972-5973
19. B. Dmitry, G. V. Ponomarev, O. S. Wolfbeis, *Spectrochim. Acta, Part A*, **1996**, *52*, 1629-1638
20. Q. Yao, A. W. Maverick, *Inorg. Chem.*, **1988**, *27*, 1669-1670
21. A. Ambroise, B. G. Maiya, *Inorg. Chem.*, **2000**, *39*, 4256-4263
22. A. Ambroise, B. G. Maiya, *Inorg. Chem.*, **1996**, *35*, 4267-4270
23. J. Tsuji, in *Palladium Reagents and Catalysts, Innovation in Organic Synthesis*, Wiley, Chichester, **1995**
24. S. Kotha, K. Lahiri, D. Kashinath, *Tetrahedron*, **2002**, *58*, 9633-9695
25. M. Sauthier, J. Forniés-Cámer, L. Toupet, R. Réau, *Organometallics*, **2000**, *19*, 553-562
26. J. Tsuji, H. Takahashi, M. Morikawa, *Tetrahedron Lett.*, **1965**, *49*, 4387-4388
27. B. M. Trost, T. R. Verhoeven, *J. Am. Chem. Soc.*, **1976**, *98*, 630-632
28. A. Satake, T. Nakata, *J. Am. Chem. Soc.*, **1998**, *120*, 10391-10396
29. M. C. Carrión, A. Díaz, A. Guerrero, F. A. Jalón, B. R. Manzano, A. Rodríguez, R. L. Paul, J. C. Jeffery, *J. Organomet. Chem.*, **2002**, *650*, 210-222
30. A. Ambroise, B. G. Maiya, *Inorg. Chem.*, **2000**, *39*, 4264-4272
31. C. D. Pietro, S. Serroni, S. Campagna, M. T. Gandolfi, R. Ballardini, S. Fanni, W. R. Browne, J. G. Vos, *Inorg. Chem.*, **2002**, *41*, 2871-2878
32. A. C. Laemmel, J. P. Collin, J. P. Sauvage, *Eur. J. Inorg. Chem.*, **1999**, 383-386
33. E. Baranoff, J. P. Collin, Y. Furusho, A. C. Laemmel, J. P. Sauvage, *Chem. Commun.*, **2000**, 1935-1936
34. B. H. Ye, X. M. Chen, T. X. Zeng, L. N. Ji, *Inorg. Chim. Acta*, **1995**, *240*, 5-11
35. E. Amouyal, A. Homsi, J. C. Chambron, J. P. Sauvage, *J. Chem. Soc., Dalton Trans.*, **1990**, 1841-1845
36. M. K. DeArmond, C. M. Carlin, *Coord. Chem. Rev.*, **1981**, *36*, 325-355

37. G. Albano, P. Belser, L. De Cola, M. T. Gandolfi, *Chem. Commun.*, **1999**, 1171-1172
38. R. Thummel, F. Lefoulon, J. D. Korp, *Inorg. Chem.*, **1987**, *26*, 2370-2376
39. T. J. Meyer, *Pure Appl. Chem.*, **1986**, *58*, 1193-1206
40. T. C. Strekas, H. D. Gafney, S. A. Tysoe, R. P. Thummel, F. Lefoulon, *Inorg. Chem.*, **1989**, *28*, 2964-2967
41. (a) N. Tsukada, T. Sato, H. Mori, S. Sugawara, C. Kabuto, S. Miyano, Y. Inoue, *J. Organomet. Chem.*, **2001**, *627*, 121-126; (b) A. Satake, H. Koshino, T. Nakata, *Organometallics*, **1999**, *18*, 5108-5111; (c) L. Canovese, F. Visentin, G. Chessa, A. Niero, P. Uguagliati, *Inorg. Chim. Acta*, **1999**, *293*, 44-52
42. I. Aiello, M. Ghedini, M. La Deda, *J. Lumin.*, **2002**, *96*, 249-259
43. N. Armaroli, L. De Cola, V. Balzani, J. P. Sauvage, C. O. Dietrich-Buchecker, J. Kern, *J. Chem. Soc., Faraday Trans.*, **1992**, *88*, 553-556
44. B. N. Bandyopadhyay, A. Harriman, *J. Chem. Soc., Faraday Trans.*, **1977**, *73*, 663-674
45. M. Hashimoto, K. Sakata, *Polyhedron*, **1997**, *16*, 975-981
46. K. Ohta, Y. Inagaki-Oka, H. Hasebe, I. Yamamoto, *Polyhedron*, **2000**, *19*, 267-274
47. K. Ohta, H. Hasebe, M. Moriya, T. Fujimoto, I. Yamamoto, *Mol. Cryst. Liq. Cryst.*, **1991**, *208*, 33-41
48. M. Beley, J. P. Collin, J. P. Sauvage, *Inorg. Chem.*, **1993**, *32*, 4539-4543
49. P. T. Herwig, V. Enkelmann, O. Schmelz, K. Müllen, *Chem. Eur. J.*, **2000**, *6*, 1834-1839

CHAPTER FOUR

POLYARYL FERROCENE COMPOUNDS - TOWARD THE SYNTHESIS OF FERROCENE SUBSTITUTED PAHs

4.1 INTRODUCTION

Carbon-rich organometallic compounds represent a rapidly growing subfield at the interface of organic and organometallic chemistry. Carbon-rich ligands provide important properties, such as facile electron transfer to and from the metal surface, allowing these compounds to be used as molecular wires. As such, in recent years organometallic fragments assembled on substituted benzenes, polyaromatics and heteroaromatics, such as pyridines, have received immense interest as potential models for organometallic polymers[1] and as targets for the study of electron-transfer processes.[2]

The discovery of ferrocene, the first dicyclopentadienyl "sandwich" complex, revolutionised the field of organometallic chemistry.[3] As such, ferrocene remains the prime representative of this class of organometallic compound. Ferrocene based compounds have found many applications in synthetic organic chemistry and material sciences, owing to the stable coordination of the cyclopentadienyl ligands, the possibility of introducing chirality and the reversible redox behaviour of the metal centre.[4] This stable inorganic compound can, therefore, be regarded as an aromatic molecule within which the encapsulated iron provides an additional source of optical, structural and electrochemical properties. These properties have lead to the application of ferrocene into a number of sensor devices. Examples include, ferrocene mediated electron transfer in glucose oxidase, anion and cation sensors and DNA biosensors.[5] Fundamental to its success has been its well-developed organic chemistry, which allows functionalization of the ferrocene cyclopentadienyl rings *via* simple synthetic methods. This provides access to a wide variety of derivatives designed to serve particular functions.

Ferrocene, as a robust electron-rich organometallic group, has also been used in the preparation of new molecular materials exhibiting non-linear optical (NLO)[6] and ferromagnetic properties.[7] There is growing interest in the synthesis of new materials with large optical nonlinearities and organometallic compounds have been shown to be useful in this regard.[6] An important feature of such molecular materials is the packing arrangement they adopt in the solid state, as this can have a major influence on the bulk properties of the molecular material. One parameter important in an attempt to obtain favourable packing arrangements is molecular shape.[7] Geometrically the ferrocenyl group is suitable for this purpose since the spacing between the cyclopentadienyl rings, is about 3.3 Å, similar to the interplanar spacing in π-π stacking arrangements.[7] Most ferrocene complexes that are investigated for their optical nonlinearities consist of ferrocene as a donor and an organic moiety such as a -CN or -CHO substituted benzene, stilbene, or azobenzene-derivative, as an acceptor.[8]

The work described in the following Chapter is concerned with linking organometallics to large PAH and N-doped PAH molecules. The strategy defined in this work to achieve this goal introduces the metal complex at an early synthetic stage. In such a scheme, the metal complex must then withstand all subsequent synthetic steps without decomposition. Given its good chemical stability and attractive materials properties, ferrocene seemed an ideal first choice. These new compounds may show attractive NLO behaviour and could potentially act as molecular redox switches due to their electronic structure.

PAHs have a number of attributes which could make them useful as linking groups in donor-acceptor organometallic systems. They are planar, relatively rigid with a fixed geometry and have various isomeric positions through which the organometallic moieties may be bound. Their highly delocalised π-systems with small HOMO-LUMO energy separations and low energy vacant π^*-orbitals are likely to facilitate electronic communication between donors and acceptors. Although large polycyclic materials incorporating up to 222 carbon atoms have been characterised, very few of these systems include an organometallic moiety. The only known examples are Bunz's ethynylated cyclobutadienes,[9,10,11,12] and recently (2000) the incorporation of tricarbonylchromium into an HBC derivative (figure 4.1).[13] Yet, as stated, the introduction of an organometallic moiety would confer very interesting geometric and electronic properties to such molecules with attractive characteristics for use in material science.

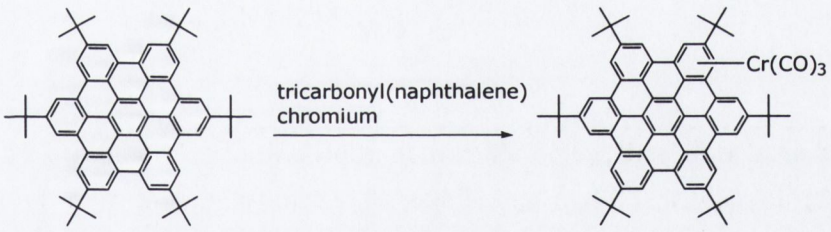


Figure 4.1. The synthesis of tricarbonyl(arene)chromium complex.[13]

The novel, L-shaped 4-(2-ferrocenyl-vinyl)-pyrene compound (figure 4.2), which links a ferrocene donor group to a planar polyaromatic moiety, was synthesized in 1998[7] and conveys fascinating solid state electrical conductivity properties.

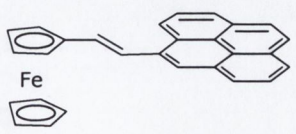


Figure 4.2. The structure of 4-(2-ferrocenyl-vinyl)-pyrene.

Relevant to our long term-goal of preparing ferrocene intercalated graphitic sheets, and in continuation of our interest in the study of PAH compounds, the following Chapter describes the synthesis, characterization, electronic and redox properties of a series of novel polyphenylene systems incorporating the ferrocenyl (Fc) moiety. The first step in the formation of ferrocenyl polyphenylene systems would be to use ferrocenyl acetylenes such as ethynylferrocene, although several modifications can also be envisaged, for example diferrocenylbutadiyne. The ferrocene based polyphenylene systems were then synthesized, *via* Diels-Alder reaction, and subjected to spectroscopic (IR, NMR and UV-vis) and ESI-mass spectrometry and electrochemical study.

Also reported herein is the successful cyclodehydrogenation to ferrocenyl PAH derivative **(41)** (a model of an iron intercalated graphitic sheet), and its comprehensive characterisation, including electrochemical data. Never before has ferrocene been incorporated onto such PAH derivatives. Modification of the ferrocene electrophore was found to give rise to site-specific redox chemistry.

4.2 RESULTS AND DISCUSSION

4.2.1 Synthesis and Characterisation

In general, the new ferrocenyl compounds synthesized in this work are yellow/red, crystalline, air-stable solids, soluble in common chlorinated and aromatic solvents, but mostly insoluble in hexane. The orange to red colour is a result of an absorption in the UV-vis at around 440 nm, characteristic of ferrocene compounds. The one exception was the ferrocene substituted cylopentadienyl **(44)**, which was a deep blue amorphous powder. All the complexes were studied spectroscopically, and characterised by ^{1}H and ^{13}C NMR and IR spectroscopy and accurate mass and ESI-mass spectrometry (see experimental for full details). Repeated attempts to grow X-ray quality crystals failed for derivatives **(41)** and **(46)**.

Alkynes are reactive building blocks for organic and organometallic synthesis. There has been huge interest in ferrocenylacetylenes as they offer a wide range of potential applications in NLO, catalysis, as models of charge transfer and in the synthesis of more complex molecules with well-defined magnetic and electronic properties.[14,15] Because ethynylferrocene is a common starting material for more complicated molecules incorporating acetylene units, its synthesis has been widely investigated. Several different synthetic methods have been employed. The Rosenblum method[16] consists of treating acetylferrocene with an excess of phosphorus oxychloride and DMF to give the 3-chloro-3-ferrocenyl-propenal. This is carefully purified and heated in a basic aqueous solution and transformed into ethynylferrocene **(37)** in a 42% overall yield.

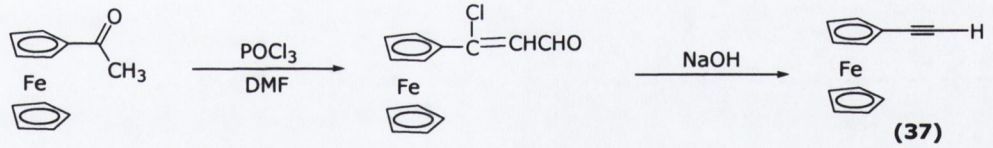


Figure 4.3. The synthesis of ethynylferrocene **(37)**.

As a new direction for ethynylferrocene chemistry this work focusses on the [2+4]-cycloaddition reaction of tetraphenylcyclopentadienone (tetracyclone) with ethynylferrocene **(37)**. A Diels-Alder reaction of this type would normally occur at 600 K, however ethynylferrocene decomposes over 558 K. Based on the work of Elise Champeil,[17] tetracyclone and ethynylferrocene were reacted in molten benzophenone and the temperature gradually increased until a new product formed.

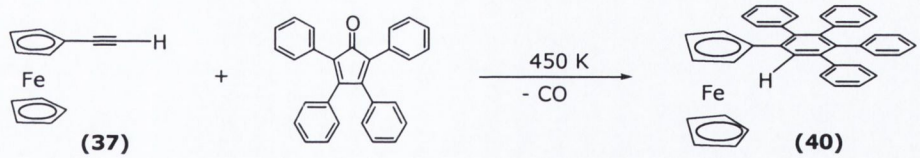
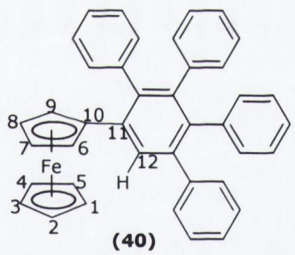


Figure 4.4. The synthesis of 1,2,3,4-tetraphenyl-5-ferrocenylbenzene **(40)**.

The reaction occurred at 363 K and the temperature was maintained until most of the starting materials had reacted. The product, 1,2,3,4-tetraphenyl-5-ferrocenylbenzene **(40)**, was purified by column chromatography on silica using a hexane/dichloromethane mixture as eluent. Crystallisation from hexane gave **(40)** as an air-stable orange to red crystalline solid in 70% yield. The orange product was re-crystallised from hexane at 273 K, and suitable crystals for single-crystal analysis were obtained.

The ^{1}H NMR spectrum of the ferrocenyl complex **(40)**, shows a downfield signal at δ 7.95, which is assigned to H12. The multiplet between δ 7.17 and δ 6.66 is due to the other 20 phenyl protons and the peaks at δ 4.06, δ 3.96 and δ 3.89 are assigned to the ferrocene moiety.



		NMR Spectroscopic Data, δ Chemical shift.	
^{1}H NMR		H12	7.95 (s)
		H phenyls	7.16 - 6.66 (m)
		H1-H5	4.06 (s)
		H(9,6) or H(7,8)	3.89 (t), 3.96 (t)
^{13}C NMR	$C_{quat/phenyl}$	141.2, 140.3, 139.7, 139.4, 139.2, 139.1, 137.0, 136.9, 136.0	
	C_{phenyl}	130.7 - 124.2 (21 aromatic Carbons)	
	$C_{ferrocene}$	85.7 (C10), 69.4 and 66.7 (Cp (C6,9 or C7,8)), 68.5 (Cp (C1-5))	

Figure 4.5. The atom labelling scheme and NMR spectroscopic data for 1,2,3,4-tetraphenyl-5-ferrocenylbenzene **(40)**.

Polyphenylene **(40)** gives rise to the expected pattern for the ferrocene unit in the δ 3.80 - δ 4.10 range. The unsubstituted C_5H_5 ring shows up as an intense singlet at δ 4.06 and the monosubstituted C_5H_4 ring gives an unsymmetrical pair of 'pseudo'-triplets at δ 3.89 and δ 3.96, corresponding to the spectrum of an A_2B_2 system.

The ^{13}C NMR shows 9 signals corresponding to phenyl quaternary carbons in the region of δ 136 - δ 142, and the characteristic ferrocene signals in the region of δ 66 - δ 86. The molecular formula of **(40)** was also confirmed by ESI-MS and the molecular ion

peak for $[M]^+$ was detected at m/z=566.3, corresponding to that calculated for $[C_{40}H_{30}Fe]^+$ (m/z=566.4).

Having proved the formation of ferrocenyl derivative **(40)**, the obvious direction for this work was to cyclodehydrogenate the system, create bonds between the phenyl rings and form a closed 'planar' system. If the polyaromatic ferrocenyl compound **(41)** could be produced, it would represent a model for an intercalated graphitic sheet, with a large π-delocalisation and exciting geometric and electronic properties. Several attempts at the cyclodehydrogenation reaction using various conditions including: $Cu(SO_3CF_3)_2$, $AlCl_3$, 14 d; Li powder, 12 h, reflux; $FeCl_3$, CH_3NO_2, 24 h, reflux; did not yield the desired product (see Chapter 6). NMR spectroscopic evidence suggested that the ferrocene group tended to decompose during the reaction. The reaction conditions used to obtain N-HBC **(17)** (see Chapter 2), were also investigated. This showed some promise, as **(40)** survived the first 24 h without the loss of the ferrocene group, unlike the other methods. A longer reaction period was explored and with careful work up led to the ferrocenyl substituted PAH derivative **(41)**. The synthesis of this novel ferrocenyl complex is represented in figure 4.6.

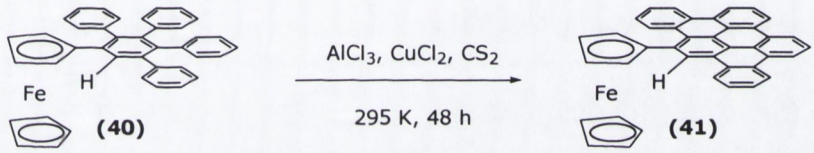
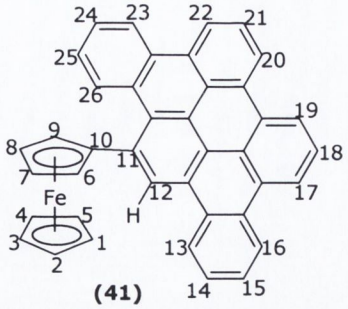


Figure 4.6. The cyclodehydrogenation of **(40)** to produce ferrocenyl PAH derivative **(41)**.

The $AlCl_3$ and $CuCl_2$ ring closure of **(40)** in CS_2 resulted in the corresponding cyclodehydrogenated ferrocene compound **(41)** in a 15% yield, as the sole isolable product. The residue is black, insoluble and intractable, a consequence of the partial oxidative decomposition of the ferrocene nuclei by Cu^{II} salts. Low yields in copper-catalysed reactions of ferrocene derivatives have been observed before.[10] The material was purified by column chromatography to give **(41)** as a pale yellow powder, which is stable as a solid at ambient temperature, but decomposes on prolonged solvation at room temperature. It was, however, stable in solution for longer periods at a temperature below 250 K. In this work, compound **(41)** was successfully characterised by NMR and IR spectroscopy, and mass spectrometry.

In this compound, ferrocene is directly attached to the aromatic hydrocarbon to create a ferrocenyl substituted PAH. As far as we are aware this is the first time an organometallic moiety has been incorporated onto the periphery of a PAH of this type. Unfortunately there was no ring closure to ferrocene's cyclopentadienyl ring, by removal of the *ortho*-proton of the mono-substituted cyclopentadienyl ring. The failure

of cyclopentadienyl to fuse to the adjacent phenyl ring may be as a result of the slightly longer distance between C9 and C26 (see figure 4.7). This allows, however, the ferrocene unit free rotation about the carbon-carbon σ-bond, that attaches it to the PAH moiety. This rotation is apparent, as seen through the symmetric nature of the ferrocene protons in the ^{1}H NMR spectral analysis. Rotation of the ferrocene unit is restricted only by the phenyl ring containing C23-C26, and the protons at C26 and C25 attached to it (see figure 4.7).



(41)

Figure 4.7. The atom labelling scheme of tetra-*peri*-benzo-*peri*-ferrocenylcoronene, **(41)**.

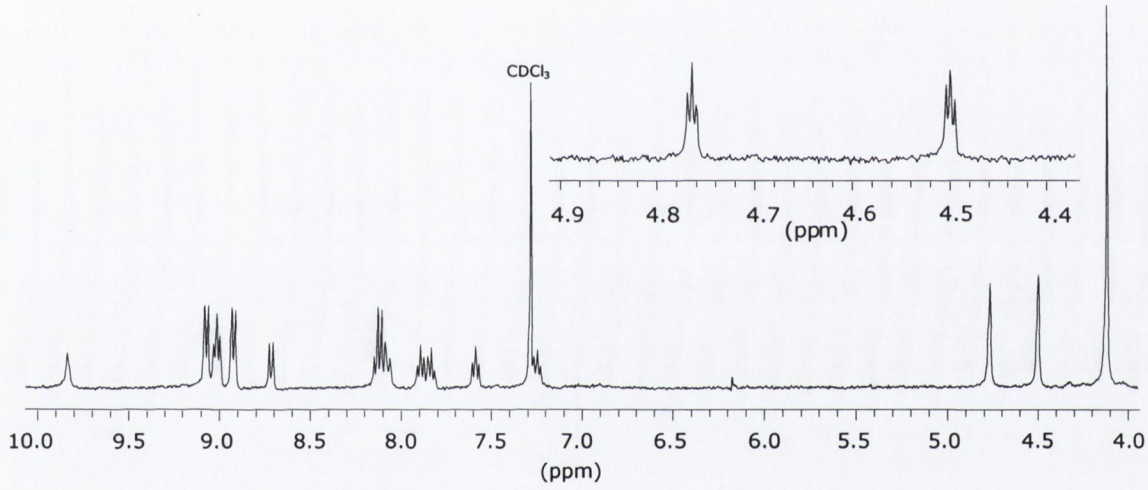


Figure 4.8. The ^{1}H NMR spectrum of ferrocenyl compound **(41)** ($CDCl_3$, RT, 400 MHz).

The ^{1}H NMR spectrum of the ferrocenyl PAH derivative, is shown in figure 4.8. Again the characteristic signal pattern for the monosubstituted ferrocene is observed, with two 'pseudo'-triplets at δ 4.77 (intensity 2H) and δ 4.50 (intensity 2H) for the PAH substituted Cp ring. The singlet at δ 4.12 (intensity 5H) for the unsubstituted Cp ring is also easily recognised.

In the aromatic region of the ^{1}H NMR spectrum (figure 4.8) we see five triplet signals, three doublets, a multiplet and a lowfield singlet. The most downfield signal at δ 9.83 appears as a singlet and is attributed to the proton at C12. The five triplet signals in the ^{1}H NMR at δ 9.01 (2H), 7.89 (1H), 7.83 (1H), 7.59 (1H) and 7.24 (1H), correspond to the six aromatic protons at carbon positions C14, C15, C18, C21, C24 and C25 (see figure 4.7). The three doublet signals at δ 9.07 (2H), 8.92 (2H) and 8.71 (1H), along

with the multiplet at δ 8.11 (3H), which is made up of three overlapping doublets, are assigned to the eight proton resonances at carbon positions C13, C16, C17, C19, C20, C22, C23 and C26 (see figure 4.7). Tables 4.1 and 4.2 show the results from Homonuclear HH COSY (TOCSY), and Heteronuclear CH COSY (HMQC) experiments.

Carbon Atom Label	1H NMR assignment (ppm)	Mulitiplicity	Integration	Coupled signals
C12	9.83	broad singlet	1 H	-
C_{Phenyl}, C13-C26	9.07	doublet	2 H	8.11
C_{Phenyl}, C13-C26	9.01	triplet	2 H	7.89, 8.11
C_{Phenyl}, C13-C26	8.92	doublet	2 H	7.83, 8.11
C_{Phenyl}, C13-C26	8.71	doublet	1 H	7.59
C_{Phenyl}, C13-C26	8.11	multiplet	3 H	8.92, 9.01
C_{Phenyl}, C13-C26	7.89	triplet	1 H	9.01
C_{Phenyl}, C13-C26	7.83	triplet	1 H	8.92
C_{Phenyl}, C13-C26	7.59	triplet	1 H	7.24, 8.71
C_{Phenyl}, C13-C26	7.24	triplet	1 H	7.59, 8.92
C(9,6) or C(7,8)	4.77	triplet	2 H	4.50
C(9,6) or C(7,8)	4.50	triplet	2 H	4.77
C1-C5	4.12	singlet	5 H	-

Table 4.1. Coupling information from the ^{1}H NMR and TOCSY experiments on **(41)**.

Although these NMR experiments were carried out, it is still not possible to unambiguously assign each of the proton signals in **(41)** to their specific position in the molecule. The experiments do, however, offer insight as to the relative groupings of some of these proton signals. It is possible, from the TOCSY data (table 4.1), to confirm the assignment for the singlet at δ 9.83, as the proton at C12. (This proton is not coupled to any other in the TOCSY). TOCSY information also allows the assignment of the doublet:triplet:triplet:doublet system at δ 8.71, δ 7.59, δ 7.24 and δ 8.92 as either C13-C16 or C23-C26. The doublet:triplet:doublet system at δ 8.92, δ 7.83 and δ 8.11 is either C17-C19 or C20-C22. HH coupling between the triplets at δ 9.01 and δ 7.89 allows assignment of these peaks to either C14 and C15 or C24 and C25, leaving the second, underlying triplet at δ 9.01 as C18 or C21, and the doublets at δ 8.11 (2H) and δ 9.07 (2H) as the corresponding doublets to these last two systems.

The HMQC experiment (table 4.2) allows confirmation of the Cp carbon signals at δ 67.9 and δ 70.7 in the ^{13}C NMR experiment as the carbons at positions C6-C9 and the carbon signal at δ 69.5 as C1-C5. Interestingly the signal at 126.7, in the ^{13}C NMR spectrum, is shown to correlate to C12 in the HMQC experiment.

Carbon atom Label	^{1}H NMR assignment (ppm)	^{13}C NMR assignment (ppm)
C1-C5; CH, Fc	4.12	69.5
C(9,6) or C(7,8); CH, Fc	4.50	67.9
C(9,6) or C(7,8); CH, Fc	4.77	70.7
C12; CH	9.83	126.7

Table 4.2. Assignment of major ^{13}C and ^{1}H NMR signals from HMQC experiments on **(41)**.

As further evidence for the success of the cyclodehydrogenation reaction to **(41)**, large shifts were observed in the ^{1}H NMR spectrum for the aromatic protons when comparing to ferrocenyl polyphenylene **(40)**. The aromatic proton signals in the δ 6.6 - δ 7.2 range, for compound **(40)**, appear downfield in the δ 7.2 - δ 9.1 region for **(41)**, as a direct result of the ring closure, and a corresponding increase in ring current-induced deshielding. Similarly the signal for the proton at C12 appears 1.88 ppm downfield, of δ 7.95 in **(40)**, to δ 9.83 in the PAH derivative **(41)**. Finally, the ferrocene unit conveys the deshielding effect of the directly attached PAH compound, with downfield shifts of the order of 1 ppm for the protons of the mono-substituted cyclopentadienyl ring. These signals appear well downfield of the C_5H_5 unsubstituted cyclopentadienyl ring singlet of **(41)**, indicating that all four ring protons of the substituted ring are deshielded by the aryl rings of the PAH system. Signals associated with the PAH protons were present, having a total integration of 15 with respect to the 9 ferrocenyl protons.

Accurate mass and ESI-mass spectrometry support the formation of **(41)**. The ESI-mass spectrum of ferrocenyl derivative **(41)** in toluene (figure 4.9) shows the isotopic distribution pattern for the $[M]^+$ ion at m/z=559.8, which is in agreement with the theoretically expected value for $[C_{40}H_{24}Fe]^+$ (m/z=560.4).

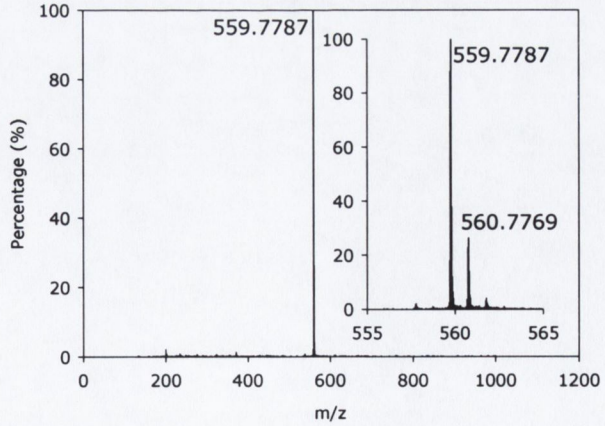


Figure 4.9. The ESI-mass spectrum of ferrocenyl PAH complex **(41)** in toluene.

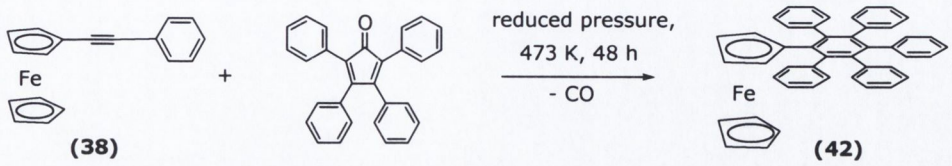
The resulting mass spectrum (figure 4.9) also gave an indication of the purity of **(41)**, as it was the only signal observed. Again, as elemental analysis could not be obtained for **(41)**, due to the extremely high thermal stability of the aromatic core, accurate mass spectral analysis was obtained for **(41)**. In toluene, the ferrocenyl PAH derivative, **(41)**, gave a $[C_{40}H_{24}Fe]^+$ peak of 560.1226, correct to within 5 ppm for that calculated.

Polyphenylene **(41)** is a yellow microcrystalline powder, soluble in common chlorinated and aromatic solvents. Its solubility is in fact curious. Compound **(41)** can be described as an L-shaped molecule in which a ferrocene donor group is linked to a planar polyaromatic moiety. It is well known that the solubility of this simple PAH ($C_{30}H_{16}$), the type attached to the ferrocene unit in complex **(41)**, is extremely low. It is necessary, in order to obtain soluble analogues of this PAH, to attach long solubilising chains at the periphery of the compound.[18] Nonetheless, the fact that the Fc analogue **(41)** is soluble in organic solvents suggests there is an underlying factor preventing aggregation in **(41)**. Aggregation of the PAH unit is caused by a π-π stacking interaction which, in **(41)**, could be prohibited by the bulky Fc group. There appears to be little perturbation of the PAH fluorophore in **(41)**. The $\pi \rightarrow \pi^*$ transitions in the UV-vis spectra of the alkyl substituted PAH are at the same energy as for the soluble ferrocene analogue (see table 4.7). It is suggested, therefore, that steric interactions between individual ferrocenyl molecules impact on the ability of the PAH subunit to stack or form dimers. This has been seen similarly in X-ray single-crystal studies of ferrocenylnaphthalimide molecules,[19] which place the bulky ferrocenyl moieties on the periphery of a columnar network.

It is important to expand this family of ferrocenyl polyphenylene compounds and incorporate further functionality onto the periphery of the polyphenylene unit. The incorporation of pyrimidine rings and further ferrocenyl acetylene units is the focus of the remainder of this section. Extension of the above synthetic strategies has led to the ferrocenyl polyphenylenes **(42)**, **(45)** and **(46)**.

Interest in the fluxional processes of sterically demanding chiral propeller compounds of type C_nAr_n, with molecular paddle wheels, has led to the limited examples of ferrocenyl polyphenylene compounds in the literature to date. The sterically crowded molecule C_6Ph_5Fc **(42)**, shown in figure 4.10, was unfortunately reported in literature during the course of this work, in 1999, and its crystal structure elucidated.[20] No information, however, concerning its electrochemical or electronic spectroscopic properties appears in literature.

The reported synthesis involves the Diels-Alder addition of 3-ferrocenyl-2,4,5-triphenylcyclopentadienone and diphenyl acetylene to yield **(42)**.[20] The alternative approach applied in this work is the one pot Diels-Alder synthesis of C_6Ph_5Fc **(42)**, from phenylethynylferrocene and tetracyclone.



(38) **(42)**

Figure 4.10. The synthesis of ferrocene substituted polyphenylbenzene **(42)**, *via* phenylethynylferrocene **(38)**.

Phenylethynylferrocene was prepared by the Sonogashira coupling reaction of ethynylferrocene **(37)** and bromobenzene. Phenylethynylferrocene **(38)** and tetracyclone were then sealed under vacuum in a glass tube and heated at 473 K for 48 h. After the Diels-Alder reaction, purification by column chromatography afforded **(42)** as an orange-yellow air-stable solid in 36% yield. This is a very slight improvement on the reported yield of 34%.[20]

Ferrocenyl polyphenylene derivative **(42)** was characterised by NMR and IR spectroscopy, and mass spectrometry and agreement was found with the reported literature values.[20] In the ^{1}H NMR spectrum, the aromatic protons of the phenyl rings of **(42)** are found in the δ 6.8 - δ 7.1 region. The ferrocene unit shows a sharp singlet at δ 3.73 and two singlets at δ 3.80 and δ 3.88 corresponding to the downfield protons of the mono-substituted cyclopentadienyl ring. Initial attempts to cyclodehydrogenate ferrocenyl polyphenylene **(42)** to form the planar, ring-closed system, have been unsuccessful. Unfortunately only a black, insoluble and uncharacterisable solid is obtained.

The novel cyclopentadienone, **(44)**, was synthesized as a ferrocene derivative with *tert*-butyl substitution incorporated into the system. These groups were included in **(44)** to aid the solubility of future cyclodehydrogenated derivatives. The synthesis of 2,5-bis-(4-*tert*-butylphenyl)-3-ferrocenyl-4-phenylcyclopentadienone **(44)** is depicted in figure 4.11. It has been noted in the literature[20] that 3-ferrocenyl-2,4,5-triphenyl cyclopentadienone is an effective diene in the Diels-Alder reaction. It differs from the novel cyclopentadienone, **(44)**, only through the absence of the *tert*-butyl substitution on the phenyl rings in the 2 and 5 positions of the cyclopentadienone. Thus it was anticipated that **(44)** would undergo the Diels-Alder reaction effectively.

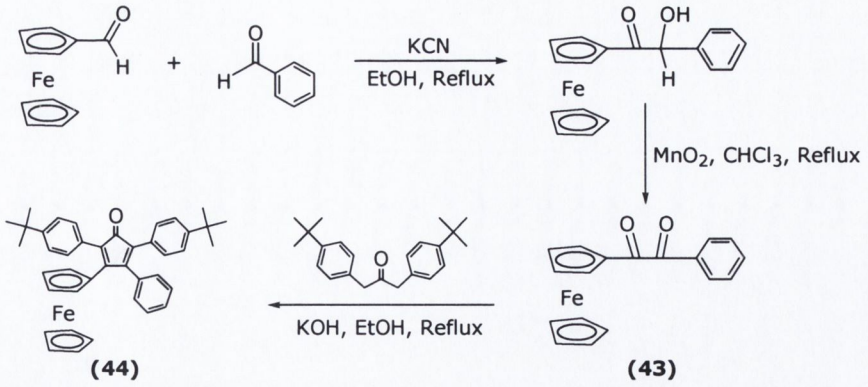
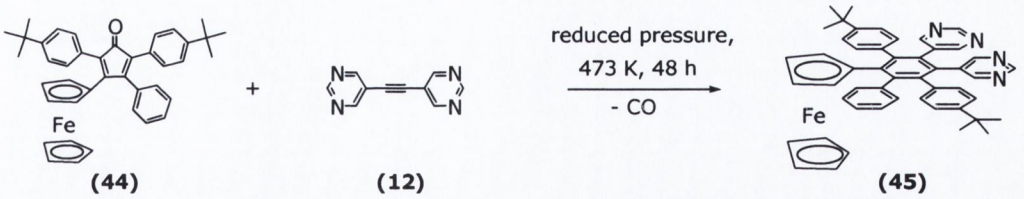


Figure 4.11. Synthetic route to the *tert*-butyl substituted ferrocenyl cyclopentadienone **(44)**.

Ferrocenecarboxyaldehyde was synthesized using the established protocol.[21] Mandeloylferrocene, formed from the mixed benzoin condensation reaction of ferrocenecarboxyaldehyde and benzaldehyde, was oxidised using activated manganese dioxide in refluxing chloroform solution, to form 1-ferrocenyl-2-phenylethane-1,2-dione **(43)**.[22] The infrared spectrum of **(43)** exhibits two characteristic carbonyl absorptions at 1679 and 1644 cm^{-1}.

Finally, the ferrocene substituted cyclopentadienone, **(44)**, was synthesized from the reaction of 1-ferrocenyl-2-phenylethane-1,2-dione, **(43)**, and 1,3-bis-(4-*tert*-butylphenyl)propan-2-one, **(14)**, in refluxing ethanolic potassium hydroxide, using a modification of the literature procedure.[22] Ferrocene derivative **(44)** was produced as a light blue-purple amorphous solid in 32% yield. Its infrared spectrum exhibited a carbonyl band at 1697 cm^{-1}, which is characteristic of cyclopentadienone systems. The formulation of all these compounds was confirmed by IR and NMR spectroscopy, elemental analysis and by mass spectrometry (see Chapter 6).

Heteroatoms can be introduced using dipyrimidine acetylene as the alkyne source in the [2+4]-cycloaddition reaction (see figure 4.12). 2,5-bis-(4-*tert*-butylphenyl)-3-ferrocenyl-4-phenylcyclopentadienone, **(44)**, was treated with dipyrimidine acetylene **(12)**, to form the ferrocenyl polyphenylene **(45)**, after extrusion of carbon monoxide. This synthesis employs the conditions published by McGlinchey *et al.*,[20] used to form the all-carbon ferrocenyl derivative **(42)**. To my knowledge, however, pyrimidine acetylenes have never been used in this synthetic method.



(44) **(12)** **(45)**

Figure 4.12. The synthesis of ferrocene substituted N-doped polyphenylbenzene **(45)**.

Under the reaction conditions, ferrocenyl complex **(44)** and dipyrimidine acetylene were sealed under vacuum in a glass tube and heated at 473 K for 48 h. After cooling to room temperature and extraction into dichloromethane, **(45)** was purified using column chromatography to afford an orange-red air-stable solid in a 40% yield (figure 4.12). IR, NMR spectroscopy, and mass spectrometry confirmed the formation of the ferrocenyl polyphenylene **(45)**.

The ^{1}H NMR spectrum (figure 4.13) displays three signals for the ferrocenyl unit in the δ 3.6 - δ 3.9 region. Again the characteristic signal pattern for monosubstituted ferrocenes is observed with two 'pseudo'-triplets at δ 3.77 and δ 3.89 for the four cyclopentadienyl protons of the polyphenylene substituted Cp ring. The singlet at δ 3.66 is assigned to the five protons of the unsubstituted cyclopentadienyl ring.

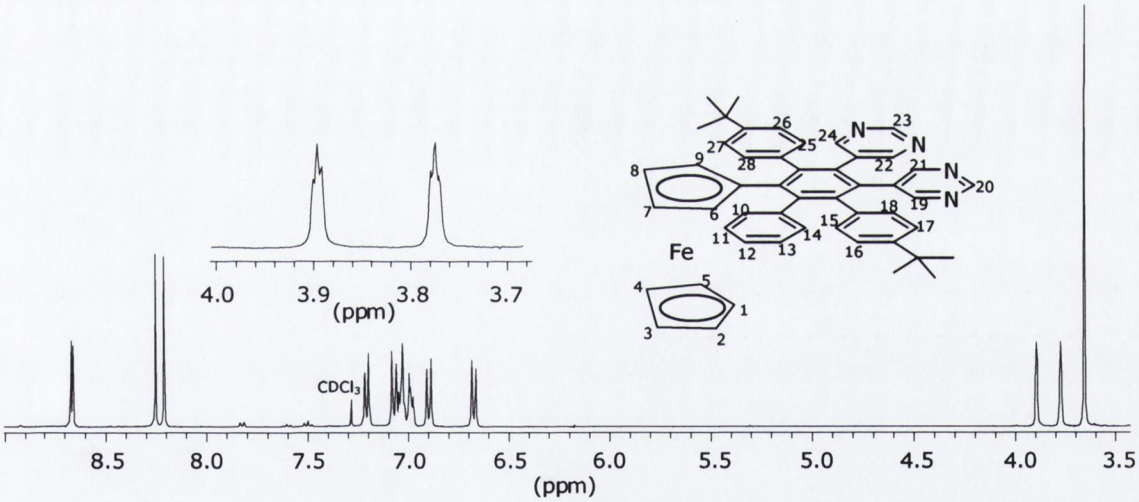


Figure 4.13. The atom labelling scheme and the aromatic region of the ^{1}H NMR spectrum of ferrocenyl compound **(45)** ($CDCl_3$, RT, 400 MHz).

The asymmetric nature of ferrocenyl polyphenylene **(45)** is demonstrated through the two singlets at δ 8.67 and δ 8.66 (each integrating for 1H), which correspond to the non-equivalent aromatic protons at C20 and C23, between the nitrogens of the pyrimidine rings. Likewise two singlets are observed at δ 8.25 and δ 8.21 (each integrating for 2H), which can be assigned to the pyrimidine protons at C19/21 and C22/24. The doublets at δ 7.21, δ 7.07, δ 6.90 and δ 6.67 (each integrating for 2H) are

assigned to the protons of the *tert*-butyl substituted phenyl rings at C15/18, C16/17, C25/28 and C26/27. The multiplet at δ 7.03 (3H) can be assigned to the phenyl protons at C11-13, with the doublet at δ 6.98 completing this particular mono-substituted phenyl ring as the aromatic protons at C10/14. In the aliphatic region of the ^{1}H NMR spectrum there are only two signals. These signals, at δ 1.25 and δ 1.10, correspond to the methyl protons of the two *tert*-butyl groups, each integrating for 9 hydrogens. The ESI-mass spectrum of **(45)** contained a single molecular ion at *m/z*=758.6 in accord with the formation of $[C_{50}H_{47}FeN_4]^+$ (calculated as *m/z*=759.7).

The diferrocenyl polyphenylene derivative **(46)** was formed according to figure 4.14.

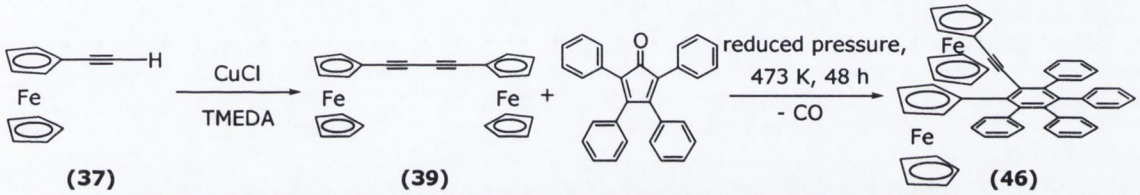


Figure 4.14. The synthesis of diferrocenyl substituted polyphenylbenzene **(46)**.

The synthesis of 1,4-bis(ferrocenyl)butadiyne **(39)** has been widely investigated and its crystal structure published.[23] Its synthesis was carried out according to literature procedure and is achieved *via* the copper catalysed oxidative homo-coupling of ethynylferrocene (Hay's coupling).[24] The diacetylene **(39)** reacted efficiently in a 1:1 molar ratio with tetracyclone under Diels-Alder conditions in a sealed tube, under vacuum, at 473 K. Compound **(46)** was isolated in a 75% yield, after chromatographic separation, as a red air-stable solid (figure 4.14). Again, IR and NMR spectroscopy and mass spectrometry were used to confirm the formulation of diferrocenyl polyphenylene **(46)**.

Complex **(46)** is asymmetric in nature, as evident in the ^{1}H NMR spectrum (figure 4.15), which exhibits two sets of ferrocenyl signals.

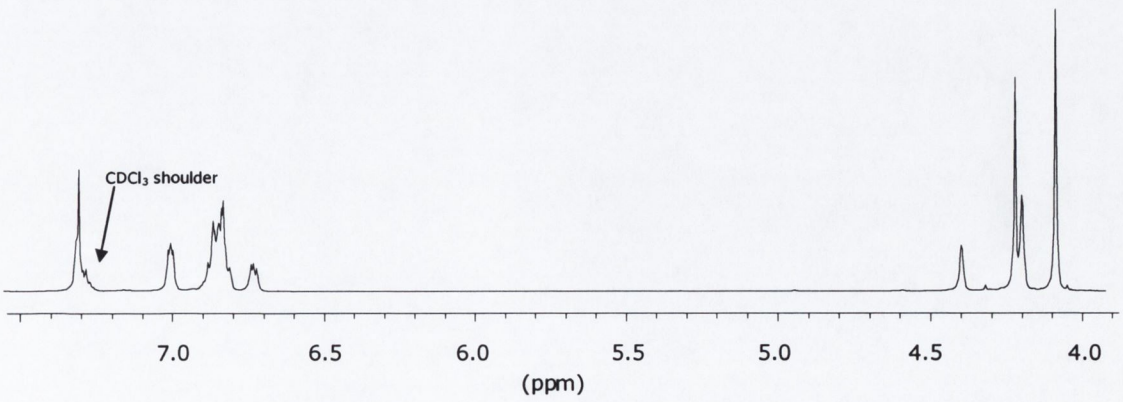


Figure 4.15. The ^{1}H NMR spectrum of diferrocenyl polyphenylene **(46)** ($CDCl_3$, RT, 400 MHz).

In the cyclopentadienyl region of the ^1H NMR spectrum, **(46)** displays four signals corresponding to the two sets of ferrocene hydrogen atoms. The singlets at δ 4.40 (2H) and at δ 4.20 (4H) represent three of the four sets of signals for the protons of two mono-substituted C_5H_4 rings. One of the unsubstituted C_5H_5 rings gives rise to a singlet at δ 4.22 (5H) and the singlet at δ 4.09 (7H) is assigned as the overlapping signals from (a) the fourth set of protons from one of the mono-substituted C_5H_4 rings (2H) and (b) the second unsubstituted C_5H_5 ring protons (5H).

In the aromatic region of the ^1H NMR spectrum we see four signals at δ 7.29, δ 7.00, δ 6.84 and δ 6.72, which integrate 5:3:10:2, respectively. These downfield shifts are assigned to the 20 aromatic protons of the phenyl rings of **(46)**. These rings are free to rotate about their single bonds to the central aromatic ring.

The CH COSY (HMQC) experiment verifies the above assignments (see table 4.3 and figure 4.16).

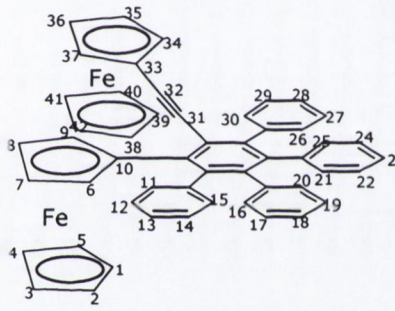


Figure 4.16. The atom labelling scheme of diferrocenyl derivative **(46)**.

Carbon atom Label	^1H NMR assignment (ppm)	^1H NMR Integration		^{13}C NMR assignment (ppm)
C(6,9) or C(7,8) or C(34, 37) or C(35, 36), H(Cp)	4.40	2H		71.3
C1-C5 or C38-C42, H(Cp)	4.22	5H		69.4
C(6,9) or C(7,8) or C(34, 37) or C(35, 36), H(Cp)	4.20	4H	(2H)	68.3
			(2H)	70.2
C1-C5 or C38-C42, H(Cp); C(6,9) or C(7,8) or C(34, 37) or C(35, 36), H(Cp)	4.09	7H	(5H)	69.4
			(2H)	66.5

Table 4.3. Assignment of major ^{13}C and ^1H NMR signals from HMQC experiments on **(46)**.

Due to the close nature of the signals in the ^{13}C NMR spectrum, it was not possible to make further assignments for the phenyl rings of **(46)**, C11-C30.

The results of the CH COSY (HMBC) NMR experiment on the ferrocene unit of **(46)** are summarised in table 4.4. The long-range correlation between the ^1H NMR signal at δ 4.20 and the ^{13}C NMR signal at δ 100.8, in the HMBC experiment, has allowed the additional assignment of acetylene carbons C31 and C32 as δ 87.2 and δ 100.8, respectively. The ferrocene units can also be distinguished. The ferrocene directly attached to the polyphenylene group displays two signals in the ^1H NMR spectrum; the two signals at δ 4.09 and δ 4.40, correspond to the mono-substituted C_5H_4 ring; the unsubstituted C_5H_5 ring gives rise to a singlet at essentially the same shift, δ 4.09.

There is a correlation in the long-range HMBC experiment between these ^{1}H NMR signals and the quaternary carbon C10 at (δ 84.6 in the ^{13}C NMR). The ferrocene with the ethynyl link to the polyphenylene also provides two broad singlets in the ^{1}H NMR spectrum; the unsubstituted C_5H_5 ring shows up as a strong singlet at δ 4.22, and the monosubstituted C_5H_4 ring gives a single peak at δ 4.20. In the long-range HMBC experiment these ^{1}H NMR signals show a correlation to the quaternary carbon at C33, which gives the signal in the ^{13}C NMR spectrum at δ 65.9 and to the acetylene carbon C32 (δ 100.8 in the ^{13}C NMR).

^{1}H NMR assignment (ppm)	**Carbon atom label; ^{13}C NMR assignment (ppm)**	**Carbon atom label and ^{13}C NMR assignment (ppm) Long-range Coupling HMBC Data**
4.40	C(6,9) or C(7,8); 71.3	C10, 84.6; C(6,9) or C(7,8), 66.5
4.22	C38-C42; 69.4	C33, 65.9
4.20	C34-C37; 68.3, 70,2	C33, 65.9; C32, 100.8
4.09	C(6,9) or C(7,8); 66.5 and C1-C5; 69.4	C10, 84.6; C1-C5, 69.4; C(6,9) and C(7,8), 71.3 and 66.5

Table 4.4. Assignment of ^{13}C and ^{1}H NMR signals from HMBC experiments on **(46)**.

The ESI-MS shows the corresponding $[M]^+$ peak at m/z=774.2 as the only peak in the mass spectrum, corresponding to $[C_{52}H_{38}Fe_2]^+$ (calculated as m/z=774.5). Its infrared spectrum exhibits a characteristic weak absorption for the C≡C stretch at 2211 cm^{-1}.

4.2.1.1 Derivative Comparisons

Table 4.5 summarises the main spectroscopic data for all the ferrocenyl compounds in this study. In all cases, mass spectra were obtained by electro-spray ionisation (ESI). Under these conditions a single peak corresponding to either the $[M]^+$ or the $[MH]^+$ ion were obtained for each complex.

Compound	**Mass Spectrum (m/z)**	**^{1}H NMR chemical shifts for Fc protons (ppm)**	
		Unsubstituted C_5H_5 ring	***meta*- and *ortho*-Hs of the substituted Cp ring**
(37)	210.0	4.22	4.19, 4.46
(38)	286.1	4.29	4.28, 4.55
(39)	418.0	4.29	4.27, 4.53
(40)	566.3	4.06	3.89, 3.96
(41)	560.3	4.12	4.50, 4.77
(42)	642.6	3.73	3.80, 3.88
(45)	758.6	3.66	3.77, 3.89
(46)	774.2	4.22, 4.09	4.40, 4.20, 4.20, 4.09

Table 4.5. Spectroscopic data for complexes **(37)**, **(38)**, **(39)**, **(40)**, **(41)**, **(42)**, **(45)** and **(46)**.

The ^1H NMR spectra of these ferrocenyl complexes all contain the expected signals arising from the ferrocenyl group. It is worth noting that the ^1H NMR spectrum of compound **(40)** shows a sharp singlet at δ 4.06 and two 'pseudo'-triplets corresponding to an A_2B_2 system at δ 3.89 and δ 3.96. These resonances are similar to those of **(42)** (δ 3.73, δ 3.80 and δ 3.88, respectively) and **(45)** (δ 3.66, δ 3.77 and δ 3.89, respectively), while for **(41)** these resonances appear at δ 4.12, δ 4.50 and δ 4.77, respectively. The downfield shift of the mono-substituted cyclopentadienyl ring protons in **(41)** is consistent with the electron-withdrawing effect of the polycyclic aromatic group, which is directly attached to the ferrocenyl moiety. The ferrocenyl acetylenes **(37)**, **(38)** and **(39)** experience a deshielding effect in the ^1H NMR, similar to **(41)**, due to the directly attached acetylene unit.

4.2.1.2 X-Ray Crystallographic Analysis

Single-crystal X-ray diffraction studies of **(40)** and **(45)** were carried out to determine their room temperature, solid-state molecular arrangements. Orange crystals of **(40)** were obtained, in air, from slow evaporation of hexane. Red crystals of **(45)** were grown, in air, from a solution of the compound in dichloromethane over which a layer of hexane was present.

Both **(40)** and **(45)** produce structures in which the outer aryl rings, which are free to rotate about their carbon-carbon single bond to the central phenyl ring, twist apart from each other like propeller blades. In the solid state, C_6Ph_5Fc **(42)**, has been reported to exhibit an unusual configuration.[20] It can be contrasted to the structure of the polyphenylenes in Chapter 2 and to the structure C_6Ph_6, which adopt a regular propeller configuration with approximate interplanar angles of 67° between the outer phenyl groups and the central ring. C_6Ph_5Fc provides a series of peripheral rings, each displaced slightly more than its preceding neighbour, starting with ferrocene at 51° to the central plane, through to the phenyl ring at 120° to the plane.[20]

All investigated crystals of **(40)** proved to be heavily twinned. The sample finally chosen consisted of at least five domains, four of which could be investigated. The structure was solved and refined for two domains, with an R_1 of 4.72%. It crystallized in space group P-1, and its molecular structure is shown in figure 4.17 (a). The molecular structure of **(40)** shows twisting of the phenyl and ferrocene subunits with respect to the central phenyl ring. Starting with ferrocene at C1, which is twisted by 36° from the central plane, the phenyl ring at C5 is then twisted by 56°, the phenyl ring at C4 by 58°, the phenyl ring at C3 by 70° and the phenyl ring at C2 by 72°.

Similar to the structure reported for **(42)**,[20] as we move around the central phenyl ring in **(40)** we see a progessive increase in the twist of the propeller blades.

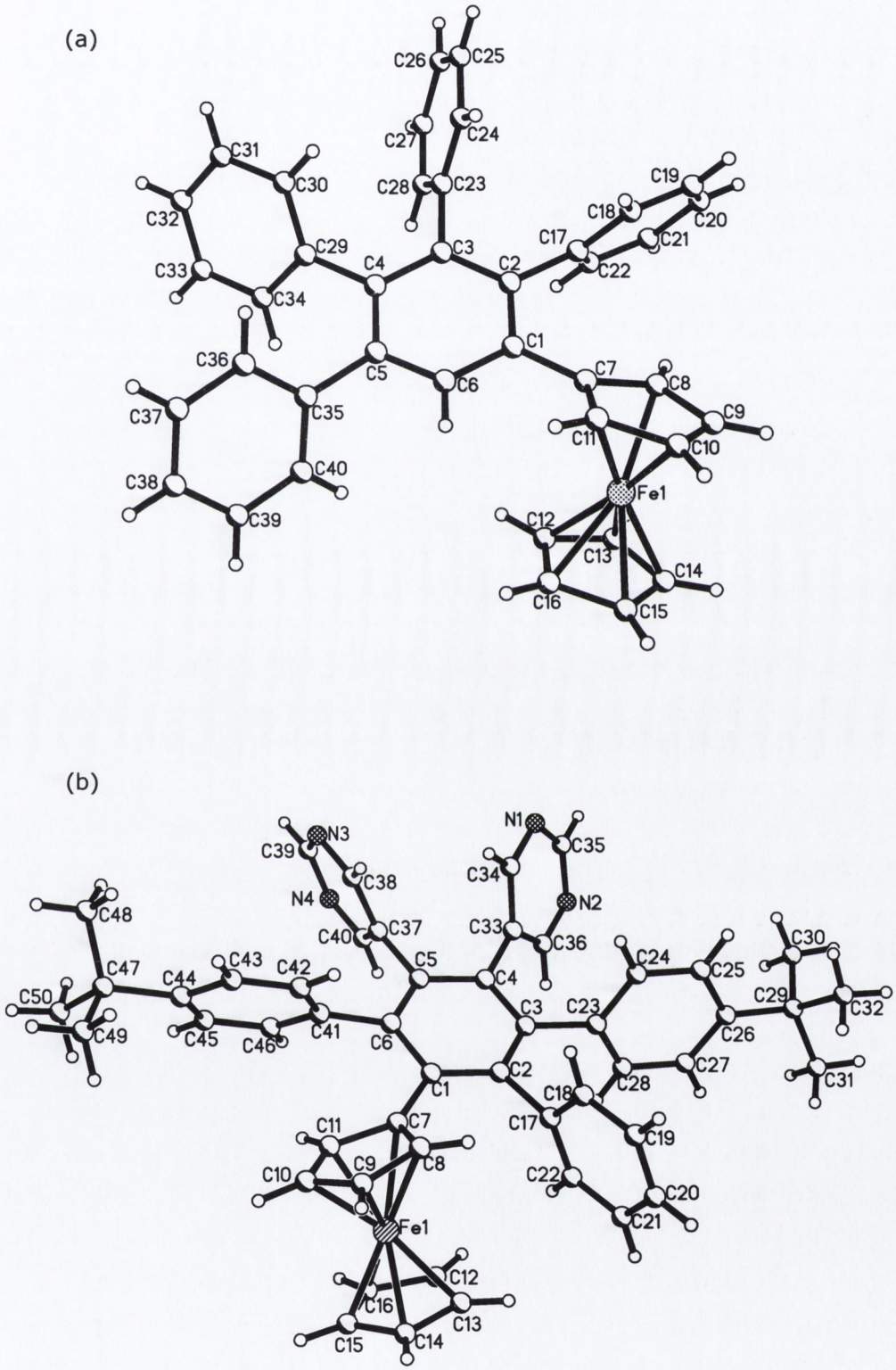


Figure 4.17. The X-ray crystal structures of ferrocenyl polyphenylenes (a) **(40)** and (b) **(45)**.

The crystals of **(45)** produced a structure in which there is no such regular displacement in the twist angles around the central ring, see figure 4.17 (b). The interplanar angles between the peripheral aryl groups and the central ring at C1 through to C6 are 36, 90, 73, 62, 75 and 71° respectively. Removal of the trend observed for **(40)** and **(42)** is attributed to the pyrimidine rings at C4 and C5. Compound **(45)** crystallized in space group $P2_1/c$, with an R_1 of 6.70%.

Molecules of **(40)** are offset stacked, with 180° rotation around the central phenyl ring, so that the bulky ferrocenyl units are not stacked upon each other. Instead these appear on alternating sides of the network.

Similarly, molecules of **(45)** are offset stacked. Unlike **(40)**, however, the bulky ferrocenyl moieties, which are on the periphery of the molecule, tend to stack on the same side of the network. Intermolecular hydrogen-bonding is also evident in the structure of **(45)**. The distance of 2.7(1) Å between N2 and H25 is indicative of moderately strong hydrogen-bonding in **(45)**.

X-ray analysis also provides information on the tilted conformation of the ferrocene units in **(40)** and **(45)**. In **(40)** the two cyclopentadienyl rings are only tilted by 3°. This is almost tripled by the ferrocene unit of **(45)** in which the cyclopentadienyl rings are tilted by 8°. The crystallographic data for both these molecules are given in tables E to F in Appendix 1.

4.2.2 UV-vis Absorption Spectroscopy

Past studies of the electronic absorption spectra of ferrocene and substituted ferrocenes have revealed that in ferrocene the metal centred d_{z2} orbital is generally the HOMO, and the combination of the d_{xz} and d_{yz} is the LUMO.[8] The absorption around 440 nm in ferrocene is thus assigned as the $^1E_{1g} \leftarrow {}^1A_{1g}$ ligand field (LF) transition and the higher energy band around 325 nm as the $^1E_{2g} \leftarrow {}^1A_{1g}$ LF transition. Substitution of the Cp ring with conjugated acceptor groups is generally followed by drastic changes in the spectrum.[8] LF, otherwise known as "*d-d*" transitions, correspond to electronic transitions between the *d*-orbitals on the metal. Organometallics are highly covalent, so these metal centred *d*-orbitals actually have considerable ligand character and since they are involved in metal-ligand bonding, the electronic transitions involving *d*-orbitals are sensitive to ligand binding.[25]

The electronic absorption spectra of all the ferrocene complexes in this study (**(37)**, **(38)**, **(39)**, **(40)**, **(41)**, **(42)**, **(45)** and **(46)**) were recorded in toluene and the data presented in table 4.6. Excluding **(41)**, each of the complexes displays two or three prominent absorption bands in the region 300-600 nm. Similar to other ferrocenyl species, they exhibit a weak low energy band attributable to the *d-d* transition arising from the ferrocene moiety.[25,26] These broad, low energy features account for the orange to red colours for these compounds. The two weak absorption bands of the ferrocene unit (λ=327.0 nm and 438.5 nm) are magnified, in some instances, indicating perturbation of the ferrocene frontier orbitals upon substitution.

Compound	λ_{max} nm, (Molar Extinction Coefficient L mol^{-1} cm^{-1} x10^3)	
		Low energy *d-d* transition
Fc	327.0 (0.5)	438.5 (0.5)
(37)	333.0 (sh) (0.5)	443.0 (0.5)
(38)	337.5 (sh) (3.0)	444.0 (1.0)
(39)	327.0 (sh) (19.0), 356.0 (sh) (7.0)	451.5 (3.0)
(40)	344.0 (2.0)	447.5 (0.5)
(42)	350.5 (2.5)	464.5 (0.5)
(45)	368.0 (3.0)	461.5 (1.0)
(46)	324.0 (sh) (11.0), 359.0 (sh) (3.5)	453.0 (1.0)
(41)	302.5 (10.0), 312.0 (14.0), 355.0 (4.0), 371.5 (4.0), 405.0 (0.5)	*ca.* 440

Table 4.6. The UV-vis data for ferrocenyl complexes **(37)**, **(38)**, **(39)**, **(40)**, **(41)**, **(42)**, **(45)** and **(46)** in toluene.

In figure 4.18 the UV-vis spectra of Ferrocene, **(40)**, **(42)**, **(45)** and **(46)** are superimposed. In ferrocene there is a very weak feature at around 450 nm. The

ferrocene derivatives also display this typical ferrocenyl transition in the visible region, at about 450 nm (figure 4.18), although it is noteworthy that the ferrocenyl transition varies in the range of 438.5 to 464.5 nm, for the complexes in this study, again suggesting frontier orbital interaction between donor and acceptor.

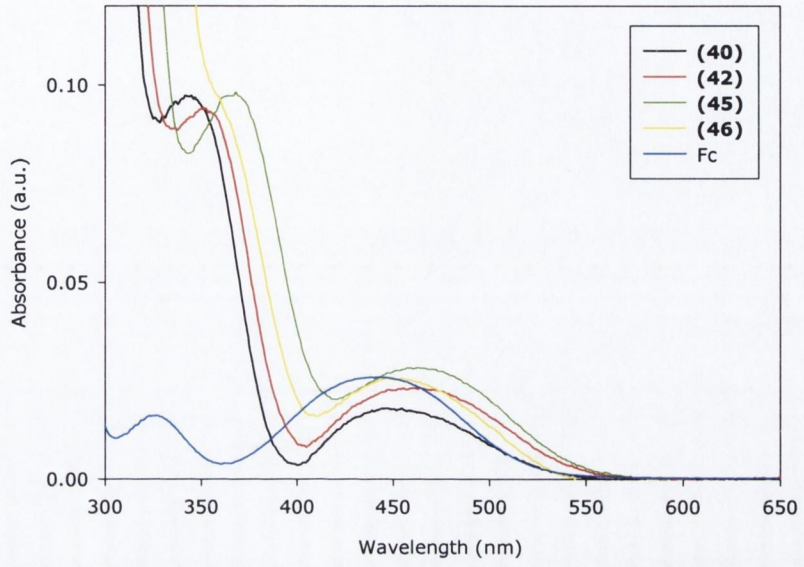


Figure 4.18. The UV-vis absorption spectrum of ferrocenyl complexes **(40)**, **(42)**, **(45)** and **(46)** in toluene, with ferrocene for comparison.

In the UV-vis spectrum of **(40)** there is a peak at 344.0 nm and an additional broad feature at 447.5 nm. There are similar features in the spectrum of **(42)** at 350.5 and 464.5 nm, and in the spectrum of **(45)** at 368.0 and 461.5 nm. The spectrum of **(46)** has a shoulder at 359.0 and a broad absorption at 453.0 nm, and an additional shoulder at 324.0 nm. As a consequence, **(40)**, **(42)**, **(45)** and **(46)** show similar electronic properties, with smaller HOMO-LUMO energy gaps than ferrocene being reflected in the lower energy transitions.

An interesting question concerns the influence on the electronic properties of ferrocene upon closing the rings of ferrocenyl polyphenylene **(40)**. The UV-vis spectrum of ferrocenyl PAH derivative **(41)** is very different from polyphenylene **(40)**, with four intense features in the 300-425 nm region (figure 4.19). In the UV-vis spectrum of **(41)**, the broad signature of the ferrocene *d-d* transition has mostly vanished and instead only a small shoulder at around 440 nm occurs. It is likely that the weaker ferrocenyl band is hidden beneath the broad 404 nm band, which is assigned to a $\pi \rightarrow \pi^*$ transition. In addition, **(41)** is highly absorbing between 300 and 450 nm. In general, the spectrum of **(41)** is dominated by $\pi \rightarrow \pi^*$ absorption bands with high absorption coefficients (table 4.6), and is reminiscent of spectra obtained for PAH derivatives.

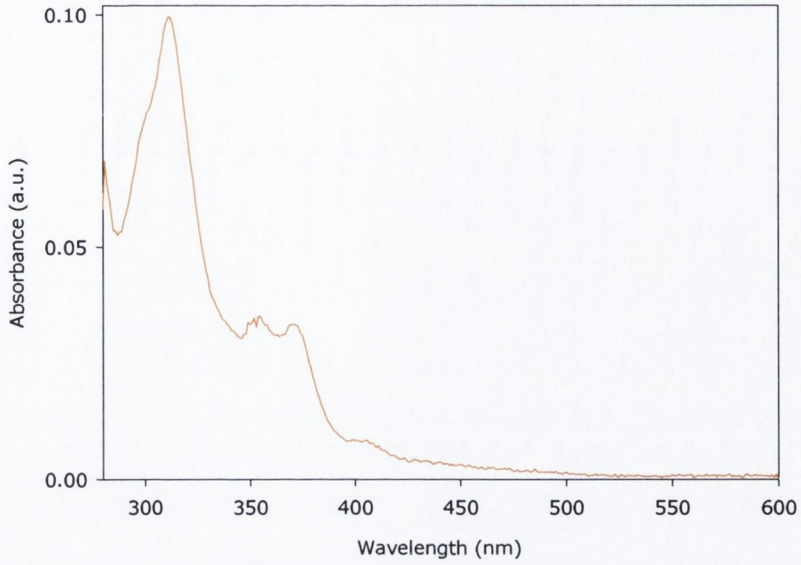
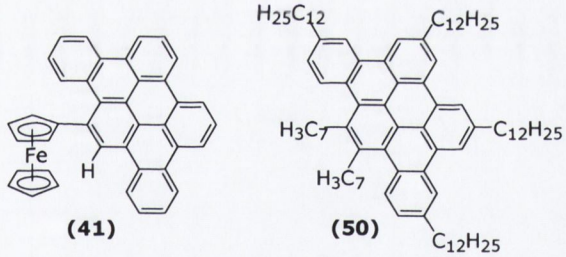


Figure 4.19. The UV-vis absorption spectrum of ferrocenyl complex **(41)** in toluene.

Due to insolubility, the UV-vis spectra for PAHs are often restricted to measurement by thin films (solid-state characterisation), unless they are substituted by large solubilising chains.[18] In table 4.7, ferrocenyl derivative **(41)** is compared to the long chain substituted PAH **(50)**.[18]



Compound	λ_{max} (nm)			
(41)	312.0	355.0	371.5	405.0
(50)	315	365	384	418

Table 4.7. UV-vis data comparing **(41)** (toluene) and **(50)**[18] (chloroform).

Figure 4.20. Ferrocenyl PAH **(41)** and PAH **(50)**.

The UV-vis spectra of **(41)** and **(50)** show extremely similar shape and λ_{max} values. Both spectra show three types (groups) of bands (α, β, *p*), which are typical of aromatic hydrocarbons. The β-bands appear around 315 nm, and the *p*-bands around 370 nm. The α-band at 410 nm is an extremely low intensity absorption band.

Comparison of the spectral properties of **(41)** to PAH **(50)** serves as further evidence for the success of the cyclodehydrogenation reaction in forming the closed ring system of **(41)**. It has also shown, therefore, that the $\pi \rightarrow \pi^*$ transitions of the PAH unit are dominating the absorption spectrum of **(41)**.

Investigations into the oxidation of substituted ferrocenes with air in acidic solutions has been carried out by numerous workers.[27] It has been reported that the rate of the oxidation is influenced by the coordination facility of the proton to the iron atom. A greater reactivity can be accounted for by a specific, tilted conformation of the two cyclopentadienyl rings.[27] The same authors also report a correlation between the wavelength of the low energy band at around 450 nm (see table 4.6), which is found to be sensitive to the inclination of the cyclopentadienyl rings of ferrocene,[27] therefore to the rate of oxidation in acidic solution. Therefore, the band of [2]ferrocenophane, for example, which has tilted cyclopentadienyl rings due to its bridged conformation, has a longer wavelength absorption.[27] In fact, [2]ferrocenophane has a high basicity and protonation of the iron atom is facile.[27]

The low energy bands of the ferrocene derivatives in this work are shown in table 4.6. The bands of **(37)**, **(38)** and **(40)** are almost equal (443.0, 444.0 and 447.5 nm, respectively), on the other hand, the bands of the ferrocene derivatives **(39)** and **(46)** are shifted by about 10 nm to longer wavelengths (451.5 and 453.0 nm, respectively), and those bands for **(42)** and **(45)** are shifted by around 20 nm (464.5 and 461.5 nm, respectively). These results suggest that although the cyclopentadienyl rings of the ferrocene complexes **(37)**, **(38)** and **(40)** are not tilted, those of **(39)**, **(46)** and especially **(42)** and **(45)** derivatives are. This is in agreement with the X-ray crystallographic results obtained for **(40)** and **(45)**, as discussed earlier. Such an inclination is rare in a non-bridged derivative.[27]

As with the above example, the basicity of the iron atom in **(42)** and **(45)** would be expected to be high because of the inclination of the cyclopentadienyl rings, and thus protonation would be accelerated.[27] This may have serious implications in the highly acidic conditions of the oxidative cyclodehydrogenation reactions and perhaps explains the failure in the cyclodehydrogenation of **(42)** to the PAH derivative, as compared to the success obtained for polyphenylene **(40)**.

4.2.3 Electrochemistry

Ferrocene/ferrocenium itself represents a strictly reversible one-electron redox couple.[14] In the case of some ferrocenium derivatives, however, reversibility may be significantly lowered by a subsequent decomposition of the electrogenerated ferrocenium species.[14] The ferrocene substituent may also be regarded as a redox active probe on a molecular level, since following the ferrocene/ferrocenium redox potentials offers a unique opportunity to detect alterations in the electronic structure of the ferrocene-derived molecules, as well as in the nature of the metal-π-ligand

bonding. This provides information about the changes of electron density distribution and HOMO energies in a series of related compounds.[14]

The following compares the electrochemistry of compounds **(37)**, **(38)**, **(40)**, **(41)**, **(42)**, **(45)** and **(46)** by cyclic voltammetry (CV), in dichloromethane (0.1 M $(TBA)PF_6$ as electrolyte). Under the applied experimental conditions, all derivatives studied, except diferrocenyl **(46)**, exhibit a fully reversible one-electron oxidation attributable to the ferrocene/ferrocenium couple. Derivative **(46)** displays two such reversible one-electron oxidations in its cycic voltammogram. The relevant electrochemical data for the studied compounds, in dichloromethane solution, are compiled in table 4.8.

Complex	$E°$ (V)	ΔE_p (mV)
Fc	0.51	160
(37)	0.64	170
(38)	0.63	115
(40)	0.46	117
(41)	0.55	70
(42)	0.43	81
(45)	0.46	79
(46)	0.45, 0.66	76, 76

Table 4.8. Electrochemical data for complexes **(37)**, **(38)**, **(40)**, **(41)**, **(42)**, **(45)** and **(46)**. Supporting electrolyte: $(TBA)PF_6$ (0.1 M) in CH_2Cl_2; platinum disc working electrode, Pt wire auxiliary electrode, Ag/AgCl reference electrode, 100 mV s^{-1} scan rate; measured for $(0.2\text{-}1.0)\times10^{-4}$ M solutions. ΔE_p is given by $(E_{pa}-E_{pc})$.

All potentials are quoted together with the $[Fc/Fc^+]$ couple, which had a potential of 0.51 V *vs* the Ag/AgCl non-aqueous reference electrode used in this work. Peak separations are in the range of ΔE=70-120 mV, close to the reversible limit. These values are similar to that of the ferrocene standard (160 mV under the same voltammetric conditions), indicating that the one-electron $[Fc/Fc^+]$ oxidation processes are electrochemically reversible in dichloromethane.

Typical cyclic voltammograms for the ferrocenyl complexes **(41)** and **(46)**, on a platinum electrode, in dichloromethane solution containing 0.1 M $(TBA)PF_6$ as a supporting electrolyte, are displayed in figure 4.21. For **(41)** (figure 4.21 (a)), a reversible one-electron redox process has been observed at $E°$=0.55 V with ΔE=70 mV, while the Bis(ferrocene), complex **(46)** (figure 4.21 (b)), exhibits two redox processes in the CV experiment at $E°$=0.45 and 0.66 V. The peak separations (ΔE=76 mV) and virtually equal peak currents indicate two reversible one-electron oxidations occurring independently at each ferrocenyl centre.

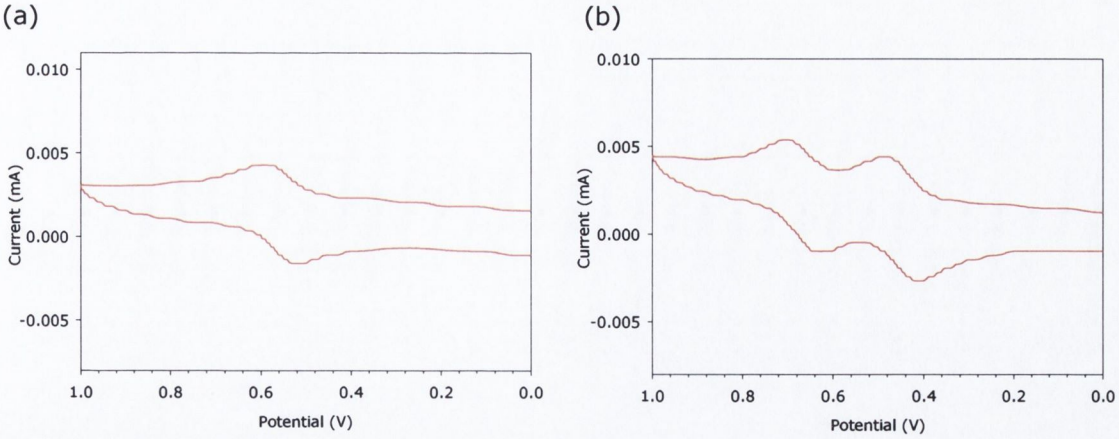


Figure 4.21. The cyclic voltammetric response of a (0.2-1.0)x10^{-4} M solution of ferrocene complexes (a) **(41)** and (b) **(46)**. Supporting electrolyte: (TBA)PF_6 (0.1 M) in CH_2Cl_2; platinum disc working electrode, Pt wire auxiliary electrode, Ag/AgCl reference electrode, 100 mV s^{-1} scan rate.

Although all ferrocenyl compounds show reversible one-electron oxidation, it is interesting to note that the redox potentials of the ferrocene units show a broad range of values from 0.43-0.66 V, caused through altering the substituent on the ferrocene ring. Molecular orbitals of the ferrocene group consist of the HOMO and LUMO of the iron atom and the ligand. The ligand offers electron density to the iron atom, while the iron atom feeds electron density back to the ligand simultaneously. The net result of the two synergic interactions and the E° of the resulting Fc/Fc^+ couple is, therefore, dependent on the substitution of the ligand.[6]

Compared to the ferrocene standard, the oxidation potentials of the ferrocenyl units in **(40)**, **(42)** and **(45)** exhibit a slight cathodic shift (less positive shift) by 50-80 mV. The redox potentials of these ferrocenyl complexes are similar (0.45 V ± 20 mV) (table 4.8), indicating that the chemical environment of the ferrocene units in these compounds are similar, irrespective of the type of polyphenylene substituent. The relatively low value for the ferrocene oxidation potential indicates that these ferrocenyl species are electron rich. The ease in oxidation in the three related compounds could be attributed to the electron donating ability of the polyphenylene core, stabilising the oxidised form with respect to ferrocene itself.

The cyclic voltammogram of **(41)** exhibits a redox potential of E°=0.55 V. The anodic shift (by 100 mV) of the $[Fc/Fc^+]$ couple as compared to the oxidation potential for **(40)** (E°=0.46 V), is due to the strong electron-withdrawing effect of the fully cyclised polyaromatic substituent, which is bound directly to the ferrocenyl moiety. This makes oxidation of the ferrocene unit in **(41)** thermodynamically more difficult than that of uncyclised **(40)** and of the unsubstituted metallocene (Fc). The loss of electron density

from the ferrocenyl donor unit to the net electron-accepting polyaromatic moiety therefore gives an anodically shifted oxidation wave. The acetylene derivatives **(37)** and **(38)** possess even higher oxidation potentials ($E°$=0.64 and 0.63 V, respectively). This is clearly the result of the electron-withdrawing alkyne unit which is directly connected to the ferrocene segment.[25]

The diferrocenyl complex **(46)**, as already stated, exhibits two redox processes. The two steps could be assigned to the oxidation of the Fe(II)-Fe(II) complex to the mixed valence Fe(II)-Fe(III) complex, and at a more positive potential, oxidation to the Fe(III)-Fe(III) complex. The first, ($E°$=0.45 V) which is essentially the same as **(40)** ($E°$=0.46), is assigned to the Fc(polyphenylene) group and the second ($E°$=0.66 V) to oxidation of the ethynylferrocene substituent (ethynylferrocene: $E°$=0.64 V).

The formal oxidation potential values, as indicated in table 4.8, show that the oxidation of the ferrocenyl units in **(37)**, **(38)** and **(41)** occur at a potential significantly more positive (by 100-200 mV) than the corresponding process in **(40)**, **(42)** and **(45)** (see also NMR, table 4.5). This is due to the strong electron-withdrawing groups bound directly to the cyclopentadienyl ring of the ferrocenyl moiety, which decreases the ease of the [Fc/Fc^+] oxidation. This feature agrees with the downfield shifts observed in the ^1H NMR spectral data for **(37)**, **(38)** and **(41)** as already discussed.

4.3 SUMMARY

New ferrocenyl complexes with polyphenylene derivatives have been prepared in excellent yields. All the compounds have been characterised by IR, ^{1}H and ^{13}C NMR and UV-vis spectroscopies and mass spectrometry. The redox chemistry of these ferrocenyl derivatives has been investigated by cyclic voltammetry and the molecular structures of **(40)** and **(45)** have been elucidated by single-crystal X-ray analyses. Three novel ferrocene polyphenylene derivatives **(40)**, **(45)** and **(46)** were prepared and characterized as air-stable products. This work has also developed a synthesis for the novel cyclodehydrogenated ferrocenyl PAH derivative **(41)**, *via* treatment of organometallic substrate **(40)** with $CuCl_2$ and $AlCl_3$ in CS_2. The work demonstrates for the first time that cyclodehydrogenation is possible in the presence of organometallic compounds, namely ferrocene, with **(41)** being synthesized in acceptable yields. Having proven the formation of a model for an intercalated graphite sheet, in a controlled and systematic fashion, this project may have wide-reaching applications for the future study and application of molecular materials.

Also presented is a preliminary investigation of electrochemical and spectroscopic properties. The electronic spectra of the complexes were measured in toluene. Derivatives **(40)**, **(42)**, **(45)** and **(46)** display similar features in their absorption spectra. However, UV-vis spectral data suggested that the two cyclopentadienyl rings are not parallel, but are tilted in **(42)**, **(45)** and **(46)**. Comparison of the X-ray data for compounds **(40)** and **(45)** adds support to this theory. Consequently, protonation of the iron atom of the ferrocene unit is expected to be accelerated, and the oxidation reactivity increased in acidic media. In general, the spectrum of ferrocenyl complex **(41)** is dominated by $\pi \rightarrow \pi^*$ absorption bands, with high absorption coefficients, corresponding to the polycyclic aromatic substituent. The lower energy weak absorption, ascribed to the *d-d* transition, is effectively swamped in **(41)**. The electrochemistry of all compounds was investigated by CV, in dichloromethane and all derivatives exhibit the one-electron reversible oxidation wave associated with the ferrocene/ferrocenium couple. The corresponding E° value is influenced by the electronic effects of the substituent, in support of the findings obtained from the NMR data. The potential value for ferrocenyl derivative **(41)** is considerably more positive than that of **(40)**, due to the electron-withdrawing effect of the polyaromatic function directly attached to the ferrocene unit. The diferrocenyl polyphenylene derivative **(46)** displayed separated, reversible, one-electron-oxidation steps (E°=0.45 and 0.66 V), occurring independently at each ferrocenyl centre. Oxidation of **(46)** thus involves two consecutive one-electron steps to give the corresponding mono- and then diferrocenium species in the potential region between 0.0-1.0 V.

4.4 FUTURE WORK

Ring closure *via* cyclodehydrogenation, to form the PAH substituted ferrocenyl compounds, should be investigated for polyphenylenes **(42)**, **(45)** and **(46)**. Alternative cyclodehydrogenation methods such as photochemical approaches may be necessary and should be considered.

Substituted cyclopentadienone **(44)** was utilised as a synthon for the novel **(45)**. The success of this reaction allows the incorporation of both ferrocene and pyrimidine elements into the polyphenylene precursor. It is envisaged that this synthetic strategy could be extended to incorporate further ferrocenyl units into the cylopentadienone, for example a tetra-ferrocenyl cyclopentadienone.

The NLO properties and photochemistry of all these novel ferrocene derivatives, especially **(41)**, have yet to be investigated. Conjugated organometallic systems that contain electronically coupled photo- and/or redox-active sites across an unsaturated organic bridge are also of considerable current interest.[28] With regards to this goal, tremendous efforts have been devoted to the design and synthesis of ferrocene-based materials with π-conjugation.[28] These types of ferrocene-containing molecule have been shown to exhibit a variety of intriguing electronic, optical, redox and structural properties.[28] Cyclodehydrogenation of **(45)** and incorporation of a second metal (*e.g.* Ru(II), Chapter 2), *via* chelation at the pyrimidine nitrogens would provide a highly novel complex with unique properties. The conjugated N-HBC linker would be expected to act as a communication channel between the two metal centres in the bimetallic complex.

4.5 REFERENCES

1. I. Manners, *Angew. Chem., Int. Ed. Engl.*, **1996**, *35*, 1602-1621
2. A. C. Ribou, J. P. Launay, M. L. Sachtleben, H. Li, C. W. Spangler, *Inorg. Chem.*, **1996**, *35*, 3735-3740
3. (a) G. Wilkinson, M. Rosenblum, M. C. Whiting, R. B. Woodward, *J. Am. Chem. Soc.*, **1952**, *74*, 2125-2126; (b) W. Steffen, M. Laskoski, G. Collins, U. H. F. Bunz, *J. Organomet. Chem.*, **2001**, *630*, 132-138
4. P. Molina, A. Tárraga, D. Curiel, M. D. Velasco, *J. Organomet. Chem.*, **2001**, *637-639*, 258-265
5. J. Sehnert, A. Hess, N. Metzler-Nolte, *J. Organomet. Chem.*, **2001**, *637-639*, 349-355
6. (a) N. Long, *Angew. Chem., Int. Ed. Engl.*, **1995**, *34*, 21-38; (b) X. Wang, Z. Deng, B. Jin, Y. Tian, X. Lin, *Electrochim. Acta*, **2002**, *47*, 1537-1543
7. J. D. McKinney, P. A. Anderson, T. A. Hamor, C. J. Jones, K. Paxton, A. Porch, *J. Organomet. Chem.*, **1998**, *558*, 147-153
8. (a) J. C. Calabrese, L. T. Cheng, J. C. Green, S. R. Marder, W. Tam, *J. Am. Chem. Soc.*, **1991**, *113*, 7227-7232; (b) K. N. Jayaprakash, P. C. Ray, I. Matsuoka, M. M. Bhadbhade, V. G. Puranik, P. K. Das, H. Nishihara, A. Sarkar, *Organometallics*, **1999**, *18*, 3851-3858
9. U. H. F. Bunz, J. E. C. Wiegelmann-Kreiter, *Chem. Ber.*, **1996**, *129*, 785-797
10. M. Laskoski, W. Steffen, M. D. Smith, U. H. F. Bunz, *Chem. Commun.*, **2001**, 691-692
11. M. Laskoski, G. Roidl, M. D. Smith, U. H. F. Bunz, *Angew. Chem., Int. Ed. Engl.*, **2001**, *40*, 1460-1463
12. M. Laskoski, J. G. M. Morton, M. D. Smith, U. H. F. Bunz, *J. Organomet. Chem.*, **2002**, *652*, 21-30
13. P. T. Herwig, V. Enkelmann, O. Schmelz, K. Müllen, *Chem. Eur. J.*, **2000**, *6*, 1834-1839
14. P. Štěpniča, L. Trojan, J. Kubišta, J. Ludvík, *J. Organomet. Chem.*, **2001**, *637-639*, 291-299
15. R. Hsung, C. Chidsey, L. Sita, *Organometallics*, **1995**, *14*, 4808-4815
16. M. Rosenblum, N. Brawn, J. Papenmeier, M. Applebaum, *J. Organomet. Chem.*, **1966**, *6*, 173-180
17. E. Champeil, Ph.D. Thesis, Trinity College Dublin, **1999**
18. F. Dötz, J. D. Brand, S. Ito, L. Gherghel, K. Müllen, *J. Am. Chem. Soc.*, **2000**, *122*, 7707-7717
19. C. J. McAdam, B. H. Robinson, J. Simpson, *Organometallics*, **2000**, *19*, 3644-3653
20. H. K. Gupta, S. Brydges, M. J. McGlinchey, *Organometallics*, **1999**, *18*, 115-122
21. G. D. Broadhead, J. M. Osgerby, P. L. Pauson, *J. Chem. Soc.*, **1958**, 650-656
22. M. D. Rausch, A. Siegel, *J. Org. Chem.*, **1968**, *33*, 4545-4547
23. Z. Yuan, G. Stringer, I. R. Jobe, D. Kreller, K. Scott, L. Koch, N. J. Taylor, T. B. Marder, *J. Organomet. Chem.*, **1993**, *452*, 115-120
24. A. S. Hay, *J. Org. Chem.*, **1962**, *27*, 3320-3321
25. K. R. J. Thomas, J. T. Lin, *J. Organomet. Chem.*, **2001**, *637-639*, 139-144
26. Y. S. Sohn, D. Hendrickson, H. B. Gray, *J. Am. Chem. Soc.*, **1971**, *93*, 3603-3612
27. Y. Okada, T. Nakagawa, T. Hayashi, *Inorg. Chim. Acta*, **2001**, *312*, 197-200
28. (a) W. Y. Wong, G. L. Lu, K. F. Ng, C. K. Wong, K. H. Choi, *J. Organomet. Chem.*, **2001**, *637-639*, 159-166; (b) N. J. Long, A. J. Martin, R. Vilar, A. J. P. White, D. J. Williams, M. Younus, *Organometallics*, **1999**, *18*, 4261-4269; (c) H. Fink, N. J. Long, A. J. Martin, G. Opromolla, A. J. P. White, D. J. Williams, P. Zanello, *Organometallics*, **1997**, *16*, 2646-2650

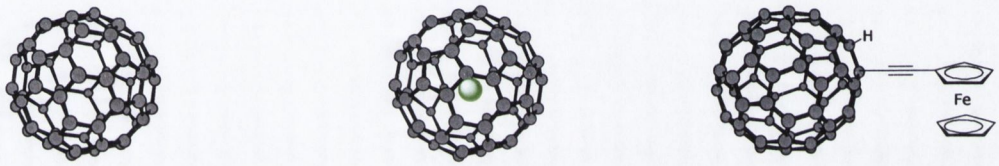
CHAPTER FIVE

THE HETEROFULLERENE, AZA[60]FULLERENE

5.1 INTRODUCTION

Buckminster fullerene is the third well-characterised allotrope of carbon after graphite and diamond and has many desirable electronic and optical properties for incorporation into future molecular devices. C_{60} contains two types of bonds (6:5 fusion and 6:6 fusion)[1] and all carbon sites are equivalent.[2]

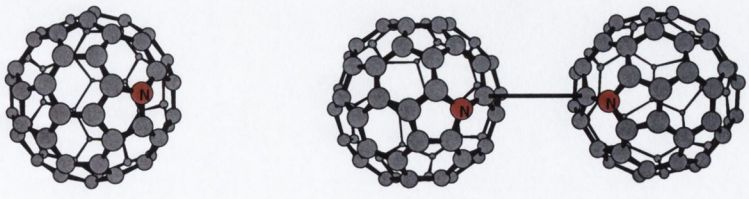
Since the discovery of the bulk production of fullerenes in 1990,[3] synthetic chemists have been fascinated by the idea of developing chemical modifications of the all-carbon cages (see figure 5.1). For the structural variation of fullerenes, three strategies can in principle be considered. Guest atoms such as atomic nitrogen atoms have been encapsulated within the cage using ion implantation to form what is called an endohedral fullerene derivative,[4] or chemistry at the surface of the C_{60} cage will produce exohedral derivatives such as the ferrocenylethynyl derivative shown below.[5]



(a) (b) (c)

Figure 5.1. (a) fullerene, C_{60}, (b) endohedral fullerene, $N@C_{60}$, (c) exohedral fullerene, 1-ferrocenylethynyl-2-hydro-1,2-dihydro-[60]fullerene.[5]

Heterofullerenes, the third fundamental group of modified fullerenes, is the least explored. In heterofullerenes, one or more carbon atoms of the cage are substituted by heteroatoms, such as the trivalent nitrogen atom. If an odd number of carbon atoms are substituted by nitrogens, radicals are formed which can be stabilised by dimerisation. Replacement of an even number of carbon atoms would lead directly to closed-shell systems. So far this group of compounds is limited to the simplest form of nitrogen heterofullerene, $C_{59}N$ and its dimer $(C_{59}N)_2$,[6] although this method has also been extended more recently for the synthesis of aza[70]fullerenes $(C_{69}N)_2$,[7] and mixed $C_{59}N/C_{69}N$ heterodimers.[8]

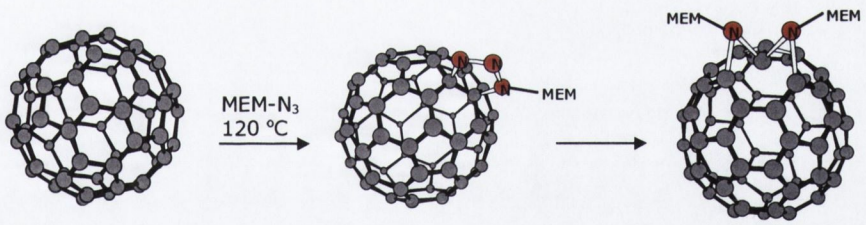


(a) (b)

Figure 5.2. (a) The aza[60]fullerene $C_{59}N^{\cdot}$ radical and its dimer (b).

The systematic substitution of cage carbon atoms by nitrogen atoms represents the 3-dimensional counterpart of the planar aromatics discussed in Chapter 2, which could be doped with nitrogen to form heteroaromatics. So by doping the fullerene cage with nitrogen to form the heterofullerene, we would expect the same gain in structural and functional qualities that we did for the doped PAH's.[6] The chemical and physical properties of heterofullerenes, are expected to be tunable for potential application as new materials.[6,8,9]

Before 1995, experimental evidence for the existence of heterofullerenes was very rare. For example in 1991, the preparation of a number of C_nN_m clusters were reported,[10] however none of these species have been isolated or structurally characterised. In 1995 exohedral fullerene chemistry had developed and it was discovered that certain epiminofullerenes and azahomofullerenes (azafulleroids) were suitable precursors for the formation of heterofullerenes, $C_{59}N^+$, in the gas phase,[11] under the conditions of FAB and DCI mass spectrometry.[12] The first chemical synthesis of aza[60]fullerene was published by Wudl in 1995.[13] Shortly after, Hirsch[7] published an alternative method after his successful conversion of bisazahomofullerene (figure 5.3 (c)) to the aza[60]fullerene dimer. The Diazabis-(1,6);(1,9)-homofullerenes are formed from a two-fold reaction of C_{60} with alkyl azides. This bisazafulleroid formation is the most regioselective reaction in fullerene chemistry to date, and is believed to proceed *via* a triazoline intermediate (figure 5.3 (b)).[14]



(b) (c)

Figure 5.3. The formation of bisazafulleroid (c) from C_{60}, *via* the triazoline intermediate (b) MEM=$CH_2O(CH_2)_2OMe$.

The bisazafulleroid is then treated with *n*-butylamine and a strong base (DBU) to produce an amine adduct, which is reacted with excess *para*-toluenesulfonic acid, to produce the dimer and an alkoxy-substituted monomeric compound (see figure 5.4)

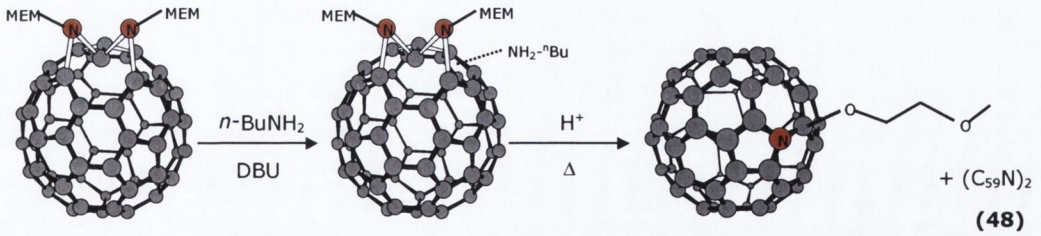


Figure 5.4. The formation of heterofullerene **(48)** and adduct $C_{59}NO(CH_2)_2OMe$, *via* the green aminofullerides.

The mechanism for this reaction is not fully understood at present, although the acidic cleavage of the MEM group with reduction to the heterofullerene monomeric radical $C_{59}N^{\cdot}$, and subsequent dimerisation is the most likely pathway.[6]

Mono-azafullerenes are still the only known heterofullerenes which can be isolated as pure substances. The substitution of one carbon atom of the fullerene framework with nitrogen leads to the formation of an open-shell system. Consequently, the simplest nitrogen heterofullerene can only be isolated as a dimer. In this compound two $C_{59}N$ moieties are connected by an sp^3-carbon adjacent to the nitrogen.

For $(C_{59}N)_2$, theoretical calculations predict a relatively low binding energy of only 18 Kcal/mol,[15] with an interdimer bond length of 160.9 pm (average C-C bond 154 pm). This bond undergoes homolytic cleavage thermally or photochemically.

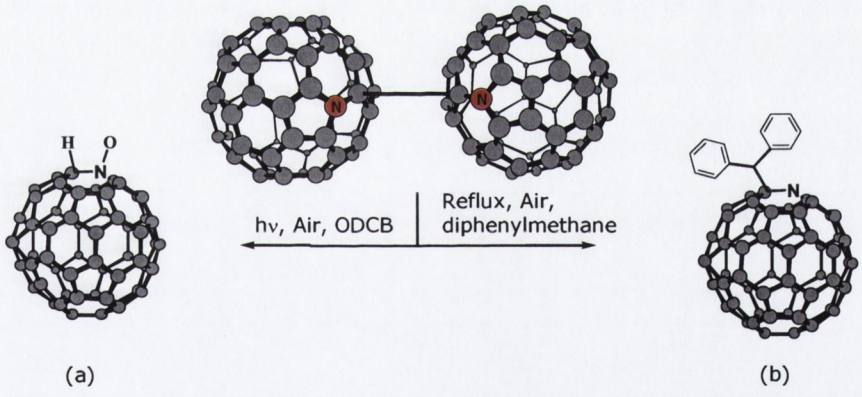


Figure 5.5. The (a) photochemical[16] and (b) thermal[17] cleavage of the heterofullerene dimer.

The monomeric radical has valuable synthetic potential, demonstrated by the thermal treatment of $(C_{59}N)_2$ with diphenylmethane (figure 5.5).[18] Interestingly, treatment of the dimer under photolytic conditions produces an N-oxide.

Although the synthesis of pure $(C_{59}N)_2$ in reasonable quantities is possible at present, very few derivatisation methods have been published to date. Several arylated

heterofullerene derivatives, $ArC_{59}N$, can be formed under thermal conditions, with electron-rich aromatics, in yields up to 90%, *via* electrophilic aromatic substitution by $C_{59}N^{+}$.[19] This was formed *via* thermal homolysis of the dimer, followed by oxidation of the $C_{59}N$ radical. Similarly, Mannich bases, $RC_{59}N$ [R=CH(R')COR''] have been obtained in almost quantitative yields, by the analogous treatment of the $(C_{59}N)_2$ dimer with enolizable aldehydes, ketones, and 1,3-diketones as nucleophiles.[20] Arylated heterofullerenes are, in general, stable and more soluble than the parent dimer, and as such are more suitable compounds for the investigation of the chemistry of azafullerene.

The alternative synthetic approach to derivatisation is the photochemical treatment of $(C_{59}N)_2$ in 1,2-dichlorobenzene (ODCB), in the presence of a trapping agent, such as $^{n}Bu_3SnH$. Here $C_{59}HN$ is obtained *via* a free radical chain mechanism.[16]

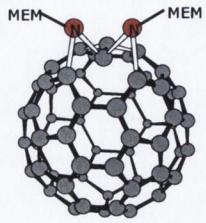
The above represents the only chemistry that has been done on these heterofullerene systems to date. So far, no organometallic compounds have been incorporated into what would be a completely novel nitrogen containing ligand system. The incorporation of an acetylene unit onto the periphery of the heterofullerene, simultaneously provides a handle for the introduction of organometallic compounds, and may also provide a compound suitable for Diels-Alder conditions, resulting in aza[60]fullerene substituted polyaromatics.

This work has explored the two methods of derivatisation of aza[60]fullerene, but with acetylene substituents. The first method is based on the thermal homolysis of the dimer and oxidation of the resulting aza[60]fullerenyl radical to the aza[60]fulleronium ion $C_{59}N^{+}$ by oxidation. The second method utilizes the photolytic cleavage of the dimer and subsequent attempted trapping by tributyl(phenylethynyl)tin.

5.2 RESULTS AND DISCUSSION

The 2-fold addition of MEM azide, which was formed *in situ* from MEM chloride and sodium azide, gives the diazabis-(1,6);(1,9)-heterofullerene in a 50% yield with 40% recovery of unreacted C_{60}. The reaction is carried out under reflux in chlorobenzene, and the black microcrystalline bisazafulleroid, **(47)**, was isolated by chromatography.

^{1}H NMR (CS_2/20% $CDCl_3$):
5.58 (d, 1H), 5.42 (d, 1H)
4.18 (dt, 1H), 4.03 (dt, 1H)
3.73 (t, 2H), 3.47 (s, 3H)



(47)

Figure 5.6. ^{1}H NMR spectroscopic data for bisazafulleroid **(47)**, MEM=$CH_2O(CH_2)_2OMe$ (RT, 400 MHz).

The ^{1}H NMR spectrum shows signals only for the alkyl side chain. The diastereotopic protons of the methylene groups, at the cage end of the alkyl chain, are split into doublets. The fullerene cage does not influence the other end of the alkyl chain and we see equivalence in the protons within the methylene and methyl groups.

Treatment of **(47)** with *n*-butylamine and strong base (DBU), in toluene leads to the formation and precipitation of the amine adduct as dark green amino-fullerides. The solution is reduced *in vacuo* and reacted without purification in the presence of 20 equivalents of *para*-toluenesulfonic acid, in dichlorobenzene. This mixture is brought to reflux for only 8 minutes to afford the azafullerene dimer **(48)**, which is purified by column chromatography, on silica using toluene as eluent.

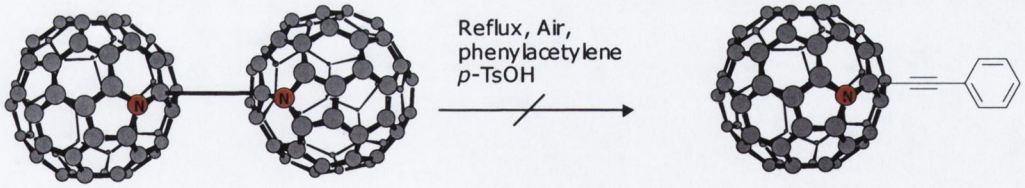
$(C_{59}N)_2$ **(48)** is obtained in an overall yield of 10-20%, a similar yield to that reported for this reaction by Hirsch.[8] The formation of **(48)** is proven unambiguously through ESI-mass spectral analysis and UV-vis spectroscopy, which are identical to that published in every way.[7] Having developed the synthesis of **(48)** to suit my conditions, and with the ability to produce quantities of $(C_{59}N)_2$ in reliable yields, I intended to react it in an attempt to introduce acetylene substituents onto the cage. This may offer a route for the introduction of metal centres and a totally new form of inorganic complex.

Very recent research demonstrates that homolytic cleavage of the interdimer C-C bond can be achieved thermally or photochemically, and leads to the monomeric radical $C_{59}N^{\cdot}$.[18] This species either dimerizes back to $(C_{59}N)_2$, or is trapped to form monomeric $C_{59}N$ derivatives. This has led to the development of two synthetic strategies for the derivatization of $(C_{59}N)_2$.[21]

Strategy 1: $C_{59}N^+$, which is isoelectronic to C_{60}, is formed *via* the thermal homolysis of the dimer, followed by oxidation of the radical. Arylation of the cation, $C_{59}N^+$, proceeds *via* electrophilic substitution.[19] The reaction requires the presence of an excess of *p*-TsOH. Its role is not yet clear, although it has been suggested that it traps the reduced oxygen species formed,[19] or that the redox potential of $C_{59}N$/ $C_{59}N^+$ may depend on pH.[9] In this way $C_{59}N$-Ar adducts, where Ar is for example phenyl or tolyl, are accessible in good yields. The direct addition of phenol is not possible, however, as the protonation of the oxygen is expected to cause deactivation relative to the electrophilic aromatic substitution.[9]

This synthetic strategy has also led to the Mannich functionalisation of $C_{59}N$ using such reactants as acetone or acetophenone.[20] Under the acidic reaction conditions the intermediate $C_{59}N^+$ is again formed, by the oxidation of the $C_{59}N$ radical, and is able to attack the enol form of the ketone generating the α-azafullerenated ketone. Interestingly, acetophenone, a compound which offers an aromatic as well as an enolic moiety shows preferred attack at the α-CH_3 position.[21] Likewise, phenylacetylene is not an electron rich aromatic system, and it is thought possible to undergo a similar Mannich type reaction at the acetylene. With this as encouragement, it was decided to proceed with the thermal reaction.

The treatment of $(C_{59}N)_2$ in ODCB with 20 equivalents of phenylacetylene and 40 equivalents of *p*-TsOH at 423 K in a constant stream of air (figure 5.7), unfortunately did not yield the phenylacetylene derivative. Instead, polymerisation of phenylacetylene occurred. ESI-mass spectral analysis showed no trace of $C_{59}N$ or indeed any derivative of $C_{59}N$.



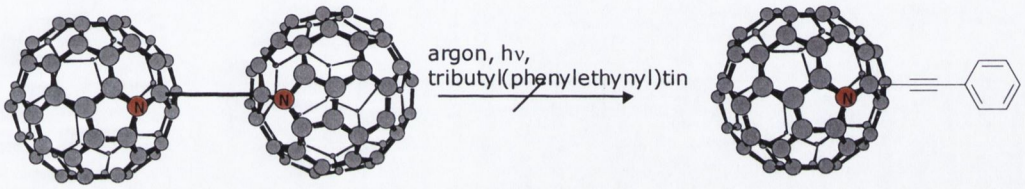
(51)

Figure 5.7. The attempted thermal synthesis of $C_{59}N$ ethynyl benzene, **(51)**, using *p*-TsOH, and oxygen.

The thermal polymerisation of aryl acetylenes is known to take place above 403 K, without catalyst,[22,23] and occurs *via* a radical mechanism. The high reaction temperature is clearly a disadvantage in this case.

Strategy 2: After photolysis of $(C_{59}N)_2$, in the presence of a good radical source, the resulting azafullerenyl radical is expected to undergo free radical reactions.[18] $C_{59}HN$, where one $C_{59}N$ moiety is substituted with an H-atom, is the simplest closed-shell azafullerene. It is obtained by the thermal or photochemical treatment of $(C_{59}N)_2$ in 1,2-dichlorobenzene (ODCB) in the presence of the trapping agent $^nBu_3SnH$.[16] Room temperature photolysis was therefore proposed, as a good alternative for the synthesis of an ethynyl substituted azafullerene, thus preventing the thermal acetylenic polymerisation, that hindered the previous route.

$(C_{59}N)_2$ was reacted photochemically with tributyl(phenylethynyl)tin (**(5)**, Chapter 1), under argon, in degassed ODCB, using light irradiation (125-W Mercury lamp), as illustrated in figure 5.8.



(51)

Figure 5.8. The attempted photochemical synthesis of $C_{59}N$ ethynyl benzene, **(51)**.

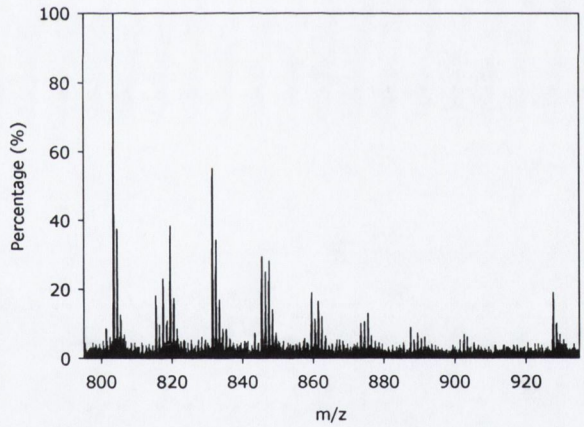


Figure 5.9. The 780 – 940 *m/z* region of the ESI-mass spectrum showing the products of the photochemical reaction of $(C_{59}N)_2$ and tributyl(phenylethynyl)tin.

Although ESI-mass spectral analysis (figure 5.9) shows the presence of molecular units in the *m/z*=800-950 region, it was not possible to purify the mixture further. The fragmentation pattern at around *m/z*=820 is promising ($C_{59}N$ ethynylbenzene is 823.7), however it does not serve as evidence for the formation of **(51)**. Consecutive spectral envelopes at 831.5, 845.5, 859.5, 873.5, and 887.5, consistently separated by *m/z*=14, perhaps indicate the loss of CH_2 groups from an incorporated butyl group.

Unfortunately, in this case, the radical process is likely to drive many reactions, including free radical additions across the triple bond.

Although attempts, thus far, have been unsuccessful in the incorporation of acetylenic units onto the heterofullerene cage, our group continues to work in this area. Currently the research group of Hirsch is attempting to develop alternative oxidising conditions, such as the use of ferrocenium hexafluorophosphate and chloranil, away from the successful, yet extremely limited, oxygen, *p*-TsOH system. This is at the forefront of azafullerene research.[21]

An alternative approach may be to utilize the aldehyde adducts, recently formed in the Mannich type reaction of the azafulleronium ion, $C_{59}N^+$, with ketones and aldehydes.[20] These aldehyde adducts may serve as handles for further functionalization, toward acetylenic substituted heterofullerenes.

Further, pincer ligands, such as those studied in Chapter 1, may be incorporated onto the surface of $C_{59}N$, *via* the electrophilic aromatic substitution type reactions discussed above, as an alternative approach to the incorporation of organometallics.

5.3 REFERENCES

1. R. Haden, *Science*, **1993**, *261*, 1545-1560
2. R. Taylor, J. Hare, A. Abdul-Sada, H. Kroto, *Chem. Commun.*, **1990**, 1423-1425
3. W. Krätschmer, L. Lamb, K. Fostiropoulos, D. Huffman, *Nature*, **1990**, *347*, 354-358
4. *Electronic Properties of Novel Materials: XII International Winterschool*, Edited by H. Kuzmany, **1998**, The American Institute of Physics, 363-367, 392-395, 223-226
5. E. Champeil, Ph.D. Thesis, Trinity College Dublin, **1999**
6. A. Hirsch, B. Nuber, *Acc. Chem. Res.*, **1999**, *32*, 795-804
7. B. Nuber, A. Hirsch, *Chem. Commun.*, **1996**, 1421-1422
8. J. Hummelen, C. Bellavia-Lund, F. Wudl, *Top. Curr. Chem.*, **1999**, *199*, 93-134
9. U. Reuther, A. Hirsch, *Carbon*, **2000**, *38*, 1539-1549
10. T. Pradeep, V. Vijayakrishnan, A. Santa, C. Rao, *J. Phys. Chem.*, **1991**, *95*, 10564-10565
11. J. Hummelen, B. Knight, J. Pavlovich, R. Gonzalez, F. Wudl, *Science*, **1995**, *269*, 1554-1556
12. I. Lamparth, B. Nuber, G. Schick, A. Skiebe, T. Grösser, A. Hirsch, *Angew. Chem., Int. Ed. Engl.*, **1995**, *34*, 2257-2259
13. J. C. Hummelen, M. Prato, F. Wudl, *J. Am. Chem. Soc.*, **1995**, *117*, 7003-7004
14. B. Nuber, F. Hampel, A. Hirsch, *Chem. Commun.*, **1996**, 1799-1800
15. W. Andreoni, A. Curioni, K. Holczer, K. Prassides, M. Keshavarz-K, J. Hummelen, F. Wudl, *J. Am. Chem. Soc.*, **1996**, *118*, 11335-11336
16. M. Keshavarz-K, R. González, R. G. Hicks, G. Srdanov, V. I. Srdanov, T. Collins, J. C. Hummelen, C. Bellavia-Lund, J. Pavlovich, F. Wudl, K. Holczer, *Nature*, **1996**, *383*, 147-150
17. C. Bellavia-Lund, M. Keshavarz-K, T. Collins, F. Wudl, *J. Am. Chem. Soc.*, **1997**, *119*, 8101-8102
18. C. Bellavia-Lund, R. González, J. C. Hummelen, R. G. Hicks, A. Sastre, F. Wudl, *J. Am. Chem. Soc.*, **1997**, *119*, 2946-2947
19. B. Nuber, A. Hirsch, *Chem. Commun.*, **1998**, 405-406
20. F. Hauke, A. Hirsch, *Chem. Commun.*, **1999**, 2199-2200
21. F. Hauke, A. Hirsch, *Tetrahedron*, **2001**, *57*, 3697-3708
22. S. Gandon, P. Mison, M. Bartholin, R. Mercier, B. Sillion, E. Geneve, P. Grenier, M. F. Grenier-Loustalot, *Polymer*, **1997**, *38*, 1439-1447
23. S. Gandon, P. Mison, B. Sillion, *Polymer*, **1997**, *38*, 1449-1459

CHAPTER SIX

EXPERIMENTAL

6 EXPERIMENTAL

General comments

Unless otherwise stated, all reactions were carried out under an argon atmosphere using standard schlenck techniques. All Solvents were distilled under nitrogen from appropriate drying agents and degassed prior to use. The deuterated solvents $CDCl_3$ and C_6D_6 were distilled from molecular sieves. Flash chromatography was performed using silica gel or activated alumina (Brockman I, Aldrich Chemical) as the stationary phase. Separations were undertaken in the air.

IR spectra were recorded on a Perkin-Elmer Paragon 1000 Fourier transform spectrophotometer. Solution IR spectra were recorded using standard NaCl solution cells. Solid-state IR spectra were recorded from KBr disks. NMR spectra were recorded on DPX 400 spectrometer operating at 400.13 MHz for ^1H, and 100.62 MHz for ^{13}C, and were standardized with respect to TMS. Specific assignments have been made for the NMR spectra where possible according to the labelled diagram for that product. Electrospray mass spectra were recorded on a micromass LCT electrospray mass spectrometer. Accurate mass spectra were referenced against Leucine Enkephalin (555.6 $gmol^{-1}$), and were reported within 5 ppm.

UV-vis absorption spectra were recorded on a Shimadzu UV-2401PC, UV-vis Recording Spectrophotometer. Emission spectra were not corrected and were recorded at 25°C using a Perkin Elmer LS50B Luminescence Spectrometer, equipped with a Hamamatsu R928 red sensitive detector (185-900 nm range), employing Perkin-Elmer Fl Win Lab software. Quartz cells (10 mm path length) were used. Emission quantum yields were measured at room temperature using $[Ru(bpy)_3]^{2+}$ or quinine sulphate in deaerated solutions as quantum yield standards assuming a value of 0.042 and 0.546, respectively.[1] Luminescence lifetime measurements were obtained using an Edinburgh Analytical Instruments (EAI) time-correlated single-photon counting apparatus (TCSPC) composed of two model J-yA monochromators (emission and excitation), a single photon photomultiplier detection system model 5300, and a F900 nanosecond flashlamp (N_2 filled at 1.1 atm pressure, 40 kHz), interfaced with a personal computer *via* a Norland MCA card. A 500 nm cut-off filter was used in emission to attenuate scatter of the excitation light (337 nm). Data correlation and manipulation were carried out using EAI F900 software version 5.1.3. Samples were deaerated for 20 min using Ar gas before measurements were carried out. Emission lifetimes were calculated using a single-exponential fitting function; a Levenberg-Marquardt algorithm with iterative reconvolution Edinburgh instruments F900 software was used; uncertainty is ±10%. The reduced χ^2 and residual plots were used to judge the quality of the fits.

Electrochemical measurements were carried out on a Model 660 electrochemical workstation (CH Instruments). Typical concentrations were $0.2\text{-}1.0\text{x}10^{-4}$ M in anhydrous solutions containing 0.1 M tetrabutylammonium hexafluorophosphate ($TBA.PF_6$). Conventional voltammetric measurements were carried out using a standard three-electrode cell arrangement. Either a) A teflon shrouded glassy carbon working electrode, a Pt wire auxiliary electrode, and an SCE reference electrode, or b) A Pt working electrode, a Pt wire auxiliary electrode, and a pseudo-Ag/AgCl reference electrode were employed. Solutions were deoxygenated by purging with N_2 or Ar gas for 15 min prior to the measurement. Measurements were made in the range –2.0 to 2.0 versus SCE.

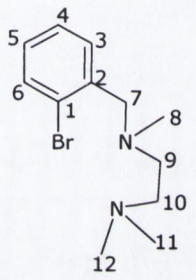
Spectroelectrochemistry was carried out using an OTTLE setup composed of a homemade Pyrex glass, thin layer cell (2 mm). The optically transparent working electrode was made from platinum-rhodium gauze, a platinum wire counter electrode, and the reference electrode, which was a pseudo-Ag/AgCl reference electrode. The working electrode was held at the required potential throughout the measurement using an EG&G PAR Model 362 potentiostat. UV-vis absorption spectra were recorded on a Shimadzu UV-vis-NIR 3100 spectrophotometer interfaced with an Elonex PC466 using UV-vis data manager.

Crystal data and X-ray experimental details are summarised in Appendix 1. Single-crystal analyses were performed with a Bruker SMART APEX CCD or CAD4 diffractometer using graphite monochromised Mo-K_α (λ=0.71073 Å) radiation at 25°C. A full sphere of data was obtained for each using the omega scan method. The data reduction was performed using SMART and SAINT-NT (v. 6.2). Intensities were corrected for Lorentz and polarization effects and for absorption using SADABS (v. 2). Space groups were determined from systematic absences and checked for higher symmetry. The structures were solved by direct methods using SHELXS (v. 5.1) and refined on F^2 using all data by full-matrix least-squares procedures with SHELXL (v. 5.1). All non-hydrogen atoms were refined with anisotropic displacement parameters. Hydrogen atoms were included in calculated positions with isotropic displacement parameters 1.3 times the isotropic equivalent of their carrier carbons. The functions minimised were $\sum w(F_o^2\text{-}F_c^2)$, with $w=[\sigma^2(F_o^2)+(aP)^2+bP]^{-1}$, where $P=[\max(F_o)^2+2F_c^2]/3$. In all cases, final Fourier syntheses showed no significant residual electron density in chemically sensible positions.

6.1 COMPLEXES OF AN ARYL DIAMINE LIGAND

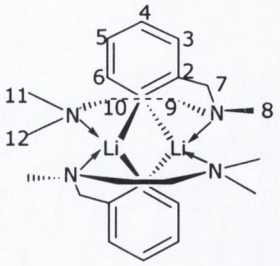
6.1.1 DiamBr, (1)

To a solution of *N,N,N'*-trimethylethylenediamine (13.3 mL; 102 mmol) and NEt_3 (40 mL) in C_6H_6 (100 mL) was added dropwise a solution of 2-bromobenzyl bromide (25.3 g; 101 mmol) in C_6H_6 (110 mL). After 1 h the resulting white suspension was filtered and washed with C_6H_6 (25 mL). The filtrate was concentrated by removing the solvent *in vacuo*. This resulted in a pale yellow oil, which was purified by chromatography (alumina, 1:1 hexane:dichloromethane) to produce a colourless oil. Yield: 17.8 g, 65%. ^{1}H NMR (C_6D_6): δ 7.65 (d, 1H, $^3J_{HH}$=7.5, H6), 7.51 (d, 1H, $^3J_{HH}$=8.0, H3), 7.11 (t, 1H, $^3J_{HH}$=7.5, H4 or H5), 6.83 (t, 1H, $^3J_{HH}$=8.0, H4 or H5), 3.69 (s, 2H, H7), 2.61 (t, 2H, $^3J_{HH}$=7.0, H9), 2.46 (t, 2H, $^3J_{HH}$=7.0, H10), 2.24 (s, 3H, H8), 2.19 (s, 6H, H11, H12). ^{13}C NMR ($CDCl_3$): δ 138.7 (1C, C1), 132.2, 130.3, 127.7, 126.6 (1C, C_{aryl}), 124.0 (1C, C2), 61.4 (1C, C7), 57.5, 55.6 (1C, C9, C10), 45.2 (2C, C11, C12), 41.9 (1C, C8).



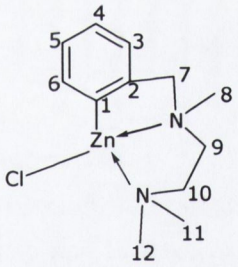
6.1.2 $(DiamLi)_2$, (2)

To a solution of **(1)** (7.74 g; 28.5 mmol) in Et_2O (25 mL) was added slowly at -70°C *n*-BuLi (20 mL of a 1.5 M solution in hexane; 30 mmol), which resulted in immediate precipitation of a white solid. The reaction mixture was stirred for 1.5 h, during which time the temperature was allowed to rise to RT. The resulting suspension was allowed to settle and the supernatant removed by cannula. The solid obtained was washed with pentane (3 x 10 mL) and dried *in vacuo* to afford **(2)** as a white powder. Yield: 5.65 g, 97%. ^{1}H NMR (C_6D_6): δ 8.32 (d, 1H, $^3J_{HH}$=7, H6), 7.38 (t, 1H, $^3J_{HH}$=7, H4 or H5), 7.27 (t, 1H, $^3J_{HH}$=7, H4 or H5), 7.18 (d, 1H, $^3J_{HH}$=7, H3), 4.23 (d, 1H, $^2J_{HH}$=12, H7), 3.28 (d, 1H, $^2J_{HH}$=12, H7), 2.75 (m, 1H, H9), 2.49 (s, 3H, H8), 2.10 (m, 1H, H9), 1.70 (m, 1H, H10), 1.55 (m, 1H, H10), 1.53 (br s, 6H, H11, H12). ^{13}C NMR (C_6D_6): δ 150.5 (1C, C2), 142.6, 125.6, 124.3, 124.0 (1C, C_{aryl}), 71.5 (1C, C7), 57.6, 52.1 (1C, C9, C10), 46 (2C, br, C11, C12), 44.8 (1C, br, C8), C_{ipso} not observed.



6.1.3 DiamZnCl, (3)

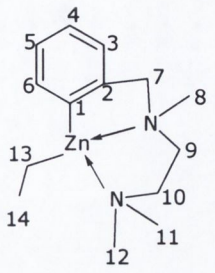
A suspension of **(2)** (14 mmol) in 1:1 Et_2O:benzene (30 mL) was added dropwise to a solution of $ZnCl_2$ (3.82 g; 28 mmol) in 1:1 Et_2O:benzene (40 mL) and the mixture was allowed to stir for 2 h. A white precipitate formed which was removed by filtration. The filtrate was concentrated and cooled. Colourless crystals of **(3)** slowly formed. ^{1}H NMR (C_6D_6): δ 8.02 (d, 1H, $^3J_{HH}$=7, H6), 7.35 (t, 1H, $^3J_{HH}$=7, H4 or H5), 7.25 (dt, 1H, $^3J_{HH}$=7, H4 or H5), 6.95 (d, 1H, $^3J_{HH}$=7, H3), 3.44 (d, 1H, $^2J_{HH}$=14, H7), 3.00 (d, 1H, $^2J_{HH}$=14, H7), 2.16, 2.12 (s, 3H, H11, H12), 2.02 (d, 1H, J_{HH}=12, H10), 1.92 (d, 1H, J_{HH}=12, H10) 1.47 (s, 3H, H8), 1.36 (td, 1H, J_{HH}=4-12, H9), 1.18 (td, 1H, J_{HH}=4-12, H9). ^{13}C NMR (C_6D_6): δ 154.2 (1C, C1), 145.3 (1C, C2), 139.3, 126.6, 126.3, 125.0 (1C, C_{aryl}), 65.0 (1C, C7), 57.6, 53.2 (1C, C9, C10), 48.2 (1C, C11 or C12), 45.8 (1C, C8), 43.4 (1C, C11 or C12).



6.1.4 DiamZnEt, (4)

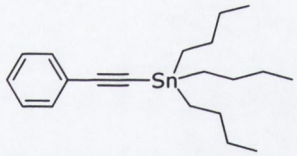
To an *in situ* prepared solution of EtZnCl from $ZnCl_2$ (10.5 mL of an 0.32 M solution in Et_2O; 3.37 mmol) and $ZnEt_2$ (3.56 mL of a 1.0 M solution in hexane; 3.57 mmol) in C_6H_6 (30 mL), was added **(2)** (15 mL of an 0.22 M suspension in Et_2O; 3.33 mmol) dropwise over 10 min with stirring. The solution was allowed to stir for 3 h and the resulting white precipitate filtered. The pale yellow filtrate was reduced *in vacuo*, to a colourless solid. ^{1}H NMR (C_6D_6): δ 8.03 (d, 1H, $^3J_{HH}$=7, H6), 7.37 (t, 1H, $^3J_{HH}$=7, H4 or H5), 7.30 (dt, 1H, $^3J_{HH}$=7, H4 or H5), 7.10 (d, 1H, $^3J_{HH}$=7, H3), 3.66 (d, 1H, $^2J_{HH}$=14, H7), 3.16 (d, 1H, $^2J_{HH}$=14, H7), 2.35 (td, 1H, J_{HH}=4-12, H10), 2.18, 2.14 (s, 3H, H11, H12), 2.01 (td, 1H, J_{HH}=4-12, H10) 1.78 (m, 6H, H8, H14), 1.62 (td, 1H, J_{HH}=4-12, H9), 1.50 (td, 1H, J_{HH}=4-12, H9), 0.56 (m, 2H, H13). ^{13}C NMR (C_6D_6): δ 161.2 (1C,

C1), 145.7 (1C, C2), 138.7, 125.2, 124.6, 123.8 (1C, C_{aryl}), 66.0 (1C, C7), 56.9, 53.6 (1C, C9, C10), 46.1, 43.6 (1C, C11, C12), 42.9 (1C, C8), 13.4 (1C, C14), -0.9 (1C, C13).



6.1.5 Tributyl(phenylethynyl)tin, (5)

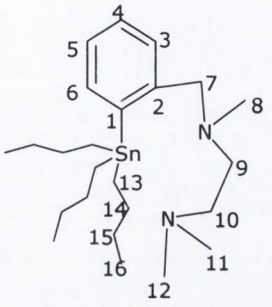
Phenylacetylene (1 mL; 9.1 mmol) was dissolved in 10 mL of THF and cooled to -78°C. To this solution was added *n*-BuLi (5.7 mL of a 1.6 M solution in hexane; 9.1 mmol). The mixture was allowed to stir for 20 min at 0°C, after which tributyltinchloride (2.5 mL; 9.1 mmol) was used to quench the solution. After stirring for an hour at RT, the solvent was removed. The crude product was dissolved in hexane, washed with water and chromatographed (SiO_2, 9:1 hexane:ethyl acetate), to produce **(5)** as a colourless oil. Yield: 3.2 g, 90%. ^{1}H NMR ($CDCl_3$): δ 7.51 (m, 2H, H_{aryl}), 7.32 (m, 3H, H_{aryl}), 1.70 (quintet, 6H, $^3J_{HH}$=7.5, H_{alkyl}), 1.46 (sextet, 6H, $^3J_{HH}$=7.5, H_{alkyl}), 1.13 (t, 6H, $^3J_{HH}$=8, H_{alkyl}), 1.01 (t, 9H, $^3J_{HH}$=7.5, H_{alkyl}). ^{13}C NMR ($CDCl_3$): δ 131.5 (2C), 127.6 (2C), 127.3 (1C) (C_{aryl}), 123.7 (1C, $C_{quat/aryl}$), 109.7 (1C, -C≡C-), 92.7 (1C, -C≡C-), 28.5 (3C, CH_2), 26.5 (3C, CH_2), 13.2 (3C, $-CH_3$), 10.8 (3C, CH_2).



6.1.6 DiamSn(Bu)$_3$, (6)

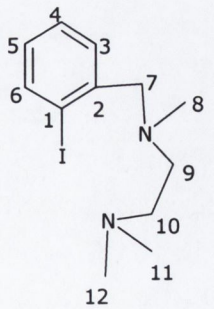
To a suspension of **(2)** (1.19 g; 3.0 mmol) in Et_2O (20 mL) at -15°C was added Bu_3SnCl (1.6 mL; 6.0 mmol). The solution was warmed to RT over 6 h and a white precipitate formed. The filtrate was collected, washed with water and aqueous sodium chloride, and dried over $MgSO_4$. The solvent was removed to afford a yellow oil. Compound **(6)** was isolated by chromatography (alumina, 1:1 hexane:dichloromethane). Yield: 1.88 g, 65%. ^{1}H NMR (C_6D_6): δ 7.75 (d, 1H, $^3J_{HH}$=7, H6), 7.45 (d, 1H, $^3J_{HH}$=7, H3), 7.29 (t, 1H, $^3J_{HH}$=7, H4 or H5), 7.21 (t, 1H, $^3J_{HH}$=7, H4 or H5), 3.62 (s, 2H, H7), 2.67 (t, 2H, $^3J_{HH}$=7, H9), 2.53 (t, 2H, $^3J_{HH}$=7, H10), 2.22 (s,

6H, H11, H12), 2.19 (s, 3H, H8), 1.77 (quintet, 6H, $^3J_{HH}$=8, H14), 1.55 (sextet, 6H, $^3J_{HH}$=8, H15), 1.29, (t, 6H, $^3J_{HH}$=8, H13), 1.05 (t, 9H, $^3J_{HH}$=8, H16). ^{13}C NMR (C_6D_6): δ 146.3 (1C, C1), 142.2 (1C, C2), 137.5, 129.6, 128.5, 126.9 (1C, C_{aryl}), 66.3 (1C, C7), 57.7, 56.4 (1C, C9, C10), 45.9 (2C, C11, C12), 41.9 (1C, C8), 29.7 (3C, C14), 28.0 (3C, C15), 13.6 (3C, C16), 10.9 (3C, C13); ESI-MS (CH_3CN) *m/z*(%) $[M\text{-}Sn(Bu)_3]^+$ 191.1 (100), $[MH]^+$ 483.3 (25); (calcd 483.3); ESI-MS (CH_3CN); calculated for $C_{24}H_{47}N_2Sn$: $[MH]^+$ *m/z* 483.2761, found: 483.2749.



6.1.7 DiamI, (7)

Iodine (3.2 g; 12.6 mmol), was added to **(6)** (5.45 g; 11.3 mmol) in dichloromethane (50 mL). The solution was stirred for 5 d at RT. It was then washed with aqueous sodium thiosulphate and dried over $MgSO_4$. After removal of the solvent the crude product was washed with hexane to produce an orange oil. Yield: 1.98 g, 55%. ^{1}H NMR ($CDCl_3$): δ 7.82 (d, 1H, $^3J_{HH}$=7, H6), 7.46 (d, 1H, $^3J_{HH}$=7, H3), 7.35 (t, 1H, $^3J_{HH}$=7, H4 or H5), 6.97 (t, 1H, $^3J_{HH}$=7, H4 or H5), 3.62 (s, 2H, H7), 3.27 (t, 2H, $^3J_{HH}$=7, H9), 2.91 (t, 2H, $^3J_{HH}$=7, H10), 2.84 (s, 6H, H11, H12), 2.34 (s, 3H, H8). ^{13}C NMR ($CDCl_3$): δ 139.3 (1C, C2), 139.2, 130.9, 129.0, 128.1 (1C, C_{aryl}), 100.5 (1C, C1), 65.9 (1C, C7), 54.3, 50.8 (1C, C9, C10), 43.4 (2C, C11, C12), 41.6 (1C, C8). ESI-MS (CH_3CN) *m/z*(%) $[MH]^+$ 319.0 (100); (calcd 319.2); ESI-MS (CH_3CN); calculated for $C_{12}H_{20}N_2I$: $[MH]^+$ *m/z* 319.0671, found: 319.0681.



Attempted Synthesis of Ethynyl substituted Diam, (8)

(i): Catalytic amounts of CuI (0.010 g), $Pd(OAc)_2$ (0.011 g) and PPh_3 (0.030 g) in diisopropylamine (50 mL) were stirred at 0°C for 10 min. Phenylacetylene (0.05 mL; 0.47 mmol) and **(1)** (0.127 g; 0.47 mmol) were added and the stirring continued for 1 h. The mixture was allowed to rise to RT and then refluxed for 2 h. After filtration and evaporation, the residue was washed with dilute HCl, sodium bicarbonate solution, water and then subjected to column chromatography (alumina, 4:1 hexane:dichloromethane). NMR analysis revealed only unreacted starting materials.

(ii): $Pd(PPh_3)_2Cl_2$ (0.010 g) and CuI (0.002 g) were added to **(1)** (0.380 g; 1.40 mmol) and phenylacetylene (0.19 mL; 1.68 mmol) in diethylamine (10 mL). The mixture was stirred for 3 h at RT and the solvent evaporated under reduced pressure. After the addition of water the mixture was extracted with diethyl ether and purified by column chromatography (SiO_2, Et_2O). NMR analysis revealed only unreacted starting materials.

(iii): $Pd(PPh_3)_2Cl_2$ (0.026 g) and CuI (0.009 g) were added to **(1)** (1 g; 3.69 mmol) and 2-methyl-3-butyn-2-ol (0.43 mL; 4.42 mmol) in diethylamine (10 mL). The mixture was stirred for 12 h at RT and the solvent evaporated under reduced pressure. After purification by chromatography (SiO_2, Et_2O), NMR analysis revealed only starting material.

(iv): A solution of **(2)** (15 mL of an 0.23 M solution in 1:1 Et_2O:C_6H_6; 3.39 mmol) was added dropwise to phenylacetylene (0.75 mL; 6.77 mmol) in Et_2O (5 mL) at 0°C. After stirring for 2 h the solution was reduced to a black oil. NMR analysis of the crude reaction mixture revealed only phenylacetylene and DiamH.

(v): Phenylacetylene (1 mL; 9.1 mmol) was dissolved in 10 mL of THF and cooled to -78°C. To this solution was added *n*-BuLi (5.7 mL of a 1.6 M solution in hexane; 9.1 mmol). The mixture was allowed to stir for 20 min at 0°C, after which **(1)** (10 mL of a 0.91 M solution in THF; 9.1 mmol) was used to quench the solution. A brown suspension formed as the solution was stirred. After removal of the solvent, NMR analysis of the crude reaction mixture revealed only starting materials.

(vi): Stille Coupling. Compound **(5)** (0.25 mL; 0.69 mmol) was added dropwise to **(7)** (0.220; 0.69 mmol) and $Pd(PPh_3)_4$ (0.020 g) in THF (15 mL). The mixture was stirred at 70°C for 24 h, cooled and the solvent removed *in vacuo*. NMR and ESI-mass spectral analysis indicated the presence of triphenylphosphine, unreacted **(7)** (*m/z*=318), and **(9)** (*m/z*=424.6).

6.2 NITROGEN-HETEROSUPERBENZENES

6.2.1 Hexaphenylbenzene, (10)

(Reaction carried out in air)

Benzophenone (4 g), tetraphenylcyclopentadienone (0.4 g; 1.05 mmol) and diphenylacetylene (0.42 g; 2.3 mmol) were mixed in a round bottom flask attached to an air condenser. The reaction mixture was heated over a microburner to reflux for 1 h. Carbon monoxide was evolved and the colour changed from purple to red/brown. After cooling the solution to RT, it was washed with methanol to remove any unreacted starting material and the benzophenone. The resulting crystals were washed with toluene. Yield 0.42 g, 75%. ^{1}H NMR ($CDCl_3/CS_2$): δ 6.84-6.78 (m, 30H, H_{aryl}). ^{13}C NMR ($CDCl_3/CS_2$): δ 140.0 (6C, $C_{quat/aryl}$), 139.9 (6C, $C_{quat/aryl}$), 130.9 (12C, C_{aryl}), 126.2 (12C, C_{aryl}), 124.8 (6C, C_{aryl}).



6.2.2 Hexabenzocoronene, (11)

10 equivalents of $AlCl_3$ (500 mg; 3.74 mmol) and $CuCl_2$ (503 mg; 3.74 mmol) were added to **(10)** (200 mg; 0.37 mmol) and dissolved in CS_2 (50 mL). The reaction was stirred at RT for 5 d, then reduced *in vacuo* and purified by fractional sublimation in high vacuum. Pale yellow crystals of **(11)** were collected. Yield: 75 mg, 40%. IR (KBr disk, cm^{-1}): 3083, 3044, 3012, 1602, 1584, 1491, 1410, 1376, 1227; UV-vis (1,2,4-trichlorobenzene): λ_{max} (nm) 342.5, 358.5, 388.5.



6.2.3 Dipyrimidinyl acetylene, (12)

(a): Synthesis of 2-methyl-4-pyrimidin-5-yl-but-3-yn-2-ol.

Bis(triphenylphosphine)palladium(II) dichloride (0.044 g), CuI (0.007 g), 5-bromopyrimidine (1 g; 6.29 mmol) and 2-methyl-3-butyn-2-ol (0.73 mL; 7.53 mmol) were stirred in 15 mL diethylamine at RT for 3 hours. The solvent was evaporated under reduced pressure and the solid extracted into dichloromethane. After washing with water the organic layer was dried over $MgSO_4$. Chromatography (SiO_2, Et_2O), and recrystallisation (ethyl acetate/petroleum ether) gave 0.895 g of 2-methyl-4-pyrimidin-5-yl-but-3-yn-2-ol (88% yield).

(b): Synthesis of 5-ethynylpyrimidine (reaction carried out in air).

A toluene solution (70 mL) of the same was heated under reflux with 0.178 g of NaOH for 2 h. The reaction mixture was filtered and washed with water. The organic layer was dried over $MgSO_4$, and reduced *in vacuo*. The white solid was chromatographed (SiO_2, 1:9 methanol:dichloromethane) to yield 0.315 g of 5-ethynylpyrimidine (55% yield).

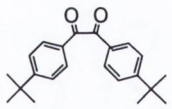
(c): Synthesis of dipyrimidinyl acetylene.

A triethyl amine solution (50 mL) of the same was added to a mixture of 5-bromopyrimidine (0.458 g; 2.88 mmol), $Pd(PPh_3)_2Cl_2$ (0.224 g) and CuI (0.034 g) in DMF (100 mL) and stirred at 55°C for 1 h, then at 25°C for 24 h. The reaction mixture was reduced *in vacuo*, washed with water and extracted with dichloromethane. The organic layer was chromatographed (SiO_2, Et_2O) and recrystallised (ethyl acetate/petroleum ether) to obtain 0.388 g of dipyrimidinyl acetylene (74% yield). m.p: 172-174°C; ^1H NMR ($CDCl_3$): δ 9.19 (s 1H, H_{aryl}), 8.89 (s, 2H, H_{aryl}). ^{13}C NMR ($CDCl_3$): δ 158.3 (2C, C_{aryl}), 157.1 (1C, C_{aryl}), 118.3 (1C, $C_{quat/aryl}$), 88.6 (1C, -C≡C-); ESI-MS (CH_3CN) *m/z*(%) $[MH]^+$ 183.5 (100); (calcd 183.2); Anal. Calcd for $C_{10}H_6N_4$: C, 65.92; H, 3.32; N, 30.76. Found: C, 65.39; H, 3.42; N, 30.64; IR ($CHCl_3$, cm^{-1}): ν(C≡C st): 2260, ν(C=N st): 1546.



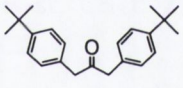
6.2.4 1,2-bis-(4-*tert*-butylphenyl)ethane-1,2-dione, (13)

To a solution of 1-bromo-4-*tert*-butyl-benzene (1.3 mL; 7.50 mmol) in THF (15mL) was added dropwise *n*-BuLi (5.9 mL of a 1.6 M solution in hexane; 9.44 mmol) in THF (30 mL). The solution was stirred for 0.5 h at -78°C, then added to a flask containing 1,4-dimethylpiperazine-2,3-dione (0.66 g; 4.65 mmol) in THF (20 mL) at -78°C. The reaction mixture was stirred and allowed to raise to RT over 1.5 h, and stirred for a further 1 h. The product solution was hydrolysed with 60 mL of 5% HCl and extracted with dichloromethane. The organic washings were combined, dried over $MgSO_4$, and reduced to a yellow oil. Chromatography (SiO_2, 4:5 hexane:dichloromethane) and recrystallisation from hexane yielded white crystals of **(13)**. Yield: 1.054 g, 87%. m.p: 100.5-103.5°C; ^1H NMR ($CDCl_3$): δ 7.93 (d, 4H, $^3J_{HH}$=8.5, H_{aryl}), 7.54 (d, 4H, $^3J_{HH}$=8.5, H_{aryl}), 1.36 (s, 18H, $-C(CH_3)_3$). ^{13}C NMR ($CDCl_3$): δ 194.0 (2C, C=O), 158.4 (2C, $C_{quat/aryl}$), 130.2 (2C, $C_{quat/aryl}$), 129.4 (4C, C_{aryl}), 125.5 (4C, C_{aryl}), 34.9 (2C, $C_{quat/alkyl}$), 30.5 (6C, $-CH_3$); ESI-MS (CH_3CN) *m/z*(%) $[MH]^+$ 323.6 (100); (calcd 323.4).



6.2.5 1,3-bis-(4-*tert*-butylphenyl)propan-2-one, (14)

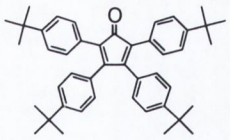
$Ca(OH)_2$ (1.3 g; 17.6 mmol) and $(Bu)_4NHSO_4$ (0.75 g; 2.2 mmol) were dissolved in 1:1 dichloromethane:water (90 mL) and stirred at 1000 rpm. 4-*tert*-butylbenzyl bromide (2 g; 8.8 mmol) was added followed by $Fe(CO)_5$ (0,58 mL; 4.4 mmol) and the reaction was stirred at RT for 5 h with a constant stream of argon circulated over the reaction. The reaction mixture was oxidised in air and acidified with 10% HCl solution (30 mL). The aqueous phase was extracted with dichloromethane and the organic washings combined and reduced to a yellow oil. Chromatography (SiO_2, 1:1 hexane:dichloromethane) and recrystallisation from hexane yielded white crystals of **(14)**. Yield: 0.921 g, 65%. m.p: 84-85°C; ^1H NMR ($CDCl_3$): δ 7.36 (dt, 4H, J_{HH}=2-8, H_{aryl}), 7.12 (dt, 4H, J_{HH}=2-8, H_{aryl}), 3.72 (s, 4H, Aryl-CH_2-), 1.35 (s, 18H, -$C(CH_3)_3$). ^{13}C NMR ($CDCl_3$): δ 205.7 (1C, C=O), 149.4 (2C, $C_{quat/aryl}$), 130.6 (2C, $C_{quat/aryl}$), 128.6 (4C, C_{aryl}), 125.1 (4C, C_{aryl}), 48.1 (2C, Aryl-CH_2-), 34.0 (2C, $C_{quat/alkyl}$), 30.9 (6C, -CH_3); ESI-MS (CH_3CN) *m/z*(%) $[MH]^+$ 323.7 (100); (calcd 323.5); Anal. Calcd for $C_{23}H_{30}O_1$: C, 85.66; H, 9.38. Found: C, 85.36; H, 9.41.



6.2.6 2,3,4,5-tetra-(4-*tert*-butylphenyl)cyclopenta-2,4-dienone, (15)

(Reaction carried out in air)

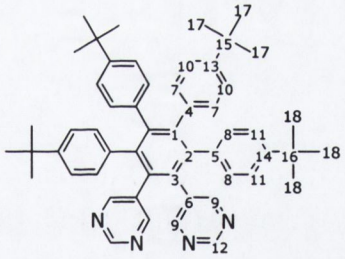
Compound **(13)** (400 mg; 1.24 mmol), **(14)** (400 mg; 1.24 mmol) and KOH (125 mg) were refluxed in ethanol (100 mL) for 3 h. The red/brown solution was reduced and chromatographed (SiO_2, 1:1 hexane:dichloromethane) to produce **(15)** as a deep red crystalline product. Yield: 0.491 g, 65%. m.p: 237-239°C; ^1H NMR ($CDCl_3$): δ 7.28 (m, 8H, H_{aryl}), 7.19 (d, 4H, $^3J_{HH}$=9, H_{aryl}), 6.88 (d, 4H, $^3J_{HH}$=9, H_{aryl}), 1.33 (s, 18H, -CH_3), 1.32 (s, 18H, -CH_3). ^{13}C NMR ($CDCl_3$): δ 200.9 (1C, C=O), 153.8 (2C, $C_{quat/Cp}$), 150.9 (2C, $C_{quat/aryl}$), 149.6 (2C, $C_{quat/aryl}$), 130.1 (2C, $C_{quat/aryl}$), 129.2 (4C, C_{aryl}), 128.6 (4C, C_{aryl}), 127.7 (2C, $C_{quat/aryl}$), 124.4 (4C, C_{aryl}), 124.1 (4C, C_{aryl}), 123.9 (2C, $C_{quat/Cp}$), 34.18 (2C, $C_{quat/alkyl}$), 34.10 (2C, $C_{quat/alkyl}$), 30.78 (6C, -CH_3), 30.81 (6C, -CH_3); ESI-MS (CH_3CN) *m/z*(%) $[MH]^+$ 609.6 (100); (calcd 609.9); Anal. Calcd for $C_{45}H_{52}O$: C, 88.76; H, 8.60. Found: C, 87.77; H, 8.70; IR (KBr disk, cm^{-1}): ν(C-H st, CH aromatic): 3032, ν(C-H st, CH_3): 2961, 2903, 2868, ν(C=O st): 1710, ν(C=C st): 1607, ν(CH_3 δ): 1462, ν(CH_3 δ sy): 1405.



6.2.7 1,2-dipyrimidyl-3,4,5,6-tetra-(4-*tert*-butylphenyl)benzene, (16)

(Reaction carried out in air)

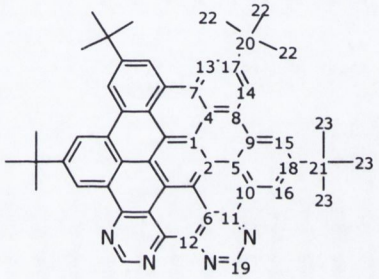
Benzophenone (4.5 g), **(12)** (120 mg; 0.657 mmol) and **(15)** (400 mg; 0.657 mmol) were mixed in a round bottom flask attached to an air condenser. The reaction mixture was heated over a microburner to reflux for 1 h. Carbon monoxide was evolved and the colour changed from purple to red/brown. After cooling, chromatography (SiO_2, Et_2O) and recrystallisation from ethyl acetate/petroleum ether gave colourless crystals. Yield: 0.406 g, 81%. m.p: >300°C; ^{1}H NMR ($CDCl_3$): δ 8.77 (s 2H, H12), 8.26 (s, 4H, H9), 6.93 (d, 4H, $^3J_{HH}$=9, H8 or H11), 6.86 (d, 4H, $^3J_{HH}$=9, H7 or H10), 6.71 (d, 4H, $^3J_{HH}$=9, H8 or H11), 6.69 (d, 4H, $^3J_{HH}$=9, H7 or H10), 1.13, 1.11 (s, 18H, H17, H18). ^{13}C NMR ($CDCl_3$): δ 157.6 (4C, C9), 155.4 (2C, C12), 148.6, 147.9, 142.6, 141.2, 136.0, 135.2, 133.7, 132.2 (2C, $C_{quat/aryl}$), 130.4 (4C, C8 or C11), 130.1 (4C, C7 or C10), 123.7 (4C, C8 or C11), 122.9 (4C, C7 or C10), 33.7, 33.6 (2C, $C_{quat/alkyl}$), 30.70, 30.68 (6C, -CH_3); ESI-MS (CH_3CN) *m/z*(%) $[MH]^+$ 763.5 (100); (calcd 764.1); Anal. Calcd for $C_{54}H_{58}N_4$: C, 84.99; H, 7.66; N, 7.34. Found: C, 84.84; H, 8.01; N, 6.92; IR (KBr disk, cm^{-1}): ν(C-H st, CH aromatic): 3031, ν(C-H st, CH_3): 2960, 2903, 2867, ν(C=N st): 1550, 1511.



6.2.8 Tetra-*peri*-(*tert*-butyl-benzo)-di-*peri*-(pyrimidino)-coronene, (17)

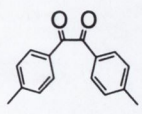
Compound **(16)** (200 mg; 0.262 mmol), $AlCl_3$ (555 mg; 4.16 mmol) and $CuCl_2$ (564 mg; 4.19 mmol) were stirred in CS_2 (60 mL) at 25°C for 72 h. The black solid was allowed to settle and the CS_2 removed by cannula. The solid was dried *in vacuo* and stirred in dilute ammonia solution. The product was extracted into chloroform and dried over $MgSO_4$. Chromatogarphy (SiO_2, 1:9 methanol:toluene) and recrystallisation from toluene/petroleum ether gave a red/orange microcrystalline sloid. Yield: 0.096 g, 49%. m.p: >300°C; ^{1}H NMR ($CDCl_3$): δ 9.79 (s 2H, H19), 9.42 (s, 2H, H16), 9.07 (s, 2H, H15), 9.01 (s, 2H, H13 or H14), 8.94 (s, 2H, H13 or H14), 1.95 (s, 18H, H23), 1.87 (s, 18H, H22). ^{13}C NMR ($CDCl_3$): δ 155.5 (2C, C19), 153.1 (2C, C11), 149.5 (2C, C18),

149.3 (2C, C12), 149.1 (2C, C17), 129.5 (2C, C7 or C8), 128.9 (2C, C9), 128.8 (2C, C7 or C8), 127.4 (2C, $C_{quat/aryl}$), 124.0 (2C, C10), 122.3 (2C, C15), 121.6 (2C, C16), 121.4 (2C, $C_{quat/aryl}$), 119.8 (2C, $C_{quat/aryl}$), 118.7 (2C, C13 or C14), 118.4 (2C, C13 or C14), 117.6 (2C, $C_{quat/aryl}$), 117.3 (2C, C6), 114.1 (2C, $C_{quat/aryl}$), 35.42 (2C, C21), 35.40 (2C, C20), 31.7 (6C, C23), 31.6 (6C, C22); ESI-MS (toluene) *m/z*(%) $[MH]^+$ 751.3 (100); (calcd 752.0); ESI-MS (toluene); calculated for $C_{54}H_{47}N_4$: $[MH]^+$ *m/z* 751.3801, found: 751.3840; IR (KBr disk, cm^{-1}): ν(C-H st, CH aromatic): 3021, ν(C-H st, CH_3): 2970, 2900, 2859, ν(C=N st): 1623, 1556, 1524; UV-vis (toluene): λ_{max} (nm) 284.0, 325.0, 339.5, 355.0, 376.5, 393.0, 413.5, 452.0, 482.0 nm; fluorescence (toluene): λ_{max} (nm) 498.0, 524.0 nm.



6.2.9 1,2-bis-(4-methyl-phenyl)ethane-1,2-dione, (18)

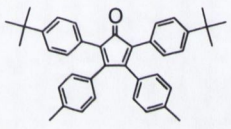
To a solution of 1-bromo-4-methyl-benzene (2 g; 11.69 mmol) in THF (15mL) was added dropwise *n*-BuLi (7.3 mL of a 1.6 M solution in hexane; 11.69 mmol) in THF (30 mL). The solution was stirred for 2 h at -78°C, then added to a flask containing 1,4-dimethyl-piperazine-2,3-dione (0.831 g; 5.85 mmol) in THF (20 mL) at -78°C. The reaction mixture was stirred and allowed to raise to RT over 1.5 h, and stirred for a further 1 h. The product solution was hydrolysed with 60 mL of 5% HCl and extracted with dichloromethane. The organic washings were combined, dried over $MgSO_4$ and reduced to a yellow oil. Chromatography (SiO_2, 2:3 hexane:dichloromethane) and recrystallisation from hexane yielded white crystals of **(18)**. Yield: 0.560 g, 40%. m.p: 101°C; ^1H NMR ($CDCl_3$): δ 7.88 (d, 4H, $^3J_{HH}$=8.5, H_{aryl}), 7.31 (d, 4H, $^3J_{HH}$=8.5, H_{aryl}), 2.45 (s, 6H, $-CH_3$). ^{13}C NMR ($CDCl_3$): δ 194.0 (2C, C=O), 145.6 (2C, $C_{quat/aryl}$), 130.3 (2C, $C_{quat/aryl}$), 129.5 (4C, C_{aryl}), 129.2 (4C, C_{aryl}), 21.4 (2C, $-CH_3$); ESI-MS (CH_3CN) *m/z*(%) $[MNa]^+$ 261.1 (100), $[MH]^+$ 239.1 (5); (calcd 239.3).



6.2.10 2,5-bis-(4-*tert*-butylphenyl)-3,4-bis-(4-methyl-phenyl)cyclopenta-2,4-dienone, (19)

(Reaction carried out in air)

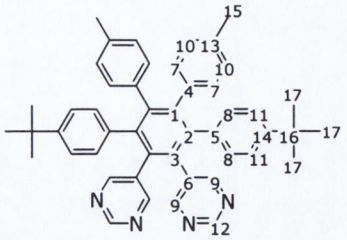
Comound **(18)** (400 mg; 1.68 mmol), **(14)** (541 mg; 1.68 mmol) and KOH (100 mg) were refluxed in ethanol (100 mL) for 4 h. The red/brown solution was reduced and chromatographed (SiO_2, 1:1 hexane:dichloromethane) to produce **(19)** as a deep red crystalline product. Yield: 0.353 g, 40%. m.p: 240-241°C; ^{1}H NMR ($CDCl_3$): δ 7.28 (d, 4H, $^3J_{HH}$=8.5, H_{aryl}), 7.20 (d, 4H, $^3J_{HH}$=8.5, H_{aryl}), 7.01 (d, 4H, $^3J_{HH}$=8, H_{aryl}), 6.86 (d, 4H, $^3J_{HH}$=8, H_{aryl}), 2.35 (s, 6H, -CH_3), 1.32 (s, 18H, -CH_3). ^{13}C NMR ($CDCl_3$): δ 200.7 (1C, C=O), 153.6 (2C, $C_{quat/Cp}$), 149.6 (2C, $C_{quat/aryl}$), 137.7 (2C, $C_{quat/aryl}$), 130.0 (2C, $C_{quat/aryl}$), 129.2 (4C, C_{aryl}), 128.9 (4C, C_{aryl}), 128.1 (4C, C_{aryl}), 127.6 (2C, $C_{quat/aryl}$), 124.4 (4C, C_{aryl}), 124.2 (2C, $C_{quat/Cp}$), 34.1 (2C, $C_{quat/alkyl}$), 30.8 (6C, -CH_3), 21.0 (2C, -CH_3); ESI-MS (CH_3CN) *m/z*(%) $[MH]^+$ 525.3 (100); (calcd 525.7); Anal. Calcd for $C_{39}H_{40}O$: C, 89.27; H, 7.68. Found: C, 88.76; H, 7.73; IR (KBr disk, cm^{-1}): ν(C-H st, CH aromatic): 3033, ν(C-H st, CH_3): 2961, 2902, 2867, ν(C=O st): 1710, ν(C=C st): 1609, 1504 ν(CH_3 δ): 1461.



6.2.11 1,2-dipyrimidyl-3,6-bis-(4-*tert*-butylphenyl)-4,5-bis-(4-methyl-phenyl)benzene, (20)

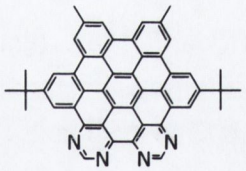
(Reaction carried out in air)

Benzophenone (2 g), **(12)** (115 mg; 0.631 mmol) and **(19)** (328 mg; 0.625 mmol) were mixed in a round bottom flask attached to an air condenser. The reaction mixture was heated over a microburner to reflux for 1 h. Carbon monoxide was evolved and the colour changed from purple to red/brown. After cooling and chromatography (SiO_2, Et_2O), recrystallisation from ethyl acetate/petroleum ether gave colourless crystals of **(20)**. Yield: 0.305 g, 72%. m.p: 293-295°C; ^{1}H NMR ($CDCl_3$): δ 8.66 (s 2H, H12), 8.14 (s, 4H, H9), 6.87 (d, 4H, $^3J_{HH}$=8.5, H_{aryl}), 6.62 (m, 12H, H_{aryl}), 2.02 (s, 6H, H15), 1.06 (s, 18H, H17). ^{13}C NMR ($CDCl_3$): δ 157.4 (4C, C9), 155.3 (2C, C12), 148.5, 142.2, 141.1, 136.0, 135.3, 134.3, 133.6, 132.5 (2C, $C_{quat/aryl}$), 130.3, 130.2, 126.9, 123.6 (4C, C_{aryl}), 33.6 (2C, C16), 30.5 (6C, C17), 20.3 (2C, C15); ESI-MS (CH_3CN) *m/z*(%) $[MH]^+$ 679.4 (100); (calcd 679.9); ESI-MS (CH_3CN); calculated for $C_{48}H_{47}N_4$: $[MH]^+$ *m/z* 679.3801, found: 679.3803; Anal. Calcd for $C_{48}H_{46}N_4$: C, 84.92; H, 6.83; N, 8.25. Found: C, 84.78; H, 7.29; N, 7.70; IR (KBr disk, cm^{-1}): ν(C-H st, CH aromatic): 3046, 3028, ν(C-H st, CH_3): 2961, 2925, 2865, ν(C=N st): 1548, 1513, ν(CH_3 δ sy): 1389.



6.2.12 Di-*peri*-(*tert*-butyl-benzo)-di-*peri*-(methyl-benzo)-di-*peri*-(pyrimidino)-coronene, (21)

Compound **(20)** (125 mg; 0.184 mmol), $AlCl_3$ (390 mg; 2.92 mmol) and $CuCl_2$ (393 mg; 2.92 mmol) were stirred in CS_2 (45 mL) at 25°C for 72 h. The black solid was allowed to settle and the CS_2 removed by cannula. The solid was dried *in vacuo* and stirred in dilute ammonia solution. The product was extracted into chloroform and dried over $MgSO_4$. The red/orange solution was passed through an alumina plug column using 1:19 methanol:chloroform to elute the product. The solid was washed with 10% HCl solution, water, 10% NH_4OH solution, water, and diethyl ether and dried *in vacuo* to afford **(21)** as a red/brown powder. Yield: 0.035 g, 30%. m.p: >300°C; ESI-MS (toluene) *m/z*(%) $[MH]^+$ 667.0 (100); (calcd 667.8); ESI-MS (toluene); calculated for $C_{48}H_{35}N_4$: $[MH]^+$ *m/z* 667.2862, found: 667.2915; IR (KBr disk, cm^{-1}): ν(C-H st, CH_3): 2959, 2924, 2852, ν(C=N st): 1655, 1610, 1560; UV-vis ($CHCl_3$): λ_{max} (nm) 291.0, 342.0, 355.5, 377.0, 394.5, 418.0, 459.0, 491.0 nm; fluorescence (toluene): λ_{max} (nm) 500.0, 524.0 nm.

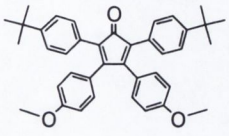


6.2.13 2,5-bis-(4-*tert*-butylphenyl)-3,4-bis-(4-methoxyphenyl)cyclopenta-2,4-dienone, (22)

(Reaction carried out in air)

4,4′-Dimethoxybenzil (536 mg; 1.98 mmol), **(14)** (639 mg; 1.98 mmol) and KOH (110 mg) were refluxed in ethanol (100 mL) for 14 h. The red/brown solution was reduced and chromatographed (SiO_2, 1:1 hexane:dichloromethane) to produce **(22)** as a deep red crystalline product. Yield: 0.305 g, 28%. m.p: 210-212°C; ^1H NMR ($CDCl_3$): δ 7.28 (d, 4H, $^3J_{HH}$=8.5, H_{aryl}), 7.20 (d, 4H, $^3J_{HH}$=8.5, H_{aryl}), 6.91 (d, 4H, $^3J_{HH}$=9, H_{aryl}), 6.75 (d, 4H, $^3J_{HH}$=8.5, H_{aryl}), 3.82 (s, 6H, $-CH_3$), 1.32 (s, 18H, $-CH_3$). ^{13}C NMR ($CDCl_3$): δ 200.6 (1C, C=O), 159.2 (2C, $C_{quat/aryl}$), 153.1 (2C, $C_{quat/aryl}$), 149.6 (2C, $C_{quat/aryl}$),

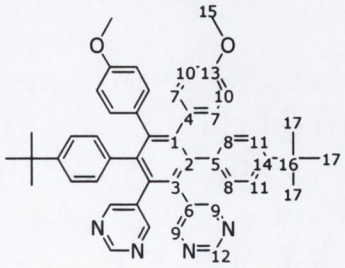
130.7 (4C, C_{aryl}), 129.2 (4C, C_{aryl}), 127.7 (2C, $C_{quat/aryl}$), 125.2 (2C, $C_{quat/aryl}$), 124.5 (4C, C_{aryl}), 123.9 (2C, $C_{quat/aryl}$), 112.9 (4C, C_{aryl}), 54.7 (2C, -CH_3), 34.1 (2C, $C_{quat/alkyl}$), 30.8 (6C, -CH_3); ESI-MS (CH_3CN) *m/z*(%) $[MH]^+$ 557.6 (100); (calcd 557.5); Anal. Calcd for $C_{39}H_{40}O_3$: C, 84.13; H, 7.24. Found: C, 83.56; H, 7.56; IR (KBr disk, cm^{-1}): ν(C-H st, CH aromatic): 3036, ν(C-H st, CH_3): 2961, 2903, 2865, ν(C-H st, 0-CH_3): 2837, ν(C=O st): 1706, ν(C=C st): 1604, ν(CH_3 δ): 1462, ν(CH_3 δ sy): 1405, ν(C-0 st, 0-CH_3): 1250.



6.2.14 1,2-dipyrimidyl-3,6-bis-(4-*tert*-butylphenyl)-4,5-bis-(4-methoxyphenyl)benzene, (23)

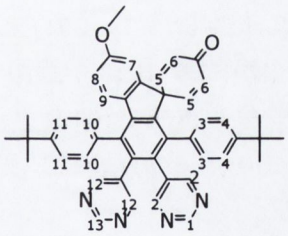
(Reaction carried out in air)

Benzophenone (3 g), **(12)** (106 mg; 0.582 mmol) and **(22)** (324 mg; 0.582 mmol) were mixed in a round bottom flask attached to an air condenser. The reaction mixture was heated over a microburner to reflux for 1 h. Carbon monoxide was evolved and the colour changed from purple to red/brown. After cooling, chromatography (SiO_2, Et_2O) and recrystallisation from acetone/water gave colourless crystals. Yield: 0.320 g, 77%. m.p: 277-278°C; ^1H NMR ($CDCl_3$): δ 8.75 (s 2H, H12), 8.21 (s, 4H, H9), 6.96 (d, 4H, $^3J_{HH}$=8.0, H8 or H11), 6.709 (d, 4H, $^3J_{HH}$=8.5, H7 or H10), 6.705 (d, 4H, $^3J_{HH}$=8.0, H8 or H11), 6.45 (d, 4H, $^3J_{HH}$=8.5, H7 or H10), 3.63 (s, 6H, H15), 1.15 (s, 18H, H17). ^{13}C NMR ($CDCl_3$): δ 157.5 (4C, C9), 156.8 (2C, C13), 155.4 (2C, C12), 148.7 (2C, C14), 142.0, 141.3, 135.3, 133.7, 132.5 (2C, $C_{quat/aryl}$), 131.6 (4C, C_{aryl}), 131.5 (2C, $C_{quat/aryl}$), 130.3, 123.9, 111.9 (4C, C_{aryl}), 54.5 (2C, C15), 33.8 (2C, C16), 30.6 (6C, C17); ESI-MS (CH_3CN) *m/z*(%) $[MH]^+$ 711.5 (100); (calcd 711.9); Anal. Calcd for $C_{48}H_{46}N_4O_2$: C, 81.09; H, 6.52; N, 7.88. Found: C, 81.40; H, 6.58; N, 7.64; IR (KBr disk, cm^{-1}): ν(C-H st, CH aromatic): 3039, ν(C-H st, CH_3): 2962, 2905, 2868, ν(C-H st, 0-CH_3): 2838, ν(C=C st): 1611, ν(C=N st): 1549, 1514, ν(C-0 st, 0-CH_3): 1248.



6.2.15 Attempted Synthesis of Di-*peri*-(*tert*-butyl-benzo)-di-*peri*-(methoxy-benzo)-di-*peri*-(pyrimidino)-coronene, (24)

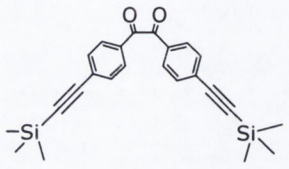
To a stirred solution of **(23)** (100 mg; 0.141 mmol) in dichloromethane (20 mL), a solution of iron(III) chloride (2.252 g; 13.883 mmol) in nitromethane (6 mL) was added dropwise. An argon stream was bubbled through the mixture throughout the course of the reaction. After stirring for another 30 min, the reaction was quenched with methanol (6 mL). The resulting mixture was poured into water and extracted with dichloromethane. The organic washings were combined, dried over $MgSO_4$, and reduced. The extract was purified by column chromatography (SiO_2, Et_2O) and recrystallised from dichloromethane to afford colourless crystals of **(24)**. Yield: 84 mg, 86%. m.p: >300°C; ^{1}H NMR ($CDCl_3$): δ 8.78, 8.73 (s, 1H, H1, H13), 8.31, 8.29 (s, 2H, H2, H12), 7.40 (d, 2H, $^3J_{HH}$=8, H_{aryl}), 7.17 (d, 2H, $^3J_{HH}$=8, H_{aryl}), 7.09 (d, 2H, $^3J_{HH}$=8, H_{aryl}), 6.91 (d, 2H, $^3J_{HH}$=8, H_{aryl}), 6.62 (dd, 1H, J_{HH}=2.5-8.5, H8), 6.57 (d, 1H, $^4J_{HH}$=2.5, H7), 6.51 (d, 2H, $^3J_{HH}$=9.5, H_{aryl}), 6.32 (d, 1H, $^3J_{HH}$=8.5, H9), 6.08 (d, 2H, $^3J_{HH}$=10, H_{aryl}), 3.72 (s, 3H, -CH_3), 1.34 (s, 9H, -CH_3), 1.23 (s, 9H, -CH_3). ^{13}C NMR ($CDCl_3$): δ 184.9 (1C, C=O), 159.9 (1C, $C_{quat/aryl}$), 157.3, 157.2 (2C, C2, C12), 155.9, 155.8 (1C, C1, C13), 153.3, 151.1, 150.9 (1C, $C_{quat/aryl}$), 148.2 (2C, C_{aryl}), 144.6, 141.8, 140.5, 140.3, 135.8, 135.1, 133.7, 132.5, 132.2, 131.8 ($C_{quat/aryl}$), 129.4 (2C), 128.9 (2C), 128.8 (2C), 125.5 (2C), 124.7 (1C), 123.8 (2C), 114.7 (1C), 108.8 (1C) (C_{aryl}), 55.1 (1C, -CH_3), 34.2, 34.0 (1C, $C_{quat/alkyl}$), 30.8, 30.6 (3C, -CH_3); ESI-MS (toluene) *m/z*(%) $[MH]^+$ 695.3 (100); (calcd 695.9); ESI-MS (toluene); calculated for $C_{47}H_{43}N_4O_2$: $[MH]^+$ *m/z* 695.3386, found: 695.3411; IR (KBr disk, cm^{-1}): ν(C-H st, CH aromatic): 3040, ν(C-H st, CH_3): 2960, 2906, 2868, ν(C=O st): 1663, ν(C=C st): 1604, ν(C=N st): 1549, ν(CH_3 δ): 1399, ν(C-0 st, 0-CH_3): 1244.



6.2.16 1,2-bis(4-trimethylsilylethynylphenyl)ethane-1,2-dione, (25)

Bis(triphenylphosphine)palladium(II) dichloride (56 mg) and CuI (15 mg) were added successively to 4,4'-dibromobenzil (1.355 g; 3.68 mmol) in THF (20 mL) and diethylamine (15 mL), the mixture was heated to 80°C. (Trimethylsilyl)acetylene (2.74 mL; 7.36 mmol) in THF (10 mL) and diethylamine (10 mL) were added dropwise and the mixture was stirred for 3 h at 80°C. The reaction mixture was allowed to cool to RT and the diethylamine was evaporated under reduced pressure. The black solid was

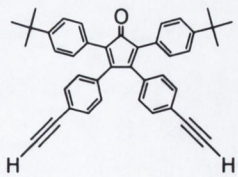
extracted with hexane. Column chromatography (SiO_2, 1:1 hexane:dichloromethane) and recrystallisation from hexane yielded white crystals of **(25)**. Yield: 0.910 g, 62%. m.p: 124-126°C; ^1H NMR ($CDCl_3$): δ 7.92 (d, 4H, $^3J_{HH}$=8.5, H_{aryl}), 7.59 (d, 4H, $^3J_{HH}$=8.5, H_{aryl}), 0.29 (s, 18H, $-CH_3$). ^{13}C NMR ($CDCl_3$): δ 192.6 (2C, C=O), 131.9 (4C, C_{aryl}), 131.7 (2C, $C_{quat/aryl}$), 129.5 (2C, $C_{quat/aryl}$), 129.2 (4C, C_{aryl}), 103.2 (2C, -C≡C-), 99.4 (2C, -C≡C-), -0.7 (6C, $-CH_3$); ESI-MS (CH_3CN) *m/z*(%) $[M_2Na]^+$ 827.3 (100), $[MNa]^+$ 425.2 (75), $[MH]^+$ 403.2 (25); (calcd 403.6); IR (KBr disk, cm^{-1}): ν(C-H st, CH_3): 2960, 2899, ν(C≡C st): 2155, ν(C=O st): 1671, ν(C=C st): 1599.



6.2.17 3,4-bis(4-ethynylphenyl)-2,5-bis(4-*tert*-butylphenyl)-cyclopenta-2,4-dienone, (26)

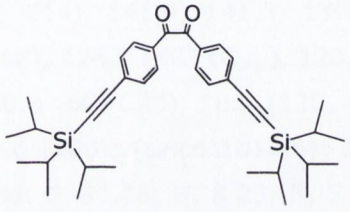
(Reaction carried out in air)

Compound **(25)** (600 mg; 1.49 mmol), **(14)** (481 mg; 1.49 mmol) and KOH (90 mg) were refluxed in ethanol (100 mL) for 4 h. The red/brown solution was reduced and chromatographed (SiO_2, 1:1 hexane:dichloromethane), to produce **(26)** as a deep red crystalline product. Yield: 0.300 g, 30%. m.p: >300°C (decomp. 210°C); ^1H NMR ($CDCl_3$): δ 7.34 (d, 4H, $^3J_{HH}$=8, H_{aryl}), 7.29 (d, 4H, $^3J_{HH}$=8.5, H_{aryl}), 7.16 (d, 4H, $^3J_{HH}$=8, H_{aryl}), 6.93 (d, 4H, $^3J_{HH}$=8, H_{aryl}), 1.60 (s, 2H, -C≡CH), 1.31 (s, 18H, $-CH_3$). ^{13}C NMR ($CDCl_3$): δ 200.0 (1C, C=O), 152.0 (2C, $C_{quat/aryl}$), 150.3 (2C, $C_{quat/aryl}$), 133.3 (2C, $C_{quat/aryl}$), 131.4 (4C, C_{aryl}), 129.2 (4C, C_{aryl}), 128.9 (4C, C_{aryl}), 126.8 (2C, $C_{quat/aryl}$), 125.0 (2C, $C_{quat/aryl}$), 124.7 (4C, C_{aryl}), 121.6 (2C, $C_{quat/aryl}$), 82.9 (2C, -C≡C-), 78.0 (2C, -C≡C-), 34.2 (2C, $C_{quat/alkyl}$), 30.8 (6C, $-CH_3$); IR (KBr disk, cm^{-1}): ν(C≡C-H st): 3254, ν(C-H st, CH aromatic): 3083, 3033, ν(C-H st, CH_3): 2961, 2867, ν(C≡C st): 2109, ν(C=O st): 1708, ν(C=C st): 1603, 1499, ν(CH_3 δ): 1459.



6.2.18 1,2-bis(4-triisopropylsilylethynylphenyl)ethane-1,2-dione, (27)

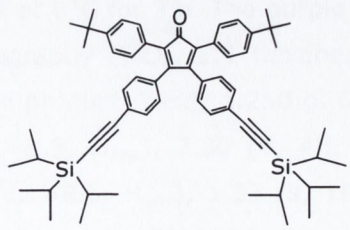
Bis(triphenylphosphine)palladium(II) dichloride (56 mg) and CuI (16 mg) were added successively to 4,4'-dibromobenzil (1.50 g; 4.08 mmol) in toluene (40 mL) and triethyl amine (20 mL). (Triisopropylsilyl)acetylene (2.74 mL; 12.0 mmol) was injected and the mixture was stirred for 4 h at 90°C. After cooling to RT, the solvent was removed *in vacuo* and the black solid was extracted into hexane. Column chromatography (SiO_2, 4:1, hexane:dichloromethane) gave a yellowish oil **(27)**. Yield: 2.030 g, 87%. ^{1}H NMR ($CDCl_3$): δ 7.93 (d, 4H, $^3J_{HH}$=8.5, H_{aryl}), 7.61 (d, 4H, $^3J_{HH}$=8.5, H_{aryl}), 1.16 (s, 36H, -CH_3), 1.15 (s, 6H, CH). ^{13}C NMR ($CDCl_3$): δ 192.8 (2C, C=O), 132.0 (4C, C_{aryl}), 131.5 (2C, $C_{quat/aryl}$), 129.8 (2C, $C_{quat/aryl}$), 129.2 (4C, C_{aryl}), 105.3 (2C, -C≡C-), 96.3 (2C, -C≡C-), 18.2 (12C, -CH_3), 10.8 (6C, CH).



6.2.19 2,5-bis(4-*tert*-butylphenyl)-3,4-bis(4-triisopropylsilylethynylphenyl)cyclopenta-2,4-dienone, (28)

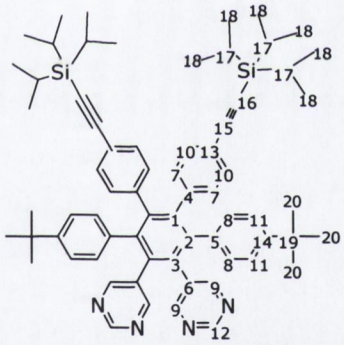
(Reaction carried out in air)

Compound **(27)** (790 mg; 1.38 mmol), **(14)** (446 mg; 1.38 mmol) and KOH (125 mg) were refluxed in ethanol (20 mL) for 2 h. The red/brown solution was allowed to cool to RT, and was kept at 0°C for 3 h. The purple black solid was filtered off as **(28)**. Yield: 0.960 g, 81%. m.p: 281-283°C; ^{1}H NMR ($CDCl_3$): δ 7.33 (d, 4H, $^3J_{HH}$=8.5, H_{aryl}), 7.30 (d, 4H, $^3J_{HH}$=8.5, H_{aryl}), 7.18 (d, 4H, $^3J_{HH}$=8.5, H_{aryl}), 6.93 (d, 4H, $^3J_{HH}$=8, H_{aryl}), 1.33 (s, 18H, -CH_3), 1.17 (s, 42H, CH, -CH_3). ^{13}C NMR ($CDCl_3$): δ 200.0 (1C, C=O), 152.2 (2C, $C_{quat/aryl}$), 150.2 (2C, $C_{quat/aryl}$), 132.8 (2C, $C_{quat/aryl}$), 131.3 (4C, C_{aryl}), 129.3 (4C, C_{aryl}), 128.8 (4C, C_{aryl}), 127.0 (2C, $C_{quat/aryl}$), 125.1 (2C, $C_{quat/aryl}$), 124.7 (4C, C_{aryl}), 123.0 (2C, $C_{quat/aryl}$), 106.4 (2C, -C≡C-), 91.7 (2C, -C≡C-), 34.2 (2C, $C_{quat/alkyl}$), 30.8 (6C, -CH_3), 18.2 (12C, -CH_3), 10.9 (6C, -CH); ESI-MS (CH_3CN) *m/z*(%) $[MH]^+$ 857.3 (100); (calcd 857.5); IR (KBr disk, cm^{-1}): ν(C-H st, CH aromatic): 3082, 3038, ν(C-H st, CH_3): 2954, 2893, 2865, ν(C≡C st): 2152, ν(C=O st): 1711, ν(C=C st): 1602, ν(CH_3 δ): 1462.



6.2.20 1,2-dipyrimidyl-3,6-bis-(4-*tert*-butylphenyl)-4,5-bis-(4-triisopropylsilylethynylphenyl)benzene, (29)

Compound **(12)** (130 mg; 0.714 mmol) and **(28)** (612 mg; 0.714 mmol) were sealed under vacuum in a glass tube and heated at 200°C for 48 h. The reaction mixture was subsequently cooled to RT, the tube broken carefully, the residue extracted into dichloromethane (50 mL) and filtered. After removal of the solvent the recovered material was subjected to flash chromatography (SiO_2, Et_2O). Recrystallisation from acetone/water gave colourless crystals. Yield: 0.470 g, 65%. m.p: >300°C; ^1H NMR ($CDCl_3$): δ 8.76 (s 2H, H12), 8.22 (s, 4H, H9), 7.04 (d, 4H, $^3J_{HH}$=8, H7 or H10), 6.97 (d, 4H, $^3J_{HH}$=8, H8 or H11), 6.77 (d, 4H, $^3J_{HH}$=8, H7 or H10), 6.70 (d, 4H, $^3J_{HH}$=8, H8 or H11), 1.15 (s, 18H, H20), 1.08 (s, 42H, H17, H18). ^{13}C NMR ($CDCl_3$): δ 157.4 (4C, C9), 155.6 (2C, C12), 149.2 (2C, C14), 141.4, 141.3, 139.0, 134.6, 133.3, 133.1 (2C, $C_{quat/aryl}$), 130.3 (8C), 130.2 (4C), 124.1 (4C) (C_{aryl}), 120.5 (2C, C13), 106.6, 89.9 (1C, C15, C16), 33.8 (2C, C19), 30.6 (6C, C20), 18.1 (12C, C18), 10.8 (6C, C17); ESI-MS (CH_3CN) *m/z*(%) $[MH]^+$ 1012.6 (100); (calcd 1012.6); Anal. Calcd for $C_{68}H_{82}N_4Si_2$: C, 80.74; H, 8.17; N, 5.54. Found: C, 80.46; H, 8.23; N, 5.51; IR (KBr disk, cm^{-1}): ν(C-H st, CH aromatic): 3034, ν(C-H st, CH_3): 2945, 2893, 2865, ν(C≡C st): 2153, ν(C=N st): 1549, 1510.

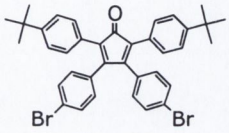


6.2.21 2,5-bis-(4-*tert*-butylphenyl)-3,4-bis-(4-bromo-phenyl)cyclopenta-2,4-dienone, (30)

(Reaction carried out in air)

4,4'-Dibromobenzil (1.211 g; 3.29 mmol), **(14)** (1.056 g; 3.27 mmol) and KOH (177 mg) were refluxed in ethanol (400 mL) for 2 h. The red/brown solution was allowed to cool to RT, and was then kept at 0°C for 3 h. The purple black solid was filtered off and purified by column chromatography (SiO_2, 1:1 hexane:dichloromethane), to produce **(30)** as a deep red crystalline product. Yield: 1.250 g, 60%. m.p: 289-290°C; ^1H NMR ($CDCl_3$): δ 7.37 (d, 4H, $^3J_{HH}$=8.5, H_{aryl}), 7.30 (d, 4H, $^3J_{HH}$=8.5, H_{aryl}), 7.17 (d, 4H, $^3J_{HH}$=8, H_{aryl}), 6.85 (d, 4H, $^3J_{HH}$=8.5, H_{aryl}), 1.33 (s, 18H, $-CH_3$). ^{13}C NMR ($CDCl_3$): δ 199.8 (1C, C=O), 151.5 (2C, $C_{quat/aryl}$), 150.4 (2C, $C_{quat/aryl}$), 131.6 (2C, $C_{quat/aryl}$), 131.0

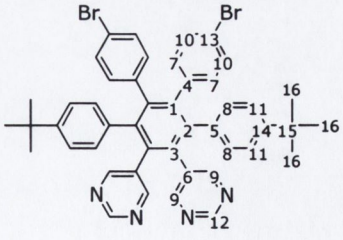
(4C, C_{aryl}), 130.5 (4C, C_{aryl}), 129.2 (4C, C_{aryl}), 126.8 (2C, $C_{quat/aryl}$), 125.1 (2C, $C_{quat/aryl}$), 124.7 (4C, C_{aryl}), 122.4 (2C, $C_{quat/aryl}$), 34.2 (2C, $C_{quat/alkyl}$), 30.8 (6C, $-CH_3$); ESI-MS (CH_3CN) *m/z*(%) $[MH]^+$ 655.3 (100); (calcd 655.5); Anal. Calcd for $C_{37}H_{34}OBr_2$: C, 67.90; H, 5.24. Found: C, 67.83; H, 5.44; IR (KBr disk, cm^{-1}): ν(C-H st, CH aromatic): 3035, ν(C-H st, CH_3): 2961, 2902, 2866, ν(C=O st): 1713, ν(C=C st): 1586, ν(CH_3 δ): 1484, ν(CH_3 δ sy): 1392.



6.2.22 1,2-dipyrimidyl-3,6-bis-(4-*tert*-butylphenyl)-4,5-bis-(4-bromo-phenyl)benzene, (31)

(Reaction carried out in air)

Benzophenone (5 g), **(12)** (223 mg; 1.22 mmol) and **(30)** (800 mg; 1.22 mmol) were mixed in a round bottom flask attached to an air condenser. The reaction mixture was heated over a microburner to reflux for 1 h. Carbon monoxide was evolved and the colour changed from purple to red/brown. After cooling and chromatography (SiO_2, Et_2O), recrystallisation from ethyl acetate/petroleum ether gave colourless crystals. Yield: 0.840 g, 85%. m.p: >300°C; ^1H NMR ($CDCl_3$): δ 8.77 (s 2H, H12), 8.21 (s, 4H, H9), 7.06 (d, 4H, $^3J_{HH}$=8, H7 or H10), 6.98 (d, 4H, $^3J_{HH}$=8, H8 or H11), 6.69 (d, 4H, $^3J_{HH}$=8, H8 or H11), 6.68 (d, 4H, $^3J_{HH}$=8, H7 or H10), 1.15 (s, 18H, H16). ^{13}C NMR ($CDCl_3$): δ 157.4 (4C, C9), 155.6 (2C, C12), 149.3 (2C, C14), 141.2, 140.7, 137.7, 134.4, 133.3, 133.2 (2C, $C_{quat/aryl}$), 132.0, 130.1, 129.8, 124.1 (4C, C_{aryl}), 119.9 (2C, C13), 33.9 (2C, C15), 30.6 (6C, C16); ESI-MS (CH_3CN) *m/z*(%) $[MH]^+$ 809.2 (100); (calcd 809.6); Anal. Calcd for $C_{46}H_{40}N_4Br_2$: C, 68.32; H, 4.99; N, 6.93. Found: C, 67.77; H, 5.03; N, 6.74; IR (KBr disk, cm^{-1}): ν(C-H st, CH aromatic): 3034, ν(C-H st, CH_3): 2959, 2902, 2867, ν(C=N st): 1549, 1490, ν(CH_3 δ sy): 1400.



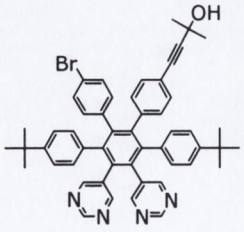
6.2.23 1,2-dipyrimidyl-3,6-bis-(4-*tert*-butylphenyl)-4,5-bis-(4-(3-methyl-3-hydroxy-butynyl)phenyl)benzene, (32)

Bis(triphenylphosphine)palladium(II) dichloride (42 mg) and CuI (12 mg) were added successively to **(31)** (200 mg; 0.247 mmol) in DMF (10 mL) and triethyl amine (5 mL).

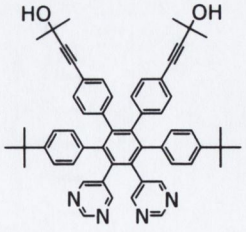
2-Methyl-3-butyn-2-ol (0.10 mL; 1.03 mmol) was injected and the mixture was stirred for 24 h at 90°C. The reaction mixture was washed with water (20 mL) and extracted with chloroform (3 x 40 mL). The organic fractions were combined, dried over $MgSO_4$, and reduced *in vacuo*. Column chromatography (SiO_2, Et_2O) was used to separate the products. Unreacted starting material **(31)** (rf=0.5), monosubstituted **(32a)** (rf=0.4), and disubstituted **(32b)** (rf=0.3) were collected. Recrystallisation from acetone and water yielded colourless crystals. Yield: 0.075 mg, 38% of **(32a)**, and 0.064 g, 30% of **(32b)**.

(32a): m.p: 253-255°C; ^{1}H NMR ($CDCl_3$): δ 8.77, 8.76 (s, 1H, H_{aryl}), 8.21, 8.20 (s, 2H, H_{aryl}), 7.05 (d, 2H, $^3J_{HH}$=8.5, H_{aryl}), 6.99 (m, 6H, H_{aryl}), 6.78 (d, 2H, $^3J_{HH}$=8.5, H_{aryl}), 6.70 (m, 6H, H_{aryl}), 1.74 (s, 1H, -OH), 1.57 (s, 6H, $-CH_3$), 1.15 (s, 18H, $-CH_3$). ^{13}C NMR ($CDCl_3$): δ 157.4, 157.3 (2C, C_{aryl}), 155.6, 155.5 (1C, C_{aryl}), 149.34 (1C), 149.27 (1C), 141.24 (1C), 141.20 (1C), 140.8 (1C), 138.9 (1C), 137.8 (1C), 134.50 (2C), 134.47 (1C), 133.4 (1C), 133.3 (1C) ($C_{quat/aryl}$), 132.0 (2C), 130.3 (2C), 130.1 (4C), 130.0 (2C), 129.7 (2C) (C_{aryl}), 129.60, 129.57 (1C, $C_{quat/aryl}$), 124.11, 124.08 (2C, C_{aryl}), 119.88, 119.79 (1C, $C_{quat/aryl}$), 93.4, 81.5 (1C, -C≡C-), 65.1 (1C), 33.8 (2C) ($C_{quat/alkyl}$), 31.0 (2C, $-CH_3$), 30.6 (6C, $-CH_3$); ESI-MS (CH_3CN) *m/z*(%) $[MH]^+$ 812.6 (100); (calcd 812.8); ESI-MS (CH_3CN); calculated for $C_{51}H_{48}BrN_4O_2$: $[MH]^+$ *m/z* 811.3011, found: 811.3002.

(32b): m.p: 264-266°C; ^{1}H NMR ($CDCl_3$): δ 8.76 (s, 2H, H_{aryl}), 8.20 (s, 4H, H_{aryl}), 6.98 (dd, 8H, J_{HH}=2-8, H_{aryl}), 6.77 (d, 4H, $^3J_{HH}$=8, H_{aryl}), 6.71 (d, 4H, $^3J_{HH}$=8.5, H_{aryl}), 1.97 (s, 2H, -OH), 1.58 (s, 12H, $-CH_3$), 1.16 (s, 18H, $-CH_3$). ^{13}C NMR ($CDCl_3$): δ 157.4 (4C, C_{aryl}), 155.5 (2C, C_{aryl}), 149.2, 141.3, 141.1, 140.0, 134.5, 133.4, 133.3 (2C, $C_{quat/aryl}$), 130.4, 130.2, 130.0, 124.1 (4C, C_{aryl}), 119.7 (2C, $C_{quat/aryl}$), 93.2, 81.6 (2C, -C≡C-), 65.4, 33.8 (2C, $C_{quat/alkyl}$), 30.0 (4C, $-CH_3$), 30.6 (6C, $-CH_3$); ESI-MS (CH_3CN) *m/z*(%) $[MH]^+$ 815.4 (100); (calcd 816.1); ESI-MS (CH_3CN); calculated for $C_{56}H_{55}N_4O_2$: $[MH]^+$ *m/z* 815.4323, found: 815.4334.



(32a)



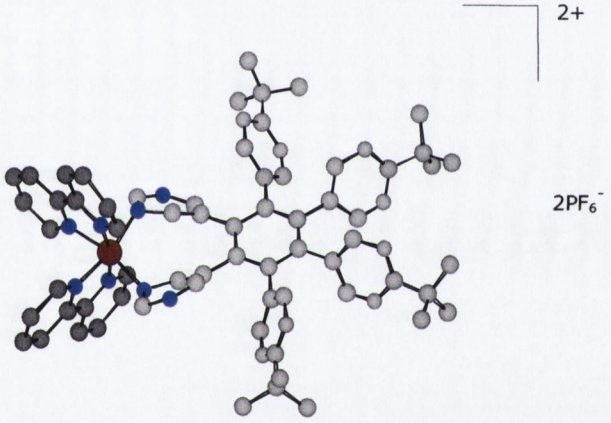
(32b)

6.3 TRANSITION METAL COMPLEXES OF N-HETEROSUPERBENZENES

$[Ru(bpy)_2Cl_2].2H_2O$[2] and $[Ru(bpy)_3](PF_6)_2$[3] were made according to literature procedures.

6.3.1 $[Ru(bpy)_2(16)](PF_6)_2$, (34)

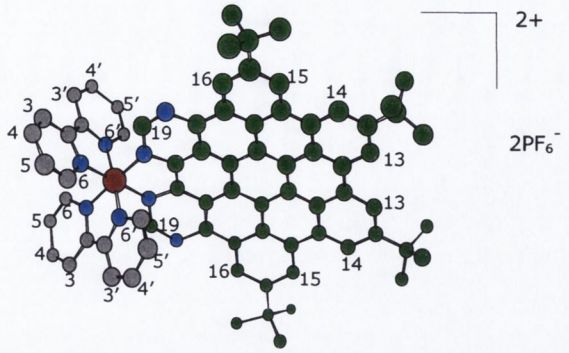
A mixture of $[Ru(bpy)_2Cl_2].2H_2O$ (15.0 mg; $2.88x10^{-2}$ mmol) and $AgBF_4$ (13.0 mg; 6.54 $x10^{-2}$ mmol) was refluxed in acetone (20 mL) for 1.5 h. The silver chloride formed was filtered off and washed with acetone. n-BuOH (20 mL) was added and the acetone evaporated. Compound **(16)** (20 mg; 2.62 $x10^{-2}$ mmol) was dissolved in dichloromethane, n-BuOH (10 mL) was added and the dichloromethane evaporated. This solution was added to the reaction mixture, and refluxed for 72 h under an argon atmosphere. After cooling to RT and filtration through a G4 Frit, the solvent was removed *in vacuo*. The minimum amount of acetonitrile was added to dissolve the solid and a saturated NH_4PF_6 aqueous solution was added to the mixture to form a red-brown solid, which was filtered off and washed with water and diethyl ether. Yield: 0.019 mg, 55%. ESI-MS (CH_3CN) *m/z*(%) $[M-2PF_6]^{2+}$ 588.2 (100); (calcd 588.2); ESI-MS (CH_3CN); calculated for $C_{74}H_{74}N_8Ru$: $[M-2PF_6]^{2+}$ *m/z* 588.2540, found: 588.2537.



6.3.2 $[Ru(bpy)_2(N\text{-}HBC_{17})](PF_6)_2$, (35)

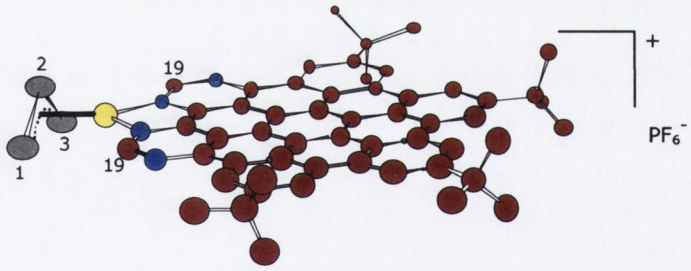
Compound **(17)** (20 mg; $2.66x10^{-2}$ mmol) and $[Ru(bpy)_2Cl_2].2H_2O$ (15.4 mg; $2.96x10^{-2}$ mmol) were sonicated in diethylene glycol ethyl ether (5 mL) for 10 mins. The brown solution was degassed by passing a stream of argon through the solution for 30 min. After heating the solution for 20 h at 127°C under an argon atmosphere, it was allowed to cool to RT and filtered through a G4 Frit. To the mixture was added a saturated NH_4PF_6 aqueous solution to form a dark green solid, which was filtered off and washed with water and diethyl ether. Chromatography (SiO_2, 100:10:1 acetonitrile:water:KNO_3 (aq)) followed by anion exchange gave $[Ru(bpy)_2(N\text{-}HBC_{17})](PF_6)_2$ as a black-green solid. Yield: 0.023 mg, 60%. ^1H NMR (CD_3CN): δ 9.94 (s, 2H, H_{aryl}), 9.80 (s, 2H, H_{aryl}), 9.60 (s, 4H, H_{aryl}), 9.31 (s, 2H, H19), 8.67 (d, 2H, $^3J_{HH}$=8.2, H3), 8.58 (br d, 2H, $^3J_{HH}$=7.5, H3'), 8.25 (t, 2H, $^3J_{HH}$=8.2, H4), 8.10 (d, 2H, $^3J_{HH}$=5.5, H6), 8.00 (m, 4H,

H4', H6'), 7.63 (t, 2H, $^3J_{HH}$=6.0-7.5, H5), 7.17 (br s, 2H, H5'), 1.88, 1.83 (s, 18H, -CH_3); ESI-MS (CH_3CN) *m/z*(%) $[M\text{-}2PF_6]^{2+}$ 581.6 (100); (calcd 582.2); ESI-MS (CH_3CN); calculated for $C_{74}H_{62}N_8Ru$: $[M\text{-}2PF_6]^{2+}$ *m/z* 582.2070, found: 582.2042.



6.3.3 $[Pd(\eta^3\text{-}C_3H_5)(N\text{-}HBC_{17})]PF_6$, (36)

Bis(chloro-η^3-allyl palladium) (4.9 mg; $1.33x10^{-2}$ mmol) was dissolved in acetonitrile (2 mL) with 5 drops of dichloromethane. $AgNO_3$ (7 mg; $4.1x10^{-2}$ mmol) was added and the solution stirred at RT for 6 h. The white precipitate of AgCl was removed by filtration through celite. Compound **(17)** (20 mg; $2.66x10^{-2}$ mmol) in toluene (5 mL) was added to the filtrate dropwise and the reaction mixture stirred for 12 h. The red precipitate was collected, taken up in a minimum of acetonitrile, and a saturated NH_4PF_6 aqueous solution added, to form a dark red solid which was filtered off. Yield: 20 mg, 84%. ^{1}H NMR ($CDCl_3$): δ 9.45, 9.40, 9.34, 9.18 (s, 2H, H_{aryl}), 8.56 (s, 2H, H19), 5.61 (s, 1H, $H2_{allyl}$), 4.24 (s, 2H, $H1^{syn}$, $H3^{syn}$), 2.87 (s, 2H, $H1^{anti}$, $H3^{anti}$), 1.96 (s, 18H, -CH_3), 1.86 (s, 18H, -CH_3); ESI-MS (CH_3OH) *m/z*(%) $[M\text{-}PF_6]^+$ 898.1 (100); (calcd 898.4); ESI-MS (CH_3OH); calculated for $C_{57}H_{51}N_4Pd$: $[M\text{-}PF_6]^+$ *m/z* 897.3148, found: 897.3182; IR (KBr disk, cm^{-1}): ν(C-H st, CH_3): 2960, 2930, 2868, ν(C=C st): 1605, ν(C=N st): 1535, 1465, 1398, 1380, 1249, 1065, 1025, 842, 558.



6.4 POLYARYL FERROCENE COMPOUNDS

6.4.1 Ethynylferrocene, (37)[4]

(a): Synthesis of acetylferrocene (reaction carried out in air).

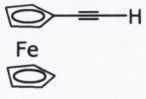
A stirred solution of ferrocene (4.6 g; 25 mmol) and acetic anhydride (4.7 mL; 50 mmol) in dichloromethane (60 mL) was cooled to -10°C in an acetone ice bath. Boron trifluoride etherate (30 mL; 239 mmol) was added quickly and the solution turned purple. The mixture was allowed to stir for 0.5 h at -10°C and then warmed to RT for 3.5 h. Sodium acetate (34 g; 414 mmol) in water (100 mL) was added while stirring the solution and cooling it to 0°C. The organic layer was set apart and the aqueous layer was extracted with dichloromethane. The organic fractions were combined and washed with water, sodium bicarbonate solution and dried over $MgSO_4$. After removal of the solvent, acetylferrocene crystallised as orange needles following a hot filtration in hexane. Yield: 4.6 g, 81%.

(b): Synthesis of 3-chloro-3-ferrocenyl-propenal.

Acetylferrocene (4.5 g; 20 mmol) was dissolved in dry DMF (30 mL). The solution was cooled to 0°C and phosphorus oxychloride (6.1 mL; 60 mmol) in DMF (20 mL) was added dropwise to the previously stirred solution. The reaction was allowed to proceed for 15 min at 0°C and 2h at RT. A 20% sodium acetate solution (150 mL) was then poured into the reaction mixture and the solution stirred for 1.5 h at RT. The solution was extracted with dichloromethane, washed with water, dried over $MgSO_4$ and concentrated to a red oil. The product was purified by crystallisation from 1:1 hexane:dichloromethane. Yield: 3.3 g, 60%.

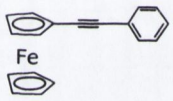
(c): Synthesis of ethynylferrocene.

3-Chloro-3-ferrocenyl-propenal (0.95 g; 3.45 mmol) in dioxane (30 mL) was heated to reflux. Aqueous NaOH (20 mL; 0.5 M; 10 mmol) was added rapidly to this solution. The reaction was allowed to continue for 25 min and was poured onto cold water (50 mL). After acidification with 0.5 M HCl, the solution was extracted with dichloromethane, washed with water and dried over $MgSO_4$. The solvent was removed and the residue subjected to chromatography (SiO_2, hexane). Yield: 0.64 g, 88%. m.p: 52-54°C; ^1H NMR ($CDCl_3$): δ 4.46 (t, 2H, J_{HH}=1.8, H(Cp)), 4.22 (s, 5H, H(Cp)), 4.19 (t, 2H, J_{HH}=1.8, H(Cp)), 2.72 (s, 1H, C≡CH). ^{13}C NMR ($CDCl_3$): δ 82.5 (1C, C≡C), 73.4 (1C, -C≡C-), 71.7 (2C, Cp), 70.0 (5C, Cp), 68.7 (2C, Cp), 63.9 (1C, Cp_{quat}); ESI-MS (CH_3CN) *m/z*(%) $[M]^+$ 210.0 (100); (calcd 210.0); Anal. Calcd for $C_{12}H_{10}Fe$: C, 68.61; H, 4.80. Found: C, 67.85; H, 4.83; IR (KBr disk, cm^{-1}): ν(C≡C-H st): 3280, ν(C≡C st): 2103, ν(C-H st, Cp): 3104, 3086, ν(CH rock, Cp): 1108, 1050, 1035, 1022, 993.



6.4.2 Phenylethynylferrocene, (38)

Compound **(37)** (0.400 g; 1.90 mmol), copper iodide (0.015 g) and {1,1 bis(diphenylphosphinoferrocene)}dichloropalladium (0.12 g) were stirred in DMF (15 mL) and diethylamine (20 mL) at 80°C under argon. Bromobenzene (0.3 mL; 2.86 mmol) was injected into the reaction vessel over 10 min. The reaction was stirred at 80°C for 2 h, and at RT for a further 10 h. The solvent was removed *in vacuo* and the black solid extracted several times with hot hexane. Phenylethynylferrocene crystallised from the hexane extraction. Flash chromatography (SiO_2, 2:1 hexane:dichloromethane) and crystallisation from hexane afforded the pure **(38)**. Yield: 0.377 g, 70%. m.p: 118-120°C; ^{1}H NMR ($CDCl_3$): δ 7,54 (dd, 2H, J_{HH}=2.0-7.5, H_{aryl}), 7.36 (m, 3H, H_{aryl}), 4.55 (t, 2H, J_{HH}=2, H(Cp)), 4.29 (s, 5H, H(Cp)), 4.28 (t, 2H, J_{HH}=2, H(Cp)). ^{13}C NMR ($CDCl_3$): δ 131.0 (2C, C_{aryl}), 127.8 (2C, C_{aryl}), 127.2 (1C, C_{aryl}), 123.6 (1C, $C_{quat/aryl}$), 87.9 (1C, -C≡C-), 85.3 (1C, -C≡C-), 71.0 (2C, Cp), 69.5 (5C, Cp), 68.4 (2C, Cp), 64.9 (1C, Cp_{quat}); ESI-MS (CH_3CN) *m/z*(%) $[M]^+$ 286.1 (100); (calcd 286.1); ESI-MS (CH_3CN); calculated for $C_{18}H_{14}Fe$: $[M]^+$ *m/z* 286.0445, found: 286.0469; IR (KBr disk, cm^{-1}): ν(C-H st, Cp): 3090, 3061, ν(C≡C st): 2224, ν(C=C st): 1493, 1439, ν(CH rock, Cp): 1102, 1068, 1024, 999.



6.4.3 1,4-bis(ferrocenyl)butadiyne, (39)[5]

(Reaction carried out in air)

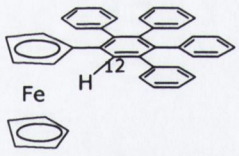
Compound **(37)** (0.350 g; 1.6 mmol) was dissolved in hexane (125 mL) in a 3-necked round bottomed flask attached to a drying tube filled with calcium hydride. CuCl (0.070 g; 0.70 mmol) and tetramethylethylenediamine (0.082 g; 0.70 mmol) were added and the reaction mixture stirred overnight at RT. After acidification with HCl (50 mL; 0.1 M) the reaction mixture was extracted with dichloromethane, washed with water and dried over $MgSO_4$. The solvent was removed *in vacuo*. Column chromatography (SiO_2, dichloromethane) eluted unreacted **(37)** and **(39)**. Yield: 0.150 g, 45%. m.p: 191-192°C; ^{1}H NMR ($CDCl_3$): δ 4.53 (t, 4H, J_{HH}=2, H(Cp)), 4.29 (s, 10H, H(Cp)), 4.27 (t, 4H, J_{HH}=1.8, H(Cp)). ^{13}C NMR ($CDCl_3$): δ 79.1 (2C, -C≡C-), 72.1 (4C, Cp), 71.0 (2C, -C≡C-), 70.1 (10C, Cp), 69.2 (4C, Cp), 63.7 (2C, Cp_{quat}); ESI-MS (CH_3CN) *m/z*(%) $[M]^+$ 418.0 (100); (calcd 418.1); IR (KBr disk, cm^{-1}): ν(C≡C st): 2152, ν(CH Cp ring): 1105, 1060, 1047, 1028, 1003.



6.4.4 1,2,3,4-tetraphenyl-5-ferrocenylbenzene, (40)

(Reaction carried out in air)

Compound **(37)** (200 mg; 0.95 mmol), benzophenone (4 g), and tetraphenylcyclopentadienone (0.36 g; 0.97 mmol) were mixed in a round bottom flask and attached to an air condenser. The mixture was heated at 90°C for 4 h. Compound **(40)** and unreacted **(37)** were separated from the reaction mixture by chromatography (SiO_2, 1:1 hexane:dichloromethane). The mixture of **(37)** and **(40)** was extracted with hexane to remove **(37)**. The product was crystallised in pure form from hexane at 0°C. Yield: 0.372 g, 70%. m.p: 213°C; ^{1}H NMR ($CDCl_3$): δ 7.95 (s, 1H, H12), 7.17-6.66 (m, 20H, H_{aryl}), 4.06 (s, 5H, H(Cp)), 3.96 (t, 2H, J_{HH}=2, H(Cp)), 3.89 (t, 2H, J_{HH}=2, H(Cp)). ^{13}C NMR ($CDCl_3$): δ 141.2, 140.3, 139.7, 139.4, 139.2, 139.1, 137.0, 136.9, 136.0 ($C_{quat/aryl}$), 130.7 (1C), 130.5 (2C), 130.4 (2C), 130.2 (2C), 128.9 (2C), 126.7 (2C), 126.1 (2C), 125.8 (2C), 125.5 (2C), 125.2 (1C), 124.8 (1C), 124.4 (1C), 124.2 (1C) (C_{aryl}), 85.7 (1C, Cp_{quat}), 69.4 (2C, Cp), 68.5 (5C, Cp), 66.7 (2C, Cp); ESI-MS (CH_3CN) *m/z*(%) $[M]^+$ 566.3 (100); (calcd 566.4); Anal. Calcd for $C_{40}H_{30}Fe$: C, 84.80; H, 5.33. Found: C, 84.68; H, 5.38; IR (KBr disk, cm^{-1}): ν(C-H st): 3080, 3055, 3022, ν(C=C st): 1599, 1494, 1441, 696.



6.4.5 Tetra-*peri*-benzo-*peri*-ferrocenylcoronene, (41)

Attempted synthesis of Tetra-*peri*-benzo-*peri*-ferrocenylcoronene, (41)

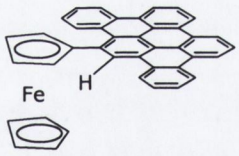
(i): $AlCl_3$ (470 mg; 3.5 mmol) and $Cu(SO_3CF_3)_2$ (1280 mg; 3.5 mmol) were added to **(40)** (200 mg; 0.35 mmol) in CS_2 (50 mL). The reaction was stirred at RT for 14 d. The solvent was evaporated *in vacuo* and the resulting black solid subjected to column chromatography. NMR analysis revealed no product formation.

(ii): A suspension of Li powder (626 mg; 90.2 mmol) in THF (70 mL) was stirred vigorously under reflux. **(40)** (20 mL of a 0.018 M solution in THF; 0.35 mmol) was added quickly and reflux maintained for 5 h. The black solution was cooled to -5°C and quenched with bubbling oxygen for 5 min. The red solution was filtered, the solvent evaporated and the residue dissolved in methanol. After chromatography, NMR analysis revealed no product formation.

(iii): $FeCl_3$ (460 mg; 2.8 mmol) and CH_3NO_2 (0.5 mL) were added to **(40)** (200 mg; 0.35 mmol) in dichloromethane (50 mL). The mixture was refluxed for 2 d. The black precipitate was filtered and the yellow filtrate reduced to a brown oil. Chromatography was followed by NMR, which revealed no product formation.

Synthesis of Tetra-*peri*-benzo-*peri*-ferrocenylcoronene, (41)

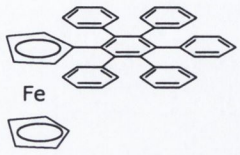
Compound **(40)** (180 mg; 0.318 mmol), $AlCl_3$ (700 mg; 5.25 mmol) and $CuCl_2$ (700 mg; 5.21 mmol) were stirred in CS_2 (60 mL) at 25°C for 48 h. The black solid was allowed to settle and the CS_2 removed by cannula. The solid was dried *in vacuo* and stirred in dilute ammonia solution. The product was extracted into chloroform and dried over $MgSO_4$. Chromatography (SiO_2, 7:3 hexane:diethyl ether) gave a pale yellow powder, **(41)**. Yield: 0.027 g, 15%. m.p: >300°C; ^1H NMR ($CDCl_3$): δ 9.83 (s, 1H, H_{aryl}), 9.07 (d, 2H, $^3J_{HH}$=8, H_{aryl}), 9.01 (t, 2H, $^3J_{HH}$=7, H_{aryl}), 8.92 (d, 2H, $^3J_{HH}$=8, H_{aryl}), 8.71 (d, 1H, $^3J_{HH}$=8, H_{aryl}), 8.11 (m, 3H, H_{aryl}), 7.89 (t, 1H, $^3J_{HH}$=7, H_{aryl}), 7.83 (t, 1H, $^3J_{HH}$=7, H_{aryl}), 7.59 (t, 1H, $^3J_{HH}$=7.5, H_{aryl}), 7.24 (t, 1H, $^3J_{HH}$=7.5, H_{aryl}), 4.77 (t, 2H, J_{HH}=2, 1.5, H(Cp)), 4.50 (t, 2H, J_{HH}=2, 1.5, H(Cp)), 4.12 (s, 5H, H(Cp)). ^{13}C NMR ($CDCl_3$): δ 133.8, 130.7, 130.1, 130.0, 129.8, 129.7, 129.6, 129.5, 129.4, 127.5, 125.8, 124.7, 124.4, 124.3, 124.0 (1C, $C_{quat/aryl}$), 130.2, 127.4, 127.1, 126.7, 126.4, 126.2, 126.0, 124.1, 123.4, 123.1, 122.9, 121.6, 121.4, 121.2, 120.8 (1C, C_{aryl}), 70.7 (2C, Cp), 69.5 (5C, Cp), 67.9 (2C, Cp); ESI-MS (toluene) *m/z*(%) $[M]^+$ 559.8 (100); (calcd 560.4); ESI-MS (toluene); calculated for $C_{40}H_{24}Fe$: $[M]^+$ *m/z* 560.1227, found: 560.1226; IR (KBr disk, cm^{-1}): ν(C-H st): 3083, 3071, ν(C=C st): 1459, 1383, 1261, ν(CH rock, Cp): 1096, 1075, 1021.



6.4.6 1,2,3,4,5-pentaphenyl-6-ferrocenylbenzene, (42)

Compound **(38)** (0.324 g; 1.13 mmol) and tetraphenylcyclopentadienone (0.522 g; 1.40 mmol) were sealed under vacuum in a glass tube and heated at 200°C for 48 h. The reaction mixture was subsequently cooled to RT, the tube broken carefully, and the residue extracted into dichloromethane (50 mL) and filtered. After removal of the solvent the recovered material was subjected to flash chromatography (SiO_2, 1:1, hexane:dichloromethane). The orange-yellow band was collected and evaporated to afford **(42)** as an orange-yellow solid. Yield: 0.260 g, 36%. m.p: >300°C; ^1H NMR ($CDCl_3$): δ 7.08 (m 10H, H_{aryl}), 6.81 (m, 15H, H_{aryl}), 3.88 (s, 2H, H(Cp)), 3.80 (s, 2H, H(Cp)), 3.73 (s, 5H, H(Cp)). ^{13}C NMR ($CDCl_3$): δ 131.7 (4C), 130.8 (4C), 130.6 (2C),

126.2 (4C), 125.8 (6C), 125.3 (2C), 124.6 (1C), 124.5 (2C) (C_{aryl}), 72.8 (2C, Cp), 68.9 (5C, Cp), 66.5 (2C, Cp), $C_{quat/aryl}$ are not listed; ESI-MS (CH_3CN) *m/z*(%) $[M]^+$ 642.6 (100); (calcd 642.6); ESI-MS (CH_3CN); calculated for $C_{46}H_{34}Fe$: $[M]^+$ *m/z* 642.2010, found: 642.2036; IR (KBr disk, cm^{-1}): ν(C-H st): 3080, 3056, 3022, ν(C=C st): 1599, 1497, 1441, 699, ν(CH rock, Cp): 1108, 1070, 1029, 1006.



6.4.7 1-ferrocenyl-2-phenylethane-1,2-dione, (43)

(a): Synthesis of ferrocenecarboxyaldehyde (reaction carried out in air).

N-Methylformanilide (4.4 g; 32 mmol) and phosphorus oxychloride (5 g; 32 mmol) were mixed and left at RT for 1 h. Ferrocene (2.99 g; 16 mmol) was then added in small portions with vigorous shaking during 30 min, the mixture being kept cool throughout. It was then left in a stoppered flask for 72 h. After addition of ice-water, the mixture was left to stand for 2 h. The product was extracted with chloroform, dried over $MgSO_4$ and evaporated. Column chromatography (SiO_2, dichloromethane) was used to separate the product from unreacted ferrocene. The main red band of ferrocenecarboxyaldehyde was eluted, evaporated and crystallised from 25% aqueous ethanol. Yield: 2.56 g, 75%.

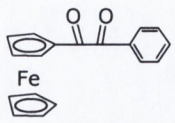
(b): Synthesis of mandeloylferrocene (reaction carried out in air).

A mixture of ferrocenecarboxyaldehyde (1.07 g; 5.0 mmol), benzaldehyde (0.53 g; 5.0 mmol), ethanol (15 mL) and aqueous potassium cyanide (0.5 g in 1 mL water) was refluxed for 1.5 h. After dilution with water and refrigeration for 2 h, the product was filtered off and recrystallised from aqueous alcohol. The product formed pink needles. Yield: 0.37 g, 25%.

(c): Synthesis of 1-ferrocenyl-2-phenylethane-1,2-dione (reaction carried out in air).

Mandeloylferrocene (5.0 g; 16 mmol) and activated manganese dioxide (20 g) were refluxed in chloroform (100 mL) for 6 h. The mixture was cooled to RT and filtered. The residue was extracted with chloroform until the extracts were colourless. The extracts and the filtrate were combined and were evaporated to dryness. Recrystallisation of the residue from hexane produced diketone **(43)** as ruby red plates. Yield: 4.7 g, 92%. m.p: 75-76°C; ^{1}H NMR ($CDCl_3$): δ 8.06 (d, 2H, $^3J_{HH}$=7.5, H_{aryl}), 7.64 (t, 1H, $^3J_{HH}$=7.5, H_{aryl}), 7.52 (t, 2H, $^3J_{HH}$=7.5, H_{aryl}), 4.88 (t, 2H, J_{HH}=2, H(Cp)), 4.68 (t, 2H, J_{HH}=2, H(Cp)), 4.27 (s, 5H, H(Cp)). ^{13}C NMR ($CDCl_3$): δ 198.5, 192.4 (1C, C=O), 133.9 (1C, C_{aryl}), 132.6 (1C, $C_{quat/aryl}$), 129.5, 128.4 (2C, C_{aryl}), 74.1 (1C, Cp_{quat}), 73.4 (2C, Cp), 70.1 (5C, Cp), 70.0 (2C, Cp); ESI-MS (CH_3CN) *m/z*(%) $[MNa]^+$ 341.0 (100), $[MH]^+$

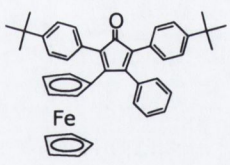
319.1 (20); (calcd 319.1); Anal. Calcd for $C_{18}H_{14}FeO_2$: C, 67.95; H, 4.44. Found: C, 67.65; H, 4.26; IR (KBr Disk, cm^{-1}): ν(C-H st, Cp): 3106, ν(C=O st): 1679, 1644, ν(C=C st): 1445.



6.4.8 2,5-bis-(4-*tert*-butylphenyl)-3-ferrocenyl-4-phenylcyclopenta-2,4-dienone, (44)

(Reaction carried out in air)

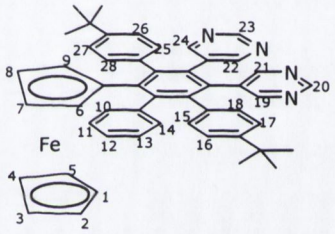
Compound **(43)** (350 mg; 1.10 mmol), **(14)** (355 mg; 1.10 mmol) and KOH (50 mg) were refluxed in ethanol (15 mL) for 2 h. The brown solution was kept at 0°C for 12 h. A blue/black solid formed and was filtered off and washed with a small amount of cold hexane. Column chromatography (SiO_2, 3:1 hexane:dichloromethane) was used to purify **(44)** as a deep blue amorphous powder. Yield: 0.210 g, 32%. m.p: 181-182°C; ^{1}H NMR ($CDCl_3$): δ 7.47 (m, 7H, H_{aryl}), 7.33 (d, 2H, $^3J_{HH}$=8.0, H_{aryl}), 7.23 (d, 2H, $^3J_{HH}$=8.5, H_{aryl}), 7.17 (d, 2H, $^3J_{HH}$=8.0, H_{aryl}), 4.27 (s, 2H, H(Cp)), 4.01 (s, 5H, H(Cp)), 3.94 (s, 2H, H(Cp)), 1.41 (s, 9H, -CH_3), 1.28 (s, 9H, -CH_3). ^{13}C NMR ($CDCl_3$): δ 199.9 (1C, C=O), 155.3, 151.8, 149.9, 149.6 (1C, $C_{quat/Cp}$), 135.7, 130.0 (1C, $C_{quat/aryl}$), 129.4 (2C), 129.2 (2C), 128.7 (2C), 127.9 (1C), 127.7 (2C) (C_{aryl}), 127.5, 124.9 (1C, $C_{quat/aryl}$), 124.7 (2C, C_{aryl}), 124.5 (1C, $C_{quat/aryl}$), 124.3 (2C, C_{aryl}), 70.7 (2C, Cp), 70.4 (2C, Cp), 69.7 (5C, Cp), 65.4 (1C, Cp_{quat}), 34.3, 34.1 (1C, $C_{quat/alkyl}$), 31.0, 30.8 (3C, -CH_3); ESI-MS (CH_3CN) *m/z*(%) $[MH]^+$ 605.4 (100); (calcd 605.6); IR (KBr disk, cm^{-1}): ν(C-H st): 3087, 3057, ν(C-H st, CH_3): 2960, 2928, 2903, 2867, ν(C=O st): 1697, ν(CH rock, Cp): 1100, 1021.



6.4.9 1,2-dipyrimidyl-3,6-bis-(4-*tert*-butylphenyl)-4-ferrocenyl-5-phenylbenzene, (45)

Compound **(44)** (0.135 g; 0.22 mmol) and **(12)** (0.040 g; 0.22 mmol) were sealed under vacuum in a glass tube and heated at 200°C for 48 h. The reaction mixture was subsequently cooled to RT, the tube broken carefully, the residue extracted from dichloromethane (20 mL) and filtered. After removal of the solvent the recovered material was subjected to flash chromatography (SiO_2, Et_2O). The red band was

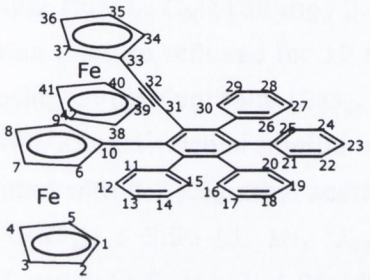
collected, evaporated and recrystallised from 1:1 hexane:dichloromethane, to afford **(45)** as red crystals. Yield: 0.066 g, 40%. m.p: 260-261°C; ^{1}H NMR ($CDCl_3$): δ 8.67, 8.66 (s, 1H, H20, H23), 8.25, 8.21 (s, 2H, H(19,21), H(22,24)), 7.21 (d, 2H, $^{3}J_{HH}$=8, H_{aryl}), 7.07 (d, 2H, $^{3}J_{HH}$=8, H_{aryl}), 7.03 (m, 3H, H11-H13), 6.98 (d, 2H, $^{3}J_{HH}$=8, H(10,14)), 6.90 (d, 2H, $^{3}J_{HH}$=8.5, H_{aryl}), 6.67 (d, 2H, $^{3}J_{HH}$=8, H_{aryl}), 3.89 (t, 2H, J_{HH}=2-1.5, H(Cp)), 3.77 (t, 2H, J_{HH}=2-1.5, H(Cp)), 3.66 (s, 5H, H(Cp)), 1.25 (s, 9H, -CH_3), 1.10 (s, 9H, -CH_3). ^{13}C NMR ($CDCl_3$): δ 157.02, 156.99 (2C, C_{aryl}), 155.4, 155.2 (1C, C_{aryl}), 149.6, 148.5, 143.7, 141.99, 141.92, 140.4, 136.9, 136.5, 135.4, 134.3, 134.1, 133.8, 131.9 (1C, $C_{quat/aryl}$), 131.1 (2C), 131.0 (2C), 129.9 (2C), 126.3 (2C), 125.6 (1C), 124.0 (2C), 123.6 (2C) (C_{aryl}), 85.5 (1C, Cp_{quat}), 72.5 (2C, Cp), 68.6 (5C, Cp), 66.7 (2C, Cp), 34.0, 33.7 (1C, $C_{quat/alkyl}$), 30.7, 30.6 (3C, -CH_3); ESI-MS (CH_3CN) *m/z*(%) $[MH]^+$ 758.6 (100); (calcd 759.7); ESI-MS (CH_3CN); calculated for $C_{50}H_{47}FeN_4$: $[MH]^+$ *m/z* 759.3150, found: 759.3162; IR (KBr disk, cm^{-1}): ν(C-H st): 3083, 3026, ν(C-H st, CH_3): 2962, 2904, 2868, ν(C=N st): 1549, ν(CH_3 δ): 1421, ν(CH_3 δ sy): 1396, ν(CH rock, Cp): 1108, 1020.



6.4.10 1,2,3,4-tetraphenyl-5-ferrocenyl-6-ferrocenylethynylbenzene, (46)

Compound **(39)** (0.120 g; 0.29 mmol) and tetraphenylcyclopentadienone (0.110 g; 0.29 mmol) were sealed under vacuum in a glass tube and heated at 200°C for 48 h. The reaction mixture was subsequently cooled to RT, the tube broken carefully, the residue extracted with dichloromethane (20 mL) and filtered. After removal of the solvent the recovered material was subjected to flash chromatography (SiO_2, 1:1 hexane:dichloromethane). The yellow-orange band was collected, evaporated and recrystallised from 1:1 hexane:dichloromethane, to afford **(46)** as orange crystals. Yield: 0.166 g, 74%. m.p: >300°C; ^{1}H NMR ($CDCl_3$): δ 7.29 (m, 5H, H_{aryl}), 7.00 (m, 3H, H_{aryl}), 6.84 (m, 10H, H_{aryl}), 6.72 (m, 2H, H_{aryl}), 4.40 (s, 2H, H(6,9) or H(7,8)), 4.22 (s, 5H, H38-H42), 4.20 (s, 4H, H34-H37), 4.09 (s, 7H, H1-H5 and either H(6,9) or H(7,8)). ^{13}C NMR ($CDCl_3$): δ 144.5, 141.4, 141.3, 140.4, 140.2, 140.1, 139.8, 138.6, 136.9 (1C, $C_{quat/aryl}$), 131.3, 130.8, 130.7, 130.4, 126.8, 126.6, 126.1, 126.0 (2C,

C_{aryl}), 125.6, 125.1, 124.8, 124.7 (1C, C_{aryl}), 122.6 (1C, $C_{quat/aryl}$), 100.8 (1C, C32), 87.2 (1C, C31), 84.6 (1C, C10), 71.3 (2C, C(6,9) or C(7,8)), 70.2 (2C, C(34,37) or C(35,36)), 69.4 (10C, C1-C5, C38-C40), 68.3 (2C, C(34,37) or C(35,36)), 66.5 (2C, C(6,9) or C(7,8)), 65.9 (1C, C33); ESI-MS (CH_3CN) *m/z*(%) $[M]^+$ 774.2 (100); (calcd 774.5); ESI-MS (CH_3CN); calculated for $C_{52}H_{38}Fe_2$: $[M]^+$ *m/z* 774.1672, found: 774.1686; IR (KBr disk, cm^{-1}): ν(C-H st): 3082, 3056, 3022, ν(C≡C st): 2211, ν(C=C st): 1600, 1496, 1441, 697, ν(CH rock, Cp): 1106, 1069, 1027, 1001.



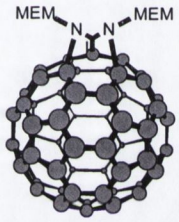
6.5 THE HETEROFULLERENE, AZA[60]FULLERENE

Modified from the literature procedure[6]

6.5.1 Diazabis-(1,6);(1,9)-homofullerene, (47),

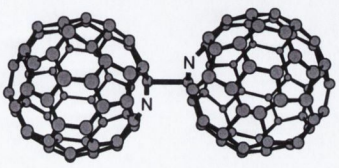
(Reaction carried out in air)

A solution of 2-methoxyethoxymethyl chloride (0.4 mL; 3.51 mmol) in chlorobenzene (10 mL) containing tetrabutylammonium bromide (15 mg) was cooled in an ice bath. Sodium azide (313 mg; 4.81 mmol), dissolved in water (5 mL), was added rapidly and the reaction mixture stirred vigorously at 25°C for 2 h. The organic phase is separated, washed with water, and dried over $MgSO_4$. C_{60} (185 mg; 0.26 mmol) in chlorobenzene (20 mL) is added and the reaction mixture refluxed for 12 h. After reduction *in vacuo*, the black residue is separated using chromatography (SiO_2, CS_2) to give unreacted C_{60}. The column was then eluted with 2:3 CS_2:dichloromethane to give trace amounts of monoazafulleroid, and finally eluted with 8:2 CS_2:ethyl acetate to give **(47)**. Yield: 108 mg, 45%. ^1H NMR (CS_2/20% $CDCl_3$): δ 5.56 (d, 1H, $^2J_{HH}$=9.5, H_{alkyl}), 5.40 (d, 1H, $^2J_{HH}$=9.5, H_{alkyl}), 4.17 (dt, 1H, J_{HH}=4.6-11.0, H_{alkyl}), 4.01 (dt, 1H, J_{HH}=4.6-11.0, H_{alkyl}), 3.71 (t, 2H, $^3J_{HH}$=4.8, H_{alkyl}), 3.42 (s, 3H, H_{alkyl}).



6.5.2 Aza[60]fullerene dimer, $(C_{59}N)_2$, (48)

1,8-Diazabicyclo[5.4.0]undec-7-ene (0.6 mL of a 0.267 M solution in toluene; 0.16 mmol) and *n*-butylamine (1.0 mL of a 0.202 M solution in toluene; 0.19 mmol) were added successively to a solution of **(47)** (150 mg; 0.16 mmol) in toluene (20 mL). The reaction mixture was stirred at 25°C for 4.5 h under argon as a green solid precipitated. After removal of the toluene, the residue was dissolved in 1,2-dichlorobenzene (20 mL) and heated with toluene-*p*-sulfonic acid (0.616 g; 3.24 mmol) under reflux for 8 min. The reaction mixture was reduced *in vacuo* and subjected to chromatography (SiO_2, CS_2) to give the heterofullerene **(48)**. Yield: 20 mg, 20%. UV-vis (cyclohexane): λ_{max} (nm) 260, 330, 436, 591, 686 nm; ESI-MS (toluene) *m/z*(%) $[C_{59}NH]^+$ 723.67 (100); (calcd 723.61).



6.6 REFERENCES

1. D. F. Eaton, *Pure Appl. Chem.*, **1988**, *60*, 1107-1114
2. B. P. Sullivan, D. J. Salmon, T. J. Meyer, *Inorg. Chem.*, **1978**, *17*, 3334-3341
3. J. V. Caspar, T. J. Meyer, *J. Am. Chem. Soc.*, **1983**, *105*, 5583-5590
4. M. Rosenblum, N. Brawn, J. Papenmeier, M. Applebaum, *J. Organomet. Chem.*, **1966**, *6*, 173-180
5. A. S. Hay, *J. Org. Chem.*, **1962**, *27*, 3320-3321
6. B. Nuber, A. Hirsch, *Chem. Commun.*, **1996**, 1421-1422

APPENDIX

APPENDIX 1

Table A1. Crystal data and structure refinement for **(23)**.

Compound		**(23)**
Empirical formula		$C_{48}H_{46}N_4O_2$
Formula weight		710.89
Temperature (K)		298(2)
Wavelength (Å)		0.71073
Crystal system		Monoclinic
Space group		P2(1)/n
Unit cell dimensions	a (Å)	12.6392(18)
	b (Å)	18.116(3)
	c (Å)	18.439(3)
	α (°)	90
	β (°)	109.418(2)
	γ (°)	90
Volume ($Å^3$)		3981.9(10)
Z		4
Density (calculated) (Mg/m^3)		1.186
Absorption coefficient (mm^{-1})		0.073
F(000)		1512
Crystal size (mm^3)		0.33 x 0.20 x 0.20
Theta range for data collection (°)		1.72 to 26.00
Index ranges		-15<=h<=15, -22<=k<=22, -22<=l<=22
Reflections collected		40174
Independent reflections		7814 [R(int) = 0.0621]
Completeness to theta = 26.00° (%)		99.9
Absorption correction		Semi-empirical from equivalents
Max. and min. transmission		1.0000 and 0.9303
Refinement method		Full-matrix least-squares on F^2
Data / restraints / parameters		7814 / 0 / 524
Goodness-of-fit on F^2		1.021
R_1 [I>2sigma(I)]		R1 = 0.0479
WR2 (all data)		wR2 = 0.1366
Largest diff. peak and hole		0.437 and -0.195 e.$Å^{-3}$

Table A2. Atomic coordinates (x 10^4) and equivalent isotropic displacement parameters ($Å^2$x 10^3) for **(23)**. U(eq) is defined as one third of the trace of the orthogonalized U^{ij} tensor.

	x	y	z	U(eq)
O(1)	4882(1)	2915(1)	1748(1)	67(1)
O(2)	7311(1)	6186(1)	3510(1)	66(1)
C(1)	8071(1)	5625(1)	-559(1)	39(1)
C(2)	7753(1)	4892(1)	-777(1)	39(1)
C(3)	7424(1)	4425(1)	-282(1)	38(1)

C(4)	7416(1)	4695(1)	430(1)	38(1)
C(5)	7765(1)	5422(1)	659(1)	38(1)
C(6)	8077(1)	5891(1)	158(1)	38(1)
C(7)	8348(1)	6147(1)	-1097(1)	42(1)
C(8)	9409(2)	6414(1)	-973(1)	64(1)
N(1)	9659(2)	6919(1)	-1413(1)	82(1)
C(9)	8801(2)	7158(1)	-1989(1)	78(1)
N(2)	7749(2)	6937(1)	-2194(1)	77(1)
C(10)	7543(2)	6426(1)	-1739(1)	60(1)
C(11)	7692(1)	4623(1)	-1553(1)	42(1)
C(12)	8610(2)	4568(1)	-1794(1)	54(1)
N(3)	8567(2)	4299(1)	-2475(1)	72(1)
C(13)	7558(2)	4091(1)	-2919(1)	77(1)
N(4)	6599(2)	4128(1)	-2775(1)	72(1)
C(14)	6685(2)	4395(1)	-2089(1)	56(1)
C(15)	7024(1)	3651(1)	-521(1)	40(1)
C(16)	7714(1)	3101(1)	-629(1)	46(1)
C(17)	7329(1)	2385(1)	-801(1)	52(1)
C(18)	6248(1)	2181(1)	-861(1)	46(1)
C(19)	5560(1)	2742(1)	-763(1)	52(1)
C(20)	5932(1)	3454(1)	-603(1)	50(1)
C(21)	5779(2)	1396(1)	-1020(1)	61(1)
C(22)	6606(2)	868(1)	-1179(2)	108(1)
C(23)	4702(2)	1400(1)	-1717(1)	95(1)
C(24)	5490(2)	1124(1)	-325(1)	92(1)
C(25)	6874(1)	4240(1)	890(1)	40(1)
C(26)	7274(1)	3561(1)	1202(1)	47(1)
C(27)	6645(1)	3107(1)	1506(1)	52(1)
C(28)	5597(1)	3331(1)	1496(1)	49(1)
C(29)	5209(1)	4021(1)	1214(1)	53(1)
C(30)	5840(1)	4470(1)	922(1)	46(1)
C(31)	5169(2)	2165(1)	1936(1)	75(1)
C(32)	7719(1)	5686(1)	1416(1)	39(1)
C(33)	8358(1)	5357(1)	2105(1)	47(1)
C(34)	8209(2)	5541(1)	2788(1)	53(1)
C(35)	7405(1)	6052(1)	2805(1)	47(1)
C(36)	6782(1)	6397(1)	2134(1)	49(1)
C(37)	6950(1)	6216(1)	1453(1)	45(1)
C(38)	6367(2)	6591(1)	3545(1)	73(1)
C(39)	8326(1)	6687(1)	358(1)	40(1)
C(40)	9284(1)	6915(1)	932(1)	49(1)
C(41)	9501(2)	7652(1)	1104(1)	54(1)
C(42)	8768(2)	8197(1)	713(1)	49(1)
C(43)	7804(2)	7965(1)	147(1)	55(1)
C(44)	7586(1)	7230(1)	-31(1)	52(1)
C(45)	9005(2)	9015(1)	913(1)	64(1)
C(46A)	10345(4)	9146(2)	1284(6)	259(12)
C(47A)	8751(13)	9444(4)	195(6)	207(8)

C(48A)	8266(10)	9222(4)	1368(7)	199(6)
C(46B)	10094(6)	9202(3)	874(7)	128(3)
C(47B)	8144(9)	9533(4)	406(4)	117(4)
C(48B)	9110(6)	9173(3)	1733(3)	87(2)

Table A3. Bond lengths [Å] and angles [°] for **(23)**.

O(1)-C(28)	1.372(2)	C(25)-C(30)	1.392(2)
O(1)-C(31)	1.419(2)	C(26)-C(27)	1.386(2)
O(2)-C(35)	1.366(2)	C(27)-C(28)	1.378(2)
O(2)-C(38)	1.422(2)	C(28)-C(29)	1.380(2)
C(1)-C(6)	1.404(2)	C(29)-C(30)	1.368(2)
C(1)-C(2)	1.407(2)	C(32)-C(37)	1.384(2)
C(1)-C(7)	1.493(2)	C(32)-C(33)	1.391(2)
C(2)-C(3)	1.405(2)	C(33)-C(34)	1.375(2)
C(2)-C(11)	1.489(2)	C(34)-C(35)	1.383(2)
C(3)-C(4)	1.404(2)	C(35)-C(36)	1.375(2)
C(3)-C(15)	1.506(2)	C(36)-C(37)	1.381(2)
C(4)-C(5)	1.409(2)	C(39)-C(40)	1.380(2)
C(4)-C(25)	1.501(2)	C(39)-C(44)	1.382(2)
C(5)-C(6)	1.406(2)	C(40)-C(41)	1.380(2)
C(5)-C(32)	1.495(2)	C(41)-C(42)	1.381(2)
C(6)-C(39)	1.497(2)	C(42)-C(43)	1.380(2)
C(7)-C(8)	1.372(2)	C(42)-C(45)	1.533(2)
C(7)-C(10)	1.375(2)	C(43)-C(44)	1.376(2)
C(8)-N(1)	1.329(2)	C(46A)-C(45)	1.620(5)
N(1)-C(9)	1.314(3)	C(45)-C(46B)	1.442(6)
C(9)-N(2)	1.318(3)	C(45)-C(47A)	1.474(10)
N(2)-C(10)	1.331(2)	C(45)-C(48A)	1.497(8)
C(11)-C(12)	1.377(2)	C(45)-C(48B)	1.502(6)
C(11)-C(14)	1.390(2)	C(45)-C(47B)	1.504(7)
C(12)-N(3)	1.330(2)		
N(3)-C(13)	1.321(3)	C(28)-O(1)-C(31)	117.72(14)
C(13)-N(4)	1.327(3)	C(35)-O(2)-C(38)	118.39(14)
N(4)-C(14)	1.325(2)	C(6)-C(1)-C(2)	120.25(13)
C(15)-C(16)	1.382(2)	C(6)-C(1)-C(7)	118.65(13)
C(15)-C(20)	1.384(2)	C(2)-C(1)-C(7)	121.01(13)
C(16)-C(17)	1.384(2)	C(3)-C(2)-C(1)	120.10(14)
C(17)-C(18)	1.384(2)	C(3)-C(2)-C(11)	119.66(13)
C(18)-C(19)	1.388(2)	C(1)-C(2)-C(11)	120.12(13)
C(18)-C(21)	1.530(2)	C(4)-C(3)-C(2)	119.55(13)
C(19)-C(20)	1.371(2)	C(4)-C(3)-C(15)	119.42(13)
C(21)-C(22)	1.516(3)	C(2)-C(3)-C(15)	120.95(13)
C(21)-C(24)	1.528(3)	C(3)-C(4)-C(5)	120.48(13)
C(21)-C(23)	1.530(3)	C(3)-C(4)-C(25)	118.91(13)
C(25)-C(26)	1.379(2)	C(5)-C(4)-C(25)	120.00(13)

C(6)-C(5)-C(4)	119.75(13)	C(27)-C(28)-C(29)	119.46(15)
C(6)-C(5)-C(32)	121.81(13)	C(30)-C(29)-C(28)	120.32(15)
C(4)-C(5)-C(32)	118.32(13)	C(29)-C(30)-C(25)	121.16(14)
C(1)-C(6)-C(5)	119.82(13)	C(37)-C(32)-C(33)	117.17(14)
C(1)-C(6)-C(39)	119.82(13)	C(37)-C(32)-C(5)	120.94(13)
C(5)-C(6)-C(39)	120.17(13)	C(33)-C(32)-C(5)	121.54(13)
C(8)-C(7)-C(10)	114.61(16)	C(34)-C(33)-C(32)	121.13(15)
C(8)-C(7)-C(1)	122.93(15)	C(33)-C(34)-C(35)	120.56(15)
C(10)-C(7)-C(1)	122.39(14)	O(2)-C(35)-C(36)	124.76(15)
N(1)-C(8)-C(7)	123.96(19)	O(2)-C(35)-C(34)	115.95(14)
C(9)-N(1)-C(8)	114.88(18)	C(36)-C(35)-C(34)	119.28(15)
N(1)-C(9)-N(2)	127.92(19)	C(35)-C(36)-C(37)	119.64(15)
C(9)-N(2)-C(10)	114.86(18)	C(36)-C(37)-C(32)	122.16(15)
N(2)-C(10)-C(7)	123.68(17)	C(40)-C(39)-C(44)	117.11(14)
C(12)-C(11)-C(14)	114.79(15)	C(40)-C(39)-C(6)	122.38(14)
C(12)-C(11)-C(2)	123.62(15)	C(44)-C(39)-C(6)	120.51(14)
C(14)-C(11)-C(2)	121.57(14)	C(41)-C(40)-C(39)	121.43(15)
N(3)-C(12)-C(11)	123.84(18)	C(40)-C(41)-C(42)	121.62(16)
C(13)-N(3)-C(12)	114.72(17)	C(43)-C(42)-C(41)	116.61(14)
N(3)-C(13)-N(4)	128.21(18)	C(43)-C(42)-C(45)	121.95(16)
C(14)-N(4)-C(13)	114.85(18)	C(41)-C(42)-C(45)	121.42(15)
N(4)-C(14)-C(11)	123.54(18)	C(44)-C(43)-C(42)	122.07(16)
C(16)-C(15)-C(20)	116.93(14)	C(43)-C(44)-C(39)	121.15(15)
C(16)-C(15)-C(3)	123.11(13)	C(46B)-C(45)-C(47A)	76.0(7)
C(20)-C(15)-C(3)	119.88(14)	C(46B)-C(45)-C(48A)	138.9(5)
C(15)-C(16)-C(17)	121.18(15)	C(47A)-C(45)-C(48A)	112.4(7)
C(16)-C(17)-C(18)	122.10(15)	C(46B)-C(45)-C(48B)	103.8(5)
C(17)-C(18)-C(19)	115.99(14)	C(47A)-C(45)-C(48B)	136.3(5)
C(17)-C(18)-C(21)	124.98(16)	C(48A)-C(45)-C(48B)	41.4(5)
C(19)-C(18)-C(21)	119.02(15)	C(46B)-C(45)-C(47B)	109.2(6)
C(20)-C(19)-C(18)	122.17(15)	C(47A)-C(45)-C(47B)	38.5(7)
C(19)-C(20)-C(15)	121.58(15)	C(48A)-C(45)-C(47B)	74.6(6)
C(22)-C(21)-C(24)	109.30(18)	C(48B)-C(45)-C(47B)	108.1(4)
C(22)-C(21)-C(23)	108.63(19)	C(46B)-C(45)-C(42)	109.1(3)
C(24)-C(21)-C(23)	108.20(18)	C(47A)-C(45)-C(42)	109.1(4)
C(22)-C(21)-C(18)	112.00(16)	C(48A)-C(45)-C(42)	105.6(3)
C(24)-C(21)-C(18)	108.97(15)	C(48B)-C(45)-C(42)	111.8(3)
C(23)-C(21)-C(18)	109.67(15)	C(47B)-C(45)-C(42)	114.2(4)
C(26)-C(25)-C(30)	117.94(14)	C(46B)-C(45)-C(46A)	26.6(7)
C(26)-C(25)-C(4)	123.50(14)	C(47A)-C(45)-C(46A)	100.8(6)
C(30)-C(25)-C(4)	118.07(13)	C(48A)-C(45)-C(46A)	119.1(5)
C(25)-C(26)-C(27)	121.17(15)	C(48B)-C(45)-C(46A)	79.4(4)
C(28)-C(27)-C(26)	119.81(15)	C(47B)-C(45)-C(46A)	127.6(5)
O(1)-C(28)-C(27)	124.84(15)	C(42)-C(45)-C(46A)	109.6(2)
O(1)-C(28)-C(29)	115.70(14)		

Symmetry transformations used to generate equivalent atoms:

Table A4. Anisotropic displacement parameters ($Å^2 x\ 10^3$) for **(23)**. The anisotropic displacement factor exponent takes the form: $-2\pi^2[h^2a^{*2}U^{11} + ... + 2hka^*b^*U^{12}]$

	U^{11}	U^{22}	U^{33}	U^{23}	U^{13}	U^{12}
O(1)	61(1)	56(1)	96(1)	23(1)	41(1)	0(1)
O(2)	84(1)	69(1)	49(1)	-4(1)	27(1)	16(1)
C(1)	37(1)	34(1)	45(1)	2(1)	13(1)	-2(1)
C(2)	37(1)	35(1)	44(1)	-2(1)	14(1)	0(1)
C(3)	35(1)	31(1)	47(1)	-1(1)	12(1)	1(1)
C(4)	37(1)	31(1)	47(1)	2(1)	14(1)	2(1)
C(5)	36(1)	34(1)	43(1)	1(1)	11(1)	2(1)
C(6)	36(1)	32(1)	45(1)	0(1)	11(1)	-1(1)
C(7)	50(1)	34(1)	48(1)	-3(1)	22(1)	-4(1)
C(8)	58(1)	70(1)	63(1)	4(1)	20(1)	-19(1)
N(1)	86(1)	80(1)	88(1)	10(1)	37(1)	-32(1)
C(9)	102(2)	56(1)	96(2)	17(1)	58(2)	-9(1)
N(2)	85(1)	75(1)	81(1)	33(1)	41(1)	13(1)
C(10)	54(1)	63(1)	66(1)	20(1)	26(1)	6(1)
C(11)	50(1)	30(1)	48(1)	2(1)	17(1)	3(1)
C(12)	61(1)	48(1)	58(1)	0(1)	26(1)	6(1)
N(3)	90(1)	73(1)	63(1)	-5(1)	40(1)	13(1)
C(13)	112(2)	73(2)	51(1)	-9(1)	31(1)	15(1)
N(4)	87(1)	71(1)	51(1)	-14(1)	12(1)	3(1)
C(14)	60(1)	53(1)	53(1)	-7(1)	16(1)	-1(1)
C(15)	43(1)	31(1)	43(1)	-1(1)	13(1)	-2(1)
C(16)	46(1)	39(1)	56(1)	-6(1)	20(1)	-3(1)
C(17)	57(1)	38(1)	64(1)	-8(1)	22(1)	5(1)
C(18)	58(1)	33(1)	43(1)	-3(1)	10(1)	-4(1)
C(19)	43(1)	40(1)	68(1)	-3(1)	12(1)	-5(1)
C(20)	41(1)	34(1)	71(1)	-6(1)	13(1)	2(1)
C(21)	80(1)	35(1)	64(1)	-6(1)	18(1)	-12(1)
C(22)	140(2)	35(1)	160(3)	-24(1)	63(2)	-9(1)
C(23)	120(2)	66(1)	77(2)	-14(1)	4(1)	-42(1)
C(24)	127(2)	61(1)	83(2)	9(1)	30(1)	-30(1)
C(25)	42(1)	32(1)	45(1)	0(1)	16(1)	-2(1)
C(26)	44(1)	40(1)	60(1)	7(1)	20(1)	5(1)
C(27)	52(1)	40(1)	67(1)	16(1)	23(1)	7(1)
C(28)	51(1)	45(1)	57(1)	10(1)	24(1)	-1(1)
C(29)	47(1)	49(1)	69(1)	8(1)	28(1)	6(1)
C(30)	49(1)	35(1)	58(1)	7(1)	21(1)	6(1)
C(31)	82(1)	54(1)	98(2)	24(1)	42(1)	-7(1)
C(32)	41(1)	30(1)	45(1)	0(1)	14(1)	-2(1)
C(33)	52(1)	38(1)	51(1)	3(1)	16(1)	9(1)
C(34)	63(1)	49(1)	43(1)	4(1)	13(1)	12(1)
C(35)	56(1)	41(1)	44(1)	-5(1)	17(1)	-1(1)
C(36)	48(1)	45(1)	55(1)	-2(1)	18(1)	10(1)
C(37)	46(1)	41(1)	44(1)	3(1)	10(1)	6(1)

C(38)	83(1)	77(1)	73(1)	-11(1)	44(1)	5(1)
C(39)	45(1)	32(1)	43(1)	0(1)	16(1)	-3(1)
C(40)	50(1)	36(1)	55(1)	2(1)	7(1)	0(1)
C(41)	54(1)	42(1)	57(1)	-5(1)	5(1)	-9(1)
C(42)	65(1)	33(1)	49(1)	-2(1)	20(1)	-6(1)
C(43)	63(1)	34(1)	58(1)	3(1)	8(1)	6(1)
C(44)	53(1)	39(1)	54(1)	-2(1)	5(1)	-1(1)
C(45)	91(2)	34(1)	65(1)	-6(1)	23(1)	-8(1)
C(46A)	136(8)	61(5)	420(20)	-60(8)	-116(11)	-23(5)
C(47A)	430(20)	40(5)	121(7)	7(4)	49(10)	-87(8)
C(48A)	279(13)	89(6)	322(16)	-128(9)	223(12)	-74(8)
C(46B)	109(6)	59(4)	216(10)	0(4)	53(7)	-39(4)
C(47B)	197(8)	31(3)	75(5)	-8(3)	-21(5)	31(4)
C(48B)	126(5)	55(3)	64(3)	-21(2)	10(3)	-14(3)

Table A5. Hydrogen coordinates (x 10^4) and isotropic displacement parameters ($Å^2$x 10^3) for **(23)**.

	x	y	z	U(eq)
H(8)	9989	6230	-555	77
H(9)	8955	7528	-2289	94
H(10)	6814	6248	-1862	72
H(12)	9300	4727	-1461	65
H(13)	7515	3893	-3394	93
H(14)	6036	4430	-1958	67
H(16)	8450	3214	-585	55
H(17)	7813	2031	-878	63
H(19)	4822	2631	-808	63
H(20)	5438	3813	-548	60
H(22A)	6914	1089	-1538	162
H(22B)	6229	418	-1391	162
H(22C)	7201	763	-707	162
H(23A)	4163	1723	-1619	142
H(23B)	4401	909	-1809	142
H(23C)	4866	1570	-2161	142
H(24A)	6157	1114	119	137
H(24B)	5180	635	-424	137
H(24C)	4950	1450	-231	137
H(26)	7978	3406	1208	57
H(27)	6928	2653	1717	62
H(29)	4514	4182	1222	63
H(30)	5574	4937	742	56
H(31A)	5306	1926	1511	113
H(31B)	4564	1922	2043	113
H(31C)	5834	2141	2380	113
H(33)	8896	5007	2102	57

H(34)	8654	5320	3242	63
H(36)	6251	6750	2140	59
H(37)	6532	6458	1005	54
H(38A)	6363	7071	3324	110
H(38B)	6408	6643	4072	110
H(38C)	5691	6334	3264	110
H(40)	9795	6563	1210	59
H(41)	10157	7786	1492	65
H(43)	7285	8316	-122	65
H(44)	6930	7097	-420	62
H(46A)	10548	9189	1833	389
H(46B)	10548	9590	1079	389
H(46C)	10735	8735	1162	389
H(47A)	7954	9459	-59	310
H(47B)	9101	9214	-136	310
H(47C)	9032	9938	314	310
H(48A)	8446	8920	1821	298
H(48B)	7495	9147	1061	298
H(48C)	8383	9732	1516	298
H(46D)	10277	9700	1046	193
H(46E)	10083	9156	353	193
H(46F)	10646	8873	1197	193
H(47D)	7430	9441	466	176
H(47E)	8086	9456	-121	176
H(47F)	8366	10034	549	176
H(48D)	9340	9676	1854	130
H(48E)	9658	8849	2068	130
H(48F)	8398	9095	1803	130

Table A6. Torsion angles [°] for **(23)**.

C(6)-C(1)-C(2)-C(3)	0.9(2)	C(25)-C(4)-C(5)-C(32)	7.9(2)
C(7)-C(1)-C(2)-C(3)	-175.73(13)	C(2)-C(1)-C(6)-C(5)	0.1(2)
C(6)-C(1)-C(2)-C(11)	176.87(13)	C(7)-C(1)-C(6)-C(5)	176.76(13)
C(7)-C(1)-C(2)-C(11)	0.3(2)	C(2)-C(1)-C(6)-C(39)	-175.03(13)
C(1)-C(2)-C(3)-C(4)	0.0(2)	C(7)-C(1)-C(6)-C(39)	1.7(2)
C(11)-C(2)-C(3)-C(4)	-176.04(13)	C(4)-C(5)-C(6)-C(1)	-1.9(2)
C(1)-C(2)-C(3)-C(15)	176.81(13)	C(32)-C(5)-C(6)-C(1)	-177.83(13)
C(11)-C(2)-C(3)-C(15)	0.8(2)	C(4)-C(5)-C(6)-C(39)	173.23(13)
C(2)-C(3)-C(4)-C(5)	-1.8(2)	C(32)-C(5)-C(6)-C(39)	-2.7(2)
C(15)-C(3)-C(4)-C(5)	-178.66(13)	C(6)-C(1)-C(7)-C(8)	71.2(2)
C(2)-C(3)-C(4)-C(25)	169.27(13)	C(2)-C(1)-C(7)-C(8)	-112.16(19)
C(15)-C(3)-C(4)-C(25)	-7.6(2)	C(6)-C(1)-C(7)-C(10)	-105.50(18)
C(3)-C(4)-C(5)-C(6)	2.7(2)	C(2)-C(1)-C(7)-C(10)	71.2(2)
C(25)-C(4)-C(5)-C(6)	-168.22(13)	C(10)-C(7)-C(8)-N(1)	2.1(3)
C(3)-C(4)-C(5)-C(32)	178.83(13)	C(1)-C(7)-C(8)-N(1)	-174.85(18)

C(7)-C(8)-N(1)-C(9)	0.4(3)	C(26)-C(27)-C(28)-O(1)	176.90(17)
C(8)-N(1)-C(9)-N(2)	-2.8(4)	C(26)-C(27)-C(28)-C(29)	-3.0(3)
N(1)-C(9)-N(2)-C(10)	2.3(4)	O(1)-C(28)-C(29)-C(30)	-177.60(16)
C(9)-N(2)-C(10)-C(7)	0.7(3)	C(27)-C(28)-C(29)-C(30)	2.3(3)
C(8)-C(7)-C(10)-N(2)	-2.7(3)	C(28)-C(29)-C(30)-C(25)	1.0(3)
C(1)-C(7)-C(10)-N(2)	174.28(17)	C(26)-C(25)-C(30)-C(29)	-3.6(2)
C(3)-C(2)-C(11)-C(12)	-119.35(17)	C(4)-C(25)-C(30)-C(29)	168.53(15)
C(1)-C(2)-C(11)-C(12)	64.6(2)	C(6)-C(5)-C(32)-C(37)	65.5(2)
C(3)-C(2)-C(11)-C(14)	59.5(2)	C(4)-C(5)-C(32)-C(37)	-110.53(16)
C(1)-C(2)-C(11)-C(14)	-116.50(17)	C(6)-C(5)-C(32)-C(33)	-121.47(16)
C(14)-C(11)-C(12)-N(3)	-1.8(2)	C(4)-C(5)-C(32)-C(33)	62.52(19)
C(2)-C(11)-C(12)-N(3)	177.12(15)	C(37)-C(32)-C(33)-C(34)	1.5(2)
C(11)-C(12)-N(3)-C(13)	0.7(3)	C(5)-C(32)-C(33)-C(34)	-171.81(15)
C(12)-N(3)-C(13)-N(4)	1.2(3)	C(32)-C(33)-C(34)-C(35)	1.0(3)
N(3)-C(13)-N(4)-C(14)	-1.7(3)	C(38)-O(2)-C(35)-C(36)	13.5(3)
C(13)-N(4)-C(14)-C(11)	0.2(3)	C(38)-O(2)-C(35)-C(34)	-168.04(17)
C(12)-C(11)-C(14)-N(4)	1.3(3)	C(33)-C(34)-C(35)-O(2)	178.90(15)
C(2)-C(11)-C(14)-N(4)	-177.64(16)	C(33)-C(34)-C(35)-C(36)	-2.5(3)
C(4)-C(3)-C(15)-C(16)	-115.92(17)	O(2)-C(35)-C(36)-C(37)	-179.99(15)
C(2)-C(3)-C(15)-C(16)	67.2(2)	C(34)-C(35)-C(36)-C(37)	1.6(3)
C(4)-C(3)-C(15)-C(20)	60.7(2)	C(35)-C(36)-C(37)-C(32)	1.0(2)
C(2)-C(3)-C(15)-C(20)	-116.09(17)	C(33)-C(32)-C(37)-C(36)	-2.5(2)
C(20)-C(15)-C(16)-C(17)	-0.9(2)	C(5)-C(32)-C(37)-C(36)	170.87(14)
C(3)-C(15)-C(16)-C(17)	175.86(15)	C(1)-C(6)-C(39)-C(40)	-113.05(17)
C(15)-C(16)-C(17)-C(18)	-1.0(3)	C(5)-C(6)-C(39)-C(40)	71.9(2)
C(16)-C(17)-C(18)-C(19)	2.0(2)	C(1)-C(6)-C(39)-C(44)	67.4(2)
C(16)-C(17)-C(18)-C(21)	-177.63(16)	C(5)-C(6)-C(39)-C(44)	-107.73(17)
C(17)-C(18)-C(19)-C(20)	-1.1(3)	C(44)-C(39)-C(40)-C(41)	-0.8(2)
C(21)-C(18)-C(19)-C(20)	178.56(16)	C(6)-C(39)-C(40)-C(41)	179.56(15)
C(18)-C(19)-C(20)-C(15)	-0.8(3)	C(39)-C(40)-C(41)-C(42)	0.4(3)
C(16)-C(15)-C(20)-C(19)	1.8(2)	C(40)-C(41)-C(42)-C(43)	0.6(3)
C(3)-C(15)-C(20)-C(19)	-175.08(15)	C(40)-C(41)-C(42)-C(45)	179.17(17)
C(17)-C(18)-C(21)-C(22)	-5.2(3)	C(41)-C(42)-C(43)-C(44)	-1.1(3)
C(19)-C(18)-C(21)-C(22)	175.17(18)	C(45)-C(42)-C(43)-C(44)	-179.67(17)
C(17)-C(18)-C(21)-C(24)	115.8(2)	C(42)-C(43)-C(44)-C(39)	0.6(3)
C(19)-C(18)-C(21)-C(24)	-63.8(2)	C(40)-C(39)-C(44)-C(43)	0.3(2)
C(17)-C(18)-C(21)-C(23)	-125.9(2)	C(6)-C(39)-C(44)-C(43)	179.94(16)
C(19)-C(18)-C(21)-C(23)	54.5(2)	C(43)-C(42)-C(45)-C(46B)	-126.6(5)
C(3)-C(4)-C(25)-C(26)	65.5(2)	C(41)-C(42)-C(45)-C(46B)	54.9(5)
C(5)-C(4)-C(25)-C(26)	-123.38(16)	C(43)-C(42)-C(45)-C(47A)	-45.2(7)
C(3)-C(4)-C(25)-C(30)	-106.16(16)	C(41)-C(42)-C(45)-C(47A)	136.3(7)
C(5)-C(4)-C(25)-C(30)	64.92(19)	C(43)-C(42)-C(45)-C(48A)	75.8(6)
C(30)-C(25)-C(26)-C(27)	2.9(2)	C(41)-C(42)-C(45)-C(48A)	-102.7(6)
C(4)-C(25)-C(26)-C(27)	-168.78(16)	C(43)-C(42)-C(45)-C(48B)	119.1(3)
C(25)-C(26)-C(27)-C(28)	0.4(3)	C(41)-C(42)-C(45)-C(48B)	-59.4(4)
C(31)-O(1)-C(28)-C(27)	-9.0(3)	C(43)-C(42)-C(45)-C(47B)	-4.1(5)
C(31)-O(1)-C(28)-C(29)	170.93(17)	C(41)-C(42)-C(45)-C(47B)	177.4(5)

C(43)-C(42)-C(45)-C(46A)	-154.8(4)	C(41)-C(42)-C(45)-C(46A)	26.7(5)

Symmetry transformations used to generate equivalent atoms:

Table B1. Crystal data and structure refinement for **(29)**.

Compound		**(29)**
Empirical formula		$C_{68}H_{82}N_4Si_2$
Formula weight		1011.56
Temperature (K)		298(2)
Wavelength (Å)		0.71073
Crystal system		Monoclinic
Space group		P2(1)/c
Unit cell dimensions	a (Å)	8.5396(11)
	b (Å)	59.842(8)
	c (Å)	12.6623(17)
	α (°)	90
	β (°)	99.555(3)
	γ (°)	90
Volume ($Å^3$)		6381.0(14)
Z		5
Density (calculated) (Mg/m^3)		1.316
Absorption coefficient (mm^{-1})		0.120
F(000)		2730
Crystal size (mm^3)		0.6 x 0.3 x 0.15
Theta range for data collection (°)		1.67 to 25.00
Index ranges		-10<=h<=10, -71<=k<=70, -14<=l<=15
Reflections collected		60586
Independent reflections		11222 [R(int) = 0.1464]
Completeness to theta = 25.00° (%)		99.9
Absorption correction		None
Refinement method		Full-matrix least-squares on F^2
Data / restraints / parameters		11222 / 0 / 667
Goodness-of-fit on F^2		0.837
R_1 [I>2sigma(I)]		R1 = 0.0797
wR2 (all data)		wR2 = 0.2286
Largest diff. peak and hole		0.328 and -0.174 e.$Å^{-3}$

Table B2. Atomic coordinates (x 10^4) and equivalent isotropic displacement parameters ($Å^2$x 10^3) for **(29)**. U(eq) is defined as one third of the trace of the orthogonalized U^{ij} tensor.

	x	y	z	U(eq)
Si(1)	13840(2)	412(1)	1859(2)	113(1)
Si(2)	56(2)	730(1)	-3194(2)	116(1)
C(1)	6808(5)	2043(1)	1062(4)	59(1)
C(2)	8213(5)	1994(1)	1765(3)	58(1)
C(3)	8802(5)	1774(1)	1851(3)	56(1)
C(4)	7977(5)	1604(1)	1231(3)	57(1)
C(5)	6562(5)	1654(1)	540(3)	58(1)

C(6)	5972(5)	1873(1)	452(4)	59(1)
C(7)	6178(5)	2275(1)	940(4)	63(1)
C(8)	4836(7)	2342(1)	1329(5)	104(2)
N(1)	4166(6)	2545(1)	1136(5)	124(2)
C(9)	4914(10)	2676(1)	567(6)	112(2)
N(2)	6202(7)	2638(1)	183(4)	105(2)
C(10)	6832(6)	2437(1)	393(4)	80(2)
C(11)	9150(6)	2170(1)	2410(4)	60(1)
C(12)	8642(6)	2275(1)	3253(5)	78(2)
N(3)	9557(7)	2413(1)	3922(4)	94(1)
C(13)	10999(9)	2443(1)	3718(6)	101(2)
N(4)	11628(6)	2359(1)	2926(5)	100(2)
C(14)	10675(6)	2224(1)	2279(4)	84(2)
C(15)	10340(5)	1722(1)	2577(4)	58(1)
C(16)	10543(5)	1747(1)	3672(4)	65(1)
C(17)	11973(6)	1698(1)	4300(4)	66(1)
C(18)	13268(5)	1622(1)	3879(4)	64(1)
C(19)	13024(6)	1597(1)	2791(4)	89(2)
C(20)	11605(6)	1643(1)	2163(4)	87(2)
C(21)	14865(6)	1566(1)	4554(4)	87(2)
C(22)	14919(6)	1608(1)	5722(5)	140(3)
C(23)	16174(7)	1705(1)	4208(5)	162(3)
C(24)	15212(10)	1323(1)	4382(8)	240(6)
C(25)	8670(5)	1372(1)	1280(4)	63(1)
C(26)	8930(5)	1251(1)	2212(4)	76(2)
C(27)	9779(6)	1055(1)	2273(5)	86(2)
C(28)	10359(6)	974(1)	1397(5)	78(2)
C(29)	10036(6)	1090(1)	443(4)	82(2)
C(30)	9190(6)	1285(1)	389(4)	75(2)
C(31)	11387(7)	780(1)	1512(5)	93(2)
C(32)	12319(7)	626(1)	1614(5)	99(2)
C(33)	13719(19)	297(4)	3200(20)	580(30)
C(34)	12110(30)	210(2)	3060(20)	580(20)
C(35)	14532(18)	34(2)	3145(13)	419(11)
C(36)	15787(11)	572(2)	1960(15)	321(9)
C(37)	15779(16)	738(3)	2975(14)	407(13)
C(38)	17199(12)	417(2)	2117(14)	370(9)
C(39)	13680(20)	235(3)	560(10)	308(9)
C(40)	12038(18)	125(3)	396(19)	460(20)
C(41)	14305(17)	408(2)	-275(9)	324(9)
C(42)	5655(5)	1467(1)	-65(4)	63(1)
C(43)	5052(6)	1293(1)	484(4)	73(1)
C(44)	4096(6)	1131(1)	-52(4)	76(2)
C(45)	3718(6)	1133(1)	-1150(4)	78(2)
C(46)	4379(6)	1300(1)	-1715(4)	90(2)
C(47)	5329(6)	1462(1)	-1177(4)	79(2)
C(48)	2609(7)	975(1)	-1742(4)	88(2)
C(49)	1627(7)	856(1)	-2252(5)	98(2)

C(50)	569(14)	448(2)	-3470(10)	257(6)
C(51)	-554(14)	349(2)	-4514(9)	312(7)
C(52)	2090(18)	365(2)	-3338(12)	344(10)
C(53)	17(17)	913(2)	-4497(9)	243(6)
C(54)	-102(15)	1143(2)	-4370(10)	308(9)
C(55)	1740(19)	866(3)	-4848(11)	359(11)
C(56)	-1809(14)	835(5)	-2745(13)	485(19)
C(57)	-1684(19)	649(3)	-1670(15)	427(14)
C(58)	-3223(17)	727(3)	-3268(17)	451(13)
C(59)	4457(5)	1919(1)	-291(4)	60(1)
C(60)	3081(6)	1829(1)	-78(4)	109(2)
C(61)	1663(6)	1844(1)	-776(5)	105(2)
C(62)	1572(5)	1953(1)	-1748(4)	62(1)
C(63)	2947(5)	2053(1)	-1929(4)	64(1)
C(64)	4355(5)	2036(1)	-1213(4)	60(1)
C(65)	22(5)	1944(1)	-2558(4)	74(2)
C(66)	-1403(6)	2008(1)	-2032(5)	115(2)
C(67)	79(6)	2100(1)	-3517(4)	106(2)
C(68)	-189(6)	1707(1)	-2980(5)	116(2)

Table B3. Bond lengths [Å] and angles [°] for **(29)**.

Si(1)-C(32)	1.813(6)	C(9)-N(2)	1.294(7)
Si(1)-C(33)	1.851(18)	N(2)-C(10)	1.328(6)
Si(1)-C(36)	1.906(12)	C(11)-C(12)	1.370(6)
Si(1)-C(39)	1.940(12)	C(11)-C(14)	1.379(6)
Si(2)-C(50)	1.792(10)	C(12)-N(3)	1.341(6)
Si(2)-C(49)	1.806(6)	N(3)-C(13)	1.311(7)
Si(2)-C(56)	1.884(16)	C(13)-N(4)	1.314(7)
Si(2)-C(53)	1.975(11)	N(4)-C(14)	1.328(6)
C(1)-C(2)	1.401(5)	C(15)-C(20)	1.361(6)
C(1)-C(6)	1.401(6)	C(15)-C(16)	1.376(5)
C(1)-C(7)	1.484(6)	C(16)-C(17)	1.375(5)
C(2)-C(3)	1.412(6)	C(17)-C(18)	1.380(6)
C(2)-C(11)	1.479(6)	C(18)-C(19)	1.368(6)
C(3)-C(4)	1.398(6)	C(18)-C(21)	1.523(6)
C(3)-C(15)	1.506(6)	C(19)-C(20)	1.362(6)
C(4)-C(5)	1.400(5)	C(21)-C(22)	1.493(7)
C(4)-C(25)	1.507(6)	C(21)-C(24)	1.503(8)
C(5)-C(6)	1.402(6)	C(21)-C(23)	1.516(7)
C(5)-C(42)	1.495(6)	C(25)-C(26)	1.372(6)
C(6)-C(59)	1.493(6)	C(25)-C(30)	1.380(6)
C(7)-C(10)	1.364(6)	C(26)-C(27)	1.372(6)
C(7)-C(8)	1.381(7)	C(27)-C(28)	1.375(6)
C(8)-N(1)	1.348(6)	C(28)-C(29)	1.381(6)
N(1)-C(9)	1.302(7)	C(28)-C(31)	1.452(7)

C(29)-C(30)	1.369(6)	C(1)-C(2)-C(3)	120.0(4)
C(31)-C(32)	1.211(7)	C(1)-C(2)-C(11)	122.1(5)
C(33)-C(34)	1.45(3)	C(3)-C(2)-C(11)	117.9(4)
C(33)-C(35)	1.72(2)	C(4)-C(3)-C(2)	119.7(4)
C(36)-C(38)	1.507(12)	C(4)-C(3)-C(15)	120.1(4)
C(36)-C(37)	1.624(16)	C(2)-C(3)-C(15)	120.2(4)
C(39)-C(40)	1.53(2)	C(3)-C(4)-C(5)	120.0(4)
C(39)-C(41)	1.631(16)	C(3)-C(4)-C(25)	119.1(4)
C(42)-C(47)	1.389(6)	C(5)-C(4)-C(25)	120.8(4)
C(42)-C(43)	1.397(6)	C(4)-C(5)-C(6)	120.5(4)
C(43)-C(44)	1.375(6)	C(4)-C(5)-C(42)	118.9(5)
C(44)-C(45)	1.375(6)	C(6)-C(5)-C(42)	120.5(4)
C(45)-C(46)	1.399(6)	C(1)-C(6)-C(5)	119.6(4)
C(45)-C(48)	1.456(7)	C(1)-C(6)-C(59)	121.5(5)
C(46)-C(47)	1.374(6)	C(5)-C(6)-C(59)	118.9(4)
C(48)-C(49)	1.202(6)	C(10)-C(7)-C(8)	114.1(5)
C(50)-C(52)	1.374(12)	C(10)-C(7)-C(1)	123.0(5)
C(50)-C(51)	1.612(11)	C(8)-C(7)-C(1)	122.8(5)
C(53)-C(54)	1.394(12)	N(1)-C(8)-C(7)	123.3(6)
C(53)-C(55)	1.630(17)	C(9)-N(1)-C(8)	114.2(6)
C(56)-C(58)	1.433(18)	N(2)-C(9)-N(1)	129.1(7)
C(56)-C(57)	1.75(3)	C(9)-N(2)-C(10)	115.0(6)
C(59)-C(64)	1.354(5)	N(2)-C(10)-C(7)	124.1(5)
C(59)-C(60)	1.359(6)	C(12)-C(11)-C(14)	114.4(5)
C(60)-C(61)	1.379(6)	C(12)-C(11)-C(2)	122.9(5)
C(61)-C(62)	1.382(6)	C(14)-C(11)-C(2)	122.4(5)
C(62)-C(63)	1.372(5)	N(3)-C(12)-C(11)	123.3(5)
C(62)-C(65)	1.535(6)	C(13)-N(3)-C(12)	115.3(5)
C(63)-C(64)	1.385(5)	N(3)-C(13)-N(4)	127.9(6)
C(65)-C(68)	1.516(6)	C(13)-N(4)-C(14)	114.7(5)
C(65)-C(66)	1.530(6)	N(4)-C(14)-C(11)	124.3(5)
C(65)-C(67)	1.539(6)	C(20)-C(15)-C(16)	116.8(4)
		C(20)-C(15)-C(3)	120.3(4)
C(32)-Si(1)-C(33)	105.8(5)	C(16)-C(15)-C(3)	122.9(4)
C(32)-Si(1)-C(36)	104.4(4)	C(17)-C(16)-C(15)	120.7(4)
C(33)-Si(1)-C(36)	107.8(10)	C(16)-C(17)-C(18)	122.5(4)
C(32)-Si(1)-C(39)	106.9(4)	C(19)-C(18)-C(17)	115.3(4)
C(33)-Si(1)-C(39)	124.7(11)	C(19)-C(18)-C(21)	120.8(5)
C(36)-Si(1)-C(39)	105.6(9)	C(17)-C(18)-C(21)	123.8(5)
C(50)-Si(2)-C(49)	110.1(4)	C(20)-C(19)-C(18)	122.5(5)
C(50)-Si(2)-C(56)	128.2(9)	C(15)-C(20)-C(19)	122.0(5)
C(49)-Si(2)-C(56)	103.5(5)	C(22)-C(21)-C(24)	109.4(6)
C(50)-Si(2)-C(53)	109.2(7)	C(22)-C(21)-C(23)	106.8(5)
C(49)-Si(2)-C(53)	103.2(3)	C(24)-C(21)-C(23)	108.5(6)
C(56)-Si(2)-C(53)	99.7(9)	C(22)-C(21)-C(18)	113.2(5)
C(2)-C(1)-C(6)	120.2(5)	C(24)-C(21)-C(18)	108.3(5)
C(2)-C(1)-C(7)	121.2(5)	C(23)-C(21)-C(18)	110.5(5)
C(6)-C(1)-C(7)	118.6(4)	C(26)-C(25)-C(30)	118.5(5)

C(26)-C(25)-C(4)	121.9(5)	C(46)-C(47)-C(42)	121.3(5)
C(30)-C(25)-C(4)	119.4(5)	C(49)-C(48)-C(45)	175.6(6)
C(27)-C(26)-C(25)	120.5(5)	C(48)-C(49)-Si(2)	167.8(5)
C(26)-C(27)-C(28)	120.9(5)	C(52)-C(50)-C(51)	112.8(10)
C(27)-C(28)-C(29)	118.8(5)	C(52)-C(50)-Si(2)	124.9(9)
C(27)-C(28)-C(31)	119.7(6)	C(51)-C(50)-Si(2)	112.1(8)
C(29)-C(28)-C(31)	121.3(6)	C(54)-C(53)-C(55)	106.7(12)
C(30)-C(29)-C(28)	120.0(5)	C(54)-C(53)-Si(2)	116.3(11)
C(29)-C(30)-C(25)	121.2(5)	C(55)-C(53)-Si(2)	104.1(9)
C(32)-C(31)-C(28)	176.2(6)	C(58)-C(56)-C(57)	90.5(17)
C(31)-C(32)-Si(1)	174.5(6)	C(58)-C(56)-Si(2)	113.5(14)
C(34)-C(33)-C(35)	92.8(18)	C(57)-C(56)-Si(2)	94.4(14)
C(34)-C(33)-Si(1)	102.6(19)	C(64)-C(59)-C(60)	116.3(4)
C(35)-C(33)-Si(1)	102.5(14)	C(64)-C(59)-C(6)	124.3(4)
C(38)-C(36)-C(37)	112.3(13)	C(60)-C(59)-C(6)	119.3(4)
C(38)-C(36)-Si(1)	111.7(9)	C(59)-C(60)-C(61)	122.9(5)
C(37)-C(36)-Si(1)	104.0(10)	C(60)-C(61)-C(62)	121.0(5)
C(40)-C(39)-C(41)	125.2(15)	C(63)-C(62)-C(61)	115.6(4)
C(40)-C(39)-Si(1)	106.5(11)	C(63)-C(62)-C(65)	124.7(5)
C(41)-C(39)-Si(1)	102.7(11)	C(61)-C(62)-C(65)	119.6(5)
C(47)-C(42)-C(43)	117.4(5)	C(62)-C(63)-C(64)	122.2(4)
C(47)-C(42)-C(5)	122.3(5)	C(59)-C(64)-C(63)	121.8(4)
C(43)-C(42)-C(5)	120.2(4)	C(68)-C(65)-C(66)	109.5(5)
C(44)-C(43)-C(42)	121.3(5)	C(68)-C(65)-C(62)	107.8(4)
C(45)-C(44)-C(43)	120.8(5)	C(66)-C(65)-C(62)	111.1(4)
C(44)-C(45)-C(46)	118.6(5)	C(68)-C(65)-C(67)	107.8(4)
C(44)-C(45)-C(48)	122.5(5)	C(66)-C(65)-C(67)	108.8(4)
C(46)-C(45)-C(48)	118.9(5)	C(62)-C(65)-C(67)	111.7(4)
C(47)-C(46)-C(45)	120.4(5)		

Symmetry transformations used to generate equivalent atoms:

Table B4. Anisotropic displacement parameters ($Å^2 x\ 10^3$) for **(29)**. The anisotropic displacement factor exponent takes the form: $-2\pi^2[h^2a^{*2}U^{11} + ... + 2hka^*b^*U^{12}]$

	U^{11}	U^{22}	U^{33}	U^{23}	U^{13}	U^{12}
Si(1)	108(1)	93(1)	136(2)	13(1)	18(1)	33(1)
Si(2)	110(2)	93(1)	128(2)	-25(1)	-25(1)	-14(1)
C(1)	41(3)	73(4)	64(3)	13(3)	12(3)	7(3)
C(2)	41(3)	72(4)	60(3)	7(3)	9(2)	-2(3)
C(3)	37(3)	77(4)	54(3)	7(3)	6(2)	8(3)
C(4)	51(3)	73(4)	46(3)	7(3)	3(2)	6(3)
C(5)	49(3)	75(4)	49(3)	7(3)	2(2)	-11(3)
C(6)	44(3)	71(4)	60(3)	13(3)	5(2)	0(3)
C(7)	39(3)	91(4)	62(3)	3(3)	12(2)	1(3)
C(8)	92(5)	122(6)	104(5)	40(4)	35(4)	22(4)

N(1)	108(4)	131(5)	142(5)	35(4)	50(4)	63(4)
C(9)	123(7)	82(5)	133(6)	1(4)	24(5)	27(5)
N(2)	83(4)	78(4)	157(5)	9(3)	25(4)	15(3)
C(10)	64(3)	71(4)	105(4)	7(4)	17(3)	3(3)
C(11)	47(3)	68(4)	63(3)	12(3)	3(3)	1(3)
C(12)	65(4)	72(4)	96(4)	-10(3)	8(4)	-5(3)
N(3)	87(4)	88(4)	106(4)	-10(3)	10(3)	-5(3)
C(13)	96(6)	100(5)	98(5)	-12(4)	-5(4)	-28(4)
N(4)	75(3)	109(4)	113(4)	7(4)	6(3)	-34(3)
C(14)	56(4)	109(5)	87(4)	2(4)	12(3)	-11(3)
C(15)	39(3)	81(4)	53(3)	7(3)	6(3)	6(2)
C(16)	47(3)	84(4)	64(4)	0(3)	12(3)	8(2)
C(17)	57(3)	91(4)	47(3)	2(3)	0(3)	-2(3)
C(18)	46(3)	82(4)	63(4)	3(3)	8(3)	1(3)
C(19)	53(3)	151(5)	62(4)	-6(4)	10(3)	25(3)
C(20)	50(3)	157(5)	52(3)	4(3)	5(3)	24(3)
C(21)	61(4)	116(5)	75(4)	10(3)	-14(3)	4(3)
C(22)	74(4)	254(8)	84(5)	41(5)	-16(3)	3(5)
C(23)	65(4)	301(10)	117(5)	35(6)	3(4)	-41(5)
C(24)	193(8)	134(7)	329(13)	-27(7)	-142(8)	86(6)
C(25)	55(3)	78(4)	53(3)	0(3)	1(3)	7(3)
C(26)	69(3)	95(4)	63(4)	18(3)	7(3)	21(3)
C(27)	87(4)	94(5)	75(4)	25(4)	9(3)	22(3)
C(28)	73(4)	76(4)	83(4)	-7(4)	12(3)	16(3)
C(29)	77(4)	101(5)	67(4)	-9(4)	7(3)	22(3)
C(30)	72(4)	85(4)	63(4)	6(3)	-1(3)	14(3)
C(31)	84(4)	88(5)	106(5)	-4(4)	14(4)	16(4)
C(32)	89(4)	83(4)	125(5)	1(4)	17(4)	14(4)
C(33)	317(19)	620(40)	890(50)	660(40)	350(30)	320(20)
C(34)	790(50)	194(14)	890(50)	290(20)	510(50)	140(20)
C(35)	400(20)	360(18)	530(30)	293(19)	175(19)	177(17)
C(36)	110(8)	237(13)	590(30)	-27(15)	-20(12)	78(9)
C(37)	222(13)	360(20)	570(30)	-240(20)	-129(16)	54(13)
C(38)	142(9)	277(13)	680(30)	3(17)	35(13)	34(10)
C(39)	470(30)	243(14)	228(13)	15(12)	122(15)	244(16)
C(40)	250(16)	310(20)	760(50)	-230(20)	-90(20)	-18(14)
C(41)	450(20)	338(16)	212(12)	98(13)	154(14)	231(16)
C(42)	58(3)	74(4)	54(3)	15(3)	1(3)	-3(3)
C(43)	66(3)	92(4)	56(3)	7(3)	-5(3)	-9(3)
C(44)	80(4)	77(4)	65(4)	16(3)	-3(3)	-12(3)
C(45)	73(4)	92(4)	63(4)	9(3)	-3(3)	-15(3)
C(46)	99(4)	114(5)	49(3)	8(4)	-11(3)	-19(4)
C(47)	85(4)	99(4)	51(4)	15(3)	2(3)	-19(3)
C(48)	92(4)	81(4)	83(4)	5(3)	-8(4)	-9(4)
C(49)	104(5)	89(4)	91(4)	0(4)	-11(4)	-16(4)
C(50)	209(11)	202(11)	328(14)	-148(10)	-51(11)	27(9)
C(51)	301(14)	251(12)	352(15)	-205(12)	-40(12)	-24(10)
C(52)	370(20)	247(13)	383(18)	-92(12)	-49(16)	190(14)

C(53)	297(15)	180(10)	189(10)	44(8)	-142(11)	-56(11)
C(54)	333(17)	137(9)	377(18)	64(10)	-167(14)	-22(10)
C(55)	317(18)	510(30)	225(13)	56(15)	-38(14)	-80(20)
C(56)	98(8)	1060(60)	282(18)	-190(30)	-17(10)	-142(18)
C(57)	320(20)	580(30)	420(20)	-260(20)	160(20)	-330(20)
C(58)	188(13)	570(30)	580(30)	-200(30)	41(17)	-51(16)
C(59)	41(3)	80(4)	56(3)	18(3)	2(2)	-4(3)
C(60)	55(4)	178(6)	91(4)	77(4)	-2(3)	-9(4)
C(61)	49(3)	163(6)	97(4)	64(4)	-1(3)	-19(3)
C(62)	47(3)	64(3)	74(4)	9(3)	3(3)	6(2)
C(63)	51(3)	78(4)	61(3)	19(3)	3(3)	7(3)
C(64)	43(3)	67(3)	69(3)	19(3)	8(3)	0(2)
C(65)	55(3)	80(4)	79(4)	-9(3)	-14(3)	6(3)
C(66)	52(3)	156(6)	128(5)	-9(4)	-8(3)	23(4)
C(67)	88(4)	130(5)	87(4)	18(4)	-28(3)	17(4)
C(68)	94(4)	108(5)	132(5)	-20(4)	-20(4)	-1(4)

Table B5. Hydrogen coordinates (x 10^4) and isotropic displacement parameters ($Å^2$x 10^3) for **(29)**.

	x	y	z	U(eq)
H(8)	4370	2242	1746	125
H(9)	4460	2815	415	135
H(10)	7778	2404	153	96
H(12)	7610	2248	3368	94
H(13)	11657	2534	4192	121
H(14)	11063	2161	1701	101
H(16)	9703	1798	3989	78
H(17)	12072	1716	5038	79
H(19)	13858	1546	2467	106
H(20)	11497	1619	1428	104
H(22A)	14126	1519	5978	211
H(22B)	14716	1763	5833	211
H(22C)	15950	1569	6104	211
H(23A)	15995	1860	4343	243
H(23B)	16175	1683	3457	243
H(23C)	17181	1660	4605	243
H(24A)	14397	1233	4603	360
H(24B)	16221	1285	4797	360
H(24C)	15239	1298	3637	360
H(26)	8527	1302	2808	91
H(27)	9965	977	2915	103
H(29)	10393	1036	-162	99
H(30)	8962	1361	-260	90
H(33)	14091	390	3829	697
H(34A)	11954	131	3697	874

H(34B)	11936	110	2461	874
H(34C)	11366	332	2939	874
H(35A)	14415	-48	3778	628
H(35B)	15639	48	3099	628
H(35C)	13995	-43	2525	628
H(56)	15784	661	1309	385
H(37A)	16729	826	3081	610
H(37B)	15735	650	3606	610
H(37C)	14869	834	2838	610
H(38A)	18158	504	2188	556
H(38B)	17139	320	1511	556
H(38C)	17198	330	2754	556
H(39)	14465	115	701	370
H(40A)	11911	34	-235	691
H(40B)	11233	239	314	691
H(40C)	11942	34	1006	691
H(41A)	14275	336	-955	486
H(41B)	15375	452	2	486
H(41C)	13633	538	-363	486
H(43)	5301	1287	1227	88
H(44)	3701	1017	333	91
H(46)	4175	1300	-2460	108
H(47)	5762	1572	-1565	95
H(50)	153	368	-2900	308
H(51A)	-277	196	-4612	468
H(51B)	-408	434	-5133	468
H(51C)	-1644	358	-4418	468
H(52A)	2057	208	-3486	516
H(52B)	2604	390	-2614	516
H(52C)	2672	440	-3822	516
H(53)	-832	861	-5060	291
H(54A)	-129	1216	-5050	462
H(54B)	798	1196	-3876	462
H(54C)	-1059	1177	-4097	462
H(55A)	1809	947	-5495	538
H(55B)	1857	709	-4968	538
H(55C)	2567	916	-4289	538
H(56)	-1873	995	-2590	582
H(57A)	-2574	671	-1308	641
H(57B)	-716	675	-1181	641
H(57C)	-1694	498	-1932	641
H(58A)	-4114	777	-2958	676
H(58B)	-3110	568	-3178	676
H(58C)	-3394	762	-4017	676
H(60)	3097	1754	568	131
H(61)	754	1780	-591	126
H(63)	2933	2135	-2555	77
H(64)	5256	2108	-1369	72

H(66A)	-1460	1910	-1439	172
H(66B)	-2360	1996	-2546	172
H(66C)	-1282	2160	-1780	172
H(67A)	960	2059	-3859	160
H(67B)	202	2251	-3271	160
H(67C)	-890	2086	-4019	160
H(68A)	-233	1606	-2396	174
H(68B)	691	1668	-3327	174
H(68C)	-1157	1697	-3486	174

Table B6. Torsion angles [°] for **(29)**.

C(6)-C(1)-C(2)-C(3)	0.7(6)	C(8)-C(7)-C(10)-N(2)	-4.2(7)
C(7)-C(1)-C(2)-C(3)	-178.8(4)	C(1)-C(7)-C(10)-N(2)	173.1(5)
C(6)-C(1)-C(2)-C(11)	178.9(4)	C(1)-C(2)-C(11)-C(12)	70.5(6)
C(7)-C(1)-C(2)-C(11)	-0.7(7)	C(3)-C(2)-C(11)-C(12)	-111.3(5)
C(1)-C(2)-C(3)-C(4)	0.1(6)	C(1)-C(2)-C(11)-C(14)	-116.4(5)
C(11)-C(2)-C(3)-C(4)	-178.1(4)	C(3)-C(2)-C(11)-C(14)	61.8(6)
C(1)-C(2)-C(3)-C(15)	177.9(4)	C(14)-C(11)-C(12)-N(3)	-2.0(7)
C(11)-C(2)-C(3)-C(15)	-0.3(6)	C(2)-C(11)-C(12)-N(3)	171.7(5)
C(2)-C(3)-C(4)-C(5)	-0.9(6)	C(11)-C(12)-N(3)-C(13)	-0.2(8)
C(15)-C(3)-C(4)-C(5)	-178.7(4)	C(12)-N(3)-C(13)-N(4)	2.3(9)
C(2)-C(3)-C(4)-C(25)	176.2(4)	N(3)-C(13)-N(4)-C(14)	-1.8(10)
C(15)-C(3)-C(4)-C(25)	-1.6(6)	C(13)-N(4)-C(14)-C(11)	-0.8(8)
C(3)-C(4)-C(5)-C(6)	0.8(6)	C(12)-C(11)-C(14)-N(4)	2.5(7)
C(25)-C(4)-C(5)-C(6)	-176.2(4)	C(2)-C(11)-C(14)-N(4)	-171.2(5)
C(3)-C(4)-C(5)-C(42)	-176.5(4)	C(4)-C(3)-C(15)-C(20)	61.1(6)
C(25)-C(4)-C(5)-C(42)	6.5(6)	C(2)-C(3)-C(15)-C(20)	-116.8(5)
C(2)-C(1)-C(6)-C(5)	-0.8(6)	C(4)-C(3)-C(15)-C(16)	-118.0(5)
C(7)-C(1)-C(6)-C(5)	178.7(4)	C(2)-C(3)-C(15)-C(16)	64.2(6)
C(2)-C(1)-C(6)-C(59)	179.0(4)	C(20)-C(15)-C(16)-C(17)	1.0(7)
C(7)-C(1)-C(6)-C(59)	-1.4(6)	C(3)-C(15)-C(16)-C(17)	-179.9(4)
C(4)-C(5)-C(6)-C(1)	0.0(6)	C(15)-C(16)-C(17)-C(18)	0.4(7)
C(42)-C(5)-C(6)-C(1)	177.2(4)	C(16)-C(17)-C(18)-C(19)	-0.9(7)
C(4)-C(5)-C(6)-C(59)	-179.8(4)	C(16)-C(17)-C(18)-C(21)	-179.8(5)
C(42)-C(5)-C(6)-C(59)	-2.6(6)	C(17)-C(18)-C(19)-C(20)	0.1(8)
C(2)-C(1)-C(7)-C(10)	74.5(6)	C(21)-C(18)-C(19)-C(20)	179.0(5)
C(6)-C(1)-C(7)-C(10)	-105.0(5)	C(16)-C(15)-C(20)-C(19)	-1.9(8)
C(2)-C(1)-C(7)-C(8)	-108.5(5)	C(3)-C(15)-C(20)-C(19)	179.0(5)
C(6)-C(1)-C(7)-C(8)	72.0(6)	C(18)-C(19)-C(20)-C(15)	1.4(9)
C(10)-C(7)-C(8)-N(1)	3.8(8)	C(19)-C(18)-C(21)-C(22)	178.9(5)
C(1)-C(7)-C(8)-N(1)	-173.5(5)	C(17)-C(18)-C(21)-C(22)	-2.3(8)
C(7)-C(8)-N(1)-C(9)	-1.4(9)	C(19)-C(18)-C(21)-C(24)	-59.5(8)
C(8)-N(1)-C(9)-N(2)	-1.0(11)	C(17)-C(18)-C(21)-C(24)	119.3(7)
N(1)-C(9)-N(2)-C(10)	0.7(10)	C(19)-C(18)-C(21)-C(23)	59.1(7)
C(9)-N(2)-C(10)-C(7)	2.1(8)	C(17)-C(18)-C(21)-C(23)	-122.1(6)

C(3)-C(4)-C(25)-C(26)	61.7(6)	C(44)-C(45)-C(46)-C(47)	-2.8(8)
C(5)-C(4)-C(25)-C(26)	-121.2(5)	C(48)-C(45)-C(46)-C(47)	174.7(5)
C(3)-C(4)-C(25)-C(30)	-112.5(5)	C(45)-C(46)-C(47)-C(42)	-0.2(8)
C(5)-C(4)-C(25)-C(30)	64.6(6)	C(43)-C(42)-C(47)-C(46)	3.4(7)
C(30)-C(25)-C(26)-C(27)	4.2(7)	C(5)-C(42)-C(47)-C(46)	-174.4(5)
C(4)-C(25)-C(26)-C(27)	-170.0(4)	C(44)-C(45)-C(48)-C(49)	114(8)
C(25)-C(26)-C(27)-C(28)	-1.3(8)	C(46)-C(45)-C(48)-C(49)	-63(8)
C(26)-C(27)-C(28)-C(29)	-1.7(8)	C(45)-C(48)-C(49)-Si(2)	30(10)
C(26)-C(27)-C(28)-C(31)	173.8(5)	C(50)-Si(2)-C(49)-C(48)	141(3)
C(27)-C(28)-C(29)-C(30)	1.8(8)	C(56)-Si(2)-C(49)-C(48)	-79(3)
C(31)-C(28)-C(29)-C(30)	-173.6(5)	C(53)-Si(2)-C(49)-C(48)	24(3)
C(28)-C(29)-C(30)-C(25)	1.1(8)	C(49)-Si(2)-C(50)-C(52)	-22.8(16)
C(26)-C(25)-C(30)-C(29)	-4.1(7)	C(56)-Si(2)-C(50)-C(52)	-150.0(14)
C(4)-C(25)-C(30)-C(29)	170.3(4)	C(53)-Si(2)-C(50)-C(52)	89.8(15)
C(27)-C(28)-C(31)-C(32)	-96(10)	C(49)-Si(2)-C(50)-C(51)	-165.4(8)
C(29)-C(28)-C(31)-C(32)	79(10)	C(56)-Si(2)-C(50)-C(51)	67.4(13)
C(28)-C(31)-C(32)-Si(1)	35(15)	C(53)-Si(2)-C(50)-C(51)	-52.8(10)
C(33)-Si(1)-C(32)-C(31)	74(6)	C(50)-Si(2)-C(53)-C(54)	-169.7(11)
C(36)-Si(1)-C(32)-C(31)	-40(6)	C(49)-Si(2)-C(53)-C(54)	-52.6(12)
C(39)-Si(1)-C(32)-C(31)	-151(6)	C(56)-Si(2)-C(53)-C(54)	53.9(13)
C(32)-Si(1)-C(33)-C(34)	60.4(18)	C(50)-Si(2)-C(53)-C(55)	-52.7(10)
C(36)-Si(1)-C(33)-C(34)	171.6(15)	C(49)-Si(2)-C(53)-C(55)	64.4(10)
C(39)-Si(1)-C(33)-C(34)	-63.9(16)	C(56)-Si(2)-C(53)-C(55)	170.9(11)
C(32)-Si(1)-C(33)-C(35)	156.2(10)	C(50)-Si(2)-C(56)-C(58)	-40(2)
C(36)-Si(1)-C(33)-C(35)	-92.6(13)	C(49)-Si(2)-C(56)-C(58)	-170.0(17)
C(39)-Si(1)-C(33)-C(35)	31.9(15)	C(53)-Si(2)-C(56)-C(58)	83.8(19)
C(32)-Si(1)-C(36)-C(38)	-177.5(11)	C(50)-Si(2)-C(56)-C(57)	52.2(11)
C(33)-Si(1)-C(36)-C(38)	70.3(15)	C(49)-Si(2)-C(56)-C(57)	-77.6(10)
C(39)-Si(1)-C(36)-C(38)	-65.0(14)	C(53)-Si(2)-C(56)-C(57)	176.2(8)
C(32)-Si(1)-C(36)-C(37)	61.2(10)	C(1)-C(6)-C(59)-C(64)	69.7(6)
C(33)-Si(1)-C(36)-C(37)	-50.9(11)	C(5)-C(6)-C(59)-C(64)	-110.4(5)
C(39)-Si(1)-C(36)-C(37)	173.8(9)	C(1)-C(6)-C(59)-C(60)	-113.8(6)
C(32)-Si(1)-C(39)-C(40)	-63.1(12)	C(5)-C(6)-C(59)-C(60)	66.0(6)
C(33)-Si(1)-C(39)-C(40)	60.7(13)	C(64)-C(59)-C(60)-C(61)	3.5(9)
C(36)-Si(1)-C(39)-C(40)	-173.8(11)	C(6)-C(59)-C(60)-C(61)	-173.2(6)
C(32)-Si(1)-C(39)-C(41)	70.0(10)	C(59)-C(60)-C(61)-C(62)	0.2(10)
C(33)-Si(1)-C(39)-C(41)	-166.3(8)	C(60)-C(61)-C(62)-C(63)	-3.6(8)
C(36)-Si(1)-C(39)-C(41)	-40.8(10)	C(60)-C(61)-C(62)-C(65)	173.3(5)
C(4)-C(5)-C(42)-C(47)	-120.7(5)	C(61)-C(62)-C(63)-C(64)	3.4(7)
C(6)-C(5)-C(42)-C(47)	62.0(6)	C(65)-C(62)-C(63)-C(64)	-173.3(4)
C(4)-C(5)-C(42)-C(43)	61.6(6)	C(60)-C(59)-C(64)-C(63)	-3.8(7)
C(6)-C(5)-C(42)-C(43)	-115.7(5)	C(6)-C(59)-C(64)-C(63)	172.7(5)
C(47)-C(42)-C(43)-C(44)	-3.7(7)	C(62)-C(63)-C(64)-C(59)	0.3(7)
C(5)-C(42)-C(43)-C(44)	174.2(4)	C(63)-C(62)-C(65)-C(68)	107.1(5)
C(42)-C(43)-C(44)-C(45)	0.7(7)	C(61)-C(62)-C(65)-C(68)	-69.4(6)
C(43)-C(44)-C(45)-C(46)	2.6(8)	C(63)-C(62)-C(65)-C(66)	-132.9(5)
C(43)-C(44)-C(45)-C(48)	-174.9(5)	C(61)-C(62)-C(65)-C(66)	50.5(6)

C(63)-C(62)-C(65)-C(67)	-11.1(7)	C(61)-C(62)-C(65)-C(67)	172.3(5)

Symmetry transformations used to generate equivalent atoms:

Table C1. Crystal data and structure refinement for **(31)**.

Compound		**(31)**
Empirical formula		$C_{46}H_{40}Br_2N_4$
Formula weight		808.64
Temperature (K)		298(2)
Wavelength (Å)		0.71073
Crystal system		Monoclinic
Space group		P2(1)/c
Unit cell dimensions	a (Å)	13.219(4)
	b (Å)	25.156(7)
	c (Å)	12.258(4)
	α (°)	90
	β (°)	106.442(5)
	γ (°)	90
Volume ($Å^3$)		3910(2)
Z		4
Density (calculated) (Mg/m^3)		1.374
Absorption coefficient (mm^{-1})		2.111
F(000)		1656
Crystal size (mm^3)		0.60 x 0.10 x 0.10
Theta range for data collection (°)		1.61 to 23.34
Index ranges		-14<=h<=14, -27<=k<=27, -13<=l<=13
Reflections collected		31177
Independent reflections		5658 [R(int) = 0.1146]
Completeness to theta = 23.34° (%)		99.6
Absorption correction		Semi-empirical from equivalents
Max. and min. transmission		1.0000 and 0.6102
Refinement method		Full-matrix least-squares on F^2
Data / restraints / parameters		5658 / 0 / 475
Goodness-of-fit on F^2		0.939
R_1 [I>2sigma(I)]		R1 = 0.0458
wR2 (all data)		wR2 = 0.1053
Largest diff. peak and hole		1.042 and -0.511 e.$Å^{-3}$

Table C2. Atomic coordinates (x 10^4) and equivalent isotropic displacement parameters ($Å^2$x 10^3) for **(31)**. U(eq) is defined as one third of the trace of the orthogonalized U^{ij} tensor.

	x	y	z	U(eq)
Br(1)	2991(1)	1446(1)	749(1)	41(1)
Br(2)	7225(1)	2196(1)	5114(1)	34(1)
C(1)	4187(3)	4946(2)	1691(3)	19(1)
C(2)	3292(3)	4758(2)	858(3)	20(1)
C(3)	3108(3)	4207(2)	722(3)	19(1)
C(4)	3819(3)	3851(2)	1432(3)	19(1)

C(5)	4723(3)	4041(2)	2271(3)	20(1)
C(6)	4905(3)	4592(2)	2394(3)	20(1)
C(7)	4369(3)	5533(2)	1837(3)	21(1)
C(8)	5098(3)	5799(2)	1430(3)	26(1)
N(1)	5262(3)	6321(2)	1519(3)	32(1)
C(9)	4673(4)	6576(2)	2062(4)	31(1)
N(2)	3945(3)	6380(1)	2509(3)	28(1)
C(10)	3800(3)	5853(2)	2374(3)	25(1)
C(11)	2524(3)	5143(2)	137(3)	20(1)
C(12)	2820(3)	5529(2)	-521(4)	27(1)
N(3)	2165(3)	5900(2)	-1126(3)	32(1)
C(13)	1182(4)	5867(2)	-1066(4)	34(1)
N(4)	780(3)	5511(2)	-500(3)	34(1)
C(14)	1470(3)	5150(2)	94(4)	26(1)
C(15)	2178(3)	3977(2)	-169(3)	22(1)
C(16)	2086(3)	4023(2)	-1325(4)	24(1)
C(17)	1301(3)	3754(2)	-2120(4)	30(1)
C(18)	579(3)	3423(2)	-1802(4)	27(1)
C(19)	650(3)	3404(2)	-648(4)	30(1)
C(20)	1434(3)	3673(2)	158(4)	28(1)
C(21)	-250(3)	3089(2)	-2656(4)	34(1)
C(22)	-216(4)	3171(2)	-3883(4)	53(2)
C(23)	-1352(3)	3235(2)	-2579(4)	41(1)
C(24)	-30(4)	2500(2)	-2344(5)	55(2)
C(25)	3627(3)	3269(2)	1292(3)	22(1)
C(26)	3774(3)	3007(2)	352(4)	28(1)
C(27)	3589(3)	2467(2)	203(4)	27(1)
C(28)	3230(3)	2189(2)	981(4)	28(1)
C(29)	3074(3)	2434(2)	1932(4)	27(1)
C(30)	3274(3)	2971(2)	2078(4)	26(1)
C(31)	5437(3)	3636(2)	3010(3)	20(1)
C(32)	6022(3)	3290(2)	2542(4)	28(1)
C(33)	6589(3)	2874(2)	3178(4)	26(1)
C(34)	6554(3)	2805(2)	4286(4)	24(1)
C(35)	6025(3)	3154(2)	4785(4)	29(1)
C(36)	5468(3)	3572(2)	4139(4)	25(1)
C(37)	5852(3)	4788(2)	3308(3)	19(1)
C(38)	6874(3)	4628(2)	3381(4)	26(1)
C(39)	7720(3)	4793(2)	4272(4)	28(1)
C(40)	7585(3)	5114(2)	5154(3)	21(1)
C(41)	6565(3)	5268(2)	5076(3)	21(1)
C(42)	5718(3)	5121(2)	4164(3)	22(1)
C(43)	8540(3)	5269(2)	6157(3)	23(1)
C(44)	9343(3)	5590(2)	5710(4)	32(1)
C(45)	8225(3)	5614(2)	7030(4)	32(1)
C(46)	9074(3)	4769(2)	6749(4)	36(1)

Table C3. Bond lengths [Å] and angles [°] for **(31)**.

Br(1)-C(28)	1.904(4)	C(34)-C(35)	1.370(6)
Br(2)-C(34)	1.911(4)	C(35)-C(36)	1.394(6)
C(1)-C(6)	1.403(5)	C(37)-C(38)	1.388(5)
C(1)-C(2)	1.408(5)	C(37)-C(42)	1.394(6)
C(1)-C(7)	1.500(6)	C(38)-C(39)	1.387(6)
C(2)-C(3)	1.409(6)	C(39)-C(40)	1.401(6)
C(2)-C(11)	1.498(6)	C(40)-C(41)	1.381(5)
C(3)-C(4)	1.408(5)	C(40)-C(43)	1.542(6)
C(3)-C(15)	1.510(5)	C(41)-C(42)	1.390(5)
C(4)-C(5)	1.420(5)	C(43)-C(46)	1.523(6)
C(4)-C(25)	1.489(6)	C(43)-C(45)	1.524(6)
C(5)-C(6)	1.408(6)	C(43)-C(44)	1.552(6)
C(5)-C(31)	1.505(6)		
C(6)-C(37)	1.507(5)	C(6)-C(1)-C(2)	121.1(4)
C(7)-C(8)	1.378(6)	C(6)-C(1)-C(7)	119.6(4)
C(7)-C(10)	1.388(6)	C(2)-C(1)-C(7)	119.3(4)
C(8)-N(1)	1.328(5)	C(1)-C(2)-C(3)	119.8(4)
N(1)-C(9)	1.326(6)	C(1)-C(2)-C(11)	120.1(4)
C(9)-N(2)	1.330(5)	C(3)-C(2)-C(11)	120.1(4)
N(2)-C(10)	1.343(5)	C(4)-C(3)-C(2)	119.4(4)
C(11)-C(14)	1.380(6)	C(4)-C(3)-C(15)	117.9(4)
C(11)-C(12)	1.386(6)	C(2)-C(3)-C(15)	122.8(4)
C(12)-N(3)	1.345(5)	C(3)-C(4)-C(5)	120.7(4)
N(3)-C(13)	1.325(5)	C(3)-C(4)-C(25)	119.5(4)
C(13)-N(4)	1.331(6)	C(5)-C(4)-C(25)	119.7(4)
N(4)-C(14)	1.345(5)	C(6)-C(5)-C(4)	119.5(4)
C(15)-C(16)	1.392(5)	C(6)-C(5)-C(31)	122.9(4)
C(15)-C(20)	1.392(6)	C(4)-C(5)-C(31)	117.6(4)
C(16)-C(17)	1.384(6)	C(1)-C(6)-C(5)	119.6(4)
C(17)-C(18)	1.403(6)	C(1)-C(6)-C(37)	121.6(4)
C(18)-C(19)	1.391(6)	C(5)-C(6)-C(37)	118.8(4)
C(18)-C(21)	1.534(6)	C(8)-C(7)-C(10)	114.7(4)
C(19)-C(20)	1.388(6)	C(8)-C(7)-C(1)	122.7(4)
C(21)-C(22)	1.531(7)	C(10)-C(7)-C(1)	122.6(4)
C(21)-C(23)	1.531(6)	N(1)-C(8)-C(7)	124.4(4)
C(21)-C(24)	1.535(7)	C(9)-N(1)-C(8)	114.5(4)
C(25)-C(26)	1.388(6)	N(1)-C(9)-N(2)	128.6(4)
C(25)-C(30)	1.400(6)	C(9)-N(2)-C(10)	114.2(4)
C(26)-C(27)	1.383(6)	N(2)-C(10)-C(7)	123.6(4)
C(27)-C(28)	1.370(6)	C(14)-C(11)-C(12)	114.7(4)
C(28)-C(29)	1.384(6)	C(14)-C(11)-C(2)	122.7(4)
C(29)-C(30)	1.381(6)	C(12)-C(11)-C(2)	122.6(4)
C(31)-C(36)	1.382(6)	N(3)-C(12)-C(11)	124.3(4)
C(31)-C(32)	1.391(6)	C(13)-N(3)-C(12)	114.4(4)
C(32)-C(33)	1.391(6)	N(3)-C(13)-N(4)	127.9(4)
C(33)-C(34)	1.383(6)	C(13)-N(4)-C(14)	115.2(4)

N(4)-C(14)-C(11)	123.4(4)	C(36)-C(31)-C(32)	118.5(4)
C(16)-C(15)-C(20)	118.3(4)	C(36)-C(31)-C(5)	121.2(4)
C(16)-C(15)-C(3)	121.5(4)	C(32)-C(31)-C(5)	120.1(4)
C(20)-C(15)-C(3)	120.0(4)	C(33)-C(32)-C(31)	121.0(4)
C(17)-C(16)-C(15)	120.6(4)	C(34)-C(33)-C(32)	118.8(4)
C(16)-C(17)-C(18)	121.9(4)	C(35)-C(34)-C(33)	121.4(4)
C(19)-C(18)-C(17)	116.6(4)	C(35)-C(34)-Br(2)	119.7(3)
C(19)-C(18)-C(21)	120.3(4)	C(33)-C(34)-Br(2)	118.8(3)
C(17)-C(18)-C(21)	123.1(4)	C(34)-C(35)-C(36)	119.0(4)
C(20)-C(19)-C(18)	121.9(4)	C(31)-C(36)-C(35)	121.2(4)
C(19)-C(20)-C(15)	120.6(4)	C(38)-C(37)-C(42)	117.0(4)
C(22)-C(21)-C(23)	108.7(4)	C(38)-C(37)-C(6)	122.9(4)
C(22)-C(21)-C(18)	112.5(4)	C(42)-C(37)-C(6)	120.0(4)
C(23)-C(21)-C(18)	109.5(4)	C(39)-C(38)-C(37)	121.2(4)
C(22)-C(21)-C(24)	108.6(4)	C(38)-C(39)-C(40)	122.0(4)
C(23)-C(21)-C(24)	109.4(4)	C(41)-C(40)-C(39)	116.3(4)
C(18)-C(21)-C(24)	108.1(4)	C(41)-C(40)-C(43)	123.2(4)
C(26)-C(25)-C(30)	118.1(4)	C(39)-C(40)-C(43)	120.5(4)
C(26)-C(25)-C(4)	120.2(4)	C(40)-C(41)-C(42)	122.0(4)
C(30)-C(25)-C(4)	121.7(4)	C(41)-C(42)-C(37)	121.3(4)
C(27)-C(26)-C(25)	121.0(4)	C(46)-C(43)-C(45)	108.6(4)
C(28)-C(27)-C(26)	119.4(4)	C(46)-C(43)-C(40)	109.6(4)
C(27)-C(28)-C(29)	121.6(4)	C(45)-C(43)-C(40)	112.3(3)
C(27)-C(28)-Br(1)	118.1(3)	C(46)-C(43)-C(44)	109.0(3)
C(29)-C(28)-Br(1)	120.2(3)	C(45)-C(43)-C(44)	107.6(4)
C(30)-C(29)-C(28)	118.4(4)	C(40)-C(43)-C(44)	109.7(3)
C(29)-C(30)-C(25)	121.5(4)		

Symmetry transformations used to generate equivalent atoms:

Table C4. Anisotropic displacement parameters ($Å^2 x\ 10^3$) for **(31)**. The anisotropic displacement factor exponent takes the form: $-2\pi^2[\ h^2a^{*2}U^{11} + ... + 2hka^*b^*U^{12}]$

	U^{11}	U^{22}	U^{33}	U^{23}	U^{13}	U^{12}
Br(1)	57(1)	21(1)	41(1)	-7(1)	9(1)	-7(1)
Br(2)	38(1)	25(1)	29(1)	3(1)	-4(1)	3(1)
C(1)	18(2)	23(3)	17(2)	0(2)	8(2)	0(2)
C(2)	17(2)	24(3)	18(2)	5(2)	3(2)	1(2)
C(3)	15(2)	27(3)	15(2)	1(2)	6(2)	0(2)
C(4)	22(3)	20(3)	18(2)	-2(2)	7(2)	0(2)
C(5)	23(3)	22(3)	15(2)	0(2)	6(2)	2(2)
C(6)	19(2)	27(3)	17(2)	1(2)	8(2)	2(2)
C(7)	15(2)	32(3)	13(2)	2(2)	0(2)	2(2)
C(8)	25(3)	28(3)	26(3)	-3(2)	10(2)	0(2)
N(1)	30(2)	25(2)	38(3)	2(2)	7(2)	-5(2)
C(9)	32(3)	24(3)	31(3)	2(2)	-2(2)	1(2)

N(2)	28(2)	18(2)	35(2)	-3(2)	6(2)	3(2)
C(10)	20(3)	28(3)	26(3)	4(2)	5(2)	2(2)
C(11)	20(2)	20(2)	18(2)	-3(2)	3(2)	-4(2)
C(12)	17(2)	34(3)	25(3)	1(2)	-1(2)	0(2)
N(3)	31(3)	28(2)	29(2)	5(2)	-2(2)	0(2)
C(13)	28(3)	30(3)	34(3)	8(2)	-8(2)	6(2)
N(4)	25(2)	35(3)	35(2)	3(2)	-1(2)	6(2)
C(14)	30(3)	23(3)	24(3)	2(2)	4(2)	-3(2)
C(15)	20(3)	20(3)	25(3)	-4(2)	6(2)	0(2)
C(16)	21(3)	26(3)	24(3)	0(2)	3(2)	-3(2)
C(17)	29(3)	42(3)	16(3)	0(2)	4(2)	1(2)
C(18)	20(3)	28(3)	28(3)	-7(2)	0(2)	-1(2)
C(19)	25(3)	32(3)	33(3)	-3(2)	8(2)	-7(2)
C(20)	26(3)	34(3)	23(3)	-1(2)	7(2)	-2(2)
C(21)	26(3)	41(3)	30(3)	-9(2)	2(2)	-9(2)
C(22)	44(3)	68(4)	40(4)	-17(3)	1(3)	-20(3)
C(23)	28(3)	41(3)	45(3)	-7(3)	-3(2)	-11(2)
C(24)	55(4)	38(4)	60(4)	-18(3)	-4(3)	-12(3)
C(25)	16(2)	31(3)	13(3)	1(2)	-3(2)	1(2)
C(26)	32(3)	32(3)	19(3)	0(2)	7(2)	-5(2)
C(27)	34(3)	27(3)	19(3)	-6(2)	8(2)	1(2)
C(28)	27(3)	25(3)	27(3)	-2(2)	-1(2)	1(2)
C(29)	34(3)	21(3)	24(3)	0(2)	6(2)	-2(2)
C(30)	25(3)	32(3)	17(3)	-3(2)	2(2)	5(2)
C(31)	23(3)	18(2)	19(3)	-4(2)	3(2)	-3(2)
C(32)	32(3)	32(3)	21(3)	5(2)	8(2)	1(2)
C(33)	29(3)	20(3)	28(3)	0(2)	6(2)	5(2)
C(34)	25(3)	17(3)	24(3)	3(2)	0(2)	3(2)
C(35)	30(3)	34(3)	18(3)	2(2)	0(2)	0(2)
C(36)	29(3)	19(3)	27(3)	-4(2)	5(2)	2(2)
C(37)	20(2)	20(3)	15(2)	4(2)	3(2)	0(2)
C(38)	22(3)	32(3)	24(3)	-5(2)	6(2)	-1(2)
C(39)	15(2)	41(3)	27(3)	0(2)	5(2)	2(2)
C(40)	21(2)	23(3)	17(3)	2(2)	4(2)	1(2)
C(41)	26(3)	17(2)	19(3)	0(2)	7(2)	-6(2)
C(42)	14(2)	25(3)	26(3)	6(2)	3(2)	1(2)
C(43)	16(2)	30(3)	22(3)	-1(2)	2(2)	-1(2)
C(44)	20(3)	40(3)	35(3)	-5(2)	4(2)	-4(2)
C(45)	24(3)	44(3)	23(3)	-5(2)	1(2)	-1(2)
C(46)	32(3)	40(3)	32(3)	-2(2)	0(2)	-2(2)

Table C5. Hydrogen coordinates (x 10^4) and isotropic displacement parameters ($Å^2$x 10^3) for **(31)**.

	x	y	z	U(eq)
H(8)	5503	5601	1070	31
H(9)	4782	6941	2139	38
H(10)	3291	5694	2655	30
H(12)	3517	5530	-545	32
H(13)	716	6123	-1467	41
H(14)	1223	4891	497	31
H(16)	2557	4237	-1564	29
H(17)	1250	3794	-2888	36
H(19)	160	3204	-410	36
H(20)	1461	3650	923	33
H(22A)	-351	3538	-4088	79
H(22B)	-744	2953	-4384	79
H(22C)	468	3074	-3945	79
H(23A)	-1385	3181	-1815	61
H(23B)	-1867	3014	-3089	61
H(23C)	-1494	3601	-2786	61
H(24A)	662	2409	-2389	83
H(24B)	-545	2284	-2865	83
H(24C)	-71	2441	-1584	83
H(26)	4002	3197	-185	33
H(27)	3706	2294	-421	32
H(29)	2840	2240	2460	32
H(30)	3171	3140	2714	31
H(32)	6034	3338	1794	34
H(33)	6984	2645	2863	32
H(35)	6037	3113	5543	35
H(36)	5110	3812	4474	31
H(38)	6994	4407	2823	31
H(39)	8397	4687	4284	34
H(41)	6440	5477	5651	25
H(42)	5047	5248	4124	26
H(44A)	9501	5398	5102	49
H(44B)	9979	5641	6316	49
H(44C)	9046	5930	5437	49
H(45A)	7947	5946	6687	48
H(45B)	8833	5680	7663	48
H(45C)	7697	5434	7291	48
H(46A)	8586	4572	7042	54
H(46B)	9677	4866	7363	54
H(46C)	9297	4553	6214	54

Table C6. Torsion angles [°] for **(31)**.

C(6)-C(1)-C(2)-C(3)	0.1(6)	C(12)-C(11)-C(14)-N(4)	-2.4(6)
C(7)-C(1)-C(2)-C(3)	-179.3(4)	C(2)-C(11)-C(14)-N(4)	176.3(4)
C(6)-C(1)-C(2)-C(11)	178.5(4)	C(4)-C(3)-C(15)-C(16)	-112.5(4)
C(7)-C(1)-C(2)-C(11)	-0.9(6)	C(2)-C(3)-C(15)-C(16)	66.8(6)
C(1)-C(2)-C(3)-C(4)	0.6(6)	C(4)-C(3)-C(15)-C(20)	62.1(5)
C(11)-C(2)-C(3)-C(4)	-177.9(4)	C(2)-C(3)-C(15)-C(20)	-118.6(5)
C(1)-C(2)-C(3)-C(15)	-178.7(4)	C(20)-C(15)-C(16)-C(17)	-2.8(6)
C(11)-C(2)-C(3)-C(15)	2.9(6)	C(3)-C(15)-C(16)-C(17)	171.9(4)
C(2)-C(3)-C(4)-C(5)	-0.7(6)	C(15)-C(16)-C(17)-C(18)	-0.7(7)
C(15)-C(3)-C(4)-C(5)	178.6(4)	C(16)-C(17)-C(18)-C(19)	3.8(6)
C(2)-C(3)-C(4)-C(25)	180.0(4)	C(16)-C(17)-C(18)-C(21)	-175.5(4)
C(15)-C(3)-C(4)-C(25)	-0.7(6)	C(17)-C(18)-C(19)-C(20)	-3.7(6)
C(3)-C(4)-C(5)-C(6)	0.3(6)	C(21)-C(18)-C(19)-C(20)	175.7(4)
C(25)-C(4)-C(5)-C(6)	179.6(4)	C(18)-C(19)-C(20)-C(15)	0.3(7)
C(3)-C(4)-C(5)-C(31)	179.0(4)	C(16)-C(15)-C(20)-C(19)	3.0(6)
C(25)-C(4)-C(5)-C(31)	-1.7(6)	C(3)-C(15)-C(20)-C(19)	-171.8(4)
C(2)-C(1)-C(6)-C(5)	-0.5(6)	C(19)-C(18)-C(21)-C(22)	179.0(4)
C(7)-C(1)-C(6)-C(5)	178.8(4)	C(17)-C(18)-C(21)-C(22)	-1.7(6)
C(2)-C(1)-C(6)-C(37)	-178.6(4)	C(19)-C(18)-C(21)-C(23)	58.1(6)
C(7)-C(1)-C(6)-C(37)	0.8(6)	C(17)-C(18)-C(21)-C(23)	-122.7(5)
C(4)-C(5)-C(6)-C(1)	0.4(6)	C(19)-C(18)-C(21)-C(24)	-61.1(5)
C(31)-C(5)-C(6)-C(1)	-178.3(4)	C(17)-C(18)-C(21)-C(24)	118.2(5)
C(4)-C(5)-C(6)-C(37)	178.4(4)	C(3)-C(4)-C(25)-C(26)	72.0(5)
C(31)-C(5)-C(6)-C(37)	-0.2(6)	C(5)-C(4)-C(25)-C(26)	-107.3(5)
C(6)-C(1)-C(7)-C(8)	77.5(5)	C(3)-C(4)-C(25)-C(30)	-106.6(5)
C(2)-C(1)-C(7)-C(8)	-103.1(5)	C(5)-C(4)-C(25)-C(30)	74.0(5)
C(6)-C(1)-C(7)-C(10)	-103.7(5)	C(30)-C(25)-C(26)-C(27)	-0.6(6)
C(2)-C(1)-C(7)-C(10)	75.7(5)	C(4)-C(25)-C(26)-C(27)	-179.3(4)
C(10)-C(7)-C(8)-N(1)	-0.6(6)	C(25)-C(26)-C(27)-C(28)	1.5(6)
C(1)-C(7)-C(8)-N(1)	178.3(4)	C(26)-C(27)-C(28)-C(29)	-1.6(7)
C(7)-C(8)-N(1)-C(9)	1.3(6)	C(26)-C(27)-C(28)-Br(1)	-179.7(3)
C(8)-N(1)-C(9)-N(2)	-0.7(7)	C(27)-C(28)-C(29)-C(30)	0.9(6)
N(1)-C(9)-N(2)-C(10)	-0.5(6)	Br(1)-C(28)-C(29)-C(30)	178.9(3)
C(9)-N(2)-C(10)-C(7)	1.3(6)	C(28)-C(29)-C(30)-C(25)	-0.1(6)
C(8)-C(7)-C(10)-N(2)	-0.8(6)	C(26)-C(25)-C(30)-C(29)	-0.1(6)
C(1)-C(7)-C(10)-N(2)	-179.7(4)	C(4)-C(25)-C(30)-C(29)	178.6(4)
C(1)-C(2)-C(11)-C(14)	-121.9(4)	C(6)-C(5)-C(31)-C(36)	71.3(6)
C(3)-C(2)-C(11)-C(14)	56.5(6)	C(4)-C(5)-C(31)-C(36)	-107.3(5)
C(1)-C(2)-C(11)-C(12)	56.7(6)	C(6)-C(5)-C(31)-C(32)	-113.5(5)
C(3)-C(2)-C(11)-C(12)	-124.9(4)	C(4)-C(5)-C(31)-C(32)	67.8(5)
C(14)-C(11)-C(12)-N(3)	2.7(6)	C(36)-C(31)-C(32)-C(33)	2.9(6)
C(2)-C(11)-C(12)-N(3)	-176.0(4)	C(5)-C(31)-C(32)-C(33)	-172.4(4)
C(11)-C(12)-N(3)-C(13)	-1.2(6)	C(31)-C(32)-C(33)-C(34)	0.6(6)
C(12)-N(3)-C(13)-N(4)	-1.0(7)	C(32)-C(33)-C(34)-C(35)	-3.7(6)
N(3)-C(13)-N(4)-C(14)	1.3(7)	C(32)-C(33)-C(34)-Br(2)	174.3(3)
C(13)-N(4)-C(14)-C(11)	0.6(6)	C(33)-C(34)-C(35)-C(36)	3.2(6)

Br(2)-C(34)-C(35)-C(36)	-174.8(3)	C(38)-C(39)-C(40)-C(43)	177.3(4)
C(32)-C(31)-C(36)-C(35)	-3.4(6)	C(39)-C(40)-C(41)-C(42)	-1.1(6)
C(5)-C(31)-C(36)-C(35)	171.8(4)	C(43)-C(40)-C(41)-C(42)	-179.8(4)
C(34)-C(35)-C(36)-C(31)	0.4(6)	C(40)-C(41)-C(42)-C(37)	3.2(6)
C(1)-C(6)-C(37)-C(38)	-125.5(5)	C(38)-C(37)-C(42)-C(41)	-2.7(6)
C(5)-C(6)-C(37)-C(38)	56.5(6)	C(6)-C(37)-C(42)-C(41)	173.9(4)
C(1)-C(6)-C(37)-C(42)	58.1(6)	C(41)-C(40)-C(43)-C(46)	120.0(4)
C(5)-C(6)-C(37)-C(42)	-119.9(4)	C(39)-C(40)-C(43)-C(46)	-58.6(5)
C(42)-C(37)-C(38)-C(39)	0.3(6)	C(41)-C(40)-C(43)-C(45)	-0.7(6)
C(6)-C(37)-C(38)-C(39)	-176.3(4)	C(39)-C(40)-C(43)-C(45)	-179.4(4)
C(37)-C(38)-C(39)-C(40)	1.8(7)	C(41)-C(40)-C(43)-C(44)	-120.3(4)
C(38)-C(39)-C(40)-C(41)	-1.4(6)	C(39)-C(40)-C(43)-C(44)	61.1(5)

Symmetry transformations used to generate equivalent atoms:

Table D1. Crystal data and structure refinement for **(24)**.

Compound		**(24)**
Empirical formula		$C_{95}H_{90}Cl_2N_8O_6$
Formula weight		1502.59
Temperature (K)		298(2)
Wavelength (Å)		0.71073
Crystal system		Triclinic
Space group		P-1
Unit cell dimensions	a (Å)	14.670(4)
	b (Å)	15.583(4)
	c (Å)	22.191(5)
	α (°)	72.098(5)
	β (°)	83.945(6)
	γ (°)	61.999(4)
Volume ($Å^3$)		4257.8(18)
Z		2
Density (calculated) (Mg/m^3)		1.172
Absorption coefficient (mm^{-1})		0.134
F(000)		1580
Crystal size (mm^3)		0.4 x 0.2 x 0.2
Theta range for data collection (°)		1.57 to 23.36
Index ranges		-16<=h<=16, -17<=k<=17, -24<=l<=24
Reflections collected		34980
Independent reflections		12237 [R(int) = 0.3789]
Completeness to theta = 23.36° (%)		98.8
Absorption correction		None
Refinement method		Full-matrix least-squares on F^2
Data / restraints / parameters		12237 / 0 / 997
Goodness-of-fit on F^2		0.990
R_1 [I>2sigma(I)]		R1 = 0.1596
wR2 (all data)		wR2 = 0.4683
Largest diff. peak and hole		1.088 and -0.428 $e.Å^{-3}$

Table D2. Atomic coordinates (x 10^4) and equivalent isotropic displacement parameters ($Å^2$x 10^3) for **(24)**. U(eq) is defined as one third of the trace of the orthogonalized U^{ij} tensor.

	x	y	z	U(eq)
O(1)	2944(7)	7266(5)	7642(4)	111(3)
O(2)	4827(7)	3853(6)	10661(4)	91(2)
O(3)	9865(6)	8504(5)	8145(3)	85(2)
O(4)	9530(8)	4173(6)	10111(4)	113(3)
O(5)	5740(6)	7204(5)	7032(3)	85(2)
O(6)	4117(11)	1322(8)	2600(6)	185(5)

Cl(1)	5248(9)	1004(7)	5128(7)	374(7)
Cl(2)	6076(12)	1182(11)	6206(6)	506(12)
C(1)	2706(7)	2006(6)	8404(5)	51(3)
C(2)	2584(8)	2816(6)	7834(4)	53(3)
C(3)	2805(7)	3594(6)	7870(4)	53(3)
C(4)	3020(7)	3605(6)	8449(4)	50(2)
C(5)	3156(7)	2779(6)	9015(4)	51(2)
C(6)	2933(7)	2020(6)	8982(5)	51(2)
C(7)	2601(8)	1136(6)	8326(4)	54(3)
C(8)	1733(11)	1061(8)	8360(6)	103(4)
N(1)	1585(9)	318(8)	8244(5)	96(3)
C(9)	2480(14)	-405(9)	8130(5)	89(4)
N(2)	3361(9)	-442(7)	8103(5)	93(3)
C(10)	3427(10)	314(8)	8206(6)	86(4)
C(11)	2297(9)	2818(7)	7221(5)	61(3)
C(12)	1312(11)	3403(9)	6968(6)	78(3)
N(3)	1041(10)	3408(9)	6416(6)	98(3)
C(13)	1773(14)	2836(11)	6106(8)	99(5)
N(4)	2710(12)	2263(9)	6279(5)	98(4)
C(14)	2968(10)	2264(8)	6830(6)	83(3)
C(15)	2822(8)	4368(6)	7281(4)	55(3)
C(16)	2010(8)	5358(7)	7050(4)	63(3)
C(17)	2148(8)	6050(7)	6545(5)	64(3)
C(18)	3063(9)	5801(7)	6225(5)	62(3)
C(19)	3834(9)	4837(7)	6413(5)	66(3)
C(20)	3752(8)	4105(7)	6942(5)	63(3)
C(21)	3203(11)	6607(8)	5668(5)	86(4)
C(22)	2144(15)	7497(12)	5417(9)	232(12)
C(23)	3910(20)	6139(13)	5203(9)	241(14)
C(24)	3841(17)	6966(13)	5947(7)	199(10)
C(25)	3313(7)	4358(6)	8608(4)	51(2)
C(26)	2328(8)	5324(7)	8607(5)	66(3)
C(27)	2239(8)	6258(7)	8280(5)	71(3)
C(28)	3007(9)	6415(7)	7922(5)	70(3)
C(29)	3968(9)	5498(7)	7883(5)	72(3)
C(30)	4103(8)	4555(7)	8213(4)	66(3)
C(31)	3549(8)	2941(6)	9531(5)	57(3)
C(32)	3679(8)	3790(7)	9305(4)	57(3)
C(33)	4092(8)	4115(8)	9674(5)	68(3)
C(34)	4433(10)	3491(9)	10304(6)	87(4)
C(35)	4285(9)	2650(8)	10522(5)	81(3)
C(36)	3870(8)	2331(7)	10155(5)	60(3)
C(37)	5105(10)	3238(9)	11284(6)	105(4)
C(38)	2946(8)	1239(6)	9568(4)	53(3)
C(39)	2167(9)	1499(8)	9994(5)	82(3)
C(40)	2206(9)	832(7)	10599(5)	78(3)
C(41)	3077(9)	-112(6)	10780(5)	66(3)
C(42)	3833(9)	-387(6)	10346(4)	69(3)

C(43)	3758(8)	279(6)	9775(4)	59(3)
C(44)	3149(12)	-812(8)	11481(5)	98(4)
C(45)	2949(18)	-247(12)	11945(7)	186(9)
C(46)	4075(17)	-1797(12)	11570(6)	282(18)
C(47)	2201(15)	-963(13)	11601(9)	200(10)
C(48)	8096(8)	4912(6)	7004(5)	59(3)
C(49)	8184(8)	5602(7)	6444(5)	64(3)
C(50)	8539(8)	6309(7)	6459(5)	58(3)
C(51)	8719(7)	6330(6)	7055(5)	52(3)
C(52)	8677(7)	5624(6)	7605(4)	51(3)
C(53)	8342(7)	4921(6)	7592(5)	56(3)
C(54)	7748(9)	4203(8)	6958(4)	61(3)
C(55)	6817(12)	4390(10)	7009(7)	126(6)
N(5)	6453(11)	3735(10)	6889(6)	142(4)
C(56)	7169(12)	2948(10)	6768(6)	109(4)
N(6)	8122(12)	2642(10)	6736(6)	138(4)
C(57)	8432(12)	3299(11)	6825(9)	145(7)
C(58)	7959(9)	5569(7)	5816(5)	55(3)
C(59)	6965(12)	6115(9)	5553(6)	90(4)
N(7)	6677(10)	6126(9)	5019(6)	106(4)
C(60)	7408(18)	5567(12)	4732(7)	111(6)
N(8)	8417(13)	4971(9)	4916(6)	120(4)
C(61)	8641(11)	5044(9)	5457(6)	97(4)
C(62)	8578(9)	7048(7)	5866(4)	59(3)
C(63)	7747(10)	7961(8)	5619(5)	81(3)
C(64)	7863(10)	8634(8)	5086(6)	93(4)
C(65)	8760(10)	8460(8)	4786(5)	72(3)
C(66)	9542(9)	7543(7)	5042(5)	70(3)
C(67)	9470(9)	6848(7)	5562(5)	66(3)
C(68)	8861(12)	9261(9)	4199(6)	96(4)
C(69)	7804(16)	10062(12)	3863(7)	174(8)
C(70)	9460(20)	8773(13)	3696(7)	268(17)
C(71)	9354(19)	9759(15)	4441(9)	228(12)
C(72)	9030(8)	6998(7)	7241(5)	62(3)
C(73)	9198(9)	7820(7)	6854(5)	76(3)
C(74)	9462(9)	8337(7)	7155(5)	73(3)
C(75)	9594(9)	8033(7)	7813(6)	75(3)
C(76)	9434(9)	7235(7)	8195(6)	78(3)
C(77)	9141(8)	6733(7)	7879(5)	62(3)
C(78)	10206(10)	9199(8)	7807(6)	103(4)
C(79)	8967(8)	5795(6)	8187(4)	53(3)
C(80)	8187(7)	5996(7)	8688(6)	64(3)
C(81)	8353(10)	5483(9)	9313(6)	71(3)
C(82)	9363(12)	4677(9)	9536(5)	78(4)
C(83)	10194(9)	4413(7)	9125(6)	75(3)
C(84)	10012(8)	4901(7)	8491(5)	63(3)
C(85)	8274(8)	4186(7)	8199(4)	50(2)
C(86)	7405(10)	4368(8)	8491(6)	95(4)

C(87)	7358(9)	3737(8)	9080(5)	82(4)
C(88)	8168(9)	2857(7)	9362(5)	60(3)
C(89)	9017(10)	2643(8)	9040(6)	100(4)
C(90)	9082(9)	3299(8)	8473(5)	88(4)
C(91)	8162(11)	2158(8)	10026(5)	84(4)
C(92)	7267(14)	1914(13)	10056(6)	164(8)
C(93)	7920(20)	2732(14)	10479(6)	230(13)
C(94)	9027(18)	1200(14)	10167(9)	360(30)
C(95)	5090(20)	1601(15)	5728(11)	189(9)

Table D3. Bond lengths [Å] and angles [°] for **(24)**.

O(1)-C(28)	1.242(10)	C(16)-C(17)	1.369(12)
O(2)-C(37)	1.391(12)	C(17)-C(18)	1.392(13)
O(2)-C(34)	1.398(13)	C(18)-C(19)	1.352(13)
O(3)-C(75)	1.382(12)	C(18)-C(21)	1.543(13)
O(3)-C(78)	1.384(11)	C(19)-C(20)	1.403(12)
O(4)-C(82)	1.256(11)	C(21)-C(23)	1.481(19)
Cl(1)-C(95)	1.78(2)	C(21)-C(22)	1.53(2)
Cl(2)-C(95)	1.63(3)	C(21)-C(24)	1.550(18)
C(1)-C(6)	1.368(12)	C(25)-C(30)	1.469(13)
C(1)-C(2)	1.441(11)	C(25)-C(26)	1.520(12)
C(1)-C(7)	1.496(12)	C(25)-C(32)	1.534(12)
C(2)-C(3)	1.420(11)	C(26)-C(27)	1.362(12)
C(2)-C(11)	1.465(13)	C(27)-C(28)	1.383(14)
C(3)-C(4)	1.363(11)	C(28)-C(29)	1.482(14)
C(3)-C(15)	1.488(11)	C(29)-C(30)	1.354(12)
C(4)-C(5)	1.445(11)	C(31)-C(32)	1.359(11)
C(4)-C(25)	1.564(11)	C(31)-C(36)	1.397(12)
C(5)-C(6)	1.390(11)	C(32)-C(33)	1.393(13)
C(5)-C(31)	1.471(12)	C(33)-C(34)	1.416(14)
C(6)-C(38)	1.477(12)	C(34)-C(35)	1.362(14)
C(7)-C(8)	1.324(15)	C(35)-C(36)	1.386(14)
C(7)-C(10)	1.366(13)	C(38)-C(43)	1.374(12)
C(8)-N(1)	1.372(14)	C(38)-C(39)	1.393(13)
N(1)-C(9)	1.332(16)	C(39)-C(40)	1.410(13)
C(9)-N(2)	1.263(16)	C(40)-C(41)	1.392(13)
N(2)-C(10)	1.313(12)	C(41)-C(42)	1.388(13)
C(11)-C(12)	1.361(15)	C(41)-C(44)	1.582(14)
C(11)-C(14)	1.395(14)	C(42)-C(43)	1.343(11)
C(12)-N(3)	1.323(14)	C(44)-C(46)	1.467(17)
N(3)-C(13)	1.320(17)	C(44)-C(45)	1.474(18)
C(13)-N(4)	1.257(16)	C(44)-C(47)	1.50(2)
N(4)-C(14)	1.320(14)	C(48)-C(53)	1.395(12)
C(15)-C(16)	1.406(12)	C(48)-C(49)	1.411(12)
C(15)-C(20)	1.430(13)	C(48)-C(54)	1.451(13)

C(49)-C(50)	1.432(12)	C(88)-C(89)	1.319(14)
C(49)-C(58)	1.489(13)	C(88)-C(91)	1.543(13)
C(50)-C(51)	1.387(12)	C(89)-C(90)	1.384(13)
C(50)-C(62)	1.475(12)	C(91)-C(94)	1.398(18)
C(51)-C(52)	1.388(11)	C(91)-C(93)	1.455(17)
C(51)-C(72)	1.489(12)	C(91)-C(92)	1.520(18)
C(52)-C(53)	1.403(11)		
C(52)-C(79)	1.535(12)	C(37)-O(2)-C(34)	113.2(10)
C(53)-C(85)	1.507(12)	C(75)-O(3)-C(78)	118.0(9)
C(54)-C(55)	1.255(16)	C(6)-C(1)-C(2)	121.8(8)
C(54)-C(57)	1.394(16)	C(6)-C(1)-C(7)	121.8(7)
C(55)-N(5)	1.452(16)	C(2)-C(1)-C(7)	116.3(9)
N(5)-C(56)	1.270(16)	C(3)-C(2)-C(1)	118.5(9)
C(56)-N(6)	1.250(16)	C(3)-C(2)-C(11)	119.9(8)
N(6)-C(57)	1.368(15)	C(1)-C(2)-C(11)	121.5(7)
C(58)-C(61)	1.330(14)	C(4)-C(3)-C(2)	118.8(8)
C(58)-C(59)	1.377(15)	C(4)-C(3)-C(15)	121.0(8)
C(59)-N(7)	1.294(15)	C(2)-C(3)-C(15)	120.2(9)
N(7)-C(60)	1.28(2)	C(3)-C(4)-C(5)	121.6(7)
C(60)-N(8)	1.350(19)	C(3)-C(4)-C(25)	128.3(8)
N(8)-C(61)	1.328(15)	C(5)-C(4)-C(25)	109.5(8)
C(62)-C(67)	1.351(13)	C(6)-C(5)-C(4)	119.2(8)
C(62)-C(63)	1.358(14)	C(6)-C(5)-C(31)	133.0(8)
C(63)-C(64)	1.374(13)	C(4)-C(5)-C(31)	107.8(7)
C(64)-C(65)	1.358(15)	C(1)-C(6)-C(5)	119.2(8)
C(65)-C(66)	1.334(14)	C(1)-C(6)-C(38)	120.8(8)
C(65)-C(68)	1.552(14)	C(5)-C(6)-C(38)	120.0(9)
C(66)-C(67)	1.352(12)	C(8)-C(7)-C(10)	112.4(9)
C(68)-C(70)	1.509(18)	C(8)-C(7)-C(1)	125.8(10)
C(68)-C(71)	1.51(2)	C(10)-C(7)-C(1)	121.9(9)
C(68)-C(69)	1.54(2)	C(7)-C(8)-N(1)	127.7(11)
C(72)-C(77)	1.353(12)	C(9)-N(1)-C(8)	110.4(10)
C(72)-C(73)	1.419(12)	N(2)-C(9)-N(1)	128.1(11)
C(73)-C(74)	1.386(13)	C(9)-N(2)-C(10)	117.4(11)
C(74)-C(75)	1.393(13)	N(2)-C(10)-C(7)	123.9(11)
C(75)-C(76)	1.380(12)	C(12)-C(11)-C(14)	112.8(12)
C(76)-C(77)	1.415(13)	C(12)-C(11)-C(2)	121.6(10)
C(77)-C(79)	1.539(11)	C(14)-C(11)-C(2)	125.7(11)
C(79)-C(80)	1.501(13)	N(3)-C(12)-C(11)	122.2(12)
C(79)-C(84)	1.542(14)	C(13)-N(3)-C(12)	117.3(12)
C(80)-C(81)	1.352(13)	N(4)-C(13)-N(3)	127.5(15)
C(81)-C(82)	1.429(16)	C(13)-N(4)-C(14)	114.5(13)
C(82)-C(83)	1.418(15)	N(4)-C(14)-C(11)	125.7(12)
C(83)-C(84)	1.364(13)	C(16)-C(15)-C(20)	117.4(8)
C(85)-C(86)	1.313(13)	C(16)-C(15)-C(3)	124.9(9)
C(85)-C(90)	1.335(13)	C(20)-C(15)-C(3)	117.6(8)
C(86)-C(87)	1.391(13)	C(17)-C(16)-C(15)	120.2(10)
C(87)-C(88)	1.335(13)	C(16)-C(17)-C(18)	122.2(9)

C(19)-C(18)-C(17)	118.7(9)	C(45)-C(44)-C(47)	95.9(14)
C(19)-C(18)-C(21)	120.4(11)	C(46)-C(44)-C(41)	109.6(10)
C(17)-C(18)-C(21)	120.9(10)	C(45)-C(44)-C(41)	111.1(10)
C(18)-C(19)-C(20)	121.6(10)	C(47)-C(44)-C(41)	109.6(13)
C(19)-C(20)-C(15)	119.6(9)	C(53)-C(48)-C(49)	119.8(8)
C(23)-C(21)-C(22)	117.5(15)	C(53)-C(48)-C(54)	121.0(8)
C(23)-C(21)-C(18)	111.4(10)	C(49)-C(48)-C(54)	119.2(9)
C(22)-C(21)-C(18)	109.3(11)	C(48)-C(49)-C(50)	121.7(10)
C(23)-C(21)-C(24)	102.0(15)	C(48)-C(49)-C(58)	119.9(8)
C(22)-C(21)-C(24)	109.9(13)	C(50)-C(49)-C(58)	118.3(8)
C(18)-C(21)-C(24)	105.8(9)	C(51)-C(50)-C(49)	116.4(8)
C(30)-C(25)-C(26)	112.9(8)	C(51)-C(50)-C(62)	123.1(8)
C(30)-C(25)-C(32)	113.1(8)	C(49)-C(50)-C(62)	120.1(9)
C(26)-C(25)-C(32)	106.3(7)	C(50)-C(51)-C(52)	121.9(8)
C(30)-C(25)-C(4)	115.0(7)	C(50)-C(51)-C(72)	130.4(8)
C(26)-C(25)-C(4)	108.6(8)	C(52)-C(51)-C(72)	107.7(8)
C(32)-C(25)-C(4)	99.8(7)	C(51)-C(52)-C(53)	121.5(9)
C(27)-C(26)-C(25)	121.4(9)	C(51)-C(52)-C(79)	110.3(7)
C(26)-C(27)-C(28)	124.1(10)	C(53)-C(52)-C(79)	128.0(8)
O(1)-C(28)-C(27)	124.3(10)	C(48)-C(53)-C(52)	118.3(8)
O(1)-C(28)-C(29)	118.8(10)	C(48)-C(53)-C(85)	121.4(8)
C(27)-C(28)-C(29)	116.9(8)	C(52)-C(53)-C(85)	120.3(9)
C(30)-C(29)-C(28)	121.0(9)	C(55)-C(54)-C(57)	117.0(11)
C(29)-C(30)-C(25)	123.6(10)	C(55)-C(54)-C(48)	121.9(11)
C(32)-C(31)-C(36)	119.8(9)	C(57)-C(54)-C(48)	121.0(10)
C(32)-C(31)-C(5)	109.6(8)	C(54)-C(55)-N(5)	121.6(15)
C(36)-C(31)-C(5)	130.4(8)	C(56)-N(5)-C(55)	113.5(15)
C(31)-C(32)-C(33)	123.2(9)	N(6)-C(56)-N(5)	131.4(16)
C(31)-C(32)-C(25)	113.2(8)	C(56)-N(6)-C(57)	113.4(14)
C(33)-C(32)-C(25)	123.6(8)	N(6)-C(57)-C(54)	122.8(13)
C(32)-C(33)-C(34)	117.2(10)	C(61)-C(58)-C(59)	113.5(11)
C(35)-C(34)-O(2)	125.9(12)	C(61)-C(58)-C(49)	126.2(11)
C(35)-C(34)-C(33)	118.5(11)	C(59)-C(58)-C(49)	120.2(11)
O(2)-C(34)-C(33)	115.5(10)	N(7)-C(59)-C(58)	125.6(13)
C(34)-C(35)-C(36)	124.1(11)	C(60)-N(7)-C(59)	114.1(14)
C(35)-C(36)-C(31)	117.1(9)	N(7)-C(60)-N(8)	129.0(14)
C(43)-C(38)-C(39)	115.3(8)	C(61)-N(8)-C(60)	112.2(13)
C(43)-C(38)-C(6)	124.2(9)	N(8)-C(61)-C(58)	125.4(13)
C(39)-C(38)-C(6)	119.9(8)	C(67)-C(62)-C(63)	117.5(9)
C(38)-C(39)-C(40)	122.7(10)	C(67)-C(62)-C(50)	120.3(10)
C(41)-C(40)-C(39)	118.1(10)	C(63)-C(62)-C(50)	122.2(10)
C(42)-C(41)-C(40)	119.0(9)	C(62)-C(63)-C(64)	118.7(11)
C(42)-C(41)-C(44)	123.6(9)	C(65)-C(64)-C(63)	124.7(11)
C(40)-C(41)-C(44)	117.4(10)	C(66)-C(65)-C(64)	113.9(9)
C(43)-C(42)-C(41)	120.3(9)	C(66)-C(65)-C(68)	123.4(12)
C(42)-C(43)-C(38)	124.4(9)	C(64)-C(65)-C(68)	122.7(11)
C(46)-C(44)-C(45)	119.5(15)	C(65)-C(66)-C(67)	124.0(11)
C(46)-C(44)-C(47)	110.0(15)	C(62)-C(67)-C(66)	121.3(10)

C(70)-C(68)-C(71)	114.1(16)	C(81)-C(80)-C(79)	126.3(9)
C(70)-C(68)-C(69)	103.5(15)	C(80)-C(81)-C(82)	118.5(10)
C(71)-C(68)-C(69)	110.4(13)	O(4)-C(82)-C(83)	118.1(13)
C(70)-C(68)-C(65)	110.8(10)	O(4)-C(82)-C(81)	119.7(12)
C(71)-C(68)-C(65)	106.3(11)	C(83)-C(82)-C(81)	122.2(10)
C(69)-C(68)-C(65)	111.9(12)	C(84)-C(83)-C(82)	119.1(11)
C(77)-C(72)-C(73)	120.2(9)	C(83)-C(84)-C(79)	124.2(9)
C(77)-C(72)-C(51)	110.2(8)	C(86)-C(85)-C(90)	115.3(9)
C(73)-C(72)-C(51)	129.5(9)	C(86)-C(85)-C(53)	122.0(10)
C(74)-C(73)-C(72)	117.7(9)	C(90)-C(85)-C(53)	122.7(9)
C(73)-C(74)-C(75)	120.9(9)	C(85)-C(86)-C(87)	122.1(11)
O(3)-C(75)-C(76)	113.7(10)	C(88)-C(87)-C(86)	122.5(10)
O(3)-C(75)-C(74)	124.2(9)	C(89)-C(88)-C(87)	114.6(9)
C(76)-C(75)-C(74)	122.1(10)	C(89)-C(88)-C(91)	121.2(11)
C(75)-C(76)-C(77)	116.1(10)	C(87)-C(88)-C(91)	124.2(10)
C(72)-C(77)-C(76)	123.0(8)	C(88)-C(89)-C(90)	122.9(10)
C(72)-C(77)-C(79)	110.2(8)	C(85)-C(90)-C(89)	122.1(10)
C(76)-C(77)-C(79)	126.7(9)	C(94)-C(91)-C(93)	117.5(18)
C(80)-C(79)-C(52)	117.4(8)	C(94)-C(91)-C(92)	103.2(16)
C(80)-C(79)-C(77)	110.1(7)	C(93)-C(91)-C(92)	104.1(14)
C(52)-C(79)-C(77)	101.4(7)	C(94)-C(91)-C(88)	113.2(11)
C(80)-C(79)-C(84)	109.7(8)	C(93)-C(91)-C(88)	108.2(9)
C(52)-C(79)-C(84)	109.9(7)	C(92)-C(91)-C(88)	109.9(11)
C(77)-C(79)-C(84)	107.6(7)	Cl(2)-C(95)-Cl(1)	118.4(16)

Symmetry transformations used to generate equivalent atoms:

Table D4. Anisotropic displacement parameters ($Å^2 x\ 10^3$) for **(24)**. The anisotropic displacement factor exponent takes the form: $-2\pi^2[h^2a^{*2}U^{11} + ... + 2hka^*b^*U^{12}]$

	U^{11}	U^{22}	U^{33}	U^{23}	U^{13}	U^{12}
O(1)	127(8)	56(5)	139(7)	-11(5)	9(6)	-45(5)
O(2)	101(7)	90(5)	84(6)	-33(5)	-24(5)	-37(5)
O(3)	132(7)	75(5)	89(5)	-33(4)	5(5)	-76(5)
O(4)	162(9)	128(7)	71(6)	-4(5)	5(6)	-99(7)
O(5)	85(6)	94(5)	84(5)	-60(4)	51(4)	-35(4)
O(6)	233(14)	124(8)	212(12)	-68(8)	86(11)	-96(9)
Cl(1)	330(14)	267(9)	562(18)	-225(11)	170(13)	-134(9)
Cl(2)	590(20)	600(20)	349(15)	174(15)	-228(16)	-430(20)
C(1)	47(6)	32(5)	64(7)	-10(5)	13(5)	-14(4)
C(2)	73(7)	53(6)	51(6)	-29(5)	2(5)	-36(5)
C(3)	61(7)	32(5)	57(7)	-15(5)	17(5)	-17(5)
C(4)	60(7)	43(5)	53(6)	-21(5)	-9(5)	-22(5)
C(5)	64(7)	47(5)	44(6)	-9(5)	-6(5)	-28(5)
C(6)	49(6)	46(5)	56(7)	-23(5)	2(5)	-17(5)
C(7)	63(7)	41(5)	57(6)	-7(4)	6(5)	-29(6)

C(8)	93(10)	56(7)	165(13)	-39(7)	34(9)	-40(7)
N(1)	81(8)	70(6)	154(10)	-34(7)	-3(7)	-46(6)
C(9)	157(15)	60(8)	74(8)	-8(6)	-12(9)	-73(10)
N(2)	111(9)	82(7)	128(9)	-62(6)	30(7)	-63(7)
C(10)	79(9)	72(7)	130(11)	-43(7)	12(8)	-47(7)
C(11)	70(8)	34(5)	77(8)	-16(5)	18(7)	-27(6)
C(12)	79(10)	82(8)	80(9)	-40(7)	9(8)	-35(8)
N(3)	95(10)	103(8)	97(9)	-27(7)	-23(7)	-42(7)
C(13)	88(12)	94(10)	122(13)	-21(9)	-30(11)	-48(10)
N(4)	142(12)	121(9)	66(7)	-64(7)	18(8)	-70(9)
C(14)	84(9)	72(7)	88(9)	-29(7)	13(8)	-30(7)
C(15)	81(8)	38(5)	46(6)	-10(5)	-7(6)	-28(6)
C(16)	82(8)	47(6)	60(7)	-20(5)	7(6)	-28(6)
C(17)	62(8)	36(5)	69(7)	2(5)	0(6)	-13(5)
C(18)	78(8)	57(7)	58(7)	-9(5)	-8(6)	-40(6)
C(19)	75(8)	64(7)	63(7)	-11(6)	2(6)	-40(7)
C(20)	69(8)	53(6)	65(7)	-17(5)	-4(6)	-25(6)
C(21)	124(11)	73(8)	72(8)	-1(7)	9(8)	-67(8)
C(22)	177(19)	139(14)	210(20)	128(15)	6(16)	-48(14)
C(23)	450(40)	151(16)	164(17)	-54(14)	150(20)	-190(20)
C(24)	370(30)	205(18)	131(14)	9(12)	-11(16)	-250(20)
C(25)	55(7)	50(5)	56(6)	-22(5)	7(5)	-27(5)
C(26)	61(7)	51(6)	88(8)	-35(5)	12(6)	-21(5)
C(27)	56(7)	38(6)	109(9)	-21(6)	-3(7)	-14(5)
C(28)	81(9)	46(6)	82(8)	-12(6)	-2(7)	-31(6)
C(29)	88(9)	67(7)	83(8)	-21(6)	13(7)	-55(7)
C(30)	78(8)	66(7)	67(7)	-32(6)	3(6)	-35(6)
C(31)	60(7)	40(5)	61(7)	-16(5)	6(6)	-14(5)
C(32)	80(8)	53(6)	45(6)	-24(5)	13(6)	-34(6)
C(33)	68(8)	61(6)	81(8)	-33(6)	-3(6)	-25(6)
C(34)	91(10)	67(7)	93(10)	-16(7)	-20(8)	-28(7)
C(35)	103(10)	65(7)	59(7)	-31(6)	0(7)	-19(7)
C(36)	67(7)	46(5)	52(7)	-19(5)	1(6)	-12(5)
C(37)	97(11)	113(10)	99(11)	-46(9)	-25(9)	-29(8)
C(38)	69(7)	39(5)	47(6)	-9(5)	4(5)	-25(5)
C(39)	71(8)	63(7)	76(8)	-2(6)	13(7)	-16(6)
C(40)	81(9)	54(6)	66(7)	-8(5)	16(6)	-14(6)
C(41)	81(8)	36(5)	62(7)	1(5)	-1(6)	-21(6)
C(42)	90(9)	30(5)	57(7)	-9(5)	23(6)	-11(5)
C(43)	73(8)	45(6)	56(7)	-21(5)	14(6)	-23(6)
C(44)	126(12)	61(7)	62(8)	-3(6)	13(8)	-19(8)
C(45)	280(30)	124(13)	85(11)	-15(10)	-55(14)	-34(15)
C(46)	260(30)	153(15)	74(11)	82(10)	51(13)	107(16)
C(47)	180(20)	146(15)	220(20)	-4(13)	115(17)	-82(14)
C(48)	82(8)	46(5)	53(7)	-16(5)	6(6)	-31(6)
C(49)	72(8)	49(6)	77(8)	-28(6)	20(6)	-29(6)
C(50)	57(7)	63(6)	69(7)	-31(6)	16(6)	-35(6)
C(51)	67(7)	47(5)	56(7)	-16(5)	7(5)	-39(5)

C(52)	65(7)	54(5)	46(6)	-23(5)	17(5)	-34(5)
C(53)	56(7)	43(5)	71(7)	-21(5)	5(6)	-22(5)
C(54)	61(7)	74(7)	63(7)	-10(5)	5(6)	-49(6)
C(55)	122(13)	125(11)	178(15)	-20(10)	-26(11)	-103(11)
C(57)	116(12)	111(10)	280(20)	-112(13)	55(13)	-90(10)
C(58)	69(8)	43(5)	60(7)	-18(5)	0(7)	-27(6)
C(59)	107(13)	99(9)	65(9)	-41(7)	2(8)	-38(9)
N(7)	110(10)	114(9)	99(10)	-65(8)	14(8)	-38(8)
C(60)	200(20)	91(10)	72(10)	7(9)	-51(13)	-99(13)
N(8)	163(14)	108(9)	97(10)	-65(7)	-8(9)	-44(9)
C(61)	92(11)	97(9)	75(9)	-39(8)	-19(8)	-8(8)
C(62)	90(9)	47(6)	44(6)	-6(5)	8(6)	-39(6)
C(63)	100(10)	56(7)	63(7)	5(6)	4(7)	-32(7)
C(64)	77(9)	53(7)	96(9)	2(6)	18(8)	-5(6)
C(65)	102(10)	61(7)	71(8)	-17(6)	6(7)	-53(7)
C(66)	85(9)	53(6)	59(7)	-11(6)	8(6)	-26(6)
C(67)	75(8)	55(6)	62(7)	-11(5)	20(6)	-32(6)
C(68)	127(12)	61(7)	80(9)	-5(7)	18(9)	-40(8)
C(69)	250(20)	126(13)	113(13)	37(11)	-21(15)	-101(16)
C(70)	560(50)	146(15)	119(14)	-49(12)	180(20)	-210(20)
C(71)	410(40)	230(20)	169(17)	-2(14)	22(19)	-280(30)
C(72)	82(8)	51(6)	53(7)	-6(5)	11(6)	-39(6)
C(73)	116(10)	70(7)	61(7)	-22(6)	10(7)	-57(7)
C(74)	114(10)	60(6)	54(7)	-3(5)	3(7)	-56(7)
C(75)	81(9)	50(6)	95(10)	-16(6)	4(7)	-33(6)
C(76)	100(9)	55(6)	105(9)	-42(6)	27(7)	-48(7)
C(77)	85(8)	53(6)	44(7)	2(5)	8(6)	-40(6)
C(78)	115(11)	85(8)	140(11)	-35(8)	11(9)	-71(8)
C(79)	57(7)	53(6)	69(7)	-27(5)	20(6)	-38(5)
C(80)	35(6)	57(6)	99(9)	-21(6)	-2(6)	-20(5)
C(81)	79(9)	84(8)	69(8)	-38(7)	27(7)	-48(8)
C(82)	132(13)	82(8)	47(8)	-7(6)	19(8)	-83(9)
C(83)	83(9)	62(7)	66(8)	15(6)	-18(7)	-39(7)
C(84)	59(7)	52(6)	96(9)	-45(6)	23(6)	-29(6)
C(85)	67(7)	48(6)	45(6)	-13(5)	10(6)	-36(6)
C(86)	76(9)	72(7)	96(9)	14(7)	18(8)	-26(7)
C(87)	65(8)	65(7)	78(8)	-4(6)	24(7)	-13(6)
C(88)	80(8)	54(6)	66(7)	-28(6)	22(7)	-45(6)
C(89)	76(9)	53(7)	105(10)	18(6)	24(8)	-6(6)
C(90)	63(8)	55(7)	104(9)	-7(6)	36(7)	-11(6)
C(91)	137(12)	60(7)	57(7)	-1(6)	9(7)	-56(8)
C(92)	230(20)	209(17)	96(11)	27(11)	-7(12)	-181(18)
C(93)	490(40)	218(19)	48(9)	-37(11)	76(15)	-230(30)
C(94)	270(30)	167(17)	220(20)	145(17)	150(20)	101(18)
C(95)	250(30)	169(17)	186(19)	-99(16)	54(19)	-113(18)

Table D5. Hydrogen coordinates (x 10^4) and isotropic displacement parameters ($Å^2$x 10^3) for **(24)**.

	x	y	z	U(eq)
H(8)	1156	1572	8476	123
H(9)	2452	-952	8060	107
H(10)	4075	288	8196	103
H(12)	813	3813	7190	93
H(13)	1573	2860	5715	118
H(14)	3657	1861	6971	99
H(16)	1378	5543	7242	75
H(17)	1611	6709	6411	77
H(19)	4433	4656	6187	80
H(20)	4300	3452	7071	76
H(22A)	1770	7279	5222	348
H(22B)	2231	8039	5110	348
H(22C)	1766	7734	5762	348
H(23A)	4233	6551	4985	362
H(23B)	3521	6093	4902	362
H(23C)	4427	5471	5420	362
H(24A)	4509	6404	6098	299
H(24B)	3487	7218	6293	299
H(24C)	3922	7497	5625	299
H(26)	1775	5276	8833	79
H(27)	1623	6826	8299	85
H(29)	4487	5572	7627	87
H(30)	4729	4001	8189	79
H(33)	4142	4717	9513	82
H(35)	4474	2266	10944	97
H(36)	3806	1736	10318	71
H(37A)	5359	2541	11298	158
H(37B)	4513	3433	11539	158
H(37C)	5636	3315	11445	158
H(39)	1597	2139	9875	98
H(40)	1665	1018	10870	93
H(42)	4393	-1034	10449	83
H(43)	4292	76	9502	71
H(45A)	2964	-679	12363	279
H(45B)	2282	338	11849	279
H(45C)	3470	-33	11925	279
H(46A)	4238	-2136	12015	423
H(46B)	4644	-1692	11374	423
H(46C)	3948	-2208	11378	423
H(47A)	1998	-1027	11226	301
H(47B)	1651	-389	11709	301
H(47C)	2348	-1569	11945	301
H(56)	6944	2523	6690	130

H(59)	6459	6509	5780	108
H(60)	7219	5571	4344	133
H(61)	9332	4698	5596	117
H(63)	7113	8128	5806	97
H(64)	7285	9253	4920	111
H(66)	10175	7372	4852	84
H(67)	10045	6221	5713	79
H(69A)	7352	10384	4159	261
H(69B)	7508	9738	3702	261
H(69C)	7894	10564	3518	261
H(70A)	9266	9276	3288	403
H(70B)	9295	8243	3695	403
H(70C)	10183	8489	3784	403
H(71A)	9855	9261	4776	343
H(71B)	8831	10290	4599	343
H(71C)	9687	10042	4102	343
H(73)	9134	8005	6415	91
H(74)	9552	8894	6914	87
H(76)	9515	7038	8634	94
H(78A)	9645	9786	7544	154
H(78B)	10756	8893	7547	154
H(78C)	10454	9399	8097	154
H(80)	7527	6525	8556	77
H(81)	7821	5651	9592	85
H(83)	10854	3915	9286	90
H(84)	10552	4680	8225	75
H(86)	6801	4937	8297	114
H(87)	6739	3935	9286	98
H(89)	9598	2025	9202	120
H(90)	9709	3116	8275	105
H(92A)	7254	1497	10475	246
H(92B)	7352	1556	9754	246
H(92C)	6629	2534	9958	246
H(93A)	8534	2497	10729	345
H(93B)	7402	2636	10752	345
H(93C)	7668	3441	10256	345
H(94A)	8970	793	10579	546
H(94B)	9641	1275	10164	546
H(94C)	9064	874	9856	546

Table D6. Torsion angles [°] for **(24)**.

C(6)-C(1)-C(2)-C(3)	6.2(13)	C(1)-C(2)-C(3)-C(4)	-6.7(13)
C(7)-C(1)-C(2)-C(3)	-172.1(8)	C(11)-C(2)-C(3)-C(4)	176.8(9)
C(6)-C(1)-C(2)-C(11)	-177.3(9)	C(1)-C(2)-C(3)-C(15)	172.0(9)
C(7)-C(1)-C(2)-C(11)	4.4(13)	C(11)-C(2)-C(3)-C(15)	-4.5(14)

C(2)-C(3)-C(4)-C(5)	7.9(14)	C(16)-C(17)-C(18)-C(21)	-178.5(9)
C(15)-C(3)-C(4)-C(5)	-170.8(9)	C(17)-C(18)-C(19)-C(20)	-3.5(15)
C(2)-C(3)-C(4)-C(25)	178.2(9)	C(21)-C(18)-C(19)-C(20)	176.2(9)
C(15)-C(3)-C(4)-C(25)	-0.5(15)	C(18)-C(19)-C(20)-C(15)	1.9(14)
C(3)-C(4)-C(5)-C(6)	-8.3(14)	C(16)-C(15)-C(20)-C(19)	2.0(13)
C(25)-C(4)-C(5)-C(6)	179.7(8)	C(3)-C(15)-C(20)-C(19)	-174.9(8)
C(3)-C(4)-C(5)-C(31)	170.5(9)	C(19)-C(18)-C(21)-C(23)	30.1(18)
C(25)-C(4)-C(5)-C(31)	-1.5(10)	C(17)-C(18)-C(21)-C(23)	-150.2(15)
C(2)-C(1)-C(6)-C(5)	-6.6(14)	C(19)-C(18)-C(21)-C(22)	161.7(13)
C(7)-C(1)-C(6)-C(5)	171.6(9)	C(17)-C(18)-C(21)-C(22)	-18.6(17)
C(2)-C(1)-C(6)-C(38)	173.5(9)	C(19)-C(18)-C(21)-C(24)	-79.9(14)
C(7)-C(1)-C(6)-C(38)	-8.3(14)	C(17)-C(18)-C(21)-C(24)	99.8(14)
C(4)-C(5)-C(6)-C(1)	7.4(13)	C(3)-C(4)-C(25)-C(30)	-46.4(13)
C(31)-C(5)-C(6)-C(1)	-171.0(9)	C(5)-C(4)-C(25)-C(30)	124.8(9)
C(4)-C(5)-C(6)-C(38)	-172.7(8)	C(3)-C(4)-C(25)-C(26)	81.2(11)
C(31)-C(5)-C(6)-C(38)	8.9(15)	C(5)-C(4)-C(25)-C(26)	-107.5(9)
C(6)-C(1)-C(7)-C(8)	90.8(14)	C(3)-C(4)-C(25)-C(32)	-167.8(9)
C(2)-C(1)-C(7)-C(8)	-90.9(13)	C(5)-C(4)-C(25)-C(32)	3.5(9)
C(6)-C(1)-C(7)-C(10)	-89.4(12)	C(30)-C(25)-C(26)-C(27)	-1.8(13)
C(2)-C(1)-C(7)-C(10)	88.9(12)	C(32)-C(25)-C(26)-C(27)	122.8(10)
C(10)-C(7)-C(8)-N(1)	-5.2(19)	C(4)-C(25)-C(26)-C(27)	-130.6(9)
C(1)-C(7)-C(8)-N(1)	174.6(11)	C(25)-C(26)-C(27)-C(28)	0.8(16)
C(7)-C(8)-N(1)-C(9)	4.6(19)	C(26)-C(27)-C(28)-O(1)	-177.2(10)
C(8)-N(1)-C(9)-N(2)	-2.1(19)	C(26)-C(27)-C(28)-C(29)	1.9(16)
N(1)-C(9)-N(2)-C(10)	1(2)	O(1)-C(28)-C(29)-C(30)	175.5(10)
C(9)-N(2)-C(10)-C(7)	-1.3(19)	C(27)-C(28)-C(29)-C(30)	-3.7(15)
C(8)-C(7)-C(10)-N(2)	3.3(17)	C(28)-C(29)-C(30)-C(25)	2.7(15)
C(1)-C(7)-C(10)-N(2)	-176.5(10)	C(26)-C(25)-C(30)-C(29)	0.0(13)
C(3)-C(2)-C(11)-C(12)	-82.2(12)	C(32)-C(25)-C(30)-C(29)	-120.8(10)
C(1)-C(2)-C(11)-C(12)	101.4(11)	C(4)-C(25)-C(30)-C(29)	125.5(10)
C(3)-C(2)-C(11)-C(14)	96.4(11)	C(6)-C(5)-C(31)-C(32)	177.0(10)
C(1)-C(2)-C(11)-C(14)	-80.0(12)	C(4)-C(5)-C(31)-C(32)	-1.5(10)
C(14)-C(11)-C(12)-N(3)	1.7(14)	C(6)-C(5)-C(31)-C(36)	3.3(17)
C(2)-C(11)-C(12)-N(3)	-179.6(9)	C(4)-C(5)-C(31)-C(36)	-175.2(10)
C(11)-C(12)-N(3)-C(13)	-1.6(17)	C(36)-C(31)-C(32)-C(33)	-2.2(15)
C(12)-N(3)-C(13)-N(4)	1(2)	C(5)-C(31)-C(32)-C(33)	-176.7(9)
N(3)-C(13)-N(4)-C(14)	-1(2)	C(36)-C(31)-C(32)-C(25)	178.5(8)
C(13)-N(4)-C(14)-C(11)	1.3(17)	C(5)-C(31)-C(32)-C(25)	4.1(11)
C(12)-C(11)-C(14)-N(4)	-1.5(15)	C(30)-C(25)-C(32)-C(31)	-127.3(9)
C(2)-C(11)-C(14)-N(4)	179.8(9)	C(26)-C(25)-C(32)-C(31)	108.2(9)
C(4)-C(3)-C(15)-C(16)	-81.3(13)	C(4)-C(25)-C(32)-C(31)	-4.6(10)
C(2)-C(3)-C(15)-C(16)	100.0(11)	C(30)-C(25)-C(32)-C(33)	53.5(12)
C(4)-C(3)-C(15)-C(20)	95.3(10)	C(26)-C(25)-C(32)-C(33)	-71.0(11)
C(2)-C(3)-C(15)-C(20)	-83.4(11)	C(4)-C(25)-C(32)-C(33)	176.2(9)
C(20)-C(15)-C(16)-C(17)	-4.2(13)	C(31)-C(32)-C(33)-C(34)	3.1(15)
C(3)-C(15)-C(16)-C(17)	172.4(9)	C(25)-C(32)-C(33)-C(34)	-177.7(10)
C(15)-C(16)-C(17)-C(18)	2.7(15)	C(37)-O(2)-C(34)-C(35)	2.2(17)
C(16)-C(17)-C(18)-C(19)	1.2(15)	C(37)-O(2)-C(34)-C(33)	177.1(10)

C(32)-C(33)-C(34)-C(35)	-3.7(16)	C(79)-C(52)-C(53)-C(48)	178.6(9)
C(32)-C(33)-C(34)-O(2)	-179.0(9)	C(51)-C(52)-C(53)-C(85)	-178.1(9)
O(2)-C(34)-C(35)-C(36)	178.4(10)	C(79)-C(52)-C(53)-C(85)	-2.5(15)
C(33)-C(34)-C(35)-C(36)	3.7(18)	C(53)-C(48)-C(54)-C(55)	85.1(15)
C(34)-C(35)-C(36)-C(31)	-2.6(16)	C(49)-C(48)-C(54)-C(55)	-94.8(14)
C(32)-C(31)-C(36)-C(35)	1.8(14)	C(53)-C(48)-C(54)-C(57)	-98.0(14)
C(5)-C(31)-C(36)-C(35)	174.9(10)	C(49)-C(48)-C(54)-C(57)	82.2(15)
C(1)-C(6)-C(38)-C(43)	80.7(12)	C(57)-C(54)-C(55)-N(5)	-4(2)
C(5)-C(6)-C(38)-C(43)	-99.3(11)	C(48)-C(54)-C(55)-N(5)	172.7(11)
C(1)-C(6)-C(38)-C(39)	-108.6(11)	C(54)-C(55)-N(5)-C(56)	4(2)
C(5)-C(6)-C(38)-C(39)	71.5(13)	C(55)-N(5)-C(56)-N(6)	0(2)
C(43)-C(38)-C(39)-C(40)	0.5(16)	N(5)-C(56)-N(6)-C(57)	-3(3)
C(6)-C(38)-C(39)-C(40)	-171.0(10)	C(56)-N(6)-C(57)-C(54)	2(2)
C(38)-C(39)-C(40)-C(41)	1.9(18)	C(55)-C(54)-C(57)-N(6)	2(2)
C(39)-C(40)-C(41)-C(42)	-4.6(16)	C(48)-C(54)-C(57)-N(6)	-175.5(14)
C(39)-C(40)-C(41)-C(44)	175.1(11)	C(48)-C(49)-C(58)-C(61)	-92.1(13)
C(40)-C(41)-C(42)-C(43)	4.9(16)	C(50)-C(49)-C(58)-C(61)	84.7(13)
C(44)-C(41)-C(42)-C(43)	-174.8(11)	C(48)-C(49)-C(58)-C(59)	87.8(12)
C(41)-C(42)-C(43)-C(38)	-2.4(16)	C(50)-C(49)-C(58)-C(59)	-95.4(12)
C(39)-C(38)-C(43)-C(42)	-0.4(15)	C(61)-C(58)-C(59)-N(7)	1.4(17)
C(6)-C(38)-C(43)-C(42)	170.8(10)	C(49)-C(58)-C(59)-N(7)	-178.5(10)
C(42)-C(41)-C(44)-C(46)	-4(2)	C(58)-C(59)-N(7)-C(60)	0.2(18)
C(40)-C(41)-C(44)-C(46)	175.9(16)	C(59)-N(7)-C(60)-N(8)	1(2)
C(42)-C(41)-C(44)-C(45)	129.9(15)	N(7)-C(60)-N(8)-C(61)	-3(2)
C(40)-C(41)-C(44)-C(45)	-49.8(18)	C(60)-N(8)-C(61)-C(58)	5.1(19)
C(42)-C(41)-C(44)-C(47)	-125.4(14)	C(59)-C(58)-C(61)-N(8)	-4.4(18)
C(40)-C(41)-C(44)-C(47)	55.0(15)	C(49)-C(58)-C(61)-N(8)	175.5(11)
C(53)-C(48)-C(49)-C(50)	1.1(15)	C(51)-C(50)-C(62)-C(67)	91.2(12)
C(54)-C(48)-C(49)-C(50)	-179.0(9)	C(49)-C(50)-C(62)-C(67)	-96.5(12)
C(53)-C(48)-C(49)-C(58)	177.8(9)	C(51)-C(50)-C(62)-C(63)	-86.0(14)
C(54)-C(48)-C(49)-C(58)	-2.3(15)	C(49)-C(50)-C(62)-C(63)	86.3(13)
C(48)-C(49)-C(50)-C(51)	-4.6(14)	C(67)-C(62)-C(63)-C(64)	-1.3(16)
C(58)-C(49)-C(50)-C(51)	178.7(9)	C(50)-C(62)-C(63)-C(64)	176.0(10)
C(48)-C(49)-C(50)-C(62)	-177.4(9)	C(62)-C(63)-C(64)-C(65)	-0.8(19)
C(58)-C(49)-C(50)-C(62)	5.9(14)	C(63)-C(64)-C(65)-C(66)	2.1(18)
C(49)-C(50)-C(51)-C(52)	7.4(14)	C(63)-C(64)-C(65)-C(68)	-177.7(11)
C(62)-C(50)-C(51)-C(52)	179.9(10)	C(64)-C(65)-C(66)-C(67)	-1.4(16)
C(49)-C(50)-C(51)-C(72)	-176.3(10)	C(68)-C(65)-C(66)-C(67)	178.4(10)
C(62)-C(50)-C(51)-C(72)	-3.7(17)	C(63)-C(62)-C(67)-C(66)	2.0(15)
C(50)-C(51)-C(52)-C(53)	-6.9(14)	C(50)-C(62)-C(67)-C(66)	-175.3(9)
C(72)-C(51)-C(52)-C(53)	176.0(8)	C(65)-C(66)-C(67)-C(62)	-0.6(17)
C(50)-C(51)-C(52)-C(79)	176.8(9)	C(66)-C(65)-C(68)-C(70)	44(2)
C(72)-C(51)-C(52)-C(79)	-0.3(11)	C(64)-C(65)-C(68)-C(70)	-135.9(17)
C(49)-C(48)-C(53)-C(52)	-0.2(14)	C(66)-C(65)-C(68)-C(71)	-80.1(16)
C(54)-C(48)-C(53)-C(52)	179.9(9)	C(64)-C(65)-C(68)-C(71)	99.7(16)
C(49)-C(48)-C(53)-C(85)	-179.1(9)	C(66)-C(65)-C(68)-C(69)	159.4(12)
C(54)-C(48)-C(53)-C(85)	1.1(15)	C(64)-C(65)-C(68)-C(69)	-20.9(17)
C(51)-C(52)-C(53)-C(48)	3.0(14)	C(50)-C(51)-C(72)-C(77)	-178.6(10)

C(52)-C(51)-C(72)-C(77)	-1.9(12)	C(77)-C(79)-C(80)-C(81)	-118.4(11)
C(50)-C(51)-C(72)-C(73)	2.1(18)	C(84)-C(79)-C(80)-C(81)	-0.2(12)
C(52)-C(51)-C(72)-C(73)	178.8(10)	C(79)-C(80)-C(81)-C(82)	1.1(15)
C(77)-C(72)-C(73)-C(74)	-0.8(16)	C(80)-C(81)-C(82)-O(4)	-178.3(9)
C(51)-C(72)-C(73)-C(74)	178.4(10)	C(80)-C(81)-C(82)-C(83)	1.0(15)
C(72)-C(73)-C(74)-C(75)	2.3(17)	O(4)-C(82)-C(83)-C(84)	175.2(9)
C(78)-O(3)-C(75)-C(76)	169.6(10)	C(81)-C(82)-C(83)-C(84)	-4.1(15)
C(78)-O(3)-C(75)-C(74)	-12.1(16)	C(82)-C(83)-C(84)-C(79)	5.2(14)
C(73)-C(74)-C(75)-O(3)	179.4(10)	C(80)-C(79)-C(84)-C(83)	-3.1(11)
C(73)-C(74)-C(75)-C(76)	-2.4(17)	C(52)-C(79)-C(84)-C(83)	-133.6(9)
O(3)-C(75)-C(76)-C(77)	179.2(9)	C(77)-C(79)-C(84)-C(83)	116.7(10)
C(74)-C(75)-C(76)-C(77)	0.8(16)	C(48)-C(53)-C(85)-C(86)	-85.1(13)
C(73)-C(72)-C(77)-C(76)	-0.7(16)	C(52)-C(53)-C(85)-C(86)	96.1(12)
C(51)-C(72)-C(77)-C(76)	179.9(9)	C(48)-C(53)-C(85)-C(90)	93.6(13)
C(73)-C(72)-C(77)-C(79)	-177.4(9)	C(52)-C(53)-C(85)-C(90)	-85.2(13)
C(51)-C(72)-C(77)-C(79)	3.3(12)	C(90)-C(85)-C(86)-C(87)	7.1(17)
C(75)-C(76)-C(77)-C(72)	0.8(16)	C(53)-C(85)-C(86)-C(87)	-174.1(10)
C(75)-C(76)-C(77)-C(79)	176.8(9)	C(85)-C(86)-C(87)-C(88)	-6(2)
C(51)-C(52)-C(79)-C(80)	122.0(9)	C(86)-C(87)-C(88)-C(89)	0.9(18)
C(53)-C(52)-C(79)-C(80)	-54.0(13)	C(86)-C(87)-C(88)-C(91)	177.3(11)
C(51)-C(52)-C(79)-C(77)	2.0(10)	C(87)-C(88)-C(89)-C(90)	3.2(18)
C(53)-C(52)-C(79)-C(77)	-174.0(9)	C(91)-C(88)-C(89)-C(90)	-173.4(11)
C(51)-C(52)-C(79)-C(84)	-111.7(9)	C(86)-C(85)-C(90)-C(89)	-3.1(18)
C(53)-C(52)-C(79)-C(84)	72.3(11)	C(53)-C(85)-C(90)-C(89)	178.1(11)
C(72)-C(77)-C(79)-C(80)	-128.3(10)	C(88)-C(89)-C(90)-C(85)	-2(2)
C(76)-C(77)-C(79)-C(80)	55.2(14)	C(89)-C(88)-C(91)-C(94)	-15(2)
C(72)-C(77)-C(79)-C(52)	-3.2(10)	C(87)-C(88)-C(91)-C(94)	168.6(19)
C(76)-C(77)-C(79)-C(52)	-179.7(10)	C(89)-C(88)-C(91)-C(93)	117.0(16)
C(72)-C(77)-C(79)-C(84)	112.2(10)	C(87)-C(88)-C(91)-C(93)	-59.3(18)
C(76)-C(77)-C(79)-C(84)	-64.3(13)	C(89)-C(88)-C(91)-C(92)	-130.0(14)
C(52)-C(79)-C(80)-C(81)	126.2(10)	C(87)-C(88)-C(91)-C(92)	53.8(15)

Symmetry transformations used to generate equivalent atoms:

Table E1. Crystal data and structure refinement for **(40)**.

Compound		**(40)**
Empirical formula		$C_{40}H_{30}Fe$
Formula weight		566.49
Temperature (K)		298(2)
Wavelength (Å)		0.71073
Crystal system		Triclinic
Space group		P-1
Unit cell dimensions	a (Å)	11.870(3)
	b (Å)	12.538(3)
	c (Å)	13.071(3)
	α (°)	112.588(3)
	β (°)	95.517(3)
	γ (°)	115.055(3)
Volume ($Å^3$)		1547.3(6)
Z		2
Density (calculated) (Mg/m^3)		1.216
Absorption coefficient (mm^{-1})		0.513
F(000)		592
Crystal size (mm^3)		0.4 x 0.3 x 0.1
Theta range for data collection (°)		1.77 to 24.99
Index ranges		-13<=h<=14, -14<=k<=14, -15<=l<=15
Reflections collected		10367
Independent reflections		5333 [R(int) = 0.0237]
Completeness to theta = 24.99° (%)		98.0
Absorption correction		None
Refinement method		Full-matrix least-squares on F^2
Data / restraints / parameters		5333 / 0 / 370
Goodness-of-fit on F^2		0.978
R_1 [I>2sigma(I)]		R1 = 0.0472
wR2 (all data)		wR2 = 0.1066
Largest diff. peak and hole		0.285 and -0.317 $e.Å^{-3}$

Table E2. Atomic coordinates (x 10^4) and equivalent isotropic displacement parameters ($Å^2$x 10^3) for **(40)**. U(eq) is defined as one third of the trace of the orthogonalized U^{ij} tensor.

	x	y	z	U(eq)
Fe(1)	2196(1)	-1156(1)	9001(1)	52(1)
C(1)	714(2)	-412(2)	7408(2)	46(1)
C(2)	-595(2)	-938(2)	6728(2)	44(1)
C(3)	-986(2)	-40(2)	6614(2)	43(1)
C(4)	-130(2)	1373(2)	7226(2)	43(1)
C(5)	1158(2)	1897(2)	7958(2)	45(1)
C(6)	1547(2)	999(2)	8011(2)	48(1)

C(7)	1269(2)	-1273(2)	7489(2)	47(1)
C(8)	631(3)	-2542(2)	7500(2)	61(1)
C(9)	1562(3)	-2981(3)	7569(2)	67(1)
C(10)	2792(3)	-1995(3)	7615(2)	61(1)
C(11)	2617(2)	-941(2)	7563(2)	51(1)
C(12)	2006(4)	196(4)	10377(2)	88(1)
C(13)	1399(3)	-1071(4)	10349(3)	89(1)
C(14)	2377(3)	-1442(4)	10455(3)	82(1)
C(15)	3583(3)	-411(4)	10560(2)	81(1)
C(16)	3360(4)	618(3)	10521(2)	86(1)
C(17)	-1599(2)	-2418(2)	6181(2)	46(1)
C(18)	-1559(3)	-3399(2)	5224(2)	64(1)
C(19)	-2483(3)	-4759(3)	4779(3)	84(1)
C(20)	-3457(3)	-5160(3)	5283(3)	85(1)
C(21)	-3509(3)	-4203(3)	6234(3)	80(1)
C(22)	-2599(3)	-2845(3)	6674(2)	62(1)
C(23)	-2346(2)	-641(2)	5789(2)	45(1)
C(24)	-2585(2)	-1307(2)	4583(2)	59(1)
C(25)	-3808(3)	-1845(3)	3792(2)	74(1)
C(26)	-4812(3)	-1721(3)	4206(3)	75(1)
C(27)	-4597(3)	-1077(3)	5401(3)	71(1)
C(28)	-3365(2)	-530(2)	6197(2)	58(1)
C(29)	-595(2)	2309(2)	7140(2)	46(1)
C(30)	-1065(2)	2214(2)	6056(2)	56(1)
C(31)	-1505(3)	3080(3)	5998(3)	72(1)
C(32)	-1505(3)	4022(3)	7009(3)	79(1)
C(33)	-1044(3)	4134(3)	8092(3)	72(1)
C(34)	-581(2)	3286(2)	8158(2)	56(1)
C(35)	2145(2)	3385(2)	8681(2)	51(1)
C(36)	2557(3)	4243(3)	8179(3)	69(1)
C(37)	3487(3)	5610(3)	8881(3)	91(1)
C(38)	4017(3)	6135(3)	10077(3)	95(1)
C(39)	3628(3)	5296(3)	10582(3)	87(1)
C(40)	2704(3)	3929(3)	9890(2)	66(1)

Table E3. Bond lengths [Å] and angles [°] for **(40)**.

Fe(1)-C(12)	2.054(3)	Fe(1)-C(7)	2.088(2)
Fe(1)-C(8)	2.065(2)	C(1)-C(6)	1.423(3)
Fe(1)-C(13)	2.067(3)	C(1)-C(2)	1.434(3)
Fe(1)-C(16)	2.068(3)	C(1)-C(7)	1.512(3)
Fe(1)-C(9)	2.070(3)	C(2)-C(3)	1.436(3)
Fe(1)-C(14)	2.073(3)	C(2)-C(17)	1.523(3)
Fe(1)-C(10)	2.074(3)	C(3)-C(4)	1.429(3)
Fe(1)-C(11)	2.076(2)	C(3)-C(23)	1.532(3)
Fe(1)-C(15)	2.080(3)	C(4)-C(5)	1.439(3)

C(4)-C(29)	1.527(3)	C(12)-Fe(1)-C(14)	68.14(13)
C(5)-C(6)	1.407(3)	C(8)-Fe(1)-C(14)	121.72(13)
C(5)-C(35)	1.526(3)	C(13)-Fe(1)-C(14)	40.58(12)
C(7)-C(8)	1.451(3)	C(16)-Fe(1)-C(14)	67.52(14)
C(7)-C(11)	1.455(3)	C(9)-Fe(1)-C(14)	106.46(13)
C(8)-C(9)	1.438(3)	C(12)-Fe(1)-C(10)	162.56(14)
C(9)-C(10)	1.435(4)	C(8)-Fe(1)-C(10)	68.53(11)
C(10)-C(11)	1.447(3)	C(13)-Fe(1)-C(10)	156.30(13)
C(12)-C(13)	1.423(4)	C(16)-Fe(1)-C(10)	126.53(13)
C(12)-C(16)	1.431(5)	C(9)-Fe(1)-C(10)	40.52(11)
C(13)-C(14)	1.436(4)	C(14)-Fe(1)-C(10)	122.06(12)
C(14)-C(15)	1.414(4)	C(12)-Fe(1)-C(11)	125.19(12)
C(15)-C(16)	1.440(4)	C(8)-Fe(1)-C(11)	68.42(10)
C(17)-C(18)	1.400(3)	C(13)-Fe(1)-C(11)	159.95(12)
C(17)-C(22)	1.409(3)	C(16)-Fe(1)-C(11)	110.69(12)
C(18)-C(19)	1.407(4)	C(9)-Fe(1)-C(11)	68.26(11)
C(19)-C(20)	1.390(5)	C(14)-Fe(1)-C(11)	158.98(11)
C(20)-C(21)	1.386(4)	C(10)-Fe(1)-C(11)	40.80(9)
C(21)-C(22)	1.402(4)	C(12)-Fe(1)-C(15)	68.45(13)
C(23)-C(24)	1.401(3)	C(8)-Fe(1)-C(15)	158.42(12)
C(23)-C(28)	1.406(3)	C(13)-Fe(1)-C(15)	67.84(13)
C(24)-C(25)	1.406(3)	C(16)-Fe(1)-C(15)	40.62(13)
C(25)-C(26)	1.398(4)	C(9)-Fe(1)-C(15)	123.71(12)
C(26)-C(27)	1.392(4)	C(14)-Fe(1)-C(15)	39.80(12)
C(27)-C(28)	1.415(3)	C(10)-Fe(1)-C(15)	109.38(12)
C(29)-C(30)	1.412(3)	C(11)-Fe(1)-C(15)	124.99(11)
C(29)-C(34)	1.414(3)	C(12)-Fe(1)-C(7)	106.83(11)
C(30)-C(31)	1.412(4)	C(8)-Fe(1)-C(7)	40.89(9)
C(31)-C(32)	1.394(4)	C(13)-Fe(1)-C(7)	121.87(11)
C(32)-C(33)	1.399(4)	C(16)-Fe(1)-C(7)	123.41(12)
C(33)-C(34)	1.413(4)	C(9)-Fe(1)-C(7)	68.77(10)
C(35)-C(36)	1.408(3)	C(14)-Fe(1)-C(7)	158.14(12)
C(35)-C(40)	1.411(3)	C(10)-Fe(1)-C(7)	69.02(10)
C(36)-C(37)	1.412(4)	C(11)-Fe(1)-C(7)	40.92(9)
C(37)-C(38)	1.393(5)	C(15)-Fe(1)-C(7)	160.17(12)
C(38)-C(39)	1.392(5)	C(6)-C(1)-C(2)	118.0(2)
C(39)-C(40)	1.409(4)	C(6)-C(1)-C(7)	118.3(2)
		C(2)-C(1)-C(7)	123.71(19)
C(12)-Fe(1)-C(8)	120.15(13)	C(1)-C(2)-C(3)	119.31(19)
C(12)-Fe(1)-C(13)	40.40(13)	C(1)-C(2)-C(17)	121.24(19)
C(8)-Fe(1)-C(13)	105.01(13)	C(3)-C(2)-C(17)	119.37(19)
C(12)-Fe(1)-C(16)	40.61(13)	C(4)-C(3)-C(2)	121.5(2)
C(8)-Fe(1)-C(16)	157.49(13)	C(4)-C(3)-C(23)	120.42(19)
C(13)-Fe(1)-C(16)	67.75(14)	C(2)-C(3)-C(23)	118.03(19)
C(12)-Fe(1)-C(9)	155.38(15)	C(3)-C(4)-C(5)	118.74(19)
C(8)-Fe(1)-C(9)	40.69(10)	C(3)-C(4)-C(29)	120.48(19)
C(13)-Fe(1)-C(9)	119.89(14)	C(5)-C(4)-C(29)	120.74(19)
C(16)-Fe(1)-C(9)	161.53(14)	C(6)-C(5)-C(4)	118.9(2)

C(6)-C(5)-C(35)	117.5(2)	C(12)-C(16)-Fe(1)	69.17(18)
C(4)-C(5)-C(35)	123.59(19)	C(15)-C(16)-Fe(1)	70.13(17)
C(5)-C(6)-C(1)	123.4(2)	C(18)-C(17)-C(22)	117.5(2)
C(8)-C(7)-C(11)	106.5(2)	C(18)-C(17)-C(2)	123.3(2)
C(8)-C(7)-C(1)	129.5(2)	C(22)-C(17)-C(2)	119.2(2)
C(11)-C(7)-C(1)	124.0(2)	C(17)-C(18)-C(19)	120.9(3)
C(8)-C(7)-Fe(1)	68.70(13)	C(20)-C(19)-C(18)	120.6(3)
C(11)-C(7)-Fe(1)	69.10(13)	C(21)-C(20)-C(19)	119.2(3)
C(1)-C(7)-Fe(1)	127.36(15)	C(20)-C(21)-C(22)	120.4(3)
C(9)-C(8)-C(7)	108.8(2)	C(21)-C(22)-C(17)	121.3(3)
C(9)-C(8)-Fe(1)	69.87(15)	C(24)-C(23)-C(28)	118.4(2)
C(7)-C(8)-Fe(1)	70.41(13)	C(24)-C(23)-C(3)	119.3(2)
C(10)-C(9)-C(8)	108.4(2)	C(28)-C(23)-C(3)	122.3(2)
C(10)-C(9)-Fe(1)	69.88(14)	C(23)-C(24)-C(25)	121.3(3)
C(8)-C(9)-Fe(1)	69.44(14)	C(26)-C(25)-C(24)	119.9(3)
C(9)-C(10)-C(11)	107.6(2)	C(27)-C(26)-C(25)	119.6(3)
C(9)-C(10)-Fe(1)	69.60(16)	C(26)-C(27)-C(28)	120.5(3)
C(11)-C(10)-Fe(1)	69.66(13)	C(23)-C(28)-C(27)	120.3(2)
C(10)-C(11)-C(7)	108.7(2)	C(30)-C(29)-C(34)	118.4(2)
C(10)-C(11)-Fe(1)	69.54(14)	C(30)-C(29)-C(4)	121.6(2)
C(7)-C(11)-Fe(1)	69.98(13)	C(34)-C(29)-C(4)	120.0(2)
C(13)-C(12)-C(16)	107.7(3)	C(31)-C(30)-C(29)	120.6(2)
C(13)-C(12)-Fe(1)	70.30(18)	C(32)-C(31)-C(30)	120.3(3)
C(16)-C(12)-Fe(1)	70.22(17)	C(31)-C(32)-C(33)	120.2(3)
C(12)-C(13)-C(14)	107.9(3)	C(32)-C(33)-C(34)	119.8(3)
C(12)-C(13)-Fe(1)	69.30(17)	C(33)-C(34)-C(29)	120.8(2)
C(14)-C(13)-Fe(1)	69.93(16)	C(36)-C(35)-C(40)	118.1(2)
C(15)-C(14)-C(13)	108.6(3)	C(36)-C(35)-C(5)	122.3(2)
C(15)-C(14)-Fe(1)	70.35(16)	C(40)-C(35)-C(5)	119.5(2)
C(13)-C(14)-Fe(1)	69.49(16)	C(35)-C(36)-C(37)	120.3(3)
C(14)-C(15)-C(16)	107.5(3)	C(38)-C(37)-C(36)	120.9(3)
C(14)-C(15)-Fe(1)	69.85(17)	C(39)-C(38)-C(37)	119.4(3)
C(16)-C(15)-Fe(1)	69.25(16)	C(38)-C(39)-C(40)	120.2(3)
C(12)-C(16)-C(15)	108.2(3)	C(39)-C(40)-C(35)	121.1(3)

Symmetry transformations used to generate equivalent atoms:

Table E4. Anisotropic displacement parameters ($Å^2 x\ 10^3$) for **(40)**. The anisotropic displacement factor exponent takes the form: $-2\pi^2[h^2a^{*2}U^{11} + ... + 2hka^*b^*U^{12}]$

	U^{11}	U^{22}	U^{33}	U^{23}	U^{13}	U^{12}
Fe(1)	52(1)	55(1)	52(1)	29(1)	14(1)	26(1)
C(1)	47(1)	41(1)	42(1)	17(1)	10(1)	19(1)
C(2)	47(1)	40(1)	38(1)	15(1)	9(1)	19(1)
C(3)	43(1)	44(1)	35(1)	15(1)	9(1)	19(1)
C(4)	46(1)	41(1)	38(1)	18(1)	10(1)	20(1)

C(5)	48(1)	40(1)	40(1)	17(1)	9(1)	20(1)
C(6)	43(1)	45(1)	45(1)	19(1)	5(1)	19(1)
C(7)	50(1)	39(1)	41(1)	12(1)	3(1)	21(1)
C(8)	52(2)	43(1)	73(2)	24(1)	2(1)	18(1)
C(9)	64(2)	43(2)	81(2)	23(1)	0(1)	26(1)
C(10)	65(2)	61(2)	56(2)	19(1)	10(1)	40(2)
C(11)	55(2)	51(1)	42(1)	19(1)	14(1)	26(1)
C(12)	131(3)	107(3)	55(2)	38(2)	38(2)	80(3)
C(13)	82(2)	138(3)	83(2)	72(2)	47(2)	63(2)
C(14)	88(2)	117(3)	78(2)	70(2)	35(2)	58(2)
C(15)	76(2)	115(3)	56(2)	46(2)	17(2)	46(2)
C(16)	98(3)	71(2)	46(2)	15(2)	13(2)	20(2)
C(17)	45(1)	42(1)	45(1)	18(1)	5(1)	20(1)
C(18)	70(2)	49(2)	57(2)	17(1)	16(1)	26(1)
C(19)	103(3)	45(2)	71(2)	7(2)	1(2)	32(2)
C(20)	69(2)	46(2)	106(3)	34(2)	-12(2)	12(2)
C(21)	60(2)	70(2)	111(3)	57(2)	19(2)	22(2)
C(22)	59(2)	54(2)	69(2)	27(1)	15(1)	27(1)
C(23)	42(1)	37(1)	49(1)	19(1)	7(1)	16(1)
C(24)	52(2)	60(2)	50(2)	19(1)	7(1)	23(1)
C(25)	65(2)	70(2)	53(2)	21(2)	-7(1)	18(2)
C(26)	48(2)	65(2)	86(2)	35(2)	-10(2)	13(2)
C(27)	48(2)	67(2)	101(2)	43(2)	21(2)	29(2)
C(28)	54(2)	51(2)	61(2)	25(1)	13(1)	23(1)
C(29)	40(1)	39(1)	51(1)	21(1)	9(1)	15(1)
C(30)	50(2)	53(2)	58(2)	30(1)	8(1)	19(1)
C(31)	57(2)	66(2)	88(2)	49(2)	2(2)	20(2)
C(32)	55(2)	57(2)	123(3)	48(2)	8(2)	25(2)
C(33)	63(2)	47(2)	95(2)	24(2)	19(2)	29(1)
C(34)	53(2)	49(2)	61(2)	25(1)	14(1)	23(1)
C(35)	44(1)	40(1)	58(2)	17(1)	5(1)	19(1)
C(36)	61(2)	52(2)	78(2)	32(2)	3(2)	18(1)
C(37)	68(2)	52(2)	128(3)	44(2)	-1(2)	14(2)
C(38)	64(2)	43(2)	122(3)	11(2)	-14(2)	13(2)
C(39)	77(2)	62(2)	70(2)	4(2)	-9(2)	22(2)
C(40)	64(2)	51(2)	57(2)	14(1)	1(1)	21(1)

Table E5. Hydrogen coordinates (x 10^4) and isotropic displacement parameters ($Å^2$x 10 ^{3}) for **(40)**.

	x	y	z	U(eq)
H(6)	2392	1345	8465	57
H(8)	-283	-3020	7468	73
H(9)	1390	-3807	7591	80
H(10)	3604	-2030	7671	74
H(11)	3297	-131	7587	61

H(12)	1577	701	10326	106
H(13)	475	-1599	10268	107
H(14)	2232	-2275	10450	99
H(15)	4419	-399	10643	97
H(16)	4021	1457	10575	103
H(18)	-913	-3149	4877	77
H(19)	-2441	-5396	4141	101
H(20)	-4066	-6060	4986	102
H(21)	-4151	-4463	6583	96
H(22)	-2657	-2214	7304	74
H(24)	-1922	-1394	4301	71
H(25)	-3948	-2283	2995	88
H(26)	-5619	-2067	3685	90
H(27)	-5268	-1005	5678	85
H(28)	-3229	-96	6994	69
H(30)	-1085	1577	5376	67
H(31)	-1796	3021	5281	87
H(32)	-1813	4578	6964	95
H(33)	-1041	4765	8767	86
H(34)	-264	3371	8880	67
H(36)	2216	3907	7382	83
H(37)	3749	6168	8541	109
H(38)	4624	7039	10534	114
H(39)	3979	5638	11379	105
H(40)	2459	3376	10236	79

Table E6. Torsion angles [°] for **(40)**.

C(6)-C(1)-C(2)-C(3)	4.4(3)	C(2)-C(1)-C(6)-C(5)	-1.1(3)
C(7)-C(1)-C(2)-C(3)	-173.7(2)	C(7)-C(1)-C(6)-C(5)	177.1(2)
C(6)-C(1)-C(2)-C(17)	-172.3(2)	C(6)-C(1)-C(7)-C(8)	146.3(2)
C(7)-C(1)-C(2)-C(17)	9.6(3)	C(2)-C(1)-C(7)-C(8)	-35.6(4)
C(1)-C(2)-C(3)-C(4)	-4.3(3)	C(6)-C(1)-C(7)-C(11)	-34.3(3)
C(17)-C(2)-C(3)-C(4)	172.4(2)	C(2)-C(1)-C(7)-C(11)	143.8(2)
C(1)-C(2)-C(3)-C(23)	174.2(2)	C(6)-C(1)-C(7)-Fe(1)	54.2(3)
C(17)-C(2)-C(3)-C(23)	-9.1(3)	C(2)-C(1)-C(7)-Fe(1)	-127.7(2)
C(2)-C(3)-C(4)-C(5)	0.9(3)	C(12)-Fe(1)-C(7)-C(8)	-116.90(18)
C(23)-C(3)-C(4)-C(5)	-177.6(2)	C(13)-Fe(1)-C(7)-C(8)	-75.4(2)
C(2)-C(3)-C(4)-C(29)	-176.8(2)	C(16)-Fe(1)-C(7)-C(8)	-158.26(17)
C(23)-C(3)-C(4)-C(29)	4.7(3)	C(9)-Fe(1)-C(7)-C(8)	37.44(15)
C(3)-C(4)-C(5)-C(6)	2.4(3)	C(14)-Fe(1)-C(7)-C(8)	-43.8(3)
C(29)-C(4)-C(5)-C(6)	-180.0(2)	C(10)-Fe(1)-C(7)-C(8)	81.02(16)
C(3)-C(4)-C(5)-C(35)	-178.2(2)	C(11)-Fe(1)-C(7)-C(8)	118.33(19)
C(29)-C(4)-C(5)-C(35)	-0.5(3)	C(15)-Fe(1)-C(7)-C(8)	170.1(3)
C(4)-C(5)-C(6)-C(1)	-2.3(3)	C(12)-Fe(1)-C(7)-C(11)	124.77(17)
C(35)-C(5)-C(6)-C(1)	178.2(2)	C(8)-Fe(1)-C(7)-C(11)	-118.33(19)

C(13)-Fe(1)-C(7)-C(11)	166.28(16)	C(13)-Fe(1)-C(9)-C(8)	77.9(2)
C(16)-Fe(1)-C(7)-C(11)	83.41(18)	C(16)-Fe(1)-C(9)-C(8)	-172.1(4)
C(9)-Fe(1)-C(7)-C(11)	-80.89(15)	C(14)-Fe(1)-C(9)-C(8)	119.82(17)
C(14)-Fe(1)-C(7)-C(11)	-162.1(3)	C(10)-Fe(1)-C(9)-C(8)	-119.8(2)
C(10)-Fe(1)-C(7)-C(11)	-37.31(14)	C(11)-Fe(1)-C(9)-C(8)	-81.74(17)
C(15)-Fe(1)-C(7)-C(11)	51.8(4)	C(15)-Fe(1)-C(9)-C(8)	159.83(17)
C(12)-Fe(1)-C(7)-C(1)	7.2(2)	C(7)-Fe(1)-C(9)-C(8)	-37.62(15)
C(8)-Fe(1)-C(7)-C(1)	124.1(3)	C(8)-C(9)-C(10)-C(11)	-0.6(3)
C(13)-Fe(1)-C(7)-C(1)	48.8(3)	Fe(1)-C(9)-C(10)-C(11)	-59.50(17)
C(16)-Fe(1)-C(7)-C(1)	-34.1(3)	C(8)-C(9)-C(10)-Fe(1)	58.93(19)
C(9)-Fe(1)-C(7)-C(1)	161.6(2)	C(12)-Fe(1)-C(10)-C(9)	-160.8(4)
C(14)-Fe(1)-C(7)-C(1)	80.3(4)	C(8)-Fe(1)-C(10)-C(9)	-37.45(15)
C(10)-Fe(1)-C(7)-C(1)	-154.8(2)	C(13)-Fe(1)-C(10)-C(9)	40.8(3)
C(11)-Fe(1)-C(7)-C(1)	-117.5(2)	C(16)-Fe(1)-C(10)-C(9)	161.80(18)
C(15)-Fe(1)-C(7)-C(1)	-65.7(4)	C(14)-Fe(1)-C(10)-C(9)	77.40(19)
C(11)-C(7)-C(8)-C(9)	-0.5(3)	C(11)-Fe(1)-C(10)-C(9)	-118.9(2)
C(1)-C(7)-C(8)-C(9)	178.9(2)	C(15)-Fe(1)-C(10)-C(9)	119.61(17)
Fe(1)-C(7)-C(8)-C(9)	-59.55(19)	C(7)-Fe(1)-C(10)-C(9)	-81.46(16)
C(11)-C(7)-C(8)-Fe(1)	59.03(15)	C(12)-Fe(1)-C(10)-C(11)	-41.9(4)
C(1)-C(7)-C(8)-Fe(1)	-121.5(2)	C(8)-Fe(1)-C(10)-C(11)	81.42(15)
C(12)-Fe(1)-C(8)-C(9)	-159.54(18)	C(13)-Fe(1)-C(10)-C(11)	159.7(3)
C(13)-Fe(1)-C(8)-C(9)	-118.66(19)	C(16)-Fe(1)-C(10)-C(11)	-79.3(2)
C(16)-Fe(1)-C(8)-C(9)	173.5(3)	C(9)-Fe(1)-C(10)-C(11)	118.9(2)
C(14)-Fe(1)-C(8)-C(9)	-78.0(2)	C(14)-Fe(1)-C(10)-C(11)	-163.73(16)
C(10)-Fe(1)-C(8)-C(9)	37.30(16)	C(15)-Fe(1)-C(10)-C(11)	-121.52(17)
C(11)-Fe(1)-C(8)-C(9)	81.32(17)	C(7)-Fe(1)-C(10)-C(11)	37.41(14)
C(15)-Fe(1)-C(8)-C(9)	-51.3(4)	C(9)-C(10)-C(11)-C(7)	0.3(3)
C(7)-Fe(1)-C(8)-C(9)	119.6(2)	Fe(1)-C(10)-C(11)-C(7)	-59.21(16)
C(12)-Fe(1)-C(8)-C(7)	80.83(19)	C(9)-C(10)-C(11)-Fe(1)	59.46(18)
C(13)-Fe(1)-C(8)-C(7)	121.71(17)	C(8)-C(7)-C(11)-C(10)	0.2(3)
C(16)-Fe(1)-C(8)-C(7)	53.9(4)	C(1)-C(7)-C(11)-C(10)	-179.3(2)
C(9)-Fe(1)-C(8)-C(7)	-119.6(2)	Fe(1)-C(7)-C(11)-C(10)	58.93(16)
C(14)-Fe(1)-C(8)-C(7)	162.36(15)	C(8)-C(7)-C(11)-Fe(1)	-58.78(16)
C(10)-Fe(1)-C(8)-C(7)	-82.33(16)	C(1)-C(7)-C(11)-Fe(1)	121.7(2)
C(11)-Fe(1)-C(8)-C(7)	-38.31(14)	C(12)-Fe(1)-C(11)-C(10)	165.83(18)
C(15)-Fe(1)-C(8)-C(7)	-170.9(3)	C(8)-Fe(1)-C(11)-C(10)	-81.71(16)
C(7)-C(8)-C(9)-C(10)	0.7(3)	C(13)-Fe(1)-C(11)-C(10)	-156.0(3)
Fe(1)-C(8)-C(9)-C(10)	-59.20(19)	C(16)-Fe(1)-C(11)-C(10)	122.43(18)
C(7)-C(8)-C(9)-Fe(1)	59.88(17)	C(9)-Fe(1)-C(11)-C(10)	-37.77(15)
C(12)-Fe(1)-C(9)-C(10)	166.3(3)	C(14)-Fe(1)-C(11)-C(10)	41.4(4)
C(8)-Fe(1)-C(9)-C(10)	119.8(2)	C(15)-Fe(1)-C(11)-C(10)	78.99(19)
C(13)-Fe(1)-C(9)-C(10)	-162.38(16)	C(7)-Fe(1)-C(11)-C(10)	-120.0(2)
C(16)-Fe(1)-C(9)-C(10)	-52.4(4)	C(12)-Fe(1)-C(11)-C(7)	-74.18(19)
C(14)-Fe(1)-C(9)-C(10)	-120.41(17)	C(8)-Fe(1)-C(11)-C(7)	38.29(13)
C(11)-Fe(1)-C(9)-C(10)	38.03(15)	C(13)-Fe(1)-C(11)-C(7)	-36.0(4)
C(15)-Fe(1)-C(9)-C(10)	-80.40(19)	C(16)-Fe(1)-C(11)-C(7)	-117.57(17)
C(7)-Fe(1)-C(9)-C(10)	82.15(16)	C(9)-Fe(1)-C(11)-C(7)	82.22(14)
C(12)-Fe(1)-C(9)-C(8)	46.5(3)	C(14)-Fe(1)-C(11)-C(7)	161.4(3)

C(10)-Fe(1)-C(11)-C(7)	120.0(2)	C(12)-Fe(1)-C(14)-C(13)	37.5(2)
C(15)-Fe(1)-C(11)-C(7)	-161.02(16)	C(8)-Fe(1)-C(14)-C(13)	-75.3(2)
C(8)-Fe(1)-C(12)-C(13)	77.3(2)	C(16)-Fe(1)-C(14)-C(13)	81.6(2)
C(16)-Fe(1)-C(12)-C(13)	-118.2(3)	C(9)-Fe(1)-C(14)-C(13)	-117.0(2)
C(9)-Fe(1)-C(12)-C(13)	44.1(4)	C(10)-Fe(1)-C(14)-C(13)	-158.4(2)
C(14)-Fe(1)-C(12)-C(13)	-37.71(19)	C(11)-Fe(1)-C(14)-C(13)	170.9(3)
C(10)-Fe(1)-C(12)-C(13)	-166.8(3)	C(15)-Fe(1)-C(14)-C(13)	119.7(3)
C(11)-Fe(1)-C(12)-C(13)	160.89(17)	C(7)-Fe(1)-C(14)-C(13)	-43.1(4)
C(15)-Fe(1)-C(12)-C(13)	-80.7(2)	C(13)-C(14)-C(15)-C(16)	0.1(3)
C(7)-Fe(1)-C(12)-C(13)	119.72(19)	Fe(1)-C(14)-C(15)-C(16)	59.2(2)
C(8)-Fe(1)-C(12)-C(16)	-164.54(19)	C(13)-C(14)-C(15)-Fe(1)	-59.2(2)
C(13)-Fe(1)-C(12)-C(16)	118.2(3)	C(12)-Fe(1)-C(15)-C(14)	81.3(2)
C(9)-Fe(1)-C(12)-C(16)	162.3(3)	C(8)-Fe(1)-C(15)-C(14)	-36.7(4)
C(14)-Fe(1)-C(12)-C(16)	80.5(2)	C(13)-Fe(1)-C(15)-C(14)	37.6(2)
C(10)-Fe(1)-C(12)-C(16)	-48.6(5)	C(16)-Fe(1)-C(15)-C(14)	118.8(3)
C(11)-Fe(1)-C(12)-C(16)	-80.9(2)	C(9)-Fe(1)-C(15)-C(14)	-74.4(2)
C(15)-Fe(1)-C(12)-C(16)	37.52(19)	C(10)-Fe(1)-C(15)-C(14)	-117.2(2)
C(7)-Fe(1)-C(12)-C(16)	-122.1(2)	C(11)-Fe(1)-C(15)-C(14)	-160.03(17)
C(16)-C(12)-C(13)-C(14)	-1.1(3)	C(7)-Fe(1)-C(15)-C(14)	161.1(3)
Fe(1)-C(12)-C(13)-C(14)	59.5(2)	C(12)-Fe(1)-C(15)-C(16)	-37.5(2)
C(16)-C(12)-C(13)-Fe(1)	-60.5(2)	C(8)-Fe(1)-C(15)-C(16)	-155.5(3)
C(8)-Fe(1)-C(13)-C(12)	-119.2(2)	C(13)-Fe(1)-C(15)-C(16)	-81.2(2)
C(16)-Fe(1)-C(13)-C(12)	38.3(2)	C(9)-Fe(1)-C(15)-C(16)	166.78(19)
C(9)-Fe(1)-C(13)-C(12)	-160.47(19)	C(14)-Fe(1)-C(15)-C(16)	-118.8(3)
C(14)-Fe(1)-C(13)-C(12)	119.2(3)	C(10)-Fe(1)-C(15)-C(16)	124.0(2)
C(10)-Fe(1)-C(13)-C(12)	170.2(3)	C(11)-Fe(1)-C(15)-C(16)	81.2(2)
C(11)-Fe(1)-C(13)-C(12)	-51.3(4)	C(7)-Fe(1)-C(15)-C(16)	42.3(4)
C(15)-Fe(1)-C(13)-C(12)	82.3(2)	C(13)-C(12)-C(16)-C(15)	1.1(3)
C(7)-Fe(1)-C(13)-C(12)	-78.2(2)	Fe(1)-C(12)-C(16)-C(15)	-59.5(2)
C(12)-Fe(1)-C(13)-C(14)	-119.2(3)	C(13)-C(12)-C(16)-Fe(1)	60.6(2)
C(8)-Fe(1)-C(13)-C(14)	121.6(2)	C(14)-C(15)-C(16)-C(12)	-0.7(3)
C(16)-Fe(1)-C(13)-C(14)	-80.9(2)	Fe(1)-C(15)-C(16)-C(12)	58.9(2)
C(9)-Fe(1)-C(13)-C(14)	80.3(2)	C(14)-C(15)-C(16)-Fe(1)	-59.6(2)
C(10)-Fe(1)-C(13)-C(14)	51.0(4)	C(8)-Fe(1)-C(16)-C(12)	37.0(4)
C(11)-Fe(1)-C(13)-C(14)	-170.5(3)	C(13)-Fe(1)-C(16)-C(12)	-38.10(19)
C(15)-Fe(1)-C(13)-C(14)	-36.9(2)	C(9)-Fe(1)-C(16)-C(12)	-156.4(4)
C(7)-Fe(1)-C(13)-C(14)	162.56(18)	C(14)-Fe(1)-C(16)-C(12)	-82.2(2)
C(12)-C(13)-C(14)-C(15)	0.6(4)	C(10)-Fe(1)-C(16)-C(12)	163.74(18)
Fe(1)-C(13)-C(14)-C(15)	59.7(2)	C(11)-Fe(1)-C(16)-C(12)	120.4(2)
C(12)-C(13)-C(14)-Fe(1)	-59.1(2)	C(15)-Fe(1)-C(16)-C(12)	-119.5(3)
C(12)-Fe(1)-C(14)-C(15)	-82.1(2)	C(7)-Fe(1)-C(16)-C(12)	76.3(2)
C(8)-Fe(1)-C(14)-C(15)	165.01(18)	C(12)-Fe(1)-C(16)-C(15)	119.5(3)
C(13)-Fe(1)-C(14)-C(15)	-119.7(3)	C(8)-Fe(1)-C(16)-C(15)	156.6(3)
C(16)-Fe(1)-C(14)-C(15)	-38.1(2)	C(13)-Fe(1)-C(16)-C(15)	81.4(2)
C(9)-Fe(1)-C(14)-C(15)	123.3(2)	C(9)-Fe(1)-C(16)-C(15)	-36.9(5)
C(10)-Fe(1)-C(14)-C(15)	81.9(2)	C(14)-Fe(1)-C(16)-C(15)	37.38(18)
C(11)-Fe(1)-C(14)-C(15)	51.2(4)	C(10)-Fe(1)-C(16)-C(15)	-76.7(2)
C(7)-Fe(1)-C(14)-C(15)	-162.8(2)	C(11)-Fe(1)-C(16)-C(15)	-120.07(18)

C(7)-Fe(1)-C(16)-C(15)	-164.14(17)	C(3)-C(4)-C(29)-C(30)	-57.5(3)
C(1)-C(2)-C(17)-C(18)	-72.2(3)	C(5)-C(4)-C(29)-C(30)	124.8(2)
C(3)-C(2)-C(17)-C(18)	111.1(3)	C(3)-C(4)-C(29)-C(34)	121.4(2)
C(1)-C(2)-C(17)-C(22)	105.6(3)	C(5)-C(4)-C(29)-C(34)	-56.2(3)
C(3)-C(2)-C(17)-C(22)	-71.1(3)	C(34)-C(29)-C(30)-C(31)	0.2(3)
C(22)-C(17)-C(18)-C(19)	-0.3(4)	C(4)-C(29)-C(30)-C(31)	179.2(2)
C(2)-C(17)-C(18)-C(19)	177.6(2)	C(29)-C(30)-C(31)-C(32)	-1.3(4)
C(17)-C(18)-C(19)-C(20)	-0.1(4)	C(30)-C(31)-C(32)-C(33)	1.3(4)
C(18)-C(19)-C(20)-C(21)	-0.1(5)	C(31)-C(32)-C(33)-C(34)	-0.2(4)
C(19)-C(20)-C(21)-C(22)	0.8(5)	C(32)-C(33)-C(34)-C(29)	-0.9(4)
C(20)-C(21)-C(22)-C(17)	-1.2(4)	C(30)-C(29)-C(34)-C(33)	0.9(3)
C(18)-C(17)-C(22)-C(21)	0.9(4)	C(4)-C(29)-C(34)-C(33)	-178.1(2)
C(2)-C(17)-C(22)-C(21)	-177.0(2)	C(6)-C(5)-C(35)-C(36)	122.8(3)
C(4)-C(3)-C(23)-C(24)	107.6(3)	C(4)-C(5)-C(35)-C(36)	-56.7(3)
C(2)-C(3)-C(23)-C(24)	-71.0(3)	C(6)-C(5)-C(35)-C(40)	-55.1(3)
C(4)-C(3)-C(23)-C(28)	-71.3(3)	C(4)-C(5)-C(35)-C(40)	125.4(3)
C(2)-C(3)-C(23)-C(28)	110.2(2)	C(40)-C(35)-C(36)-C(37)	-1.2(4)
C(28)-C(23)-C(24)-C(25)	0.5(4)	C(5)-C(35)-C(36)-C(37)	-179.1(2)
C(3)-C(23)-C(24)-C(25)	-178.4(2)	C(35)-C(36)-C(37)-C(38)	0.3(5)
C(23)-C(24)-C(25)-C(26)	0.0(4)	C(36)-C(37)-C(38)-C(39)	0.4(5)
C(24)-C(25)-C(26)-C(27)	-0.7(4)	C(37)-C(38)-C(39)-C(40)	-0.2(5)
C(25)-C(26)-C(27)-C(28)	1.0(4)	C(38)-C(39)-C(40)-C(35)	-0.7(5)
C(24)-C(23)-C(28)-C(27)	-0.2(4)	C(36)-C(35)-C(40)-C(39)	1.4(4)
C(3)-C(23)-C(28)-C(27)	178.6(2)	C(5)-C(35)-C(40)-C(39)	179.3(2)
C(26)-C(27)-C(28)-C(23)	-0.5(4)		

Symmetry transformations used to generate equivalent atoms:

Table F1. Crystal data and structure refinement for **(45)**.

Compound		**(45)**
Empirical formula		$C_{50}H_{46}FeN_4$
Formula weight		758.76
Temperature (K)		298(2)
Wavelength (Å)		0.71073
Crystal system		Monoclinic
Space group		P2(1)/c
Unit cell dimensions	a (Å)	6.5053(4)
	b (Å)	31.838(2)
	c (Å)	19.9291(13)
	α (°)	90
	β (°)	91.542(2)
	γ (°)	90
Volume ($Å^3$)		4126.2(5)
Z		4
Density (calculated) (Mg/m^3)		1.221
Absorption coefficient (mm^{-1})		0.404
F(000)		1600
Crystal size (mm^3)		0.3 x 0.23 x 0.05
Theta range for data collection (°)		1.64 to 23.26
Index ranges		-7<=h<=7, -35<=k<=35, -22<=l<=22
Reflections collected		29460
Independent reflections		5919 [R(int) = 0.1196]
Completeness to theta = 23.26° (%)		99.8
Absorption correction		Semi-empirical from equivalents
Max. and min. transmission		1.0000 and 0.8662
Refinement method		Full-matrix least-squares on F^2
Data / restraints / parameters		5919 / 0 / 502
Goodness-of-fit on F^2		1.004
R_1 [I>2sigma(I)]		R1 = 0.0670
wR2 (all data)		wR2 = 0.1807
Largest diff. peak and hole		0.383 and -0.263 e.$Å^{-3}$

Table F2. Atomic coordinates (x 10^4) and equivalent isotropic displacement parameters ($Å^2$x 10^3) for **(45)**. U(eq) is defined as one third of the trace of the orthogonalized U^{ij} tensor.

	x	y	z	U(eq)
Fe(1)	2126(1)	761(1)	10201(1)	56(1)
C(1)	2453(7)	1527(2)	9042(2)	34(1)
C(2)	1806(7)	1911(1)	9321(2)	33(1)
C(3)	2381(7)	2297(1)	9042(2)	34(1)
C(4)	3598(7)	2309(1)	8467(2)	34(1)

C(5)	4241(7)	1929(2)	8181(2)	34(1)
C(6)	3656(7)	1541(1)	8453(2)	36(1)
C(7)	1876(8)	1106(2)	9304(2)	43(1)
C(8)	-79(8)	970(2)	9523(3)	56(2)
C(9)	-49(12)	525(2)	9571(3)	75(2)
C(10)	1878(13)	384(2)	9400(3)	79(2)
C(11)	3084(9)	736(2)	9258(3)	61(2)
C(12)	3578(15)	1092(2)	10950(3)	90(2)
C(13)	1645(14)	976(2)	11154(3)	89(2)
C(14)	1515(14)	535(3)	11133(3)	89(2)
C(15)	3402(15)	384(2)	10909(4)	97(2)
C(16)	4690(13)	723(3)	10805(4)	99(2)
C(17)	289(7)	1930(1)	9883(2)	36(1)
C(18)	-1771(8)	1948(2)	9717(3)	58(2)
C(19)	-3220(8)	1986(2)	10203(3)	69(2)
C(20)	-2653(9)	2013(2)	10858(3)	60(2)
C(21)	-599(9)	2007(2)	11033(3)	62(2)
C(22)	852(8)	1968(2)	10547(2)	49(1)
C(23)	1695(7)	2708(1)	9328(2)	35(1)
C(24)	245(8)	2950(2)	8987(3)	49(1)
C(25)	-326(8)	3340(2)	9223(3)	50(1)
C(26)	513(8)	3508(2)	9809(3)	42(1)
C(27)	1956(8)	3268(2)	10141(2)	48(1)
C(28)	2556(8)	2875(2)	9906(2)	47(1)
C(29)	-124(9)	3938(2)	10043(3)	60(2)
C(30)	811(17)	4261(2)	9581(5)	164(5)
C(31)	500(13)	4027(2)	10769(4)	114(3)
C(32)	-2496(11)	3973(2)	10019(4)	121(3)
C(33)	4044(7)	2714(1)	8139(2)	35(1)
C(34)	3299(8)	2799(2)	7498(2)	45(1)
N(1)	3594(8)	3162(2)	7182(2)	63(1)
C(35)	4692(10)	3442(2)	7527(3)	71(2)
N(2)	5496(7)	3402(1)	8139(2)	61(1)
C(36)	5151(7)	3037(2)	8438(3)	46(1)
C(37)	5548(7)	1939(1)	7575(2)	37(1)
C(38)	4800(8)	1845(2)	6940(3)	56(2)
N(3)	5929(8)	1858(2)	6399(2)	68(1)
C(39)	7882(11)	1964(2)	6496(3)	68(2)
N(4)	8803(7)	2061(2)	7079(3)	64(1)
C(40)	7602(8)	2043(2)	7607(3)	55(2)
C(41)	4119(8)	1151(1)	8063(2)	36(1)
C(42)	2572(8)	944(2)	7720(3)	47(1)
C(43)	2938(8)	580(2)	7381(3)	52(1)
C(44)	4882(9)	404(2)	7351(2)	48(1)
C(45)	6439(8)	619(2)	7684(3)	54(2)
C(46)	6080(8)	988(2)	8028(2)	47(1)
C(47)	5218(9)	-7(2)	6967(3)	60(2)
C(48)	4629(12)	52(2)	6229(3)	109(3)

C(49)	3849(12)	-349(2)	7265(4)	108(3)
C(50)	7419(11)	-164(2)	7028(4)	106(3)

Table F3. Bond lengths [Å] and angles [°] for **(45)**.

Fe(1)-C(11)	1.997(5)	C(25)-C(26)	1.384(7)
Fe(1)-C(10)	2.001(6)	C(26)-C(27)	1.367(7)
Fe(1)-C(9)	2.011(6)	C(26)-C(29)	1.509(7)
Fe(1)-C(15)	2.014(7)	C(27)-C(28)	1.395(7)
Fe(1)-C(16)	2.035(7)	C(29)-C(31)	1.517(8)
Fe(1)-C(12)	2.038(7)	C(29)-C(30)	1.519(8)
Fe(1)-C(14)	2.041(6)	C(29)-C(32)	1.547(8)
Fe(1)-C(13)	2.051(6)	C(33)-C(34)	1.379(6)
Fe(1)-C(8)	2.054(5)	C(33)-C(36)	1.382(6)
Fe(1)-C(7)	2.100(5)	C(34)-N(1)	1.333(6)
C(1)-C(2)	1.414(6)	N(1)-C(35)	1.324(7)
C(1)-C(6)	1.429(6)	C(35)-N(2)	1.320(7)
C(1)-C(7)	1.490(6)	N(2)-C(36)	1.330(6)
C(2)-C(3)	1.404(6)	C(37)-C(40)	1.376(7)
C(2)-C(17)	1.513(6)	C(37)-C(38)	1.377(7)
C(3)-C(4)	1.410(6)	C(38)-N(3)	1.322(6)
C(3)-C(23)	1.499(6)	N(3)-C(39)	1.324(7)
C(4)-C(5)	1.404(6)	C(39)-N(4)	1.328(7)
C(4)-C(33)	1.480(6)	N(4)-C(40)	1.329(6)
C(5)-C(6)	1.405(6)	C(41)-C(42)	1.370(6)
C(5)-C(37)	1.496(6)	C(41)-C(46)	1.381(6)
C(6)-C(41)	1.501(6)	C(42)-C(43)	1.366(7)
C(7)-C(11)	1.420(7)	C(43)-C(44)	1.386(7)
C(7)-C(8)	1.424(7)	C(44)-C(45)	1.378(7)
C(8)-C(9)	1.419(8)	C(44)-C(47)	1.533(7)
C(9)-C(10)	1.384(8)	C(45)-C(46)	1.382(7)
C(10)-C(11)	1.402(8)	C(47)-C(50)	1.518(8)
C(12)-C(13)	1.382(9)	C(47)-C(48)	1.521(8)
C(12)-C(16)	1.413(9)	C(47)-C(49)	1.537(8)
C(13)-C(14)	1.406(9)		
C(14)-C(15)	1.403(9)	C(11)-Fe(1)-C(10)	41.1(2)
C(15)-C(16)	1.384(9)	C(11)-Fe(1)-C(9)	68.3(3)
C(17)-C(22)	1.369(6)	C(10)-Fe(1)-C(9)	40.3(2)
C(17)-C(18)	1.373(6)	C(11)-Fe(1)-C(15)	120.2(3)
C(18)-C(19)	1.374(7)	C(10)-Fe(1)-C(15)	103.0(3)
C(19)-C(20)	1.350(7)	C(9)-Fe(1)-C(15)	119.0(3)
C(20)-C(21)	1.372(7)	C(11)-Fe(1)-C(16)	106.4(3)
C(21)-C(22)	1.376(7)	C(10)-Fe(1)-C(16)	118.9(3)
C(23)-C(28)	1.373(6)	C(9)-Fe(1)-C(16)	154.0(3)
C(23)-C(24)	1.383(6)	C(15)-Fe(1)-C(16)	40.0(3)
C(24)-C(25)	1.382(6)	C(11)-Fe(1)-C(12)	124.0(3)

C(10)-Fe(1)-C(12)	157.0(4)	C(6)-C(5)-C(37)	119.7(4)
C(9)-Fe(1)-C(12)	162.6(4)	C(5)-C(6)-C(1)	120.4(4)
C(15)-Fe(1)-C(12)	67.6(3)	C(5)-C(6)-C(41)	117.9(4)
C(16)-Fe(1)-C(12)	40.6(3)	C(1)-C(6)-C(41)	121.4(4)
C(11)-Fe(1)-C(14)	156.3(3)	C(11)-C(7)-C(8)	105.5(5)
C(10)-Fe(1)-C(14)	120.1(3)	C(11)-C(7)-C(1)	125.4(5)
C(9)-Fe(1)-C(14)	106.6(3)	C(8)-C(7)-C(1)	128.1(5)
C(15)-Fe(1)-C(14)	40.5(3)	C(11)-C(7)-Fe(1)	65.9(3)
C(16)-Fe(1)-C(14)	67.5(3)	C(8)-C(7)-Fe(1)	68.2(3)
C(12)-Fe(1)-C(14)	67.2(3)	C(1)-C(7)-Fe(1)	138.9(3)
C(11)-Fe(1)-C(13)	160.7(3)	C(9)-C(8)-C(7)	108.3(5)
C(10)-Fe(1)-C(13)	158.2(3)	C(9)-C(8)-Fe(1)	67.9(3)
C(9)-Fe(1)-C(13)	125.5(3)	C(7)-C(8)-Fe(1)	71.7(3)
C(15)-Fe(1)-C(13)	67.7(3)	C(10)-C(9)-C(8)	108.7(5)
C(16)-Fe(1)-C(13)	67.3(3)	C(10)-C(9)-Fe(1)	69.5(4)
C(12)-Fe(1)-C(13)	39.5(3)	C(8)-C(9)-Fe(1)	71.2(3)
C(14)-Fe(1)-C(13)	40.2(3)	C(9)-C(10)-C(11)	107.7(5)
C(11)-Fe(1)-C(8)	67.9(2)	C(9)-C(10)-Fe(1)	70.2(4)
C(10)-Fe(1)-C(8)	68.3(3)	C(11)-C(10)-Fe(1)	69.3(3)
C(9)-Fe(1)-C(8)	40.8(2)	C(10)-C(11)-C(7)	109.7(5)
C(15)-Fe(1)-C(8)	157.1(3)	C(10)-C(11)-Fe(1)	69.6(3)
C(16)-Fe(1)-C(8)	162.8(3)	C(7)-C(11)-Fe(1)	73.7(3)
C(12)-Fe(1)-C(8)	128.0(3)	C(13)-C(12)-C(16)	108.3(7)
C(14)-Fe(1)-C(8)	124.2(3)	C(13)-C(12)-Fe(1)	70.8(4)
C(13)-Fe(1)-C(8)	112.3(3)	C(16)-C(12)-Fe(1)	69.6(4)
C(11)-Fe(1)-C(7)	40.5(2)	C(12)-C(13)-C(14)	108.2(7)
C(10)-Fe(1)-C(7)	68.4(2)	C(12)-C(13)-Fe(1)	69.7(4)
C(9)-Fe(1)-C(7)	68.1(2)	C(14)-C(13)-Fe(1)	69.5(4)
C(15)-Fe(1)-C(7)	158.2(3)	C(15)-C(14)-C(13)	107.4(7)
C(16)-Fe(1)-C(7)	125.3(3)	C(15)-C(14)-Fe(1)	68.7(4)
C(12)-Fe(1)-C(7)	112.2(2)	C(13)-C(14)-Fe(1)	70.3(4)
C(14)-Fe(1)-C(7)	161.1(3)	C(16)-C(15)-C(14)	108.6(7)
C(13)-Fe(1)-C(7)	127.1(3)	C(16)-C(15)-Fe(1)	70.8(4)
C(8)-Fe(1)-C(7)	40.1(2)	C(14)-C(15)-Fe(1)	70.8(4)
C(2)-C(1)-C(6)	118.1(4)	C(15)-C(16)-C(12)	107.5(8)
C(2)-C(1)-C(7)	124.1(4)	C(15)-C(16)-Fe(1)	69.2(4)
C(6)-C(1)-C(7)	117.7(4)	C(12)-C(16)-Fe(1)	69.8(4)
C(3)-C(2)-C(1)	121.1(4)	C(22)-C(17)-C(18)	117.6(4)
C(3)-C(2)-C(17)	116.5(4)	C(22)-C(17)-C(2)	123.8(4)
C(1)-C(2)-C(17)	122.1(4)	C(18)-C(17)-C(2)	118.4(4)
C(2)-C(3)-C(4)	120.4(4)	C(17)-C(18)-C(19)	121.2(5)
C(2)-C(3)-C(23)	121.8(4)	C(20)-C(19)-C(18)	120.8(5)
C(4)-C(3)-C(23)	117.8(4)	C(19)-C(20)-C(21)	118.9(5)
C(5)-C(4)-C(3)	119.2(4)	C(20)-C(21)-C(22)	120.3(5)
C(5)-C(4)-C(33)	120.4(4)	C(17)-C(22)-C(21)	121.2(5)
C(3)-C(4)-C(33)	120.2(4)	C(28)-C(23)-C(24)	116.9(4)
C(4)-C(5)-C(6)	120.9(4)	C(28)-C(23)-C(3)	122.6(4)
C(4)-C(5)-C(37)	119.4(4)	C(24)-C(23)-C(3)	120.3(4)

C(25)-C(24)-C(23)	121.4(5)	C(38)-C(37)-C(5)	122.9(4)
C(24)-C(25)-C(26)	122.0(5)	N(3)-C(38)-C(37)	123.6(5)
C(27)-C(26)-C(25)	116.2(5)	C(38)-N(3)-C(39)	116.1(5)
C(27)-C(26)-C(29)	123.3(5)	N(3)-C(39)-N(4)	126.6(5)
C(25)-C(26)-C(29)	120.5(5)	C(39)-N(4)-C(40)	114.9(5)
C(26)-C(27)-C(28)	122.3(5)	N(4)-C(40)-C(37)	124.4(5)
C(23)-C(28)-C(27)	121.2(5)	C(42)-C(41)-C(46)	117.4(4)
C(26)-C(29)-C(31)	113.2(5)	C(42)-C(41)-C(6)	120.1(4)
C(26)-C(29)-C(30)	108.0(5)	C(46)-C(41)-C(6)	122.5(4)
C(31)-C(29)-C(30)	110.6(6)	C(43)-C(42)-C(41)	121.3(5)
C(26)-C(29)-C(32)	109.7(5)	C(42)-C(43)-C(44)	122.4(5)
C(31)-C(29)-C(32)	104.9(6)	C(45)-C(44)-C(43)	115.9(5)
C(30)-C(29)-C(32)	110.3(6)	C(45)-C(44)-C(47)	123.4(5)
C(34)-C(33)-C(36)	114.9(4)	C(43)-C(44)-C(47)	120.6(5)
C(34)-C(33)-C(4)	120.8(4)	C(44)-C(45)-C(46)	121.9(5)
C(36)-C(33)-C(4)	124.3(4)	C(41)-C(46)-C(45)	121.0(5)
N(1)-C(34)-C(33)	123.8(5)	C(50)-C(47)-C(48)	109.3(5)
C(35)-N(1)-C(34)	114.9(5)	C(50)-C(47)-C(44)	112.8(5)
N(2)-C(35)-N(1)	127.5(5)	C(48)-C(47)-C(44)	110.0(5)
C(35)-N(2)-C(36)	115.6(5)	C(50)-C(47)-C(49)	106.9(5)
N(2)-C(36)-C(33)	123.3(5)	C(48)-C(47)-C(49)	109.1(6)
C(40)-C(37)-C(38)	114.4(4)	C(44)-C(47)-C(49)	108.7(5)
C(40)-C(37)-C(5)	122.7(4)		

Symmetry transformations used to generate equivalent atoms:

Table F4. Anisotropic displacement parameters ($Å^2 x\ 10^3$) for **(45)**. The anisotropic displacement factor exponent takes the form: $-2\pi^2[h^2a^{*2}U^{11} + ... + 2hka^*b^*U^{12}]$

	U^{11}	U^{22}	U^{33}	U^{23}	U^{13}	U^{12}
Fe(1)	76(1)	43(1)	50(1)	6(1)	2(1)	-5(1)
C(1)	32(3)	38(3)	32(3)	2(2)	0(2)	0(2)
C(2)	34(3)	38(3)	28(3)	5(2)	1(2)	0(2)
C(3)	32(3)	37(3)	33(3)	-1(2)	-3(2)	5(2)
C(4)	30(3)	37(3)	36(3)	-2(2)	0(2)	-6(2)
C(5)	31(3)	42(3)	30(3)	-2(2)	-4(2)	-1(2)
C(6)	37(3)	35(3)	36(3)	3(2)	-1(2)	-3(2)
C(7)	53(3)	38(3)	37(3)	3(2)	6(3)	-1(3)
C(8)	54(4)	58(4)	55(4)	12(3)	-7(3)	-13(3)
C(9)	108(6)	51(4)	65(4)	14(3)	-3(4)	-36(4)
C(10)	139(7)	37(4)	62(4)	-3(3)	23(4)	-1(4)
C(11)	86(4)	41(4)	59(4)	13(3)	26(3)	10(3)
C(12)	143(7)	69(5)	58(4)	11(4)	-26(5)	-31(6)
C(13)	143(7)	76(6)	49(4)	0(4)	14(4)	-10(5)
C(14)	133(7)	85(6)	50(4)	22(4)	-3(4)	-35(5)
C(15)	131(7)	63(5)	94(6)	25(4)	-39(5)	-8(6)

C(16)	98(6)	84(6)	112(6)	21(5)	-27(5)	-12(5)
C(17)	37(3)	32(3)	39(3)	3(2)	6(2)	-2(2)
C(18)	46(4)	90(5)	37(3)	10(3)	-3(3)	-2(3)
C(19)	37(3)	105(5)	64(4)	7(4)	3(3)	4(3)
C(20)	47(4)	76(4)	57(4)	-5(3)	22(3)	0(3)
C(21)	63(4)	84(5)	40(3)	-9(3)	13(3)	-3(4)
C(22)	40(3)	67(4)	41(3)	-7(3)	2(3)	1(3)
C(23)	36(3)	30(3)	37(3)	0(2)	1(2)	0(2)
C(24)	50(3)	46(3)	50(3)	-16(3)	-11(3)	0(3)
C(25)	44(3)	39(3)	66(4)	-1(3)	-7(3)	9(3)
C(26)	46(3)	31(3)	49(3)	-1(3)	6(3)	1(3)
C(27)	65(4)	47(3)	32(3)	-9(3)	-2(3)	-1(3)
C(28)	54(3)	44(3)	41(3)	-1(3)	-6(3)	5(3)
C(29)	74(4)	35(3)	71(4)	-4(3)	5(3)	5(3)
C(30)	286(13)	42(4)	171(9)	9(5)	118(9)	0(6)
C(31)	182(8)	62(5)	97(6)	-40(4)	-18(5)	21(5)
C(32)	128(7)	91(6)	145(8)	-47(5)	8(6)	54(5)
C(33)	40(3)	33(3)	34(3)	-1(2)	3(2)	0(2)
C(34)	61(4)	34(3)	39(3)	1(2)	-6(3)	-9(3)
N(1)	90(4)	46(3)	51(3)	7(2)	-13(3)	-13(3)
C(35)	96(5)	49(4)	68(5)	24(3)	-10(4)	-17(4)
N(2)	78(4)	43(3)	62(3)	9(3)	-12(3)	-19(3)
C(36)	46(3)	50(4)	43(3)	6(3)	0(3)	-2(3)
C(37)	41(3)	38(3)	34(3)	-3(2)	5(2)	-2(3)
C(38)	51(4)	70(4)	46(4)	-2(3)	10(3)	-11(3)
N(3)	70(4)	89(4)	46(3)	-12(3)	15(3)	-13(3)
C(39)	82(5)	73(5)	51(4)	-3(3)	34(4)	-3(4)
N(4)	56(3)	80(4)	59(3)	2(3)	21(3)	-14(3)
C(40)	53(4)	69(4)	44(3)	2(3)	6(3)	-9(3)
C(41)	45(3)	27(3)	38(3)	1(2)	9(2)	1(3)
C(42)	43(3)	42(3)	58(4)	-9(3)	1(3)	4(3)
C(43)	53(4)	48(4)	53(3)	-10(3)	-12(3)	-5(3)
C(44)	59(4)	39(3)	46(3)	-6(3)	5(3)	6(3)
C(45)	41(3)	53(4)	66(4)	-8(3)	9(3)	9(3)
C(46)	44(3)	41(3)	57(4)	-13(3)	1(3)	-5(3)
C(47)	78(4)	41(4)	61(4)	-15(3)	1(3)	12(3)
C(48)	185(8)	81(5)	61(5)	-26(4)	-8(5)	45(5)
C(49)	146(7)	42(4)	137(7)	-18(4)	20(5)	4(5)
C(50)	113(6)	82(5)	124(6)	-53(5)	-8(5)	43(5)

Table F5. Hydrogen coordinates (x 10^4) and isotropic displacement parameters ($Å^2$x 10^3) for **(45)**.

	x	y	z	U(eq)
H(8)	-1244	1152	9625	67
H(9)	-1204	348	9700	89

H(10)	2319	90	9379	95
H(11)	4525	727	9128	74
H(12)	4094	1380	10916	108
H(13)	550	1168	11286	107
H(14)	325	365	11254	107
H(15)	3763	88	10849	116
H(16)	6113	709	10658	118
H(18)	-2193	1935	9268	69
H(19)	-4607	1993	10078	82
H(20)	-3639	2035	11186	72
H(21)	-186	2028	11482	74
H(22)	2240	1968	10672	59
H(24)	-358	2848	8591	59
H(25)	-1304	3494	8979	60
H(27)	2558	3370	10537	58
H(28)	3557	2724	10144	56
H(30A)	2283	4252	9628	247
H(30B)	333	4536	9697	247
H(30C)	408	4200	9124	247
H(31A)	-33	3810	11051	171
H(31B)	-46	4294	10901	171
H(31C)	1972	4032	10814	171
H(32A)	-2993	3943	9564	182
H(32B)	-2896	4243	10187	182
H(32C)	-3070	3756	10291	182
H(34)	2548	2590	7274	54
H(35)	4924	3697	7313	86
H(36)	5681	2996	8872	56
H(38)	3425	1768	6889	67
H(39)	8691	1972	6119	82
H(40)	8189	2104	8026	66
H(42)	1246	1054	7719	57
H(43)	1843	446	7161	62
H(45)	7771	513	7676	64
H(46)	7173	1127	8238	57
H(48A)	5432	275	6046	163
H(48B)	3195	121	6186	163
H(48C)	4888	-203	5990	163
H(49A)	4061	-609	7032	162
H(49B)	2432	-268	7215	162
H(49C)	4198	-385	7732	162
H(50A)	7508	-438	6830	160
H(50B)	7832	-180	7494	160
H(50C)	8309	26	6800	160

Table F6. Torsion angles [°] for **(45)**.

C(6)-C(1)-C(2)-C(3)	-2.0(7)	C(11)-Fe(1)-C(7)-C(1)	-116.8(7)
C(7)-C(1)-C(2)-C(3)	-178.9(4)	C(10)-Fe(1)-C(7)-C(1)	-155.0(6)
C(6)-C(1)-C(2)-C(17)	171.3(4)	C(9)-Fe(1)-C(7)-C(1)	161.4(6)
C(7)-C(1)-C(2)-C(17)	-5.6(7)	C(15)-Fe(1)-C(7)-C(1)	-84.8(9)
C(1)-C(2)-C(3)-C(4)	0.9(7)	C(16)-Fe(1)-C(7)-C(1)	-44.1(7)
C(17)-C(2)-C(3)-C(4)	-172.7(4)	C(12)-Fe(1)-C(7)-C(1)	0.2(6)
C(1)-C(2)-C(3)-C(23)	179.5(4)	C(14)-Fe(1)-C(7)-C(1)	84.3(9)
C(17)-C(2)-C(3)-C(23)	5.9(6)	C(13)-Fe(1)-C(7)-C(1)	42.7(7)
C(2)-C(3)-C(4)-C(5)	-0.5(7)	C(8)-Fe(1)-C(7)-C(1)	123.5(7)
C(23)-C(3)-C(4)-C(5)	-179.1(4)	C(11)-C(7)-C(8)-C(9)	-3.0(6)
C(2)-C(3)-C(4)-C(33)	174.5(4)	C(1)-C(7)-C(8)-C(9)	165.8(5)
C(23)-C(3)-C(4)-C(33)	-4.2(6)	Fe(1)-C(7)-C(8)-C(9)	-58.3(4)
C(3)-C(4)-C(5)-C(6)	1.1(7)	C(11)-C(7)-C(8)-Fe(1)	55.4(3)
C(33)-C(4)-C(5)-C(6)	-173.8(4)	C(1)-C(7)-C(8)-Fe(1)	-135.9(5)
C(3)-C(4)-C(5)-C(37)	-179.5(4)	C(11)-Fe(1)-C(8)-C(9)	81.9(4)
C(33)-C(4)-C(5)-C(37)	5.6(7)	C(10)-Fe(1)-C(8)-C(9)	37.5(4)
C(4)-C(5)-C(6)-C(1)	-2.2(7)	C(15)-Fe(1)-C(8)-C(9)	-33.8(9)
C(37)-C(5)-C(6)-C(1)	178.4(4)	C(16)-Fe(1)-C(8)-C(9)	155.8(10)
C(4)-C(5)-C(6)-C(41)	170.7(4)	C(12)-Fe(1)-C(8)-C(9)	-161.4(5)
C(37)-C(5)-C(6)-C(41)	-8.7(6)	C(14)-Fe(1)-C(8)-C(9)	-75.0(5)
C(2)-C(1)-C(6)-C(5)	2.6(7)	C(13)-Fe(1)-C(8)-C(9)	-119.0(4)
C(7)-C(1)-C(6)-C(5)	179.7(4)	C(7)-Fe(1)-C(8)-C(9)	119.3(5)
C(2)-C(1)-C(6)-C(41)	-170.1(4)	C(11)-Fe(1)-C(8)-C(7)	-37.5(3)
C(7)-C(1)-C(6)-C(41)	7.1(7)	C(10)-Fe(1)-C(8)-C(7)	-81.9(3)
C(2)-C(1)-C(7)-C(11)	-150.9(5)	C(9)-Fe(1)-C(8)-C(7)	-119.3(5)
C(6)-C(1)-C(7)-C(11)	32.1(7)	C(15)-Fe(1)-C(8)-C(7)	-153.1(8)
C(2)-C(1)-C(7)-C(8)	42.4(7)	C(16)-Fe(1)-C(8)-C(7)	36.5(11)
C(6)-C(1)-C(7)-C(8)	-134.6(5)	C(12)-Fe(1)-C(8)-C(7)	79.3(5)
C(2)-C(1)-C(7)-Fe(1)	-58.0(7)	C(14)-Fe(1)-C(8)-C(7)	165.7(4)
C(6)-C(1)-C(7)-Fe(1)	125.0(5)	C(13)-Fe(1)-C(8)-C(7)	121.7(4)
C(10)-Fe(1)-C(7)-C(11)	-38.2(4)	C(7)-C(8)-C(9)-C(10)	1.1(7)
C(9)-Fe(1)-C(7)-C(11)	-81.8(4)	Fe(1)-C(8)-C(9)-C(10)	-59.6(4)
C(15)-Fe(1)-C(7)-C(11)	32.0(8)	C(7)-C(8)-C(9)-Fe(1)	60.7(4)
C(16)-Fe(1)-C(7)-C(11)	72.7(5)	C(11)-Fe(1)-C(9)-C(10)	38.3(3)
C(12)-Fe(1)-C(7)-C(11)	117.0(4)	C(15)-Fe(1)-C(9)-C(10)	-75.1(5)
C(14)-Fe(1)-C(7)-C(11)	-158.9(7)	C(16)-Fe(1)-C(9)-C(10)	-44.7(8)
C(13)-Fe(1)-C(7)-C(11)	159.5(4)	C(12)-Fe(1)-C(9)-C(10)	176.4(8)
C(8)-Fe(1)-C(7)-C(11)	-119.7(5)	C(14)-Fe(1)-C(9)-C(10)	-117.2(4)
C(11)-Fe(1)-C(7)-C(8)	119.7(5)	C(13)-Fe(1)-C(9)-C(10)	-157.2(4)
C(10)-Fe(1)-C(7)-C(8)	81.5(4)	C(8)-Fe(1)-C(9)-C(10)	119.2(5)
C(9)-Fe(1)-C(7)-C(8)	37.9(4)	C(7)-Fe(1)-C(9)-C(10)	82.0(4)
C(15)-Fe(1)-C(7)-C(8)	151.7(7)	C(11)-Fe(1)-C(9)-C(8)	-80.9(4)
C(16)-Fe(1)-C(7)-C(8)	-167.6(4)	C(10)-Fe(1)-C(9)-C(8)	-119.2(5)
C(12)-Fe(1)-C(7)-C(8)	-123.3(4)	C(15)-Fe(1)-C(9)-C(8)	165.6(4)
C(14)-Fe(1)-C(7)-C(8)	-39.2(9)	C(16)-Fe(1)-C(9)-C(8)	-164.0(6)
C(13)-Fe(1)-C(7)-C(8)	-80.8(5)	C(12)-Fe(1)-C(9)-C(8)	57.2(9)

C(14)-Fe(1)-C(9)-C(8)	123.6(4)	C(9)-Fe(1)-C(12)-C(13)	34.7(11)
C(13)-Fe(1)-C(9)-C(8)	83.6(4)	C(15)-Fe(1)-C(12)-C(13)	-81.5(5)
C(7)-Fe(1)-C(9)-C(8)	-37.2(3)	C(16)-Fe(1)-C(12)-C(13)	-119.0(6)
C(8)-C(9)-C(10)-C(11)	1.3(7)	C(14)-Fe(1)-C(12)-C(13)	-37.5(5)
Fe(1)-C(9)-C(10)-C(11)	-59.4(4)	C(8)-Fe(1)-C(12)-C(13)	79.0(5)
C(8)-C(9)-C(10)-Fe(1)	60.7(4)	C(7)-Fe(1)-C(12)-C(13)	122.0(4)
C(11)-Fe(1)-C(10)-C(9)	-118.8(5)	C(11)-Fe(1)-C(12)-C(16)	-74.7(5)
C(15)-Fe(1)-C(10)-C(9)	119.8(4)	C(10)-Fe(1)-C(12)-C(16)	-32.3(9)
C(16)-Fe(1)-C(10)-C(9)	159.4(4)	C(9)-Fe(1)-C(12)-C(16)	153.7(8)
C(12)-Fe(1)-C(10)-C(9)	-177.3(6)	C(15)-Fe(1)-C(12)-C(16)	37.4(5)
C(14)-Fe(1)-C(10)-C(9)	80.1(5)	C(14)-Fe(1)-C(12)-C(16)	81.4(5)
C(13)-Fe(1)-C(10)-C(9)	58.1(9)	C(13)-Fe(1)-C(12)-C(16)	119.0(6)
C(8)-Fe(1)-C(10)-C(9)	-37.9(3)	C(8)-Fe(1)-C(12)-C(16)	-162.1(4)
C(7)-Fe(1)-C(10)-C(9)	-81.1(4)	C(7)-Fe(1)-C(12)-C(16)	-119.0(5)
C(9)-Fe(1)-C(10)-C(11)	118.8(5)	C(16)-C(12)-C(13)-C(14)	-0.6(8)
C(15)-Fe(1)-C(10)-C(11)	-121.4(5)	Fe(1)-C(12)-C(13)-C(14)	59.1(5)
C(16)-Fe(1)-C(10)-C(11)	-81.8(5)	C(16)-C(12)-C(13)-Fe(1)	-59.7(5)
C(12)-Fe(1)-C(10)-C(11)	-58.5(8)	C(11)-Fe(1)-C(13)-C(12)	-36.5(11)
C(14)-Fe(1)-C(10)-C(11)	-161.1(4)	C(10)-Fe(1)-C(13)-C(12)	149.6(8)
C(13)-Fe(1)-C(10)-C(11)	176.9(7)	C(9)-Fe(1)-C(13)-C(12)	-168.0(4)
C(8)-Fe(1)-C(10)-C(11)	80.9(4)	C(15)-Fe(1)-C(13)-C(12)	81.5(5)
C(7)-Fe(1)-C(10)-C(11)	37.6(3)	C(16)-Fe(1)-C(13)-C(12)	38.1(4)
C(9)-C(10)-C(11)-C(7)	-3.2(7)	C(14)-Fe(1)-C(13)-C(12)	119.5(7)
Fe(1)-C(10)-C(11)-C(7)	-63.2(4)	C(8)-Fe(1)-C(13)-C(12)	-123.3(5)
C(9)-C(10)-C(11)-Fe(1)	59.9(4)	C(7)-Fe(1)-C(13)-C(12)	-80.0(5)
C(8)-C(7)-C(11)-C(10)	3.8(6)	C(11)-Fe(1)-C(13)-C(14)	-156.0(8)
C(1)-C(7)-C(11)-C(10)	-165.3(5)	C(10)-Fe(1)-C(13)-C(14)	30.1(11)
Fe(1)-C(7)-C(11)-C(10)	60.7(4)	C(9)-Fe(1)-C(13)-C(14)	72.6(6)
C(8)-C(7)-C(11)-Fe(1)	-56.8(3)	C(15)-Fe(1)-C(13)-C(14)	-38.0(5)
C(1)-C(7)-C(11)-Fe(1)	134.0(5)	C(16)-Fe(1)-C(13)-C(14)	-81.4(5)
C(9)-Fe(1)-C(11)-C(10)	-37.6(4)	C(12)-Fe(1)-C(13)-C(14)	-119.5(7)
C(15)-Fe(1)-C(11)-C(10)	74.2(5)	C(8)-Fe(1)-C(13)-C(14)	117.2(5)
C(16)-Fe(1)-C(11)-C(10)	115.4(5)	C(7)-Fe(1)-C(13)-C(14)	160.6(5)
C(12)-Fe(1)-C(11)-C(10)	156.3(5)	C(12)-C(13)-C(14)-C(15)	-0.3(8)
C(14)-Fe(1)-C(11)-C(10)	44.2(9)	Fe(1)-C(13)-C(14)-C(15)	58.9(5)
C(13)-Fe(1)-C(11)-C(10)	-176.5(8)	C(12)-C(13)-C(14)-Fe(1)	-59.2(5)
C(8)-Fe(1)-C(11)-C(10)	-81.8(4)	C(11)-Fe(1)-C(14)-C(15)	41.8(9)
C(7)-Fe(1)-C(11)-C(10)	-118.9(5)	C(10)-Fe(1)-C(14)-C(15)	73.8(6)
C(10)-Fe(1)-C(11)-C(7)	118.9(5)	C(9)-Fe(1)-C(14)-C(15)	115.5(5)
C(9)-Fe(1)-C(11)-C(7)	81.3(4)	C(16)-Fe(1)-C(14)-C(15)	-37.6(5)
C(15)-Fe(1)-C(11)-C(7)	-166.9(4)	C(12)-Fe(1)-C(14)-C(15)	-81.8(5)
C(16)-Fe(1)-C(11)-C(7)	-125.7(4)	C(13)-Fe(1)-C(14)-C(15)	-118.7(7)
C(12)-Fe(1)-C(11)-C(7)	-84.8(4)	C(8)-Fe(1)-C(14)-C(15)	156.7(4)
C(14)-Fe(1)-C(11)-C(7)	163.1(6)	C(7)-Fe(1)-C(14)-C(15)	-173.8(6)
C(13)-Fe(1)-C(11)-C(7)	-57.6(10)	C(11)-Fe(1)-C(14)-C(13)	160.5(6)
C(8)-Fe(1)-C(11)-C(7)	37.1(3)	C(10)-Fe(1)-C(14)-C(13)	-167.6(5)
C(11)-Fe(1)-C(12)-C(13)	166.3(4)	C(9)-Fe(1)-C(14)-C(13)	-125.8(5)
C(10)-Fe(1)-C(12)-C(13)	-151.2(6)	C(15)-Fe(1)-C(14)-C(13)	118.7(7)

C(16)-Fe(1)-C(14)-C(13)	81.1(5)	C(1)-C(2)-C(17)-C(18)	-89.1(6)
C(12)-Fe(1)-C(14)-C(13)	36.9(5)	C(22)-C(17)-C(18)-C(19)	-2.7(8)
C(8)-Fe(1)-C(14)-C(13)	-84.6(5)	C(2)-C(17)-C(18)-C(19)	-176.8(5)
C(7)-Fe(1)-C(14)-C(13)	-55.1(10)	C(17)-C(18)-C(19)-C(20)	1.1(9)
C(13)-C(14)-C(15)-C(16)	1.1(8)	C(18)-C(19)-C(20)-C(21)	0.7(9)
Fe(1)-C(14)-C(15)-C(16)	61.0(5)	C(19)-C(20)-C(21)-C(22)	-0.8(9)
C(13)-C(14)-C(15)-Fe(1)	-59.9(5)	C(18)-C(17)-C(22)-C(21)	2.6(8)
C(11)-Fe(1)-C(15)-C(16)	79.4(6)	C(2)-C(17)-C(22)-C(21)	176.4(5)
C(10)-Fe(1)-C(15)-C(16)	119.9(6)	C(20)-C(21)-C(22)-C(17)	-0.9(9)
C(9)-Fe(1)-C(15)-C(16)	159.8(5)	C(2)-C(3)-C(23)-C(28)	76.3(6)
C(12)-Fe(1)-C(15)-C(16)	-38.0(5)	C(4)-C(3)-C(23)-C(28)	-105.1(5)
C(14)-Fe(1)-C(15)-C(16)	-118.6(7)	C(2)-C(3)-C(23)-C(24)	-108.4(5)
C(13)-Fe(1)-C(15)-C(16)	-80.9(5)	C(4)-C(3)-C(23)-C(24)	70.2(6)
C(8)-Fe(1)-C(15)-C(16)	-175.6(6)	C(28)-C(23)-C(24)-C(25)	-0.8(7)
C(7)-Fe(1)-C(15)-C(16)	56.0(9)	C(3)-C(23)-C(24)-C(25)	-176.4(5)
C(11)-Fe(1)-C(15)-C(14)	-162.0(4)	C(23)-C(24)-C(25)-C(26)	-0.2(8)
C(10)-Fe(1)-C(15)-C(14)	-121.5(5)	C(24)-C(25)-C(26)-C(27)	0.6(7)
C(9)-Fe(1)-C(15)-C(14)	-81.6(5)	C(24)-C(25)-C(26)-C(29)	178.9(5)
C(16)-Fe(1)-C(15)-C(14)	118.6(7)	C(25)-C(26)-C(27)-C(28)	-0.1(7)
C(12)-Fe(1)-C(15)-C(14)	80.6(5)	C(29)-C(26)-C(27)-C(28)	-178.4(5)
C(13)-Fe(1)-C(15)-C(14)	37.7(4)	C(24)-C(23)-C(28)-C(27)	1.3(7)
C(8)-Fe(1)-C(15)-C(14)	-57.0(9)	C(3)-C(23)-C(28)-C(27)	176.7(4)
C(7)-Fe(1)-C(15)-C(14)	174.6(5)	C(26)-C(27)-C(28)-C(23)	-0.9(8)
C(14)-C(15)-C(16)-C(12)	-1.5(8)	C(27)-C(26)-C(29)-C(31)	-16.7(8)
Fe(1)-C(15)-C(16)-C(12)	59.5(5)	C(25)-C(26)-C(29)-C(31)	165.1(5)
C(14)-C(15)-C(16)-Fe(1)	-61.0(5)	C(27)-C(26)-C(29)-C(30)	106.2(7)
C(13)-C(12)-C(16)-C(15)	1.3(8)	C(25)-C(26)-C(29)-C(30)	-72.0(8)
Fe(1)-C(12)-C(16)-C(15)	-59.2(5)	C(27)-C(26)-C(29)-C(32)	-133.5(6)
C(13)-C(12)-C(16)-Fe(1)	60.5(5)	C(25)-C(26)-C(29)-C(32)	48.3(7)
C(11)-Fe(1)-C(16)-C(15)	-117.6(6)	C(5)-C(4)-C(33)-C(34)	60.4(6)
C(10)-Fe(1)-C(16)-C(15)	-74.9(6)	C(3)-C(4)-C(33)-C(34)	-114.5(5)
C(9)-Fe(1)-C(16)-C(15)	-43.5(10)	C(5)-C(4)-C(33)-C(36)	-121.6(5)
C(12)-Fe(1)-C(16)-C(15)	118.9(7)	C(3)-C(4)-C(33)-C(36)	63.6(6)
C(14)-Fe(1)-C(16)-C(15)	38.1(5)	C(36)-C(33)-C(34)-N(1)	-0.3(7)
C(13)-Fe(1)-C(16)-C(15)	81.8(5)	C(4)-C(33)-C(34)-N(1)	178.0(5)
C(8)-Fe(1)-C(16)-C(15)	174.2(9)	C(33)-C(34)-N(1)-C(35)	0.7(8)
C(7)-Fe(1)-C(16)-C(15)	-157.8(5)	C(34)-N(1)-C(35)-N(2)	-0.5(9)
C(11)-Fe(1)-C(16)-C(12)	123.5(5)	N(1)-C(35)-N(2)-C(36)	-0.1(9)
C(10)-Fe(1)-C(16)-C(12)	166.2(4)	C(35)-N(2)-C(36)-C(33)	0.5(8)
C(9)-Fe(1)-C(16)-C(12)	-162.4(6)	C(34)-C(33)-C(36)-N(2)	-0.4(7)
C(15)-Fe(1)-C(16)-C(12)	-118.9(7)	C(4)-C(33)-C(36)-N(2)	-178.5(5)
C(14)-Fe(1)-C(16)-C(12)	-80.8(5)	C(4)-C(5)-C(37)-C(40)	74.9(6)
C(13)-Fe(1)-C(16)-C(12)	-37.1(4)	C(6)-C(5)-C(37)-C(40)	-105.7(6)
C(8)-Fe(1)-C(16)-C(12)	55.3(12)	C(4)-C(5)-C(37)-C(38)	-105.2(6)
C(7)-Fe(1)-C(16)-C(12)	83.3(5)	C(6)-C(5)-C(37)-C(38)	74.3(6)
C(3)-C(2)-C(17)-C(22)	-89.3(6)	C(40)-C(37)-C(38)-N(3)	-1.0(8)
C(1)-C(2)-C(17)-C(22)	97.1(6)	C(5)-C(37)-C(38)-N(3)	179.0(5)
C(3)-C(2)-C(17)-C(18)	84.5(6)	C(37)-C(38)-N(3)-C(39)	0.7(9)

C(38)-N(3)-C(39)-N(4)	-0.5(9)	C(42)-C(43)-C(44)-C(47)	179.6(5)
N(3)-C(39)-N(4)-C(40)	0.5(9)	C(43)-C(44)-C(45)-C(46)	0.2(8)
C(39)-N(4)-C(40)-C(37)	-0.8(8)	C(47)-C(44)-C(45)-C(46)	-179.7(5)
C(38)-C(37)-C(40)-N(4)	1.1(8)	C(42)-C(41)-C(46)-C(45)	-2.8(7)
C(5)-C(37)-C(40)-N(4)	-179.0(5)	C(6)-C(41)-C(46)-C(45)	177.6(5)
C(5)-C(6)-C(41)-C(42)	-105.0(5)	C(44)-C(45)-C(46)-C(41)	1.4(8)
C(1)-C(6)-C(41)-C(42)	67.8(6)	C(45)-C(44)-C(47)-C(50)	3.5(8)
C(5)-C(6)-C(41)-C(46)	74.5(6)	C(43)-C(44)-C(47)-C(50)	-176.4(5)
C(1)-C(6)-C(41)-C(46)	-112.7(5)	C(45)-C(44)-C(47)-C(48)	-118.8(6)
C(46)-C(41)-C(42)-C(43)	2.8(7)	C(43)-C(44)-C(47)-C(48)	61.2(7)
C(6)-C(41)-C(42)-C(43)	-177.7(5)	C(45)-C(44)-C(47)-C(49)	121.8(6)
C(41)-C(42)-C(43)-C(44)	-1.2(8)	C(43)-C(44)-C(47)-C(49)	-58.1(7)
C(42)-C(43)-C(44)-C(45)	-0.3(8)		

Symmetry transformations used to generate equivalent atoms:

APPENDIX 2

The dipole moment was calculated using semi-empirical quantum mechanics (AM1 parameter set)

For comparison phenol, pyridine and toluene were also calculated using the same method. The results are presented in the table below, and show good correlation to literature values (quoted from the "CRC Handbook of Chemistry and Physics 57th Edition", CRC Press 1976, table E65).

Compound	Calculated Dipole Moment (using quantum mechanics)	Actual Dipole Moment
Phenol	1.2 D	1.45 D
Pyridine	2.0 D	2.19 D
Toluene	0.3 D	0.36 D
N-HBC **(17)**	6.2 D	-